TEKA

KOMISJI MOTORYZACJI
I ENERGETYKI ROLNICTWA
POLITECHNIKA LUBELSKA
WSCHODNIOUKRAIŃSKI NARODOWY UNIWERSYTET
IM. WOŁODYMYRA DALA W ŁUGAŃSKU

COMMISSION OF MOTORIZATION
AND POWER INDUSTRY IN AGRICULTURE
LUBLIN UNIVERSITY OF TECHNOLOGY
THE VOLODYMIR DAHL EAST-UKRAINIAN
NATIONAL UNIVERSITY OF ŁUGAŃSK

POLSKA AKADEMIA NAUK ODDZIAŁ W LUBLINIE
POLITECHNIKA LUBELSKA
WSCHODNIOUKRAIŃSKI NARODOWY UNIWERSYTET
IM. WOŁODYMYRA DALA W ŁUGAŃSKU

TEKA

KOMISJI MOTORYZACJI I ENERGETYKI ROLNICTWA

POLITECHNIKI LUBELSKIEJ

WSCHODNIOUKRAIŃSKIEGO NARODOWEGO UNIWERSYTETU IM. WOŁODYMYRA DALA W ŁUGAŃSKU

Tom XI

LUBLIN 2011

POLISH ACADEMY OF SCIENCES BRANCH IN LUBLIN
LUBLIN UNIVERSITY OF TECHNOLOGY
THE VOLODYMIR DAHL EAST-UKRAINIAN
NATIONAL UNIVERSITY OF ŁUGAŃSK

TEKA

COMMISSION OF MOTORIZATION AND POWER INDUSTRY IN AGRICULTURE

LUBLIN UNIVERSITY OF TECHNOLOGY

THE VOLODYMIR DAHL EAST-UKRAINIAN NATIONAL UNIVERSITY OF ŁUGAŃSK

Volume XI

LUBLIN 2011

Linguistic consultant: *Małgorzata Wojcieszuk*
Technical editor: *Robert Kryński*
Typeset: *Robert Kryński, Hanna Krasowska-Kołodziej*
Cover design: *Barbara Jarosik*

Commission of Motorization and Power Industry in Agriculture
Wielkopolska Str. 62, 20-725 Lublin, Poland
e-mail: eugeniusz.krasowski@up.lublin.pl

ISSN 1641-7739

Edition 150 + 16 vol.

Anniversary of "Teka"- journal of the Commission of Motorization and Power Industry in Agriculture at the Polish Academy of Sciences Branch in Lublin

In 2001 the first volume of "Teka" was released. The editor in chief, prof. dr hab. inż Eugeniusz Krasowski invited the most prominent publishing specialists from many research centers in the country and abroad, mostly members of the Commission of Motorization and Power Industry in Agriculture at the Polish Academy of Sciences - Branch in Lublin.

The fast-growing cooperation has resulted in the integration of research centers, which became a solid basis for the development of publishing. Success has been achieved by the obtainment for the journal "Teka" of 9 points from the Ministry of Science and Higher Education. This success has been made possible through the cooperation of research centers such as: Cracow University of Technology, Poznan University of Technology, Lublin University of Technology, Czestochowa University of Technology, Szczecin University of Technology, Warsaw University of Technology, Bialystok University of Technology, Rzeszów University of Technology, Wrocław University of Technology, Koszalin University of Technology, Kielce University of Technology, Radom University of Technology, ART in Bydgoszcz, University of Warmia and Mazury, Warsaw University of Life Sciences, West Pomeranian University of Technology in Szczecin, University of Life Sciences in Lublin, Warsaw IBMER, PIMR in Poznan, Agricultural University in Krakow, AGH in Krakow, College of Engineering and Economics in Rzeszow, Institute of Foundry in Krakow. Among the foreign research centers most involved in the co-operation are: the National Agrarian University in Kiev, W. Dahl East-Ukrainian National University in Lugansk, State University of Agriculture in Mykolayev, University of Lutsk, Lviv National University of Agriculture in Dublany, Odessa University, University of Agriculture in Chersonia. Agricultural engineering specialists from Lithuania, Belarus, Greece, Russia, Romania, Holland, Belgium, Latvia and Slovakia have also been invited to participate in the editorial.

In appreciation of the high scientific level of "Teka", the editor-in-chief Eugeniusz Krasowski received an offer of co-operation from the Rector of W. Dahl East-Ukrainian National University in Lugansk, academician prof. dr hab. inż. Alexander Holubenko. He proposed to establish close partnership in the joint publication of the journal "Teka". The Rector's proposal was accepted, as a result in 2009 we jointly issued one volume and five other volumes were scheduled to follow.

To celebrate ten years of "Teka"publishing, the editor has received numerous letters of congratulations from prominent scholars from home and abroad, reflecting the high level of the editorial work.

Research published in the "Teka":

1. Research in the field of internal combustion engines.
2. Issues concerning the design solutions and operating machinery.
3. Energy intensity in the use of machinery and food processing.
4. Research on the development of biofuels and emissions of combustion products
5. Dynamics of vibration systems and work processes, diagnosis of technical working groups.
6. Study of statics and dynamics of biological materials
7. Use of solar energy, wind and falling water.
8. Research on combines related to the construction and optimization.
9. Research on the use of plastic materials in the hydraulic and agricultural machinery.
10. Planning of research experiments.
11. Simulation studies of machine units.
12. Ergonomic problems in agriculture, for example, research on the operator's seat.

13. Grinding and pelleting of biological materials in the context of rational use of energy.
14. In the research on new machine constructions the latest modelling and simulation testing methods were presented, this theme appears in almost all the volumes of "Teka."

The ten years of publishing can be summarized as follows: 17 volumes of "Teka" have been published containing 516 pages and 683 articles, 1424 authors have participated in their writing, 900 reviewers have evaluated their work.

Authors from the following countries have taken part in the creation of the "Teka": Poland, Ukraine, Belarus, Lithuania, Russia, Latvia, Moldova, Romania, Greece, Slovakia, the Netherlands, Belgium, Luxembourg, USA, the Czech Republic.

The authors represented the following universities or other research institutions:

West Pomeranian University of Technology in Szczecin, Warsaw University of Technology, Lublin University of Technology, Cracow University of Technology, Poznan University of Technology, Rzeszów University of Technology, Częstochowa University of Technology, Kharkov University of Technology , Lviv University of Technology, Technical University of Civil Engineering and Architecture in Kharkov, Donetsk University of Technology, Ostrogród University of Technology, Radom University of Technology, Koszalin University of Technology, Kielce University of Technology, Agricultural University in Kharkov, Agricultural University in Chersonia , University of Life Sciences in Lublin, Luck University of Technology, University of Warmia and Mazury in Olsztyn, Latvian University of Life Sciences, Agricultural University in Gembloux - Belgium, Langwies, Junglinster, GD Luxembourg, Chelyabinsk Agricultural Engineering University - Russia, Wageningen University, Oklahoma State University - USA, University of Agriculture in Kamieniec Podolski - Ukraine, Agricultural University in Nitra - Slovakia, Gdynia Maritime University, National University of Romania, National Agrarian University in Lugansk, Bostwana University, Hopkins University - USA, W. Dahl East-ukrainian National University in Lugansk, National Agrarian University in Odessa, University of Civil Engineering and Architecture in Donbas, Odessa National Maritime University, Kiev University of Civil Engineering and Architecture, University of Niagara, Department of Mathematics - USA, Holding Company 'Luganskteplovos' in Lugansk - Ukraine, Vinny National Agrarian University, Transilvania University of Brasov - Romania, TEI Kalamata-Greece, Chelyabinsk State University of Agriculture - Russia, Kharkov Technical University of Agriculture in Kharkov - Ukraine, Agricultural University of Warsaw, University of Groningen - The Netherlands, National University of Lviv in Dublany , Agricultural University in Krakow, National University of Construction and Architecture in Kiev, Belarus National Technical University, University of Rzeszow - Poland, University of Mining and Metallurgy in Krakow, the National Academy for Nature Conservation and Construction of Sanatory Objects in Simferopol, University of Technology and Agriculture in Bydgoszcz, Belarus State University of Agriculture in Gorki, Belarus State Polytechnic University in Minsk, Institute of Agrophysics in Lublin, Institute of Oil and Gas, Institute of Agricultural Engineering in Bucharest - Romania, Institute of Chemical Technology in Prague - Czech Republic, Institute of Agricultural Engineering in Poznan, Institute of Building Mechanization and Electrification of Agriculture in Warsaw, College of Engineering and Economics in Rzeszów, Foundry Research Institute in Cracow, Pohoviłoho Institute of Agricultural Engineering and Electrification - Ukraine, Institute of Agricultural Engineering in Chlevache, National Academy of Agricultural Sciences of Ukraine, Kerch Maritime Technological Institute - Ukraine, Academy of Sciences in Vilnius - Lithuania.

In connection with the 10th anniversary of "Teka" - the Commission of Motorization and Power Industry in Agriculture at the Polish Academy of Sciences Branch in Lublin would like to express the warmest thank you to all those who have contributed to the launching and development of this publication, namely: prof. dr hab. inż. Zbigniew Burski, the Secretary of the Editor, to whom

we owe a lot of reasonable ideas that have improved the quality of the journal. Please accept our sincere wishes for good health and further fruitful work on the occasion of the 45th anniversary of scientific work and 70th birthday. Zbyszek, you have been the hub of our publication, we do hope you will change your mind and stay with the Editorial Committee.

Thanks to all the authors of articles, without them the 'Teka' would simply not exist. We also express deep gratitude to the Reviewers, the journal has obtained high scores due to their tremendous contribution, i.e. the most careful and strict reviews. And finally, last but not least, thank you very much to the editorial team: mgr Małgorzata Wojcieszuk, mgr Robert Krynski and, tireless since the beginning of the "Teka", mgr Hanna Krasowska - Kołodziej.

Editor -in- Chief
Prof. Eugeniusz Krasowski

TEKA Kom. Mot. Energ. Roln. – OL PAN, 2011, 11, 9–17

APPLICATION OF IP MONITORING IN THE SUPERVISING SYSTEM OF A BUILDING

Artur Boguta

Lublin University of Technology

Summary. Thanks to the development of modern technologies in the electronics field it is possible to directly connect the camera to computer networks. The purpose of this solution is to display the images from cameras installed in the object being monitored. Therefore, we can watch the image from any camera by means of any computer connected to the Internet or the telephone situated in GSM network range. The camera is provided with network interface and with assigned individual IP address or uses a domain with corresponding redirection of ports. No cabling is necessary for monitoring if WiFi radio transmission is used but the camera should be situated within WiFi network range and provided with power supply.

Key words: WiFi networks, IP camera, monitoring

INTRODUCTION

IP monitoring uses Internet devices; every device is provided with an IP address assigned in a static or dynamic manner. This address consists of a series of digits separated by means of dots (4 groups containing 3 digits each or 5 groups containing 3 digits each in new systems). All devices working in the network are identified on the basis of their assigned IP addresses. If the devices working in the network are provided with statically assigned IP addresses and with the corresponding software, their remote operation is possible from any location by means of the search engine.

Owing to limited number of IP addresses and to the fees associated with the static address, they are dynamically assigned by many service providers to DHCP (e.g. Internet network Neostrada TP). In such case it is difficult to localize the devices with variable address and for this purpose we can use a domain enabling the localization of the actual IP address of our router. The domain is defined as an unique string (universally unique identifier) precisely identifying IP address of our router. In order to use this opportunity we have to register the domain on one of DNS servers and to enter the relevant data into the router thereafter. After entering the domain name and password into our router, the redirection to IP address assigned to our device will take place after the domain name entry into the search engine.

The study presents the manner of configuration for the router and IP cameras in order to create the system monitoring a residential building. The building is connected to Internet network by means of Neostrada TP link with variable IP address.

Vigor DrayTek 2820Vn has been applied owing to stable operation and advanced configuration menu i.e. ADSL router. The router has been integrated with FI8916W and FI8905W IP cameras manufactured by Foscam and equipped with LAN and WLAN interface. FI8916W camera designed for indoor installation is provided with built-in loudspeaker and microphone and FI8905W camera is designed for outdoor installation. The both cameras are equipped with diode infrared radiators to enable the monitoring in complete darkness.

The layout diagram for the monitoring is illustrated in Fig.1.

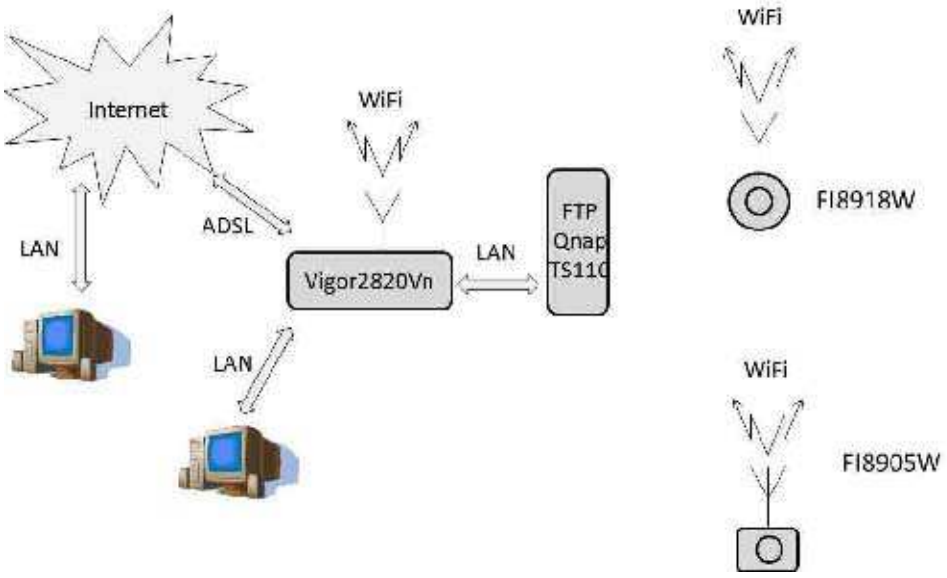

Fig. 1. Hardware structure for Internet network including WiFi cameras.

Figure 1 illustrates the hardware structure used for the creation of the object monitoring system. The system consists of the following components:

- ADSL Vigor2820Vn router,
- five (5) FI8918W indoor cameras,
- three (3) FI 8905W outdoor cameras,
- FTP Qnap TS110 server,
- PC computers in the internal and external Internet network.

The cameras are connected with the router via WiFi radio network using WPA2 encryption and MAC filtration as the data transmission protection.

CAMERA CONFIGURATION

The camera configurations have been carried out by means of Internet Explorer as the search engine and IP Camera Tool program. The program makes it possible to detect IP cameras which are initially connected with operating router by means of a cable. After the starting of IP Camera Tool program, the window is displayed (Fig. 2); this window contains IP addresses of all cameras con-

nected to our router. Having selected the correct camera we have to perform its configuration to enable easy detection of and connection with the camera.

Fig. 2. Program window used for IP cameras searching

The first step of the camera configuration is the setting of administrator password. Figure 3 illustrates the configuration menu window enabling the change of the camera administrator password and addition of the new users.

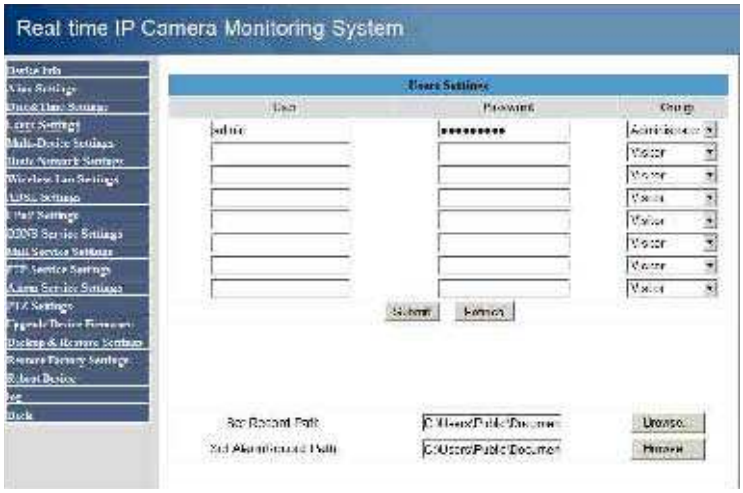

Fig. 3. Menu window for camera users

After the setting of administrator password, the assignment of the static IP address and port has been commenced. It should be emphasized that the camera IP address setting should be included in the router addresses pool assigned dynamically to DHCP and that the port should not be used by other devices in the network. The settings for the address and port are illustrated in Fig. 4.

Fig. 4. Window containing the camera IP address settings menu

The next phase consists in the setting of WiFi radio interface between the camera and router. Therefore we have to open Wireless Lan Settings tab between the camera and router and to find the radio networks as well as to select our network and to enter WPA encryption password thereafter. If MAC filtration is activated we have to enter mac-address of the camera into router menu and to enable radio connection with the camera. An example of WiFi network in camera is illustrated in Fig. 5.

Fig. 5. Window containing the settings of wireless WLAN network

An image can be transmitted and recorded by the camera in case of movement detection in its field of view. Additionally the camera activates a sound signal informing the operator about the zone infringement. Furthermore it is possible to transmit the pictures from the camera to E-mail address or their registration on FTP server. The configuration of E-mail service is illustrated in Fig. 6 and FTP server configuration in Fig. 7.

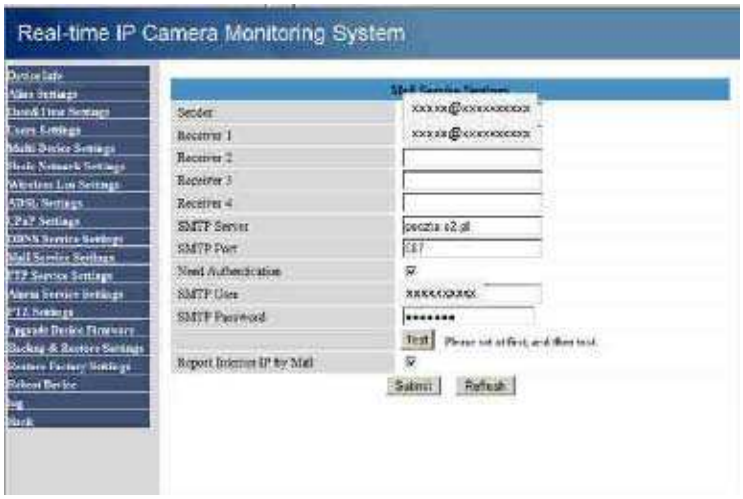

Fig. 6. Configuration of E-mail account for the transmission and receipt of pictures recorded by the camera at the time of zone infringement

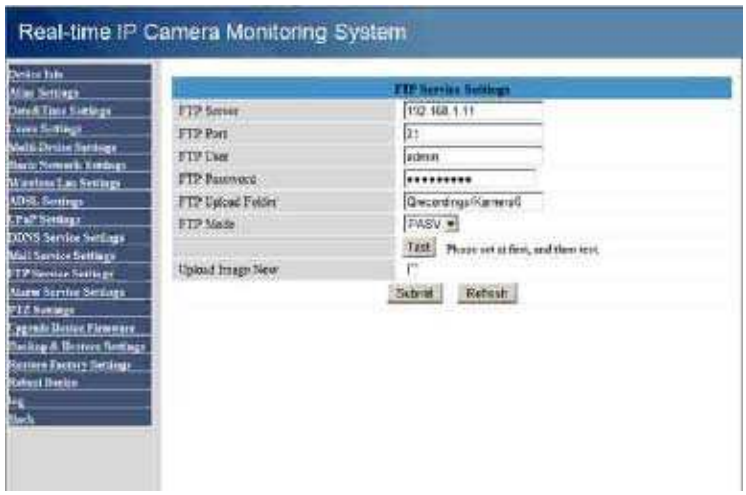

Fig. 7. Configuration of the account on FTP server for the transmission and receipt of pictures recorded by the camera at the time of zone infringement

In order to enable the transmission of the pictures by the camera in case of detected movement, it is necessary to set the camera sensitivity and the sequence of the transmission of the pictures. Additionally it is possible to set the time of picture recording by the camera. An example of settings for the camera is illustrated in Fig. 8.

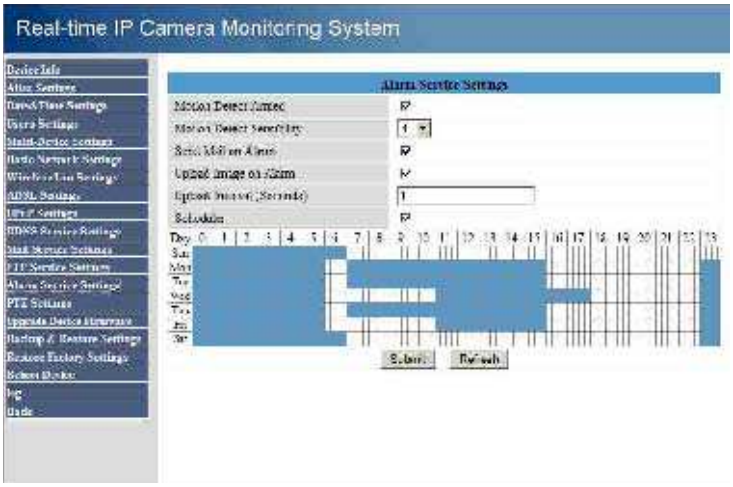

Fig. 8. Settings for alarm and sequence of the transmission of pictures at the time of zone infringement

ROUTER SETTINGS

After these settings the camera will be visible in internal network and will send recorded pictures to the E-mail address and will record them on FTP server. In order to enable the access to the cameras from the computers connected to the external network, it is necessary to set the domain and to redirect the ports to IP addresses. An example of settings for the router is illustrated in Fig. 9.

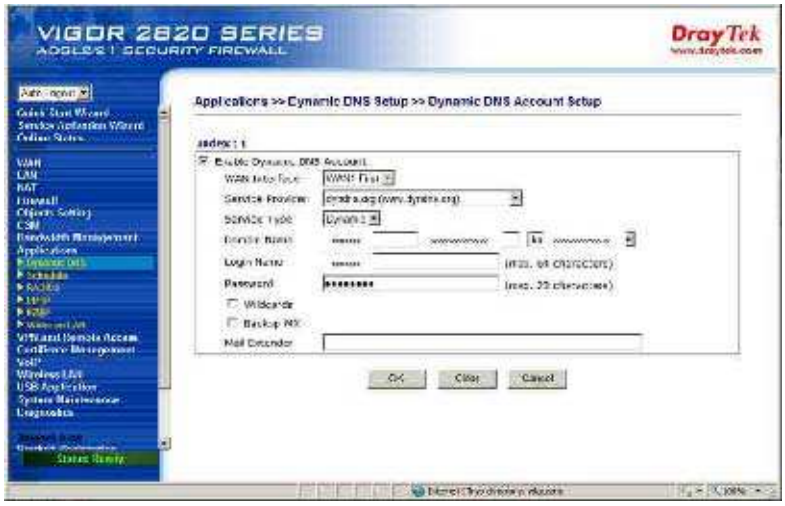

Fig. 9. Domain setting in router menu

Having redirected the ports (Fig. 10) we can watch the situation in the object being monitored in real time.

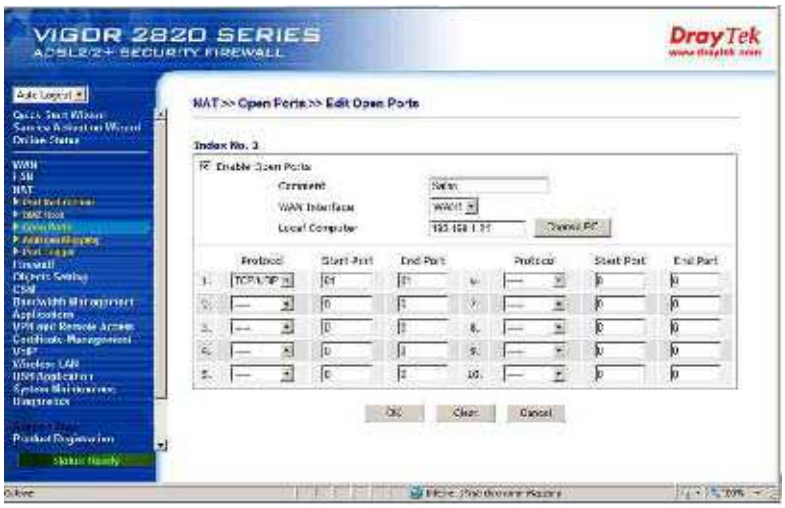

Fig. 10. Ports redirection window

IP cameras manipulators windows are illustrated in Fig. 11 and 12. The purpose of virtual manipulator of an indoor camera is to enable its rotation towards the object we want to watch. The manipulator can serve nine IP cameras simultaneously.

Fig. 11. Indoor camera manipulator window
OBRAZ Z KAMERY = Picture from camera

Fig. 12. Outdoor camera manipulator window
OBRAZ Z KAMERY = Picture from camera

CONCLUSION

IP cameras entering into monitoring systems eliminate the conventional cameras which have to be connected with the monitoring station by means of cables.

Owing to their unlimited capabilities created by the software of the cameras, it is possible to perform the monitoring from any location on Earth and to reproduce the record from the cameras at any place provided with the computer connected to Internet network.

The pictures can be sent by IP camera to specified E-mail address. Therefore the record can not be removed from the camera by the person infringing the zone being protected.

However there is an disadvantage of IP cameras, because they are completely dependent on the Internet network. They are unable to perform their role in case of Internet failure but the picture is recorded on local servers.

REFERENCES

Tanenbaun S. Sieci komputerowe [Computer Networks]. Published by Helion 2004

Danowski B. WiFi. Domowe sieci bezprzewodowe [Home Wireless Networks]. Published by Helion 2010

Serafin M. Sieci VPN. Zdalna praca i bezpieczeństwo danych [VPN networks. Remote work and data security]. Published by Helion 2009

Kurytnik P; Karpiński M. Bezprzewodowa transmisja informacji [Wireless transmission of information]. Published by PAK 2008

Ross J. Sieci bezprzewodowe. Przewodnik po sieciach WiFi i szerokpamowych sieciach bezprzewodowych [Wireless networks. Guide to WiFi networks and wireless networks]. Published by Helion 2009

Zieliński B. Bezprzewodowe sieci komputerowe. Published by Helion 2000
Danowski B. Domowe sieci bezprzewodowe. Ilustrowany przewodnik [Home wireless networks. Illustrated Guide]. Published by Helion 2010
Pejman R; Jonathan L. Bezprzewodowe sieci LAN 802.11. Podstawy. [Wireles LAN 802.11. Basics]. Published by MIKOM 2004
http://www.draytek.pl/
http://www.foscam.pl/

ZASTOSOWANIE MONITORINGU IP W SYSTEMIE NADZORU BUDYNKU

Streszczenie. Rozwój nowoczesnych technologii z dziedziny elektroniki umożliwił bezpośrednie łączenie kamery z sieciami komputerowymi. Rozwiązanie to pozwala na oglądanie obrazów z kamer zainstalowanych w monitorowanym obiekcie, dzięki czemu mamy możliwość oglądania obrazu z dowolnej kamery przy pomocy dowolnego komputera podłączonego do internetu lub telefonu znajdującego się w zasięgu sieci GSM. Kamera wyposażona jest w interfejs sieciowy ma przydzielony własny adres IP lub wykorzystuje ona domenę z odpowiednim przekierowaniem portów. Jeśli korzystamy z transmisji radiowej WiFi to monitoring nie wymaga rozprowadzania kabli, wystarczy, że kamera będzie umieszczona w zasięgu sieci WiFi oraz będzie miała zasilanie.

Key words: sieci WiFi, kamera IP, monitoring

TEKA Kom. Mot. Energ. Roln. – OL PAN, 2011, 11, 18–28

THE USE OF LABVIEW ENVIRONMENT FOR THE BUILDING OF SUPERVISION SYSTEM CONTROLLING THE CLIMATIC AND TECHNICAL PARAMETERS IN FARM ROOMS

Marcin Buczaj, Andrzej Sumorek

Department of Computer and Electrical Engineering
Lublin University of Technology, Nadbystrzycka 38A, 20-618 Lublin
email: m.buczaj@pollub.pl; a.sumorek@pollub.pl

Summary. Nowadays, the modern farms operate like the small manufacturing facilities specialized in the production and preliminary processing of agricultural products. The compliance with precisely determined production and storage conditions in the objects and in individual rooms is required in order to achieve required qualitative indicators of the products. This article presents the control system for the principal climatic and technical parameters in selected rooms existing at the farm. LabView environment has been used for the building of such system. The acquisition of parameters was carried out basing upon the information and signals received from the sensors supporting the measuring cards. The actual as well as archived parameters occurring in individual rooms can be displayed on the computer screen via built-in interface. Thanks to this solution, the farmer has the opportunity to review of and to supervise over the autonomous control systems operating in individual rooms.

Key words: control and supervision systems, processes inspection, LabView environment

INTRODUCTION

The modern machines as well as maintenance of precisely determined production and storage conditions for the products are the elements indispensable to improve the production effectiveness of the farm. The purpose of every room and building object at the farm is to perform different specific functions and tasks [Kuboń M. 2007]. The objects existing at the farm can be subdivided into the following groups: the buildings for livestock; utility (storage) buildings, workshops (garages) and residential buildings. All these rooms are characterized by diversified hazards to be considered as well as by the climatic and technical parameters to be maintained.

Actually the tasks to be performed by the modern electric installations installed in the farm buildings are not limited only to the reliable supply of electric energy with required parameters. The specialized systems are expected to exercise the control over the object status and to control the operation of the devices installed in this system [Buczaj M. 2009b]. Therefore the electric installations are equipped with the control systems enabling the performance of the functions and procedures intended by the user. The purpose of these systems is to perform assumed tasks associated with

the operation of the lighting, heating and ventilation in the object; to perform the role of processes control systems and to enable the permanent supervision over the processes occurring in specified rooms for the user [Buczaj M. 2010, Horyński M. 2006, Petykiewicz 2001].

The first control systems for the electric equipment operation in the farm buildings made it possible to turn on and off the energy receivers by means of the switches only. Thanks to the technological progress and introduction of relay and contact systems it is possible to perform more complex functions (e.g. startup of energy receivers in cyclic mode). When the generally available sensors appeared on the market, it became possible to create the control algorithms enabling the automatic adaptation of the actuators settings on the basis of information received from the detection and measuring elements of the system. The logic functions have been introduced into the control systems after the application of digital systems. The extension of the control systems capabilities in the form of comprehensive expert systems, database systems and even in the form of systems based upon the artificial intelligence systems became possible as a result of the introduction of microprocessor techniques.

At the moment, there are several specialized systems available on the market and enabling the accomplishment of an assumed control algorithm. The disadvantage of such solution consists in their being highly autonomous. Every such system controlling the assumed and set parameters operates independently. This system is equipped with a specific interface (different for each system) to ensure the communication with the user. The systems operate in a manner supplying a large amount of detailed data concerning the process controlled for the user. Owing to the lack of compatibility, the user is unable to determine what is going on in other rooms or what is the impact of the changes of parameters occurring in one system or another.

This article presents the concept of a virtual supervision system enabling the control and monitoring of the autonomous control systems applied at a farm. Therefore it will be possible to improve the comfort of use of the systems, to increase the work safety and simultaneously to reduce the operation costs for such systems.

INTEGRATION AND INTEROPERABILITY OF CONTROL SYSTEMS

There are two principal kinds of the systems performing the control and management functions in the electric equipment applied at farms [Buczaj M. 2009a]:

- island system – the system based upon autonomous systems with one of the systems performing only precisely assigned tasks (e.g. controlling the building's heating of performing the alarm system functions only);
- integrated system – the system based upon information exchange, sharing individual systems infrastructure or upon centralized management system.

The functions of individual circuits are the same in the autonomous systems as in the integrated circuits. The requirement to be met by the heating control circuit is all the time to create desired thermal comfort in the room. The task of the alarm system elements is to generate an alarm signal in case of detected hazard for the users or for the property being protected. The difference consists in the fact that in case of an integrated system the signals origination from the input elements (detectors, sensors) are directed to the corresponding analysing and decision making system which controls the operation of individual output elements (actuators).

The system integration process is defined as the process consisting in the interoperability of individual installations included in the object and performing autonomous functions to create one system performing all functions assigned to individual parts being the components of the system.

The tasks of integrated systems consist in multiple functions control and in the actuators control in the building. The following circuits are particularly important:

- lighting control ;
- heating control;
- ventilation and air – conditioning heating;
- equipment operation control and technological process control [Buczaj M., Buczaj A. 2009, Horyński M., Pietrzyk W. 2010];
- alarm system operation control (burglary and hold-up, fire alarm, access control system) [PN-EN 50131, PN-EN 50133, PN-EN 50136, Buczaj M. 2010, Buczaj M., Sumorek A. 2010].

The integration of the autonomous systems can be performed in the following manner [Buczaj 2009a]:

- through information exchange between the autonomous systems (Fig. 1)
- through the sharing of detection and decision making elements by the systems (Fig. 2);
- through the performance of the functions assigned to individual systems by the same control system (Fig. 3).

The integration of the systems through information exchange is the simplest manner of interoperability between the autonomous systems. All systems operate in an autonomous manner but they exchange the information about the statuses of determined inputs and outputs. In this case each autonomous system knows the statuses in determined points of the system is able to adapt its operation algorithm to determined conditions.

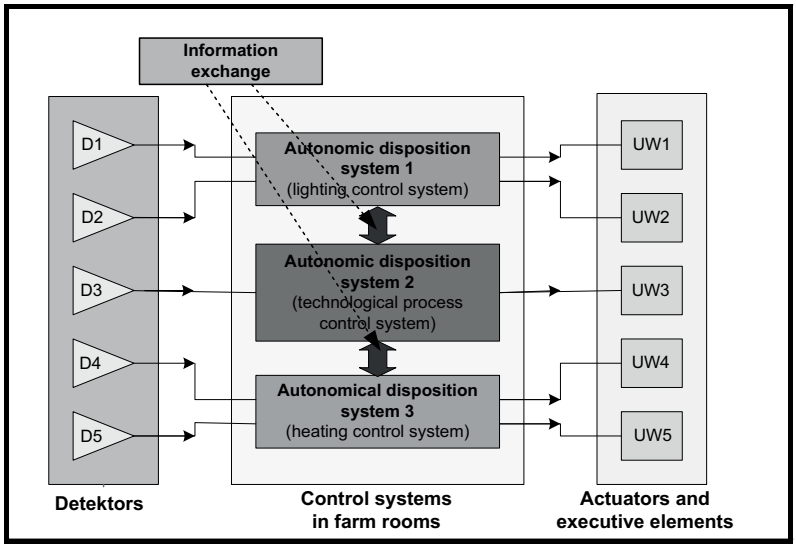

Fig. 1. The integration of the systems through information exchange

The integration of the systems through the sharing of detection and decision making elements consists in the connection of the elements constituting the common part between the systems to the central parts managing the operation of individual circuits. Such solution improves the ergonomic

features of the system use, enables its better configuration and reduction of the installation costs owing to the elimination of redundant elements performing the same function but interoperating with only one autonomous system (e.g. with I&HAS system only). However, the power supply for shared elements (particularly detectors) and the hierarchy of commands supplied from the controllers (important in case of actuators) should be well considered.

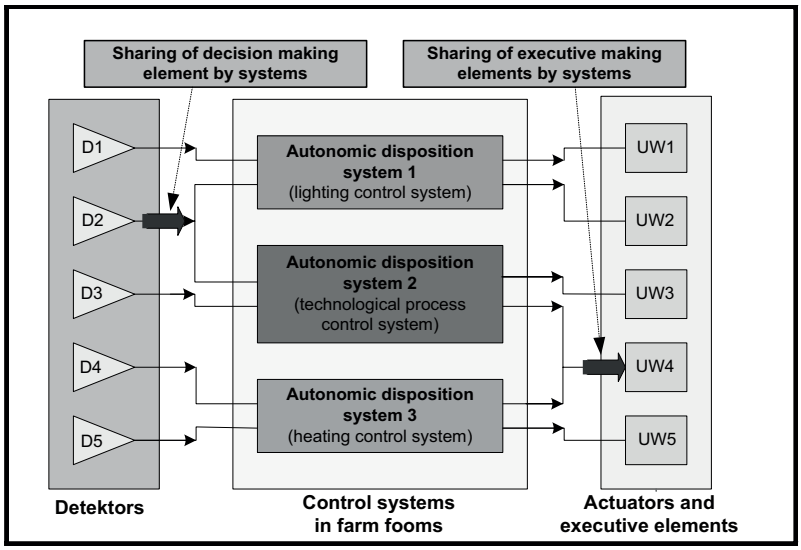

Fig. 2. The integration of the systems through the sharing of infrastructure elements

All problems associated with the autonomous systems disappear in case of the use of one system to control the operation of the whole system. All elements are connected to single controller. Thanks to such solution, there is only one supervising system having the access to all data originating from the detection elements and performing assumed functions in accordance with the operation status (mode) established by the user. The system is characterized by the lack of redundant procedures or by the shortest time of reaction to recorded events. Such solution creates much more opportunities in the building of the system operation control algorithm but it is usually associated with the necessity to know the programming languages or to cooperate with specialized service.

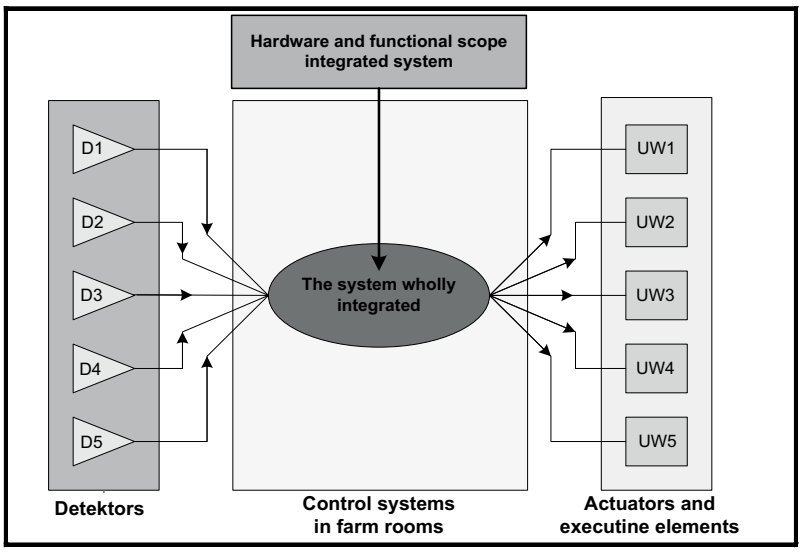

Fig. 3. The system wholly integrated in hardware and functional scope

Nowadays there are many kinds of systems enabling the performance of the function of the equipment operation automatic control systems. The most popular are the three basis groups of systems dedicated for the applications in the residential and other farm buildings [Antoniewicz B. i in. 1998, Brock S. i in. 2000, Buczaj M. Kowalik P. 2008, Horyński M. 2008, Horyński M., Pietrzyk W. 2008, Kasprzyk J. 2006]:

– the systems based upon EIB bus – applied in new installations and those mainly applied for the checking and control of climatic and lighting parameters;
– the systems based upon PLC controllers – used in case of adaptation of existing installation to the tasks of an integrated system and mainly used for the checking and control of process parameters occurring in the production processes;
– the systems based upon microprocessor built-in systems – applied in the control systems for individual machines and devices.

FUNCTIONAL ASSUMPTIONS FOR VIRTUAL SUPERVISION SYSTEM

The principal task to be performed by the virtual system under construction for the supervision over the status of infrastructure and conditions in the rooms existing in the farms is to enable the complex control of the climatic and technological process parameters exercised by the user. This task will be performed through the acquisition of measurement data collected by the supervision system from individual detection elements located in the rooms (climatic parameters) or directly in individual machines (technical parameters). Therefore the use of the model of an integrated system shared by the basic control system and by the supervising system for the same infrastructure elements will be the best solution to perform this task. Such solution will make it possible to limit the costs associated with the use of an additional system (checking supervision system). This system will be additionally characterized by identical signals transmitted to the control and supervision system enabling the correct evaluation of the situation existing in individual objects or rooms.

An additional function of the virtual supervision system additionally increasing the functionality of such system consists in the potential acquisition of measurement data and their archiving as well as the possibility to apply the mathematical models and calculation algorithms in order to determine an optimal work schedule for individual devices. It is possible to provide the program with an additional panel enabling the transmission of information about the necessity to perform planned inspections of the devices with the specification of the parts required for this purpose. The advantage of such system over a standard solution (independent autonomous systems) consists in the fact that all necessary data will be displayed and available for the user at the same location on the computer screen in order to enable more complete control over production processes occurring in the farm.

The organizational diagram of the virtual supervision system is illustrated in Fig. 4.

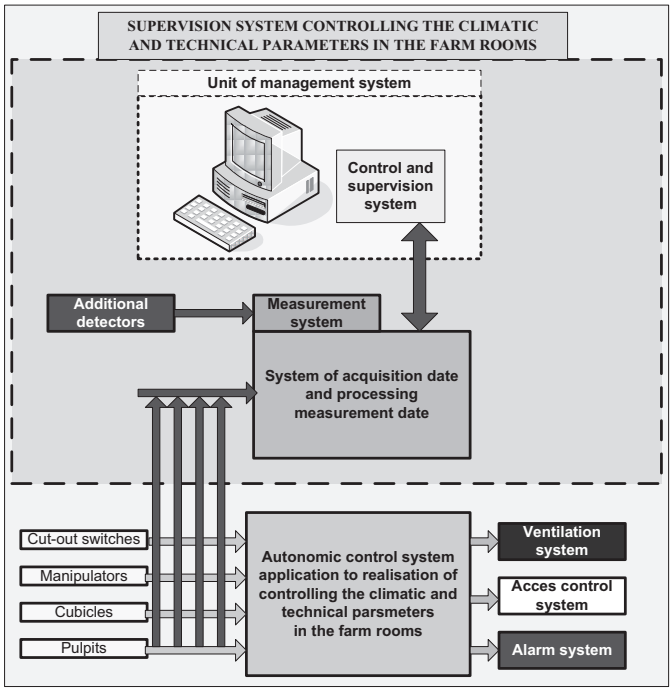

Fig. 4. The organizational block diagram of the system

The virtual supervision system controlling the climatic and technical parameters in the farm rooms consists of the following essential elements (Fig. 5):

– management unit – computer used for the system operation;
– existing control programs – designated autonomous systems supporting and performing the program determined by the system user (controllers, supplying and control systems etc.);
– detection elements – climatic and technical parameters sensors installed in sensitive points situated in the rooms being supervised and determining actual parameters in an area;
– actuators – the elements used in order to change the climatic and technical parameters in the rooms being controlled (e.g. motors, heaters, fans) as well as the systems informing about detected hazard or emergency comdition;

– intermediate elements participating in the data exchange between autonomous control systems and virtual supervision system – measuring cards used for data acquisition by the virtual supervision system.

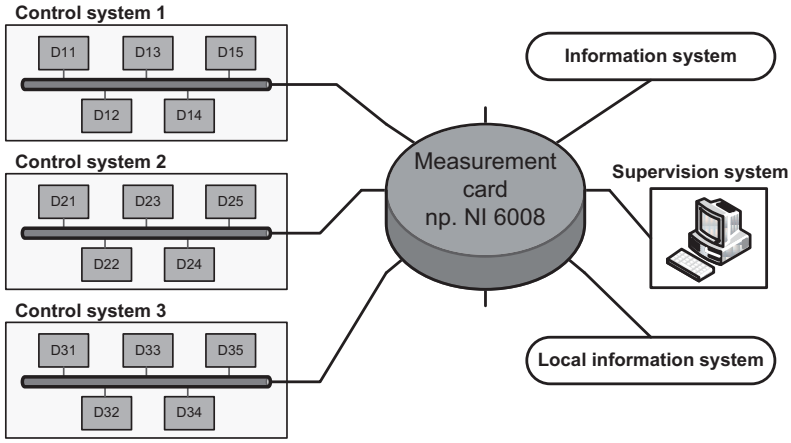

Fig. 5. Topology of the supervision system controllling the climatic and technological parameters in the farm rooms, D – detectors

VIRTUAL SUPERVISION SYSTEM CONTROLLLING THE CLIMATIC AND TECHNOLOGICAL PARAMETERS

The virtual supervision system controllling the climatic and technological parameters has been created on the basis of programmable LabView environment. LabView programming environment makes it possible to perform the complex functions in the processes encompassing the acquisition and archiving as well as measuring data processing and analysis. Therefore it is possible to freely create the program structures in measuring and simulation systems which are useful in scientific and research projects but also to create the applications enabling the building of modern control systems supervising the technological processes. This environment is characterized by great capabilities associated with the support of technological processes in the scope of measurements and control as well as with the individual approach to the creation of the systems served by many users [Nawrocki W. 2006, Tłaczała W. 2002].

Depending on their authorizations, the system access rights of individual users can be different. Therefore the system is stable and resistant to the activity of unauthorized persons. An additional advantage of applications created in LabView program consists in their individuality. It is possible to use certain schemes and to provide the programs with individual solutions. Therefore it is possible to adapt the application to sometimes dynamically varying situation in the farm (e.g. change of technology, change of production profile).

The system operation management and control application consists of the following elements:

– interface of the user (Fig. 6) – enabling (in accordance with authorizations) the system operation control, configuration change or the system operation checking;
– organizational diagram – internal relation between individual elements of application enabling the performance of tasks assigned by the user in the control panel (Fig. 7);

– I/O support (input and output devices support) – the system component responsible for data acquisition from the system detection elements and for the transmission of information to the devices ensuring the actuators operation control or to the system users (Fig. 8).

Fig. 6. User.s interface of the system

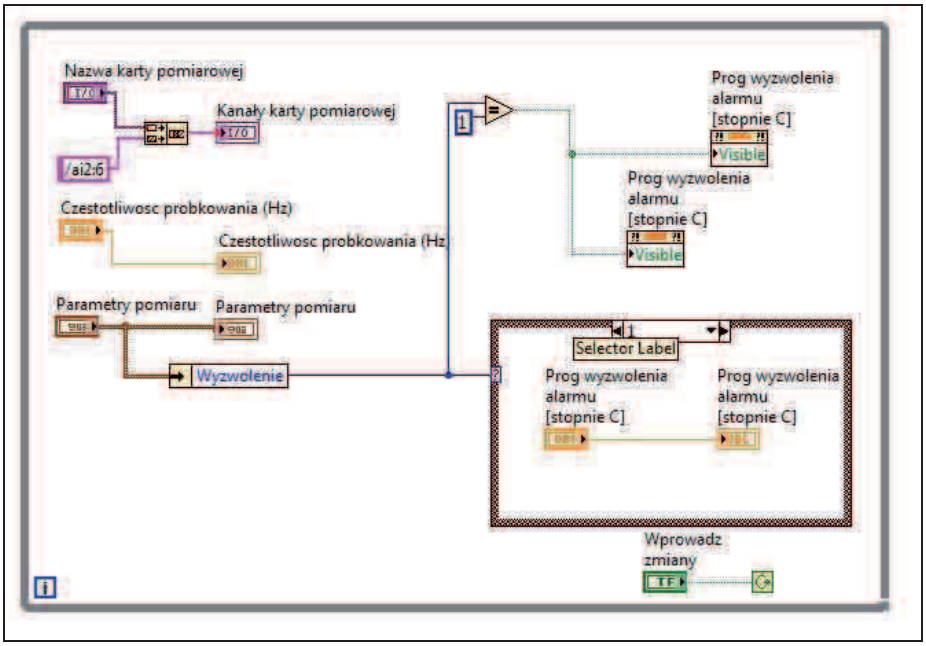

Fig. 7. The calibration date procedure of alarm threshold – a part of the head program

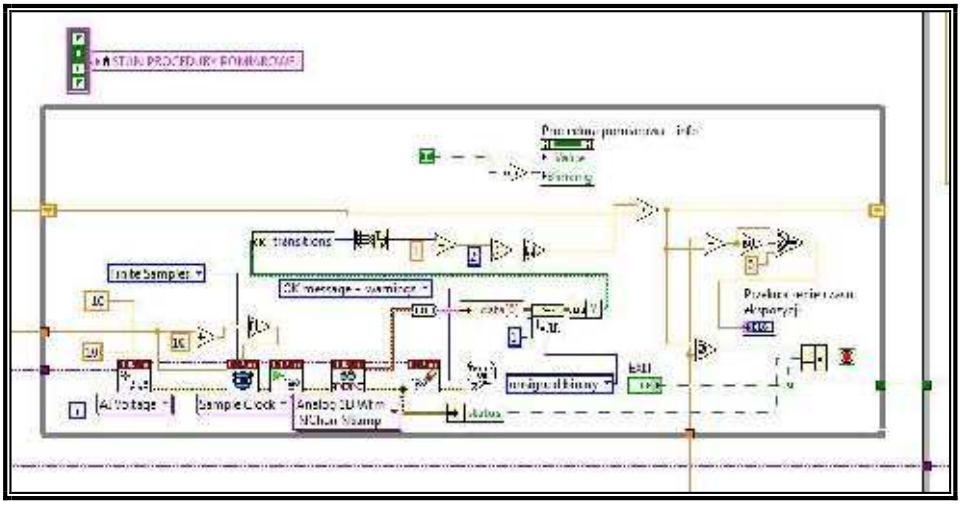

Fig. 8. One of the acquire measurement date procedure – a part of the head program

The proposed supervision system controllling the climatic and technological parameters in selected rooms at the farm can be operated in the automatic operation mode, in manual operation mode managed by the user at the work station and in emergency mode managed by the system user from the level of computer with installed supervision system. Thanks to such solution it is possible to optimize the system operation in normal conditions and to adapt to actual needs in case of occurred emergency conditions or conditions endangering the correct course of storage and production processes.

Except for the control and status checking for individual autonomous control systems, it is possible to provide the virtual supervision system with the events recording option. Therefore the work history is created for individual system elements installed in the farm and it is more easy to determine the reasons of occurred emergency conditions and to determine the periods of scheduled maintenance shudowns on the basis of the equipment operation time recording.

CONCLUSIONS

The analysis of capabilities and functionalities of the autonomous control systems, particularly those built on the basis of EIB and PLC systems of elements as well as on the basis of built-in systems demonstrated that said systems can support the virtual supervision system. Such interoperability is possible in the form of systems infrastructure sharing (particularly detection elements).

The systems integration through the creation of a uniform supervision system controlling the technical and climatic parameters occurring at the farm makes it possible to increase the capabilities of the whole management system. Thanks to the storage and processing of data from many autonomous systems, such systems enable the extension of their functions to tasks associated with planning and management of the production and storage process.

Owing to the application of the virtual supervision system integrated with the autonomous control systems applied for the execution of the production and storage processes at the farm it is possible to extend the scope of parameters and functions obtained by the user. Additionally the status of individual systems is monitored the supervision system and the user is provided with the complex access to information from one place.

Thanks to the application of LabVIEW software delivered by National Instruments, the user can have access of to advanced applications enabling the communication with external devices in several ways. In this system it is possible to use the serial and parallel ports, TCP/IP protocol as well as wireless connection with the devices. The last option increases the data transmission process efficiency. The systems are under uninterrupted control and the user is immediately informed thereof. Therefore the systems users are able to quickly localize the failure and to eliminate the defect source in case of a breakdown or danger status.

The application of LabVIEW environment for the building of the virtual supervision system makes it possible to create the systems adapting themselves to the individual needs of their user and, consequently, to implement such a system for various objects and various production processes.

REFERENCES

PN-EN 50131-1 – Systemy alarmowe. Systemy sygnalizacji włamania i napadu. Część 1: Wymagania systemowe, PKN, Warszawa 2009

PN-EN 50133-1 – Systemy alarmowe. Systemy kontroli dostępu w zastosowaniach dotyczących zabezpieczenia. Część 1: Wymagania systemowe, PKN, Warszawa 2002

PN-EN 50136-1-1 – Systemy alarmowe. Systemy i urządzenia transmisji alarmu. Wymagania ogólne dotyczące systemów transmisji alarmu, PKN, Warszawa 2001

Antoniewicz B., Koczyk H., Srocza E. 1998. Nowoczesne wyposażenie techniczne domu jednorodzinnego, Państwowe Wydawnictwo Rolnicze i Leśne, Poznań

Brock S., Muszyński R., Urbański K., Zawirski K. 2000. Sterowniki programowalne, Wydawnictwo Politechniki Poznańskiej, Poznań

Buczaj M. 2009a. Integracja systemów alarmowych i systemów zarządzających pracą urządzeń w budynku mieszkalnym. Zabezpieczenia 4(68)/2009. s. 64÷68

Buczaj M. 2009b. Czas jako kryterium skuteczności przebiegu procesu neutralizacji zagrożeń w systemach nadzorujących stan chronionego obiektu, Zabezpieczenia nr 6(70)/2009, s. 56÷61.

Buczaj M. 2010. Wykorzystanie telefonii mobilnej i Internetu w procesie przekazywania informacji w systemach nadzorujących stan chronionego obiektu, Zabezpieczenia nr 1(71)/2010, s. 56÷61

Buczaj M., Buczaj A. 2009. Komputerowy system kontroli poziomu zapylenia w młynie zbożowym. XII Ogólnopolska Konferencja Naukowa „Zastosowanie technologii informacyjnych w rolnictwie", Poznań – Puszczykowo, s. 13÷14

Buczaj M. Kowalik P. 2008. Wykorzystanie sterowników programowalnych PLC do budowy elektronicznych systemów alarmowych. Przegląd elektrotechniczny, Nr 3/2008, s. 178÷180.

Buczaj M., Sumorek A. 2010. Wirtualny system nadzoru sterujący pracą systemu sygnalizacji włamania i napadu. Motrol - Motoryzacja i Energetyka Rolnictwa, tom 12, s. 46÷53

Kuboń M. 2007. Miejsce i rola infrastruktury logistycznej w funkcjonowaniu przedsiębiorstw rolniczych, Inżynieria Rolnicza 9(97)/2007, s. 87÷93

Horyński M. 2006. Zdalne zarządzanie inteligentną instalacją elektryczną, Motrol – Motoryzacja i Energetyka Rolnictwa, tom 8A, Lublin.

Horyński M. 2008. Instalacje elektryczne EIB w inteligentnym domu – komunikacja bezprzewodowa. Przegląd elektrotechniczny, Nr 3/2008, s. 105 -107

Horyński M., Pietrzyk W. 2010. Zastosowanie inteligentnych systemów magistralnych do sterowania napędami bramowymi. Logistyka 6/2010, s. 1101÷1109

Kasprzyk J. 2006. Programowanie sterowników przemysłowych, Wydawnictwo Naukowo-Techniczne WNT, Warszawa

Nawrocki W. 2006. Komputerowe systemy pomiarowe, WKiŁ, Warszawa
Petykiewicz P. 2001. Nowoczesna instalacja elektryczna w inteligentnym budynku, Wydawnictwo COSiW SEP, Warszawa
Tłaczała W. 2002. Środowisko LabVIEW w eksperymentach wspomaganych komputerowo. WNT. Warszawa

WYKORZYSTANIE ŚRODOWISKA LABVIEW DO BUDOWY SYSTEMU NADZORU KONTROLUJĄCEGO PARAMETRY KLIMATYCZNE I TECHNICZNE W POMIESZCZENIACH W GOSPODARSTWIE ROLNYM

Streszczenie. Nowoczesne gospodarstwa rolne to dzisiaj małe zakłady produkcyjne wyspecjalizowane w produkcji i wstępnym przetwórstwie produktów rolnych. Osiągnięcie wymaganych wskaźników jakościowych produktów wymaga przestrzegania w obiektach i w poszczególnych pomieszczeniach ściśle określonych warunków produkcji i przechowywania. W artykule przedstawiono system kontroli głównych parametrów klimatycznych i technicznych w wybranych pomieszczeniach występujących w gospodarstwie rolnym. Do budowy takiego systemu zostało wykorzystane środowisko LabView. Akwizycja parametrów odbywała się na podstawie informacji i sygnałów z czujników współpracujących z kartami pomiarowymi. Zbudowany interfejs umożliwia wyświetlanie na ekranie komputera aktualnych, a także archiwalnych parametrów występujących w poszczególnych pomieszczeniach. Dzięki takiemu rozwiązaniu rolnik ma możliwość wglądu i nadzór nad autonomicznymi systemami sterującymi działającymi w poszczególnych pomieszczeniach.

Słowa kluczowe: systemy sterowania i nadzoru, kontrola procesów, środowisko LabView

TEKA Kom. Mot. Energ. Roln. – OL PAN, 2011, 11, 29–39

THE PROPERTIES OF A HDV DIESEL ENGINE FUELLED BY CRUDE RAPESEED OIL

Jerzy Cisek*), Andrzej Mruk*), Vladimir Hlavňa**)

*) Jerzy Cisek, Ph.D., M.E., Andrzej Mruk, Prof., Cracow University of Technology Poland
**) Vladimir Hlavňa, Prof. University of Žilina, Slovakia

Summary. The article presents the results of investigation of a 500 kW diesel engine fuelled by crude rapeseed oil. The authors discuss technical problems of adapting the engine to work on rapeseed oil and of using additives, which provide engine operation without breakdown. Measurements of energy parameters and of exhaust gas toxicity were done. The test methods and the measurement apparatus were in accordance with the ECE standards. As the engine was the integral part of the generating set, the measurements were conducted at constant rotational speed n=1500 rpm and at changing engine load. As a result of the performed investigation it was stated that the use of rapeseed oil instead of gas oil causes the increase of the fuel consumption per hour (without affecting the total efficiency), the increase of nitric oxides (NO_x) as well as the emission of particulate matter (PM). In consequence of the investigation it can be confirmed that high-power diesel engines can be fuelled by crude rapeseed oil, provided that both the engine and the fuel is adapted to this purpose.

Key words: crude rapeseed oil, energy parameters, exhaust gas, particulate matter

1. INTRODUCTION

The vast majority of research centres dealing with the problem of fuelling the combustion engines by vegetable fuels concentrate on the rape oil methyl esters instead on the crude vegetable oil. It is due to the fact that "crude" vegetable oils differ considerably in physical and chemical properties from the gas oil. However, manufacturing costs of the crude vegetable oil are significantly lower than the costs of the methyl esters, for example – of the rapeseed oil. Therefore, this study presents the results of examining a Perkins 2806A-E18TAG2 Diesel engine of power rating 500 kW. The engine was integral part of a generating set, fuelled by rapeseed oil without chemical modification to the RME form.

2. PHYSICAL AND CHEMICAL PROPERTIES OF RAPESEED OIL

Crude rapeseed oil is a mixture of different glycerides, i.e. compounds of fatty acids. Unfortunately, due to the different botanic forms of the rape, climatic conditions and stamping technology (cool or hot forming), physical and chemical properties of the rape oil may significantly differ [11-

16]. The Table 1 contains the mean values of the parameters characteristic for the rape oil compared with the properties of the gas oil.

Table 1. Comparison of the physical and chemical properties of the rapeseed oil and the gas oil [1-7]

Parameter \ Fuel	Unit	Gas oil	Vegetable oil
Molecular mass	-	ca 280	max. 850
Density at 20^{o}C	g/cm^{3}	0.825	max. 0.915
Kinematic viscosity at 20^{o}C	mm^{2}/s	ca 4	max. 70
Surface tension at 20^{o}C	N/m	ok. 24 10^{-3}	max. 35 10^{-3}
Calorific value	MJ/kg MJ/dm^{3}	42.6 35.2	min. 38.0 min. 34.5
Average elementary composition • C • H • O	% mas.	 87.0 13.0 0.0	 77.0 12.0 11.0
Sulphur content	% mas.	max 0.2	max. 0.001
Water content	mg/kg	-	300-max 700
Free fatty acids content.	% mas.	-	0.8-1.3
Cetane index LC	-	45-55	ok. 40
Ignition temperature	K	440	470-550
Cloud point	K	265	260 -270
Cold filter blocking temperature	K	260	285-300
Freezing temperature	K	260	250
Destillation run • Start • 50% • 85%	K	 • 450 • 565 • 600	 • 315–max.430 • ca 600 • ca 620
Heat of vaporization	kJ/kg	230	max. 830
Stoichiometric constant	kg/kg	14.5	12.5

3. ADAPTATION OF THE ENGINE TO WORK ON RAPE OIL

Due to the important differences in rape oil properties in comparison to the gas oil, adapting the engine to work on crude rapeseed oil involved not only changing the supply and control engine systems, but also applying appropriate packs of additives to the vegetable oil.

The most important changes in the engine supply system are presented below:

1. Use of separate fuel tanks for vegetable oil and gas oil. The tank containing rapeseed oil had an automatic temperature control system (60^{O}C),
2. Use of a special heated fuel filter, engaged automatically with the engine supply system, when the engine operated on vegetable oil,

Change of the control engine software consisting, among other things, in controlling the rape oil temperature, automatic switching over of the engine supply system on the rape oil after starting the engine and getting the required temperature of the vegetable fuel, as well as automatic switching over of the fuel system on the gas oil after the command "stop engine". The engine was stopped automatically only after the supply system was flushed with the gas oil.

The discussed above construction and control changes in the engine adapted to the operation on the rape oil, result from two essential facts. In the ambient temperature, the kinematic viscosity of the rape oil is more than 18 times higher in relation to the gas oil. It results in deterioration of the processes of injection, atomization, evaporation, self-ignition and combustion of the rape oil as compared with the gas oil. Heating the rape oil up to the temperature 60^{O}C equalizes these inconveniences influencing as well the engine energy parameters as the exhaust gas toxicity [8]. Moreover, vegetable oils (except for olive oil) are prone to self-oxidation [9]. Practically, it means that they dry up forming a very durable layer, which, under engine operation conditions, leads to the immobilization of the injection apparatus precise pairs during the engine standstill. For this reason, stopping of the engine followed automatically the switching over the supply system to work on gas oil.

Phot. 1. Overall view of the generating set with the examined engine Perkins 2806A-E18TAG2

Phot. 2. Engine Perkins 2806A-E18TAG2
with a special, heated rape oil filter. View of a part of supply system.

Considering the differences in physical and chemical parameters of the gas oil as compared with the rapeseed oil (crude, not degummed), in the case of the vegetable oil, two additives were used:

– the additive washing the engine injection system, produced by the firm *Kleen-flo*, 300 ml for 200 l of the rape oil,
– the additive *Nitrocet 45*, 0.5 %. This additive increased the rape oil cetane index value of about 15 units.

Vegetable oils are characterized by a run of the distillation curve different from this of the gas oil. It means, among other things, higher temperatures at the beginning of the distillation and impossibility of full evaporating of the fuel. Higher temperatures lead to a thermal cracking [6], which is the cause of important amounts of deposit on the atomizer and in the combustion chamber. This was the reason to use a commercial washing additive "Kleen-flo", very effective for the rapeseed oil. It was confirmed also by our other tests.

The rapeseed oil has considerably lower value of the cetane index than the gas oil (Tab.1). It usually causes an increase of the self-ignition delay, higher maximum speed of the combustion pressure growing (just after the self-ignition), higher maximum combustion temperatures, and, in consequence, a rise in emission of nitric oxides NO_X [9, 7]. To reduce such inconveniences, we used the additive increasing the rape oil cetane index value up to the level LC for the gas oil.

3. TEST STAND

During the investigation, the engine Perkins 2806A-E18TAG2, which was the integral part of the generating set, was stopped by changing the electric load of the generator. Main elements of the measuring line used here are connected with the analysis of the energy parameters and toxicity of the exhaust gases. Applied measurement systems were produced by the firm AVL (Austria). Here are some of them:

- computer mass fuel gauge, produced by AVL
- measurement system to determine the concentration of the exhaust gaseous components - AVL Bench Emissions System CEB II (O_2 – PMD, CO, CO_2 – NDIR, HC – FID, NO_x – CLD)
- Measurements stand with the exhaust gas diluting tunnel and computer microbalance of Sartorius (measurement accuracy – 0.001 mg) to determine the emission of the particulate matters in the engine exhaust gas.
- measurement stand to determine the smokiness level in Bosch scale – AVL Smoke Meter
- Measurement stand to determine: exhaust gas temperature, ambient temperature, pressure and humidity of the air absorbed by the engine, excess air factor λ.

Exhaust gas toxic components were measured using the apparatus in accordance with the binding standards: ISO/CD 8178-1 (RIC engines-Exhaust emissions measurement, edition 11.XI.1992) and ECE – R49/2(Uniform provisions concerning the approval of compression ignition (C.I.) engines and vehicles equipped with C.I. engines with regard to the emissions of pollutants by the engine).

4. INVESTIGATION RESULTS AND THEIR ANALYSIS

As mentioned above, the measurements were performed at the constant engine speed of 1500 rpm and at the loading of the generating set electric power 0 to 480 kW. For each of the examined fuels (gas oil, rapeseed oil), 13 measurement points of energy and ecology engine parameters have been done. Loading changes of the combustion engine (Perkins 2806A-E18TAG2), being an integral part of the generating set, were done using an electric engine dynamometer of the maximum power 500 kW.

The principal energy parameter considered in the analysis of the rape oil effect as compared with the gas oil, is the Gp fuel consumption per hour [kg/h]. The results are showed on the Fig. 1. It is visible, that supplying the examined Diesel with the rape oil causes the increase of the fuel consumption per hour, rising when the engine load grows. At 480 kW of the received electric power, the increase of the fuel consumption, in the case of rape oil supply (as compared with the gas oil) comes to 20 %. It is however to notice, that the rapeseed oil density (ρ=0.913 g/cm^3) is significantly higher than this of the gas oil (ρ=0.825 g/cm^3). For that reason, after the recalculation of the fuel consumption from the mass units (kg) to the volume units (dm^3), the increase of the fuel consumption – of the rape oil – in comparison with the gas oil, is only about 8 %. Also, we have to take into consideration the fact, that the rape oil calorific value (38.0 MJ/kg and 34.5 MJ/dm^3) is lower than this of the gas oil (42.6 MJ/kg and 35.2 MJ/dm^3). Then, if the differences in calorific values of the examined fuels were considered, the overall efficiency of the examined engine for the rape oil would be practically on the same value level, than for the gas oil.

The last important conclusion resulting from the analysis of data showed on the Fig. 1, relating to the Gp fuel consumption per hour for the gas oil and rapeseed oil (at a constant rotational speed of the engine n = 1500 rpm and changing load) concerns the measurements scatters. The

diagram shows clearly that the rapeseed oil is characterized by the higher lack of repeatability of the fuel consumption per hour than the gas oil (measurements done 3 times, on different days for each fuel), which is an important advantage. It results from the fact that the vegetable oil is characterized by a larger fluctuation of the processes: injection, atomization, evaporation, mixing with the air, self-ignition and finally – combustion process itself. However, from the point of view of the engine (generating set) user, it is not very important, because mean values are significant only in a long time.

Changes of Gp fuel consumption per hour involve changes of excess air factor λ. The values λ for both examined fuels are practically the same within the whole range of engine load. Some small changes – slightly lower values of λ for the vegetable oil – are due both to the higher fuel consumption (rapeseed oil) and to the differences in values of stoichiometric constant Lt coming to about 14.5 kg air/kg fuel for the gas oil and about 12.5 kg air/kg fuel for the rapeseed oil. The constant stoichiometric values are dependent on the elementary composition of the fuel (fuel constant), i.e. on the amount of carbon/hydrogen/oxygen/sulphur in the fuel. In principle, the amount of the sulphur in the fuel (in compliance with the European Fuel Card) is so small – 50 ppm for the gas oil – that there is no need to consider it in Lt calculation for the rapeseed oil. In the case of rapeseed oil, the situation is even more favourable, because vegetable oils, practically, do not contain the sulphur. In the conventional gas oil, there are no oxygen molecules (mixture of different hydrocarbons). The advantageous feature of the rapeseed oil is the fact that this fuel contains about 10 % of oxygen in its particle. It is favourable for the optimization of the combustion process run, disturbed otherwise, as compared with the gas oil, by a significantly higher value of viscosity, density, surface tension, distillation curve run etc., as compared with the gas oil.

The changes of the air excess factor are usually accompanied by the changes of the exhaust gas temperature. In accordance with the statement above, the change of the examined engine supply system from gas oil to rapeseed oil, without significantly changing the air excess factor value, in spite of a small increase of the fuel consumption, does not influence the exhaust gas temperature. It is important, because it indicates a similar situation of the combustion process for the rapeseed oil as for the gas oil. If the vegetable oil combustion happened disadvantageously too late (relative to the top dead centre) in the case of the rapeseed oil as compared with the gas oil, which would deteriorate the combustion efficiency, the exhaust gas temperatures would be showed as higher. The test results presented on the Fig. 2 show, that in the case of this particular supply system of a Diesel, equipped with the injection units, the rapeseed oil supply does not cause a delayed combustion. It is importantly due to the high maximum fuel pressures, which equalizes partly the negative effect of the high viscosity of the rape oil in the process of injection and atomization of such a fuel on its combustion and enables a good preparation of the mixture rapeseed oil-air, ensuring the similar time and situation of the combustion process as for the gas oil.

The results of measuring the concentration of the nitric oxides NO_X in the exhaust gases, for the examined fuels, are presented on the Fig. 3. The data on the diagram indicate that the application of the rapeseed oil supply in a Diesel causes an increase of the nitric oxides concentration at higher loads (above 128 kW), as compared to the gas oil supply. Probably, this range of the generating set loading will be realized most often in practice. At maximum engine loads, the increase of the NO_X concentration in the exhaust gas comes to about 18 %. This tendency maintains within 250 to 480 kW of the electric power developed by the combustion engine. It is important, because the nitric oxides NO_X are the most toxic of the exhaust gas components. It must be however noticed, that the NO_X forming is due to the maximum combustion temperatures (so called “maximum maximorum of the temperature”) appearing locally and temporarily in the combustion chamber. If there were no application, in the case of the rape oil, of the additive (“Nitrocet” or any other increasing the cetane index value), the concentrations of NO_X in the exhaust gases would be certainly higher. It results from the fact that the crude rape oil has significantly lower cetane index value than the gas

oil. In this case, a lower value of the cetane index causes a reduction of the vegetable oil tendency to self-ignition. In consequence, the time between the beginning of the fuel injection (of the rape oil as compared with the gas oil) and the beginning of the self-ignition is longer. In this longer time – between the beginning of the injection and the beginning of the self-ignition – in the combustion chamber gathers a great amount of the fuel supplied by the injection units. A greater fuel mass in the combustion chamber, gathered before the self-ignition, in the moment of the fuel (rape oil) ignition, ignites incomparably more violently (explodes) than the gas oil. It results in increasing the values: of maximum combustion pressure, maximum speed of the combustion pressure growing $(dp/d\alpha)$ max, "hardness of engine operation", maximum combustion temperature and of NO_X concentration [7, 9]. The additive "Nitrocet", raising the cetane index value and increasing by this the tendency of the rape oil to self-ignition, equalizes considerably these problems. Paradoxically, it is also important that the application of a modern Diesel, equipped with the injection system with very high maximum pressures of the fuel injection, improves the processes of the rape oil injection and atomization reducing the fuel consumption – of the rape oil), but on the other hand, it enlarge, in the determined time of the self-ignition delay τ_S, the amount of the fuel in the combustion chamber, in the time between the beginning of the injection and the beginning of the self-ignition, which increases the maximum speed of kinetic combustion and causes higher concentrations of NO_X in the exhaust gases. From this point of view, Diesel engines equipped with traditional injection pumps with lower maximum pressures of the fuel injection, turn out to be a little more advantageous, though the engines with such supply systems involve a greater consumption of the fuel.

It must be remembered that, at the values of the air excess factor λ applied in Diesel engines and measured on the examined engine, the application of conventional, in series production, catalytic converters, will reduce only the emission of carbon monoxide CO and of unburned hydrocarbons THC, without lowering the concentration and emission of NO_X in the exhaust gases. To achieve this, some special systems reducing NO_X should be used, as well as the filters of particulate matters for the emission of the application of such NO_X reducers and particulate matter filters with a continuous regeneration (CR) requires further investigations. In the case of generating sets, it is much simpler than in the case of traction engines because of the constant rotational speed of the engine.

The concentration of the carbon monoxide CO in the exhaust gas of the examined Diesel engine, connected with a generator, analysed in relation to the loading, for the gas oil and rapeseed oil, are similar (qualitatively). The test results indicate that the CO concentration values are, at low engine loads, very similar to these of the gas oil. At higher engine loads (above 256 kW), the concentration and the emission CO are lower for the rape oil than for the gas oil. The difference comes to 35 % as related to the gas oil.

A similar tendency is also observed for the concentration (Fig. 5) of unburned hydrocarbons HC. At high engine loadings, the amount of emitted unburned hydrocarbons in exhaust gases is lower for the engine supplied with the rape oil than in the case of the gas oil. It results mainly from the favourable effect of high combustion temperatures (extremely important in the case of the rapeseed oil) on the oxidation of hydrocarbons in the engine cylinder. If there were necessity of reducing carbon monoxide and unburned hydrocarbons emissions, a good solution would be in this case the mass-produced catalytic converter, selected to match the temperatures and rate of the fuels flow.

The effect of growing load of the examined engine on the particulate matter emission (Fig. 6) is quite different. In the case of gas oil, for which the producer optimized the examined engine, the emission of particulate matter changes only slightly. While in the case of the rapeseed oil, an increase in the engine power involves an intense growth of the particulate matter emission. At the full engine loading, the emission of PM is higher for the rape oil even of about 275 % as compared with the gas oil. At the electric power 480 kW, the emission per hour of the particulate matters comes to about 20 g/h for the gas oil and about 75 g/h for the rape oil. Moreover, the test results presented

on Fig. 6 show clearly, that the mean standard deviations calculated from 3 repeat measurements of the PM emission are considerably higher for the rape oil than for the gas oil. It is due directly to the larger fluctuations of proportioning the rape oil in relation to the gas oil, which was already mentioned in the analysis of the fuel consumption per hour (Fig. 1).

Unfortunately, no change of the engine control parameters (for instance, the beginning of the fuel injection or/and the supercharging pressure) can be considered as a remedial measure. It is so, because any construction or regulation changes of the engine, reducing the emission of the particulate matters, would cause at the same time an increase of the nitric oxides NO_X emission. This emission is anyway higher for the rape oil than for the gas oil. The only, theoretically possible solution would be shaping the fuel injection characteristic in such a way that the maximum speed of kinetic combustion is reduced in purpose to lower the NO_X emission and raise the maximum speed of diffusion combustion to reduce the emission of PM. It is however impossible in the case of injection pumps. The unique supply system allowing shaping the fuel injection characteristic is the common-rail system. In the case of the examined engine with injection pumps, the only sensible method of reducing the emission of particulate matter would be the application of a particulate matter filter with the continuous regeneration, but such a solution involves considerable expenses.

5. CONCLUSIONS

The investigation of the effect of fuelling a modern Diesel Engine with the crude rapeseed oil allows formulating a few essential conclusions:

1. The work of a Diesel engine on the crude rapeseed oil is possible, which was confirmed by the operation during many months of operating a generating set with the engine Perkins 2806A-E18TAG2 of the power rating 500 kW, but it is necessary to adapt the supply and control systems of such an engine as well as to use appropriate additives to the vegetable oil.
2. The use of the crude rapeseed oil in a modern Diesel high-power engine involves, among other things, an increase of the fuel consumption per hour (at the principally stable values of the engine total efficiency), and the increase of both the nitric oxides concentration and of the particulate matter emission.

The concentrations of the gaseous compounds of the incomplete combustion remain in principle on a similar level as those for the gas oil.

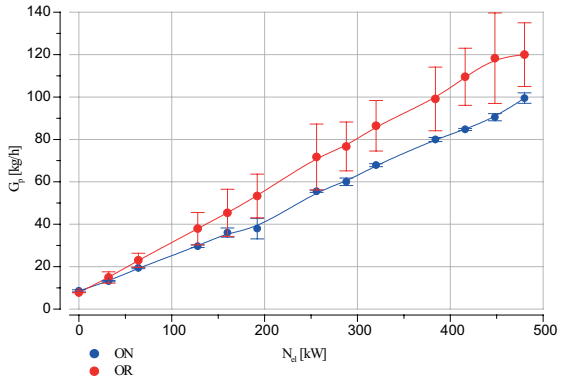

Fig. 1. Consumption per hour in the examined engine for the gas oil and for the rape oil.

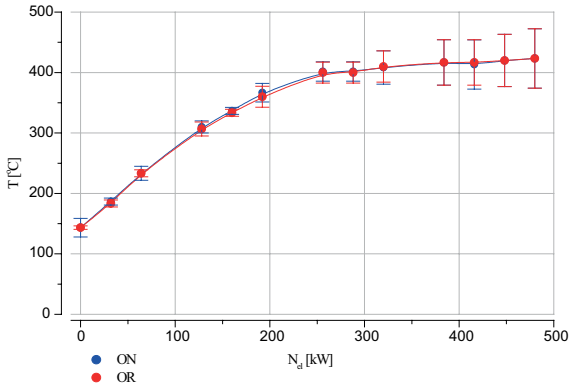

Fig. 2. Exhaust gas temperature in the examined engine for the gas oil and for the rape oil.

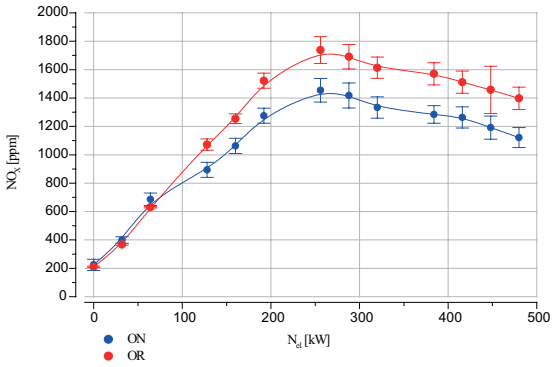

Fig. 3. Concentration of nitric oxides NOx in the engine exhaust gas for the gas oil and for the rape oil

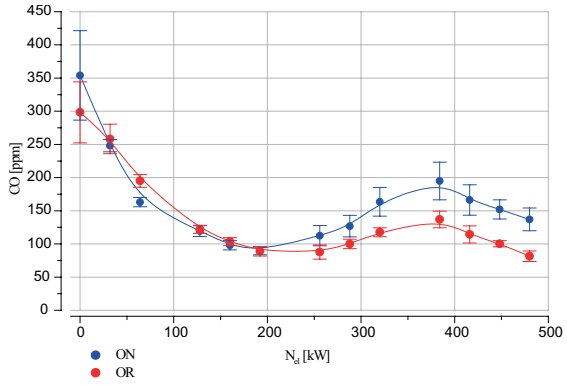

Fig. 4. Concentration of the carbon monoxide CO
in the engine exhaust gas for the gas oil and for the rape oil.

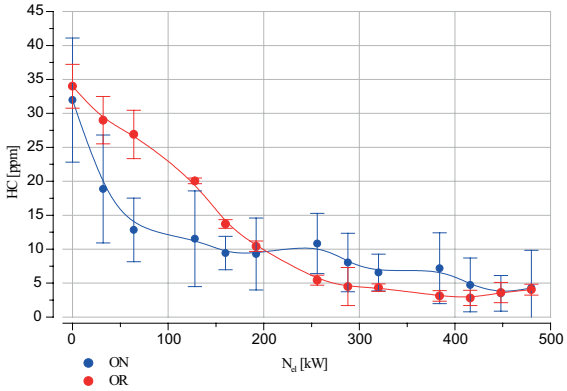

Fig. 5. Concentration of the unburned hydrocarbons in the exhaust gas for the gas oil and for the rape oil.

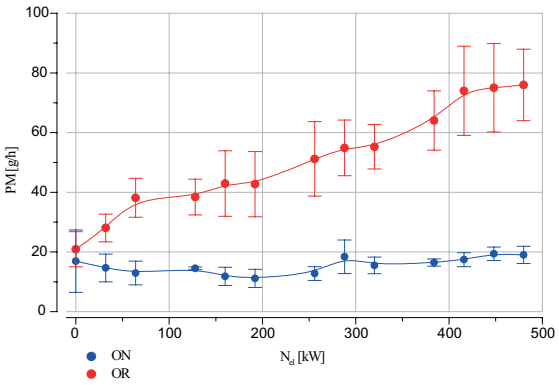

Fig. 6. Emission of particulate matter PM in the exhaust gas for the gas oil and for the rape oil.

REFERENCES

Goering C.E., Schwab A.W., Daughewrty M.J., Pryde E.H., Heakin A. *Fuel Properties of Eleven Vegetables Oils.* Transactions of the Society of Agricultural Engineers, 1982.

Zabłocki M. *Olej rzepakowy jako paliwo dla szybkoobrotowych silników wysokoprężnych.* PAN Teka Komisji Naukowo-Problemowej, Kraków 1990.

Vellguth G. *Performance of Vegetable Oils and their Monoesters as Fuels for Diesel Engines.* SAE Transactions, 1983, nr 83 1358.

Murayama T., Oh Y., Miyamoto N., Chikahisa T., Itow K. *Low Carbon Flawer Buildup, Low Smoke and Efficient Diesel Operation with Vegetable Oils by Conversion to Mono-Esters and Blending with Diesel Oil or Alkohols.* SAE Transactions, 1984, nr 84 1161.

Cisek J. *Wpływ dodatków do oleju rzepakowego w postaci mieszanin lub emulsji na parametry pracy silnika wysokoprężnego*. Materiały *International Science Conference on Combustion Engines ‚Kones 95',* Poznań 1995.

May H., Hattingen U., Birkner C., Adt U., Dietrich W. *Entwicklung eines Nutzfahrzeug-Vorkammer-Dieselmotors für Rohe Pflanzenole als Kraftstoff.* 14. Wiener Motorensymposium, 1993.

Mruk. A., Szlachta Z., Cisek.J. Efekty zastosowania ceramicznej powłoki na denku tłoka silnika wysokoprężnego. *IV Sympozjum Naukowo-Technicznego 'Silniki spalinowe w zastosowaniach wojskowych'*. Jurata, 13-15.10.1999

Cisek J. *Wpływ podgrzewania oleju rzepakowego na parametry pracy silnika wysokoprężnego.* Prace Naukowo-Badawcze Instytutu Pojazdów Samochodowych i Silników Spalinowych Politechniki Krakowskiej w Roku Jubileuszowym 50-Lecia Politechniki Krakowskiej. Politechnika Krakowska, Kraków 1995.

Cisek J., Szlachta Z. *The autoignition delay of vegetable fuels at varied air temperature inside combustion chamber of diesel engine.* Międzynarodowa Konferencja Agrotech Nitra 2001. Nitra, Słowacja 05-6.06.2001.

Sureshkumar K. et al *Performance and Charakteristics of the Use of Environment Friendly Pongamia Pinnata Methyl Ester in C.I. Engines.* Journal of Energy & Environment, Vol.5, May 2007.

Uzdowski M. *Możliwości wykorzystania paliw alternatywnych w rolnictwie.* Motrol. Motoryzacja i Energetyka w Rolnictwie, tom 4. Lublin 2001.

Lisowski M. *Ekonomiczne i ekologiczne aspekty zasilania silnika ZS olejami roślinnymi i ich mieszaninami z olejem napędowym.* Motrol. Motoryzacja i Energetyka w Rolnictwie, tom 7. Lublin 2005.

Wcisło G. *Determination of Rapeseed Oils Combustion Heat in Calorimeter Bomb and an Assesment of The Heat Value.* Teka Komisji Motoryzacji i Energetyki w Rolnictwie PAN, Lublin 2005.

Lotko W. *Ocena emisji składników spalin silnika wysokoprężnego zasilanego mieszaninami oleju napędowego z estrami metylowymi oleju rzepakowego.* Archiwum Motoryzacji. Lublin 2006.

Lotko W. *Ocena opóźnienia samozapłonu silnika wysokoprężnego z wtryskiem bezpośrednim zasilanego mieszaninami oleju napędowego z estrami metylowymi oleju rzepakowego.* Archiwum Motoryzacji. Lublin 2005.

Lotko W. *Paliwa roślinne a emisja składników toksycznych spalin.* Archiwum Motoryzacji. Lublin 2000.

WŁAŚCIWOŚCI SILNIKA DIESLA ZASILANEGO NATURALNYM OLEJEM RZEPAKOWYM

Streszczenie. W artykule przedstawiono wyniki badań silnika diesla o mocy 500 kW zasilanego naturalnym olejem rzepakowym. Podano techniczne aspekty przystosowania silnika do pracy na oleju rzepakowym oraz stosowane dodatki do oleju, pozwalające na bezawaryjną pracę silnika. Mierzono parametry energetyczne i toksyczność spalin. Stosowano metody badań i aparaturę pomiarową zgodną z normami ECE. Ze względu na fakt, że silnik był integralną częścią agregatu prądotwórczego, pomiary przeprowadzono przy stałej prędkości obrotowej n=1500 obr/min. i zmiennych obciążeniach silnika. W wyniku przeprowadzonych badań stwierdzono między innymi, że zastosowanie oleju rzepakowego, w miejsce oleju napędowego, powoduje wzrost godzinowego zużycia paliwa (przy niezmiennych zasadniczo wartościach sprawności ogólnej), wzrost stężenia zarówno tlenków azotu NO_X jak i emisji cząstek stałych (PM).

W konkluzji przeprowadzonych badań można stwierdzić, że istnieje możliwość zasilania silników wysokoprężnych dużej mocy naturalnym olejem rzepakowym, pod warunkiem przystosowania do tego celu zarówno silnika jak i paliwa

Słowa kluczowe: naturalny olej rzepakowy, parametry energetyczne, spaliny, cząstki stałe

TEKA Kom. Mot. Energ. Roln. – OL PAN, 2011, 11, 40–47

ELASTIC HYSTERESIS DETERMINATION FOR THE SKIN OF TOMATO FRUIT DURING UNIAXIAL TENSION TEST

Anna Ciupak and Bożena Gładyszewska

Departments of Physics, University of Life Sciences,
Akademicka 13, 20-950 Lublin, Poland
e-mail: anna.ciupak@up.lublin.pl

Summary. The presented work covers the problem of hysteresis loop characteristic determination during uniaxial stretching of the tomato fruit skin cv. *Admiro* stored in a controlled environment chamber at 21°C in the cycle load-unload process. The force and strain, as well as the absorbed energy, degree of elasticity and hysteresis losses were determined with the use of the random markers method. The absorbed energy values for the skin of fresh fruits ranged from $2.1 \cdot 10^{-3}$ mJ to $18.6 \cdot 10^{-3}$ mJ, while the hysteresis losses fall between 12.3 % and 54.2 %, depending on tensile force value. The absorbed energy and hysteresis losses were defined for the stored fruit stabilized at the level of $20.3 \cdot 10^{-3}$ mJ and 50.8%, respectively. The degree of elasticity ranged between 40% and 71 %.

Keywords: tomato skin, absorbed energy, degree of elasticity, hysteresis losses

INTRODUCTION

The knowledge of mechanical properties of plant origin materials (vegetables and fruit), is of major importance when it comes to the storage, transport and converting processes as well as the machines and devices design [Thiagu 1993].

Fruit and vegetables damage, which may occur at each stage of the production and processing, is considered the fundamental problem in the area of nowadays crop production [Machado 1999; Dobrzański 2008]. Therefore, the maintenance of high quality products, which also means material damage minimising, plays a significant role in nowadays production, mainly because loads and stresses that cause mechanical defects considerably reduce their nutritional and trade value [Desmet 2004; Van Zeebroeck 2005; Singh 2006; Van Linden 2006].

Mohsenin (1986), among the parameters that characterise the crop material in the respect of its mechanical capacity, mentions ultimate compressive strength, tensile and shear strength, stress relaxation, Young's modulus, Poisson's ratio and elastic hysteresis. It needs to be emphasized [Stopa 2010], that a correct determination of the mentioned quantities is highly dependent on both the crop material type and the applied test method.

In the opinion of Chaib's (2007), rheological measurements and hysteresis characteristics are an important source of knowledge on the mechanical properties of the whole fruits as well as their structural elements (e.g. skin, pericarp tissue).

The skin of fruit e.g. tomato functions mainly as the protection of the soft internal tissue against external factors, affects the product's integrity and growth process [Andrews 2002; Bargel 2005] and determines its mechanical properties – elasticity, resistance and load response. Due to the above-mentioned, determination of mechanical properties of coat layers seems to be of the utmost importance considering the end product quality and safety, its storage, processing and the structural design of machines and devices used in food processing systems [Thiagu 1993].

Elastic hysteresis is a measure of energy dissipation, which is caused by the internal friction and material structure destruction. What is more, it allows to describe both the structure and its changes during deformation [Bohdziewicz 2003; Łysiak 2006]. The energy dissipation may be also developed by the mechanical vulnerability such as cracking or disintegration [Dobraszczyk 1994; Fossdal 2005].

Recent year's data indicate the growing popularity of rheological investigation applications, connected with determination of hysteresis loop with reference to the crop materials. Gindl (2006) in the cycling stretching test applied repeated loading and unloading with recuperated cellulose fibre. Spatz (1999) used the stretching test during the rheological examination of the *sklerenchym tissue. Hysteresis loop was also determined in the* compression tests with respect to the apples [Holt 1983; Blahovec 1997], pears [Blahovec 2002], potato bulbs [Holt 1983], sugar beet roots [Bzowska-Bakalarz 1994] and wheat grain [Łysiak 2006]. The rheological properties of the isolated tomato skin were defined by Petracek (1995) and Edelmann (2005).

The determination of hysteresis loop characteristics is usually connected with load and unload energy, absorbed energy value and hysteresis losses [Holt 1983; Bzowska-Bakalarz 1994; Doherty 1998; Blahovec 2002; Malkin 2006; Bohdziewicz 2007]. The elasticity of the fruit tissue might be characterised by the value of elasticity modulus (degree of elasticity) expressing the participation of accumulated elastic strain energy in the general deformation force balance [Bohdziewicz 2007].

On account of the shortage of data concerning the hysteresis loop losses for the skin of the soft fruits, the authors of the present article decided to conduct the research focusing on the determination of the absorbed energy, degree of elasticity and loses of hysteresis loop for the skin of the tomato put through the tension in the process of loading and unloading.

MATERIALS AND METHODS

Laboratory tests were carried out on tomato fruits (*Lycopersicon esculentum* Mill) cv. *Admiro*, ripe and similar in size, supplied by the Leonów Greenhouse Gardening Company in Niemce near Lublin.

The experiment was conducted on the measuring stand assigned for the determination of mechanical properties of biological materials [Gładyszewska 2006].

After washing and drying the surface of the fruit, skin specimens were procured for tensile tests. The incision was made from the base of the tomato to the stalk. Longitudinal strips were sliced off from each fruit with a profiled, single-blade knife with a limiter. Parameters such as length, width and thickness were measured with the use of a caliper before the examination. The samples had the shape of a strip with the length of 30 mm ± 0.1 mm and the width of 10 mm ± 0.1 mm. The thickness of each sample was measured under an optical microscope with the accuracy of ± 0.05 mm.

The prepared samples were placed in clamping grips of the tensile machine, which allows constant and measurable increase of the tensile force value. Powdered graphite markers were ran-

domly sprayed on the sample surface. The strips were at first stretched, up to the chosen force value (increment in the force during uniaxal tension was equal to 1.4 $N \cdot min^{-1}$). Then the sample was unloaded by decreasing the tensile force to zero. The force value as well as the sample tensile strain was determined on the grounds of the method of random markers [Gładyszewska 2007].

The obtained relations of force-tensile strain, derived from 15 repetitions were used to determine the average value of absorbed energy W_a [mJ], which relates to the area between the load and unload curves (Fig. 1). Degree of elasticity t_{sp} and the hysteresis loss degree S_h were determined according to the relations 2 and 3, respectively.

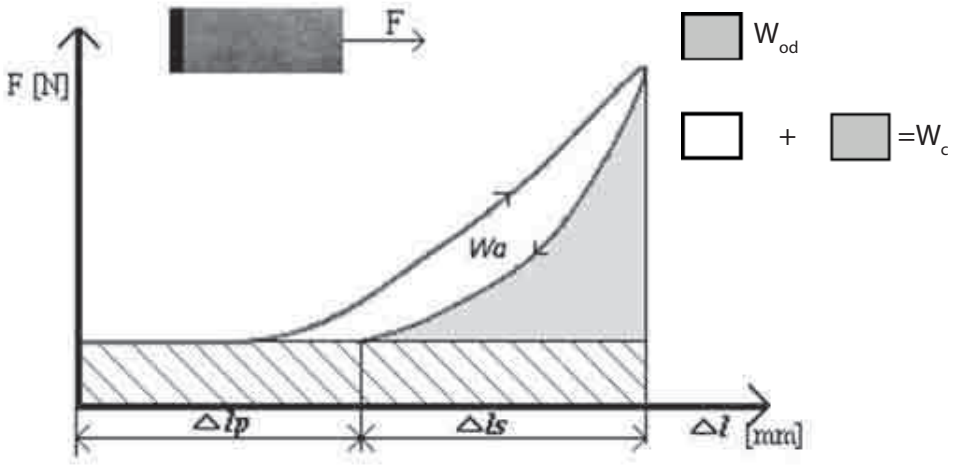

Fig. 1. Load curve for tomato fruit skin with marked parameters: W_c, W_a, Δl_p i , Δl_s

$$W_a = W_c - W_d \tag{1}$$

$$t_{sp} = \frac{\Delta l_s}{\left(\Delta l_s + \Delta l_p\right)} \cdot 100\% \tag{2}$$

$$S_h = \frac{W_a}{W_c} \cdot 100\% \tag{3}$$

where: W_c – total energy [mJ], W_{od} – unload energy [mJ], Δl_s – elastic strain [mm], Δl_p – plastic strain [mm].

RESULTS AND DISCUSSION

Figure 2 presents the exemplary characteristic of the load-unload test for the tomato skin sample. Along with the tensile force increase, strain growth could be observed. The specimen, which was cut from the fruit directly after harvesting, could be loaded and unloaded several times. The first loading of the examined sample was conducted until the tensile force reached 1.7 N. Then, the sample was completely unloaded, after which the specimen was subjected to a load of 2.3 N. The sample damage was observed in the presence of tensile force of 3.5 N (Fig.2).

Table 1 shows the absorbed energy values W_a, material degree of elasticity t_{sp}, and hysteresis losses S_h, for the first (I) and second (II) load (Fig. 1).

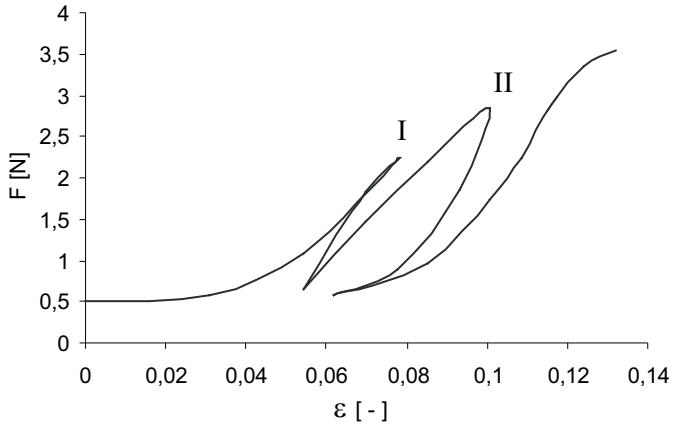

Fig. 2. Force – relative strain relation F(ε) during the cyclic load-unload test for tomato skin sample, harvested directly from the plant

Table 1. Average values of absorber energy W_a, degree of elasticity t_{sp} and hysteresis losses for the fresh tomato fruits during load I and II.

	Load I	Load II
Force [N]	1.7	2.3
W_a [mJ]	$2.1 \cdot 10^{-3}$	$18.6 \cdot 10^{-3}$
t_{sp} [%]	40	71
S_h [%]	12.3	54.2

In case of the first load (I), the amount of absorbed energy was 8 times lower than during the second one (load of 2.3 N). For the second load (II) over fourfold increase in hysteresis losses degree was observed compared to load I. The degree of elasticity value, determined during the first load-unload cycle stayed in the region of 40 % while through the second one reached 71% (Tab.1).

It was possible to load only once (one load and one unload) the samples that were cut from the stored fruits and kept at the temperature of 21°C in the controlled environment chamber for 2 days. The research showed that the time and storage conditions of the tomato fruit as well as its ripening process had a huge impact on the skin structure and mechanical properties [Ciupak 2010].

Figure 3 presents the sample graph of the tensile force in the function of specimen relative strain F(ε), which was determined in the load-unload cycle. The value of the tensile force was not higher than 3 N for all the examined cases, which allows to load the sample completely and to avoid sudden rupture at the same time. The obtained hysteresis loops were used in the average absorbed energy values W_a, degree of elasticity t_{sp} and hysteresis losses S_h determination. The parameters were calculated on the basis of 15 repetitions and presented in Table 2.

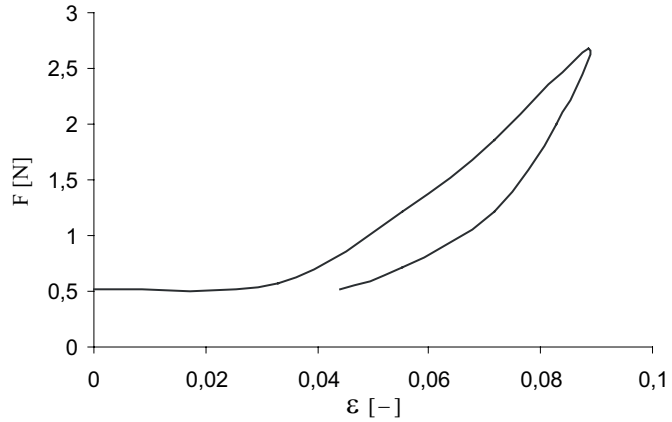

Fig. 3. Sample graph of the tensile force in the function of relative strain F(ε)

For the examined tomato skin the 50 % hysteresis loss could be observed (Tab.2). The skin of the fruits stored in an environment chamber and samples from tomatoes harvested directly from the plant (I load) were comparable with respect to degree of elasticity t_{sp}, which reached the level of 40 % (Tab. 1 and Tab. 2).

Table 2. Average values of absorbed energy W_a, degree of elasticity t_{sp} and hysteresis losses S_h determined for stored tomato fruits.

W_a [mJ]	$20.3 \cdot 10^{-3}$
t_{sp} [%]	41
S_h [%]	50.8

It might be expected that with the material and skin cells damage growth during uniaxal tension test, the values of absorbed energy and hysteresis losses would increase while on the other hand the decrease in degree of elasticity value should be observed. Blahovec (2002) obtained similar results during compression tests with respect to pears.

On account of the lack of information concerning determination of absorbed energy, degree of elasticity and hysteresis losses for the skin of the tomato, the received results cannot be compared with other outcomes. Admittedly, Pertacek (1995) established rheological characteristics of isolated tomato skin, while Edelmann (2005) described the cuticle participation in rheological tomato skin properties, but the numerical values of the determined parameters were not provided.

It might be observed, that the absorbed energy values (Tab. 1, Tab. 2) are significantly lower than the energy obtained during e.g. apple compression test, contained in the 0,1 J to 0.4 J range [Blahovec 1997] and pears ($3.6 \cdot 10^{-3}$ J to 0.3 mJ) [Blahovec 2002]. The absorbed energy value during the cycle load of wheat grain and its increase with the humidity escalation was determined by Łysiak (2006) at the level of 2.5 mJ – 23 mJ.

The degree of elasticity for tomato skin, determined on the level of 40 % < t_s < 71 % (Tab. 1 i Tab. 2), might be compared with the data obtained during tests on the pears – 28.3 % < t_{sp} < 75.9 % [Blahovec et al. 2002] and sugar beet roots – 64 % < t_{sp} < 88 % [Bzowska-Bakalarz 1994].

The calculated hysteresis losses for tomato skin S_h ranged from 12.3 % to 54.2 %. Blahovec (2002) presented similarly wide range for that parameter, establishing it between 35 % - 85 % for

pears. Hoolt (1983) determined the hysteresis losses for the potato at the level of 75 % and for apples at 30 %. Bzowska-Bakalarz (1994) conducted investigation on hysteresis losses in the first load-unload cycle with reference to fresh and withered sugar beet roots. The outcome of this study showed that the hysteresis losses value ranged from 34 % to 62 % and was about 35 % higher for fresh roots than the one determined for the withered roots.

CONCLUSIONS

1. Absorbed energy values for the skin of tomato harvested directly from the plant ranged from $2.1 \cdot 10^{-3}$ mJ to $18.6 \cdot 10^{-3}$ mJ while the degree of elasticity and hysteresis losses – 40% to 71% and 12.3 % to 54.2 % respectively, depending on tensile force value.
2. Absorbed energy, hysteresis losses and degree of elasticity defined for stored fruits was stabilized at the level of $20.3 \cdot 10^{-3}$ mJ, 41 % and 50.8 %, respectively.
3. The outcome of this study shows that the random markers method might be applied for elastic hysteresis determination with reference to soft fruits. It should be pointed out that the presented research provided a preliminary characteristic in the field of mechanical properties of soft fruit and its continuation is required.

REFERENCES

Andrews J., Adams S. R., Burton K. S., Edmondson R. N. (2002). Partial purification of tomato fruit peroxidase and its effect on the mechanical properties of tomato fruit skin. Journal of Experimental Botany 53 (379), 2393-2399.

Bargel H., Neinhuis C. (2005). Tomato (Lycopersicon esculentum Mill.) fruit growth and ripening as related to the biomechanical properties of fruit skin and isolated cuticle. Journal of Experimental Botany 56 (413), 1049-1060.

Blahovec J., Vlačkova M.; Paprštein F. (2002). Static low-level bruising in pears. Research in Agricultural Engineering 48 (2), 41-46.

Blahovec J., Potočka K., Bareš J. (1997). Low-level bruising of stored apples due to quasistatic loading up to constant compression strain. Journal of Texture Studies 28, 87-99.

Bohdziewicz J. (2007). Modelowanie przebiegu odkształcenia tkanek parenchymy warzyw w warunkach quasi-statycznych zmian obciążenia. Zeszyty Naukowe Uniwersytetu Przyrodniczego we Wrocławiu. Rozprawy CCXLIX.

Bohdziewicz J. (2003). Histereza odkształceń miąższu wybranych warzyw. Acta Agrophysica 2, (4), 707-716

Bzowska-Bakalarz M. (1994). Właściwości mechaniczne korzeni buraków cukrowych. Rozprawy Naukowe z. 166. Lublin: Wydawnictwo Akademii Rolniczej.

Chaib J., Devaux M. F., Grotte M. G., Robini K., Causse M., Lahaye M., Marty I. (2007). Physiological relationships among physical, sensory and morphological attributes of texture in tomato fruits. Journal of Experimental Botany 58 (8), 1915-1925.

Ciupak A. (2010) Wpływ warunków przechowywania owoców pomidora na mechaniczne właściwości ich skórki. Rozprawa doktorska. Uniwersytet Przyrodniczy w Lublinie.

Desmet M., Lammertyn J., Van linden V., Verlinden B. E., Darius P., Nicolaï B. M. (2004). The relative influence of stem and fruit properties on stem puncture injury in tomatoes. Postharvest Biology and Technology 33, strony 101-109.

Dobraszczyk B. J. (1994). Fracture mechanics of vitreous and mealy wheat endosperm. Journal of Cereal Science 25, 927-933.

Dobrzański jr. B., Rybczyński R. (2008). Właściwości fizyczne i biochemiczne materiałów roślinnych. Problemy pomiaru mechanicznych właściwości owoców w aspekcie oceny ich jędrności. Lublin: Wyd. Nauk. FRNA, Komitet Agrofizyku PAN.

Edelmann H. G., Neinhuis C. Bargel H. (2005). Influence of hydration and temperature on the rheological properties of plant cuticles and their impact on plant organ integrity. Plant Physiology 24, 116-126.

Fossdal A., Einarsrud M. A., Grande T. (2005) Mechanical properties of LaFeO3 ceramics. Journal of the European Ceramics society, 25, 927-933.

Gindl W., Keckes J. (2006). Strain hardening in regenerated cellulose fibres. Composites Science and Technology 66, 2049-2053.

Gładyszewska B. (2007). Metoda badania wybranych mechanicznych właściwości cienkowarstwowych materiałów biologicznych. Rozprawy Naukowe z. 325. Lublin: Wydawnictwo Akademii Rolniczej w Lublinie.

Gładyszewska B. (2006). Testing machine for assessing the mechanical properties of biological materials. Technical Science 9, 21-31.

Holt J. E., Schoorl D. (1983). Fracture in potatoes and apples. Journal of Materials Science 18, 2017-2028.

Łysiak G., Laskowski J., Gagłowski S. (2006). Wpływ wilgotności na histerezę odkształceń ziarna pszenicy odmiany Kobra. Inżynieria Rolnicza 13, 333-339.

Machado R. M., Rodriguez del Rincon A., Portas C. A. (1999). Mechanical harvest of processing tomatoes: influence on percentage of damaged fruit and importance of the relation green fruit/rotten fruits. Acta Horticulturae 487, 237-241.

Malkin A. Ya., Isayev A. I. (2006). Rheology: concept, methods and applications. ChemTec Publishing, Toronto.

Mohsenin N. N. (1986). Physical properties of plant and animal materials. I. Structure, physical characteristic and mechanical properties. New York, London, Paris: Gordon and Breach Science Publishers.

O'Brien M., Goddard W. B., Gyasi S. (1972). Tomato damage during harvesting and handling. Transactions of the ASAE 15 (4), 653-655.

Petracek P. D., Bukovac M. J. (1995). Rheological properties of enzymatically isolated tomato fruit cuticle. Plant Physiology 109, 675-679.

Singh K. K., Reddy B. S. (2006). Post-harvest physico-mechanical properties of orange peel and fruit. Journal of Food Engineering 73, 112-120.

Spatz H.-Ch., Köhler L., Niklas K. J. (1999). Mechanical behaviour of plant tissues: composite materials or structures ? The Journal of Experimental Biology 202, 3269-3272.

Stopa R. (2010). Modelowanie deformacji korzenia marchwi w warunkach obciążeń skupionych metodą elementów skończonych. Monografie XCIII Wrocław: Wydawnictwo Uniwersytetu Przyrodniczego.

Thiagu R., Chand N., Ramana K. V. (1993). Evolution of mechanical characteristics of tomatoes of two varieties during ripening. Journal of the Science of Food and Agriculture 62, 175-183.

Van Linden V., De Ketelaere B., Desmet, M., De Baerdemaeker J. (2006). Determination of bruise susceptibility of tomato fruit by means of an instrumented pendulum. *Postharvest Biology and Technology 40*, 7-14.

Van Zeebroeck M. (2005). The discrete element method (DEM) to simulate fruit impact damage during transport and handling. Leuven: Katholieke Universiteit Leuven.

WYZNACZANIE HISTEREZY ODKSZTAŁCEŃ SKÓRKI OWOCÓW POMIDORA W TESCIE JEDNOOSIOWEGO ROZCIĄGANIA

Streszczenie. W pracy przedstawiono charakterystykę pętli histerezy skórki owoców pomidora odmiany Admiro przechowywanych w komorze klimatycznej w temperaturze 21 ºC, otrzymaną podczas rozciągania próbki w procesie obciążenie-odciążenie. W oparciu o metodę losowych znaczników wyznaczono wartości siły i odkształcenia próbki, a następnie wartość energii zaabsorbowanej, stopnia sprężystości materiału oraz strat histerezy. W zależności od siły obciążającej wartość energii zaabsorbowanej dla skórki owoców świeżych zawierała się w przedziale $2{,}1 \cdot 10^{-3}$ mJ do $18{,}6 \cdot 10^{-3}$ mJ, a straty histerezy od 12,3 % do 54,2 %. Dla owoców przechowywanych energia zaabsorbowana wynosiła $20{,}3 \cdot 10^{-3}$ mJ, zaś starty histerezy 50,8 %. Stopień sprężystości badanego materiału zawierał się w przedziale od 40 % do 71 %.

Słowa kluczowe: skórka pomidora, energia zaabsorbowana, stopień sprężystości, strata histerezy

TEKA Kom. Mot. Energ. Roln. – OL PAN, 2011, 11, 48–64

DUAL-FUEL FEEDING OF DIESEL ENGINE WITH GENERATOR GAS AND LIQUID FUEL

Karol Cupiał, Adam Dużyński, Michał Gruca, Janusz Grzelka, Stanisław Szwaja*

* Czestochowa University of Technology, Poland

Summary. The paper presents the results of research carried out at the Institute of Internal Combustion Engines and Control Technology of the Czestochowa University of Technology in the period from 2007 to 2010 under Research & Development Project R10 019 02 "The piston combustion engine in the sewage sludge gasification installation" financed by the Ministry of Science and Higher Education in Warsaw. Testing results for a turbocharged piston engine fed with generator gas obtained from a dried sewage sludge gasification plant are discussed.

Key words: piston engine, generator gas, sewage sludge, gasification.

INTRODUCTION

Sewage sludge is generated in a sewage treatment plant as a by-product of the biochemical processes of sewage treatment. The calorific value of dried sludge is approx. 11 MJ/kg and is comparable with the calorific value of crude wood (8 MJ/kg), brown coal (9-11 MJ/kg), and dry peat (14 MJ/kg), and this means that the dried sludge can be utilized as an energy raw material. Sewage sludge with a moisture content not exceeding 10% and a calorific value not lower that 10 MJ/kg is not biodegradable and may only be disposed of by thermal transformation [21]. Within the meaning of the waste management regulations in force, sewage sludge is regarded as hazardous waste of category B33, Annex no. 2 [24], and therefore its storage and processing is subject to regulatory restrictions. The gasification of sewage sludge and using thus obtained generator gas for feeding an internal combustion engine to drive a stationary electric current generator is a variation of the waste thermal neutralization process.

With a view to the applicable EU environmental regulations and requirements [21, 19], the Institute of Internal Combustion Engines and Control Technology of the Czestochowa University of Technology has carried out, under Research & Development Project R10 019 02 financed by the Ministry of Science and Higher Education of Warsaw, research aimed at investigating the possibility of gasifying dried sewage sludge generated by sewage treatment plants, and utilizing it for double-fuel feeding a piston engine to drive a generating set.

The fuel gasification process is a variation of the incomplete combustion process conducted with a considerable oxygen deficiency. Installations gasifying various organic substances, mainly

lumped wood, charcoal, peat, etc., were fairly common at the turn of the 19th and 20th centuries, and are extensively described in both archival [1, 6] and contemporary literature, e.g. [13, 14, 15, 23], which indicates some renaissance of interests in this technology. The available literature lacks, however, relevant data on any plants enabling gasification of dried sewage sludge.

Table 1 gives generator gas composition obtained from measurements on the installation, at an average bed temperature of 850°C.

Table 1. Averaged values of composition of the generator gas obtained from sewage sludge gasification, along with calorific values and theoretical air demand values

	H_2	CO	CO_2	CH_4	W_{dm}	W_{dg}	L_t	O_2
	[%]	[%]	[%]	[%]	[MJ/m^3]	[MJ/m^3]	[m^3/m^3]	[%]
Average value	3.81	13.40	7.69	0.97	1.63	2.44	0.50	3.84
Maximum value	4.17	14.18	8.10	0.98	1.67	2.54	0.52	3.99
Standard deviation	0.13	0.79	0.41	0.01	0.04	0.09	0.02	3.69

INDICATING OF THE DOUBLE-FUEL PISTON ENGINE FED WITH LIQUID FUEL AND GENERATOR GAS

The generating set driven by the 6CT107 turbocharged engine [20] was adapted to double-fuel operation by furnishing it with an additional gas supply system [3, 22, 24] and liquid and gaseous fuel dosage control systems completed from parts supplied by WOODWARD. The engine of this set was adapted to simultaneous indication of all the six cylinders and equipped with measuring instrumentation necessary for taking measurements of basic load characteristics and with a set of analyzers to measure chemical composition of generator gas supplied to the engine. The engine and electric generator control systems allow either the powering of a group of loads isolated from the power grid or parallel operation with this power grid. The final tests of the sewage sludge gasification installation and the generating set were carried out on the premises of PPUH „MARSZ" M. Szymor of Nowa Gorzelnia near Czestochowa [3].

The tests included simultaneous, synchronized measurements and recording of pressure variations in the individual cylinders of a turbocharged six-cylinder 6.56 dm^3 displacement engine adapted to double-fuel operation being fed with a liquid and gaseous fuels (Fig. 1). The engine drove, at a constant rotational speed of 1500 rpm, a synchronous electric generator loaded with resistances being switched on sequentially.

Fig. 1. The generating set connected to the gasification installation during the indication of the double-fuel engine [3]

Pressure variations and CRA and TDC tracer signals were recorded as a function of time at a frequency of 50 kHz. Recorded in a digital form, the signals were subjected to resampling at the moments of successive CRA tracer pulses, which made it possible to obtain the variations of pressure as a function of CRA angle with a strep of 0.5° CRA [2, 8, 12, 17]. At the same time, the basic parameters of gasification unit operation and composition of produced generator gas were also recorded. For the acquisition of all fast-varying signals, a USB HS1608 eight-channel module operated by its own program was used. In each recorded measurement series, 495 engine cycles were recorded. A schematic of the engine indication system is shown in Figure 2.

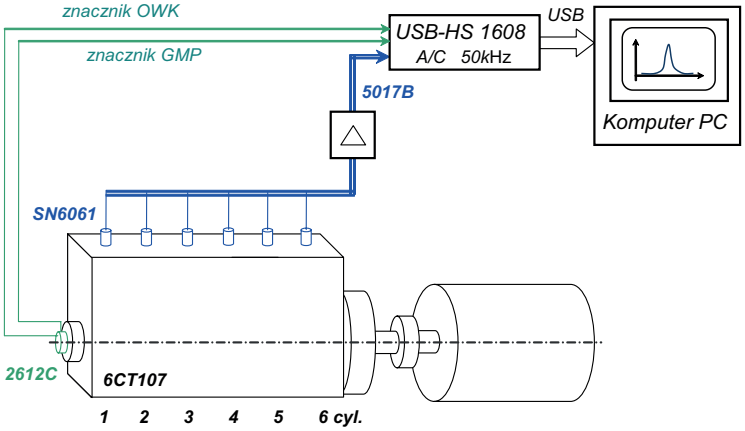

Fig. 2. A schematic of the engine indication system: 2612C – crank angle transmitter, SN6061 – piezoquartz pressure pickups , 5017B – eight-channel charge amplifier [3]

The tests performed on the supercharged piston engine double-fuel fed with generator gas and liquid fuel batched to the engine in varying energy fraction proportions have demonstrated that the double-fuel feeding of an engine is an effective method to reduce the engine susceptibility to rapid variations in chemical composition of generator gas and its calorific value [3, 7]. Some of the indication results are given in Figures 3 through 9. The most favourable engine operation conditions occur in the situation of a partial electric generator load of approx. 40 kW corresponding to approx. 50% of the generator rated power attained with the liquid fuel alone. The process of combustion of fuels in the engine double-fuel fed with generator gas (with an energy fraction of 75%) and liquid fuel (with an energy fraction of 25%) is run with an excess air factor of approx. 2.85, corresponding to 14% of oxygen content in the generator gas-air mixture and proceeds correctly. The engine attains then a high overall efficiency of 40%, which is better than the efficiency of 32% attainable when being fed with 100% liquid fuel. A maximum combustion pressure of 8.5 MPa occurs during feeding the engine with the sole liquid fuel, and then it monotonically decreases down to 7.2 MPa as the liquid fuel energy fraction is reduced to 25%. The maximum value of the cylinder pressure derivative, dp/dα, attains its highest level of 0.94 MPa/°CRA during the operation of the engine fed with the sole liquid fuel and then monotonically decreases to 0.5 MPa/°OWK as the liquid fuel energy fraction is reduced to 25%.

Under the conditions of the full load corresponding to approx. 100% of the generator's rated electric power, which is 80 kW, the fuel combustion process in the double-fuel fed engine has characteristics differing unfavourably from the respective characteristics occurring for partial loads corresponding to engine loading with a power of 40 kW. With the full engine load, the liquid fuel energy fraction could not be lower than 73%. In that case, the fuel combustion process is conducted with the excess air factor reduced to approx. 1.5, corresponding to an oxygen content of the generator gas-air mixture of 15%, and no longer proceeds correctly, since the exhaust gas smoking, the maximum combustion pressure, dp/dα and the pulsation amplitude of the variable indicated pressure component considerably increase. During engine operation with the full power, a maximum combustion pressure of 11 MPa occurs when feeding the engine with the liquid fuel alone, and then monotonically increases up to 13 MPa as the liquid fuel energy fraction is reduced to 63%. The maximum value of the cylinder pressure derivative, dp/dα, attains its lowest level of 0.70 MPa/deg during the operation of the engine fed with the sole liquid fuel, and then monotonically increases to 1.5 MPa/°CRA as the liquid fuel energy fraction is reduced to 63%.

The liquid fuel batch energy fraction equal to 25% corresponded to a liquid fuel unit consumption of approx. 52 g/kWh, as related to the generated electric energy, which, for the diesel oil price of 4.5 PLN/litre, corresponds to a rather high unit cost of this fuel, namely 0.28 PLN/kWh of generated electric energy (Fig. 9). With a view to the quite high unit cost of the liquid fuel batch as against the price for 1 kWh of electric energy possible to be achieved in settlements with power utility companies, which (according to the VATTENFALL offer valid as per Jan. 31, 2011) is within the range from 0.2934 PLN/kWh (night-time) and 0.3537 PLN/kWh (whole day) to 0.4033 PLN/kWh (day time), it can be stated that the gasification of dried sewage sludge in the installation in question will oscillate around the level of economic viability.

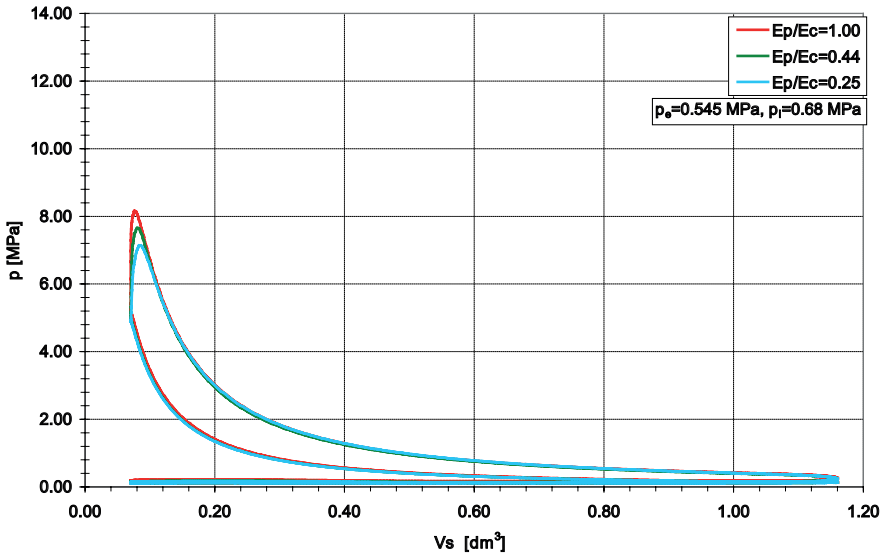

Fig. 3. Indicator diagrams of the double-fuel engine for varying magnitudes of the liquid fuel batch energy fraction (E_p) of the total energy amount contained in the liquid and gaseous fuels (E_c) (the averaged run for 495 cycles, pe=0.545 MPa)

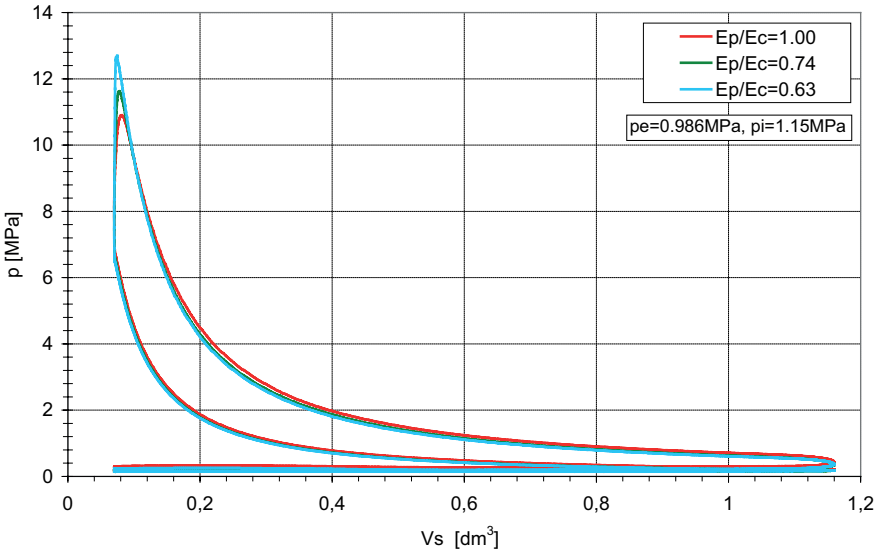

Fig. 4. Indicator diagrams of the double-fuel engine for varying magnitudes of the liquid fuel batch energy fraction (E_p) of the total energy amount contained in the liquid and gaseous fuels (E_c) (the averaged run for 495 cycles, pe=0.986 MPa)

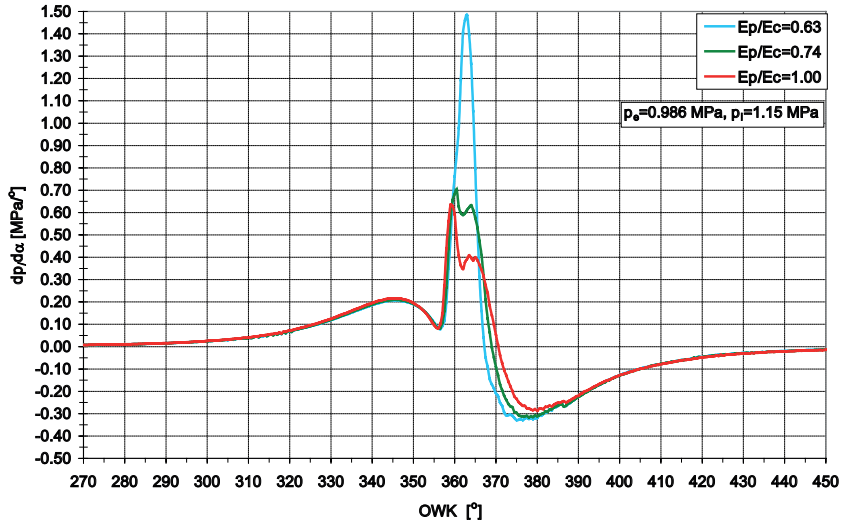

Fig. 5. Pressure derivative, dp/dα for varying magnitudes of the liquid fuel batch energy fraction (E_p) of the total energy amount contained in the liquid and gaseous fuels (E_c) (the averaged run for 495 cycles, p_e=0.986 MPa)

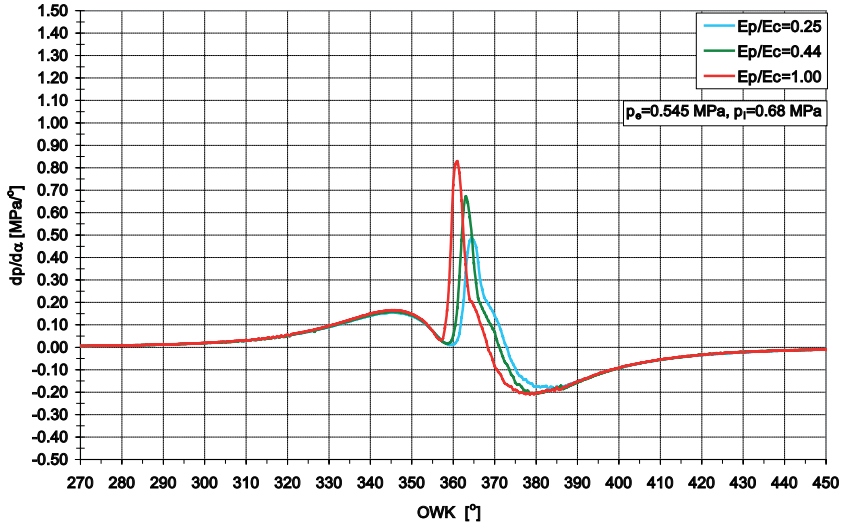

Fig. 6. Pressure derivative, dp/dα for varying magnitudes of the liquid fuel batch energy fraction (E_p) of the total energy amount contained in the liquid and gaseous fuels (E_c) (the averaged run for 495 cycles, p_e=0.545 MPa)

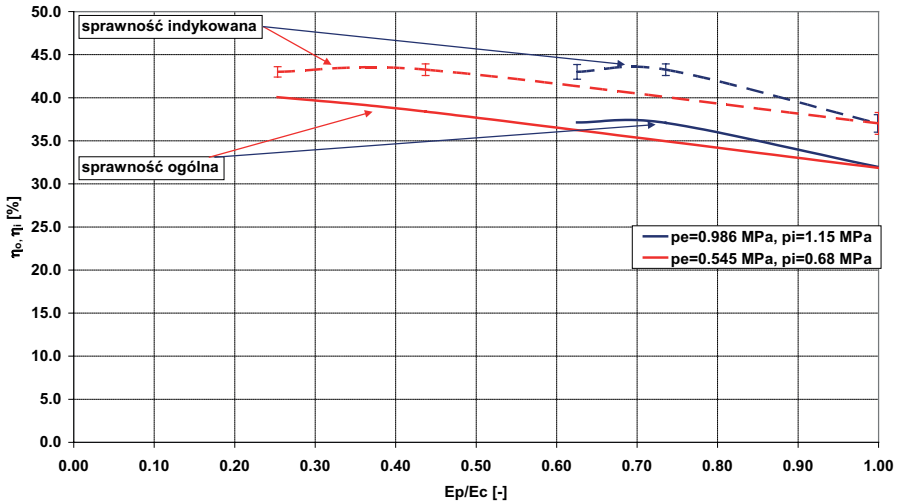

Fig. 7. Overall generating set efficiency related to the active electric power and the indicated engine efficiency as dependent on the liquid fuel batch energy fraction (E_p) of the total energy amount contained in the liquid and gaseous fuels (E_c)

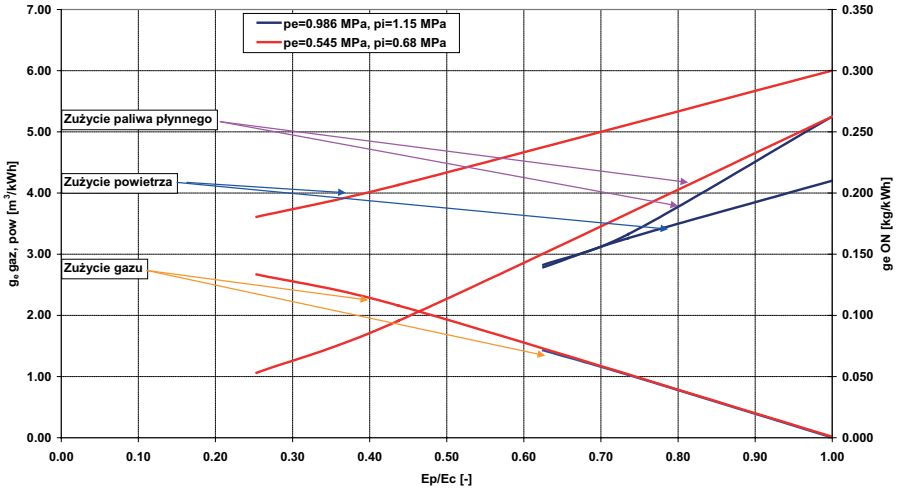

Fig. 8. Unit consumption of the gaseous and liquid fuels and air as dependent on the liquid fuel batch energy fraction (E_p) of the total energy amount contained in the liquid and gaseous fuels (E_c)

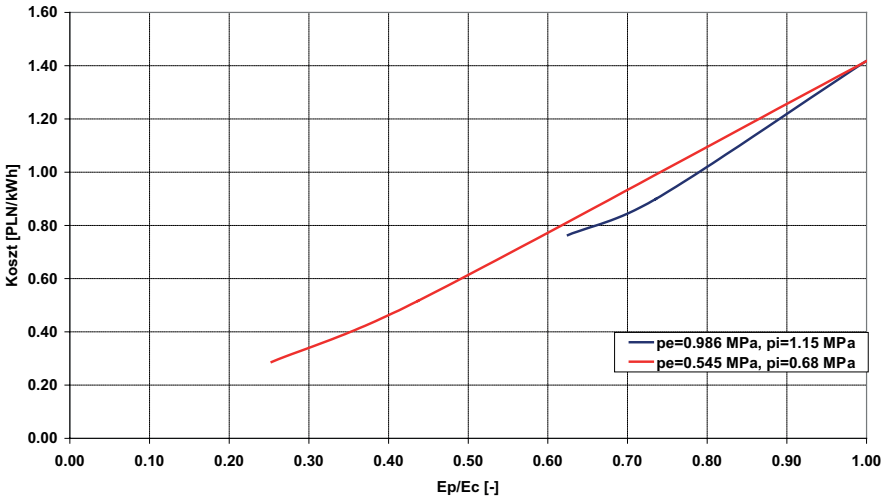

Fig. 9. Unit cost of liquid fuel as calculated for the diesel oil price of 4.5 PLN/litre related to the active electric power, as dependent on the liquid fuel batch energy fraction (E_p) of the total energy amount contained in the liquid and gaseous fuels (E_c)

EVALUATION OF OPERATION REPEATABILITY OF THE DOUBLE-FUEL INTERNAL COMBUSTION ENGINE

In order to evaluate the effect of fuel composition on the repeatability of operation of individual engine cylinders, statistical probability density distributions were made for the maximum pressure, maximum pressure derivative and indicated work for engine cylinder no. 1 based on the analysis of 495 successive operation cycles [3, 4, 16, 18]. **Figures 10 through 14 represent the statistical distributions** of selected physical quantities for the engine fed with the liquid and gaseous fuels at varying engine loads (p_e=0.545 MPa and p_e=0.986 MPa).

For a partial engine load, increasing the gas fraction of the fuel causes a reduction in the maximum values of pressures, whereas at the nominal load, increasing the amount of gas in the fuel increases the magnitudes of maximum pressures.

Figures 11 and 12 represent the statistical distribution of the maximum pressure derivative for different fuel compositions in the first engine cylinder for p_e=0.545 MPa and p_e=0.986 MPa. Similarly as for maximum pressures, for the partial engine load, too, increasing the gas fraction of the fuel results in a reduction in the maximum values of the pressure derivative. At the nominal load, on the other hand, decreasing the diesel oil amount in the fuel to a value of E_p/E_c=0.625 increases the maximum pressure derivative values, while increasing their scatter around the mean value, at the same time.

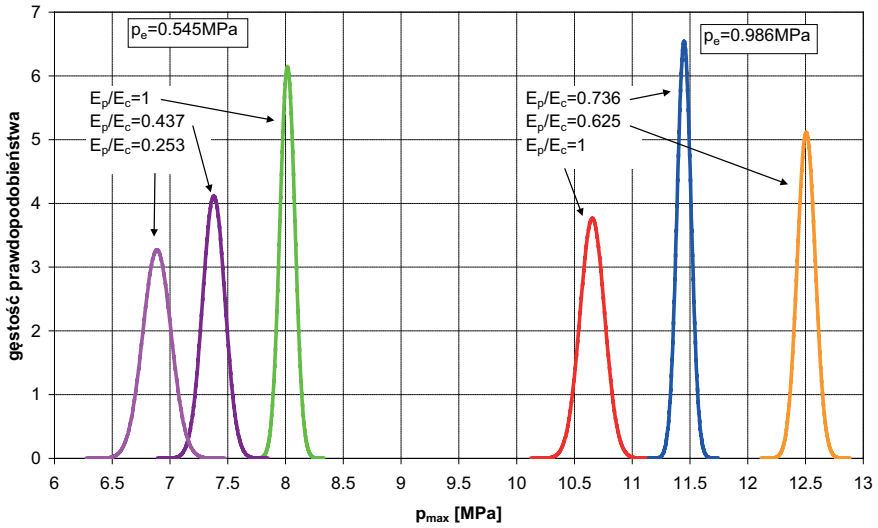

Fig. 10. Maximum pressure probability density at a load of p_e=0.545MPa and p_e=0.986 MPa in the first cylinder for varying liquid fuel energy fractions

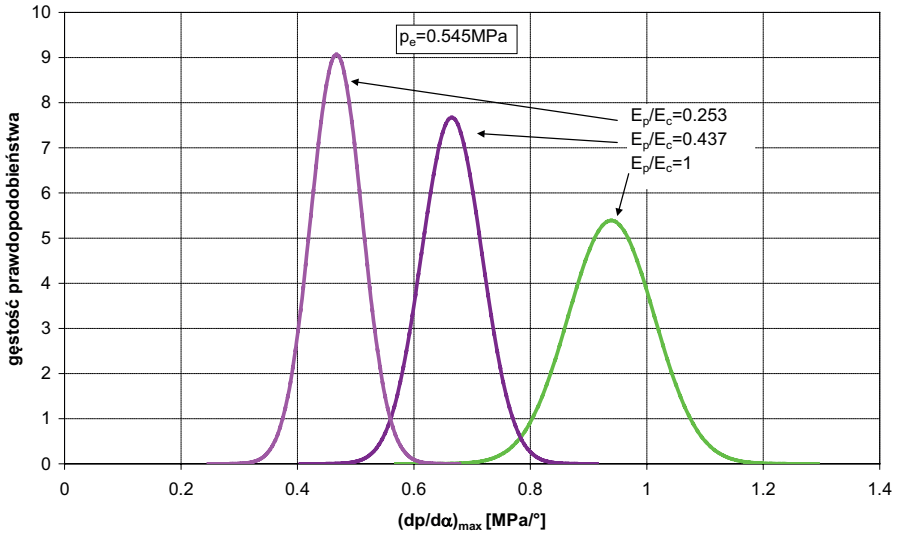

Fig. 11. Maximum pressure increment probability density at a load of p_e=0.545 MPa in the first cylinder for varying liquid fuel energy fractions

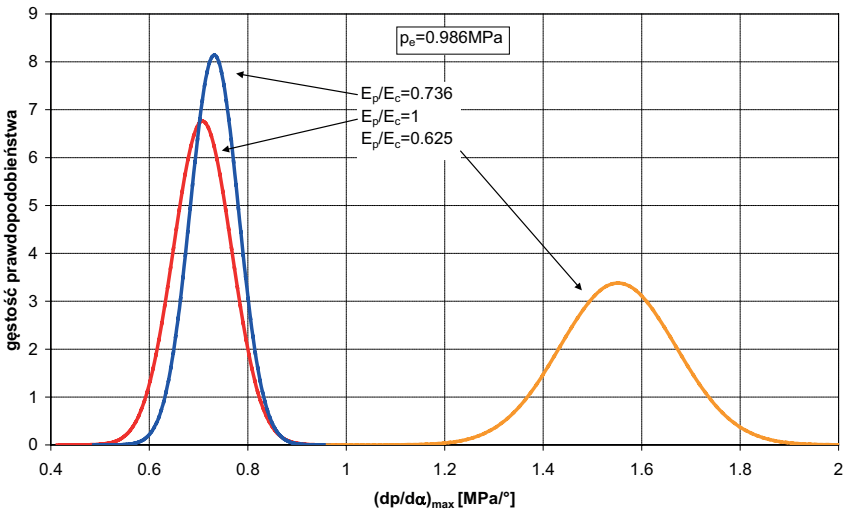

Fig. 12. Maximum pressure increment probability density at a load of p_e=0.986 MPa in the first cylinder for varying liquid fuel energy fractions

Figures 13 and 14 represent the statistical distributions of indicated work for different fuel compositions in the first engine cylinder for p_e=0.545 MPa and p_e=0.986 MPa. **For a partial engine load**, increasing the gas fraction of the fuel causes a small increase in indicated work, while simultaneously reducing its scatter around the mean value. At the minimal load, on the other hand, increasing the gas fraction of the fuel practically does not charge the value of indicated work, but markedly reduces its scatter around the mean value.

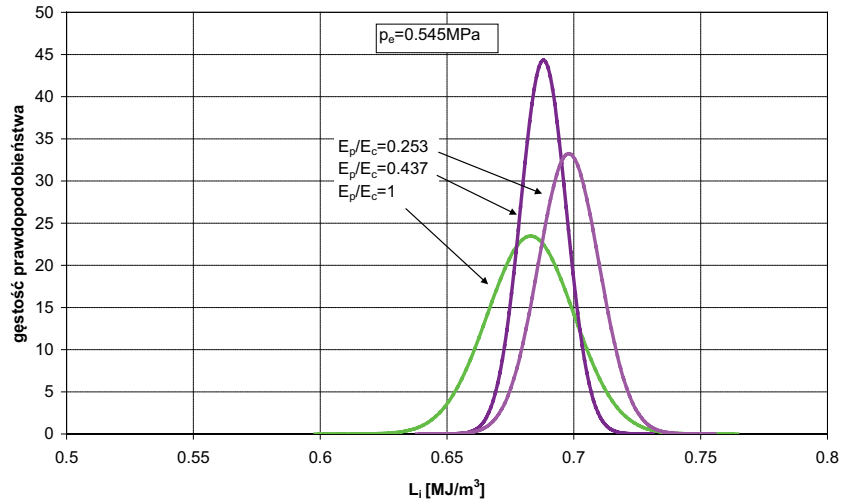

Fig. 13. Indicated work probability density at a load of p_e=0.545 MPa in the first cylinder for varying liquid fuel energy fractions

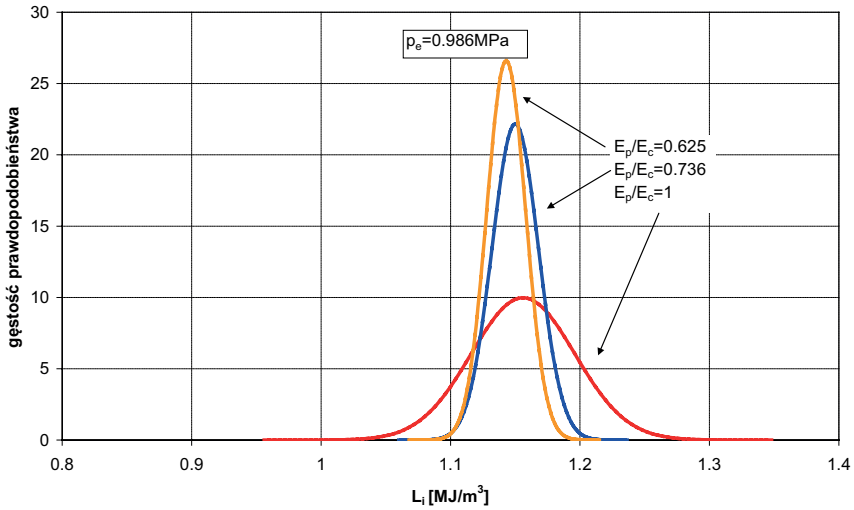

Fig. 14. Indicated work probability density at a load of p_e=0.986 MPa in the first cylinder for varying liquid fuel energy fractions

In addition, evaluation was made of the effect of the gaseous fuel energy fraction on the values of so called cycle parameters unrepeatability indicators [9] (i.e. the indicated work, X_{pi}; maximum combustion pressure, X_{pmax}; and the crank angle, for which combustion pressure attains a maximum value, X_a). Figure 15 shows the values of respective unrepeatability indicators:

- indicated pressure:

$$X_{pi} = \frac{\sigma_{pi}}{\overline{p}_i}, \tag{1}$$

- maximum combustion pressure angle:

$$X_{p\alpha} = \frac{\sigma_{p\alpha}}{\overline{\alpha}_{p\,max}}, \tag{2}$$

- maximum combustion pressure:

$$X_{p\,max} = \frac{\sigma_{p\,max}}{\overline{p}_{max}}, \tag{3}$$

where:
n – number of successive cycles,
p_{max} – mean value of the maximum combustion pressure,
$\overline{p}_i$ – mean value of indicated pressure,
$\overline{\alpha}_{p\,max}$ – mean value of the maximum combustion pressure angle.

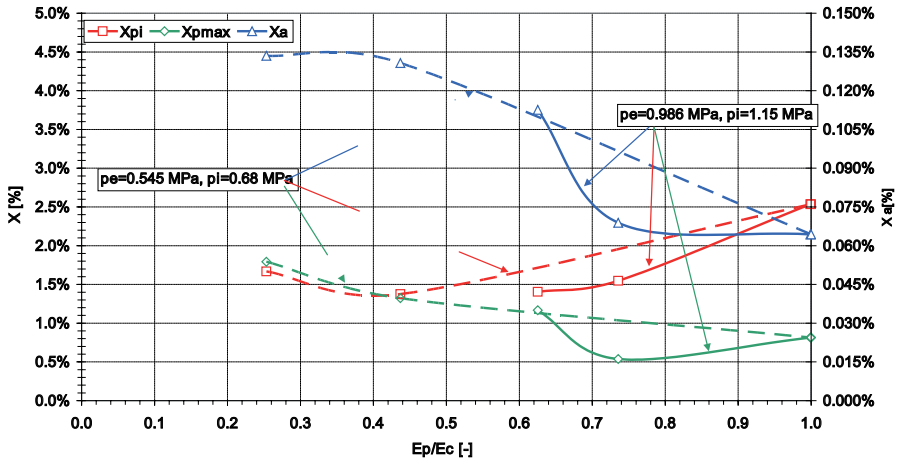

Fig. 15. Cycle unrepeatability indicators at a load of p_e=0.545 MPa and p_e=0.986 MPa in the first cylinder for varying liquid fuel energy fractions

In the graphs of cylinder pressure time variations for the engine operating under full load with a large gaseous fuel fraction, pressure pulsations of a frequency in the range of (5.5-12) kHz was observed to occur in the combustion phase. In order to determine the intensity of those pulsations recorded as a function of time at a frequency of 50 kHz, they were subjected to high-pass filtration by a filter with a limiting frequency of 4 kHz.

Figures 16 and 17 represent pressure pulsation variations obtained from this filtration, against the background of the cylinder pressure variation for p_e=0.545 MPa. It is visible that pressure pulsations in the combustion phase occur for all the fuel compositions, while attaining the greatest intensity for a fuel composed of diesel oil alone, in which case their maximum amplitude value approaches 120 kPa. Increasing the gas fraction of the fuel (decreasing the E_p/E_c ratio) causes a clear reduction in pressure oscillation intensity to a level of 10 kPa with bringing the liquid fuel energy ratio down to a value of E_p/E_c=0.253.

The maximum amplitude of the variable pressure component occurs at the beginning of the combustion process, which indicates that these pulsations are caused by the rapid combustion of the gaseous fuel-air mixture without any indication of autoignition, which would have generated considerable pulsations in the end phase of the combustion process [10, 11].

Figures 18 and 19 represent pressure pulsation variations obtained as a result of high-pass filtration, against the background of the cylinder pressure variation for p_e=0.986 MPa. It is visible that pressure pulsations in the combustion phase occur also for all the fuel compositions. Under the maximum engine load, however, their level changes with changing fluid fuel energy fraction in a different manner. For the sole diesel oil, their level is comparable with the pressure pulsations observed for p_e=0.545 MPa and does not exceed 100 kPa. Increasing the gas fraction of fuel to a level of E_p/E_c=0.736 (reducing the E_p/E_c ratio) reduces them slightly (by approx. 10%); however, further increasing the gas fraction of fuel (up to a level of E_p/E_c=0.625) results in a distinct increase in the pressure pulsation amplitude up to 200 kPa.

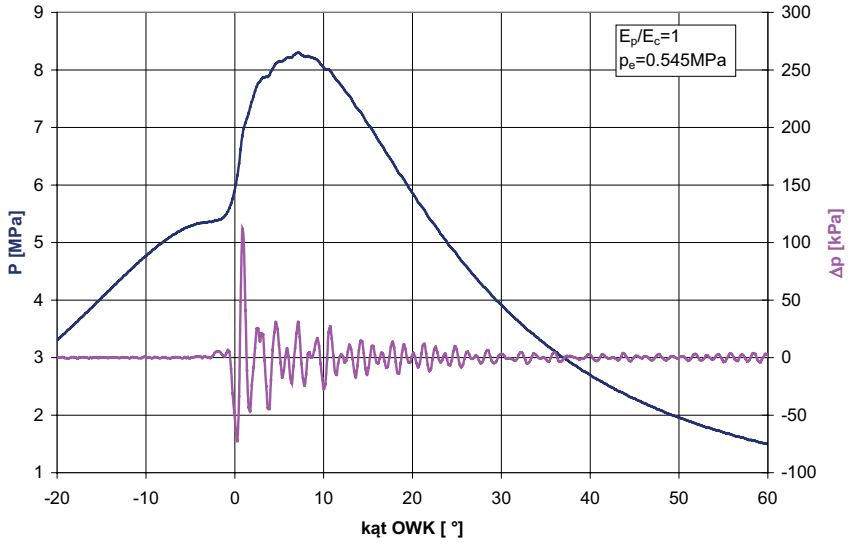

Fig. 16. The variable pressure component of one of the highest intensities with the cylinder pressure variation superposed against the background, for a liquid fuel energy fraction of E_p/E_c=1, p_e=0.545 MPa

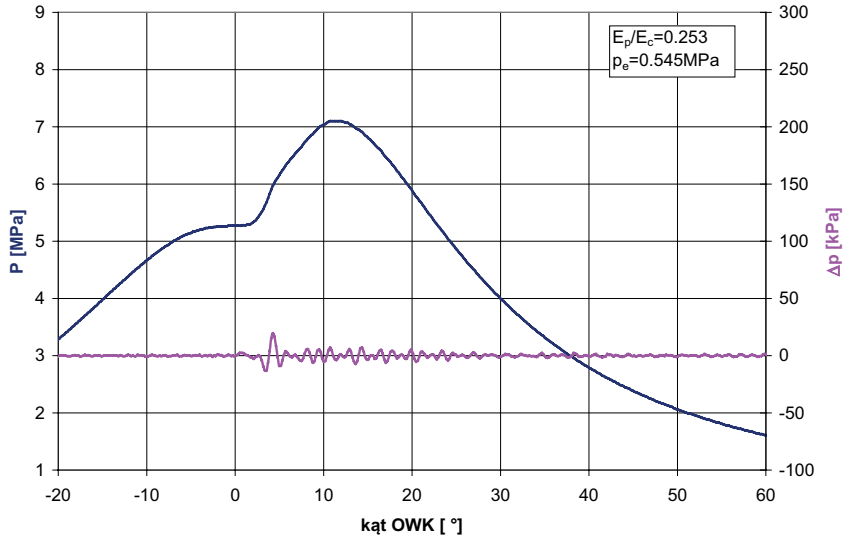

Fig. 17. The variable pressure component of one of the highest intensities with the cylinder pressure variation superposed against the background, for a liquid fuel energy fraction of E_p/E_c=0.253, p_e=0.545 MPa

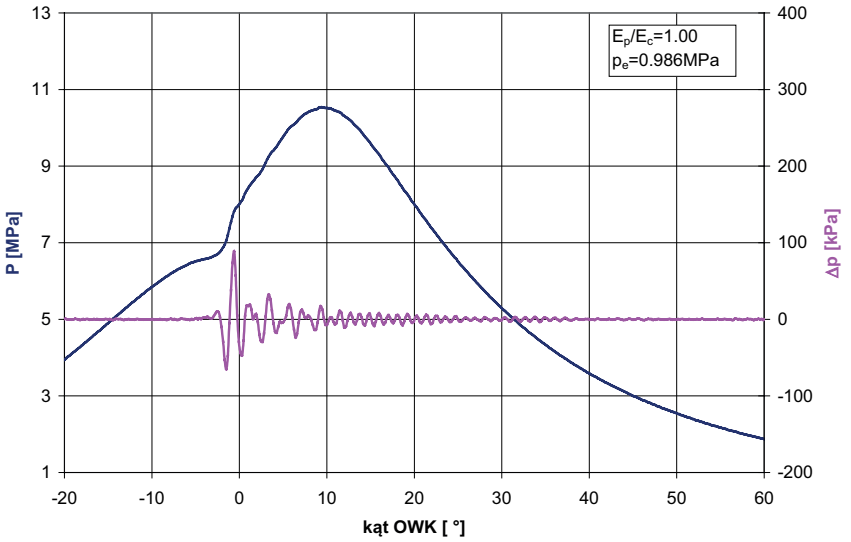

Fig. 18. The variable pressure component of one of the highest intensities with the cylinder pressure variation superposed against the background, for a liquid fuel energy fraction of E_p/E_c=1, p_e=0.986 MPa

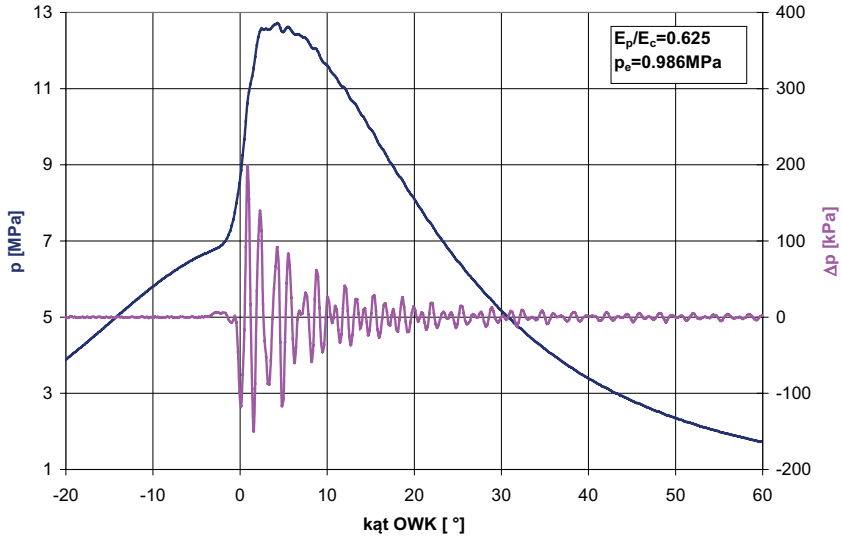

Fig. 19. The variable pressure component of one of the highest intensities with the cylinder pressure variation superposed against the background, for a liquid fuel energy fraction of E_p/E_c=0.625, p_e=0.986 MPa

The obtained results show that when the engine runs with a full power of 80 kW, the mechanical loads on the crankshaft assembly of the double-fuel fed engine increase unfavourably

compared to the respective loads occurring when the engine operates fed with the sole liquid fuel, while attaining the same power.

SUMMARY AND CONCLUSIONS

The largest combustion pressure pulsation amplitude in the case of a small and medium engine loads (up to p_e=0.545 MPa) occurred for the engine being fed with sole diesel oil (the maximum pulsation amplitudes in individual combustion cycles approached a level of about 120 kPa). During co-combustion of diesel oil with gaseous fuel, a drop in the maximum pulsation amplitude down to about 10 kPa was observed. At the same time, an elongation of the combustion process was observed, which caused a more gentle increase in combustion pressure and a delay of the moment of the maximum pressure occurring. The generator gas being fed as the additional fuel was characterized by large contents of incombustible components – with the nitrogen content being at a level of approx. (55-65) %.

Hence, it can be supposed that the generator gas acted on the combustible charge existing in the cylinder as a "diluter". The air oxygen and the combustible mixture formed from evaporated diesel oil were primarily diluted. In this case, the effect of the generator gas could be compared to that of combustion gas recirculation. The first combustion phase, which is the kinetic burning of a combustible mixture with the oxygen ratio reduced due to that combustible mixture being diluted by other gases, slows down, as can be seen in the pressure increment graph. Pressure pulsations are a result of a rapid, unstable combustion process. The largest pressure pulsations occur immediately after the combustible mixture ignition and fall into the kinetic combustion phase which, in a compression-ignition engine, proceeds fastest. Hence, as a result of the combustion process slowing down in this phase, the pressure pulsations have definitely decreased. With increasing generator gas energy fraction, the oxygen content of the generator gas-air mixture decreased to about 15% (for λ=1.4) and was significantly lower than that of the air. The hydrogen concentration in the pure generator gas was normally at a level of about (4-6)%, while in the generator gas-air mixture it was much lower. Presumably, the effect of hydrogen and carbon monoxide on the combustion process comes down to accelerating the ignition initiating reactions, and thus to the growth of H and OH radicals caused by the presence of free hydrogen.

In the case of the engine operating under a maximum possible load (p_e=0.986MPa), an increase in the maximum pressure pulsation amplitude from 100 to 200 kPa was found as the generator gas energy ratio increased. Similarly as before, the occurrence of the maximum combustion pressure pulsations was immediately after the ignition in the first, kinetic combustion phase. Increasing the amount of gas added to the air being sucked causes the acceleration of the kinetic combustion process, which results, among other things, in an increase in pressure pulsations. The faster combustion process might also have been in that case due to generator gas burning initiated by the autoignition of the diesel oil. As a result of increasing the gas ratio of the unchanged amount of the gas-air combustible mixture being forced to the cylinder, the mixture composition had changed from a lean mixture for an engine fed with the sole liquid fuel to a near-stoichiometric mixture for a double-fuel fed engine, which caused the concentrations of the combustible gases, hydrogen and carbon monoxide, to have exceeded the lower flammability limit resulting in rapid burning of these gases and the occurrence of intensive pressure pulsations. In the case at hand – a large load on the engine – intensive fuming of the combustion gas was also observed, caused by incomplete burning of the diesel oil, which could additionally confirm the claim about separate gas and diesel oil combustion. Burning faster, the gas "took away" the oxygen, whose deficiency had a strong effect of causing incomplete burning of the diesel oil and fuming. With the double-fuel

operation of the engine under large load and gas fraction conditions with associated intensive pressure pulsations at a level of 200 kPa, a high-pitch sound characteristic of knock-combustion, as determined by organoleptic methods, could be heard. This sound faded out as the load was reduced and those combustion pressure pulsations were decreased. The position of the maximum pressure pulsations in the initial combustion phase suggest that the emitted sound was caused by combustion proceeding violently in this phase, and not by knock-combustion due to a potential autoignition of the gas in the end combustion phase.

The double-fuel engine version developed within the Project can be recommended to be practically applied in a dried sewage sludge gasification installation as a double-fuel engine to drive en electric generator loaded with active electric power reduced to 40 kW (which accounts for approx. 50% of its rated power), since this is the power level at which the optimum conditions for the operation of an engine double-fuel fed with liquid fuel and generator gas are achieved. Under the round-the-clock operation conditions, a gasification installation operating with this engine will be able to gasify about 1.8 tons of dried sewage sludge containing approx. 10% of water, and to generate 8.960 MWh of electric energy during this time, while consuming approx. 50 kg diesel oil for this purpose. The amount of dried sewage sludge generated by a sewage treatment plant in a town with 250 thousand inhabitants is about 13.5 tons/day, thus being approx. 7.5 times larger than the capacity of the test installation in question. The economic relationships achieved so far could be improved by thorough modernization of the liquid fuel engine supply system to reduce the minimum liquid fuel dose necessary for assuring the correct operation of the piston engine under the conditions of double-fuel feeding with liquid fuel and a generator gas-air mixture in which the oxygen concentration could decrease to a level below 15%. In that case, the gasification of dried sewage sludge might turn out to be a technology more competitive than the incineration of sewage sludge in rotary tunnel kilns used e.g. in cement mills.

The effects achieved so far from this installation prove that the dried sewage sludge gasification installation developed within the Project, when carried out in an appropriately enlarged installation equipped with a double-fuel engine with a reduced liquid fuel energy fraction, allows the combustion of gaseous fuel of chemical composition varying as a function of time.

This scientific research has been financed from the resources allocated to science in the years 2007 to 2010 under Research Project R10 019 02 "The piston combustion engine in the sewage sludge gasification installation".

REFERENCES

Albrecht: Kraftfahrtechnischer Leitfaden. Albrecht Verlag ok.1939.

Azzoni P.M., Minelli G., Moro D., Flora R., Serra G.: Indicated and load torque estimation using crankshaft angular velocity measurement, Society of Automotive Engineers, SAE Technical Report 1999-01-0543, 1999.

Cupiał K. i inni: Sprawozdanie merytoryczne z wykonania zadań objętych projektem rozwojowym R10 019 02 „Tłokowy silnik gazowy w instalacji zgazowania osadu ściekowego". IMTiTS PCz. Częstochowa 2011.

Finney C.E.A., Green J.B., Daw C. S. Jr.: Symbolic Time-Series Analysis of Engine Combustion Measurements. Society of Automotive Engineers 980624, Inc. 1998.

Green J. B. Jr., Daw S. C., Armfield J. S., Finney C. E. A., Wagner R. M., Drallmeier J. A., Kennel M. B., Durbetaki P.: Time irreversibility and comparison of cyclic-variability models. SAE International Congress & Exposition, Detroit, Michigan USA; 1998 March 01-04.

Guldner H.: Entwerfen und Berechnen der Verbrennungsmotoren. Handbuch für Konstrukteure und Erbauer von Gas – und Ölkraftmaschinen. 2 Auflage, Verlag von Julius Springer. Berlin 1905, s. 1-626.

Heywood J.B.: Internal Combustion Engine Fundamentals, McGraw-Hill, ISBN 0-07-028637-X, 1988.

Li Y., Gu F., Harris G., Ball A., Bennett N., Travis K.: The measurement of instantaneous angular speed, Mechanical Systems and Signal Processing 19 (2005) 786–805.

Lotko W.: Niepowtarzalność ciśnień szybkozmiennych w silniku wysokoprężnym. Materiały sympozjum „Rozruch silników spalinowych". Politechnika Szczecińska. Szczecin 1998.

Marcio L. de Souza-Santos.: Solid Fuels Combustion and Gasification. Modeling, Simulation, and Equipment Operation. Marcel Dekker Inc (USA), 2004, s. 1 – 439.

Matekunas F.: Modes and Measures of Cyclic Combustion Variability, SAE Paper 830337, 1983.

Rizzoni G.: Diagnosis of individual cylinder misfires by signature analysis of crankshaft speed fluctuations, Society of Automotive Engineers, SAE Technical Report 890884, 1989.

Reed B., Das A.: Handbook of Biomass Downdraft Gasifier Engine Systems. SERI/SP-271-3022. Solar Energy Research Institute. Golden Co. March 1988, s 1-140.

Steinbrecher N., Walter J.: Marktanalyse 2000 für Holzvergasersysteme bis 5 MW. Öko- Institut (Institut für angewandte Ökologie e.V). Darmstadt 2001 s. 1-77.

Vogel A., Bolhar-Nordenkampf M., Kaltschmitt M., Hofbauer H.: Analyse und Evaluierung der thermochemischen Vergasung von Biomasse. Schriftenreihe Nachwachsende Rohstoffe, Band 29, Münster 2006, s. 1-433.

Volk W.: Statystyka dla inżynierów, WNT Warszawa 1973.

Yang J., Wang L. Pu, Z., Yan Y.Z.X.: Fault detection in a diesel engine by analysing the instantaneous angular speed, Mechanical Systems and Signal Processing 15 (2001) 549–564.

Yorita H., Miwa T., Okabe S.: Development of Ignition Analysis Method in Spark Ignition Engine, Internal Combustion Engine Symposium 20026072, 2002.

Dyrektywa Rady 1999/31/WE z dnia 26 kwietnia 1999 w sprawie składowania odpadów Dz. Urz. WE L 182 z 16.07.1999.

Instrukcja obsługi zespołu prądotwórczego ZAE6CT107-2/2/1 nr 16024 wykonanie specjalne. Andoria – Mot Sp. z o.o. Andrychów.

Krajowy plan gospodarki odpadami 2010. MP nr 90 z 29.12.2006, poz. 946.

Ścieżka gazowa do zasilania silnika spalinowego. Dokumentacja Techniczno-Ruchowa. Ga-Ma GAZ Sp. z o.o. Radlin grudzień 2008.

Ustawa o odpadach. Dz. U nr 62 z 20.06.2001, poz. 629 i Dz. U. nr 7 2003, poz.78.

www.dungs.com

DWUPALIWOWE ZASILANIE SILNIKA ZS GAZEM GENERATOROWYM I PALIWEM PŁYNNYM

Streszczenie. W referacie przedstawiono wyniki zrealizowanego w latach 2007-2010 w Instytucie Maszyn Tłokowych i Techniki Sterowania Politechniki Częstochowskiej projektu badawczego rozwojowego R10 019 02 "Tłokowy silnik spalinowy w instalacji zgazowania osadu ściekowego" sfinansowanego przez Ministerstwo Nauki i Szkolnictwa Wyższego w Warszawie. Omówiono wyniki badań doładowanego silnika tłokowego zasilanego pozyskiwanym gazem generatorowym w instalacji zgazowującej osuszony osad ściekowy.

Słowa kluczowe: silnik tłokowy, gaz generatorowy, osad ściekowy, zgazowanie.

TEKA Kom. Mot. Energ. Roln. – OL PAN, 2011, 11, 65–74

APPLICATION OF OPTIMISATION FOR DETERMINING THE EXTERNAL CHARACTERISTICS OF A TRACTION DIESEL ENGINE WITH SEQUENTIAL TURBOCHARGING

Krzysztof Danilecki

Faculty of Automotive Vehicles Operation,
the West Pomeranian University of Technology in Szczecin

Summary. The way has been shown how to shape the characteristics of a diesel engine with sequential turbocharging through a rational selection of turbochargers and the course of the speed characteristics of the maximum delivery of the injection pump, taking into account the imposed restrictions. The quality coefficients for the selection of the optimised parameters have been proposed according to the dynamic criterion, comprising the shape of the curve of the maximum torque. In order to determine the value of these coefficients, in the next steps of the optimisation procedure the gradientless Hooke-Jeeves method has been used.

Key words: combustion engine, turbocharging, optimisation

INTRODUCTION

The sequential turbocharging is based on the application of two turbochargers, most often of different sizes, working in various ranges of the engine speed and load [Borila 1986 a, b, c, Wisłocki K. 1991]. In recent years, there has been a significant increase in interest in its further development potential. This has been shown by the research and the most modern designs of e.g. BMW, Opel and others [Doll G. *et al.* 2005, Jungmann T. 2005, Kołodziejczyk A. 2008, Łęgowicz J. 2005, Pflüger, F. 1998, Saulnier S. 2004, Steinparzer F. *et al.* 2005]. An important problem in the turbocharged engines is the selection of a supercharging device and ensuring adequate conditions for its cooperation with the combustion engine [Syomin D. *et al.* 2010]. In case of the sequential turbocharging, this problem is magnified due to the necessity to choose two supercharging devices, and – additionally – due to the need to ensure adequate conditions for cooperation between them. The results of the previous research by the author indicate diverse, often contradictory effects of various factors affecting the quality of the selection of turbochargers and, consequently, on the course of the engine characteristics. Thus, considering the issue of a proper match of the characteristics of different size turbochargers, it becomes obvious that the selection of their design parameters should take place with application of optimisation methods. It is therefore essential to select a criterion for optimal proceeding (quality coefficients) that takes into account the expected effects. This in particular applies to the proper shaping of the torque curve in the conditions of the external characteristics

[Kowalczyk M. *et al.* 1990]. Ensuring proper co-operation conditions is essential in the phase of switching of operation modes between the turbochargers, and thus it requires including the control issues in the optimisation task. Full use of the air being at disposal and of the whole design also requires an appropriate adjustment of the fuel delivery while ensuring sustainable and safe operation of the engine. In case of shaping of the external characteristics of the engine with sequential turbocharging, a complete solution to the problem of optimisation therefore consists of solving the following partial tasks:

- selection of completion of turbochargers
- determination of the operational characteristics of the switching system,
- determination of the speed characteristics of the delivery of the injection pump in the position of the maximum delivery for the determined conditions of the engine supply.

The quality coefficient values in particular steps of the selection of the optimised parameters, on which appropriate constraints have been imposed, defining the area of feasible solutions, have been determined during numerical tests.

CHARACTERISTICS OF THE NUMERICAL PROGRAM

The values of the coefficient of quality of selection of turbochargers have been determined by including the simulation program developed by the author into the optimisation procedure that enables numerical determination of the engine operating parameters in conditions of the external characteristics for various completions of turbochargers at a given fuel dose course or the excess air coefficient. The simulation program has been based on mathematical models of particular system components: diesel engine, radial compressor, radial turbine [Danilecki K. 2007, Danilecki K. 2008].

A simplified model of the combustion engine, limited to the calculation of the average cycle parameters has been presented in the form of functions describing the values of selected parameters depending on the engine operating conditions. These dependencies have been determined through the identification of the engine, by the approximating with the polynomial functions of the second-degree the sets of discrete values of these parameters obtained under steady conditions in the engine test bed.

The compressor model has been presented in the form of second-degree polynomials, developed on the basis of characteristics provided by the manufacturer, describing the dependence of isentropic compression efficiency and the compression in the function of the air expenditure and the speed of the turbocharger.

For the calculation of parameters of the turbine one has used a generalised description in the form of polynomial functions of dimensionless characteristics obtained experimentally. Functional dependencies obtained in this way allow for the determination of the flow parameter value and the adiabatic efficiency for the given values of the rotor diameter and the flow cross-section of the turbine inlet box.

OPTIMAL SELECTION CRITERION

Bearing in mind the fact that the principal purpose of the application of the sequential turbocharging is to improve the shape of the torque curve on the external characteristics, the quality of selection of turbochargers in both ranges of the system operation has been assessed on the basis of the coefficient that takes into account, most of all, the dynamic properties of the engine. Assum-

ing that an engine with a constant power will be a standard [Jaskuła A. *et al.* 1998], the dynamic optimisation criterion is defined by the condition to obtain a minimum coefficient of:

$$W_d = W_{d(I)} + W_{d(II)} = \int_n \left[T_{tq(P=const)} - \left(T_{tq(I)} + T_{tq(II)} \right) \right] dn, \quad (1)$$

where:

$T_{tq(P=const)}$ – the engine torque at its defined speed n from the useful range of characteristics (n_{min}–n_N), corresponding to the condition of the constant engine power (P=const),

$T_{tq(I),} T_{tq(II)}$ – torque in the first (I) and the second sequence (II) of operation under conditions of the shaped external characteristics, with the same value of n.

The graphical illustration of the W_d coefficient has been shown in the Figure 1.

The values included in the W_d coefficient are the function of the decision variables of the optimisation process.

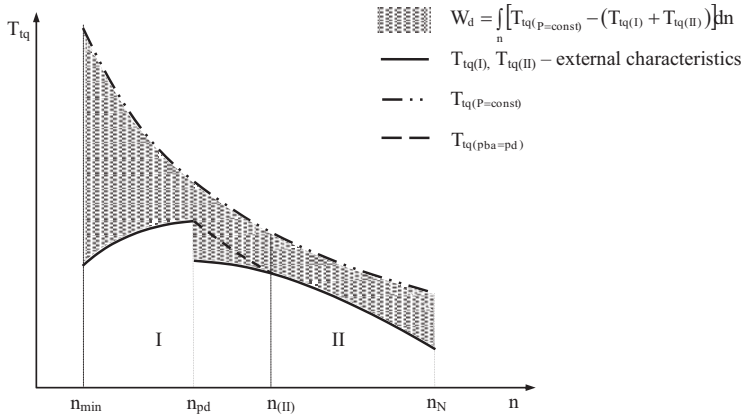

Fig. 1. Diagram illustrating the definition of the quality coefficient W_d

DECISION VARIABLES AND THEIR LIMITATIONS

Formulation of the task as a selection of turbochargers and the operational characteristics of the switching system in the conditions of the external characteristics suggests the adoption of the following decision variables:

x_1 – catalogue number of the rotor of the first sequence compressor,

x_2 – catalogue number of the rotor of the second sequence compressor,

x_3 – inlet cross section of the of the first sequence turbine box $A_{T(I),}$

x_3 – inlet cross section of the of the second sequence turbine box $A_{T(II),}$

x_5 – operating ranges of turbochargers in the conditions of the external characteristics,

x_6 – fuel delivery course.

On the basis of the initial research, the scope of changes in x_1 and x_2 with discrete values available from the particular series of compressor rotors has been limited to two – 309K and 60.

The descriptions of the characteristics of the turbines used in the model allow for determination of the required flow cross-sections that take values within a specified range. The range of variation of x_3, x_4 limits 'from the top' the value of the cross-section of A_T=21 cm^2, which corre-

sponds to the initial construction (in the conventional supercharging). The lower limit results from the conditions of not exceeding the pumping limit by the compressors and the permissible values of compression required due to the supercharging characteristics. These conditions are taken into account as internal limitations of the simulation program. They can therefore be neglected in solving the task of selection of the design of turbochargers.

The variable x_5 has been defined as the value of engine speed, at which the second turbocharger is engaged into the cycle. It can act as a function protecting the turbocharger and engine against overload, for example in case of exceeding the permissible supercharging pressure. Thus it becomes the resulting value, losing at the same time the nature of the decision variable. This is equal to adopting the required characteristics of the operation of the switching system.

The decision variable x_6 is a characteristic of the fuel delivery derived from discrete values, found for the determined speeds n in the conditions of the external characteristics of the engine. For particular values of n, the maximum delivery of fuel has been determined for a defined course of the excess air ratio (as in a conventionally supercharged engine) with taking into account the internal limitations covered by the numerical program, and resulting from not exceeding the permissible values of the exhaust gases temperature and the supercharging pressure. Given the adopted directions of search for the optimum value of the criterion function in the scope of the action of these limitations, the possibility of correcting the delivery of fuel has been allowed. In such conditions of calculations, the fuel delivery also becomes the resulting value, which is synonymous with defining the requirements put for the injection pump, operating at the maximum inclination of the control lever.

OPTIMISATION RESEARCH PROCEDURE

The torque values T_{tq} depending on the variables $\{x_1, x_2, x_3, x_4, x_5, x_6\}$ determining the objective function have been defined by including a simulation program into the optimisation procedure. The T_{tq} values have been calculated separately for each engine speed with a variable step Δn within its useful range. The characteristics obtained in this way have been used to determine the values of the W_d coefficient in the particular steps of the selection of the optimised parameters. Given that the developed simulation program allows for calculation of the parameters of the engine in a discrete and determined way, in order to solve the optimisation task, a gradientless method has been selected to search for optimum values of the decision variables. The minimum quality coefficient values have been determined using the Hooke-Jeeves method [Kusiak J. *et al.* 2009].

In order to facilitate interpretation of the results, three auxiliary coefficients have been used, which should be considered when interpreting the coefficient of optimality W_d. The first of them $W_{(I)}$ expresses the correctness of shaping the engine torque due to its driving characteristics, which requires a possibly large torque supply field within the first operating range (at low and medium engine speeds). This coefficient has been defined as follows:

$$W_{(I)} = \int_{n_{min}}^{n_{II}} \left[T_{tq(P=const)} - T_{tq(I)} \right] dn, \tag{2}$$

where:

n_{min} – the minimum engine speed,

n_{II} – speed for switching the turbochargers.

According to the adopted structure of the $W_{(I)}$ coefficient, compliance with this criterion requires obtaining the minimum of its value.

The second auxiliary coefficient W_N allows for assessing the shaping of the engine torque within the first range of operation in the conditions of the fuel dosing correction, required due to the characteristics of supercharging (for the turbine with specific flow characteristics). It is proposed to define this coefficient by the expression of:

$$W_N = \frac{\pi}{60} \cdot \left[\frac{(n_{min} + n_{pd})}{(n_{pd} - n_{min})} \cdot \int_{n_{min}}^{n_{pd}} T_{tq(I)} dn - \frac{(n_{pd} + n_{II})}{(n_{II} - n_{pd})} \cdot \int_{n_{pd}}^{n_{II}} T_{tq(I)} dn \right], \quad (3)$$

where:

n_{min} – the minimum engine speed,

n_N – rated speed,

n_{pd} – speed, at which the maximum supercharging pressure is reached,

n_{II} – speed for switching the turbochargers.

It is desirable to obtain even distribution of average power values within the range of speeds without correction and with correction of the delivery, which requires reaching the absolute minimum of the value of the W_N coefficient.

The third coefficient W_k determines the relative value of the delivery corrections required to keep the permissible values of the supercharging pressure within the first range. The changes in the positions of points of the engine operation on the compressor characteristics related to that, depending on the flow cross-section of the turbine are reflected in the values of the λ coefficient forming a part of the coefficient, which is defined by the expression:

$$W_k = \int_{n_{pd}}^{n_{II}} (\lambda - \lambda_z) dn \Big/ \int_{n_{min}}^{n_{II}} \lambda_z dn, \quad (4)$$

where:

λ_z – the set value of the excess air ratio at determined engine speed n from the range of characteristics (n_{pd}–n_{II}) – Figure 1,

λ – corrected excess air ratio in the conditions of shaped external characteristics within the range under consideration at the same speed n.

The assessment of the torque curve has also taken into account the range of speeds covered by the correction (n_{pd}–n_{II}) and the position of the point of switching of turbochargers n_{II}/n_N.

RESULTS OF CALCULATIONS

The optimisation calculations have been carried out for discrete values of the turbine inlet box cross-sections from the range of $A_{T(I)}$=16.8–15 cm^2 and $A_{T(II)}$=6.6–5.1 cm^2. Limitation of ranges has resulted both from the method of the optimisation procedure and the need for proper selection of the step of searching the ranges, and due to the area of permissible solutions defined by the characteristics of the engine supercharging. It has been arbitrarily assumed that the supercharging pressure cannot exceed the value of p_{ba}=0.18 MPa.

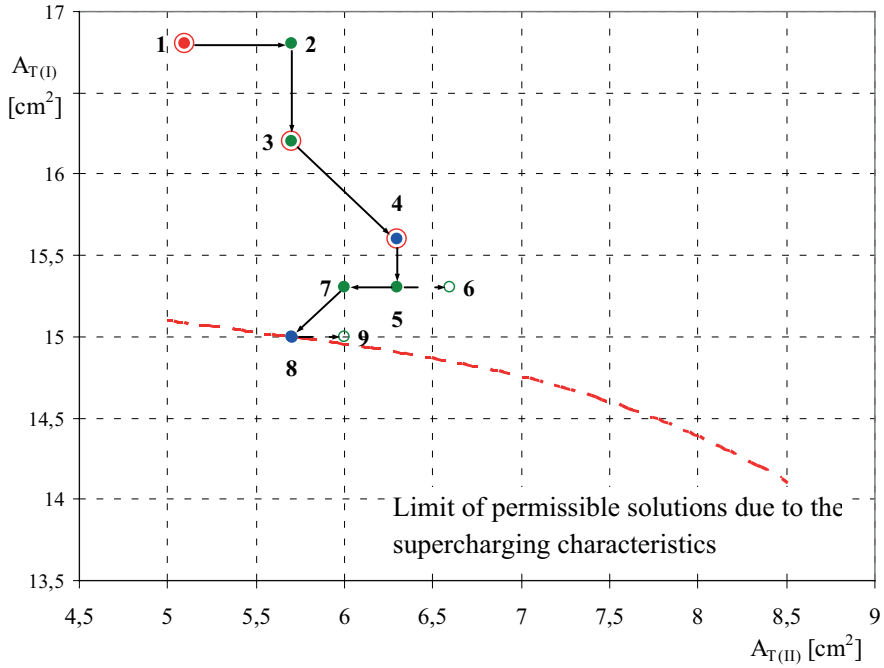

Fig. 2. Search for the minimum of the quality coefficient W_d with Hooke-Jeeves method (subsequent steps of the search have been marked with figures; green points indicate the test steps, and the blue ones – working steps; the red edge marks further basis points, and the dashed line – unsuccessful steps)

In anticipation of the practical use of the optimisation results and their experimental verification, in determining the limits of these ranges and their distinctiveness, one has also included the values of cross-sections of $A_{T(I)}$, $A_{T(II)}$ available for each series of turbochargers.

The effects of the applied optimisation procedure can be seen in the Figure 2, where subsequent steps of search for optimum values of cross-sections of $A_{T(I)}$ and $A_{T(II)}$ have been marked in the area of permissible solutions. For certain compressors, the limit of that area for various associations of the flow cross-sections $A_{T(I)}$ and $A_{T(II)}$ (dashed line) have been determined from the condition of not exceeding the permissible value of the supercharging pressure at the maximum speed of the second range (rated speed). Obtaining of the quality coefficient W_d improvement of less than 1% has been taken as the criterion for the search completion. The results of the W_d coefficient calculation and other coefficients in the next steps of this procedure have been summarised in the Table 1. As it can be seen, the completion of search for the optimum $A_{T(I)}$ and $A_{T(II)}$ cross-sections has taken place in the eighth step of the optimisation procedure due to the characteristics of the engine supercharging for the values of $A_{T(I)}$=15, $A_{T(II)}$=5.7 cm^2. The run of the limiting line does not allow for confirmation of the conjectures about the existence of the global minimum of the W_d coefficient determined in such a way. The decrease in the value of W_d results from the rapid increase in the torque for smaller cross-sections of $A_{T(I)}$ at the first range of operation, as demonstrated by favourable changes in the values of $W_{(I)}$ and $W_{N.}$ However, attention is drawn to the fact of deterioration of the W_k coefficient along with the decrease in the $A_{T(I)}$ cross-section due to the increasing value of the fuel delivery correction at increasing the speed with regards to the set course

of the λ coefficient. This confirms the decrease in the speed range covered by the correction (n_{pd} – n_{II}). This leads to the offset of the switching point for turbochargers towards smaller speed values (reduction of n_{II}/n_N).

Table 1. Values of the quality coefficient and auxiliary coefficients

Step No.	$A_{T(II)}$	$A_{T(I)}$	W_d	$W_{(I)}$	W_N	W_k	$n_{II} - n_{pd}$	n_{II}/n_N
1	5.1	16.8	123.9	90.2	-21.3	0.0435	340	0.759
2	5.7	16.8	123.6	90.2	-21.3	0.0435	340	0.759
3	5.7	16.2	119.0	87.1	-18.6	0.0505	310	0.727
4	6.3	15.6	114.6	70.8	-16.2	0.0589	300	0.705
5	6.3	15.3	111.1	69.2	-15.3	0.0596	280	0.686
6	6.6	15.3	112.7	70.2	-15.1	0.0622	290	0.691
7	6	15.3	110.3	68.3	-15.4	0.0571	270	0.682
8	**5.7**	**15**	**107.4**	**68.6**	**–14,6**	0.0616	**270**	**0.673**
9	6	15	108.3	68.7	-14.5	0.0617	270	0.673

The mentioned changes in the coefficients of quality for selection of turbochargers can be traced in the Figure 3, which compares the course of the external characteristics for the optimum values of $A_{T(I)}$ and $A_{T(II)}$ and for the cross-sections sections of $A_{T(I)}$=16.8, $A_{T(II)}$=5.7 cm^2 available for each series of turbochargers, that within the areas of permissible solutions are the most similar - in the sense of the adopted criterion - to the optimum solution. Approximately 5.5% increase in the torque value of T_{tq} and the offset of its maximum towards lower values of speed in the case of optimum completion of turbochargers (point line) result from this comparison. For the smaller cross-section of $A_{T(I)}$ one has also obtained a clear increase in the torque throughout the second range at lower specific fuel consumption b. At the same time the engine meets the imposed constraints. However, the earlier mentioned increase in the excess air ratio λ required due to the characteristics of the supercharging, leads to a too strong decrease in the torque at the increasing speed of the first range, which does not allow for further reduction of the W_d coefficient. This fact enforces the earlier engaging of the second turbocharger into the cycle.

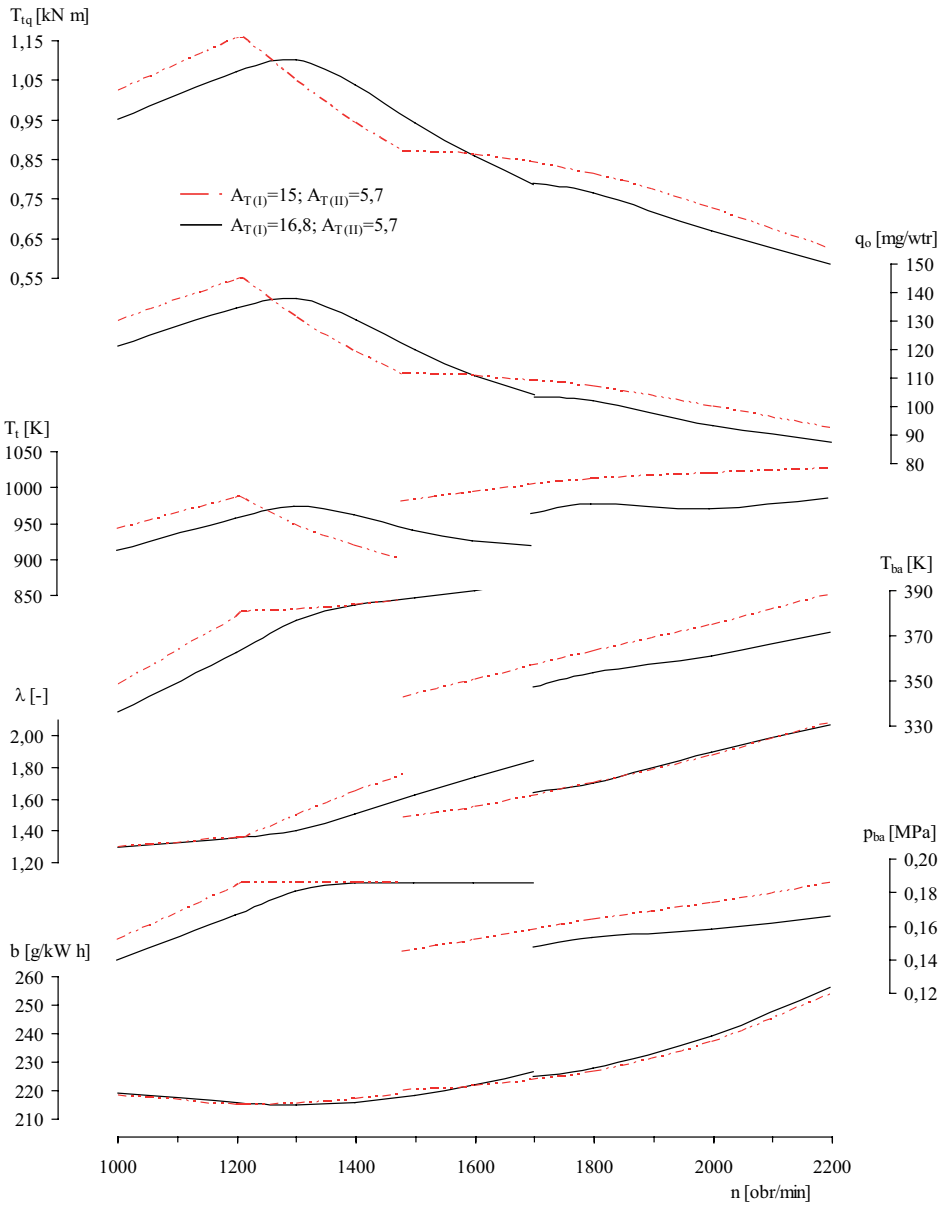

Fig. 3. Results of the optimisation of the selection of the areas of turbine inlet box cross-sections on the curve of the external characteristics of the SW 680 engine: T_{Tq} – torque, λ – excess air ratio, p_{ba} – supercharging pressure, T_{ba} – supercharging temperature, T_t – temperature of exhaust gases, q_o – delivery of fuel per cycle, b – specific fuel consumption

CONCLUSIONS

The results of the works for the optimisation of selection of parameters of turbochargers for the diesel traction engine with sequential turbocharging presented in this paper have demonstrated the usefulness of the proposed models for the simulation research in this field. On the basis of the obtained results it can be concluded that the method discussed in the article allows - in a satisfying way - for the predicting and shaping of the external characteristics of the engine, according to the imposed requirements. However, this method is laborious and requires a complex numerical program. The functions of speed determined during the execution of the optimisation task that describe the maximum values of the delivery of the injection pump as well as the coordinates of the switching points for turbochargers are essentially the solution to the problem of the optimum control. They can thus be used to develop models and algorithms for the numerical system of engine control.

REFERENCES

Borila Y.G. 1986 a: A sequential turbocharging method for highly-rated truck diesel engines. SAE Pap. 860074.

Borila Y.G. 1986 b: Sequential turbocharging helps highly-rated diesels. Automotive Engineering, Nov. 1986.

Borila Y. G. 1986 c: Same aspects of performance optimization of the sequentially turbocharged highly-rated truck diesel engine with turbochargers of unequal size and a pulse converter. IMechE. Pap. CIOS/1986.

Danilecki K. 2007: Model of turbo-charging system of traction diesel engine. Polish Scientific Society of Combustion Engines. Combustion Engines, nr 3.

Danilecki K. 2008: Simulation assessment of operation rates of an engine with sequential turbocharging. Teka Komisji Motoryzacji i Energetyki Rolnictwa Polskiej Akademii Nauk Oddział w Lublinie. Lublin. Vol. VIII.

Doll G., Fausten H., Noell R., Schommers J., Spengel Ch., Werner P. 2005: Der neue V6-Dieselmotor von Mercedes-Benz. MTZ nr 9.

Jaskuła A., Kowalczyk M., Kozak K., Wisłocki K. 1988: Kształtowanie charakterystyki turbodoładowanego trakcyjnego silnika wysokoprężnego poprzez regulację układu silnik - turbosprężarka. Teka Komisji Naukowo-Problemowej Motoryzacji, Kraków, Zeszyt 1.

Jungmann T. 2005: Ford und PSA bauen Dieselmotoren-Kooperation weiter aus. www.atzonline.de.

Kołodziejczyk A. 2008: Jaguar XF Diesel S - Sekwencyjnie doładowany. www.autogaleria.pl/news/index.php?id=1740.

Kowalczyk M., Kozak W., Wisłocki K., Jaskuła A. 1990: Zastosowanie optymalizacji do wyznaczania charakterystyki zewnętrznej silnika wysokoprężnego., Teka Komisji Naukowo - Problemowej Motoryzacji, Konstrukcja, badania, eksploatacja, technologia pojazdów samochodowych i silników spalinowych. Zeszyt 3. Kraków.

Kusiak J., Danielewska-Tułecka A., Oprocha P. 2009: Optymalizacja. Wydawnictwo Naukowe PWN.

Łęgowicz J. 2005: Doładowanie typu twin-turbo. Auto Moto Serwis, nr 3.

Pflüger, F. 1998: Die zweistufig geregelte Aufladung (R2S) – ein neues Aufladesystem für Nfz-Motoren. Motortechnische Zeitschrift MTZ nr7-8.

Syomin D., Rogovoy A. 2010: Power characteristics of superchargers With vortex work chamber. Teka Komisji Motoryzacji I Energetyki Rolnictwa PAN oddział w Lublinie, Tom XB, Lublin.

Steinparzer F., Kratochwill H., Mattes W., Stütz W. 2005: Der neue BMW Sechszylinder-Dieselmotor mit Stufenaufladung . Motortechnische Zeitschrift MTZ, nr 5.
Wisłocki K. 1991: Systemy doładowania szybkoobrotowych silników spalinowych. WKŁ. Warszawa.

ZASTOSOWANIE OPTYMALIZACJI DO WYZNACZANIA CHARAKTERYSTYKI ZEWNĘTRZNEJ TRAKCYJNEGO SILNIKA WYSOKOPRĘŻNEGO Z DOŁADOWANIEM ZAKRESOWYM

Streszczenie. Przedstawiono sposób kształtowania charakterystyki wysokoprężnego silnika z doładowaniem zakresowym przez racjonalny dobór turbosprężarek oraz przebiegu prędkościowej charakterystyki maksymalnego dawkowania pompy wtryskowej przy uwzględnieniu nałożonych ograniczeń. Zaproponowano wskaźniki jakości doboru wartości optymalizowanych parametrów według kryterium dynamicznego ujmującego ukształtowanie krzywej maksymalnego momentu obrotowego. Do wyznaczenia wartości tych wskaźników w kolejnych krokach procedury optymalizacyjnej wykorzystano bezgradientową metodę Hooke'a–Jeevesa.

Słowa kluczowe: silnik spalinowy, turbodoładowanie, optymalizacja

TEKA Kom. Mot. Energ. Roln. – OL PAN, 2011, 11, 75–82

SIMULATION PREDICTION OF OPERATIONAL PARAMETERS OF A TRACTION DIESEL ENGINE WITH SEQUENTIAL TURBOCHARGING AT SELECTION OF TURBOCHARGERS

Krzysztof Danilecki

Faculty of Automotive Vehicles Operation,
the West Pomeranian University of Technology in Szczecin

Summary. The paper presents analytical and empirical model of the system: diesel engine, radial compressor, radial turbine and a numerical program enabling prediction of the engine operating parameters at the selection of turbochargers, adapted to the case of the sequential turbocharging. The essence of the presented model is the appropriate combination of balance equations enabling calculations of thermodynamic parameters in the control points of the system for both the single-stage supercharging, as well as in the case of the parallel combination of two different turbochargers. The numerical program enables selection of turbochargers and determination of functional requirements and the values of control signals for the supercharging adjustment system.

Key words: combustion engine, turbocharging, mathematical modelling

INTRODUCTION

A parallel combination of two turbochargers, engaged successively with increasing the exhaust gas flow intensity (with the increase in the engine speed and the engine load) is most often the essence of sequential turbocharging [Wisłocki 1991]. In case of this method of supercharging, one of the most important problems is the discontinuity of the supercharging characteristics resulting from the jumping engagement of the second turbocharger into the cycle, which leads to an unfavourable course of the maximum torque curve [Borila 1986 a, b, c]. This draws attention to the special importance of a proper match of the characteristics of the turbochargers to the engine, and – additionally – to ensuring adequate conditions for cooperation between them [Danilecki K. 2008, Syomin D. *et al.* 2010:]. The selection of a proper supercharging system design is based on multiple determinations of rates of the engine operation for each successively analysed completion of turbochargers in order to find a solution to meet the assumptions. The solution of such task with an experimental method forces to carry out costly and time consuming engine bench testing, and is limited to available designs of turbochargers. Significant savings of time and financial resources can be obtained by solving this task through computer simulation tests, based on mathematical models of individual system components: diesel engine, radial compressor, and radial turbine. By adopting exactly this way of proceeding, one has assumed the possibility of simulation of operation

of the engine with sequential turbocharging over the whole area of its general characteristics, and the ability to influence on the course of the external characteristics by changing the delivery of fuel or the excess air ratio. For this purpose, a numerical program has been developed that allows for quick prediction of the engine performance at the selection of turbochargers and their switching characteristics.

ASSUMPTIONS TAKEN AT CONSTRUCTING THE MODEL

The essence of the presented model is to combine (conjugate) dependencies known from the literature [Zinner K. 1985] describing the conditions of cooperation of the engine and turbocharger, forming a system of equations enabling the balance calculation of thermodynamic parameters in the control nodes of the system. The calculations have been limited to the situation of the energy balance corresponding to the steady conditions of operation. The diagram of the sequential turbocharging system, where relevant denotation of pressures and temperatures characterising the operational conditions of turbochargers have been plotted is shown in the Figure 1.

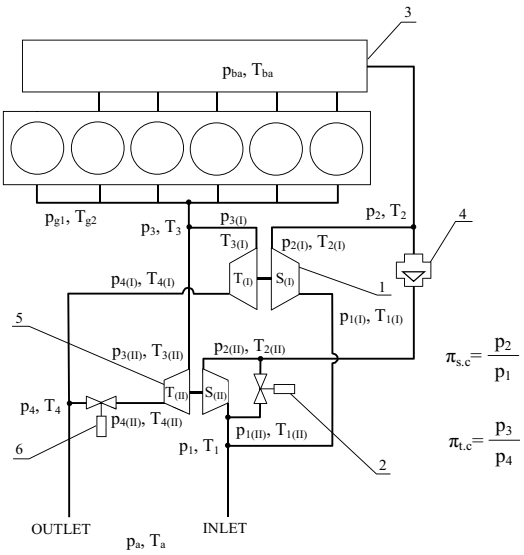

Fig. 1. Diagram for the analysis of the sequential turbocharging system performance: 1 – turbocharger of the first range, 2 – air release valve, 3 – air surge tank, 4 – valve engaging the compressor, 5 – turbocharger of the second range, 6 – valve engaging the turbine

For the case of the sequential turbocharging at parallel combination of turbochargers, the calculations are carried out for specified conditions of the air and exhaust gase flow through turbochargers, which can be taken as: $p_{1(I)} = p_{1(\mathbf{I})} = p_1$, $T_{1(I)} = T_{1(\mathbf{I})} = T_1$, $p_{2(I)} = p_{2(\mathbf{I})} = p_2$, $p_{3(I)} = p_{3(\mathbf{I})} = p_3$, $T_{3(I)} = T_{3(\mathbf{I})} = T_3$, $p_{4(I)} = p_{4(\mathbf{I})} = p_4$. By solving the balance equations for turbochargers with specified flow cross-sections of turbines, one can determine the required breakdown of the excess air W_p and the exhaust gases W_t, and the values of the characteristics of each turbocharger, for which the condition of the power balance and mass at their cooperation with the engine is met. A detailed description of the assumptions of the method of analysis of this type, determining the conditions of supply of turbochargers with different flow characteristics has been presented in the paper of the author [Danilecki K. 2009].

DESCRIPTION OF THE MODEL DEPENDENCIES

For the simulation of the engine, one has developed an analytical and empirical model of a diesel engine limited to the calculation of the average parameters of the cycle [Ćwik B. *et al.* 1993, [Danilecki K. 2007, Sobociński R. *et al.* 1986, Yusupov Ramazan Ch. *et al.* 2003]. Such a simplification of the model has been a compromise between the required accuracy of calculations and the amount of work required for its development, while ensuring the proper interpretation of the results of the model tests. Carrying out the simulation calculations in accordance with the intended purpose of the numerical program required the inclusion of specified dependencies and auxiliary factors in the numerical model, describing the engine parameters.

The actual engine cylinder volumetric efficiency η_v being the basis for the calculation of the mass air flow intensity through the engine and the compressor has been presented in the form of empirical dependence on the engine speed n, the supercharging pressure $p_{ba,}$ the supercharging temperature T_{ba} and the average exhaust gases pressure $p_{g1:}$

$$\eta_v = F_2\left(n, p_{ba}, T_{ba}, p_{g1}\right) \tag{1}$$

The engine thermal efficiency $\eta_{c,}$ necessary to determine the indicated mean effective pressure is calculated depending on the speed n, the excess air ratio λ, the supercharging pressure p_{ba} and the supercharging temperature T_{ba}:

$$\eta_c = F_1\left(n, \lambda, p_{ba}, T_{ba}\right) \tag{2}$$

The average friction pressure has been expressed by linear dependence on the engine speed. Increase in the frictional resistance depending on the supercharging pressure has been determined by means of the empirical dependence given in the paper [Cichy M. *et al.* 1989]. In determining the mechanical losses one has also included the influence of the supercharging parameters on the conditions of the charge exchange. The average pressure of the charge exchange determined from the empirical dependence given in the paper [Симсон А. Э. *et al.* 1976] has been taken as the measure of the charge exchange losses.

The exhaust gas temperature T_t has been calculated depending on the speed n, the excess air ratio λ, the supercharging pressure p_{ba} and the supercharging temperature T_{ba}.

$$T_t = F_3\left(n, \lambda, p_{ba}, T_{ba}\right) \tag{3}$$

The dependencies of (1–3) have been determined by identifying the SW-680 engine using the "black box" method through the approximation with polynomials of discrete sets of values of $\eta_{c,}$ $\eta_{v,\,T\,t}$ obtained on the engine test bench in steady conditions of the engine operation. These values have been determined for 49 points of operation from the area of the general characteristics with keeping the principles of a planned experiment. The approximation of the empirical data has been made using polynomials of four variables of the second degree.

The compressor model has been presented in the form of polynomials developed on the basis of characteristics of the compressor as specified by the manufacturer [Ćwik B. *et al.* 1993, Kowalczyk M. *et al.* 1990, Moraal P. *et al.* 1999, Wirkowski P. 2005] describing the dependence of isentropic compression efficiency η_s and the compression ratio π_s on the reduced values of the air expenditure $\dot{m}_s$ and the speed of the turbocharger n_t:

$$\eta_s = f\left(n_t, \dot{m}_s\right) \tag{4}$$

$$\pi_s = f\left(n_t, \dot{m}_s\right) \tag{5}$$

The mathematical model of a turbine [Синявский В.В. 1986] is based on the experimentally obtained dimensionless characteristics developed on the basis of the theory of dynamic flow similarity, which describe the flow parameter values $F_p = \dot{m}_t \cdot \sqrt{T_t} / p_t$, the speed parameter $u_{t.kr} = u_t / \sqrt{T_t}$ and the expansion ratio π_t and the adiabatic efficiency $\eta_{ad.t}$ on the speed parameter u_t / c_{ad} and the $u_{t.kr}$ parameter:

$$\frac{\dot{m}_t \cdot \sqrt{T_t}}{p_t} = f\left(\frac{u_t}{\sqrt{T_t}}, \pi_t\right) \tag{6}$$

$$\eta_{ad.t} = f\left(\frac{u_t}{\sqrt{T_t}}, \frac{u_t}{c_{ad}}\right) \tag{7}$$

Functional dependencies (6), (7) have been presented by means of polynomial functions of the second degree. Identification of the coefficients of polynomials has been carried out using multiple regression method based on the characteristics determined for turbines with the outer diameters of rotors ranging from 0.05 to 0.09 m with different inlet box cross-sections.

Changes in the turbine power and flow capacity at the pulsating exhaust gas flow are taken into account by means of pulsatility indices of k_N and k_f given by Wanszejdt [Wanszejdt *et al.* 1977].

PROGRAM STRUCTURE

The calculations are carried out for a given engine operating point and a selected quantity and completions of turbochargers. The commencement of calculations requires the adoption of:

- the value of the engine speed n,
- the value of the excess air ratio λ or the fuel delivery q_o.

Moreover, it is necessary to adopt the initial values of: supercharging pressure p_{ba}, pressure p_t and temperature T_t of exhaust gases in the turbine inlet cross-section, the speed of turbocharger n_t and the volumetric efficiency η_v.

Bearing in mind the permissible conditions of operation of particular components of the engine and turbocharger set system, adequate protection has been provided for in the program. Such role is fulfilled by the conditions of not exceeding the pumping limit of the compressor and the permissible exhaust gases temperature before the turbine. Also restrictions due to the variation range of input values have been introduced, on the basis of which the identification of parameters of the functions of the engine model has taken place. These restrictions apply in particular to the permissible supercharging pressure values p_{ba} (compression of the compressor) and the excess air ratio λ that cannot exceed the area covered by the experimental conditions.

Due to the need to meet the basic balance dependencies of the turbocharger at its co-operation with the engine, and in case of sequential turbocharging – the balance of the supercharging pressure ($p_{2(I)} = p_{2(II)} = p_2$) and the exhaust gases pressure ($p_{3(I)} = p_{3(II)} = p_3$) of two supercharging devices, simulation has been carried out using an iterative calculation mechanism, until the assumed accuracy of the solution has been obtained.

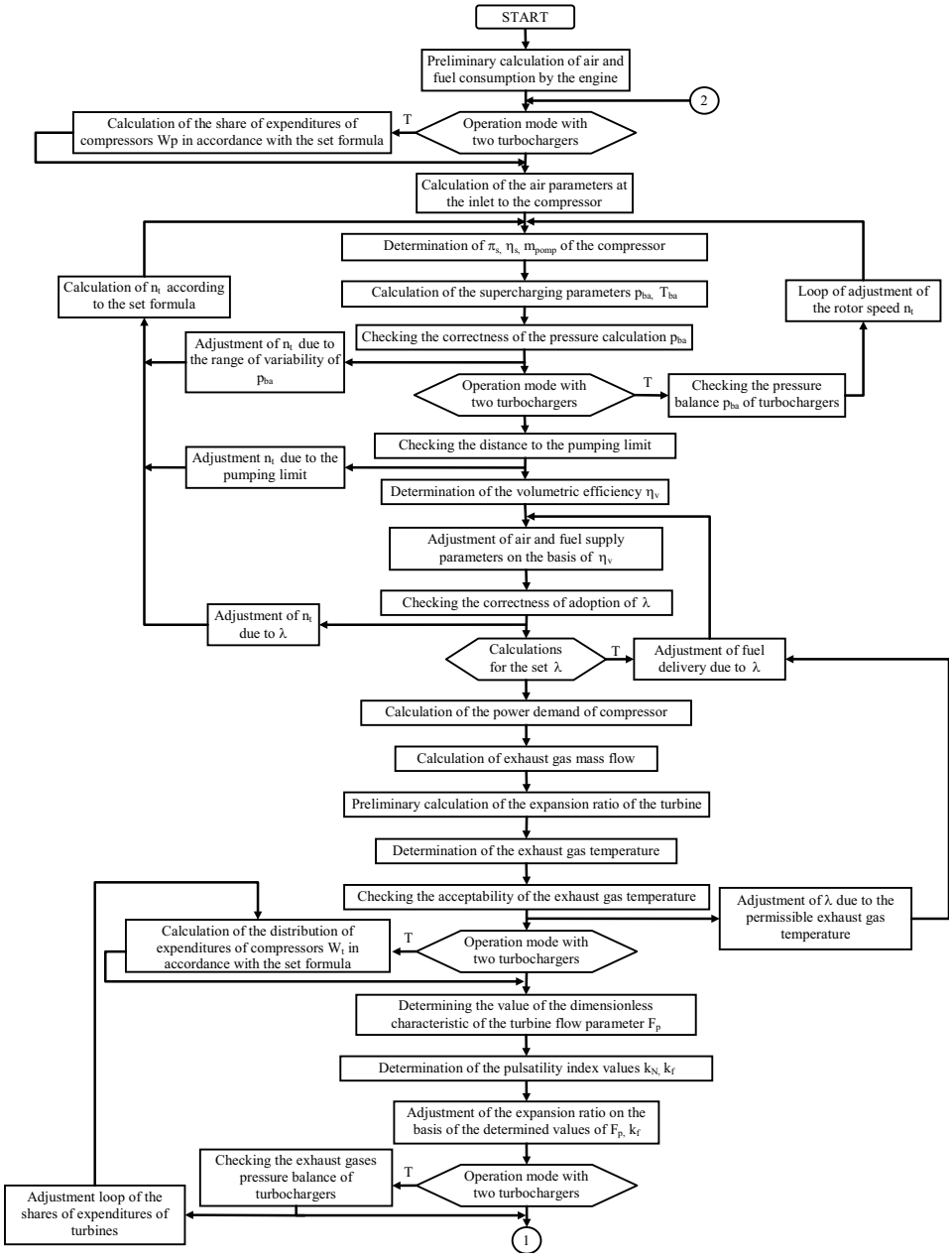

Fig. 2a. Block diagram of algorithm for calculating the characteristics of the engine and supercharging system operation

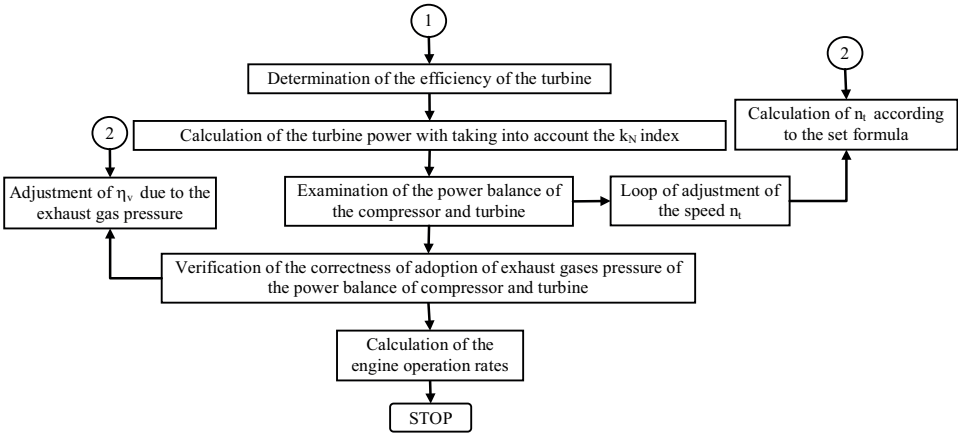

Fig. 2b. Block diagram of algorithm for calculating the characteristics of the engine and supercharging system system operation – continued of Figure 2a

In the inner iteration loop there are adjusted the values of such parameters as: speed of turbocharger n_t, fuel delivery q_o, share of expenditure of the turbine W_t of the first range and the volumetric efficiency η_v. The turbocharger speed n_t is adjusted due to the compressor pumping limit and because of the permissible range of variation of the λ ratio, the supercharging pressure p_{ba} and the pressure of exhaust gases p_{g1} in the exhaust manifold. If the calculated values of the exhaust gas pressure p_{g1}, the supercharging pressure p_{ba} and the λ ratio were at the limit of the permissible range, then regardless of the balance of power and the mass intensity of flow, the turbocharger speed n_t would be adjusted on the basis of the set increase of the turbocharger speed $\pm \Delta n_t$.

In case of simulations performed for a system with two turbochargers, the speed n_t is also adjusted due to the supercharging pressure balance of each supercharging device. The fuel delivery q_o is determined in the loop of excess air ratio adjustment (in the calculations for a set value of λ) and with taking into account the permissible temperature of exhaust gases. In the calculations carried out for a system with two turbochargers, in the loop of adjustment of the share of the expenditure of turbines W_t, the pressure of exhaust gases in the outlet manifold p_{g1} is balanced for each turbine. Due to the pressure of exhaust gases, the filling ratio is adjusted.

In the outer iteration loop, the speed of turbocharger n_t is adjusted depending on the balance of the compressor power N_s and the turbine N_t. With increasing the speed of the turbocharger n_t, the values of compression π_s increase, and consequently, the values of the λ ratio. However, the expansion ratio of π_t decreases, which should lead to a reduction in difference in the power of the turbine N_t and the compressor N_s. In the calculations with two turbochargers on the basis of the determined values of the power of compressor and the turbine, also the expenditure is adjusted for each compressor by changing the share of the expenditure of compressors of the first and the second ranges (W_p). The condition for completion of the calculations is to obtain for each turbocharger the required convergence of values of N_s and N_t.

The block diagram of algorithm for calculating the average values of selected parameters of the engine and the supercharging system is illustrated by the Figure 2.

POSSIBILITIES TO USE THE PROGRAM

The usefulness of the numerical program developed by the author for predicting the characteristics of the engine depending on the completion of turbochargers has been confirmed by comparing the calculated and the experimentally obtained external characteristics of the SW680 engine. It has been found that the deviations between them vary from less than 1 up to 3.5% depending on the observed parameter.

Use of the numerical program boils down to calculating the average values of operating parameters during the entire cycle for the given values of the fuel delivery q_o or the excess air ratio λ and the speed n. This allows for determination of the engine performance in the conditions of:

- external characteristics,
- load characteristics,
- general characteristics.

The numerical program, apart from the selection of turbochargers, also enables determination of functional requirements and the values of control signals for the supercharging adjustment system.

REFERENCES

Borila Y.G. 1986 a: A sequential turbocharging method for highly-rated truck diesel engines. SAE Pap. 860074.

Borila Y.G. 1986 b: Sequential turbocharging helps highly-rated diesels. Automotive Engineering, Nov. 1986.

Borila Y. G. 1986 c: Same aspects of performance optimization of the sequentially turbocharged highly-rated truck diesel engine with turbochargers of unequal size and a pulse converter. IMechE. Pap. CIOS/1986.

Cichy M., Friedrich E. 1989: Możliwość zastosowania mikroprocesorowego systemu pomiaru i rejestracji procesów czasowych (PRPC) na przykładzie pomiaru momentu bezwładności i momentów oporów mechanicznych silnika SW 680. Sympozjum Motorcomput ’89. Metody obliczeniowe w projektowaniu, badaniu i eksploatacji silników spalinowych. Jadwisin, 24-26.04. 1989.

Ćwik B., Szczeciński S. 1993, Koncepcja modelu systemu turbodoładowania silnika spalinowego o zapłonie samoczynnym. Eksploatacja Silników Samochodowych Materiały Seminaryjne, Szczecin.

Danilecki K. 2007: Model of turbo-charging system of traction diesel engine. Polish Scientific Society of Combustion Engines. Combustion Engines, nr 3.

Danilecki K. 2008: Simulation assessment of operation rates of an engine with sequential turbocharging. Teka Komisji Motoryzacji i Energetyki Rolnictwa Polskiej Akademii Nauk Oddział w Lublinie. Lublin. Vol. VIII.

Danilecki K. 2009: Theoretical analysis of co-operation of a turbocharger with a sequentially turbocharged engine. Combustion Engines, nr 1.

Kowalczyk M., Kozak W., Wisłocki K., Jaskuła A. 1990: Zastosowanie optymalizacji do wyznaczania charakterystyki zewnętrznej silnika wysokoprężnego., Teka Komisji Naukowo - Problemowej Motoryzacji, Konstrukcja, badania, eksploatacja, technologia pojazdów samochodowych i silników spalinowych. Zeszyt 3. Kraków.

Moraal P., Kolmanovsky I. 1999: Turbocharger Modeling for Automotive Control Applications. SAE Paper 1999-01-0908.

Синявский В.В. 1986: Обобщенные характеристики малоразмерных компрессоров и турбин. Рабочие процессы автотракторных двигателей и их агрегатов. Сборник научных трудов, МАДИ.

Симсон А. Э, Каминский В. Н., Моргулис Ю.Б. и др. 1976: Турбонаддув высокооборотных дизелей. Машиностроение. Москва.

Sobociński R., Mitka J. 1986: Zastosowanie eksperymentu planowego w opracowaniu modeli symulacji procesów roboczych tłokowego silnika spalinowego. II Konferencja Naukowo-Techniczna N.T. Pojazdy Samochodowe, Problemy Postępu i rozwoju, Autoprogres'86, Sekcja II, Badania i Urządzenia Badawcze, Jadwisin.

Syomin D., Rogovoy A. 2010: Power characteristics of superchargers With vortex work chamber. Teka Komisji Motoryzacji I Energetyki Rolnictwa PAN oddział w Lublinie, Tom XB, Lublin.

Wanszejdt W.A., Iwaczenko N. P., Kollierowa Ł. K. 1977: Dizeli. Sprawocznik. Maszinostrojenije, Moskwa.

Wirkowski P. 2005: Modelowanie charakterystyki sprężarki osiowej o zmiennej geometrii kanału przepływowego. Diagnostyka, nr 35.

Wisłocki K. 1991: Systemy doładowania szybkoobrotowych silników spalinowych. WKŁ. Warszawa.

Yusupov Ramazan Ch., Deev V. Y., Zaynishev A. V., Solomonenko M. V. 2003: Optimisation of parameters of diesel's regulator and loading. Teka Komisji Motoryzacji i Energetyki Rolnictwa Polskiej Akademii Nauk Oddział w Lublinie. Lublin. Vol. III.

Zinner K. 1985: Aufladung von Verbrennungsmotoren. Springer Verlag, Berlin-Heidelberg-New York, III Auflage

SYMULACYJNE PRZEWIDYWANIA PARAMETRÓW PRACY TRAKCYJNEGO SILNIKA WYSOKOPRĘŻNEGO Z DOŁADOWANIEM ZAKRESOWYM PRZY DOBORZE TURBOSPRĘŻAREK

Streszczenie. Przedstawiono analityczno-empiryczny model układu: silnik wysokoprężny, sprężarka promieniowa, turbina promieniowa oraz program numeryczny umożliwiający prognozowanie parametrów pracy silnika przy doborze turbosprężarek, dostosowany do przypadku doładowania zakresowego. Istotą prezentowanego modelu jest odpowiednie połączenie równań bilansowych umożliwiających obliczenia parametrów termodynamicznych w kontrolnych punktach układu zarówno dla doładowania jednostopniowego, jak i w przypadku równoległego połączenia dwóch różnych turbosprężarek. Program numeryczny umożliwia dobór turbosprężarek oraz ustalenie wymagań funkcjonalnych i wartości sygnałów sterujących dla układu regulacji doładowania.

Słowa kluczowe: silnik spalinowy, turbodoładowanie, modelowanie matematyczne

TEKA Kom. Mot. Energ. Roln. – OL PAN, 2011, 11, 83–91

SCIENTIFIC AND PRACTICAL ASPECTS OF PROJECT MANAGEMENT FOR PRODUCTION AND REPROCESSING COMPLEXES

Ihor Flys

Lviv National Agrarian University, Ukraine

Summary. The scientific and practical aspects of project management for production and reprocessing complexes which are created on the basis of new or operating agricultural enterprises have been considered. The introduction of production and reprocessing complex project will provide the additional financial funds for the agricultural enterprise and the increase of technical and technological level of its production.

Key words: project, project management, agricultural enterprise, small reprocessing enterprise, production and reprocessing complex.

INTRODUCTION

One of the new directions providing a high efficiency of modern agricultural production and leading to new technical-technological and social-economic level is the creation of complexity in agricultural enterprises (ACE) activity: from growing the raw material and its storage - to its more complete reprocessing into commodity products. Therefore the theoretical grounding of the expedience and feasibility of the production-reprocessing complexes (PRC) created on the ACE production basis is a current scientific-technical problem.

THE ANALYSIS OF SCIENTIFIC RESEARCHES AND PUBLICATIONS

Main requirements towards the innovative projects in the programs of villages and their territories development, the identification of projects value, including PRC projects, are worked out in the researches [1,2,3].

A number of scientific publications [4,5,6,7,8,9,10,11,13,14,16,21,24] have been devoted to the important problem of choice equipment and the grounding of the production programmes of small reprocessing enterprises (SRE) (their specialization and power) and management of their functional structures.

The scientific-methodological grounds of the development of projects for the complexes of agricultural raw material growing and reprocessing in ACE have been examined in the researches [11,12,15,17,18,19,20,22,23,25].

AIM AND TASK OF THE RESEARCH

The aim of this research is to find out the production and technological grounds and the evaluation of PRC projects' creation. The task of this research is to expose the scientific and practical aspects in the relation to the production and reprocessing complexes management created on the new or operating ACE production basis.

THE RESULTS OF THE RESEARCH AND THEIR ANALYSIS

The agricultural production at the present time is under the influence of both the objective (agri-technical and weather conditions) and subjective (the human factor) character. Therefore, the potential possibilities of ACE in achieving the considerable success in agricultural production are very often dependent on the poorly forecasted and uncontrolled (or not well-guided) factors. This leads to the production inefficiency and financial losses of ACE. As the process of getting the agricultural raw material from preparation to growing up to the sale is long (9-12 months), there is a high probability of substantial money losses of facilities that have invested in the production.

We consider that one of the effective ways of removal of possible risks or their minimizing on one hand, and getting additional profits without any considerable capital investments and current expenses, on the other hand, is the creation of production and reprocessing complexes on the ACE base. The production and reprocessing complex is the agrarian-industrial enterprise which is created for agricultural raw material growing and its reprocessing into the commodity products (Fig. 1).

Agricultural lands, machines, tractors and trucks, stock-raising farms with productive animals and technological equipment, compositions and depositories with equipment and also a few small reprocessing enterprises with their technological equipment are PRC components.

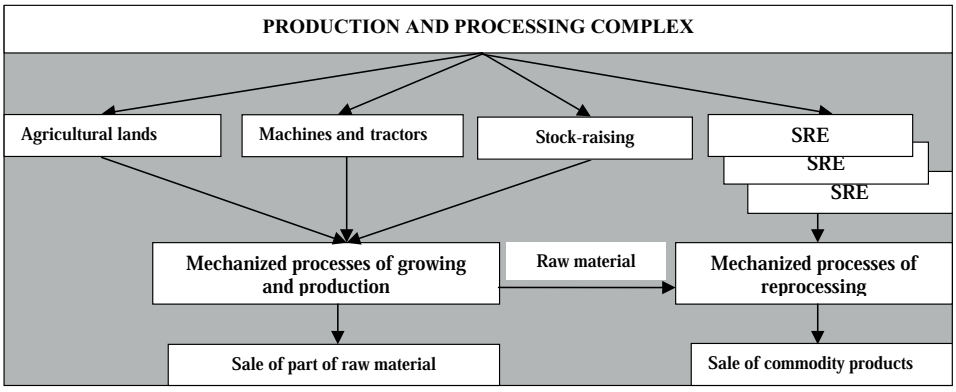

Fig. 1. Scheme of production and reprocessing complex

PRC projects development, in the first place, needs its identification. The process of PRC project identification is demonstrated on the next scheme (Fig. 2).

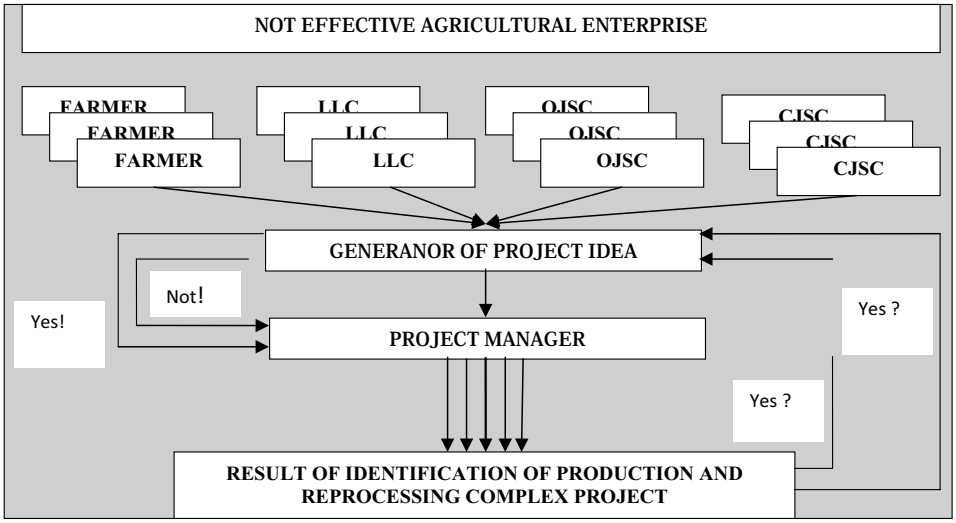

Fig. 2. Process of production and reprocessing complex project's identification LLC - Limited Liability Company; OJSC - Opened Joint-Stock Company; CJSCA - Closed Joint-Stock Company

The project management specialists operatively execute the project identification. However, there must be a person who is the most interested in such project: that is the generator of project idea. The generator of PRC project idea may be a physical or legal person who is mostly interested in this project and will exploit his product in the future. The generator of PRC project idea must expressly realize and clearly explain to the project manager the requirement in the project's product, adequately estimate its financial state and investment possibilities to formulate the project identification order. The project manager and generator of PRC project idea (more often he is the customer of the project and user of its product in future) conduct the conceptual negotiations on the project configuration, its purpose, and the ways of its achievement. The project manager conducts a preliminary technical and economic ground and multiple agreement of the preliminary configuration of PRC project with interested persons. For PRC project identification it is necessary to give the project manager some information:

- V kinds and Q volumes of agricultural raw material grown in this ACE, which is the result of agricultural production;
- S forecast specialization and W power of each small reprocessing enterprise, which will be included in PRC, which is the result of reprocessing production.

The result of every ACE agricultural production is the function of the following indexes:

$$V = f(K_T, P_S, F_G, A_g, G_Z, R_S), \quad (1)$$

Where K_T - the traditional sowing of cultures in the economies of the region; P_S - an area of agricultural lands; F_G - physical and mechanical properties of soils; A_G - agri-technical properties of soils; G_Z - configuration of fields; R_S - the demand on this raw material at the market.

$$Q = f(N_M, U_K, P_T, G_K, O_P, Z_P), \quad (2)$$

Where N_M - the quality of seminal material; U_K - the productivity of cultures; R_T - the productivity of animals; G_K - soils and climatic terms; O_P - the organization of mechanized processes in a crop-growing and husbandry; Z_P - the storage of raw material.

The efficiency of reprocessing production also depends on such factors:

$$S = f(C_P, C_S, W_P, Q_S), \tag{3}$$

Where C_P, C_S - a realized price, according to commodity products and its raw material; W_P - commodity products volumes of every SRE; Q_S - the amount of the grown raw material for the given commodity products.

$$W = f(V_P, B_P, T_P, K_P), \tag{4}$$

Where V_P - a commodity unit cost; B_P - the losses of products in raw material up to the moment of reprocessing; T_P - transport charges; K_P - capital investments on creation of SRE.

Consequently, each of the created PRC must have its own production programme activity (kinds and volumes): at first, grown agricultural raw material and, secondly, commodity products produced by such complex. On the other hand, the production programme of every SRE in the PRC structure depends on the kinds and amount of the grown raw material, and also on the demand for the commodity products produced by every SRE in the PRC structure. Making conclusions we consider that PRC will be effective enough in the case of coordination and cooperation of all the components of production structure. The growing of raw materials in PRC, on one hand, will satisfy the demand on the local market and on the other hand - will be downgraded to the group of small reprocessing enterprises.

Therefore, it is very important to scientifically establish, according to soil, climatic and socio-economic conditions, for each PRC: 1) the agricultural production programme; 2) the production programmes of each of SRE in PRC; 3) a flexible and effective interaction of growing, storage and reprocessing of PRC agricultural raw material.

That is why in modern economic conditions the agricultural production is considered as the interaction of three basic mechanized processes: plant growing, meat and milk production and the reprocessing of these types of raw material into the commodity products. Therefore, the primary purpose of PRC production is not just getting the agricultural raw material in maximally possible volumes but the production and realization of commodity products at the market.

Taking into account the stated theoretical opinions, we are planning to create the PRC project on the basis of the educational-scientific-experimental center (ESEC) of Lviv national agrarian university (LNAU).

The production and technological bases of ESEC are formed by:

- 1545 hectare of agricultural lands, including 560 hectare of plough-land;
- stock-raising-production complex comprising: 180 cattle-heads; 142 pig-heads;
- engineering and technical complex;
- tractor, truck and agricultural machine park involving: 10 tractors; 8 trucks; 4 combines harvesters; 3 forages combines; complex of agricultural machines.

After the accumulation of the basic data and the proper calculations according to the methods developed in the researches [5,8,10,14,16,17,21], the SRE optimum annual programmes were estimated according to the ESEC grown raw material production and the present socio-economic conditions can be included in the production and reprocessing complex (Table).

Table. SRE production programmes for PRC on the basis of ESEC of LNAU

SRE SREcialization	Annual power, tons
Mill: flour grain	400 350 50
Bakery: bread macaroni	85 70 15
Rape oil making enterprise	150
Milk reprocessing enterprise: pasteurized milk, 2,5% adiposeness sour cream, 15% adiposeness	115 80 35
Meat reprocessing enterprise: can beef ham smoked sausages semi smoked sausages	32 8 5 7 12

As the result of the conducted experimental researches we have grounded the specialization of five SRE: mill, bakery, rape oil making enterprise, milk and meat reprocessing enterprises. Consequently, except the present production base, the complex of small processing enterprises will be included in PRC:

- Mill: flour - 350 tons/year and grain - 50 tons/year;
- Bakery: bread - 70 tons/year and macaronis - 15 tons/year;
- Rape oil making enterprise: rape oil - 150 tons/year;
- Milk reprocessing enterprise: pasteurized milk - 80 tons/year and sour cream - 35 tons/year;
- Meat reprocessing enterprise: can beef - 8 tons/year, ham - 5 tons/year, smoked sausages - 7 tons/year, semi smoked sausages - 12 tons/year.

The organization process of PRC activity consists in the engineering and technical, organizational and technological providing of production, which is demonstrated in the next scheme (Fig.3).

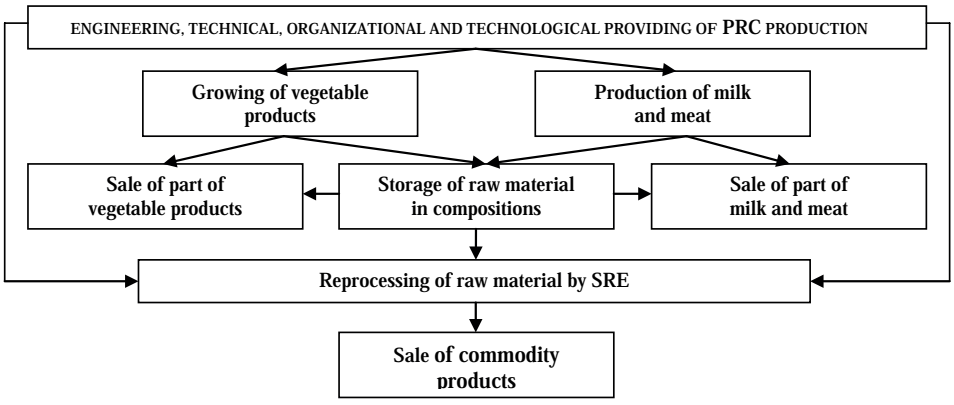

Fig. 3. Organization scheme of PRC activity on the ESEC LNAU production basis

The management of a production and processing complex has as the main purpose to provide the control over the production and effective co-operation of all the services and subsections. The scheme of PRC activity management is presented in Fig.4.

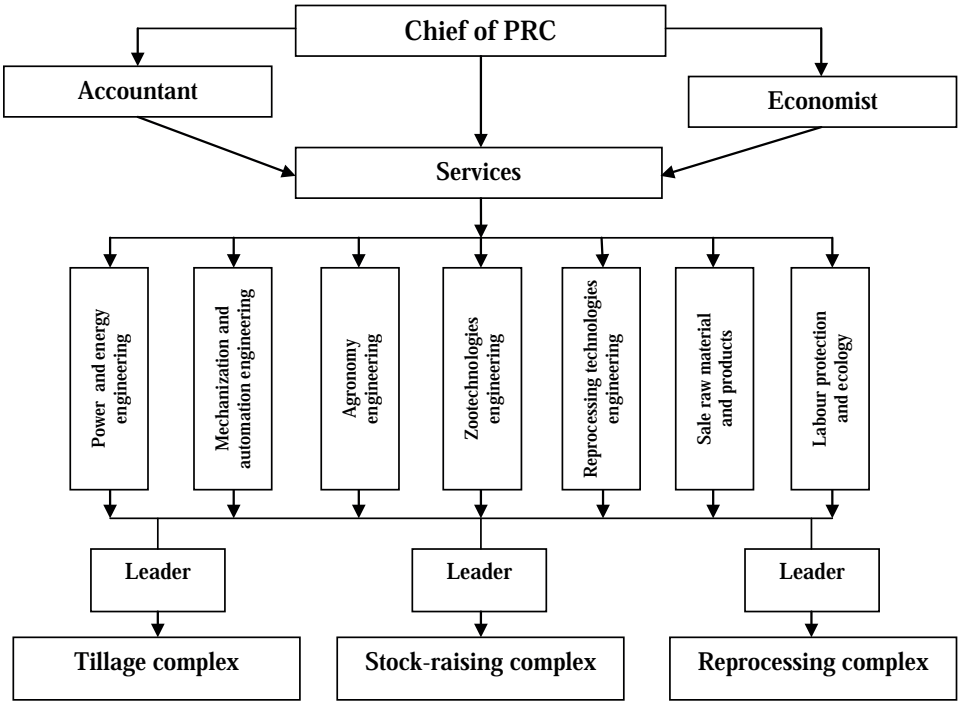

Fig. 4. Scheme of PRC activity management on the ESEC LNAU production basis

The director of production and processing complex heads the PRC management. There are two main SRE specialists - economist and accountant for providing the management wi8th object planning and accounting.

There are three production complexes: tillage, stock-raising and reprocessing and seven specialized services: power and energy engineering, mechanization and automation engineering, agronomy engineering, zootechnics engineering, reprocessing technologies and technology of food production engineering, sale of raw material and commodity products, labour and environment protection. The complexes are managed by the specialists of proper industries and the services are managed by the main specialists.

The agronomical, engineering and technical services of PRC organize the mechanized processes of plant raw material growing. Zootechnics engineering and technical services of the production and processing complex have a task to organize milk and meat production in PRC. Reprocessing technologies, mechanization and automation, and power engineering services organize mechanized processes of raw material reprocessing.

The Chief of PRC is the main co-ordinator of the three mechanized processes: crop-growing, stock-raising and reprocessing industry complexes. The preliminary trained workers are responsible for the implementation of all the technological operations in three PRC departments. The leaders of the proper services organize and test their work keeping to the technologies and regimes, proper

technical exploitation of machines and equipment, control over the labour and ecological protection. The leaders of subsections organize and control the workers' activity. The sale of raw materials and commodity products is organized by sale service. The service of labour and environmental protection must provide the normative conditions of labour and ecology in PRC activity.

We have estimated the efficiency of the production and reprocessing complex activity which will be created on the production, economic, material and technical basis of ESEC of Lviv NAU. The results of the calculations prove that the introduction of PRC in the university ESEC will provide €120-150 thousand of annual profit.

CONCLUSIONS

The development of projects for production and reprocessing complexes for growing and reprocessing of the ACE agricultural raw materials into commodity products at present will provide the agrarian enterprises with the additional financial funds for the increase of technical-technological and social-economic level of agricultural production.

We consider that the creation of PRC on the production basis of a new or operating ACE in the production and technological processes of modern agriculture is one of the effective methods of the removal of possible risks or minimizing the results of their influence, on one hand, and getting the additional profits after low capital investments and current expenses, on the other hand.

REFERENCES

Flys I.M. Main requirements to the innovative projects in the programs of the villages and their territories development / I.M.Flys // East-West Magazine of new technologies. – 2010. – 1/3(43) – p. 61-63.

Flys I.M. Identefication of projects value for rural territories / I.M.Flys // Theses of the VII International conference «The projects management in society development». Theme: Projects and programs management for organizations value development. – Account. for an issue prof. S.D.Bushuev. – K. : KNUBA, 2010 – p. 208-209.

Flys I.M. Innovative projects identefication and harmonization of project environment in the programmes of development of AIC / I.M.Flys // East-West Magazine of new technologies. – 2011. – 1/6(49) – p. 57-59.

Flys I.M. An equipment choice for small reprocessing enterprise on the coefficients of ponderability basis / I.M.Flys, S.V.Syrotjuk // Announcer of Lviv State Agrar. Un-ty: Agroengineerings researches №4. – Lviv : Lviv State Agrar. Un-ty, 2000. – p.41-43.

Flys I.M. The Scientifically methodical grounding of specialization and power of reprocessing enterprise / Ekology-ekonomical problems of development of AIC: Materials of International scientifically-practical conference, devoted 10th the anniversary of Conference of UNO on questions of guard of environment and development (t. Dublyany, September, 25-27 2002). – V.1. – Lviv : Lviv State Agrar. Un-ty, 2002. – p. 285-290.

Sydorchuk O.V. The functional structure theory development of material production / O.V.Sydorchuk // Announcer of Lviv State Agrar. Un-ty: Agroengineerings researches №7. – Lviv : Lviv State Agrar. Un-ty, 2003. – p. 3-8.

Sydorchuk O.V. A functional structure of reprocessing enterprises in their projects / O.V.Sydorchuk, I.M.Flys // Announcer of Lviv State Agrar. Un-ty: Agroengineerings researches №8. – Lviv : Lviv State Agrar. Un-ty, 2004. – p. 82-88.

Flys I.M. Grounding of the reprocessing enterprise production programme / I.M.Flys // Announcer of Lviv State Agrar. Un-ty: Agroengineerings researches №8. – Lviv : Lviv State Agrar. Un-ty, 2004. – p. 75-81.

Flys I.M. Technological features of functional structure forming of reprocessing enterprises / I.M.Flys // Announcer of Lviv State Agrar. Un-ty: Agroengineerings researches №9. – Lviv : Lviv State Agrar. Un-ty, 2004. – p.60-64.

Flys I.M. A management of the small processing enterprises production programmes in their projects / I.M.Flys // Scientific messages of the International humanitarian university: Collection / Edited by prof. Rybak A.I. – Odessa : Intern. Humanit. Un-ty, 2009. – Iss. 16.- Series : «Projects and programs management». – p. 28-33.

Flys I. Engineer project management by production and processing complexes / I. Flys // MOTROL-2010 . – Motorization and power industry in agriculture. – Tom 12. – Lublin, 2010. – p. 75-81.

Flys I.M. Engineering providing of complexity of agricultural raw material reprocessing / I.M.Flys, J.V.Shymonjuk, O.G.Gordijuk // Announcer of Lviv State Agrar. Un-ty: Agroengineerings researches №9. – Lviv : Lviv State Agrar. Un-ty, 2004. – p. 65-69.

Sydorchuk O.V. A method of determination of harvest of agricultural cultures losses as a result of ill-timed implementation of the mechanized processes of field-crop cultivation / O.V.Sydorchuk, S.R.Senchuk, P.M.Lub, A.V.Tatomyr, A.V.Burylko // MOTROL-2005 . – Motorization and power industry in agriculture. – Vol. 7. - Odessa, 2005. – p. 87-91.

Flys I.M. The reprocessing enterprises programmes management in their projects / I.M.Flys // The agroindustrial engineering in measurings of thrift / Edited by prof. O.D.Semkovich, O.V.Sydorchuk, I.M.Flys, S.J.Kovalyshyn. – Lviv : Lviv State Agrar. Un-ty, 2006. – 318 p.

Flys I.M. The projects Development of the complex reprocessing of agricultural raw material in economies // Announcer of agrarian science . – K. – 2006. – Special issue, August. – p.121-125.

Flys I.M. The production programme management of small reprocessing enterprise in its project / Theses of International conference // Projects management in society development. – Theme: The organization development programmes management in competition surroundings: Materials of the IV International conference. – K. : KNUBA, 2007. – p.153-155.

Flys I., Kupriyenko M. The engineering management of complex processing of agricultural raw materials in economies / The 31st Presentation of Scientific Papers conference at the University in Novi Sad, 19-20.11.2007. – p. 134-139.

Tatomyr A.V. A configuration management in theprojects / A.V.Tatomyr, R.E.Krygul, M.M. Babich // MOTROL-2007. – Motorization and power industry in agriculture. – Volume 9a. – Lublin, 2007. – p. 89-94.

Flys I.M. Methodology of projects identefication of production and reprocessing complexes / Theses of International conference of // Management projects are in development of society. – Theme: A professional projects management is a way to the increase of assets of organizations: Materials of the V International conference. – K.: KNUBA, 2008. – p. 210-212.

Flys I.M. Project identefication of production and reprocessing complexe / Announcer of Lviv National Agrar. Un-ty: Agroengineerings researches №12. - Vol. 1. – Lviv : Lviv Nation. Agrar. Un-ty, 2008.– p.46-50.

Flys I.M. The calculation of the production programme of processing enterprise // Engineering of agroindustrial production: Scientists of mechanics and power energy faculty for the production: Collective monograph. – Vip. 2 / by editor V.V.Snitinskij. – Lviv : Lviv Nation. Agrar. Un-ty, 2008.– p.75-76.

Sydorchuk O., Sydorchuk L., Tatomyr A. Grounding of the main tasks the project management of power supply for rural power consumers / MOTROL-2008 // Motorization and power industry in agriculture. – Volume 10. – Lublin, 2008. – p. 122-125.

Flys I.M. Development of the projects of the complex reprocessing of agricultural raw material in economies // Scientific messages of the International humanitarian university: Collection / Edited by prof. Rybak A.I. – Odessa : Intern. Humanit. Un-ty, 2008. – Iss. 10. – p. 92-95.

Flys I.M. The grounding of mill production programme for agricultural enterprise / I.M.Flys, M.J.Kuprijenko, M.I.Kozhushko // Konferencja Miedzynarodowa."Problemy inzynierii rolniczej i lesnej". – Szkola Glowna Gospodarctwa Wiejskiego w Warszawie. – Warszawa, 4-5 czerwca 2008. – Warszawa, 2008. – p. 111-115.

Flys I.M. Theoretical grounding of production and reprocessing complex projects / Theses of international conference // Thesis lectures of VI International conference «A management projects in development of society». – Theme: An acceleration of development of organization is on the basis of project management – Account. for an issue prof. S.D.Bushuev. – K. : KNUBA, 2009. – p. 197-199.

НАУЧНО-ПРАКТИЧЕСКИЕ АСПЕКТЫ УПРАВЛЕНИЯ ПРОЕКТАМИ ПРОИЗВОДСТВЕННО-ПЕРЕРАБАТЫВАЮЩИХ КОМПЛЕКСОВ

Аннотация. Рассмотрены научно-практические аспекты управления проектами производственно-перерабатывающих комплексов, которые создаются на базе новых или действующих сельскохозяйственных предприятий. Внедрение проекта производственно-перерабатывающего комплекса обеспечит получение дополнительных финансовых средств сельскохозяйственному предприятию для повышения технико-технологического уровня производства.

Ключевые слова: проект, управление проектами, сельскохозяйственное предприятие, малое перерабатывающее предприятие, производственно-перерабатывающий комплекс.

TEKA Kom. Mot. Energ. Roln. – OL PAN, 2011, 11, 92–97

CONTOUR CONTACT AREA OF THE BLOCK AND DISK OF THE DISK BRAKE UNDER THE CONDITIONS OF THERMAL DEFORMATIONS

Alexander Golubenko*, Yuriy Yu. Osenin*, Igor Sosnov*

*Volodymyr Dahl East-Ukrainian National University, Lugansk, Ukraine

Summary. The article presents the analysis of the contour contact area changes of the block and the disk of the disk brake under the action of thermal deformations of the disk which appear while braking. The design is offered which promotes the influence decrease of the thermal deformations on the value of the contour contact area.

Key words: disk brake, thermal deformations, contour contact area.

INTRODUCTION

According to classical ideas of interaction of the bodies, contour contact area is the area which is formed while touching the bodies which have macrodeviations from regular geometrical shapes.

One of the factors which influence the macrodeviations of the block and disk of the disk brake are the thermal deformations of the materials which are caused by the heating of the interacting surfaces (700 – 800 and more degrees Celsius). In connection with this, the purpose of this article is the analysis of the peculiarities of the formation of the contour contact area of the block and disk of the disk brake under the conditions of the disk thermal deformations.

The nature of thermal (reversible and irreversible) deformations of the surfaces of the block and disk is caused by the conditions of considerable non-stationarity of the process both in the quantity and durability of the cycles of the thermal heating in the result of braking and in the level of realized temperatures.

The heating of the working elements of the disk brake is characterized by irregularity of temperature spreading in the volume of the materials of the block and the disk and it causes irregular deformations of the disk surface. As the result, the working surface of the disks is distorted and acquires macrodeviations from the plane [1, 2, 5, 6, 8 – 14, 16, 17].

CALCULATION MODEL

The evaluation is given of the changes in the contour contact area of the block and disk of the disk brake under the conditions of deformations caused by the heating of the disk because of

friction (the disk is approximated by cylindrical and spherical surfaces, the block is approximated by the plane). The analysis is carried out for two cases: in the first one the block is represented by one working plane, in the second case it is represented by two planes. Calculation diagrams are given in Figure 1. The following assumptions are taken into account:

- voltage in the zone of contact does not exceed the limit of elasticity;
- the areas of contact are small in comparison with the surfaces of the touching bodies;
- pressure forces spreading along the surface of contact are normal to this surface;
- deformations of the disk surface: volume – symmetrical;
- deformations of the block are small.

The areas of contact for the case of interaction of the above surfaces are calculated with the help of dependencies known from the theory of elasticity [3, 4, 15].

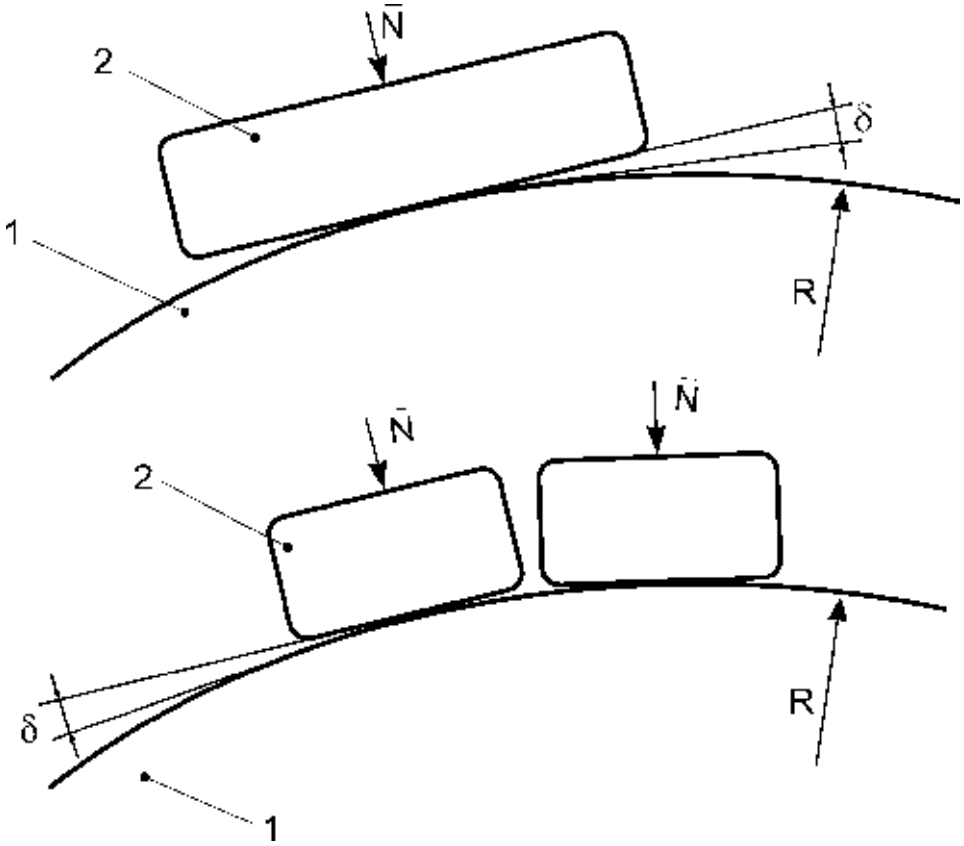

Fig. 1. Calculation diagrams in the estimation of contour contact area
of the block and the disk of the disk brake under the conditions of thermal deformations:
a) – block presented by one working plane; b) – block presented by two working planes.
1 – brake disk; 2 – block; N – pressing force of the block to the disk;
δ - level of deformation stipulated by the curvature radius of the surface R.

The contact of the flat and cylindric surfaces is estimated by the expression:

$$b = 1{,}131\sqrt{\frac{N \cdot R}{H}\left(\frac{1-\mu_1^2}{E_1}+\frac{1-\mu_2^2}{E_2}\right)}, \tag{1}$$

where: b – semi-width of the strip contact;
R – curvature radius of the surface in the zone of contact;
H – length of the contact strip (width of the block);
$\mu_{1,2}$ - Puasson coefficient of the materials of the contacting surfaces;
$E_{1,2}$ – elasticity modulus of the materials of the contacting surfaces.

Contact of flat and spheric surfaces:

$$r = 0{,}909\sqrt[3]{N \cdot R\left(\frac{1-\mu_1^2}{E_1}+\frac{1-\mu_2^2}{E_2}\right)}, \tag{2}$$

where: r – radius of the contact spot.

Curvature radius of the contacting surfaces R, which is a member of the formula (1) – (2) is determined in the following way (see Fig. 2).

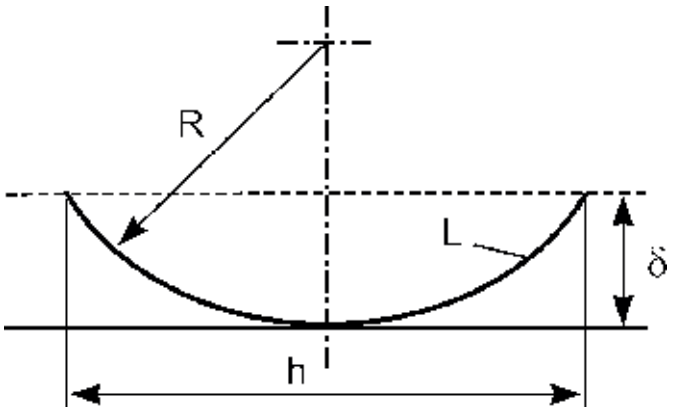

Fig. 2. Diagram in the value estimation of the curvature radius R of the contacting surfaces in the zone of contact

Lengths of the chord h and arc L (Fig. 2) are estimated as [7]:

$$h = 2\sqrt{2 \cdot \delta \cdot R - R^2}\ ;\ \ L = \sqrt{h^2 + \frac{16 \cdot \delta^2}{3}}. \tag{3}$$

Having manipulated these expressions we obtain:

$$R = \frac{L}{8 \cdot \delta} - \frac{2}{3}\delta + \frac{1}{2}\delta\,. \tag{4}$$

The value L in the calculations corresponds to the outer radius of the brake disk. The values of summary nominal areas of the working surfaces of the blocks of the brake disk for the two above-mentioned cases (a) and (b) are considered to be equal.

Cast-iron and steel with corresponding use in the formulas (1) – (2) of the average values of their mechanical characteristics are taken as the materials of the blocks and brake disk. The seize of

the block for the condition (a) (fig. 1): 0,20 ´ 0,121 m: for the condition (b): 0,10 ´ 0,121 m; outer radius of the brake disk: 0,35 m.

RESULTS OF CALCULATIONS

The results of the calculations in the above dependencies are given in Fig. 3. (Notes: the values for the condition (b) are given in the brackets, for the condition (a) the values are given without brackets; S_H – nominal area of contact of the considered surfaces before deformation.

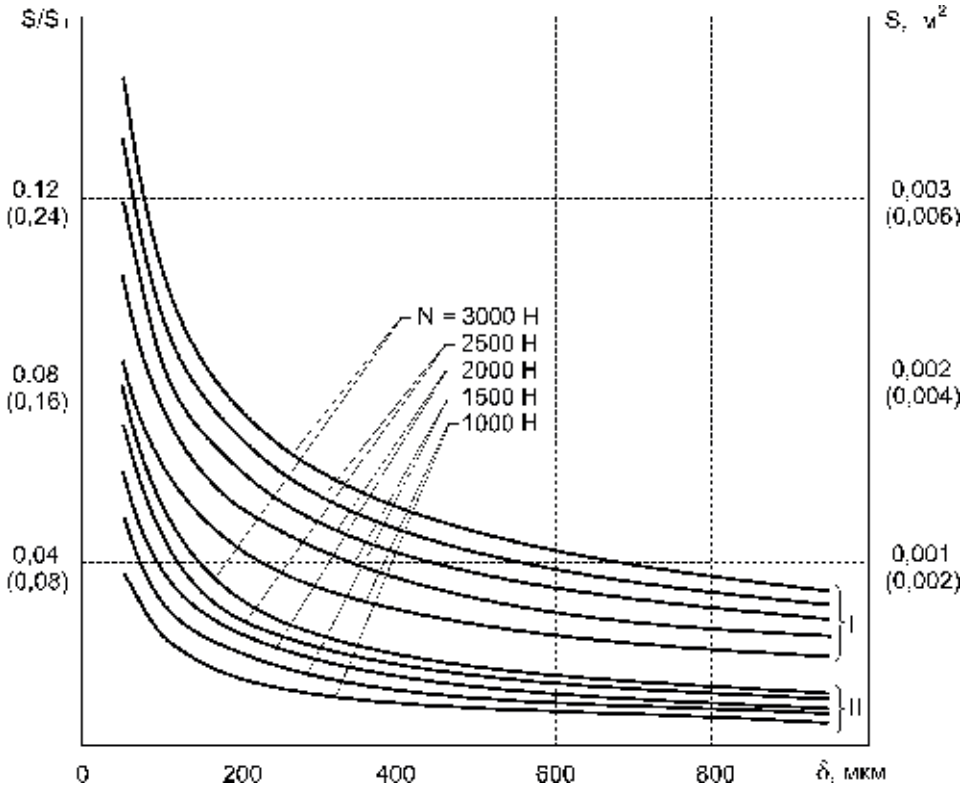

Fig. 3. Dependencies of the contour S and relative $S/S_н$ areas
on the thermal deformation δ and normal pressing force N of the block to the disk:
I – contacting surfaces: plane (block) – cylinder (disk);
II – contacting surfaces: plane (block) – sphere (disk)

The analysis of the given dependencies showed that in the result of thermal deformations of the disk its contour area of contact with the block has the tendency to decrease. While level growing of the thermal deformations (parameter δ) from 0,0 mkm to 1000 mkm a contour area of contact Has , on average, 81% of decrease.

Decrease levelling of the contour area of contact of the block and disk under the conditions of thermal deformations can be provided due to the block which is presented in the form of two

working planes (condition b). In this case the decrease of the contour area of contact under the conditions of thermal deformations can be two times less and makes 40%.

CONCLUSION

Thermal deformations of the brake disk have a considerable influence on the formation of its contour area of contact with a block under the conditions of force interaction. General tendency of influence of thermal deformations on the contour area consists in the decrease of the latter while growing deformations.

With the growth of thermal deformations from 0,0 mkm to 1000 mkm a contour area of contact decreases by mean 81% (for a block presented by one plane) and by mean 40% (for a block presented by two planes).

Design improvement of the block of the disk brake can be achieved due to the presentation of the working surface of the block as the system of kinematically connected of two and more planes.

REFERENCES

Aleksandrov M.P., Lisyakov A.G. and others, 1985. Brake devices. Reference book. / Editor M.P.Aleksandrov – M.: Engineering. – 312 p.

Asadchenko V.R., 2006. Automatic brakes of the rolling stock: Training appliances for higher schools of the railway transport. – M.: Route. – 392 p.

Berlin V.I., Zakharov B.V., Melnichenko P.A., 1982. Transport science of materials. – M.: Transport. – 287 p.

Birger I.A., Mavlyutov P.P., 1986. Resistance of materials. – M.: Science. – 560 p.

Brake disk in details (electronic resource), access mode: http://www.autogazeta.by/autogazeta/tehburo/716.

Brake disks (electronic resource), access mode: http://www.autocentre.ua/ac/Service/Exploitation/11838.html.

Bronstein I.N., Semendyaev K.A., 1981. Reference book in mathematics for engineers and students of the technical higher schools. – M.: Science. – 704 p.

Demyanushko I.V., Birger I.A., 1978. Strength calculation of the rotating disks. – M.: Engineering. – 247 p.

Design of brake discs (electronic resource), access mode: http://avtonov.svoi.info/dicol.htm.

Inozemtsev V.G., 1987. Brakes of the rolling stock. Questions and replies. 3-edition. – M.: Transport. – 207 p.

Iosilevich G.B., 1981. Voltage and deformation concentration in the machine parts. – M.: Engineering. – 224 p.

Krylov V.I., Klykov E.V., Yasentsev V.F., 1980. Rolling stock brakes. M.: Transport. – 272 p.

Otmakhov V.I. Use of MSC.Nastran for the analysis of temperature deformation of the brake disk of the automobile (electronic resource), access mode: http://www.mscsoftware.com/international/russia/conf_ru2001_4.html.

Parkhomov V.T., 1994. Design and brake operation. – M.: Transport. – 208 p.

Pisarenko G.S., Yakovlev A.P., Matveev V.V., 1988. Reference book in metal resistance. / Editor Pisarenko G.S. – 2-nd edition. – Kiev: Scientific thought. – 736 p.

Prigorovsky N.I., 1961. Voltage and deformation in the parts and units of the machines. – M.: Mashgiz. – 566 p.

Troschenko V.T., 1981. Deformation and metal failure under manycycle loading. – M.: Engineering. – 344 p.

КОНТУРНАЯ ПЛОЩАДЬ КОНТАКТА КОЛОДКИ И ДИСКА ДИСКОВОГО ТОРМОЗА В УСЛОВИЯХ ТЕРМИЧЕСКИХ ДЕФОРМАЦИЙ

Аннотация. В статье представлен анализ изменений контурной площади контакта колодки и диска дискового тормоза под воздействием термических деформаций диска, возникающих при торможении. Предложен конструктивный способ уменьшения влияния термических деформаций на величину контурной площади контакта.

Ключевые слова: дисковый тормоз, термические деформации, контурная площадь контакта.

TEKA Kom. Mot. Energ. Roln. – OL PAN, 2011, 11, 98–105

ANALYSIS OF TRACTION CHARACTERISTICS OF THE MOTOR CAR FIAT PANDA EQUIPPED WITH A 1.3 16 V MULTIJET ENGINE

Wawrzyniec Gołębiewski*, Tomasz Stoeck *

* Department of Motor Vehicle Use, the West-Pomeranian University of Technology in Szczecin

Summary. This paper presents analysis of traction characteristics of the Fiat Panda car equipped with a 1.3 16 V Multijet engine. Characteristics of the full power of the 1.3 JTD engine was prepared, along with a selection of the trend curves. On the basis of the moment curve from that graph and the car basic data, traction characteristics of the vehicle was prepared. It was a dependence of the propulsive force on the vehicle's linear velocity. On that basis, such traction qualities of the Fiat Panda as its ability to accelerate, to drive upon hills and its achieving the maximum speed were analyzed.

Key words: traction characteristics of a vehicle, theory of motion, combustion engines, external characteristic of an engine.

INTRODUCTION

Acceleration potential is one of the most important traction characteristics of a vehicle. It finds its reflection in urban traffic. A higher number of cars that manage to drive over a crossing in one light cycle results in a lower number of cars waiting before the crossing, which translates to a lower emission of combustion gases from engines working idle.

Moreover, quick passing is also important, as it shortens the time of the hazardous maneuver. This quality of the car is strongly affected by the external characteristics of the engine torque and selection of an appropriate power transmission system.

Overcoming heights by the vehicle at its maximum speed is meaningful, too.

These traction qualities describe the essence of the vehicle work and the character of its use.

PURPOSE OF THE RESEARCH

Purpose of this research was to perform analysis of traction characteristics of a motor vehicle Fiat Panda, equipped with a 1.3 16 V Multijet engine.

TESTING STATION

The testing station was composed of the following components:

- a fuel (diesel oil) tank – a 200 l fuel tank for diesel oil;
- a fuel pump – it was supposed to ensure fuel pressure from the tank and its delivery to the fuel pipes;

"Automex" fuel meter – it was an important component, necessary for measuring fuel consumption with the weighing method (not included in the scope of the tests). Unburnt fuel returned to it through the engine;

- a Fiat Multijet 1,3 JTD engine – a four-stroke turbo-charged diesel engine with direct injection, provided with the Common Rail fuel delivery system;
- an „Automex" eddy current brake – which charged the engine with any chosen anti-torque at variable rotational speeds, using the rotary current phenomenon;
- a power panel with a Fiat Panda 2 switchboard with software and the fuel meter controlling system – controlling the engine work and torque loading the engine via the brake, with a display of the basic operational parameters, including: power, engine torque, etc..

Below, Figure 1 presents the testing station arrangement.

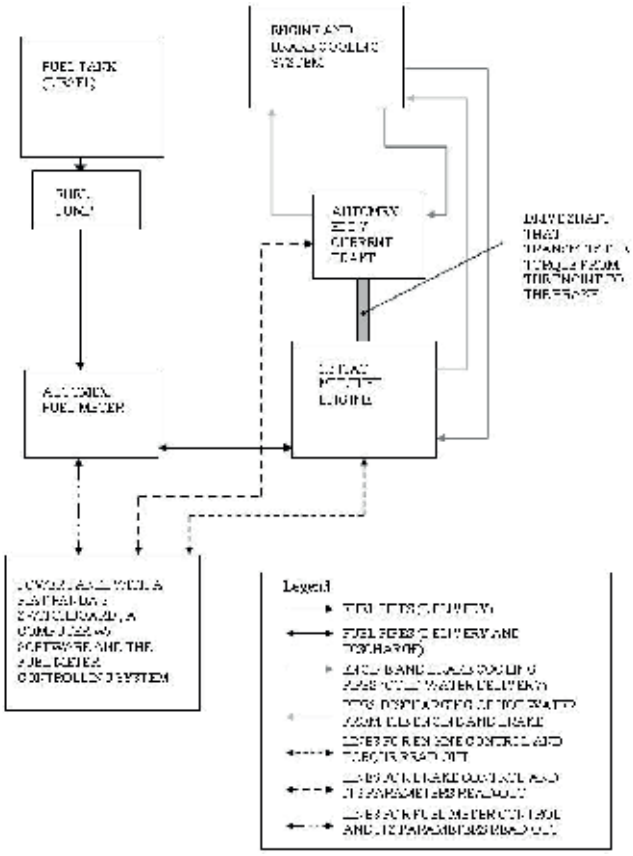

Fig. 1. Arrangement of the testing station (plan)

COURSE OF THE TESTS

During the tests, measurements on a test engine bed were conducted, by performing the engine full power speed characteristic [6,9,16] for the Fiat Multijet 1,3 JTD. It appeared as follows:

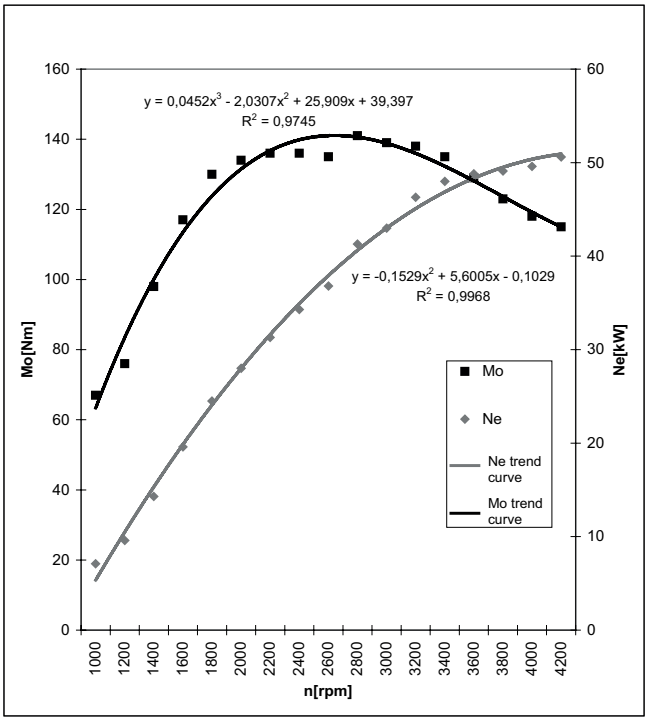

Fig. 2. Speed characteristic of a Fiat Multijet 1,3 JTD engine; Mo – engine torque, Ne – engine power output, n – engine rotational speed, R^2 – correlation coefficient

The measurements were made every 200 rpm, from 1000 rpm to 4200 rpm and the opposite. The result was the mean of the two measurements. For these values, trend curves were matched. Equations characterizing those curves are shown on the graph, where x=1,2,3,... 17 –the next measurement number. High values of the correlation coefficients (R^2) proved the good matching of the trend curves and the actual values. In the table below, results of actual measurements with theoretic values obtained from equations of the matched trend curves are presented.

Table 1. Actual values and theoretical values of the engine torque and power output

	n (rpm)	M_o[Nm]	$M_{o\,theor}$[Nm]	N_e[kW]	$N_{e\,theor}$[kW]
1	1000	67	63.32	7.1	5.34
2	1200	76	83.45	9.6	10.49
3	1400	98	100.07	14.3	15.32
4	1600	117	113.43	19.6	19.85
5	1800	130	123.82	24.5	24.08
6	2000	134	131.51	28	28.00
7	2200	136	136.76	31.3	31.61
8	2400	136	139.85	34.3	34.92
9	2600	135	141.04	36.8	37.92
10	2800	141	140.62	41.3	40.61
11	3000	139	138.84	43	43.00
12	3200	138	135.99	46.3	45.09
13	3400	135	132.33	48	46.86
14	3600	129	128.13	48.8	48.34
15	3800	123	123.67	49.1	49.50
16	4000	118	119.22	49.6	50.36
17	4200	115	115.05	50.6	50.92

where: M_o – actual engine torque, $M_{o\,theor}$ – theoretical engine torque, N_e – actual engine power output, $N_{e\,theor}$ – theoretical engine power output.

The next stage of the test was selection of parameters characterizing the vehicle and preparation of a traction graph based on the above-given theoretical characteristic of the engine torque.

VEHICLE DATA

The basic parameters that describe the vehicle include the ones given in Table 2.

Table 2. Basic data of the vehicle

Symbol	Value	Unit	where:
G_c	19325.70	[N]	vehicle weight
f_t^0	0.012	-	basic rolling resistance coefficient
A	0.00005	-	additional rolling resistance coefficient
c_x	0.3	-	non-dimensional air resistance coefficient
k	0.9	-	filling factor
B	1.578	[m]	vehicle width
H	1.54	[m]	vehicle height
F	2.19	[m^2]	vehicle end face area
η	0.9	-	propulsive system mechanical efficiency
σ	1	-	under-hood power loss factor
r_k	0.27	[m]	wheel kinematic radius

Basic assumptions for selecting values for the vehicle data:

- it was assumed that the vehicle is fully loaded, hence its weight (G_c),

- the value of the basic rolling resistance coefficient f_t^0 was adopted as for a surface similar to smooth asphalt,
- the value of the additional rolling resistance coefficient A was adopted as for most of surfaces in use,
- the value of the non-dimensional air resistance coefficient c_x was adopted as for a Fiat Panda car,
- the value of the filling factor k was adopted as for motor cars,
- the values of the width and height of the car were adopted as for a Fiat Panda, version 4x2 Van,
- the vehicle end face area was calculated based on the dependence $F=kBH$,
- the value of the propulsive system mechanical efficiency was adopted as for motor cars,
- the value of the under-hood power loss factor was adopted as for a vehicle going at elevation of 0 meters above the sea level,
- the wheel kinematic radius resulted from the tire size (at pressure recommended by the producer) and the ring, with consideration of static loads.

Table 3. Basic ratios of gearbox C514R and the final drive [18]

I gear	3.909
II gear	2.158
III gear	1.345
IV gear	0.974
V gear	0.766
Reverse gear	3.818
Final drive	3.438

TRACTION CHARATERISTIC OF THE CAR

Traction characteristic of the car was the dependence between the propelling force on the car wheels on its linear speed. The propelling force on the car wheels was calculated with the formula:

$$P_k = (M_{o\ theor}\ \sigma\ \eta_m\ i_{bi}\ i_g)/r_k, \tag{1}$$

where:
P_k – propelling force on the wheels [N],
$M_{o\ theor}$ – theoretical engine torque (value according to the trend curve) [Nm],
σ - under-hood power loss factor,
η_m – mechanical efficiency of propelling system,
i_{bi} – ratio of the actual gear of the gearbox the car is driving at (selectable ratio),
i_g – final drive ratio (permanent ratio),
r_k – wheel kinematic radius [m].

The car velocity was described with the dependence:

$$V=(0.38\, n_s r_k)/ i_{bi}\, i_g \tag{2}$$

where:
V – car linear velocity [km/h],
n_s – engine rotational speed [min^{-1}],
r_k – wheel kinematic radius [m],
i_{bi} – ratio of the actual gear of the gearbox the car is driving at (selectable ratio),
i_g – final drive ratio (permanent ratio).

The values of the propelling force and the linear velocity were calculated for five gears. The reverse gear was not taken into account.

The graph shows the vehicle motion resistances, i.e. rolling resistance, air resistance and grade resistance. The resistance curves were drawn based on dependences available in the literature [1,4,8,12,14].

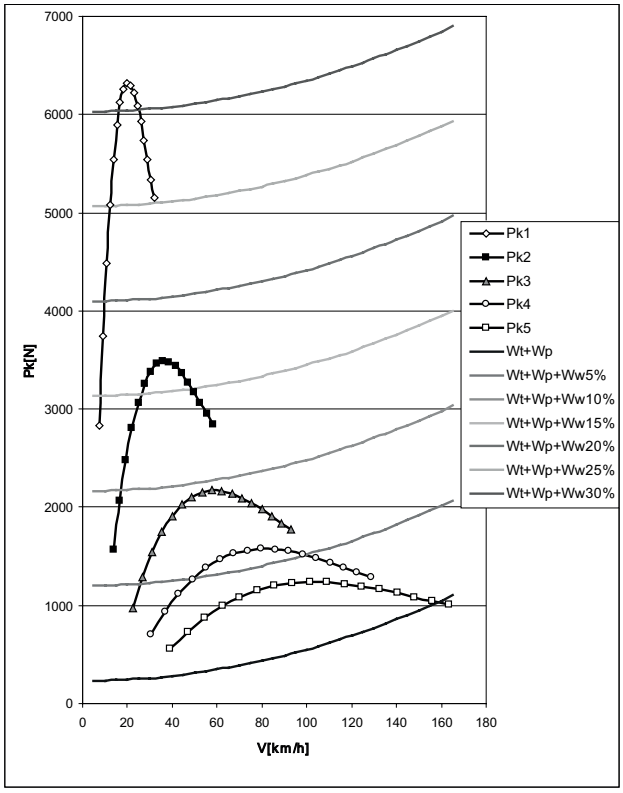

Fig. 3. Traction graph of a Fiat Panda car equipped with a 1.3 JTD engine
Pk1, Pk2, Pk3, Pk4, Pk5 – propelling force for the subsequent gears: 1, 2, 3, 4, 5;
Wt– rolling resistances; Wp – air resistance; Ww% - grade resistance
(e.g. Ww 5% - grade resistance at a 5% slope)

RESULTS

Maximum speed of the car: 155 km/h,
Maximum propelling and acceleration forces at individual gears:

Table 4. Maximum propelling and acceleration forces at individual gears

	$P_{k\,max}$[N]	a [m/s^2]
gear 1	6318.28	3.21
gear 2	3488.07	1.77
gear 3	2173.98	1.10
gear 4	1574.32	0.80
gear 5	1238.12	0.63

where: $P_{k\,max}$ – maximum value of propelling force at the given gear, a – maximum value of acceleration at the given gear

Steepest hill possible to overcome at gear 1: 30 %
Steepest hill possible to overcome at gear 2: 15 %,
Steepest hill possible to overcome at gear 3: 5%,
Steepest hill possible to overcome at gear 4: 5%.

CONCLUSIONS

Considering the fact that it was not a sports car, its maximum speed (155 km/h) was of a satisfactory level. Apart from the engine and propelling system design, that was strongly attributed to the aerodynamics of the vehicle. The basic air resistance factor had been effectively reduced throughout the years, thanks to which the car had been achieving higher and higher maximum speeds and using less and less fuel.

The ability to overcome a 30 % slope when fully loaded proved the good selection of the transmission ratio of gear 1 and utilization of the torque characteristics.

Acceleration values achieved at the other gears were important too, whereas the first selectable transmission had a high value.

It its worth consideration if it would not good to have the ratios of gears 2 and 3 increased slightly. This could make the car able to overcome steeper elevations at these gears and to achieve a better acceleration. Particularly, increasing the gear 3 ratio would make sense, as in urban traffic this gear is used most frequently.

On the other hand, increased rations of gears 2 and 3 would result in increased fuel consumption while driving at them. That would entail a general increase of fuel consumption, and thus a higher emission of exhaust gases.

To sum up, in the view of the ecology and economy, the engine and propelling system design should be qualified as good. Traction characteristics of the car result from its intended use.

REFERENCES

Arczyński S.: Mechanika ruchu samochodu. Warsaw, WNT 1994. p. 45-64, 92-104.

Bogdański J.R.: Hamownia podwoziowa – kompendium wiedzy minimalnej cd. Auto Moto Serwis. No 10/2002. Wydawnictwo Instalator Polski. Warsaw 2002.
Bogdański J.R.: Ile koni „pod maską"? Auto Moto Serwis. No 6/2004. Wydawnictwo Instalator Polski. Warsaw 2004.
Dębicki M.: Teoria samochodu. Teoria napędu. WNT. Warsaw 1976. p. 19-27, 45-60, 106-120, 161-172.
Hozer J. red.: Statystyka. Katedra Ekonometrii i Statystyki Wydziału Nauk Ekonomicznych i Zarządzania Uniwersytetu Szczecińskiego. Szczecin 1998. p. 187-201.
Kijewski J.: Silniki spalinowe. WSiP Warsaw 1997. p.81-85.
Lisowski M.: Ocena własności trakcyjnych samochodu Jelcz 317 wyposażonego w silnik SW-680 z różnymi systemami doładowania. MOTROL. Lublin 1999.
Lisowski M.: Teoria ruchu samochodu. Teoria napędu. Politechnika Szczecińska. Szczecin 2003. p. 8-13, 17-19, 43-47, 64-67.
Luft S.: Podstawy budowy silników. WKiŁ. Warsaw 2006. p.45-46.
Mysłowski J.: Ocena własności eksploatacyjnych silników wysokoprężnych na podstawie jednostkowego zużycia paliwa. Praca doktorska. Szczecin 2005. p.18-26.
Mysłowski J., Mysłowski J.: Tendencje rozwojowe silników spalinowych o zapłonie samoczynnym. Wyd. AUTOBUSY. Radom 2006. p.70-77.
Prochowski L.: Mechanika ruchu. WKiŁ. Warszawa 2007. p.53-83.
Siłka W.: Energochłonność ruchu samochodu. WNT. Warszawa 1997. p.28-36.
Siłka W.: Teoria ruchu samochodu. WNT. Warszawa 2002. p.53-144.
Ubysz A.: Teoria trakcyjnych silników spalinowych. Politechnika Śląska. Gliwice 1991. p.203-210.
Wajand J. A., Wajand J. T.: Tłokowe silniki spalinowe. WNT. Warsaw 2005. p.159-162.
Zając P., Kołodziejczyk L. M.: Silniki spalinowe. WSiP. Warsaw 2001. p.108-114.
Zembowicz J.: Fiat Panda. WKiŁ. Warsaw 2005. p.12, 50-51, 136-138.
Instrukcja obsługi panelu mocy. Automex. Gdańsk 2007.
Instrukcja obsługi modułu programatora AMX 211. Automex. Gdańsk 2007.

ANALIZA WŁASNOŚCI TRAKCYJNYCH SAMOCHODU FIAT PANDA WYPOSAŻONEGO W SILNIK 1,3 16 V MULTIJET

Streszczenie. W artykule przedstawiono analizę własności trakcyjnych samochodu Fiat Panda wyposażonego w silnik 1,3 16 V Multijet. Wykonano charakterystykę pełnej mocy silnika 1,3 JTD wraz z doborem krzywych trendu. Na podstawie krzywej momentu z tego wykresu oraz podstawowych danych pojazdu wyznaczono charakterystykę trakcyjną pojazdu. Była to zależność siły napędowej od prędkości liniowej pojazdu. Na jej podstawie analizowano własności trakcyjne pojazdu Fiat Panda, takie jak: zdolność przyspieszania, możliwość pokonywania wzniesień oraz uzyskiwanie maksymalnej prędkości.

Słowa kluczowe: własności trakcyjne pojazdu, teoria ruchu, silniki spalinowe, charakterystyka zewnętrzna silnika.

TEKA Kom. Mot. Energ. Roln. – OL PAN, 2011, 11, 106–113

CHANGES OF GEOMETRIC CHARACTERISTICS OF STORED BARLEY IN ACCORDANCE WITH SIMULATED LOADS SUBSISTING IN SILO

Tomasz Guz, Zbigniew Kobus, Elżbieta Kusińska,
Rafał Nadulski, Zbigniew Oszczak

Department of Food Engineering and Machinery
University of Life Sciences in Lublin

Summary. The paper presents methodology and results of geometric characteristics measurements of grain stored in silo-stress simulated conditions. The subject of the study was barley grains (cv. Stratus). The silo-like stress was developed by specially designed cylinders. The values of stress were 35, 52 and 70 kPa, which is commonly met in industry-scale silos. The aim of this work was to search the course of geometric changes in grains, developed by variable conditions of storage (14, 16, 18, 20, 22, 24% of moisture and 6°C and 20°C of temperature). The measurements of geometric characteristics were taken by SVISTMET system and software. The results showed that the changes of geometric characteristics were not statistically significant. Slight changes appeared only at extremely high stress (70 kPa) and at higher temperature (20°C) and moisture content (over 20%).

Key words: barley, silo, storage, geometric characteristics, image analysis

INTRODUCTION

Active ventilation in the silo enables to maintain proper conditions of grain during storage [Kamiński i in. 1978; Haque i in. 1982; Jayas, Muir 1991]. The reaction to air conditioning is flow resistance, which is estimated so far by many researchers [Al-Yahya, Moghazi 1998; Agullo i in. 2005; Molenda i in. 2005]. Grain elevators that are used in today's industry have become increasingly higher and bigger, that means the bulk resistance is still a non-solved problem [Pabis 1978; Sacilik 2004; Kusińska 2006]. The raised bulk density and low porosity of grain with the time of storage and height of grain loaded in the silo cumulates high resistance to airflow [Giner, Denisienia 1996; Łukaszuk 2005].

The keeping of grain quality is strictly determined by its moisture, temperature, and time of storage [Łuszczewski 1985; Tyburcy1997; Ciećko 2003]. Ventilation by active multiple atmosphere exchange made the intergrain space accessible to fresh air thus diminishing physiological activity of grain [Bujak 1972; Kusińska *2008]. The flow resistance of air should be known at the initial phase of conditioner construction [*Sokhansanj i in. 1990; Dziki, Laskowski 2004]. The most effectual factors of air-flow resistance are: bulk density, moisture content, porosity, shape and size of grain as well as internal friction of grain [Bekasov 1952; Giner, Denisienia 1996]. The shape and size of

grain are strictly influenced by a variety of properties as well as climate and conditions of growth [Jankowski 1988]. There is a strong relationship between shape and size of grain. The shape of grain may be spherical, egg-like, oval or wedge-shaped. It may sometimes exist as the ridge side, the abdominal side or basis and top of the particular grain. Shaken mass of grain cumulates flow-resistance which is strongly influenced by volume-to-area ratio [Lityński 1982; Grzesiuk, Górecki 1994]. Almost every grain has its length (a), thickness (b) and width (c). All these characteristics change with the moisture content in the grain. The shape of the grain may be illustrated by spherical coefficient, K1=c/a, K2=b/a.

The use of modern visual technology (digital image analysis systems) enables to calculate more complex image parameters existing in biological objects. They are based on area measurements, edge lines distance or substituted diameters [Guz 2009]. The description of phenomena and its effect on the stored material is now more specific and accurate. This is especially important in description of grain stored in high-volume silo, where the porosity is significantly diminishing [Bekasov, Denisov 1952]. The volume of intergrain spaces has a decisive influence on air-flow resistance [Bujak 1972].

Germination capacity is the most common factor studied after storage. Higher values of germination have grains of higher springness and resistance to stress, impact and thrust [Lityński 1982]. The susceptibility to deformation of grain after stress is higher due to its higher plasticity caused by high moisture content. At the low level of moisture the grains loose their plasticity and are+ very susceptible to internal break [Kolowca 1979]. Grain shape changes are by so far one of the most important factors that creates its quality and influences the conditions of ventilation process in silos [Waszkiewicz, Nowakowski, Sznajder 1999].

MATERIALS AND METHODS

Barley grains (cv Stratus) at initial moisture content of 14% were moistened to 16, 18, 20, 22 and 24% of moisture. The grain then was placed to cylindrical shaped vessels of 2l capacity. Vessels had a specially designed stress-developing mechanism (Fig. 1).

Fig. 1. Specially designed silo-stress simulator vessel

The stress values were 35,52 and 70 kPa accordingly to the stress simulation in silo conditions. Such a tension is equal to the thrust of over ten meters high bed of grain, which is common in industry plants. The grain was placed also to non-stressed vessels as reference material. The storage of commodity lasted until the stoppage of relaxation in the stressed layer. After storage 3 parts of volume of 30 ml were randomly taken from the vessel and mixed together. Every measurement was taken out with the participation of 100 grains taken from the mixture. Objects of the study were placed on specimen table that was illuminated with backlight to emboss the grain silhouette. Every measurement was taken 10 times with 10 grains which were placed on limited area to improve the measurement precision. Images taken digitally were stored for further analysis. After storage the images were digitally filtered to dual-color (binary image) (Fig. 2) which was the basis of measurements (SVISTMET).

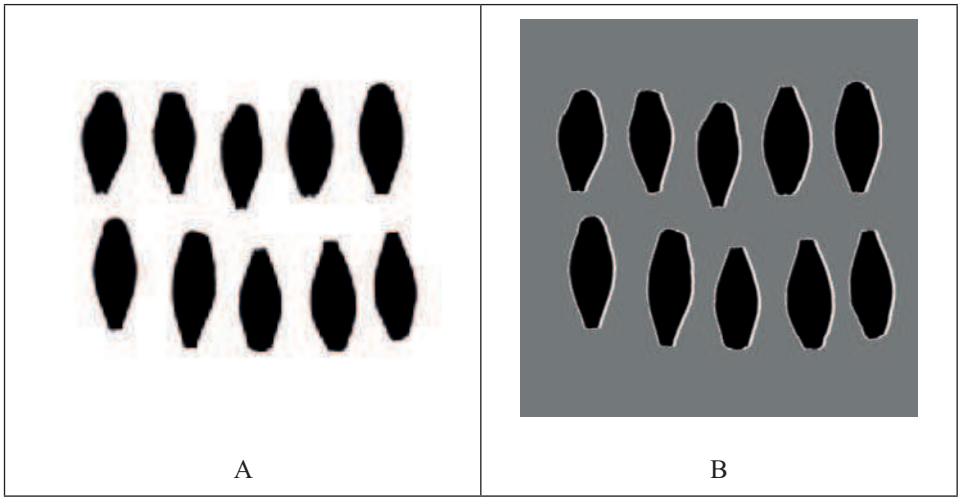

Fig. 2. Barley grain measurement images: A- digital primary image, B – binary digital image with edge line

The following data were measured: length, width, area of horizontal projection and shape coefficients:

$$K1=\frac{L}{S}$$

$$K2=\frac{4A}{PR}$$

where:
L – length of grain,
S- width of grain,
A – area of horizontal projection,
P – perimeter of grain,
R – radius of equivalent area.
RESULTS
The courses of horizontal projection area in dependence on pressure and storage temperature were shown in Fig 3 and 4. The area of grain changed insignificantly.

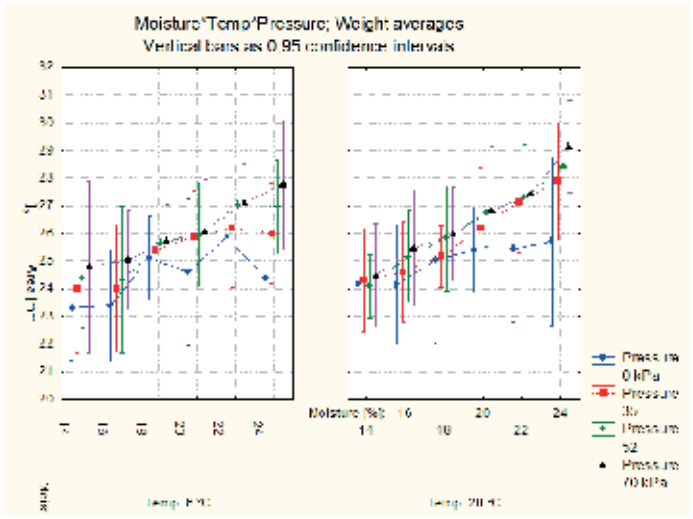

Fig. 3. Area of horizontal projection in dependence on silo pressure

The least changes were noticed for non-stressed grains. Those changes were not statistically significant. Although the commodity was a strictly selected sewing material and its dimensions were specified by sieve, there was still a problem with detecting slight deviations in grain dimension.

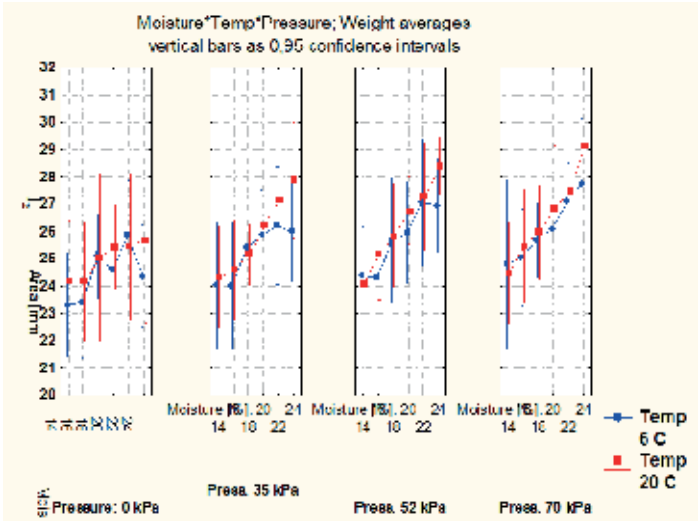

Fig. 4. Area of horizontal projection in dependence on storage temperature

The next factor analyzed in the storage was process temperature. The growth of grain plasticity after moistening at ambient storage temperature resulted in grain growth (Fig. 4). The course of area changes showed that moistening had a significant influence on grain size.

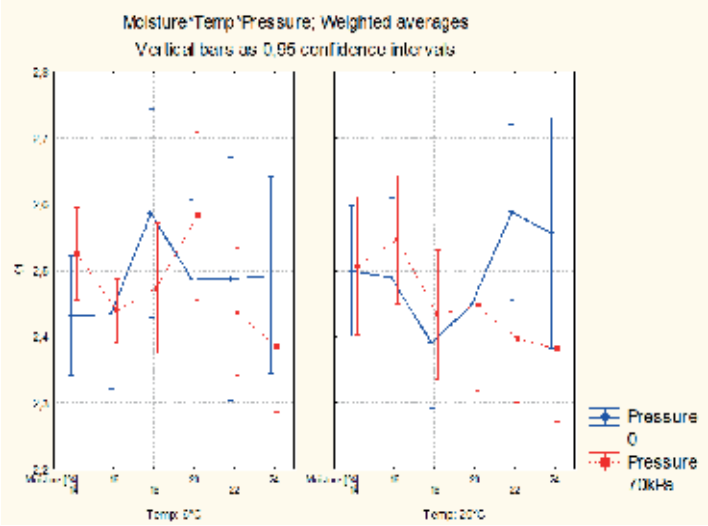

Fig. 5. The comparison of K1 changes caused by storage pressure

The pressure in the silo is not a significant factor of size changes in barley grains. The uniform pressure values were not the influent factor forming the grain size in the temperature range used in the experiment.

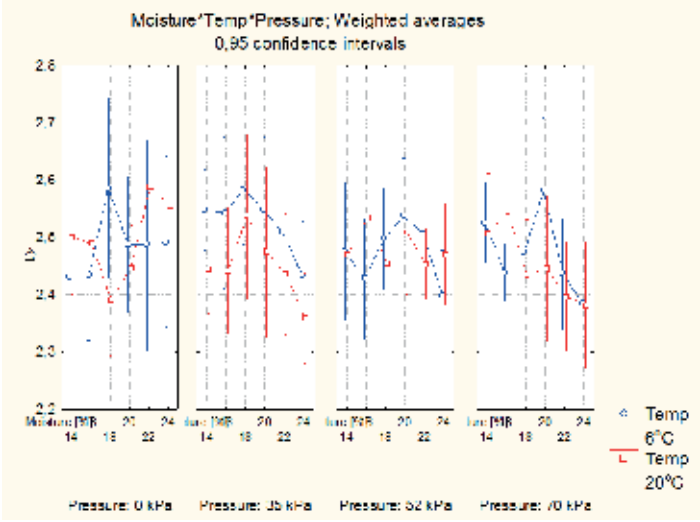

Fig. 6. The temperature course of K1 coefficient

The K1 coefficient changes were similar to the course which was independent of the silo pressure. The temperature taken into account as a factor forming the shape of barley grains was not influential to K1 slight deviations (Fig. 5) The K2 values represented stable, unchangeable factor through the whole pressure and moisture range values used in the experiment (Fig 7).

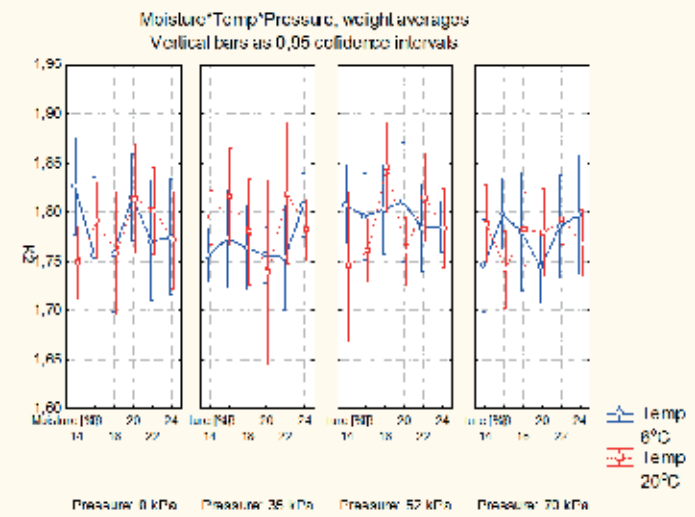

Fig. 7. The temperature course of K2 coefficient

Stability of K2 coefficient is a confirmation that the border line of the grain has a constant ratio in relation to other geometrical characteristics, taken into account during defining the K2 shape coefficient. The border line in the whole grain specimens was not distracted by deformations caused by bruises, breaks and other stable inconsistency of the grain outlines. Slight decrease of K2 value was observed only at 20°C and 52-70 kPa. (Fig. 7).

CONCLUSIONS

The experiment developed slight geometric changes of sampled barley grain caused by different factors. Among those factors moisture content, silo pressure and storage temperature were taken into account. On the basis of observations it was affirmed that moisture content and silo pressure were the most influencial factors that made these changes. The temperature of storage surprisingly wasn't the main factor significantly forming geometric parameters of barley grain measured in the experiment. Moreover, it was observed, that after storage of the commodity in silo conditions, all geometric parameters changes, expressed by shape coefficients were in aspect ratio to almost all storage conditions. This was a direct evidence that storage process was conducted without any harm to external structure of grain. This was shown by calculating the K1 and K2 shape coefficients. Only after storage at 20°C and higher pressure values a slight value drop of K2 was observed.

Acknowledgements

This research was funded by the State Committee for Scientific Research (KBN) of Poland and is part of the project N° N N313 013336.

REFERENCES

Agullo J.O., Marenya M.O. 2005. Airflow resistance of parchament arabica coffee. Biosystems engineering, 91 (2), 149-156.

Al-Yahya S.A., Moghazi H.M.M. 1998. Static pressure drop through barley grain. Canadian Agricultural Engineering. 40 (3), 213-217.

Bekasov A.G., Denisov N.I. 1952. Rukovodstvo po suške zerna. Zagotizdat, Moskva.

Bujak S. 1972. Przechowalnictwo surowców rolnych. WAR, Lublin.

Ciećko Z. 2003. Ocena jakości i przechowalnictwo produktów rolnych. WUWM, Olsztyn.

Dziki D., Laskowski J. 2004. Przewodnik do ćwiczeń z przetwórstwa zbożowo-młynarskiego. WAR, Lublin.

Giner S.A., Denisienia E. 1996. Pressure drop through wheat as affected by air velocity, moisture content and fines. J. Agicult. Eng. Res., 63, 73-86.

Grzesiuk S., Górecki R. 1994. Fizjologia plonów. Wprowadzenie do przechowalnictwa. Wydawnictwo Akademii Rolniczo-Technicznej, Olsztyn.

Guz T. 2009. The use of image analysis to estimate harvest ripeness of apples. TEKA Kom. Mpt Energ. Roln OL PAN, ,Vol 9, 61-68

Haque E., Achmed Y.N., Deyoe C.W. 1982. Static pressure drop in a fixed bed of grain as affected by grain moisture content. Trans. ASAE, 25 (4), 1095-1096.

Jankowski S. 1988. Surowce mączne i kaszowe. Przemysł Spożywczy. WNT, Warszawa.

Jayas D.S., Muir W.E. 1991. Airflow-pressure drop data for modelling fluid flow in anisotropic bulks. Trans. ASAE, 34 (1), 251-254.

Kamiński E., Cenkowski S., Zdrojewski Z. 1978 Opory przepływu powietrza przez warstwę ziarna kukurydzy. Roczniki Nauk Rolniczych, t. 73-C-2, 75-84.

Kolowca J. 1979. Wpływ obciążeń mechanicznych na uszkadzalność i wartosć biologiczną ziarna pszenicy. Rozprawa habilitacyjna nr 70. AR Kraków.

Kusińska E.*2008.* Hydraulic resistance of air flow through wheat grain in bulk *TEKA Kom. Mot. Energ. Roln. – OL PAN, , 8, 121–127*

Kusińska E 2006. Horizontal pressure on the wall of a model silo in relation to the moisture content of oats. TEKA Kom. Mot. Energ. Roln., , 6A, 115–122.

Lityński M., 1982.Biologiczne podstawy nasiennictwa. PWN.Warszawa.

Łukaszuk J. 2005. Wstępna ocena wpływu sposobu formowania złoża ziarna pszenicy na opór przepływu powietrza. Acta Agrophysica, 6 (3), 709-714.

Łuszczewski B. 1985. Uszlachetnianie i przechowywanie materiału siewnego PWRiL, Warszawa.

Molenda M. Montross M.D., McNeill S.g. Horabik J. 2005. Airflow resistance of seeds at different bulk densities using Ergun's equation. Trans ASAE, 48, (3), 1137-1145.

Pabis. J. 1978. opory przepływu powietrza przez warstwę niektórych roślin warzywnych. Roczniki Nauk Rolniczych, t. 73-C-2, 121-128.

Sacilik K. 2004. Resistance of bulk poppy seeds to airflow. Biosystems Engineering, 89 (4), 435-443.

Sokhansanj S., Falaciński A.A., Sosulski F.W, Jayas D.S., TangJ. 1990. Resistance of bulk lentils to airflow. Trans, ASAE, 33(4), 1281-1285.

Szwed G., Łukaszuk J. 2003. Ocena oporu przepływu powietrza przez warstwę nasion rzepaku. Acta Agrophysica, 2 (3), 645-650.

Tyburcy A. 1997. Prawidłowe magazynowanie ziarna zbóż. Przegląd Zbożowo-Młynarski, 11, 28-29.

Waszkiewicz C., Nowakowski T. Sznajder M. 1999. Resistance of airflow through the grain layer of amaranth. Agricultural Engineering, 34, 55-61.

ZMIANY CECH GEOMETRYCZNYCH JĘCZMIENIA PRZECHOWYWANEGO W WARUNKACH OBCIĄŻENIA PANUJĄCYCH W SILOSIE

Streszczenie. Praca przedstawia metodykę i wyniki oceny zmian cech geometrycznych ziarna jęczmienia odmiany Stratus po przechowywaniu w warunkach symulowanego laboratoryjnie obciążenia. Naprężenia o wartościach 35, 52 oraz 70 kPa były wywoływane w specjalnych cylindrach symulujących warunki przechowywania w silosie. Celem pracy było ustalenie przebiegu zmian cech geometrycznych nasion w zmiennych (wilg. 14, 16, 18 20, 22 i 24%; temp. 6°C oraz 20°C) warunkach ich przechowywania. Pomiary cech geometrycznych przeprowadzono z użyciem systemu SVISTMET. Wyniki badań wskazują, że zmiany cech geometrycznych nasion (statystycznie nieistotne) występują tylko w skrajnych warunkach przechowywania (20°C, 52 i 70 kPa) w warunkach wysokiej ich wilgotności (ponad 20%), która była głównym czynnikiem tych zmian.

Słowa kluczowe: jęczmień, silos, przechowywanie, cechy geometryczne, analiza obrazu

Publikacja powstała w ramach projektu badawczego własnego Nr N N313 013336

TEKA Kom. Mot. Energ. Roln. – OL PAN, 2011, 11, 114–122

INDOOR CLIMATE CONTROL IN EIB SYSTEM

Marek Horyński

Lublin University of Technology, Department of Computer and Electrical Engineering
20 - 618 Lublin, Nadbystrzycka 38A Str., e-mail: m.horynski@pollub.pl

Summary. The present article refers to the designing of an intelligent electric installation in the European Installation Bus (EIB) system. Its purpose is to present the problems associated with the assurance of human friendly indoor climate with particular emphasizing of the implementation of EIB TP system.

Key words: indoor climate, HVAC systems, building management systems, intelligent buildings, electric systems

INTRODUCTION

The idea of intelligent building has been created in the 70s of the 20th century in the USA. This concept was applied in the next decade in the scope of the systems designed to control the watering in greenhouses and in residential gardens. Together with the development of aforesaid systems, other installations have been automatized and connected together to form a centralized and integrated system in the building– Building Management System (BMS). The largest part of energy generated in the European Union i.e. about 40% of its total consumption is used by the buildings. The energy saving and application of renewable energy sources is considered as one of the most important methods of natural environment protection, undoubtfully contributing to the reduction of carbon compounds emissions released to atmosphere. The building operation costs and environment cleanness are affected by properly programmed climate in the rooms. The energy consumption in the building depends on the designed system and on its maintenance.

The climate in the rooms is essential for comfort, health and productivity of their occupants and increases our living standards. We spend most part of the day and night in various rooms [1, 3, 9, 10].

When designing an intelligent building, we have to pay particular attention to the balance to be maintained between our comfort and economical operation. The latter is affected by several elements established to achieve the same goal: to decrease the energy consumption, to reduce the maintenance costs, to ensure a simplified and elastic service.

The fact of diversified perception of the climate i.e. as comfortable or optimal is important in the framework of designing intelligent systems ensuring the indoor climate parameters control and constitutes the background of the present article.

DEFINITION OF VALUES DETERMING THE PARAMETERS OF INDOOR CLIMATE

Indoor microclimate is one of the most important elements included in the scope of building quality, because it is closely associated with human health and comfort. The Sick Building Syndrome term is connected with microclimate analysis. As a result of SBS (Sick Building Syndrome), some symptoms of sickness are possible e.g. headache, watery eyes, deteriorated concentration, breathing disorders. Many years research in the scope of human work environment quality contributed to the creation of the so called intelligent buildings. Their principal goal is the reduction of SBS effects and improvement of living comfort. The level of comfort perceived by occupant is essentially affected by the following factors:

- Air quality,
- Thermal comfort,
- Noise level,
- Conditions associated with ergonomics (lighting, windows, height of rooms etc.)

As a result of the research in the scope of Sick Building Syndrome – SBS, it appears that poor quality of indoor air is the main principle of illnesses in occupants of such type of buildings [2].

It is defined as a complex of factors negatively influencing the occupants of the room under consideration. SBS induces typical allergic reactions like conjunctivitis, chronic inflammation of larynx and bronchitis, asthma bronchiale and some other non- allergic symptoms are also specified – headaches, irritation, concentration disorders, humidifier fever as well as cancer diseases as the consequence of the affect of carcinogen substances e.g. tobacco smoke, asbestos or radon.

The Sick Building Syndrome has been permanently intensified, particularly in Western Europe and in USA. Therefore detailed investigations have been carried out by many companies and scientists [4].

The following factors causing SBS have been indicated:

- Improper air temperature and humidity,
- Improper lighting,
- Poor air quality,
- Noise.

The air quality is affected by several factors i.e.: ventilation of buildings, air temperature and its relative humidity, variations of pollutions originating of endogen sources, ambient air quality in direct vicinity of the building.

The natural air exchange is often minimized as a result of new technologies and use of energy saving solutions in case of a significant number of the buildings being erected actually in Poland.

The perception of comfort and the definition of comfort level are affected by subjectively perceived human impressions, but as a result of many years of scientific research and studies, the standardization of indoor climate parameters was possible [PN-78/B-03421 – Ventilation and air-conditioning. Indoor air design parameters for the rooms designed for permanent human occupation].

The optimal indoor climate is characterized by air temperature in the range between 16 up to 20°C and relative air humidity between 40 and 60%. However frequently, owing to diversified likes and likes of the occupants, the values of indoor air temperature and relative air humidity are different [5].

Every designer responsible for the designing of indoor climate control system has to resolve the problem associated with the determination of design inputs and preliminary assumptions to determine the purpose of the design and to enable its verification after the completion of the installation.

However we have to remember that the indoor climate, apart from the ventilation and air-conditioning parameters, also encompasses the interior design including, among others, the dimensions (height, width, length, height and type of windows, interior features, lighting).

In the connection with entry of EPBD Directive issued in European Union into force, it is ordered to ensure the correct energetic performance of the installation and consequently to consider the costs of object operation. Aforesaid Directive has been prepared in order to promote the improvement of the energetic performance for the buildings in the European Community. First of all the outdoor and indoor conditions of the building as well as projects rentability are considered therein.

The overheating of rooms occurs frequently, and in overdried air it is difficult to maintain the negative ionisation which is favourable for occupants.

The presence of electronic equipment, particularly the screens of TV sets and computers, floor linings made of improper materials, tobacco smoke and even dogs' hair – contribute to the generation of the climate with unfavourable ionisation.

CONTROL OF INDOOR CLIMATE FORMING INSTALLATIONS

The application of the technical solutions offering the individualization of indoor environment parameters is the most effective method contributing to increased number of occupants positively evaluating the indoor microclimate.

It refers to:

- Indoor heating control with consideration of the rooms occupancy,
- Immediate shutoff of the heater valve in case of window opening,
- Elimination of manual screwing in and out of the heaters valves and their replacement by the automatic temperature control vs. time and in accordance with individual preferences,
- Application of heating types ensuring a uniform heat supply (floor heating systems),
- Heating only the rooms where it is needed,
- Application of low temperature heating systems. A smooth heat exchange is possible as a result of low temperature on the feeding side. Thanks to the lack of continuous air circulation occurring in the vicinity of convection radiators, the amount of dust circulating in the rooms is significantly reduced. The heated floor creates less favourable conditions for mites and fungi spores living in dust.

The savings are also associated in the intelligent heating of the building. The conventional systems maintain constant temperature without considering any functions of the rooms and their occupancy periods. However our intelligent system performs temperature measurements in individual rooms and maintains it at desirable level. In the standby mode, the temperature is reduced by several degrees when it is recorded that the occupants left the building; in night operation mode - the temperature is reduced to the level preferred by the occupants.

In comfort mode, the optimal temperature is restored before the inhabitants will come back after work at programmed time. It seems to be not much, but as a result of heating control by means of individual temperature control in each room, more that 30% of energy can be saved.

In many studies in the scope of indoor climate, only HVAC installations are considered but it should be emphasized that the indoor climate is also associated with the interior arrangement and design or with correct lighting.

The analogue signals (mainly on sensors side) as well as digital signals (Fig.1) are used in EIB/KNX system. They convert analogue signals e.g. temperature into electric signals.

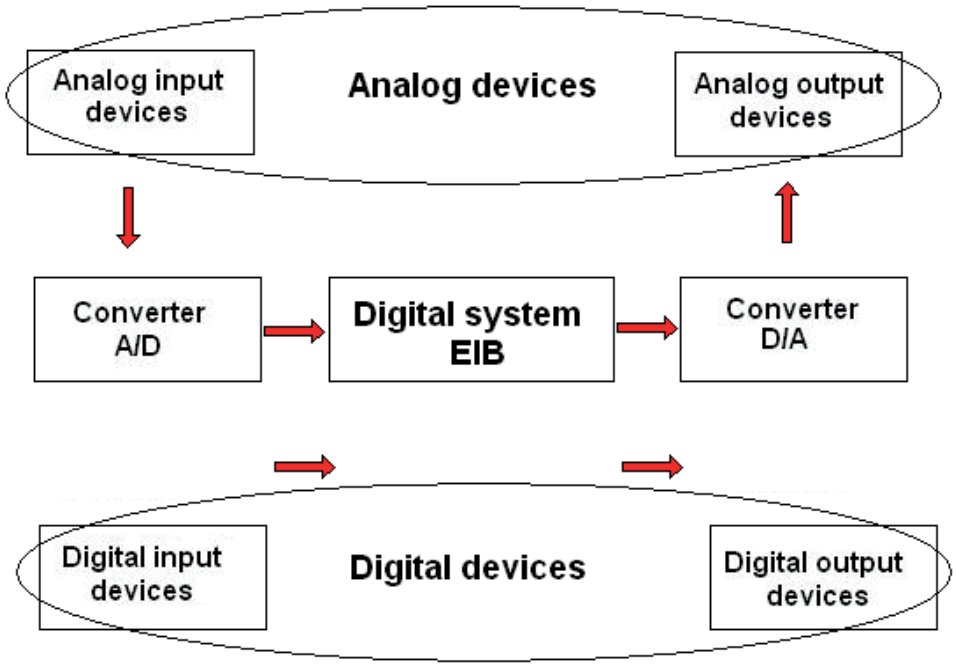

Fig. 1. Use of signals in system EIB[8]

Furthermore there are many other possibilities ensured by the indoor climate control for the users:

– Temperature control enabling diversified temperature settings in the building e.g. reduced temperature setting at night during sleep and increased temperature setting at the time of getting up and other activities before going out to work.
  In the buildings with integrated antiburglary system integration and HVAC installations control, the remote control of aforesaid systems is also possible.
– The control system installed in an intelligent building also prevents any unreasonable ventilation and air-conditioning, particularly owing to the fact that it frequently happens in the rooms which are not used at the moment. Therefore additional costs of unnecessary electric energy consumption are avoided. Thanks to the use of occupancy sensors, the information about necessity or lack of necessity to provide comfortable climate condition in an area is supplied to the system continuously.

The impact of the light is also extremely important to the indoor climate. The scope of main reasons of the sick building syndrome encompasses the improper lighting including too low or excessive illumination, its improper direction, dazzling, incorrect colour of light, strobe effect. The rooms with improper lighting make bad impression and are unfavourable for effective work or rest.

In order to ensure an efficient control for integrated systems, there many requirements to be met in all phases i.e. designing throughout their implementation, commissioning and finally the commercial operation [6]. It is one of the most important prerequisites contributing to the control systems development including lighting control systems.

The automatic lighting control by means of KNX/EIB system encompasses the following:

– Control vs. time for switching off the light sources in course of work breaks and weekends,
– Adaptation of the rooms lighting to optimal working conditions by means of the function maintaining the constant illumination and depending on natural lighting changes (Fig. 2). Therefore, in combination with intelligent heating control, it is possible to reduce the costs of energy consumption even by 30%,
– Automatic lighting control in the corridors, staircases and rarely used rooms by means of movement sensors.

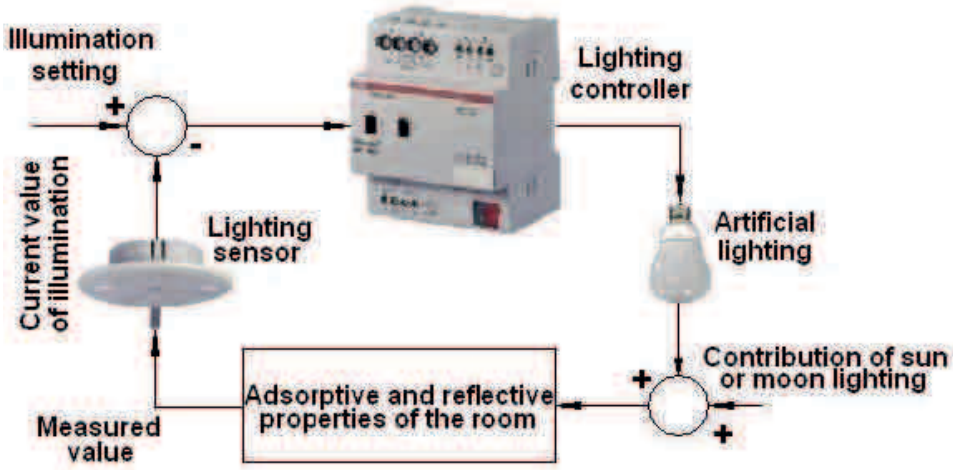

Fig. 2. Devices incorporated in EIB TP system and required to perform the function maintaining the constant illumination [7]

The lighting controller and light sensor are used in order to maintain the constant illumination in the room. This sensor is installed on the roof in order to enable the measurement of the surface lighting within its detection range. The measured value is compared with setting thereafter. As a result of this comparison, the difference between the settling and actual illumination value is minimized. The influence of the sensor surrounding is also important. If its surrounding is lighter, the contribution of artificial lighting is limited and increased in case of darker surrounding. The setting is established by means of the illumination meter, which is incorporated under the light sensor for this purpose.

The essential advantages resulting from the use of the control systems are:

– Flexibility – enabling the reconfigurations of circuits being controlled in case of any changes in interior arrangement, without any necessity of physical intervention into the installations,
– Energy saving – enabling reduced consumption of energy for lighting purposes even up to 70%,
– Improved visual conditions for work and possibility of user's intervention into lighting intervention,
– Possibility of lighting scenarios realization.

The lighting must meet several conditions, the most important ones are:
- The value of average illumination within the surface under consideration is conforming to standard
- Lighting uniformity in space and time
- Correct luminance distribution
- Light colour adapted to needs.

The average illumination *E* is determined as the ratio of total luminous flux inciding onto the surface area under consideration and the size of this surface area. The lowest permissible values of average illumination in all types of rooms are included in the standard PN-84/E 02033.

The uniformity of lighting ε on the surface consists in the maintenance of the average illumination in various points of illuminated surface area of the room.

The ratio of the lowest value of illumination to its average value should not be lower than 0.65 within the room, on the working plane.

The light colour is a very important parameter of lighting, because it may affect the human psyche as well as ability to perform the work correctly. Most favourable are the sources generating the light with the colour similar to daylight.

The lighting efficiency method as well as point method and computerized programs e.g. Dialux, Calculux, Relux are most frequently used for the lighting calculation.

Lighting efficiency method

The lighting efficiency method is based upon the general lighting efficiency and the luminaire efficiency. The lighting efficiency $\eta_{oś}$ is defined as the ratio of useful luminous flux inciding onto the surface area of the plane being illuminated to the luminous flux emitted by the light sources in the luminaire.

The reflection indices for the walls and ceiling are assumed from the calculation table containing the general lighting efficiency. The distance "h" between the light sources and working plane and the room index are calculated thereafter in:

$$h = H - H_b - L_{zw} \tag{1}$$

where:
h – distance between the light sources and working plane,
H – height of the room ,
H_b – height of the work field;
$L_{zw.}$ – length of luminaire suspension.

$$w = \frac{0.2a + 0.8b}{h} \tag{2}$$

The calculation of total luminous flux required to generate the illumination $E_{śr}$ in the room is performed after transformation of the following equation:

$$E_r = \frac{n\Phi K\eta}{ab}\frac{\eta'_{op}}{\eta_{op}}, \tag{3}$$

where:
$E_{śr}$- average illumination within working plane under consideration,
n – number of luminaries,

Φ – summarized luminous flux,

η_{op} – luminaire efficiency,

η'_{op} – actual luminaire efficiency,

η – lighting efficiency, considering the reflection indices of the ceiling, walls and floor, luminaire efficiency and index of use,

a – length of the room,

b – width of the room,

$k = 1/K$ – reserve ratio considering the reduction of illumination level parallel to the period of use, closely associated with an efficient maintenance system; included in table. The reserve ratio depends on the type of lighting, its class luminaire efficiency, room index as well as reflection indices of the ceiling and walls.

Having calculated the summarized luminous flux Φ for light sources, we can select the light sources ensuring the required values of summarized luminous flux and average illumination as recommended by standards. Then the power required for lighting and actual average illumination are calculated.

$$P = nP_n \tag{4}$$

where:

n – number of light sources,

P_n – power of single light source.

$$E^*_{r.} = E_{r.}\frac{\Phi^*}{\Phi} \tag{5}$$

where:

Φ - summarized designed luminous flux of light sources,

Φ^* - summarized actual luminous flux of light sources.

The lighting scenes system applied in intelligent installations, makes it possible to program even several lighting scenarios in the same room, lamps dimming, maintenance of constant lighting level.

Point method

In the framework of the point method, the horizontal and vertical components of the illumination in a design point are calculated:

$$E_{hA} = \frac{I}{r^2}\cos\alpha\,, \tag{6}$$

$$E_{vA} = \frac{I}{r^2}\sin\alpha\,, \tag{7}$$

$$E = \sqrt{E_{hA}^2 + E_{vA}^2} \tag{8}$$

where:

I – candle power of the lamp read from the candle power transmission curve,

α – angle used for the determination of candle power (Fig. 3.).

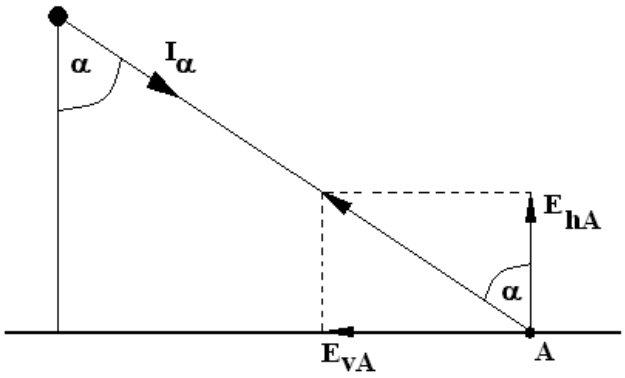

Fig. 3. Determination of horizontal E_{hA} and vertical E_{vA} illumination

RECAPITULATION

The requirements associated with indoor environment were continuously increased in recent years. As a result of the experience gained in the past, it is obvious, that the future of intelligent buildings installations is very optimistic. The dynamic development of electronic sector and its progressing miniaturization contribute to the construction of more and more modern automatic systems including the building management systems. Sick Building Syndrome and indoor climate are the essential issues associated with the modern building systems. They demonstrate the fact that the modernization of human life brings also some dangers to be continuously monitored in order to avoid or at least reduce their negative impacts.

REFERENCES

Directive 2002/91/EC issued by European Parliament and European Council on 16th December 2002 concerning the energetic quality of the buildings.

Felcyn E. W.: The air quality at home. Article available on website: http://www.creon.pl, 2004-05-02.

Jelondz, D., Spasokukotskiy, K., Ruser, H.: Concept and realisation of an EIB based automated room climate control In Proceedings of EIB Conference. Technical University Munich, 2001.

Kabza Z., Kostyrko K., Zator Sł., Łobzowski A., Szkolnikowski W.: Adjusting the microclimate of the room. AGENDA PAK Publishing Edition, 2005.

PN Standards PN-78/B-03421 - Ventilation and Air Conditioning. Calculation parameters of indoor air in rooms intended for permanent human habitation.

Olga Plaksina, Thomas Rausch: Fieldbus Systems and their Applications, Vol. 6, Part 1, 2005.

ABB Directories: Lighting. Constant lighting control, 2010.

Internet service: www.zabezpieczenia.com.pl, 2009.

Spasokukotskiy, K. Jelondz, D. Traenkler, H.-R.: Technical base for separated rooms climate automatic control. Univ. der Bundeswehr Muenchen, Neubiberg, 2002.

Spasokukotskiy, K.; Trankler, H.-R.; Lukasheva, K. Intelligent Data Acquisition and Advanced Computing Systems: Technology and Applications. Proceedings of the Second IEEE International Workshop, 2003.

STEROWANIE KLIMATEM POMIESZCZEŃ W SYSTEMIE EIB

Streszczenie. Niniejszy artykuł dotyczy projektowania inteligentnych instalacji elektrycznych w systemie EIB (European Installation Bus). Poruszono w nim zagadnienia związane z zapewnieniem przyjaznego dla człowieka klimatu pomieszczeń. Szczególną uwagę zwrócono na implementację do tego celu systemu EIB.

Słowa kluczowe: klimat pomieszczeń, systemy HVAC, systemy zarządzające budynkiem, budynek inteligentny, instalacje elektryczne

TEKA Kom. Mot. Energ. Roln. – OL PAN, 2011, 11, 123–134

COMPUTER – AIDED DESIGN OF VIRTUAL SUPERVISION SYSTEMS FOR THE ELECTRIC SYSTEM IN CONTEMPORARY BUILDINGS

Marek Horyński

Lublin University of Technology, Nadbystrzycka 38 D Str., 20-618 Lublin

Summary. The purpose of the present article is to discuss the role of the information system in the building management systems as well as the use of computers for computer – aided design and operation of intelligent electric systems in contemporary buildings. Special attention is devoted to KNX system as one of the most popular systems applied in the buildings management solutions. The article presents the basic principles of the creation of KNX system design in TP (Twisted Pair) version in ETS4 tool and the procedure of its startup.

Key words: intelligent electric systems, designing, integration, virtual supervision

INTRODUCTION

The idea of intelligent building engineering and so called intelligent systems became popular and more present in our everyday life in recent years. Nowadays "an intelligent" house is not a luxury any more but becomes a more and more commonly applied solution. The first electric systems in the buildings were equipped with conventional accessories i.e. fuses, sockets, circuit – breakers, cam switches, light fittings. Owing to continuous trends towards the improvement of the standard of contemporary buildings, further development in the scope of the conventional electrical systems is practically impossible. The development of electronic engineering and computerization in many fields of life is also reflected in the electric systems sector. New control and regulation systems are created by the manufacturers of the systems equipment introducing control engineering solutions into building management systems. Owing to their advanced development and complexity, it is necessary to find a new approach to the designing of these systems, power supply methods, as well as to the localization and elimination rate of potential disturbances [7, 8].

The intelligent electric systems have been created simultaneously with the general access to personal computers. The field of the computers applications has also been extended to the private companies and industrial centres. The reason of these changes was obvious – using the computer with proper software the companies were able to meet the investor's need in a faster and more effective manner and consequently to survive in the market. However, the role of the computer was not essential in the work of designers, because appropriate tools to be installed in the computer i.e. dedicated software are more important.

At that time it was a group of specialized computer programs enabling the creation of the diagrams of conventional electric systems e.g. CAD programs. Furthermore, the designers could perform the computations and to prepare the design documentation by means of computation support software and text editors, for example by means of MathCad and Word.

Another new application of computers in the intelligent systems consists in their use for the startup (activation) of the components of the intelligent systems as well as for the supervision over and control of the building systems [1, 5, 9, 10].

INFORMATION SYSTEM.

The information system performs an essential role in the contemporary modern buildings as an important element of automated systems. Such solution makes it possible to ensure the communication between the elements being the components of the building management systems. The adherence to relevant principles as early as in the course of its construction is important for the correct functioning of an information system.

Most often there are four levels (stages) in the structure of this system (Fig. 1):

- The system encompasses several subsystems (at least two) and constitutes an assembly of interconnected parts creating the whole. Each system performs the role of a subsystem in a higher order system (or: a higher order system performs the role of a superior system over the lower order system) e.g. heating control system in the building can perform the role of the subsystem in BMS (Building Management System). The purpose of the information system is to enable the acquisition and processing of information necessary for correct management.
- The subsystem is an element included in the higher order system. It is isolated in the system through the establishing of principles which correspond to relevant objectives in the systems and to management tasks. Another criterion used for the subsystem definition is its function performed in the system e.g. planning, records, inspection etc. or in accordance with other established principles. The subsystem is provided with a decision making member responsible for the decision making process in the determined decision area.
- The functional unit constituting a part of the subsystem is the smallest element of the whole structure of the system, which can be operated independently. The task of the functional unit consists in the processing of a separate task. The functional units are separated in a manner enabling the operation of every unit in one processing sequence.
- The module constituting a component of the functional unit encompasses a separate fragment of an issue e.g. temperature measurements in individual rooms and heating medium control in accordance with pre-programmed temperatures. The module is situated on the lowest level in the system's hierarchy structure. Its implementation is the easiest but independent operation is impossible.

The system, subsystem, functional unit and module constitute the levels (stages) in the system's structure. The structure of an information system is presented below as the model of modular structure. Such structure makes it possible to combine the simplest elements (modules) in an easy manner and to create various forms of higher order structures. Such systems are easy to design and implement and can be easily modified in accordance with varying requirements of the user.

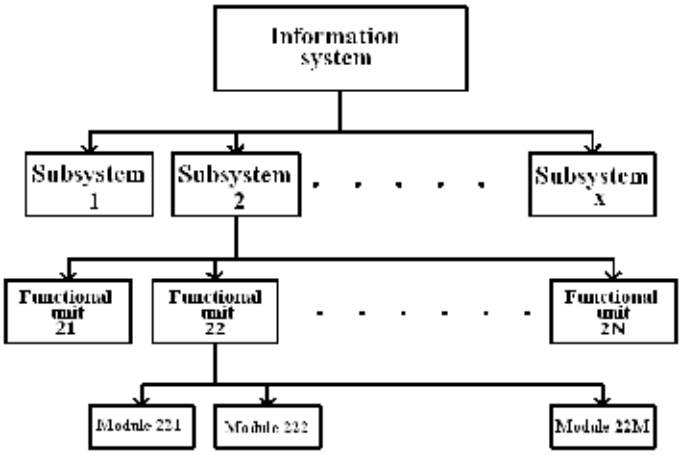

Fig. 1. Diagram of the information system structure [3]

KNX BUS SYSTEM; TP TYPE

The control structure applied in the building management systems is frequently called the complex processes control structure in the literature. The systems contain several controlled inputs with $u_1, \ldots u_j, \ldots, u_m$ signals and with the following operators A_i:

$$y_i = Ai(u_1, \ldots u_j, \ldots, u_m), \text{ where } i=1, 2, \ldots j, \ldots, n \quad (1)$$

In particular case of a multidimensional linear system the form of the equation (1) is as follows:

$$y_i = \sum_{j=1}^{m} L_{ij}(u_j), \text{ where } i=1, 2, \ldots j, \ldots, n$$

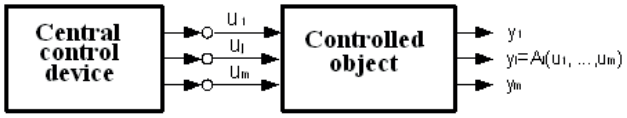

Fig. 2. Multidimensional system [10]

In case of the systems characterized by several impacts, the central control device (Fig. 2) can be substituted by several local devices C_i, i= l, 2,..., n, performing the control functions for individual subsystems. This solution is presented for m=n (Fig. 3).

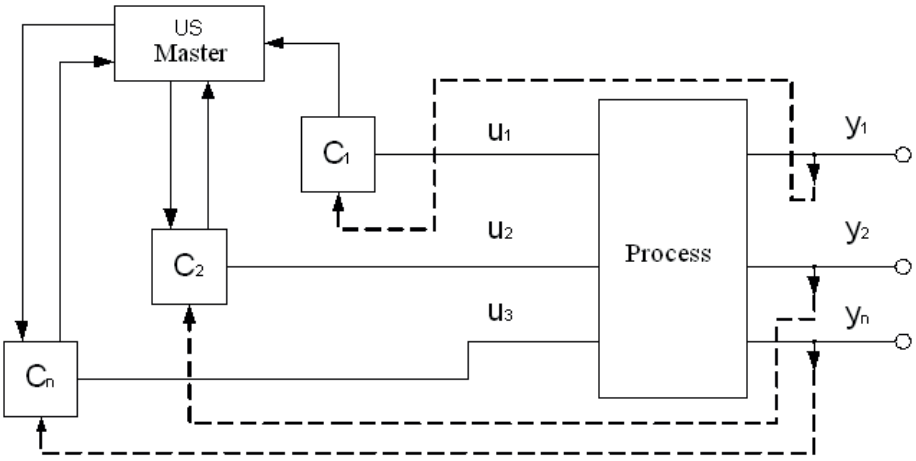

Fig. 3. Multidimensional system control by means of local devices and superior tool [3, 10]

The purpose of the superior control device is to coordinate the operation of local devices in order to subordinate to local objectives of separate subprocesses to the common global objective as well as to consider the interrelation of process outputs and inputs. The coordination is achieved through the continuous data flow between the local control devices and superior control devices.

The systems in accordance with Fig. 2 are called the centralized control systems and the systems in accordance with Fig. 3 are called the decentralized control systems.

The decentralized control systems prevail in the complex system for the processes control. Their role is important in the scope of processes automation in industry, building engineering and in other fields of our life. The principal advantage of these systems consists in their ability to perform rather complex functions by means of relatively simple tools. The volume of data to be processed by the local and superior devices is significantly lower than the volume of data to be processed by means of single control system in the centralized system.

In order to enable the correct functioning of the decentralized system, it is necessary to coordinate the functioning of the local devices and systems through the selection of the efficient links enabling fast data transfer. Unless this requirement is met, the functioning of the decentralized system will be significantly worse than the functioning of the centralized system.

In a majority of control systems, the control devices for individual processes are arranged in the form of pyramid or hierarchical structure (Fig. 4). The hierarchical structure belongs to the group of decentralized structures in case of determined freedom of the individual subsystems containing the decision making members or devices in the decision making process. The hierarchical centralized structure is also possible with all the decisions made by the member situated on the top of the hierarchy and with other members completing the orders issued by the central member. This structure contains the controlled objects O_1,..., O_n, (with interrelations ignored in order to simplify the problem), local control devices C_1^1,..., C_m^1, second level control devices C_1^2 , ... etc. Every set of objects e.g. O_1, ..., O_n and C_1, ..., C_n. C_1^1 can be considered as a subsystem (indicated in Fig. 4 by means of dashed line and letter P_1) controlled by the higher level device (in case of P_1 - C_1^2 performs the role of superior device).

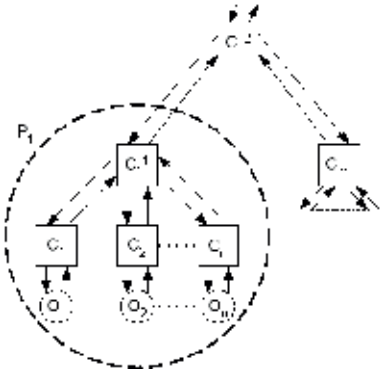

Fig. 4. Hierarchical structure [3]

The integrated systems are characterized by “distributed intelligence”. Therefore, the individual devices arranged in the whole building can perform their functions in an undisturbed manner, even in case of interrupted communication with the superior managing units. It is possible, thanks to the controllers equipped with individual microprocessors and memory used for storage of the controller operation data. Therefore, the various systems can be controlled in local mode without necessity of permanent intervention of the system operator. Such solution increases the system reliability and reduces the time of reaction to various hazards and alarm conditions. The possibility of optional modelling of the system shape should also be emphasized, because the system flexibility is ensured – enabling its continuous adaptation to the needs of an organization.

EIB (European Installation Bus) actually called KNX is defined as a bus system with tree structure (the system can be branched but without forming any loops).

The line (branch) is the basic part of the structure used for the connection of system elements (maximum 64), sensors and actuators. Several lines (max 15) can be integrated together to form an area by means of special devices, for instance linear couplings. It is possible to integrate fifteen areas into one system (Fig. 5) by means of individual area couplings.

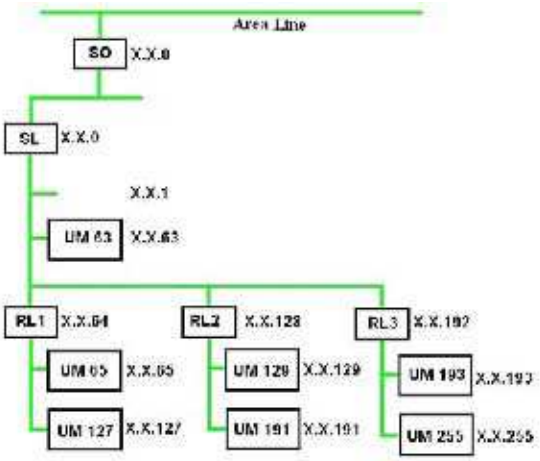

Fig. 5. KNX system: SO – Area coupler, SL – Line coupler, RL - Line Repeater, UM – bus unit [2, 4]

EIB (European Installation Bus) integrates more than 50000 bus elements together; the communication elements can communicate with each other in the form of information exchange irrespective of the location of their connection to the bus.

The system elements communicate with each other usually in local mode [12]. In case of the occurred event, determined commands are issued by the sensor in the form of telegrams transmitted between the sensor and actuator. The Carrier Sense Multiple Access /Collision Avoidance [CSMA/CA] protocol has been applied as the bus access mechanism warranting collision free and equal right access (of BCU module) to the bus [2, 6, 12, 13].

Algorithm of asynchronous CSMA/CA protocol is presented in Fig. 6.

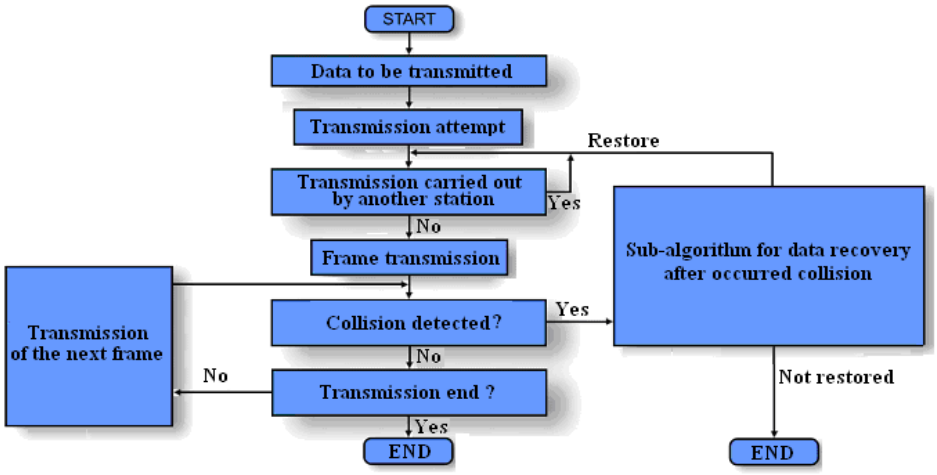

Fig. 6. Algorithm of bus access mechanism in KNX system [2, 11]

Therefore the transmission of messages can be commenced any time by the elements participating in the transmission but they have to verify if the network is not busy by other transmission. The system elements (sensors or actuators) are provided with assigned priorities. In case of transmission process commenced by two sensors simultaneously, the transmission is withheld by the sensor with lower priority and restored after the completion of the transmission by the sensor with higher priority. In case of both sensors with the same priority, the decision on transmission order depends on the physical address. The physical address is a unique number assigned to every element of the system in order to determine the telegram recipient and the localization place of the device. The element with the higher physical address releases the bus for the element with the lower address [12, 13, 14].

The communication telegram sent by the sensor propagates along the whole line. The messages are received by the actuators being the recipients of information; the receipt notification is sent by the recipient to the sender. The telegram must be ignored by other users who are not its recipients. The linear coupling preventing the propagation of information along the whole bus is extremely important in such situations. The coupling performs the role of a filter – amplifier. At the time of the system activation in the coupling, a filtering table is automatically recorded in order to determine the telegrams to be amplified and transmitted and the telegrams to be attenuated. The information flow as well as filtration is possible in both directions.

In case of a telegram sent for example by the sensor from the line 3 and to be received by the actuator situated in the line 13, this telegram is furnished to the linear coupling 3 and passed by this coupling to the main line. Then the telegram is passed through the linear coupling 13 and furnished to the recipient. At this time the telegram is locked by the linear couplings 1,2...14,15 and sent via the main line without reaching these lines. Therefor, the communication is possible within these lines in a parallel mode. Identical filtering tables are incorporated in area couplings in a manner enabling unrestricted information transfer to the elements located in other parts of system structure. The telegram transfer process to other areas is identical.

COMPUTER – AIDED DESIGN

A wide group of programs dedicated for computer – aided design of electric systems in conventional version was available at the time of the creation of intelligent electric systems. Therefore it was obvious that more advanced programs will be developed to facilitate the designing of intelligent electric systems. Furthermore it should be emphasized that the programming by means of the computer is required for some installations of intelligent electric systems.

The designing process of an intelligent system consists of several phases diversified with respect to their degree of difficulty and time consumption. All requirements included in the standards, regulations and recommendations concerning the issue under analysis should be considered and met in every phase. The majority of designing activities can be automated and optimised to a significant degree by means of computer – aided design systems.

The wide spectrum of computers with diversified hardware architecture, functioning in the framework of many various operating systems has been created as a result of intensive development of electronic engineering and information systems. However, the disadvantage of this diversity consists in the fact that the software elaborated for a hardware platform most often will not work on the computer with another platform.

ETS4 SOFTWARE TOOL

ETS4 software tool (European Installation Bus Tool Software) is required for the designing, startup and further servicing of the installations in KNX TP system. ETS4 software tool is distributed by the Association of KNX system devices manufacturers and dedicated for operation in Windows environment as the standard program for EIB systems installations. ETS4 is a modular program consisting of several parts supporting each other. The scope of basic properties of ETS4 program encompasses the automatic creation of the system documentation encompassing the plan of the system, addresses allocation list and the list of applied bus elements. At the installation startup all data and information concerning the installation functioning, diagnostics and service are transferred to the memory of corresponding bus elements.

The special symbols and names of bus elements with various application, established by Konnex Association responsible for the certification of devices in this systems, are used in KNX system designing and automatically entered by ETS4 package into the plans and diagrams of the systems i.e. into its electromagnetic part (230/400V) and bus(24V). After startup, the main window is opened (Fig. 7.) with pushbuttons enabling the access to the next parts of the program.

Fig. 7. Starting window of ETS4 program – commencing of the new design creation

The individual program windows contain: the modules responsible for the selection of design saved in the computer or for the commencement of work associated with a new design, designing, installation of KNX TP system apparatuses from the manufacturers in base program if the use of their devices is intended by the designer, program setting, option selection menu; startup and testing.

The devices can be inserted directly into the design or the building structure can be created at the beginning with subdivision into the storeys and rooms.

In the second case the devices are located at the places of their factual installation in the real object i.e. the apparatuses to be installed in switching stations are located in switching stations and control apparatuses in the rooms from which the bus telegrams are sent to the actuators. The designing principle consists in the dragging of individual “building objects” to the design, with logical reservation that the larger object must not be inserted into the smaller object.

The first step of systems designing is associated with the selection and planning of the layout of bus elements in the building. At the selection of the devices for KNX systems the following principles should be adhered to:

- For each bus line, at least one power pack should be selected with the coil with rated current sufficient to provide the power supply for all devices connected to the line.
- The length of the conductors for single line should not exceed 1000 meters. For more complex topological structures (containing the level higher than basic) one linear coupling should be selected for each subordinate line.
- When designing the line routes in the building, the quantity of devices to be directly connected to this line should be considered in order to not exceed their permissible quantity determined by the address space.

The simplest KNX system able to function in the building consists of one power pack with coil, two – wire bus cable, one actuator and one sensor as well as KNXnet/IP router coupling KNX system with the computer network of the building in order to enable the communication by means of IP network.

OPERATING PRINCIPLE OF VISUALIZATION SYSTEMS

The operation of the visualization and control systems is determined through the so called Objects determining their types, functions and interrelations [3]. The following items can be classified as the objects; editable data from panel, symbolic names of programmable controllers supporting the system, buffers of messages. The objects can be also created in the form of graphical elements, icons, windows and alarm messages pages as well as elements located on the screens. The objects enabling the control system support and its visualization are a very important group of the objects. The system support is possible by means of the following objects: virtual switches (pushbuttons, switches), real pushbuttons and input fields used for data entry. The objects enabling the visualization encompass the following scope: binary states displays, output fields (text and numerical fields) as well as virtual meters.

Analysing the hardware and software mechanisms used for the control over the object automation system on the levels of individual tiers of hierarchic model of information exchange in the object, we can find that on the level of direct control tier in KNX TP standard, the simple optical and audible signal devices as well as liquid crystal displays (LCD) and HMI panels are very often used as the system status visual presentation mechanisms.

In case of hardware elements used for the visualization and control purposes in residential objects, the aesthetical feature of the component, possibility of its integration with interior design as well as the manner of the presentation of automatic control system devices status are principal criterion for the selection of proposed solution.

The communication protocols are another criterion essential for the applications area of a visualization component.

In case of automatic control system based upon KNX standard, the elements dedicated for the visualization of and control over the system operation are usually characterized by very limited possibility of extension and their implementation in other automatic control systems. The visualization devices (mainly HMI panels) are equipped with additional interfaces (e.g. RJ-45, USB) enabling the achievement of their objective on the level of higher control tiers (mainly in superior control tier).

The interfaces applied in this standard constitute in a way the equivalents of external communication cards. The information received from the bus or sent to the bus (occurring as a result of the telegrams with the queries concerning the address group status or as a result of bus watching)

is copied to the cache of KNX interface and sent to visualization system after its conversion. In order to enable data exchange with KNX system bus, one communication program constituting and integral part of communication system is usually used. This program is completely independent of the hardware elements used in the automatic control system owing to complete standardization of BCU units construction.

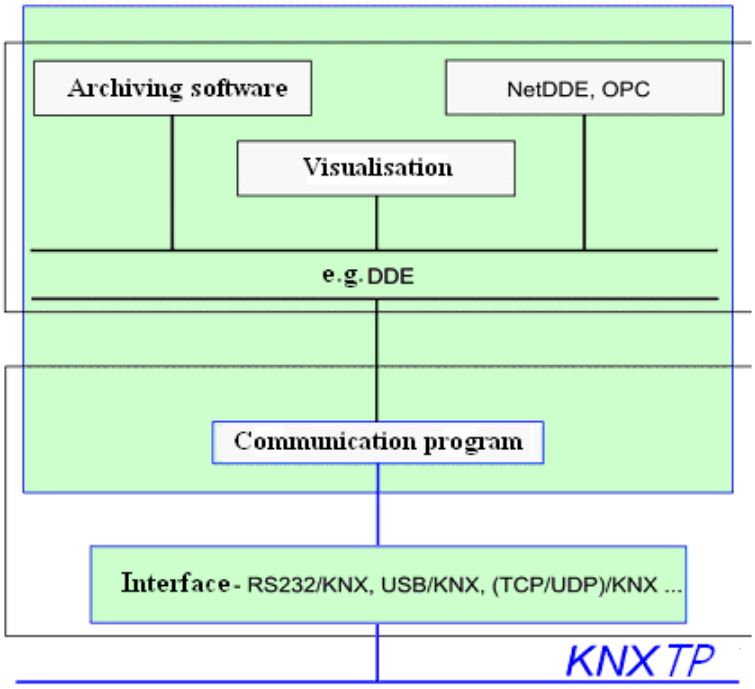

Fig. 8. Data exchange mechanism in visualisation application in KNX system [11]

In case of KNX automatic control system, the application of superior Building Management Systems (BMS) is not obligatory [8]. This type of systems is usually applied in large objects characterized by significant topological span of the automatic control system. The aim of the achievement of economical benefits associated with savings by the users in the scope of electric energy, heating medium energy etc. as well as increased comfort of object use is the principal factor contributing to the application of the Building Management System in an object. An example of such management completed by means of WinSwitch 3 program is presented in the diagram below (Fig. 9).

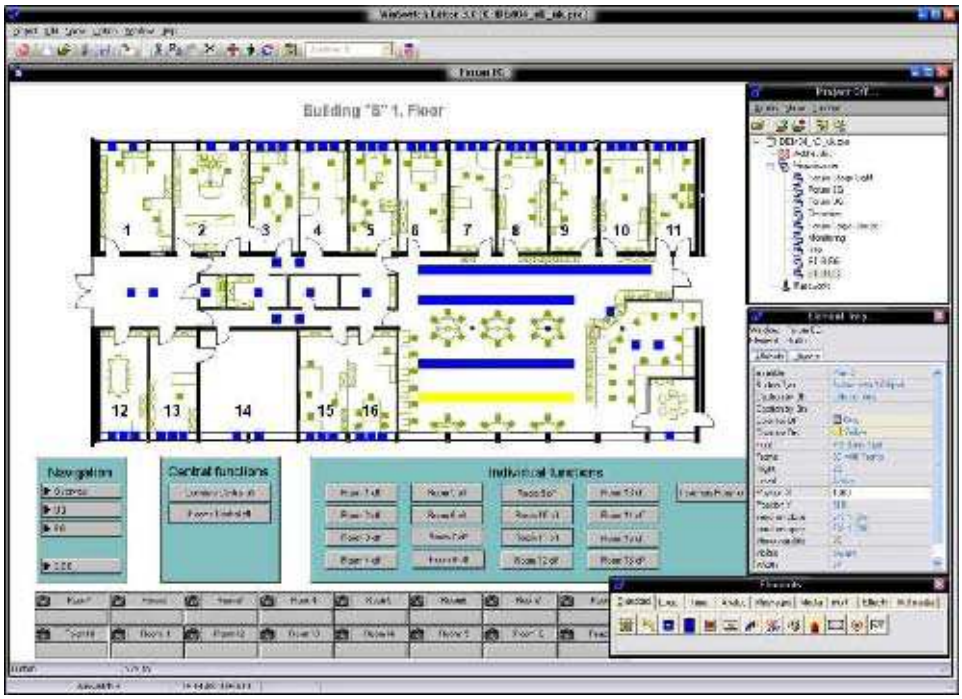

Fig. 9. Intelligent systems management by means of WinSwitch 3 program

CONCLUSIONS

The electric systems are an inherent element of every contemporary building. Initially their sole task was to provide the power supply for electric energy receivers. Owing to technology progress, the automatic control elements occurred in the systems in order to increase their safety, functionality, comfort and electric energy saving. The information systems in intelligent buildings are their indispensable component, irrespective of its scale, advancement degree and applications area. More than 20 years ago a communication standard has been created to enable the communication between distributed BMS devices. Initially called EIB and after conversions known as KNX - this open standard makes it possible that the devices from various manufacturers support each other. The application of IP network for communication between KNX system devices has been launched in recent years. This solution creates huge opportunities for the electric energy management via the Internet.

REFERENCES

Buczaj M., Sumorek A.: The virtual supervising system controlling the operation of the intrusion and hold -up alarm system. Motrol - Motoryzacja i Energetyka Rolnictwa, Volume 12.

EIBA/Konnex Org. EIB Installation Bus.: Instructors Seminar. EIB Interworking Standards. Bruksela, Belgia 1999.
Chilimoniuk T. : The analysis of intelligent installations systems in residential building. Master thesis. Lublin University of Technology 2003.
Drop D. Jastrzębski D „ The contemporary electric installations in single houses construction using the equipment manufactured by Moeller Company" COSiW SEP Warszawa 2002.
EN-50131-1:1997 Alarm system – Intrusion system – Part 1:General requirements.
Horyński M.: The application of binary inputs and outputs in management systems of an intelligent building. Electric Engineering Review 7/2010, p. 218-220.
Horyński M., Majcher J.: The possibility of installations status visualization in intelligent buildings. Drives and control – Technical and information monthly No 12(140), p. 90-92.
Kamieński K.: Programming of operator panels. Wydawnictwo Gryf. Edition I, 2007.
Koczyk H. Antoniewicz B. Sroczan E. „ The modern technical fitout for single family house" Państwowe Wydawnictwo Rolnicze i Leśne, Poznań 1998.
Kulikowski R. „ The control in large systems" WNT Second edition Warszawa 1974.
Luchowski G.: The information systems for the installations operation visualization in an intelligent building. Master thesis. Lublin University of Technology 2009.
Mikulik J.: European Installation Bus. Distributed safety and comfort control system. COSiW, Warszawa 2009.
Petykiewicz P. „ The modern electric installation in an intelligent building" COSiW SEP Warszawa 2001.
Petykiewicz, P.: The building management systems - Instabus EIB. Siemens Sp. z o.o., Warszawa 1999.

KOMPUTEROWE WSPOMAGANIE PROJEKTOWANIA WIRTUALNYCH SYSTEMÓW NADZORU INSTALACJI ELEKTRYCZNEJ WE WSPÓŁCZESNYCH BUDYNKACH

Streszczenie. W artykule omówiono rolę systemu informatycznego w systemach automatyki budynkowej oraz wykorzystanie komputera do wspomagania projektowania i uruchamiania inteligentnych instalacji elektrycznych we współczesnych budynkach. Główną uwagę poświęcono systemowi KNX TP, jednemu z najpopularniejszych systemów stosowanych w automatyce budynków. Podano podstawowe zasady tworzenia projektu instalacji KNX TP w programie narzędziowym ETS oraz procedurę jej uruchamiania.

Słowa kluczowe: inteligentne instalacje elektryczne, projektowanie, integracja, nadzór, wirtualny

TEKA Kom. Mot. Energ. Roln. – OL PAN, 2011, 11, 135–142

MUTUAL SUPPORT OF INTELLIGENT BUILDING COMPONENTS IN THE SCOPE OF LIGHTING CONTROL

Marek Horyński, Wiktor Pietrzyk

Lublin University of Technology, Nadbystrzycka 38 D Str., 20-618 Lublin.

Summary. The purpose of the present article is to discuss the components of intelligent electric systems used in the building management systems for the lighting control and to present the methodology in the scope of their design using KNX/EIB system as an example. The role performed by KNX/EIB system, previously called EIB (European Installation Bus) among the intelligent systems is important, because this system combines the tasks of a conventional system and introduces many new functions enabling the control of individual systems in the building.

Key words: lighting, control, intelligent, designing, integration, system

INTRODUCTION

The electric energy becomes more and more important in contemporary modern society. Its ineffective use means that our capabilities are lost in 60%. More effective energy use not only could help to protect limited resources of mineral fuels but also contribute to the reduction of carbon dioxide emission. The effective energy use is particularly important at the time of global energy crisis [7, 8].

Owing to the improvement in the scope of building engineering techniques and modern architectonic solutions, also the electric system is subject to transformations. The idea of intelligent building engineering and so called intelligent systems has become popular and more present in our everyday life in recent years. Nowadays "an intelligent" house is not a luxury any more but becomes a more and more commonly applied solution.

The first electric systems in the buildings were equipped with conventional accessories i.e. fuses, sockets, circuit – breakers, cam switches, light fittings. However the further development in the scope of the conventional electrical systems is practically impossible. The works associated with the new systems are continued owing to continuous trend towards the improvement of the standard of contemporary buildings. The development of electronic engineering and computerization in many fields of our life are also reflected in the electric systems sector. New control and regulation systems are created by the manufacturers of the systems equipment introducing control engineering solutions into building management systems. Owing to their advanced development and complexity, it is necessary to find a new approach to the designing of these systems, power supply methods, as well as to the localization and elimination rate of potential disturbances.

The optimisation of energy consumption in the buildings should be based upon the energy use only in case of such necessity; the amount of energy to be used should be maintained on a reasonably low level and at the highest possible efficiency. The use of intelligent building system is favourable in this case [1, 6, 12, 13].

LIGHTING CONTROL

The lighting control systems [1, 4, 6] have been created and are widely applied as a result of necessity of electric energy saving as well as the need to create proper working conditions.

In order to generate the savings, the systems installed in the building should support each other ensuring so called systems integration. It is possible by integration of all individual systems by means a superior system i.e. the building management system – BMS. Thanks to impressive spectrum of products dedicated for the lighting control, measurement, regulation and management, KNX/EIB system can perform the most demanding tasks. This system often is applied as the basic system of BMS enabling wide automation of the illumination control in the building and energy saving e.g. by lighting turnoff in the rooms with detected lack of occupants (employees). The use of daylight in order to ensure the required illumination level is also important. The wireless control is also possible by means of this system. Its advantage consists in the possibility of monitoring of the objects being controlled from any location, simple and user friendly operation, easy installation, operation reliability and safety. The achievement of individual illumination levels in various rooms and application of lighting scenarios to be activated in accordance with activity performed in those rooms e.g. writing, party, TV watching or reading is also ensured in KNX/EIB system control.

The images transmission is possible in real time through the connection with video module. An Internet Gateway automatically informs about events and alarms by means of an e-mail. The connection with Internet Gateway is possible via LAN by means of browser and its known IP address or by means of an Internet Explorer and specialized service e.g. www.domoport.de [5, 9, 10].

The security procedures applied in case of remote controlling of an intelligent electric system are similar to those used in Internet banking. All pages are encoded (SSL protocol) and 3 – level authorization is used [2, 3, 11].

The Internet Gateway is applied in commercial applications e.g. in electrical engineering systems, heating, ventilation, air-conditioning and in residential houses; for instance to extend the possibilities of already existing systems, to ensure remote supervision over summer houses and remote supervision over all-year houses.

When designing an intelligent electric system, the designer should first of all adhere to relevant standards in the scope of electric systems. The designer of the building management system should thoroughly analyse the actual needs of the building and its users.

The lighting control belongs to the group of most popular functions of an intelligent building. The lighting in modern building is something more than only the basic requirement – because the lighting can perform an important role in the architectonic design and affect the energy performance of building except of the health, safety and the good feeling of its inhabitants.

The lighting control in KNX/EIB system is understood as: automatic turning on, turning off, dimming, brightening up or maintenance of constant illumination for the light sources. The lighting control can be also supplemented in the form of window roller blinds or shutters control additionally enabling proper adjustment of natural daylight illumination [3].

In comparison to the conventional system, the energy savings are possible in the building with KNX/EIB system thanks to lighting control. However, it is impossible to determine the level of these savings in a precise manner, because they depend on many factors:

In the houses equipped with KNX/EIB system, the extension of the lighting control system is possible in a manner enabling full use of the lighting functions as well as the support of other systems of the building, among others the window roller blinds or shutters control system.

Fig. 1. Lighting control opportunities in KNX/EIB system.

The product range offered by many companies being the members of KONNEX association of the manufacturers of KNX/EIB system devices, encompasses the electric apparatuses used in the indoor lighting automatic control engineering. For instance the following electric equipment is offered by ABB[1]:

- Lighting controllers used in order to maintain the constant illumination in the rooms dedicated for work and for rest of occupants. Thanks to the combination of natural and artificial light, maximum energy consumption savings is possible.
- The movement and occupancy sensors used for the monitoring of lighting and other electric energy receivers installed indoors and outdoors.
- Illumination sensors for measurement of lighting levels.
- Dimming actuators ensuring the control of lighting consisting of incandescent and halogen lamps. They enable the control of the degree of illumination in the buildings in an economic and universal manner.
- Regulators used in order to maintain the constant illumination level in the working environment area combining the natural and artificial light in order to achieve the maximum energy consumption savings.

The construction of the lighting control by means of KNX/EIB system encompasses also the local lighting regulation in the building rooms. The dimmers and individually controlled light fittings supporting the lighting sensors are used for this purpose.

An example illustrating the lighting control possibility by means of KNX/EIB system has been presented in Figure 1. All lamps in the building can be turned on and off in individual or in group mode (Fig. 2).

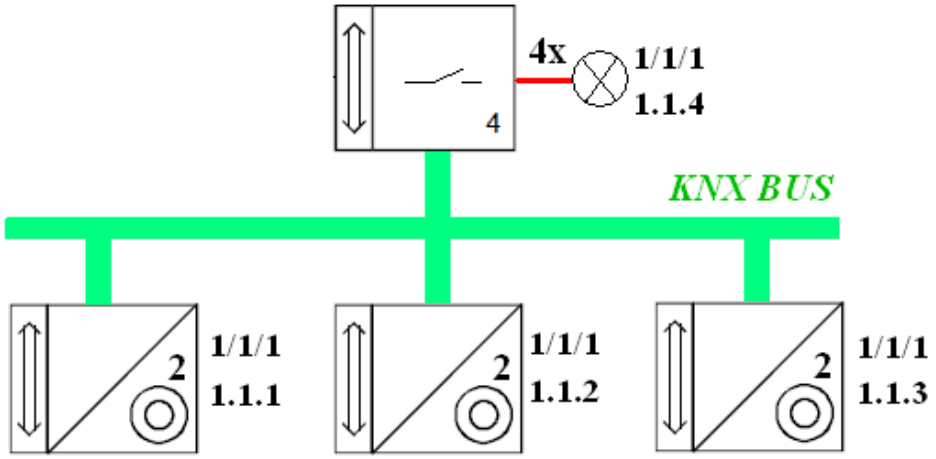

Fig. 2. Bidirectional connection in KNX control: four -channel actuator for lighting control is turned on by dual channel sensors.

A clock, movement sensors or infrared pilot (Fig. 3) can also be used. Therefore, it is possible to adapt the lighting to the needs of users. The illumination in the rooms does not have to be constant. Its level can be controlled by means of illumination sensors. It is very important for instance on the table or desktop for work where the value of illumination should be correspondingly high.

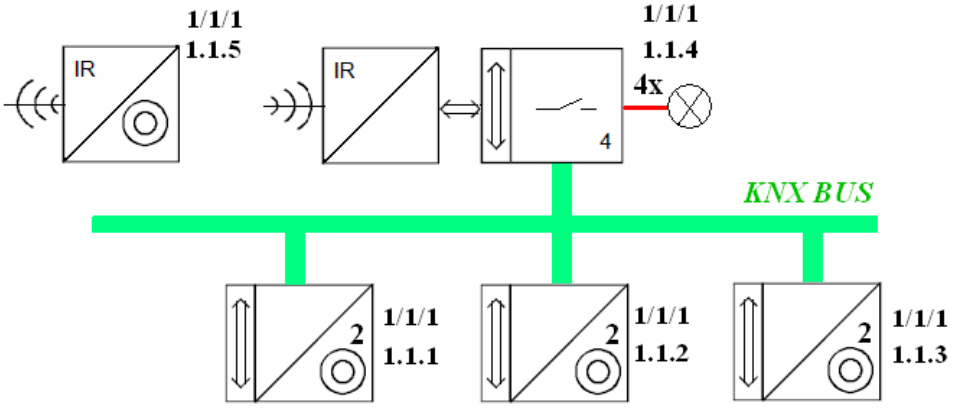

Fig. 3. Bidirectional connection in KNX control: four channel actuator for lighting control and IR control is turned on by dual channel sensors

The lighting control system is provided in the building in combination with other systems. Therefore, its analysis should be carried out against the background of the complex building management system and its relations with other systems e.g. air-conditioning, ventilation and heating system, etc. should be considered [3,4].

Therefore KNX/EIB system devices dedicated for the application in lighting system are supported by the devices provided for the purposes other than the control of lighting.

The role of the window roller blinds or shutters control is significant in the course of the lighting control. The roller blinds systems are used in the buildings in order to protect against sun lighting. If the illumination in the room is insufficient, any artificial lighting is unnecessary because the solution consisting in automatic shutter angle control vs. sun position is more favourable (Fig. 4).

Fig. 4. Shutter inclination angle control depending on sun position

The shutters are open in a manner ensuring the access to daylight without penetration of dazzling light into the room. Therefore the illumination control becomes a more efficient and economical solution. The integration of the shutter controller with the devices dedicated for the lighting system control has been illustrated in Figure 5.

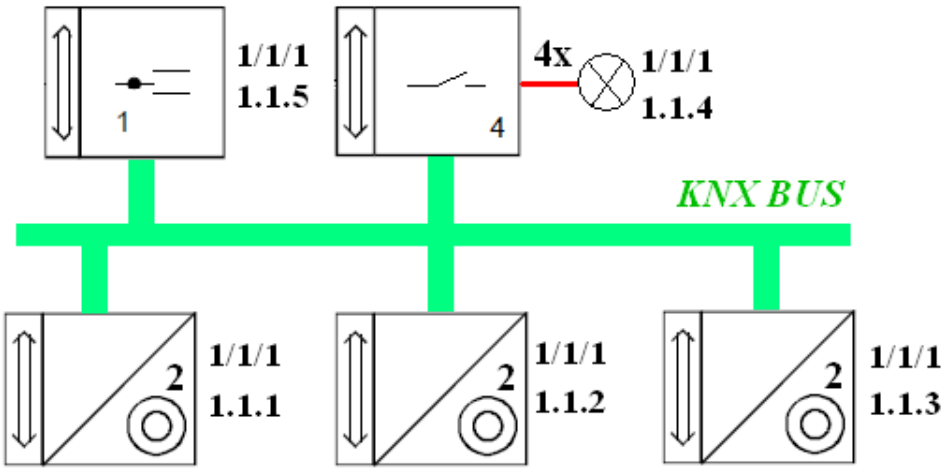

Fig. 5. Diagram of shutter inclination angle control depending on the sun's position

Another important method of the lighting regulation existing in KNX/EIB system and giving certain savings is the so called dimming. The dimming is possible in a manual mode i.e. a specified lamp is controlled individually by the user until anticipated illumination is achieved or

in automatic mode maintaining the constant illumination level in the room irrespective of varying daylight conditions.

The maintenance of the constant illumination level in the rooms with consideration of varying external conditions is an important element affecting the lighting control. The air conditioning units and illumination sensors which are installed in the rooms (Fig. 6) are used for this purpose.

Fig. 6. Principle of indoor artificial lighting control depending on varying natural light conditions [1]

An example can be presented as group of lamps situated in the closest distance from the windows; this group of lamps can be turned off during a bright day and other lamps can be dimmed to the required illumination level, depending on the amount of daylight. Therefore the energy is saved which would be used for the room lighting – wholly with artificial light. Moreover, in order to ensure the stable and comfortable conditions in the room, the lamps are dimmed or brightened up smoothly with long time constants; therefore the lighting regulation is physically invisible.

In order to enable the energy savings, PIR movement sensors are very often used in the lighting regulation circuits. Their task is to turn on the lighting in the rooms only if the human presence is detected. A turn on/ off single bit information is transmitted by the movement sensor to the bus. Certain savings of energy to be used for lighting will be possible as a result of introduction of such elements into control circuits.

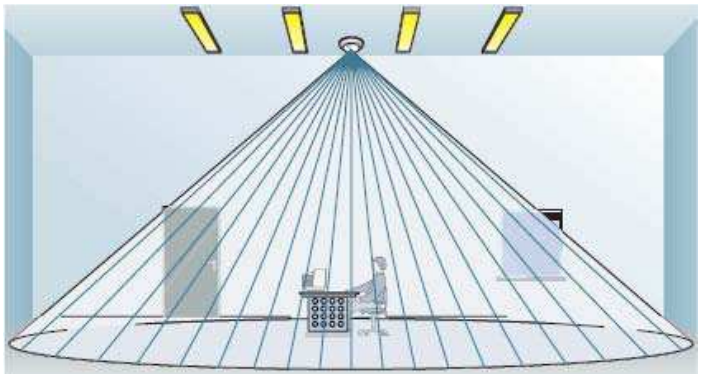

Fig. 7. Use of movement sensor detecting human occupancy in the room for lighting control [1]

The ordinary turning on or off of the circuits is the prevailing part of the lighting control. The real time clocks are often used for this purpose.

The central control mode is also possible by means of KNX/EIB system (Fig. 8). The double pole circuit-breaker with physical address 1.1.3 is dedicated for the control of an actuator with physical address 1.1.6 and simultaneously is used for the central control of both actuators in the considered circuit.

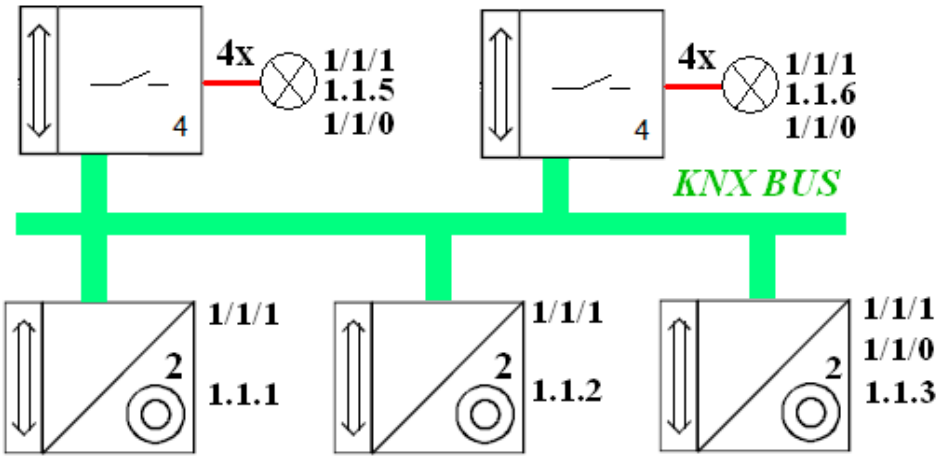

Fig. 8. Central control for lighting in KNX/EIB system

Using EIB system for the daylight and artificial light control, it is possible to save even ten percent of electric energy to be used for lighting. The lighting can be turned on in the whole building by means of EIB system and by means of only one pushbutton; e.g. with simultaneous dropping of external roller shutters.

The methods of the lighting control in the residential building presented above are used in order to ensure the comfort and to minimize the electric energy consumption. The consumption of electric energy for the lighting purposes in the buildings is significant; therefore significant savings are possible, through proper control.

CONCLUSIONS

The designer engaged in the designing of lighting systems in intelligent buildings should have the knowledge of the technical and legal issues associated with other types of systems. Many factors, among others: the quality and reliability, functionality, availability in the market, system costs, possibility of further integration with other systems as well as perspectives of development and competitiveness in the market. The correct integration of all building systems, basing upon detailed analysis of their functions is essential for a good design. On the basis of integration, the selection of devices and their correct parametrization is performed by the designer / integrator of an intelligent system. Owing to specific and unique features of each object, the reproduction of ready solutions by the designer would be a very risky approach without their critical evaluation and checking with respect to functionality in any case.

The conscious energy consumption is necessary to ensure the safety in future and leads to a more economical house. The real energy saving is commenced already in the building design phase. The energy savings achievable thanks to the lighting control depend on many factors. Therefore it is impossible to determine their level precisely without the functioning analysis of the relevant building system. It is possible in an approximated manner only.

The rational and responsible behaviours should be promoted, facilitated and strengthened in order to support the efficient energy use.

REFERENCES

ABB – Information materials, 2010.

EIBA/Konnex Org. EIB Installation Bus.: Instructors Seminar. EIB Interworking Standards. Bruksela, Belgia 1999.

Chilimoniuk T. : The analysis of intelligent installations systems in residential building. Master thesis. Lublin University of Technology. 2003.

Drop D. Jastrzębski D „The contemporary electric installations in single houses construction using the equipment manufactured by Moeller Company" COSiW SEP Warszawa 2002.

EN-50131-1:1997 Alarm system – Intrusion system – Part 1:General requirements.

Horyński M.: The application of binary inputs and outputs in management systems of an intelligent building. Electric Engineering Review 7/2010, p. 218-220.

Horyński M., Majcher J.: The possibility of installations status visualization in intelligent buildings. Drives and control – Technical and information monthly No 12(140), p. 90-92.

Koczyk H. Antoniewicz B. Sroczan E. „The modern technical fitout for single family house" Państwowe Wydawnictwo Rolnicze i Leśne, Poznań 1998.

Kulikowski R. „The control in large systems" WNT Second edition Warszawa 1974.

Luchowski G.: The information systems for the installations operation visualization in an intelligent building. Master thesis. Lublin University of Technology 2009.

Mikulik J.: European Installation Bus. Distributed safety and comfort control system. COSiW, Warszawa 2009.

Petykiewicz P. „The modern electric installation in an intelligent building" COSiW SEP Warszawa 2001.

Petykiewicz, P.:The building management systems - Instabus EIB. Siemens Sp. z o.o., Warszawa 1999.

WSPÓŁPRACA KOMPONENTÓW INTELIGENTNEGO BUDYNKU W STEROWANIU OŚWIETLENIEM

Streszczenie. W artykule omówiono komponenty inteligentnych instalacji elektrycznych wykorzystywane w systemach automatyki budynkowej do sterowania oświetleniem oraz metodykę projektowania tych instalacji na przykładzie systemu KNX/EIB. Ważne miejsce wśród systemów inteligentnych zajmuje system KNX/EIB, do niedawna znany pod nazwą EIB (Europejskiej Magistrali Instalacyjnej). Łączy on zadania tradycyjnej instalacji oraz wprowadza wiele nowych funkcjonalności umożliwiających sterowanie poszczególnymi systemami w budynku.

Słowa kluczowe: oświetlenie, sterowanie, inteligentny, projektowanie, integracja, instalacja

TEKA Kom. Mot. Energ. Roln. – OL PAN, 2011, 11, 143–156

ANALYSIS OF INDICATION ERRORS OF THE SI GAS ENGINE WITH A PRECHAMBER

Arkadiusz Jamrozik

Institute of Internal Combustion Engines and Control Engineering,
Czestochowa University of Technology, Armii Krajowej 21, 42-201 Czestochowa,
e-mail: jamrozik@imtits.pcz.czest.pl

Summary. The paper presents indication results accuracy and accuracy of thermal processes analysis which particularly occurs in the cylinder of internal combustion engine. The characteristic values of IC (internal combustion) engine thermal cycle are: indicated efficiency and pressure and non-repeatability factor of indicated work. The paper presents results of measuring errors analysis and uncertainty of the above-mentioned values obtained from indication of the spark ignition internal combustion engine with a prechamber. The analysis shows that results of the indication of the piston engine should include information on measurement accuracy and uncertainty of the calculated values. This information has a significant influence on the final measurement results. Errors are the inseparable part of measurement result. Results without given errors are not complete. The indication of the internal combustion engine is currently a standard research method which allows us to find out information on temporary parameters of processes in the cylinder of IC engine. The indication of IC engine is generally considered to be a very accurate method with repeatability of results. On the basis of error analysis and measurement uncertainty it was confirmed that the main parameters are loaded with significant errors.

Key words: engine with two-stage combustion system, excess air factor, indicated work, indicated efficiency, non-repeatability factor of the indicated work

INTRODUCTION

Experimental measurements of processes in a combustion engine are a source of necessary knowledge to optimize and improve the engine and can lead to reduction of emissions of harmful exhaust components, and reduction of fuel consumption. Basic experimental method of testing the working processes in the cylinder of internal combustion engine is indicated, consisting mainly in the measurement of fast-changing processes and instantaneous changes in the cylinder pressure. Information obtained from the indicated engine cylinder is the basis for the diagnosis and optimization of the combustion process and allows for a qualitative assessment of its work. Results of indicated engine piston analysis, in particular the results of the analysis of thermal processes occurring in the cylinder are in varying degrees dependent on the accuracy of measurements and the uncertainty of the result.

The test engine was constructed on the basis of a four-stroke compression-ignition engine manufactured by "ANDORIA" Diesel Engine Manufacturers of Andrychow, which, after some constructional changes, was designed for the combustion of gaseous fuel as a spark-ignition engine due to a new fuel supply system and an ignition installation. The main engine element that underwent modernization was the head (Fig. 1).

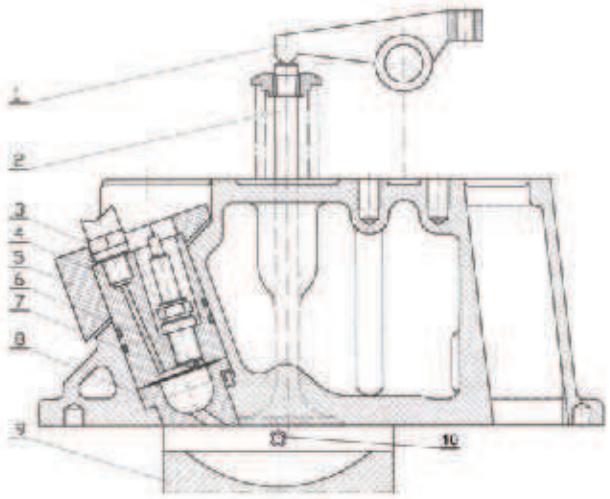

Fig. 1. Test engine head with prechamber
1 - valve rocker, 2 - inlet valve, 3 - flame suppressor,
4 - prechamber head, 5 - retaining cover, 6 - spark plug,
7 - sealing ring, 8 – prechamber body, 9 – piston, 10 – pressure sensor

Tab. 1. Main engine parameters	
displacement volume	1810 cm^3
number of cylinders	1
cylinder configuration	horizontal
cylinder bore	120 mm
connecting-rod length	275 mm
piston stroke	160 mm
compression ratio	8.6
engine speed	1000 rpm

The implemented changes allowed for an additional combustion chamber (prechamber) to be installed in the previously existing head of the S320 ER engine by setting the compression ratio to 8.6. The prechamber volume is approximately 4.5% of the total volume above the piston at TDC (top dead centre) and it is located asymmetrically regarding the cylinder axis. The applied changes have enabled the implementation of two-stage combustion system within the sectional combustion chamber.

MEASUREMENT PROCEDURE

The tests were conducted at a constant rotational speed of n = 1000 rpm. The engine was brought to full loading after prior thermal stabilisation, that is, the cooling water was brought to boiling (the evaporation cooling system). The main chamber and prechamber of the test engine was powered by propane-butane gas LPG (liquefied petroleum gas). The tests included three main measurement series allowing for a different ratio of thermal energy input with fuel to the prechamber - Q_{in}, to the thermal energy input to the whole engine - Q_{tot}. The pressures occurring in the engine combustion chambers were recorded for Q_{in}/Q_{tot} = 2.5%, for Q_{in}/Q_{tot} = 5% and for Q_{in}/Q_{tot} = 8%, while the combustion air factor changed in the range from 1.4 to 2.0 and the ignition advance angle in the range from 6 deg to 18 deg before the TDC. The recording was made for 95 successive operation cycles every 1 deg with specialised software [1]. At the same time, other quantities necessary

for the subsequent analysis of indication results [2] were three times measured, such as rotational speed, air consumption, gas fuel consumption, air temperature, combustion-gas temperature and ambient pressure and temperature.

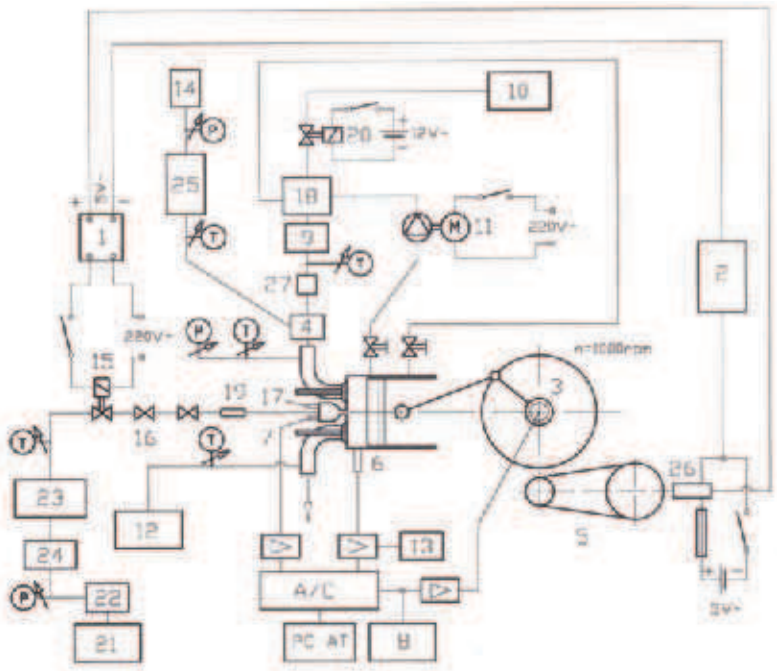

Fig. 2. Schematic diagram of the testing stand

1 – electronic relay, 2 – pulse generating system, 3 – CA angle transmitter, 4 – gas mixer, 5 – belt transmission, 6 – main chamber pressure sensor, 7 – prechamber pressure sensor, 8 – counting module, 9 – gas flowmeter, 10 – main gas fuel tank, 11 – circulating-water pump, 12 – combustion-gas analyser, 13 – oscilloscope, 14 – measuring orifice, 15 – solenoid valve prechamber, 16 – non-return valve set, 17 – spark plug, 18 – reducer-evaporator, 19 – flame suppressor, 20 – gas solenoid valve, 21 – gas fuel tank prechamber, 22 – pressure regulator, 23 – pressure fluctuation damping reservoir, 24 – set of measurement rotameters, 25 – equalizing tank, 26 – magnetic induction sensor, 27 – metering valve

The value of excess air factor of fuel mixture gas analyzer was measured by the AI Radio 9600 on the basis of the oxygen in the exhaust of the engine. For the analyzer measurement the range of excess air factor contained from 0 to 2, and the measurement resolution was 0.01.

The paper presents an analysis of measurement error of the indicated work and the indicated efficiency. The performed analysis of uncertainty determination for the indicated work which determines the dispersion (spread) around the average value calculation results indicated work in the individual cycles of the three measurements containing 95 registered engine cycles. Uncertainty analysis was performed for the indicated efficiency with the three measurements of speed, the time consumption of propane-butane gas in the cylinder, the propane-butane jet delivered to the prechamber and for the three average values indicated work was performed. The study also calculated the uncertainty of determining the non-repeatability factor of indicated work which defines the uniqueness of the engine test cycles.

ANALYSIS OF MEASUREMENT RESULTS

Characteristics based on an analysis of the measurement results show that the energetic share of enriching fuel in the prechamber in the engine with a two-stage combustion system has an influence on the indicated efficiency, the indicated work and the stability of the engine work and repeatability of the cycles. The best effects of the test engine were achieved for the lowest analysed energetic share of enriching fuel, which was 2.5%.

One of the parameters determining the performance of the combustion engine is the indicated work.

$$L_i = \frac{\sum_{0}^{720} \frac{p_n + p_{n+1}}{2}(V_{n+1} - V_n)}{V_s}, \tag{1}$$

where p_n, p_{n+1} are instantaneous values of the pressure in the cylinder [MPa], V_n, V_{n+1} are instantaneous values of the cylinder volume [m^3], V_s is displacement volume [m^3].

For Q_{in}/Q_{tot} = 2.5%, indicated work decreased with increasing excess air factor. L_i ranged from 0.72 to 0.55 MJ/m^3 (Fig. 3).

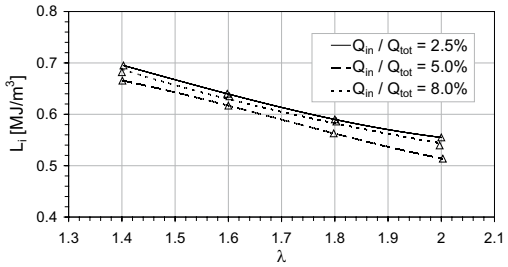

Fig. 3. Indicated work versus excess air factor

The practical measurement of physical quantities is related to measurement error and the uncertainty of the result. The measurement error of the indicated work consists of measurement error in the engine cylinder pressure and the error of measurement of the instantaneous cylinder volume. The measurement error of the indicated work can be determined from the dependence [3]:

$$\delta L_i = \sqrt{\delta p^2 + \delta V^2}, \tag{2}$$

where δp is measurement error in the cylinder pressure [%], δV is measurement error of the instantaneous cylinder volume [%].

The measurement error in the cylinder pressure is the sum of the piezo quartz pressure sensor error, the amplifier error and the error of the measurement a/d card.

$$\delta p = \sqrt{\delta cz^2 + \delta w^2 + \delta(a/d)^2}, \tag{3}$$

$$\delta cz = 0.5\% \ [4],$$

$$\delta w = 3\% \ [5],$$

where δcz is error of the piezo quartz pressure sensor [%], δw is amplifier error [%], δ(a/d) is error of the measurement card [%].

The error of the measurement card is quantization error of the a/d converter with the processing of ±10V and a resolution of 12 bit [6]:

$$\delta(a/d)=\frac{\theta}{FSR}100\%, \tag{4}$$

$$\theta=\frac{FSR}{2^r},$$

$$\delta(a/d)=0.024\%$$

where θ is quantization interval of the a/d converter [V], FSR is range of a/d converter [V], r is resolution of the a/d converter.

The measurement error of the instantaneous cylinder volume is the sum of CA crank angle transmitter error and error of measurement a/d card.

$$\delta V=\sqrt{\delta k^2+\delta(a/d)^2}, \tag{5}$$

where δk is error of CA crank angle transmitter [%].

The error of CA crank angle transmitter was calculated with respect to the perpendicular position of the connecting rod relative of the crankshaft crank arm. It is calculated as the ratio of change in volume of the cylinder, for 0.5 deg - half the value of the step crank angle transmitter, to the displacement volume.

$$\delta k=\frac{\Delta V}{V_s}100\%=0.45\%, \tag{6}$$

where ΔV is change in cylinder volume corresponding to pulse duration of the course of a rectangular tag of the crank angle transmitter [m^3].

According to relation (2) measurement error of the indicated work is equal to $\delta L_i \approx 3.1\%$.

The uncertainty designation of the indicated work, determine the dispersion (spread) around the average value calculation results of the indicated work in the individual cycles of the three measurements containing 95 registered engine cycles. It was assumed that the uncertainty designation of the indicated work has a normal distribution and it was calculated from the relation [3]:

$$\Delta L_{ii}=t_s\sigma_{Lii}, \tag{7}$$

where t_s is coefficient of the t-Student distribution for N-1 degrees of freedom and for the most commonly adopted technique in the 95% confidence level, N is the number of measurements.

The standard deviation of the indicated work:

$$\sigma_{Lii}=\sqrt{\frac{1}{N-1}\sum(L_{ii}-L_i)^2}, \tag{8}$$

where L_{ii} is value of the indicated work of cycles [MJ/m^3], L_i is average value of the indicated work of the three measurements containing 95 registered engine cycles [MJ/m^3].

The accuracy of determining the average value of a specified quantity is dependent on the number of measurements and the uncertainty limit of average value is called. For indicated work of the uncertainty the determination of the average value was calculated according to [3]:

$$\Delta L_i = t_s \frac{\sigma_{Lii}}{\sqrt{N}}. \tag{9}$$

Figure 4 shows the uncertainty intervals designation of the indicated work $\pm\Delta L_{ii}$ and the uncertainty intervals designation of the average value of the indicated work $\pm\Delta L_i$. They were placed on the characteristics of the average value of L_i changes in the function of the excess air factor, the $Q_{in}/Q_{tot} = 2.5\%$. The uncertainty value $\pm\Delta L_{ii}$ ranged from ±0.008 MPa for $\lambda = 1.6$ (1.3% of the average value of the indicated work) to ±0.03 MPa for $\lambda = 2.0$ (5% of the L_i value). The uncertainty value $\pm\Delta L_i$ ranged from ±0.0005 MPa for $\lambda = 1.6$ (0.08% of the average value of the indicated work), to ±0.002 MPa for $\lambda = 2.0$ (0.29% of the L_i value).

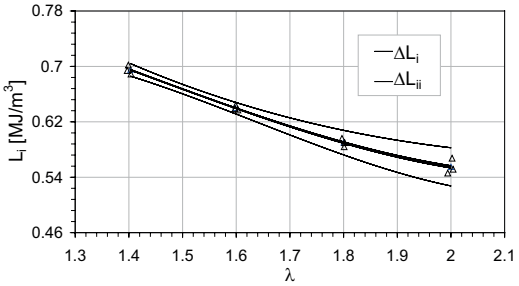

Fig. 4. Indicated work with uncertainty intervals determination of the indicated work ΔL_{ii} and its average value ΔL_i, for $Q_{in}/Q_{tot} = 2.5\%$

The highest indicated efficiency, equal to $\eta_i = 36.5\%$, test engine achieved when the share of enriching fuel mixture in the prechamber was 2.5%.

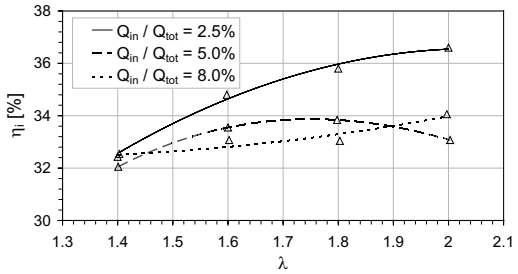

Fig. 5. Indicated efficiency versus excess air factor

The indicated efficiency is the ratio of the indicated work done in the operating cycle of the engine to the heat supplied to the engine over the cycle. During the tests the measurement of heat applied in a single cycle was not possible because the measured value was the amount of heat brought in during a few hundred cycles (about 500). The indicated efficiency was defined as the ratio of the indicated work in the cylinder volume, averaged during the measurement of fuel consumption to the average amount of heat. The measurement error of the indicated efficiency average is the sum of the measurement error of the indicated work average, and the measurement error of the total heat supplied to the engine.

The average value of the indicated efficiency, expressed in % is equal to:

$$\eta_i = \frac{L_i V_s}{Q_{tot}} 100\%,$$

$$\eta_i = \frac{L_i V_s}{Q_{cyl} + Q_{in}} 100\%, \tag{10}$$

where Q_{tot} is total heat supplied to the engine [MJ], Q_{cyl} is heat supplied to the engine cylinder [MJ], Q_{in} is heat supplied to the prechamber [MJ].

The measurement error of the average value of the indicated efficiency:

$$\delta\eta_i = \sqrt{\delta L_i^{\,2} + \delta Q_{tot}^{\,2}},$$

$$\delta Q_{tot} = \sqrt{\delta Q_{cyl}^{\,2} + \delta Q_{in}^{\,2}},$$

$$\frac{\delta Q_{tot}}{Q_{tot}} = \sqrt{\left(\frac{\delta Q_{cyl}}{Q_{tot}}\right)^2 + \left(\frac{\delta Q_{in}}{Q_{tot}}\right)^2},$$

$$\frac{\delta Q_{tot}}{Q_{tot}} = \sqrt{\left(\frac{\delta Q_{cyl}}{Q_{cyl} + Q_{in}} \frac{Q_{cyl}}{Q_{cyl}}\right)^2 + \left(\frac{\delta Q_{in}}{Q_{cyl} + Q_{in}} \frac{Q_{in}}{Q_{in}}\right)^2},$$

$$\delta Q_{tot} = \sqrt{\left(\frac{Q_{cyl}}{Q_{cyl} + Q_{in}}\right)^2 \delta Q_{cyl}^{\,2} + \left(\frac{Q_{in}}{Q_{cyl} + Q_{in}}\right)^2 \delta Q_{in}^{\,2}},$$

$$\delta\eta_i = \sqrt{\delta L_i^{\,2} + \left(\frac{Q_{cyl}}{Q_{cyl} + Q_{in}}\right)^2 \delta Q_{cyl}^{\,2} + \left(\frac{Q_{in}}{Q_{cyl} + Q_{in}}\right)^2 \delta Q_{in}^{\,2}}, \tag{11}$$

where δL_i is the measurement error of the indicated work [%], δQ_{tot} is the measurement error of the total heat supplied to the engine [%], δQ_{cyl} is the measurement error of the heat supplied to the engine cylinder [%], δQ_{in} is the measurement error of the heat supplied to the prechamber [%].

The heat supplied to the engine cylinder:

$$Q_{cyl} = \frac{V_{cyl}\,\rho_{LPG}\,W_{LPG}}{0,5\,n\,t}, \tag{12}$$

where V_{cyl} is volume of propane-butane delivered to the engine cylinder [m^3], ρ_{LPG} is density of propane-butane [kg/m^3], W_{LPG} is calorific value of propane-butane [MJ/kg], n is speed engine [rpm], t is time consumption of propane-butane delivered to the engine cylinder [min].

The measurement error of the heat supplied to the engine cylinder:

$$\delta Q_{cyl} = \sqrt{\delta V_{cyl}^{\,2} + \delta\rho_{LPG}^{\,2} + \delta W_{LPG}^{\,2} + \delta n^2 + \delta t^2}, \tag{13}$$

where δV_{cyl} is measurement error of volume of propane-butane delivered to the engine cylinder [%], $\delta\rho_{LPG}$ is an estimated error of propane-butane density [%], δW_{LPG} is estimated error of

calorific value of propane-butane [%], δn is measurement error of speed engine [%], δt is measurement error of time consumption of propane-butane delivered to the engine cylinder [%].

The measurement error of propane-butane volume delivered to the engine cylinder is expressed in % and was calculated as a ratio scale interval of gas flowmeter to the measured value of propane-butane volume:

$$\delta V_{cyl} = \frac{dz.elem.}{V_{cyl}} 100\% = 1\%. \tag{14}$$

The estimated error of propane-butane density [7]:

$$\delta \rho_{LPG} = 6.8\%.$$

The estimated error of calorific value of propane-butane [7]:

$$\delta W_{LPG} = 1.8\%.$$

The measurement error of speed engine is expressed in % and was calculated as a ratio scale interval of the speed measurement system to the measured value of speed engine:

$$\delta n = \frac{dz.elem.}{n} 100\% = 0.1\%. \tag{15}$$

The measurement error of time consumption of propane-butane in engine cylinder is expressed in % and was calculated as a ratio scale interval of the timer to the measured value of time:

$$\delta t = \frac{dz.elem.}{t} 100\% = 0.2\%. \tag{16}$$

The heat supplied to the prechamber of the engine:

$$Q_{in} = \frac{V'_{in} \rho_{LPG} W_{LPG}}{0,5n}, \tag{17}$$

where V'_{in} is propane-butane jet delivered to the prechamber [m^3/min].

The measurement error of the heat supplied to the prechamber of the engine:

$$\delta Q_{in} = \sqrt{\delta V'^{\,2}_{in} + \delta \rho^{\,2}_{LPG} + \delta W^{\,2}_{LPG} + \delta n^2}, \tag{18}$$

where $\delta V'_{in}$ is measurement error of propane-butane jet delivered to the prechamber [%].

The measurement error of propane-butane jet delivered to the prechamber of the engine is expressed in % and was calculated as a ratio scale interval of gas rotameter to the measured value of propane-butane jet:

$$\delta V'_{in} = \frac{dz.elem.}{V'_{in}} 100\% = 5\% \tag{19}$$

According to relation (11) measurement error of the average value of the indicated efficiency is equal $\delta \eta_i \approx 7.3\%$.

The uncertainty of the indicated efficiency depends on the uncertainty of the indicated work, engine speed, time consumption of propane-butane in the engine cylinder and propane-butane jet delivered to the prechamber. The uncertainty of the indicated efficiency was determined from three measurements of engine speed, consumption time of propane-butane in the engine cylinder and propane-butane jet delivered to the prechamber as well as the three average values of the indicated work.

The uncertainty of the indicated efficiency was calculated according to [3]:

$$\Delta\eta_{ii} = \sqrt{\left(\frac{\partial\eta_i}{\partial L_i}\Delta L_{ii}\right)^2 + \left(\frac{\partial\eta_i}{\partial n}\Delta n_i\right)^2 + \left(\frac{\partial\eta_i}{\partial t}\Delta t_i\right)^2 + \left(\frac{\partial\eta_i}{\partial V'_{in}}\Delta V'_{ini}\right)^2}, \tag{20}$$

$$\frac{\partial\eta_i}{\partial L_i} = \frac{0.5 V_s n t}{\left(V_{cyl}\rho_{LPG}W_{LPG} + V'_{in}W_{LPG}t\right)},$$

$$\frac{\partial\eta_i}{\partial n} = \frac{0.5 L_i V_s t}{\left(V_{cyl}\rho_{LPG}W_{LPG} + V'_{in}W_{LPG}t\right)},$$

$$\frac{\partial\eta_i}{\partial t} = \frac{0.5 L_i V_s n(V_{cyl}\rho_{LPG}W_{LPG} + V'_{in}W_{LPG}t) - 0.5 L_i V_s n t V'_{in}W_{LPG}}{\left(V_{cyl}\rho_{LPG}W_{LPG} + V'_{in}W_{LPG}t\right)^2},$$

$$\frac{\partial\eta_i}{\partial V'_{in}} = \frac{-0.5 L_i V_s n t^2 W_{LPG}}{\left(V_{cyl}\rho_{LPG}W_{LPG} + V'_{in}W_{LPG}t\right)^2}.$$

The uncertainty of the engine speed:

$$\Delta n_i = t_s \sigma_{ni}, \tag{21}$$

where σ_{ni} is the standard deviation of the engine speed [rpm].

The uncertainty of the time consumption of propane-butane in the engine cylinder:

$$\Delta t_i = t_s \sigma_{ti}, \tag{22}$$

where σ_{ti} is the standard deviation of the time consumption of propane-butane in the engine cylinder [min].

The uncertainty designation of the propane-butane jet delivered to the prechamber of the engine:

$$\Delta V'_{ini} = t_s \sigma_{V'ini}, \tag{23}$$

where $\sigma_{V'ini}$ is the standard deviation of the propane-butane jet delivered to the prechamber [m^3/min].

The uncertainty of the average value of the indicated efficiency was calculated according to [3]:

$$\Delta\eta_i = \sqrt{\left(\frac{\partial\eta_i}{\partial L_i}\Delta L_i\right)^2 + \left(\frac{\partial\eta_i}{\partial n}\Delta n\right)^2 + \left(\frac{\partial\eta_i}{\partial t}\Delta t\right)^2 + \left(\frac{\partial\eta_i}{\partial V'_{in}}\Delta V'_{in}\right)^2}, \tag{24}$$

The uncertainty of the average value of the indicated work:

$$\Delta L_i = t_s \frac{\sigma_{Lii}}{\sqrt{3}}, \tag{25}$$

The uncertainty of the average value of the engine speed:

$$\Delta n = t_s \frac{\sigma_{ni}}{\sqrt{3}}, \tag{26}$$

The uncertainty of the average value of the time consumption of propane-butane:

$$\Delta t = t_s \frac{\sigma_{ti}}{\sqrt{3}}, \tag{27}$$

The uncertainty of the average value of the propane-butane jet delivered to the prechamber:

$$\Delta V'_{in} = t_s \frac{\sigma_{V'ini}}{\sqrt{3}}, \tag{28}$$

Figure 6 shows the uncertainty intervals of the indicated efficiency $\pm\Delta\eta_{ii}$ and the uncertainty intervals of the average value of the indicated efficiency $\pm\Delta\eta_i$. They were placed on the characteristics of the average value of η_i changes in the function of the excess air factor, the Q_{in}/Q_{tot} = 2.5%. The uncertainty value $\pm\Delta\eta_{ii}$ ranged from ±1.2% for λ = 1.6 (3.6% of the average value of the indicated efficiency) to ±2.7% for λ = 2.0 (7.4% of the η_i value). The uncertainty value $\pm\Delta\eta_i$ ranged from ±0.7% for λ = 1.6 (2.1% of the average value of the indicated efficiency), to ±1.6% for λ = 2.0 (4.3% of the η_i value).

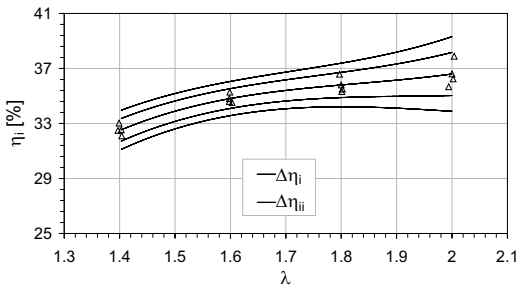

Fig. 6. Indicated efficiency with uncertainty intervals determination for indicated efficiency $\Delta\eta_{ii}$ and its average value $\Delta\eta_i$ for Q_{in}/Q_{tot} = 2.5%

One of the main criteria for evaluating the work of the internal combustion engine is non-repeatability of engine cycles. In the present study, the non-repeatability cycle phenomenon was defined by the factor of the non-repeatability factor of the indicated work engine COV_{Li}. It is expressed in % and calculated as the ratio of the standard deviation of the engine indicated work to the average value of its three measurements containing 95 registered engine cycles.

$$COV_{Li} = \frac{\sigma_{Lii}}{L_i} 100\%. \tag{29}$$

In conventional SI engines, the combustion process of the correct mixture takes place in a fairly narrow range of λ. Depletion of the fuel mixture to a level at which the value of the excess air ratio exceeds 1.5 causes irregular engine performance manifested by, inter alia, misfire and

non-repeatability of engine cycles. According to literature [10], the limit of the correct operation of the internal combustion engine, expressed by the maximum of the non-repeatability factor of the indicated engine work COV_{Li} is equal to 10%.

Figure 7 shows that the minimum value COV_{Li} coefficient equal to 0.66% for the Q_{in}/Q_{tot} = 2.5% was obtained with λ equal to approximately 1.6.

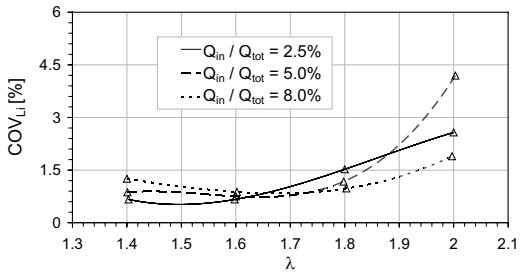

Fig. 7. Non-repeatability factor of indicated work versus excess air factor

Assuming that uncertainty of the non-repeatability factor of the indicated work COV_{Li} is normally distributed, it was calculated from the correlation [3]:

$$\Delta COV_{Li} = t_s \, \sigma_{COVLi}, \tag{30}$$

where σ_{COVLi} is the standard deviation of the coefficient COV_{Li} [%].

The standard deviation of the non-repeatability factor of the indicated work COV_{Li} depends on the uncertainty of the standard deviation of the indicated work σ_{Lii} and the uncertainty determination of the uncertainty of the indicated work L_i. The standard deviation of the non-repeatability factor of the indicated work COV_{Li} was calculated using the following dependence of the variance function of two variables [11]:

$$\sigma_{COVLi}{}^2 = \left(\frac{\partial COV_{Li}}{\partial \sigma_{Lii}} \right)^2 \sigma_{\sigma Lii}{}^2 + \left(\frac{\partial COV_{Li}}{\partial L_i} \right)^2 \sigma_{Li}{}^2, \tag{31}$$

where $\sigma_{\sigma Lii}$ is standard deviation of the standard indicated work deviation [MJ/m^3], σ_{Li} - standard deviation of the average value of the indicated work [MJ/m^3].

When you differentiate, the standard deviation of the non-repeatability factor of the indicated work COV_{Li}:

$$\sigma_{COVLi} = 100\% \sqrt{\left(\frac{1}{L_i} \right)^2 \sigma_{\sigma Lii}{}^2 + \left(-\frac{\sigma_{Lii}}{L_i{}^2} \right)^2 \sigma_{Li}{}^2}. \tag{32}$$

The standard deviation of the standard indicated work deviation (relative uncertainty σ_{Lii}) [3]:

$$\sigma_{\sigma Lii} = \sigma_{Lii} \frac{1}{\sqrt{2(N-1)}}. \tag{33}$$

The standard deviation of the average value of the indicated work:

$$\sigma_{Li} = \frac{\sigma_{Lii}}{\sqrt{N}}. \tag{34}$$

The uncertainty of the non-repeatability factor of the indicated work decreases with an increase in the number of measurements N. An increasing number of repetitions of measurements lead to a decrease in the value of $\sigma_{\sigma Lii}$ and σ_{Li} and a more reliable test. As a consequence, the uncertainty of the coefficient COV_{Li} determination is lower.

Figure 8 shows the uncertainty intervals determination of the non-repeatability factor of the indicated work $\pm\Delta COV_{Li}$. They were placed on the characteristics of the COV_{Li} changes in the function of the excess air factor, the Q_{in}/Q_{tot} = 2.5%. For the whole range λ, the value of uncertainty $\pm\Delta COV_{Li}$ was equal to 8.3% of the value of the non-repeatability factor of the indicated work COV_{Li} and ranged from 0.05% for λ = 1.6 to ±0.21% for λ = 2.0.

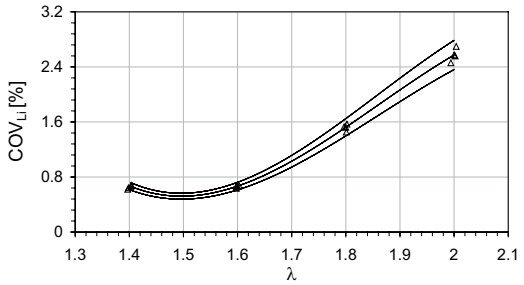

Fig. 8. Non-repeatability factor of indicated work COV_{Li} with uncertainty intervals determination COV_{Li} for Q_{in}/Q_{tot} = 2.5%

CONCLUSIONS

As practice shows, no measurement, regardless of the diligence of its execution, can provide a completely accurate result. The size of measurement errors is an integral part of the measurement process. The measurement result with unknown error is the result which tells us nothing. The indication process of the combustion engine is now the standard test method used in the field of internal combustion piston engines. It allows the registration of the instantaneous values parameters of the processes occurring in the cylinder. Indication results allow for an analysis of the impact of various factors on the parameters of the combustion process. Common opinion about the precision of the computer systems and sensors used during the indication process leads to the belief that it is a very accurate, reliable and repeatable test procedure and that it meets the requirements for measurement accuracy [12]. Based on analysis of errors and uncertainty of measurement results of the internal combustion engine, an indication process can be established that sets the main parameters characterizing the operation of the engine containing significant errors and uncertainties in measurements. The measurement error of the indicated work is equal to $\delta L_i \approx 3.1\%$. The maximum value of uncertainty determination of the indicated work: $\Delta L_{ii} = 5\%$. The measurement error of the indicated efficiency of the test engine is equal to $\delta\eta_i \approx 7.3\%$. The maximum value of uncertainty determination of the indicated efficiency is $\Delta\eta_{ii} = 7.4\%$. The uncertainty determination of the non-repeatability factor of the indicated work engine: ΔCOV_{Li}

= 8.3%. In conclusion, it can be stated that the reliable interpretation of study analysis resulting from indication of spark ignition internal combustion engine should include the values of measurement errors and measurement uncertainties. The characteristic changes in the measurement results should be supplemented by error range or measurement uncertainty intervals [14].

REFERENCES

Gruca, M., 2001: LCTXR – program for digital recording and analysis of the frequency signals, Czestochowa University of Technology, Institute of Internal Combustion Engines and Control Engineering.

Cupiał, K., 2002: SILNIK – version 2001.5 – program for develop the indicator diagram, Czestochowa University of Technology, Institute of Internal Combustion Engines and Control Engineering.

Taylor, J.R., 1995: Introduction to the analysis of measurement error. PWN Warszawa.

Kistler - Instruction Manual Water-Cooled ThermoCOMP Pressure Sensors. Type 7061B, 7063A, 6061B, 6067C1, 6041A, 6043A.

http://www.kistler.com/.

AMBEX, 1995: Instruction card LC-020-0812.

Jakóbiec, J., Janik, R., Gardyński, L., 2003: The influence of a refining additive on practical physical and chemical properties of vehicle gas. VIth International Scientific Conference Gas Engines – Design – Research – Development Renewable Fuels.

Norma PN-C-96025., 1999: Petroleum products. Engines gasoline, Leading of gasoline.

Golec, K., Stępień, Z., 1993: Fuels and engines oils. The script for students of technical colleges. Cracow University of Technology.

Heywood, J.B., 1988: Internal combustion engine fundamentals. McGraw – Hill Book Company.

Volk, W., 1973: Applied statistics for engineers. WNT Warszawa.

Ambrozik, A., Kurczyński, D., 2008: Analysis of the fast-changing speed of the AD3.152 UR engine-powered mineral fuel, fuel of vegetable origin nd mixtures of these fuels. MOTROL.

Cupiał, K., Dużyński, A., Gruca, M., Grzelka, J., 2001: Some errors of gas engine indication. Journal of Kones, Combustion Engines, Vol 8, No 1-2.

Jamrozik, A., Kociszewski, A., Tutak, W., 2009: Measurements accuracy of internal combustion engine indication. Pomiary Automatyka Kontrola, nr 12.

Jamrozik A., Kociszewski A., Tutak W., 2009: Błędy indykowania silnika ZI z dwustopniowym systemem spalania, Journal of KONES Powertrain and Transport, Vol. 16, No. 4. Warsaw.

Tutak W., Jamrozik A., Kociszewski A., Sosnowski M., 2006: Experimental Research into Turbulence Field in Combustion Chamber of Internal Combustion Engine. Journal of KONES Powertrain and Transport, Vol 13, No 2, Warsaw.

Tutak W., Jamrozik A., Kociszewski A., 2005: Procesy przepływowe w komorze wstępnej silnika gazowego. Teka Komisji Motoryzacji Polskiej Akademii Nauk oddział w Krakowie. Konstrukcja, Badania, Eksploatacja, Technologia Pojazdów Samochodowych i Silników Spalinowych. Zeszyt Nr 29-30, Kraków.

Oktawa W., 1976: Elementy statystyki matematycznej i metodyka doświadczalnictwa. PWN Warszawa.

Tutak W., 2008: Interpretacja wyników pomiaru prędkości przepływu ładunku w komorze spalania tłokowego silnika spalinowego. Pomiary Automatyka Kontrola, Vol.54, nr 2.

Cupiał K., Kociszewski A., 2002.: Wielopunktowy zapłon w silniku ZI. AUTOPROGRES-KONMOT 2002

ANALIZA BŁĘDÓW INDYKOWANIA GAZOWEGO SILNIKA ZI Z KOMORĄ WSTĘPNĄ

Streszczenie. Wyniki indykowania silnika tłokowego, a w szczególności wyniki analizy procesów termicznych zachodzących w cylindrze silnika są w różnym stopniu uzależnione od dokładności pomiarów oraz niepewność uzyskanego wyniku. Wielkościami charakteryzującymi pracę silnika spalinowego pod względem jego osiągów są wskaźniki pracy silnika takie jak: sprawność i ciśnienie indykowane oraz współczynnik niepowtarzalności pracy indykowanej. W pracy przedstawiono analizę błędów pomiarowych i niepewności uzyskanych wyników wyżej wymienionych wielkości podczas indykowania silnika spalinowego o zapłonie iskrowym z komorą wstępną. W wyniku przeprowadzonych obliczeń można stwierdzić, że aby można było wiarygodnie interpretować wyniki analizy indykowania tłokowego silnika spalinowego powinny one zawierać wartości błędów i niepewności pomiarowych, gdyż ich wielkość ma znaczący wpływ na końcowy wynik pomiaru. Na podstawie przeprowadzonej analizy błędów i niepewności pomiarowych wyników procesu indykowania silnika spalinowego można stwierdzić, że wyznaczone główne parametry charakteryzujące prace silnika są obarczone dość znacznym błędem i niepewnością pomiaru.

Słowa kluczowe: silnik z dwustopniowym systemem spalania, współczynnik nadmiaru powietrza, praca indykowana, sprawność indykowana, współczynnik niepowtarzalności pracy indykowanej

TEKA Kom. Mot. Energ. Roln. – OL PAN, 2011, 11, 157–165

NUMERICAL OPTIMIZATION OF THE IGNITION ANGLE OF SI ENGINE

Arkadiusz Jamrozik

Institute of Internal Combustion Engines and Control Engineering,
Czestochowa University of Technology, Armii Krajowej 21, 42-201 Czestochowa,
e-mail: jamrozik@imtits.pcz.czest.pl

Summary. The paper presents the results of numerical optimization of ignition advance angle of the modernized test engine Andoria 1hc102 using AVL FIRE software. Modelling allows to find the optimal ignition advance angle of the test engine during the combustion of fuel mixture with an excess air factor $\lambda = 1.2$. The optimum value of the ignition angle was that which occurred at the maximum indicated pressure and indicated efficiency, and for which there was no combustion knock. Modelling results show that the test engine powered by the mixture of $\lambda = 1.2$, should work with the ignition advance angle equal to 10 deg before TDC.

At this ignition advance angle a knock occurred in the engine and it reached the indicated pressure and the indicated efficiency was equal to, respectively, 0.99 MPa and 41.47%.

Key words: internal combustion engine, modelling, ignition advance angle, indicated pressure, indicated efficiency

INTRODUCTION

During recent years the numerical modelling research using more and more advanced mathematical models has been intensively developing. The development of numerical modelling is heightened by increasing computational power that allows modelling not only of flow processes but also combustion in 3D [1, 2, 3]. One of the more advanced numerical models used for combustion process in piston engines modelling is AVL FIRE [4]. In 2009 Institute of Internal Combustion Engines and Control Engineering at Częstochowa University of Technology began University Partnership Program with AVL Company and started using AVL FIRE software for modelling of the thermal cycle of IC engines [5,6,7].

The AVL FIRE software belongs to modern programs which are used for modelling of the thermal cycle of internal combustion engines. FIRE allows modelling flow and thermal processes occur in the intake manifold, in combustion chamber of IC engine and exhaust pipe with a catalyst and a particulate filter. This programme enables the calculation of transport phenomena, mixing, ignition and turbulent combustion in internal combustion engine. Homogeneous and not homogeneous combustion mixtures in spark ignition and compression ignition engine can also be modelled using this software. Kinetics of chemical reactions phenomena is described by combustion models

which take oxidation processes in high temperature into consideration. Several models apply to auto ignition processes. AVL FIRE allows for the modelling of the knock process which occurs in the combustion chamber of IC engine. This program allows for the creation of three-dimensional computational greed, characterized by boundary conditions of surfaces and initial conditions of simulation. The postprocessor makes it possible to visualize the results.

This paper presents results of numerical optimization of ignition advance angle in the modernized test engine Andoria 1hc102 using AVL FIRE software, during the combustion of fuel mixture with excess air factor $\lambda = 1.2$. The optimum value of the angle was that which occurred at the maximum indicated pressure p_i and indicated efficiency η_i, and for which there was no combustion knock.

The combustion knock is a type of abnormal combustion process, characterized by intensive pressure pulses in the engine combustion chamber. The knock is a type of abnormal combustion process, characterized by intense pressure pulsations in the combustion chamber, which are transferred to the block engine, generate a distinctive sound and could lead to engine damage. The source of combustion knock is auto-ignition of unburnt gases before the flame front (initiated by a spark plug) after a big increase in temperature and pressure [13, 15, 18, 19].

NUMERICAL MODEL

The test engine was constructed on the basis of a four-stroke compression-ignition engine 1hc102 manufactured by "ANDORIA" Diesel Engine Manufacturers of Andrychow. After some constructional changes, this engine was redesigned for the combustion of gasoline as a spark-ignition engine. For this reason, the engine was equipped with a new fuel supply system and an ignition installation. As a result of modernization the shape of the combustion chamber was changed and the compression ratio was reduced from 17 to 8.5. The engine is a stationary, two-valve unit with a horizontal cylinder configuration. The engine cooling system is the evaporation of the water jacket. Figure 1 shows the experimental modernized test engine Andoria 1hc102. On the basis of the real dimensions of the experimental engine, the three-dimensional mesh of combustion chamber of engine was built (Fig. 2).

Tab.1. The main engine parameters

bore cylinder	100 mm
stroke piston	120 mm
connecting rod length	216 mm
direction of cylinders	horizontal
squish	11 mm
compression ratio	8.5
engine speed	1.5e+3 rpm
number of cylinders	1

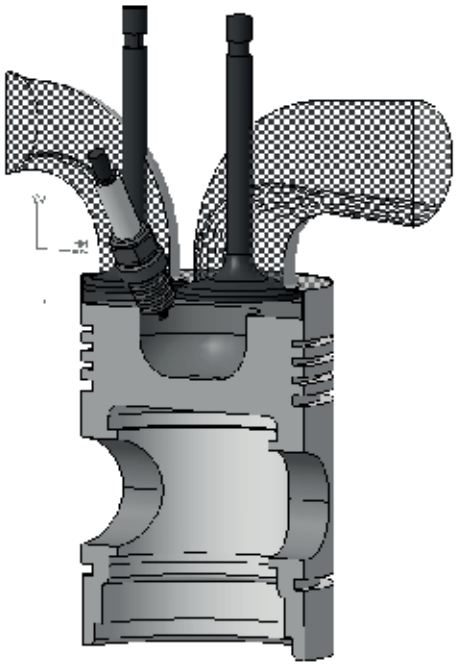

Fig. 1. Experimental engine

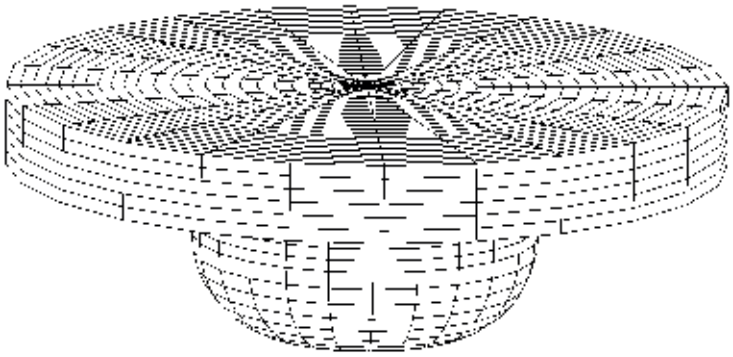

Fig. 2. Geometric grid of combustion chamber
of model engine in TDC

COURSE OF CALCULATIONS

The calculation started at BDC at the beginning of compression stroke and finished at 360 deg since the end of engine power stroke. At the beginning of compression stroke, the lean mixture of excess air factor equal to 1.2 was in the chamber.

The modelling of combustion process was conducted for a range of ignition advance angle from 38 to 8 deg of crank angle before TDC in order to optimize the thermal cycle of the test engine. On the basis of the pressure data indicated pressure and indicated efficiency were calculated. They did not include many losses both in the combustion process and flow losses or blows. Using AVL FIRE software the computational analysis was conducted of the potential combustion knock.

Tab. 2. Chosen input parameters of the modelled process

ignition advance angle	8 ÷ 36 deg
ignition duration	10 deg
fuel	gasoline
temperature fuel injection	320 K
initial pressure	0.85e+5 Pa
initial temperature	365 K
excess air factor	1.2
density	1.19 kg/m^3
turbulence kinetic energy (180 deg before TDC)	0,1 J/m^3
turbulence length scale (180 deg before TDC)	1,12 cm

One of the parameters determining the performance of the combustion engine is the indicated pressure.

$$p_i = \frac{\sum_{180}^{540} \frac{p_n + p_{n+1}}{2}(V_{n+1} - V_n)}{V_s}, \tag{1}$$

where p_n, p_{n+1} are instantaneous values of the pressure in the cylinder [MPa], V_n, V_{n+1} are instantaneous values of the cylinder volume [m^3], V_s is displacement volume [m^3].

The average value of the indicated efficiency, expressed in % is equal to:

$$\eta_i = \frac{p_i V_s}{Q} 100\%, \tag{2}$$

where Q is the total heat supplied to the engine [MJ].

The heat supplied to the engine cylinder:

$$Q = \frac{V \rho W}{0.5 n t}, \tag{3}$$

where V is volume of gasoline delivered to the engine cylinder [m^3], ρ is density of gasoline [kg/m^3], W is calorific value of gasoline [MJ/kg], n is speed engine [rpm], t is time consumption of gasoline delivered to the engine cylinder [min].

RESULTS OF CALCULATION

As a result of modelling the pressure courses were obtained as a function of crank angle for the whole analyzed range of the ignition advance angle (Fig. 3).

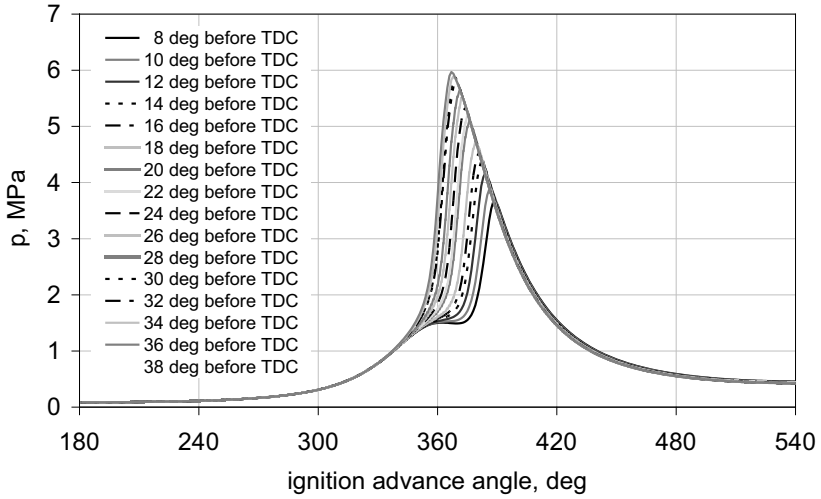

Fig. 3. Courses of pressure for the analyzed range of the ignition advance angle

Figure 4 shows the indication parameters of the engine model calculated on the basis of pressures.

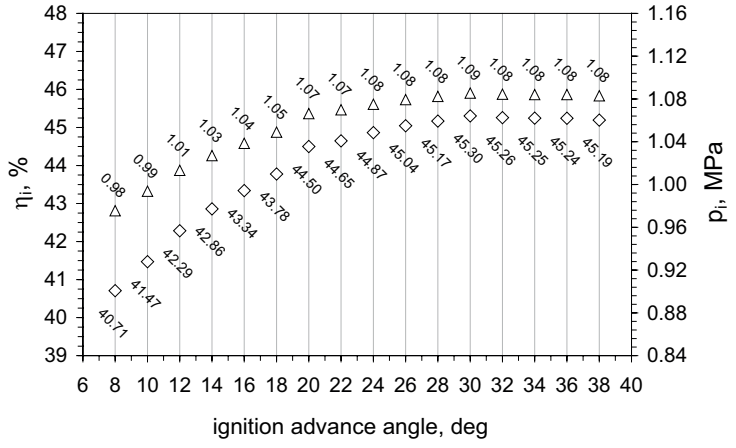

Fig. 4. The value of indicated pressure and indicated efficiency
for the analyzed range of the ignition advance angle

Figures 5 to 7 show the temperature distribution and location of the knock in the combustion chamber of test engine.

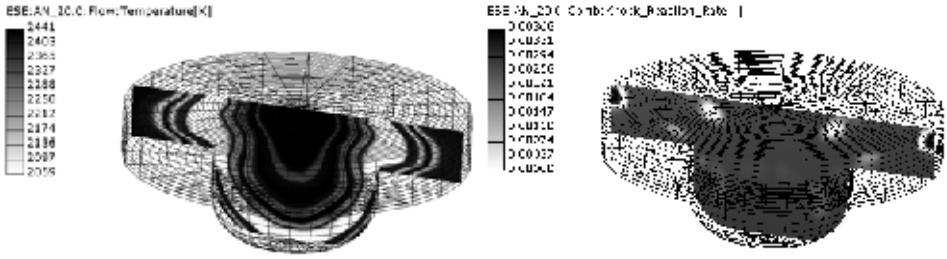

Fig. 5. Temperature distribution and location of the knock in combustion chamber of model engine at 20 deg after TDC for ignition advance angle equal to 30 deg before TDC

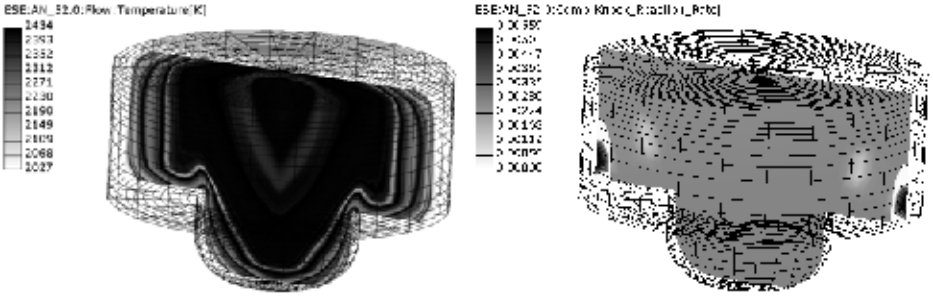

Fig. 6. Temperature distribution and location of the knock in combustion chamber of model engine at 52 deg after TDC for ignition advance angle equal to 12 deg before TDC

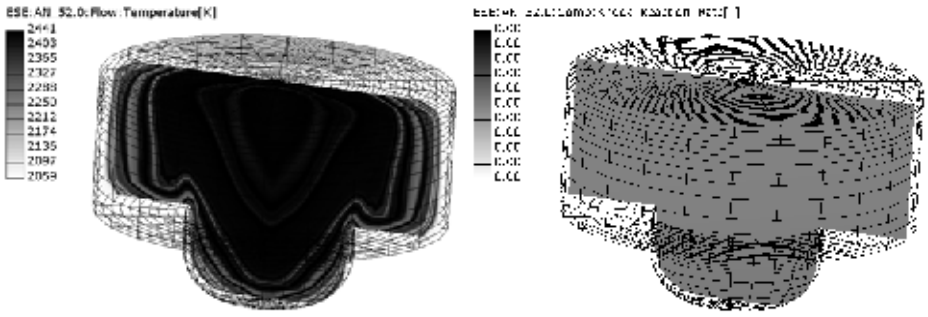

Fig. 7. Temperature distribution and location of the knock in combustion chamber of model engine at 52 deg after TDC for ignition advance angle equal to 10 deg before TDC

The obtained results of modelling show that the angle of 30 deg before TDC is the most suitable ignition advance angle for the engine parameters. For this ignition angle the maximum indicated pressure achieved is 1.09 MPa and the highest indicated efficiency is 45.3%. Unfortunately, the consequence of using such a large ignition advance in the test engine causes the creation of combustion knock. The knock combustion process occurred also at smaller advance angles, at 12

deg before TDC. For this engine, the combustion process occurs normally to the ignition angle equal to10 deg before TDC. For the ignition angles larger than 10 deg BTDC knock occurs in the engine.

CONCLUSIONS

AVL FIRE program is a modern research tool that can be successfully used to model the thermal cycle of the internal combustion engine. The AVL FIRE up-to-date numerical code used during research made it possible to generate 3D geometric mesh of combustion chambers of the test engine and allowed to perform numerical calculations of processes occurring in this engine. Conducted simulations of combustion process have delivered information concerning spatial and time-dependent pressure and temperature distribution in the combustion chamber. This information would be extremely difficult to obtain by experimental methods. The ability to detect knock in the cylinder can identify the real engine operating parameters at the optimum settings. In the paper, using AVL Fire the optimal value of ignition advance angle was found for a modernized 1hc102 Andoria engine powered by a combustible mixture with excess air factor 1.2. The optimum value of the angle was that which occurred at the maximum indicated pressure and indicated efficiency, and for which there was no combustion knock. As a result of modelling it can be concluded that during combustion of the mixture of $\lambda = 1.2$, the engine should work with the ignition advance angle equal to 10 deg before TDC. At this ignition angle no undesirable symptoms such as combustion knock occurred in the engine and the obtained values of the indicated pressure and the indicated efficiency were equal to, respectively, 0.99 MPa and 41.47%.

Numerical modelling using the AVL FIRE can be used for preliminary determination of adjustable engine parameters such as ignition advance angle, without using a real engine on the testing stand. However, the use of numerical methods to optimize engine operation can and should be verified by experiments on the measuring stand.

REFERENCES

Jamrozik A.: Modelling of two-stage combustion process in SI engine with prechamber. MEMSTECH 2009, V-th International Conference PERSPECTIVE TECHNOLOGIES AND METHODS IN MEMS DESIGN, Lviv-Polyana, UKRAINE 22 - 24 April 2009.

Jamrozik A.: Analiza numeryczna procesu tworzenia i spalania mieszanki w silniku ZI z komorą wstępną. Teka Komisji Motoryzacji Polskiej Akademii Nauk oddział w Krakowie. Konstrukcja, Badania, Eksploatacja, Technologia Pojazdów Samochodowych i Silników Spalinowych, Zeszyt Nr 33-34, Kraków 2008.

Tutak W.: Modelling of flow processes in the combustion chamber of IC engine.MEMSTECH 2009, V-th International Conference PERSPECTIVE TECHNOLOGIES AND METHODS IN MEMS DESIGN, Lviv-Polyana, UKRAINE 22 - 24 April 2009.

AVL FIRE version 2009, ICE Physics & Chemistry, Combustion, Emission, Spray, Wallfilm. AVL LIST GmbH, 2009.

Jamrozik A., Tutak W.: Modelling of combustion process in the gas test engine. Proceedings of the VI-th International Conference MEMSTECH 2010 Perspective Technologies and Methods in Mems Design. s. 14-17, Lviv – Polyana 2010.

Tutak W., Jamrozik A.: Numerical analysis of some parameters of gas engine. Teka Commission of Motorization and Power Industry in Agriculture, Volume X, s. 491-502, Polish Academy of Science Branch in Lublin. Lublin 2010.

Tutak W., Jamrozik A.: Modelling of the thermal cycle of gas engine using AVL FIRE Software. COMBUSTION ENGINES/Silniki Spalinowe. No. 2/2010 (141), s. 105-113.

Tutak W., Jamrozik A., Kociszewski A., Sosnowski M.: Numerical analysis of initial swirl profile influence on modeled piston engine work cycle parameters. SILNIKI SPALINOWE/Combustion Engines, Mixture Formation Ignition & Combustion. 2007-SC2, pp. 401-407, 2007.

Kociszewski A., Jamrozik A., Sosnowski M., Tutak W.: Simulation of combustion in multi spark plug engine in KIVA-3V. SILNIKI SPALINOWE/Combustion Engines, Mixture Formation Ignition & Combustion. 2007-SC2, pp. 212-219, 2007.

Jamrozik A., Tutak W., Kociszewski A., Sosnowski M.: Numerical Analysis of Influence of Prechamber Geometry in IC Engine with Two-Stage Combustion System on Engine Work Cycle Parameters. Journal of KONES Powertrain and Transport. Vol 13, No 2, pp. 133-142, Warsaw 2006.

Jamrozik A., Kociszewski A., Sosnowski M., Tutak W.: Simulation of combustion in SI engine with prechamber. XIV Ukrainian-Polish Conference – CAD in Machinery Design Implementation and Educational Problems CADMD'2006. Polyana, Ukraine, pp. 66-69, May 2006.

Cupiał K., Jamrozik A.: SI engine with the sectional combustion chamber. Journal of Kones, Internal Combustion Engines. Vol 9, No 3-4, pp. 62-66,Warsaw-Gdansk 2002.

Szwaja S, Jamrozik A.: Analysis of Combustion Knock in the SI Engine. PTNSS KONGRES - 2009. International Congress of Combustion Engines. The Development of Combustion Engines, Opole June 2009.

Tutak W., Jamrozik A., Kociszewski A., Sosnowski M.: Numerical analysis of initial swirl profile influence on modelled piston engine work cycle parameters. COMBUSTION ENGINES/ Silniki Spalinowe, Mixture Formation Ignition & Combustion, 2007-SC2, 2007.

Szwaja S.: Studium pulsacji ciśnienia spalania w tłokowym silniku spalinowym zasilanym wodorem. Serie monografie nr 182, Częstochowa 2010.

Tutak W.: Thermal cycle of SI engine modeling with initial swirl proces into consideration. COMBUSTION ENGINES/Silniki Spalinowe, 1/2008

Kociszewski A.: Numerical analysis of spark plugs number influence on selected parameters of combustion in piston engine. COMBUSTION ENGINES/Silniki Spalinowe, 1/2008

Szwaja S., Bhandary K.R., Naber J.D.: Comparison of hydrogen and gasoline combustion knock in a spark ignition engine. Int. J. Hydrogen Energy Vol.32 nr 18. 2007.

Szwaja S.: Combustion Knock - Heat Release Rate Correlation of a Hydrogen Fueled IC Engine Work Cycles. 9th International Conference on Heat Engines and Environmental Protection. Proceedings. Balatonfured, Hungary. 2009.

Styła S., Walusia S., Pietrzyk W.: Computer simulation possibilities in modelling of ignition advance angle control in motor and agricultural vehicles. Teka Commission of Motorization and Power Industry in Agriculture VIII/2008.

NUMERYCZNA OPTYMALIZACJA ZAPŁONU W SILNIKU SPALINOWYM ZI

Streszczenie. W ramach pracy w programie AVL FIRE przeprowadzono numeryczną optymalizację zapłonu w badawczym zmodernizowanym silniku Andoria 1hc102 o zapłonie iskrowym. Modelowanie umożliwiło znalezienie optymalnego kąta wyprzedzenia zapłonu silnika badawczego podczas spalania mieszanki palnej o współczynniku nadmiaru powietrza $\lambda = 1.2$. Optymalną wartością kąta była ta, przy której wystąpiło maksymalne ciśnienie indykowane oraz sprawność indykowana, i przy której nie zaobserwowano objawów spalania stukowego. W wyniku modelowania stwierdzono, że silnik badawczy spalając mieszankę o $\lambda = 1.2$, powinien pracować z wyprzedzeniem zapłonu równym 10^{o} przed GMP. Przy tym kącie wyprzedzenia zapłonu silnik

nie wykazywał niepożądanych objawów spalania stukowego, a osiągnięte wartości ciśnienia indykowanego i sprawności indykowanej były równe odpowiednio 0.99 MPa i 41.47%.

Słowa kluczowe: silnik spalinowy, modelowanie, kąt wyprzedzenia zapłonu, ciśnienie indykowane, sprawność indykowana

TEKA Kom. Mot. Energ. Roln. – OL PAN, 2011, 11, 166–172

EFFECT OF STORING PERIOD ON THE QUALITY OF PHYSICAL AND CHEMICAL PARAMETERS OF THE INDUSTRIAL WINTER RAPE SEEDS

Magdalena Kachel-Jakubowska[1], Agnieszka Sujak[2]

[1] Department of Machinery, Agricultural Exploitation and Management in Agricultural Engineering; University of Life Sciences in Lublin, Poland
[2] Department of Physics, University of Life Sciences in Lublin, Poland

Summary. The physical and chemical parameters of winter rape seeds stored under laboratory conditions for up to three years were analyzed. Seed humidity and crude fat were assessed in seeds as well as the chlorophyll content and kinetic viscosity measured for the oil. As a result of the seeds storage process the tendency of the decrease of crude fat in seeds was observed as well as in chlorophyll content in the pressed oil. In general, all the analyzed seed and oil quality parameters were contained within the permitted range of standards making the examined seeds a valuable material for different industrial branches.

Key words: rape seeds, seeds humidity, crude oil, chlorophyll, kinetic viscosity

INTRODUCTION

Seeds of oilseed plants and mainly rape seeds are still used for the production of edible oils. During the last years both in Poland as in the world the increase of interest in this plant is observed. Apart from utilization of the rape oil as a semi-finished foodstuff or chemical [Rojek *et al.* 2010], usage as a material for the production of bio-fuels for high-pressure engines becomes more popular [Krygier *et al*. 1995a; Bendioli et al.. 2003; Szlachta, 2002; Wawrzosek *et al.* 2006; Kachel-Jakubowska *et al.* 2010] as well as usage of oil as a heat source for drying the grains [Rosiński *et al.* 2006]. In The National Catalogue of Agricultural Plant Varieties many rape plant varieties originated from Poland as well as from France or Germany different from crude oil are registered [Heimann, 2005; Wcisło, 2006; Dz.U.UE, 2010]. In Poland cultivation of the low eruic acid and glucozynolates is recommended as these varieties are characterized by a low level of anti-nutritional components [Muśnicki, 2003]. The quality of rape oil is dependent on their physico-chemical parameters highly affected by the plant variety (genetic factor determining chemical content) and to the climatic and soil conditions where plants are cultivated. Seed humidity [Janowicz, 2004] as well as fat content and composition have the crucial impact on physical and technological properties of the seeds as the main cause of deterioration of seed quality during their storage. The presence of chlorophyll in the rape seeds is undesirable for the reason of difficulties with its removal and obtaining high quality oil and its byproducts. On the basis of long-term research, Daun [1987] found that the chlorophyll

content is related mainly to the variety and the cropping year. Seeds containing below 24 mg/kg of chlorophyll were considered as a high quality material. In the case of fuel industry oil should be characterized by a relatively high thermal stability and viscosity. Kinetic viscosity is straightforwardly related to the lipid composition and properties [Wcisło, 2008] characteristic for lipids in all of their physical states as a result of intermolecular interactions. According to Niewiadomski [1983] and Ojczyk [1996] viscosity of non eruic acid oils is somehow higher than that of refined oil. Kinetic viscosity of traditional rape oil at the temperature of 20°C is 90 mPa·s and is relatively high compared to the viscosity of soy and olive oil which are 60 mPa·s and 77 mPa·s, respectively. Kinetic viscosity is highly temperature-dependent and for non eruic acid rape seeds amounts to 17 mPa·s at the temperature of 50°C. For some varieties kinetic viscosity at 30°C amounts to about 65 mPa·s while at 60°C is at the level of about 24 mPa·s [Tremazi *et al.* 1965].

The aim of the presented work was the determination of the physical and chemical parameters of rape seeds stored up to three years under laboratory conditions and of the quality of oils pressed from these seeds in order to estimate their usability in certain industrial branches. The estimations were based on the measurements of seed humidity, seed crude fat content, chlorophyll content in oil and on the measurements of oil kinetic viscosity.

MATERIALS AND METHODS

Experimental material consisted of 0.5 kg samples of the industrial rape seeds from the Oil Plant in Bodaczów, taken randomly from the bulk raw material supplied by 17 different contractors. All the samples were from the Lublin area (South-East Poland) and consisted of a mixture of different varieties collected by individual suppliers. Seeds were collected according to PN-EN ISO 542/1997 standard and stored under laboratory conditions at the temperature between 19- 22°C and humidity between 60-70%. Seed material consisted of the variety of mixed rape species. It was not possible to find any dependence between the certain varieties of the seeds and contractors for the reason that the Oil Plants do not maintain a register of supplied varieties and that the seeds from different varieties were mixed both during collection by the producers and during seed purchase. During the time of seed collection and experiments Bodaczów Oil Plants were purchasing seeds from the following winter seeds: Bazyl, Bojan, Californium, Cabriolet, Casoar, Kaszub, Lisek and Libomir. They are cultivars registered in The National Catalogue of Agricultural Plant Varieties [Dz.U.UE, 2010]. Every seed batch was represented by two independent samples provided with labels indicating the source of the seeds.

Experiments included the analysis of physical and chemical parameters of the rape seeds as well as oil pressed from the seeds stored for a period up to three years. Seed samples were marked with numbers 1, 2 or 3 for the storing period of one, two and three years, respectively

Humidity and crude fat of the rape seeds (in %) was determined by means of Omega 10 UV-Vis-NIR Bruins Analyser equipped in 10 interference filters for organic substances. The instrument was provided with internal standard for the rape seeds. The obtained value was the arithmetic mean from 3 independent measurements under condition that the admissible error was not bigger than 0.5% of the measured value.

Chlorophylls *a* and *b* were determined spectrophotometrically in the freshly pressed oil using a double-beam Varian Model Cary 300 Bio spectrophotometer. Samples of oils were diluted 5x in acetone and the spectrum measured between 350 and 700 nm. Concentrations of chlorophylls a (c_a) and b (c_b) and total carotenoids (c_x) in μg/ml were calculated as follows

$$c_a(\mu g/ml) = 11.24A_{661.6} - 2.04A_{644.8}$$

$$c_b(\mu g/ml) = 20.13A_{644.8} - 4.19A_{661.6}$$

$$c_{car}(\mu g/ml) = \frac{(1000A_{470} - 1.9c_a - 63.14c_b)}{214}$$ [Lichtenthaler and Buschmann, 2001]

Rape oil was pressed on a laboratory pressing stand using a HYBREN 6 worm extruder equipped with micrometric mesh strainers. The process of pressing began after stabilization of the press temperature. After pressing of c.a. 1.5 kg of raw material the temperature of extruder reached 70°C. The temperature was measured with TP6 laser pyrometer. The oil was stored at 5°C until used for analysis.

Kinematic viscosity values of oils were determined by using Brookfield RVDV II digital viscosimeter. The measurements were performed at constant temperature of 24.2 °C and the speed of 100 rpm using an A-21 spindle. Measurements were taken after 1 min of stabilised process. The admissible error of the method was 0.5 mPa×s

Statistical analysis consisted in the designation of basic statistical parameters such as mean values, standard deviations and correlation matrices. Calculations were done by using Statsoft Statistica 6.0 program.

RESULTS AND DISCUSSION

Fig. 1. shows the distribution of the seed humidity after storing the seeds for 1,2 and 3 years, respectively. For all the storage years most samples were characterized by optimal humidity ranging between 6 and 8.5% which is considered secure for storing the seeds for longer periods without loses, under condition that the seeds are mature, healthy, clean, having natural color, having the seed covers undamaged and not under the process of sprouting [Niewiadomski, 1983; Janowicz, 2004].

The statistical analysis tests showed statistically significant differences in the seed humidity stored for two years in comparison to seeds stored for one or three years. It also found no statistical differences between the seeds in groups stored for one and three years.

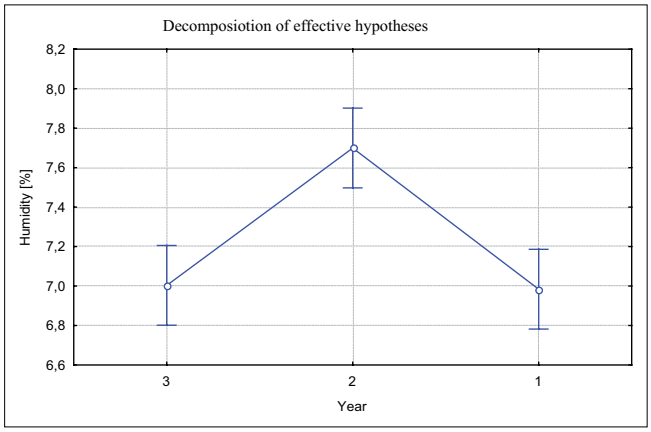

Fig. 1. Humidity of rape seeds stored for up to three years.

The seed material for the oil production in the Oil Plant in Bodaczów contained between 41.1 and 45% of d.m. of crude fat.

The results of Appelqvist [1972] show that storing time of the good quality rape seeds having the humidity at the level of about 7% can be as long as two to three years, without any change in their humidity or fat content.

The results of statistical analysis of the influence of the storing time (between one and three years) on the content of crude fat are shown in Fig. 2. Although no statistical differences were shown between the amples from particular groups, a tendency of the crude fat content's decrease can be observed for the seeds stored for three years.

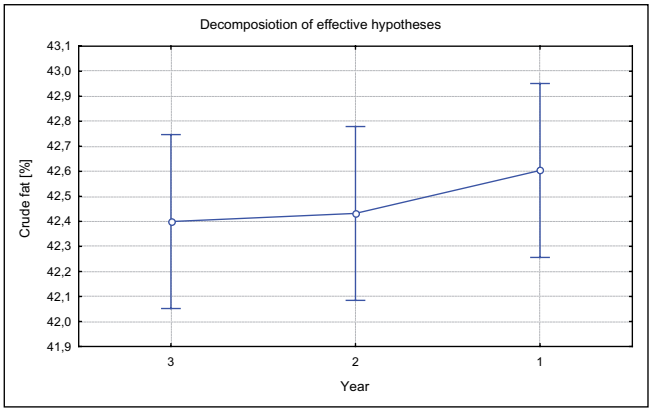

Fig. 2. Crude fat in rape seeds stored for up to three years.

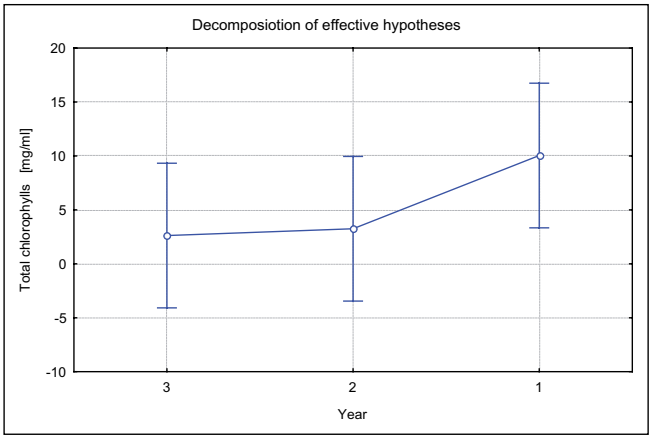

Fig.3. Chlorophyll content (sum of chlorophylls *a* and *b*)
of the rape oil pressed from seeds stored for up to three years.

Fig. 3. shows the total chlorophyll content in the rape seed oil. The samples were characterized by a varying amounts of chlorophylls (from 0.63 to 7.5 mg/ml of oil). On the basis of the data the decrease in chlorophylls was observed upon prolonged storage time (in years) although no statistical differences were observed. Such a tendency is a good information for food industry where

the smallest possible contents of chlorophylls are required due to taste and aesthetic advantages of oil depleted from chlorophylls. The cause of such a phenomenon may be not only the process of storing the material under proper conditions but also suitable seed variety or the cropping method [Tys et al., 2002; Kachel-Jakubowska, 2008].

The examined oils were characterized by similar kinetic viscosity (from 54 to 64 mPa·s), which did not differ statistically ($p \geq 0.05$). The results obtained from the samples stored for longer period showed higher multiplicity of data, caused most probably by the variety of seed stock. Statistical analysis did not show differences between samples from different years (Fig. 4.). The rape oil demonstrates 20-fold higher viscosity as compared to heating oil. This problem, however, in oil burners for boilers can be solved by application of special constructions [Jóźwiak *et al.* 2006].

Viscosity of rape oil differs significantly from this parameter for diesel fuel oil and at the temperature of 40°C is c.a twelve-fold higher, rendering impossible the proper functioning of the engines. This characteristic property forced the invention of double-fuel system eliminating some of disadvantageous phenomena arising during fuel combustion [Dzieniszewski, 2006].

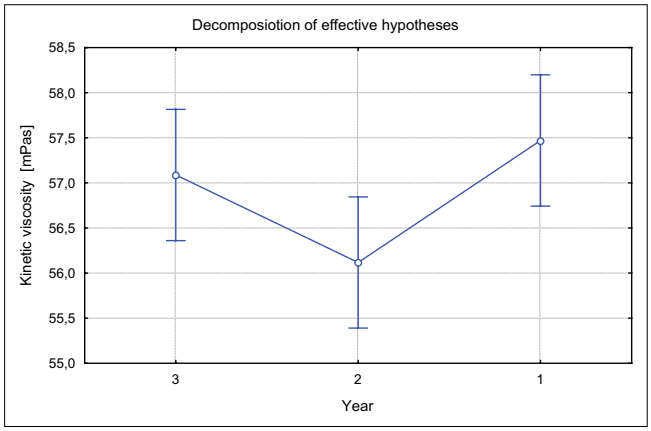

Fig.4. Kinetic viscosity of the oils pressed form the rape seeds stored for up to three years.

SUMMARY AND CONCLUSIONS

The conducted survey and the data analysis show that it is possible to determine the physico-chemical parameters of the rape seeds and the pressed oils in order to evaluate their usability in further industrial processing. The process of storing the material is the most basic element of post-cropping treatment, during which the decrease in the material quality can occur, mainly caused by the excessive humidity. Cleaned, mature rape seeds containing between 6 and 8 % of water can be stored without the risk of severe losses. The crucial problem is therefore maintaining the relative air humidity in storage rooms at the level between 30 and 70% [Janowicz, 2004].

1. The conducted experiments showed that the storage period is statistically influencing the industrial quality of seed humidity which renders a variable initial humidity of seed material supplied by different contractors in a definite year.

2. Of advantage is the decrease of chlorophyll content in oils obtained from the seeds stored for two or three years, which improves the quality of material although it seems to be statistically insignificant.
3. The basic quality parameters of the rape seeds stored under laboratory conditions assessed in this study stayed within the permitted by oil and chemical industry technical standards ranges. This can therefore indicate the favorable selection of varieties as well as good cultivation and cropping technologies.
4. The kinetic viscosity measured for the oils may be of interest for the producers of chemicals mainly because the storage period does not influence this parameter.
5. Although the rape seeds stored for longer periods proved to be useful for industrial purposes, the producers should decide whether the storing of seed material would be profitable considering the cost of storage.

REFERENCES

Abromovič, H., Klofutar, C. 1998. *A*cta. Chim. Slov, .45(1), 69.

Appelqvist L., Lööf B. 1972. Post – harvest handling and storage of rapeseed. In: Appelqvist L., Ohlson R.: Rapeseed. Elsevier, Amsterdam.

Bondioli P., Gasparoli A., Della Bella L., Tagliabauue S.. 2003. Biodisel stability under commercial storage conditions over one year. Eur. J. Lipid Sci. Technol., 105 (12). 735-741.

Daun J. K. 1987. Chlorophyll in Canadian Canola and Rapeseed and its Role in Grading. 7th International Rapeseed Congress, Poland, 1451 – 1456.

Dutt, N., V., K., Prasad, D., H., L., 1989. J. Am. Oil. Chem. Soc., 66, 701.

Dziennik Ustaw Unii Europejskiej. 2010. Wspólnotowy katalog odmian roślin rolniczych (2010/C 337 A/01).

Dzieniszewski G. 2006. Analiza możliwości zasilania silnika diesla surowym olejem rzepakowym. Inżynieria Rolnicza, 12, 117-125.

Heimann S. 2005. Zasady oceny odmian i ich wartość gospodarcza. Technologia produkcji rzepaku. Wydanie specjalne dla firmy Z. P.U.H. „Best-Pest" s.j. Warszawa. 62-67.

Janowicz L. 2004. Przechowywanie nasion rzepaku w magazynach silosowych. Rzepak – VI, 47-50.

Jóźwiak D., Szlęk A. 2006. Ocena oleju rzepakowego jako paliwa kotłowego. Energetyka i Ekologia, VI, 449-451.

Kachel-Jakubowska M., Szpryngiel M., 2008. Influence of drying condition on quality of rapeseed. Int. Agrophysics.,22, 327-331.

Kachel – Jakubowska M., Zając G. 2010. Influence of fuel rapeseed oil temperature on energetic parameters of an engine. Kom. Mot. Energ. Roln. TEKA t.10, 145-152.

Krygier K., Damian K., Drąka D. 1995a. Porównanie jakości I trwałości olejów rzepakowych tłoczonych na zimno I na gorąco oraz rafinowanego. Rośliny Oleiste IHAR, XVI. 301-306.

Lichtenthaler H.K., and Buschmann C., 2001**.** Chlorophyll and Carotenoids: Measurement and Characterisation by UV-Vis Spectroscopy. In: Current Protocols in Food Analytical Chemistry, Suppl 1, Unit F4.3.1.

Muśnicki Cz. 2003. Szczegółowa uprawa roślin. Praca zbiorowa. Tom II, WAR we Wrocławiu.

Niewiadomski H. 1983. Technologia nasion rzepaku. PWN Warszawa.

Ojczyk T. 1996. Nawożenie mineralne . W: Rzepak – produkcja surowca olejarskiego. Rozdział 10, ART. Olsztyn , 163-164.

Robak B., Gogolowski M.. 2000. Zmiany fizykochemiczne zachodzące w oleju rzepakowym w trakcie ogrzewania w wysokich temperaturach z uwzględnieniem tworzenia się transizomerów kwasów tłuszczowych. Rośliny Oleiste-Oilseed Crops, XXI. 683-692.

Rojek P., Pawlik H., Praciak A. 2010. Wpływ budowy chemicznej bio-polioli z oleju rzepakowego na właściwości wiskoelastycznych pianek poliuretanowych. Czasopismo Techniczne. WPK. Zeszyt 10, 277-284.

Rosiński M., Furtak L., Łuksa A., Stępień A. 2006. Wykorzystanie olejów roślinnych i urządzeń do ich spalania w procesach suszarniczych. MOTROL. Motorization and Power Industry In Agriculture, Lublin, VOL VIIIA, 243-250.

Szlachta Z. 2002. Zasilanie silników wysokoprężnych paliwami rzepakowymi. WkiŁ, Warszawa.

Tramazi S., Lovegner N., Feuge R. 1965. Characterisation and evaluation of some rapeseed oils. J. Am. Oil Chem., 42, 78.

Tys J., Sujak A., Bogdan A. 2002. Changes to the composition of colorants caused by the temperature of drying rapeseed. Int. Agrophysics, 16, 307-312.

Wawrzosek J., Piekarski W. 2006. Udział estrów oleju rzepakoweg w mieszance paliwowej z olejem napędowym a poziom emisji tlenków azotu. MOTROL. Motorization and Power Industry In Agriculture, Lublin, Vol. VIII, 240-249.

Wcisło G. 2006. Application of the cold stamping metod for rapeseed oil extraction. Kom. Mot. Energ. Roln. TEKA t.6, 175-181.

Wcisło G. 2008. Wyznaczenie wpływu temperatury na lepkość dynamiczną biopaliw roślinnych. Inżynieria Rolnicza . 10(108), 277-282.

WPŁYW OKRESU PRZECHOWYWANIA NASION RZEAPKU OZIMEGO NA JAKOŚĆ PARAMETRÓW FIZYKO-CHEMICZNYCH DLA CELÓW PRZEMYSŁOWYCH

Streszczenie. W pracy dokonano analizy parametrów fizyko-chemicznych nasion rzepaku ozimego przechowywanych w warunkach laboratoryjnych przez okres do trzech lat. Analizie poddano parametry dotycząc poziomu wilgotności nasion, zawartości tłuszczu surowego, zawartości chlorofilu oraz określeniu lepkości oleju rzepakowego. W wyniku procesu przechowywania nasion, zaobserwowano niewielką tendencję spadkową zawartości tłuszczu surowego w próbkach oraz chlorofilu w wytłoczonym oleju. Ogólnie badane parametry jakościowe nasion oraz oleju mieściły się w granicach dopuszczalnych przez normy branżowe, czyniąc powyższe surowce cennym dla poszczególnych gałęzi przemysłu.

Słowa kluczowe: nasiona rzepaku, wilgotność nasion, tłuszcz surowy, chlorofil, lepkość oleju

TEKA Kom. Mot. Energ. Roln. – OL PAN, 2011, 11, 173–180

APPLICATION OF A MICROCONTROLLER IN SIMULATION OF THE PHOTOVOLTAIC GENERATORS

Jacek Kapica

University of Life Sciences in Lublin
Doświadczalna 50A, 20-280 Lublin
e-mail: jacek.kapica@up.lublin.pl

Summary. The solar radiation varies in time and is unrepeatable. For this reason in researches dealing with systems powered by photovoltaic generators a device simulating the current-voltage curve of a real generator may be useful. It consists of a controlling block, which can be made of a micro controller and an output unit – voltage amplifier.

The paper presents a mathematical model of a photovoltaic module, principle of operation of the simulator and results of laboratory measurements which were undertaken to test the designed device.

Key words: solar energy, photovoltaic generator, simulator.

INTRODUCTION

Since the energy crisis in 1970's a constant growth of photovoltaic power production has been observed [Grubb et al. 1997, Sinha 1998, Lotsch et al. 2005]. One of the areas of solar energy application is agriculture [Luque et al. 2003, Tiwari et al. 2010]. This kind of energy is sometimes considered as "agro-energy" [Roszkowski 2006].

Operating state of devices powered by photovoltaic (PV) generators depends on the solar radiation intensity on the surface of photovoltaic modules. This radiation varies in time and is unrepeatable. When, during research experiments it is needed to compare the performance of various configurations of the photovoltaic system, it is difficult to have the same radiation conditions for each case [Mukerjee et al. 2007].

One of the ways to solve this problem is to apply a device which will model the current-voltage curve of a photovoltaic generator for a given radiation values. Such a device may be also useful in training in the area of photovoltaics because experiments with real PV modules may be impossible in autumn – winter season or after dark.

Recently, a PV simulator with MOSFET technology has been presented [Gonzales et al. 2010]. The main components of the PV simulator presented in this paper are: amplifier in which we can control the output voltage and a microcontroller with a set of analog inputs and outputs.

A microcontroller is a computer which has all the necessary parts of a conventional microcomputer contained in a single electronic chip. Main parts of the microcontroller are: CPU (Central

Processing Unit), memory and input/output interface [James 2001]. The memory of the chip can store algorithms of system behaviour dependent upon many different parameters [Wierzbicki 2006], which enables the device to control different processes.

This paper presents the construction of the simulator and results of the tests which were performed to verify the current-voltage characteristics modelling quality.

CURRENT-VOLTAGE CURVE OF THE PV CELL

Current-voltage curve of a photovoltaic cell is given by the following equation [Kalogirou 2009]:

$$I = I_{PH} - I_0\left(\exp\left[\frac{e(V + IR_S)}{kT}\right] - 1\right) - \frac{V + IR_S}{R_{SH}}, \tag{1}$$

in which

I is the current generated by the PV cell and flowing through the load circuit,

I_{PH} – photocurrent, current of the short-circuited cell, proportional to the solar radiation intensity,

I_0 – dark saturation current,

V – cell's voltage,

e – electronic charge,

k – Boltzmann's constant,

T – cell's temperature,

R_{SH} – shunt resistance of the cell,

R_S – series resistance of the cell.

This and other models of photovoltaic cells are also presented by Kaddour et al., (2010).

Current-voltage curve modelling by the equation (1) is very difficult. Enough accuracy can be provided by a model with three parameters [Kapica 1998], which can be obtained from eq. (1) assuming $R_{SH} \to \infty$ and $R_S = 0$:

$$I = I_{PH} - I_0\left(\exp\left(\frac{eV}{kT}\right) - 1\right). \tag{2}$$

Parameters of this equation, which are specific for the given cell (I_{PH} with full insolation, I_0) need to be obtained by measurement of the current-voltage curve of a real PV cell or module, which we want to model. Methods to obtain the equation parameters are given by Kim et al. (2010) and Xu Xiao-bing et al. (2009).

For simplicity, influence of the solar radiation upon the cell's temperature has been neglected in the simulator's algorithm, but this functionality can be easily added.

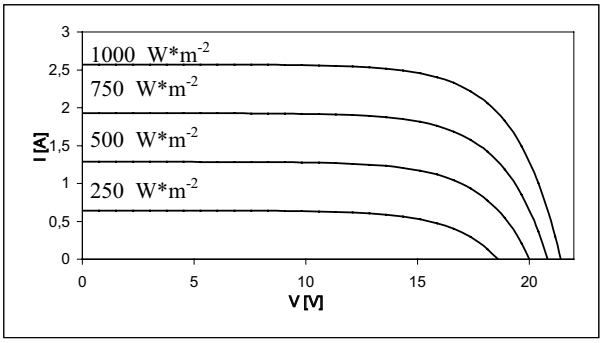

Fig. 1. Example of a current-voltage curve of a photovoltaic module for different insolation levels

THE PHOTOVOLTAIC SIMULATOR

Photovoltaic simulator is a device which is able to model current-voltage curve of a PV module or generator. Its main part is an operational amplifier, whose output voltage is proportional to the voltage applied to the input (Fig. 2). In the prototype device a high output current operational amplifier OPA 541 has been used [Texas Instruments 2000].

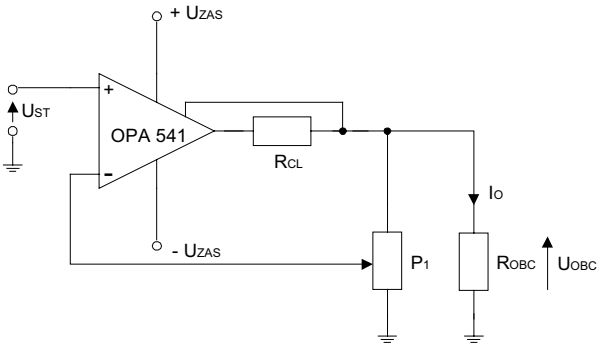

Fig. 2. Schematic diagram of a voltage amplifier used in the simulator [Marciniuk 2000]

A single chip microcomputer (microcontroller) with analog input and output circuits is used to control the amplifier. In the prototype device a ATmega8535 chip with external A/C and D/C converter chip has been used [Atmel 2006]. The analog input is connected to a Hall effect current transducer. The output voltage is fed to the input of the amplifier.

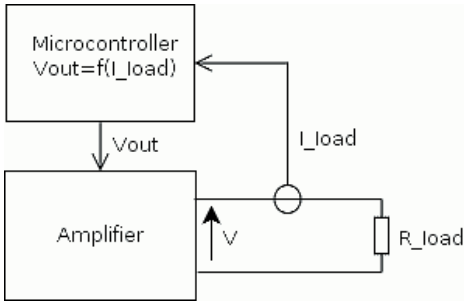

Fig. 3. Diagram of photovoltaic generators' simulator

The microcontroller sets its output voltage (Vout – see Fig. 3) based on measurements of the amplifier load current (I_load). The voltage is calculated according to the current – voltage curve equation for the simulated PV module or generator.

The current-voltage curve of the generator has been divided into two parts. In the part where the load current is lower or equal to 0.85 I_{PH}, the microcontroller's output voltage is calculated directly from the curve equation after transforming the equation (2) into a form of V=f(I).

Because the second part of the curve – for currents greater than 0.85 I_{PH} – has a large gradient of current as a function of voltage, it was necessary to employ a different procedure of the output voltage calculation. In this case, the output is changed stepwise until the working point on the current-voltage curve is reached iteratively.

TESTING PROCEDURE

In order to test the device a series of measurements have been done. All the experiments were conducted with help of the computer applications created in LabView - a graphical programming environment which is especially useful in creating software for measurement circuits [Buczaj et al. 2007].

In the first step it was checked whether the proposed single chip computer will be fast enough to calculate the required parameters in real time. This was achieved by exposing the device to rapid load resistance change when the input solar radiation was constant and by rapidly changing the input solar radiation with the load resistance unchanged. The measurement circuit is presented on Fig. 4. The time needed to set the working point was in the range of few milliseconds and on exceptional occasions to approx. 300 ms. The longer values were recorded for low radiation levels combined with low load resistance values. This is the result of the simulator working in the second part of the current-voltage curve and the iterative procedure of the working point calculation. However such cases were not frequent. Taking into account that the rate of radiation change is usually much slower, the tested microcontroller may be implemented in the simulator.

In the second step, a series of measurements were undertaken in order to compare the performance of the simulator with a real PV module. First, the voltage, current and insolation were registered over a period of several days for a real PV module connected to a load resistance. The circuit diagram is presented on Fig. 5. As a voltage transmitter a potentiometer (voltage divider) was used. The current was measured through a Hall-effect transducer. The insolation is obtained through measurement of the short-circuit current of another module which is parallel to the tested module. Also in this case a Hall-effect transducer was used.

Than the measurements for the PV simulator were performed. As the solar radiation data, the data obtained during measurements with the real module were used. In the electrical circuit used previously, the solar module was replaced with the simulator and the insolation data were fed to the simulator from a digital-to-analog converter card plugged into a computer (Fig. 4). The tests were planed in such a way that the voltage and current were saved 0.5 s after the insolation level had been set to allow time for the microcontroller to set the working point.

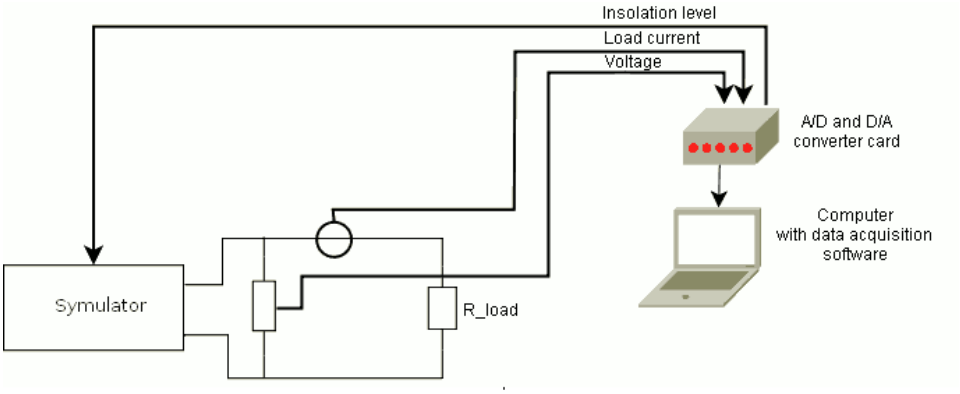

Fig. 4. Diagram of the measurement circuit for tests of the simulator of the photovoltaic generators

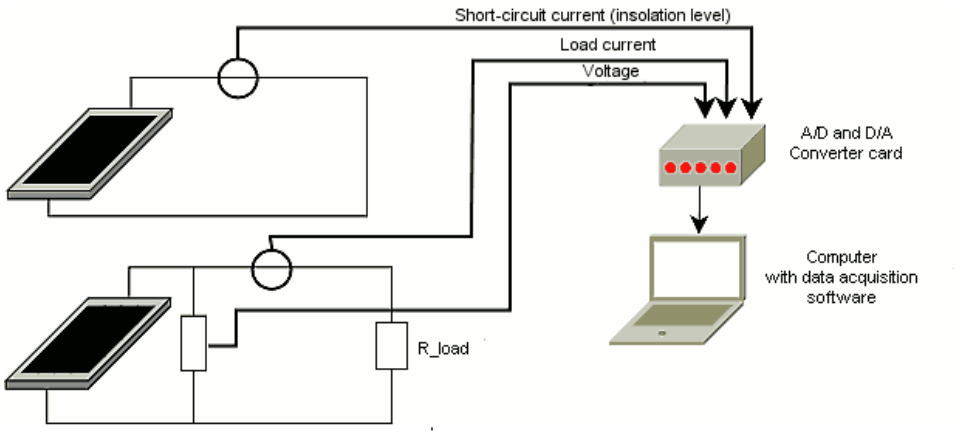

Fig. 5. Diagram of the measurement circuit for tests of a real photovoltaic module

The measurements were done in April 2010. Figures 6-9 present the results of the comparative tests from April 9th. One of the black lines shows the current or voltage of the real module whereas the grey line – of the simulator. Additionally an absolute error is presented (the other black line with lower values). For convenience, Fig. 8 to 9 present curves for a selected part of the day.

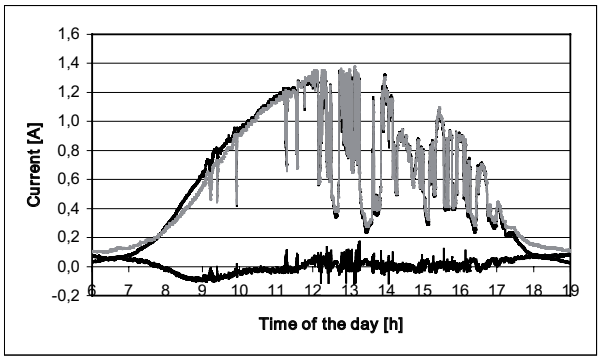

Fig. 6. Current – time curve of a real module and of the simulator for April 9th 2010

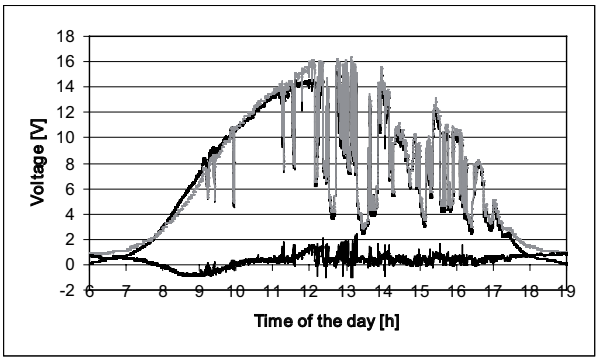

Fig. 7. Voltage – time curve of a real module and of the simulator for April 9th 2010

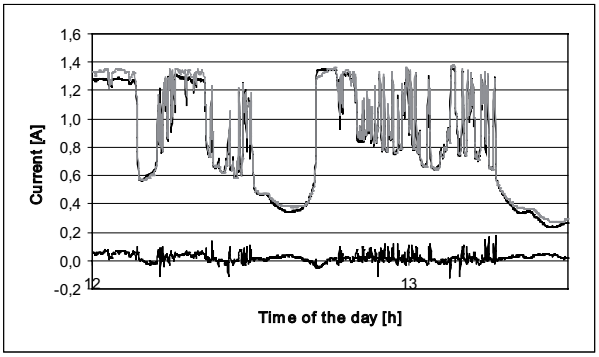

Fig. 8. Current – time curve of a real module and of the simulator for a selected part of April 9th 2010

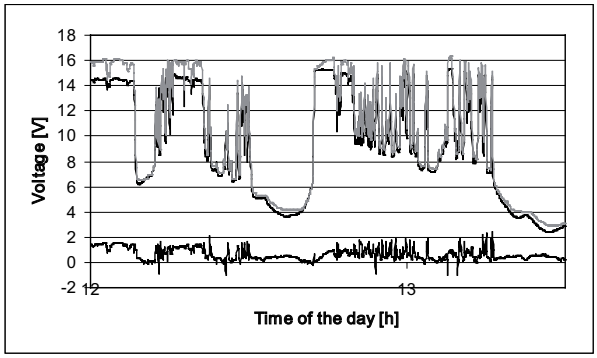

Fig. 9. Voltage – time curve of a real module and of the simulator for a selected part of April 9th 2010

After the measurements, maximum differences between the values obtained from the real module and from the simulator were calculated. Maximum absolute error for the current simulation was 0.18 A and for the voltage – 2.4 V. Additionally, the daily energies produced by the real module and the simulator were evaluated. The maximum difference was 8300 J (5 % of the value produced by the real PV module).

CONCLUSION

As the comparative tests show, the simulator resembles closely the current-voltage curve of a real PV module. The precision can be improved by employing a more accurate model and – primarily – by taking into account temperature change of the solar module with the insolation.

The time to set the working point is fair and it could be improved by using a faster CPU.

Proposed simulator of the photovoltaic generators can be used in researches aimed at performance analysis of circuits powered from photovoltaic power sources. Another area is education. In both cases application of the device gives an advantage of opportunity to repeat the tests for identical insolation curve, independent on current weather conditions and season of the year.

Additional advantage which was revealed during the tests of the device is a possibility to decrease the time needed to perform the test in case when the insolation sampling period is greater than the time needed to set the simulator's working point – which is true for most of the cases. For example, for the results presented in this paper, the simulation of the whole day was finished in less than two hours. This is because the simulator does not have to wait the full time between the points in time but only the time needed to set the working point.

REFERENCES

Atmel Corporation. 2006. 8-bit AVR Microcontroller with 8K Bytes In-System Programmable Flash.

Buczaj M., Sumorek A. 2007. Simulation of motor vehicles instrument panels in LabView environment. Teka Komisji Motoryzacji i Energetyki Rolnictwa VII. p. 52.

Gonzalez, S. Kuszmaul, S.; Deuel, D.; Lucca, R. 2010. PV array simulator development and validation. Photovoltaic Specialists Conference (PVSC), 35th IEEE. ISBN: 978-1-4244-5890-5.

Grubb M., Vigotti R. 1997. Renewable Energy Strategies for Europe: Electricity systems and primary energy sources. Royal Institute of Internetional Affairs. ISBN: 1-85383-284-7.
James M. 2001. Microcontroller cookbook. Newnes. ISBN 0-7506-4832-5. p. 4.
Kaddour A., Merad Boudia, M, Lemerini, M. 2010. Simulation and Modelling of the PEDOT/PSS Layer Effect for Organic Solar Cells with One and Two Diode Models, International Review on Modelling & Simulations.
Kalogirou S. A. 2009. Solar Energy Engineering: Processes and Systems. (p. 477). Elsevier. ISBN: 978-0-12-374501-9
Kapica J. 1998. The Influence of selection of the Solar Cell's Model on the Accuracy of Calculation of the Current-Voltage Characteristic, Proceedings of the 2nd World Conference and Exhibition on Photovoltaic Solar Energy Conversion, Vienna, Austria. ISBN 92-828-5179-6.
Kim W., Woojin C. 2010. A novel parameter extraction method for the one-diode solar cell model. Solar Energy 84.6.
Lotsch H.K.V., Goetzberger A., Hoffman V.U. 2005. Photovoltaic Solar Energy Generation. Springer Series in Optical Sciences Volume 112.
Luque A., Hegedus S. 2003. Handbook of photovoltaic science and engineering. John Wiley & Sons. p. 54.
Marciniuk K. 2000. Construction of a device to simulate the photovoltaic modules. Akademia Rolnicza w Lublinie (in Polish).
Mukerjee A.K., Dasgupta N. 2007. DC power supply used as photovoltaic simulator for testing MPPT algorithms, Renewable Energy, Volume 32, ISSN 0960-1481.
Papadopoulou E. 2011. Photovoltaic Industrial Systems: An Environmental Approach. Springer. p. 3.
Roszkowski A. 2006. Agriculture and fuels of the future. Teka Komisji Motoryzacji i Energetyki Rolnictwa VI. p. 132.
Sinha P.C. 1998. Energy Crisis. Anmol Publications. p. 184.
Texas Instruments Incorporated. 2000. OPA541 High Power Monolithic Operational Amplifier.
Tiwari G. N., Dubey S. 2010. Fundamentals of Photovoltaic Modules and their Applications. Royal Society of Chemistry. ISBN: 978-1-84973-020-4. p. 118.
Xu Xiao-bing, Wang Jian-ping, Zhang, Chong-wei. 2009. An analytical method of silicon solar cell model parameters. Chinese Journal of Power Sources, vol.33 no. 6.
Wierzbicki S. 2006. Diagnosing microrpocessor-controlled systems. Teka Komisji Motoryzacji i Energetyki Rolnictwa VI. p. 182.

ZASTOSOWANIE MIKROKONTROLERA DO SYMULACJI GENERATORÓW FOTOWOLTAICZNYCH

Streszczenie. Promieniowanie słoneczne jest zmienne w czasie i niepowtarzalne. Z tego względu w badaniach naukowych nad układami zasilanymi z generatorów fotowoltaicznych użyteczne może być urządzenie symulujące przebieg charakterystyki prądowo – napięciowej rzeczywistego generatora. Składa się ono z bloku sterującego, którym może być mikrokomputer jednoukładowy oraz bloku wyjściowego, którym jest wzmacniacz napięciowy. W artykule przedstawiono model matematyczny modułu fotowoltaicznego, zasadę działania symulatora oraz wyniki pomiarów mających na celu sprawdzenie poprawności pracy prezentowanego urządzenia.

Słowa kluczowe: energia słoneczna, generator fotowoltaiczny, symulator

TEKA Kom. Mot. Energ. Roln. – OL PAN, 2011, 11, 181–188

APPLICATION OF THE AKAIKE INFORMATION CRITERION FOR AN ASSESSMENT OF SUGAR BEET CROP DISTRIBUTION.

Andrzej Kornacki [1], Katarzyna Ostroga [2]

University of Life Sciences in Lublin
[1] Department of Applied Mathematics and Informatics
[2] Department of Agricultural Machinery

Summary. Normal distribution is commonly applied in natural sciences, as well as in technical, humanistic or social. It is also very often used for the description of phenomena and processes in investigations in the domain of agricultural engineering. Wide application of this distribution is justified by the principle of great numbers. Great importance of normal distribution results also from the following facts: 1) Normal distribution is a model for random error of measurements. 2) Many physical phenomena, even if they do not have normal distribution, can be described in terms of this distribution after suitable transformation. 3) Normal distribution is a good approximation for different distributions, 4) Every linear combination of independent random variables with normal distribution has a normal distribution.

These desirable properties cause, that research workers want to check whether the results of their experiments have normal distribution. In literature many tests checking normality of distribution of the studied feature are described both in one [Anderson at al 1954, Bowman at al 1975, Geary 1947, Green at al 1976,Tench at al 1980, Oja 1983, Pearson 1930, Shapiro at al 1965, Uthoff 1973, Vasicek, 1976] and in multidimensional case [Andrews at al 1973, Bera ay 1986, Cox at al 1978, Hawkins 1981, Henze at al 1990, Buck 1986, Royston 1983]. All of them require the application of suitable tables of critical values.

In the present work we suggest using the selection between normal and logarythm - normal distribution: Akaike information criterion (AIC). This criterion originates from the theory of information. The suggested method was applied to dataset obtained in an experiment with crops of sugar beets. Conclusions resulting from criterion Akaike were confirmed by the classic Shapiro-Wilka test.

Key words: Crop of sugar beet, Akaike information criterion, normal distribution, lognormal distribution, selection of the models.

AKAIKE INFORMATION CRITERION.

The concept of Akaike information criterion (AIC) has its source in the theory of information. This notion is based on the concept of Kullback-Leibler (K-L) information [Kulback.and Leibler 1951]. Let us consider a continuous probability distribution. Let $g(x)$ be the true density function and $f(x)$ be a model density function. Then the Kullback-Leibler information is given by [17]

$$I(g, f) = \int_{-\infty}^{+\infty} \log \frac{g(x)}{f(x)} g(x)dx, \tag{1}$$

where: log denotes the natural logarithm. $I(g, f)$ describes the distance between two probability distributions and has the following properties [Akaike 1974]:

1. $I(g, f) \geq 0$,
2. $I(g, f) = 0 \Leftrightarrow f(x) = g(x)$ almost everywhere.

Obviously, the lower the value of $I(g, f)$, the better the fitting of the model. Notice that the value of $I(g, f)$ depends on the distribution of $g(x)$, which is usually unknown. So we need an estimator of $I(g, f)$. From the definition of K-L information we have:

$$I(g, f) = \int_{-\infty}^{+\infty} g(x) \log g(x)dx - \int_{-\infty}^{+\infty} g(x) \log f(x)dx.$$

The first term in the last equality does not depend on the model distribution $f(x)$, so finding the minimum of K-L information is equivalent to finding the maximum of the value:

$$\int_{-\infty}^{+\infty} g(x) \log f(x)dx, \tag{2}$$

which is called an expected log likelihood. If we have *n* independent realizations $\{X_1,....,X_n\}$, then the value :

$$\sum_{i=1}^{n} \log f(x_i), \tag{3}$$

is called the log likelihood of the model. It is easy to prove that an expected log likelihood can be approximated by (3) times 1/n [24]. So, the higher the value of (3), the better the fitting of the model.

Assume that $f(x_1,...,x_n \mid \theta)$ is a joint distribution function of the vector $(X_1,...,X_n)$ θ, where is a parameter of the distribution. If we have *n* observations $\{x_1,....,x_n\}$ then the function $L(\theta) = f(x_1,...x_n \mid \theta)$ is called the likelihood function. When we consider the independent random variables $\{X_1,....,X_n\}$, then $L(\theta) = f(x_1 \mid \theta) \cdot ... \cdot f(x_n \mid \theta)$, where $f(x_i \mid \theta)$ is a density function of X_i, we can define the log likelihood function as

$$l(\theta) = \sum_{i=1}^{n} \log f(x_i \mid \theta).$$

Let us identify $g(x) = f(x \mid \theta^*)$, where *f* is a model with *k* parameters and θ^* is a vector of true parameters. Then the expected log likelihood of the distribution $f(\cdot \mid \theta)$ is given by [24]:

$$l^*(\theta) = E_Z[\log f(Z \mid \theta)],$$

where Z is a random variable with the same distribution as X_i and independent of X. As we said, this value is a criterion of fitting of the distribution. The higher the value of $l^*(\theta)$, the better the fitting of the model.

Let $\hat{\theta}$ be the maximum likelihood estimator of the parameters of the model maximizing the log likelihood function $l(\theta)$. So the goodness of fitting of the model can be expressed in terms of $l^*(\hat{\theta})$. Observe that this value depends on the realization of the random variable X. Therefore, in order to lose this dependence, define the mean expected log likelihood as:

$$l_n^*(k) = E_X[l^*(\hat{\theta}_k)] = \int l^*(\hat{\theta}) \prod_{i=1}^{n} g(x_i)dx.$$

As before, the higher the value of $l_n^*(k)$, the better the fitting of the model. At first sight, it would seem that the maximum log likelihood is a good estimator of the mean expected log likelihood. However, as Akaike has shown, it is a biased estimator of this value and its bias is equal to the number of the parameters. Akaike [25] has also shown that the asymptotically unbiased estimator of the mean expected log likelihood is:

AIC(k) = the maximum log likelihood – number of estimated parameters.

By historical reasons [Rao 1980] we take:

$$\mathrm{AIC}(k) = -2l(\hat{\theta}_k) + 2k. \tag{4}$$

Summarizing, the model which has the minimal value of AIC(k) is considered to be the most appropriate model.

ESTIMATION OF PARAMETERS OF NORMAL DISTRIBUTION BY THE MAXIMUM LIKELIHOOD METHOD

Let $X_1, X_2, ..., X_n$ be the independent *n* observations of the normal distribution $N(\mu, \sigma^2)$, where $\mu \in R, \sigma^2 > 0$. Let us consider the normal density function of the random variable X_i:

$$f(x_i \mid \mu, \sigma^2) = \frac{1}{\sqrt{2\pi\sigma^2}} \exp\left\{-\frac{(x_i - \mu)^2}{2\sigma^2}\right\}.$$

The likelihood function is given by

$$L(\mu, \sigma^2) = \frac{1}{\left(\sqrt{2\pi\sigma^2}\right)^n} \exp\left\{-\frac{1}{2\sigma^2}\sum_{i=1}^{n}(x_i - \mu)^2\right\}. \tag{5}$$

Thus

$$l(\mu, \sigma^2) = -\frac{1}{2\sigma^2}\sum_{i=1}^{n}(x_i - \mu)^2 - \frac{n}{2}\log 2\pi - \frac{n}{2}\log\sigma^2.$$

We also have

$$\frac{\partial l}{\partial \mu} = \frac{1}{\sigma^2}\sum_{i=1}^{n}(x_i - \mu) \text{ and } \frac{\partial l}{\partial \sigma^2} = \frac{1}{2\sigma^4}\sum_{i=1}^{n}(x_i - \mu)^2 - \frac{n}{2\sigma^2}. \tag{6}$$

We will find the maximum value of the function $l(\cdot,\cdot)$ and the corresponding maximum argument. The necessary condition for the existence of the maximum of this function is $\frac{\partial l}{\partial \mu} = 0$ and $\frac{\partial l}{\partial \sigma^2} = 0$. Solving the system

$$\begin{cases} \sum_{i=1}^{n}(x_i - \mu) = 0 \\ \sum_{i=1}^{n}(x_i - \mu)^2 - n\sigma^2 = 0, \end{cases} \tag{7}$$

we get $\mu = \frac{1}{n}\sum_{i=1}^{n} x_i$ and $\sigma^2 = \frac{1}{n}\sum_{i=1}^{n}(x_i - \mu)^2$.

We can write the solution of the above system as:

$$\hat{\mu} = \frac{1}{n}\sum_{i=1}^{n} x_i,\ \hat{\sigma}^2 = \frac{1}{n}\sum_{i=1}^{n}(x_i - \hat{\mu})^2. \tag{8}$$

Now, we should check if the function $l(\cdot,\cdot)$ has the maximum in $(\hat{\mu},\hat{\sigma}^2)$. We will check if $l(\hat{\mu},\hat{\sigma}^2) - l(\mu,\sigma^2) \geq 0$. Let us consider the difference:

$$l(\hat{\mu},\hat{\sigma}^2) - l(\mu,\sigma^2) == -\frac{1}{2\hat{\sigma}^2}\sum_{i=1}^{n}(x_i - \hat{\mu})^2 - \frac{n}{2}\log\hat{\sigma}^2 + \frac{1}{2\sigma^2}\sum_{i=1}^{n}(x_i - \mu)^2 - \frac{n}{2}\log\sigma^2 =$$

$$= -\frac{1}{2\hat{\sigma}^2}\sum_{i=1}^{n}(x_i - \hat{\mu})^2 - \frac{n}{2}\log\frac{\hat{\sigma}^2}{\sigma^2} + \frac{1}{2\sigma^2}\left[\sum_{i=1}^{n}(x_i - \hat{\mu})^2 + n(\hat{\mu} - \mu)^2\right] =$$

$$= -\frac{n}{2}\log\frac{\hat{\sigma}^2}{\sigma^2} + \left(\frac{1}{2\sigma^2} - \frac{1}{2\hat{\sigma}^2}\right)\sum_{i=1}^{n}(x_i - \hat{\mu})^2 + \frac{n(\hat{\mu} - \mu)^2}{2\sigma^2} = \frac{n}{2}\left(\frac{\hat{\sigma}^2}{\sigma^2} - 1 - \log\frac{\hat{\sigma}^2}{\sigma^2}\right) + \frac{n(\hat{\mu} - \mu)^2}{2\sigma^2}.$$

The last term in the equation is nonnegative, so we can observe the function $f(x) = \log x - x$. The function f has a maximum in $x = 1$ and $f(1) = -1$. Thus $\log x - x \leq -1$ for $x > 0$.

So we have $l(\hat{\mu},\hat{\sigma}^2) - l(\mu,\sigma^2) \geq 0$, which implies that function $l(\mu,\sigma^2)$ has the maximum at $\mu = \hat{\mu}$ and $\sigma^2 = \hat{\sigma}^2$. To summarize, $\hat{\mu}$ and $\hat{\sigma}^2$ are the maximum likelihood estimators of the parameters μ and σ^2. Also the maximum log likelihood is given by:

$$l(\hat{\mu},\hat{\sigma}^2) = -\frac{n}{2}\log 2\pi\hat{\sigma}^2 - \frac{n}{2}. \tag{9}$$

ESTIMATION OF PARAMETERS OF LOGNORMAL DISTRIBUTION BY THE MAXIMUM LIKELIHOOD METHOD.

Def. Let random variable Y have a normal distribution: $Y \sim N(\mu,\sigma^2)$. Then a random variable $X = e^Y$ has a lognormal distribution with parameters μ,σ^2. The probability density function of the lognormal random variable is given by the formula;

$$f(x) = \begin{cases} 0, & x \leq 0 \\ \dfrac{1}{x\sigma\sqrt{2\pi}} e^{-\frac{(\ln x - \mu)^2}{2\sigma^2}}, & x > 0 \end{cases} \tag{10}$$

Let $X_1, X_2, ..., X_n$ be the sample from lognormal distribution with parameters μ,σ^2. $\mu \in R, \sigma^2 > 0$. Let us consider the lognormal density function of the random variable X_i:

$$f(x_i \mid \mu,\sigma^2) = \frac{1}{x\sqrt{2\pi\sigma^2}}\exp\left\{-\frac{(\ln x_i - \mu)^2}{2\sigma^2}\right\} \text{ dla } x>0.$$

The likelihood function is given by:

$$\begin{cases} L(\mu,\sigma^2) = f(x_1, x_2, \ldots, x_n I \sigma^2, \mu) = \prod_{i=1}^{n} f(x_i I \sigma^2, \mu) \\ = (2\pi\sigma^2)^{-\frac{n}{2}} \prod_{i=1}^{n}(x_i)^{-1} \cdot e^{-\frac{\sum_{i=1}^{n}(\ln x_i - \mu)^2}{2\sigma^2}}. \end{cases} \tag{11}$$

Thus log likelihood is equal to:

$$l(x|\sigma^2,\mu) = -\frac{n}{2}(\ln 2\pi + \ln\sigma^2) - \sum_{i=1}^{n}\ln x_i - \frac{\sum_{i=1}^{n}(\ln x_i - \mu)^2}{2\sigma^2} \tag{12}$$

In order to find the maximum likelihood estimators $\hat{\mu}$ i $\hat{\sigma}^2$ of parameters of distribution we differentiate the function with respect to μ i σ^2 i and then equate it to zero. We get the following:

$$\begin{cases} \dfrac{\partial l}{\partial \mu} = -\dfrac{1}{2\sigma^2}\sum_{i=1}2(\ln x_i - \mu)(-1) = \dfrac{1}{\sigma^2}\sum_{i=1}^{n}(\ln x_i - \mu) = 0 \\ \dfrac{\partial l}{\partial \sigma^2} = -\dfrac{n}{2\sigma^2} + \dfrac{\sum_{i=1}^{n}(\ln x_i - \mu)^2}{2}\cdot\dfrac{1}{\sigma^4} = 0. \end{cases} \tag{13}$$

After the transformation of the system (13) we obtain equalities:

$$\begin{cases} \sum_{i=1}^{n}(\ln x_i - \mu) = 0 \\ -n\sigma^2 + \sum_{i=1}^{n}(\ln x_i - \mu)^2 = 0, \end{cases} \tag{14}$$

and from it the following estimators:

$$\begin{cases} \hat{\mu} = \dfrac{\sum_{i=1}^{n}\ln x_i}{n} = \overline{\ln x} \\ \hat{\sigma}^2 = \dfrac{\sum_{i=1}^{n}(\ln x_i - \hat{\mu})^2}{n} = S^2_{\ln x}. \end{cases} \tag{15}$$

Moreover, the maximum log likelihood is equal to (from(12) and (15)):

$$\left\{l(x|\hat{\sigma}^2,\hat{\mu}) = -\frac{n}{2}\ln 2\pi - \frac{n}{2}\ln\hat{\sigma}^2 - \sum_{i=1}^{n}\ln x_i - \frac{n}{2}. \right. \tag{16}$$

SELECTION OF NORMAL DISTRIBUTION BY THE AKAIKE METHOD

We want to verify if the investigated feature in population has a normal or lognormal distribution. We state hypotheses:

$$\begin{cases} H_0 : F(x) \in F_N \\ H_{1_1} : F(x) \in F_{LN}, \end{cases} \tag{17}$$

where: F_N denotes a family of normal cumulative distribution functions, F_{LN} a family of lognormal cumulative distribution functions and F(x) a cumulative distribution function of feature in population.

In Akaike method we match to each of hypotheses a model connected with specified probability distribution, evaluate Akaike information criterion AIC for each model and then we choose this hypothesis, which corresponds to the lower value of AIC.

Model (0)-the feature in population has normal distribution.

Model (1)-the feature in population has lognormal distribution.

From (4) we have $\mathrm{AIC} = -2\mathrm{l}(\hat{\theta}) + 2\mathrm{k}$. As the number of free parameters in the model (0) is 2 so AIC for it is equal to (from (9)):

$$\left\{\mathrm{AIC}(0) = \mathrm{AIC}(\mu, \sigma^2) = -2\mathrm{l}(\hat{\mu}, \hat{\sigma}^2) + 2\mathrm{x}2 = \mathrm{n}[\log 2\pi + \log \hat{\sigma}^2 + 1] + 4\right\} \tag{18}$$

where $\hat{\sigma}^2$: is given by (8).

Similarly, for model (1) we find (from (16)):

$$\mathrm{AIC}(1) = -2\mathrm{l}(\hat{\mu}, \hat{\sigma}^2) + 2\mathrm{x}2 = \mathrm{n}[\log 2\pi + \log \hat{\sigma}^2 + 1] + 2\sum_{\mathrm{i}=1}^{\mathrm{n}} \ln \mathrm{x}_{\mathrm{i}} + 4 \tag{19}$$

where in its time $\hat{\sigma}^2$ is given by (15).

APPLICATION

The Akaike theory given in previous sections we apply to an analysis of experimental data from the crop of sugar beets. Proper investigations were carried out in the years 2006-2008. [Ostroga 2010, Bzowska-Bakalarz et al 2008]. The tool for assembling the data in farms were questionnaires filled through growers. Area of questionnaires' investigations contained region of working of four sugar factories - Krasnystaw, Lublin, Werbkowice and Strzyżów. Respondents were farmers who had a chance of survival of production of sugar beets in next years. They became chosen at co-operation with workers of sections of raw material sugar factory on the basis of positive productive results. Investigations were carried out by the method of standardized interview. Analyzing dataset related to crops of sugar beet received through 100 manufacturers in 2006 year we obtain $\hat{\sigma}^2$ =75,035, n=100 while from example (18) we get:

$$\mathrm{AIC}(0) = 100 \cdot [1{,}8379 + \ln(75{,}035) + 1] + 4 = 719{,}5855. \tag{20}$$

For dataset $\hat{\sigma}^2$ =0,0364, $\sum_{\mathrm{i}=1}^{\mathrm{n}} \ln \mathrm{x}_{\mathrm{i}}$=381,89, n=100 from example (19) we receive:

$$\mathrm{AIC}(1) = 100 \cdot [1{,}8379 + \ln(0{,}0364) + 1] + 2 \cdot 381{,}89 + 4 = 720{,}2513 \tag{21}$$

In the face of inequality AIC(1)>AIC(0) we state, that normal distribution better than log normal distribution describes crops of beets. Now we will try to apply the traditional method of testing of hypotheses for analysis of experimental dataset. We will use classic test Shapiro-Wilka to this end. Test function of this test has the form [Domański 1990]:

$$\mathrm{W} = \frac{\{\sum_{\mathrm{i}=1}^{\left[\frac{\mathrm{n}}{2}\right]} \mathrm{a}_{(\mathrm{i})}(\mathrm{x}_{(\mathrm{n}-\mathrm{i}+1)} - \mathrm{x}_{(\mathrm{i})})\}^2}{\sum_{\mathrm{i}=1}^{\mathrm{n}} (\mathrm{x}_{\mathrm{i}} - \bar{\mathrm{x}})^2}, \tag{22}$$

where: $x_{(i)}$ denotes i-th; within growing crop of beet., $a_{(i)}$ fixed value in Shapiro-Wilka test read from statistical tables, meanwhile symbol [z] denotes the largest integer number less or equal to z. In our example we have: n=100, $\sum_{i=1}^{\left[\frac{n}{2}\right]} a_{(i)}(x_{(n-i+1)} - x_{(i)}) = 85,39$, $nS^2 \sum_{i=1}^{n}(x_i - \bar{x})^2 == 7503,5202$.

Therefore in the face of (22) we get:

$$W = \frac{(85,39)^2}{7503,5202} = 0,9717. \tag{23}$$

Assuming the level of significance α =0,05 we read the critical value $W_{0,05}$=0,9641. In the face of $W > W_{0,05}$ we state, that it does not have bases for rejection of hypothesis about normality of distribution of crop of sugar beets.

REFERENCES

Akaike H.1974.: A new look at the statistical model identification. IEEE.Trans.Autom.Contr, AC-19, 716-723.

Anderson T.W., Darling D.A. 1954.: A test of goodness of fit JASA 49, 765-769**.**

Andrews D.F., Gnanadesikan R., Warner J.L. 1973.:Methods for assessing multivariate normality**.** In P.R Krishnaiah, ed, Multivariate Analysis, 3rd ed., Academic Press, New York.

Bera A., John. 1986.:Test for multivariate normality with Pearson alternatives**.** Commun in Statist. 12, 103-117.

Box G.E.P**.,** 1953.:A note on regions for tests of kurtosis. Biometrika 40, 465-468.

Bowman K.O., Shenton L.R. 1975.:Omnibus test contours for depature from normality based on $\sqrt{b_1}$ and b_2.

Bzowska-Bakalarz M., Gil K. 2008.:Analiza funkcjonowania bazy danych do monitorowania systemu produkcji buraków cukrowych. Inzynieria Rolnicza 2,15-21.

Cox D.R., Small N.J.H. 1978.:Testing Multivariate normality**.** Biometrika 65, 263-262.

D'Agostino R.B. 1971.:An omnibus test for normality for moderate and large size samples. Biometrika 58, 341-348.

Domański C. 1990.:Testy statystyczne**.** PWE, Warszawa.

Franck W.E. 1981.:The most powerful invariant test of normal versus Cauchy with applications to stable alternatives**.** JASA 76, 1002-1005.

Geary, R.C. 1947.: Testing for normality. Biometrika.34, 209-242.

Green J.R., Hegazy Y.A.S. 1976. Powerful modified EDF goodness of fit test. JASA 71, 204-209.

Hawkins D.M. 1981**.:**A new test for multivariate normality and homoscedasticity. Technometrics 23, 105-110.

Henze, N., Zirkler, B. 1990.:A class of invariant consistent tests for multivariate normality**.** Commun in Statist. 19, 3595-3617.

Kozioł J.A. 1986.:Assesing multivariate normality: a compendium Commun in Statist 15, 2763-2783.

Kulback Leibler. 1951.: On information and sufficiency. Ann.Math.Statist, 22, 79-86.

Lin, C.C. Mudholkar G.S. 1980.:A simple test for normality against non-symmetric alternatives**.** Buiometrika 67, 455-461.

Locke C., Spurrier J.D. 1976.:The use of U-Statistics for testing normality against non-symmetric alternatives**.** Biometrika 63, 143-147.

Oja H. 1983.**:**New tests for normality. Biometrika 70, 297-299.
Ostroga K 2010.:Techniczne i technologiczne uwarunkowania produkcji buraków cukrowych na tle aktualnej organizacji rynku rolnego**.** Rozprawa doktorska. Wyd UP Lublin.
Pearson E.S. 1930:A further development of tests for normality. Biometrika 22, 239-249.
RaoC.R. 1980.:Modele liniowe statystyki matematycznej PWN Warszawa.
Royston J.P. 1983.:Some techniques for assessing multivariate normality based on the
Shapiro-Wilk W. Appl Statist 32, 121-133.
Sakamoto .Y., Ishiguro M., Kitagawa G. 1986.:Akaike Information Criterion Statistics. Mathematics and Its Application.

ZASTOSOWANIE KRYTERIUM AKAIKE DO OCENY ROZKŁADU PLONÓW BURAKÓW CUKROWYCH

Streszczenie. Rozkład normalny jest powszechnie stosowany w naukach przyrodniczych, technicznych jak również humanistycznych i społecznych. Bardzo często jest on również używany do opisu zjawisk i procesów w badaniach z zakresu inżynierii rolniczej. Szerokie wykorzystanie tego rozkładu tłumaczą prawa wielkich liczb. Znaczenie rozkładu normalnego wynika też z następujących faktów: 1) Rozkład normalny jest modelem dla losowych błędów pomiarów. 2) Wiele zjawisk fizycznych, choć nie podlega rozkładowi normalnemu może być opisanych za pomocą tego rozkładu po odpowiedniej transformacji. 3) Rozkład normalny jest dobrym przybliżeniem dla innych rozkładów, 4) Każda kombinacja liniowa niezależnych zmiennych losowych o rozkładzie normalnym ma rozkład normalny.

Te pożądane własności powodują, iż badacze dysponując wynikami eksperymentu chcą sprawdzić czy mają one rozkład normalny. W literaturze opisanych jest wiele testów sprawdzających normalność rozkładu badanej cechy zarówno w przypadku jedno [Anderson i in 1954, Bowman i in 1975, Geary 1947,Green i in 1976,Lin i in 1980,Oja 1983,Pearson 1930, Shapiro i in 1965, Uthoff 1973, Vasicek, 1976] jak i wielowymiarowym [Andrews i in 1973, Bera i in 1986, Cox i in 1978, Hawkins 1981, Henze i in 1990, Kozioł 1986, Royston 1983]. Wszystkie one wymagają stosowania odpowiednich tablic wartości krytycznych.

W niniejszej pracy proponuje się zastosowanie do selekcji między rozkładem normalnym i logarytmo-normalnym kryterium informacyjnego Akaike. Kryterium to wywodzi się z teorii informacji. Sugerowaną metodę zastosowano do danych uzyskanych w doświadczeniu z plonami buraków cukrowych .Wnioski wynikające z kryterium Akaike potwierdzono klasycznym testem Shapiro-Wilka.

Słowa kluczowe: Plony buraków cukrowych, kryterium informacyjne Akaike, rozkład normalny, rozkład logarytmo-normalny, selekcja modeli.

TEKA Kom. Mot. Energ. Roln. – OL PAN, 2011, 11, 189–196

THE INFLUENCE OF MOISTURE CONTENT OF SELECTED ENERGY CROPS ON THE BRIQUETTING PROCESS PARAMETERS

Alina Kowalczyk-Juśko*, Ryszard Kulig**, Janusz Laskowski**

* Department of Crop Production and Agribusiness,
**Department of Food Industry Machinery Operation,
University of Life Sciences in Lublin, ul. Doświadczalna 44, 20-280 Lublin
e-mail: ryszard.kulig@up.lublin.pl

Summary. The following paper examines the effect of pressure agglomeration process on some energy crops (miscanthus, prairie cordgrass, Virginia mallow). The materials susceptibility to briquetting was assessed, together with the relevant energy consumption levels needed for the agglomeration processes as well as the quality of the final product. The lowest electrical energy consumption was observed at the briquetting of powdered miscanthus (average 412.87 kJ·kg^{-1}), and the highest consumption was observed for Virginia mallow at about 629.23 kJ·kg^{-1}. The briquetted Virginia mallow has shown to possess the highest value of mechanical durability at about 91.45%.

Key words: energy crops, briquetting, pressure agglomeration, energy consumption, briquette quality.

INTRODUCTION

Recently, an increase in the demand for biomass of agricultural origin has been observed (Junginger et al, 2008; Kowalska, 2010; Schenkel et al, 2003; van Dam et al, 2007; van Dam et al 2009) and, consequently, there has been a quest for the most energy-efficient crops which are also well adapted to a variety of conditions (Kowalczyk-Juśko, 2007). At the same time, there has been more interest on the part of farmers and the energy sector in new plant species, among which perennial grasses with C4 photosynthesis have received the most attention. An example of such a plant is *Miscanthus x giganteus* Greef & Deuter. A major issue in its cultivation is its low resistance to low temperatures, especially in its first year of vegetation (Clinton-Brown and Lewandowski, 2000). In rather severe climatic conditions of central and eastern Europe, species more resistant to such conditions enjoy popularity, such as *Miscanthus sacchariflorus* (Maxim.) Benth. & Hook.), prairie cordgrass (*Spartina pectinata* Link.) and the perennial plant - Virginia mallow (*Sida hermaphrodita* Rusby) (Borkowska and Styk, 2006; Kościk, 2003; Lewandowski et al, 2000). The species are treated as energy crops and as fuel material both by the energy sector and in the light of the Polish law (Rozporządzenie… 2008). The plants are characterized by significant durability, estimated in the relevant sources as lasting from several to over twenty years. The yield of prairie cordgrass in

eastern England was estimated at the level of 12-14 $Mg \cdot ha^{-1}$ (Potter et al, 1994) and in northern Germany at about 12.8 $Mg \cdot ha^{-1}$ (El Bassam, 1998). Its resistance to unfavourable environmental conditions is often emphasized; inevitably such conditions will lead to lower yields, nevertheless its durability is adequate. Miscanthus is the species characterized by great expansiveness and durability and thanks to its strong shrubbing properties it replaces weeds, which in turn lowers the overall cost of plantation. In optimal soil moisture conditions, the plant can yield crops at the level of 20 $Mg \cdot ha^{-1}$ (El Bassam, 1998). Virginia mallow is found in certain areas of the United States of America as a wild, uncultivated plant, and its cultivation records in Russia and Ukraine date back to 1930s (Spooner et al, 1985). Great hopes have recently been pinned on its cultivation for energy purposes in Poland (Borkowska and Styk, 2006; Kościk, 2003).

An effective use of plant biomass in professional energy generation is closely related to the need of the biomass to be agglomerated, which allows for "energy densification." In relevant sources there is no explicit assessment of the susceptibility of the above- mentioned plant species to pellet and briquette compacting.

In the case of pressure agglomeration processes (compacting), physical and chemical properties of the processed material are of primary importance (above all, chemical composition and moisture content) (Mani et al, 2006; Niedziółka et al, 2008; Relova et al, 2009; Szymanek and Kachel-Jakubowska, 2010) as they essentially impact both the efficiency of the process and the durability properties of the final product. In terms of chemical composition of the material, the agglomeration process is determined mainly by the content levels of fats, fibres, proteins and starch (Kaliyan and Morey, 2009). Materials rich in protein and starch and low in fibre content are especially suited to such processing (Kulig and Laskowski, 2006). A fat content of 2-3% is also advisable, as the values below 1% make the pellet compacting significantly more difficult (Kulig and Laskowski, 2005). Naturally, such conditions cannot be met by energy crops whose main content is fibre. The compacting of such materials requires considerable energy expenditures.

Keeping the above-stated facts in mind, in the present paper we endeavour to examine the efficiency of briquetting process of the selected energy crops at their varying moisture content. We believe that the examination will be a valuable contribution to the popularity of the cultivation of energy crops, and that our work will provide highly needed advice for farmers, companies and staff involved in the search and production of energy efficient briquettes.

MATERIALS AND METHODS

The research material was the powdered miscanthus, prairie cordgrass, and Virginia mallow plant material. The plants under investigation came from the experimental fields of the University of Life Sciences in Lublin, Faculty of Agricultural Sciences in Zamość, Department of Agribusiness and Plant Production, and were harvested after the fifth year of vegetation (in January 2010), which means they were in their full crop capacity. The harvesting was conducted when Virginia mallow had lost its leaves, and the grasses were withered.

The material was cut into shreds of 20mm in length, and subsequently was ground in a beater mill (type ML-500), fitted with a sieve with ϕ 4mm holes. After grinding, the material's moisture was determined, using the drier method complying with the norm PN-ISO 712:2002.

The briquette compacting was conducted in the laboratory at the Department of Food Industry Machinery Operation (KEMPS) in the University of Life Sciences in Lublin. The agglomeration process was conducted with the use of a hydraulic briquette press type PBH-100. The working densification pressure was 50 MPa. Briquettes produced in this way measured 60 mm in diameter and 80 mm in length.

During the briquetting process the conditioning with water was applied. Before pressing the examined material was brought to five distinct levels of moisture content, that is 12, 14, 16, 18, and 20%, with ±0,5% accuracy. The quantity of added water was determined based on the following formula:

$$M_w = M_1 \frac{W_2 - W_1}{100 - W_2}, \quad (1)$$

where: M_w – weight of added water, g;
M_1 – weight of material sample, g;
W_1 – moisture content of material sample, %;
W_2 – required moisture content of material sample, %.

The samples were stored for 24 h in tight containers to evenly distribute moisture throughout the material.

The quality of the agglomerates was estimated on the basis of their physical properties. The density of briquette was determined on the basis of the measurement of its external dimensions and mass, after 24 hours since its production. The moisture content of the input material was determined by the drier method, according to the norm PN-ISO 712:2002. The examination of mechanical durability of briquettes was conducted according to the norm PN–EN 15210-2:2011. The measurements of agglomerate mechanical strength was conducted in test grip "brazilian " (Li et al, 2000, Ruiz et al, 2000), with the use of a Zwick Z020/TN2S tensile tester in the range of 0÷500 N tension. Individual briquette, after having their length (l) and diameter (d) measured with $\pm 10^{-1}$ mm accuracy, were placed horizontally on a stationary table and they were subsequently crushed with a measurement head moving at a steady speed of 10 mm/min. The measurement was conducted until the maximum tension (F_n) was obtained, after which the agglomerate was disintegrated. Mechanical strength of briquette [MPa] was determined using the following formula:

$$o_m = \frac{2 \cdot F_n}{\pi \cdot d \cdot l}, \quad (2)$$

In order to establish energy consumption demands for the compacting processes (electrical energy), the value of energy required by a given device was measured in the same period of time as the measurement of its efficiency. The measurements were made with the use of network parameter meter Vega 76, equipped with HT96U meter clamp.

An analysis of the dependence between the moisture content of raw materials and the parameters of the briquetting process was performed using the statistical procedures included in the STATISTICA program, at the significance level of $\alpha_i = 0.05$

RESULTS AND DISCUSSION

The results obtained during the investigation of the briquette compacting process point to the fact that the materials under examination are suitable for this form of agglomeration. In the case of all materials under study, the technological process of briquetting was successful and the end product was a durable agglomerate. The only exception was miscanthus briquettes produced from loose material with 12% moisture content. In this case, the product leaving the compacting machine did not retain the briquette shape and crumbled. However, with other moisture levels, the process was more successful. The results of the examination of the influence of moisture content in the loose input material on the briquetting compacting process are set out in Figures 1 to 5.

The changes of the agglomerate density were presented in Figure 1. For all the studied materials the highest values of the parameter were found for moisture 16%, and the smallest for moisture 20%.

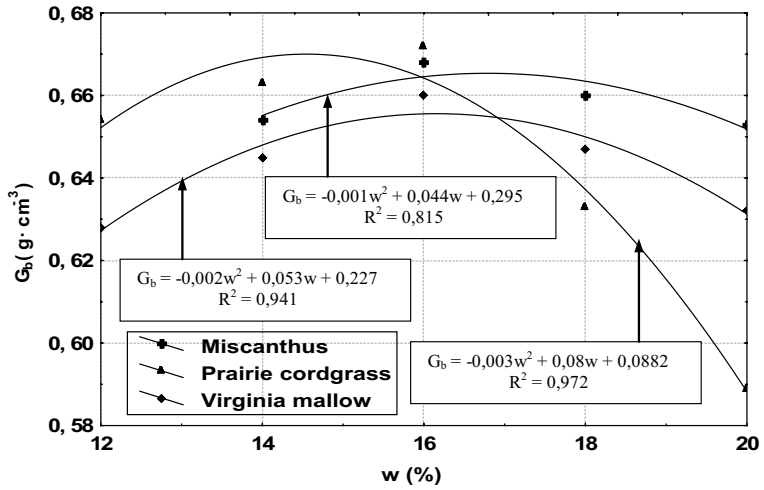

Fig. 1. Correlation between density (G_b) and moisture content (w)

Virginia mallow briquettes were characterized by the highest values of resistance parameters (Fig. 2). In the case of mechanical durability, no significant influence of moisture content was found on the value of the parameter under investigation ($p>0,05$), and the obtained differences were in the error margin.

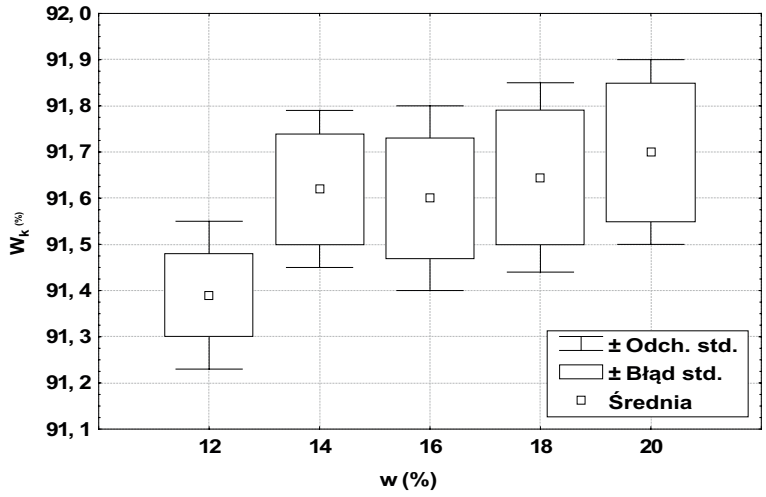

Fig. 2. Correlation between mechanical durability of Virginia mallow (W_k) and moisture content (w)

In relation to other materials (Fig. 3), the influence was more noticeable, especially in the case of miscanthus, where the increase of moisture content from 14% to 20% allowed to obtain a briquette with the mechanical durability increased by 20 proportional points.

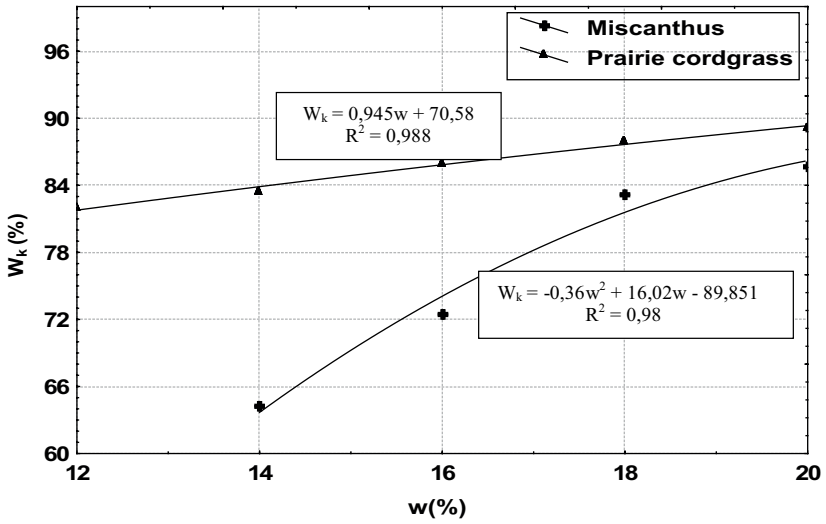

Fig. 3. Correlation between mechanical durability (W_k) and moisture content (w)

Such tendency was also observed in the examination of the mechanical strength of briquette (Fig. 4). For all the materials the highest values of mechanical strength were noted with 16% moisture content of the loose input material.

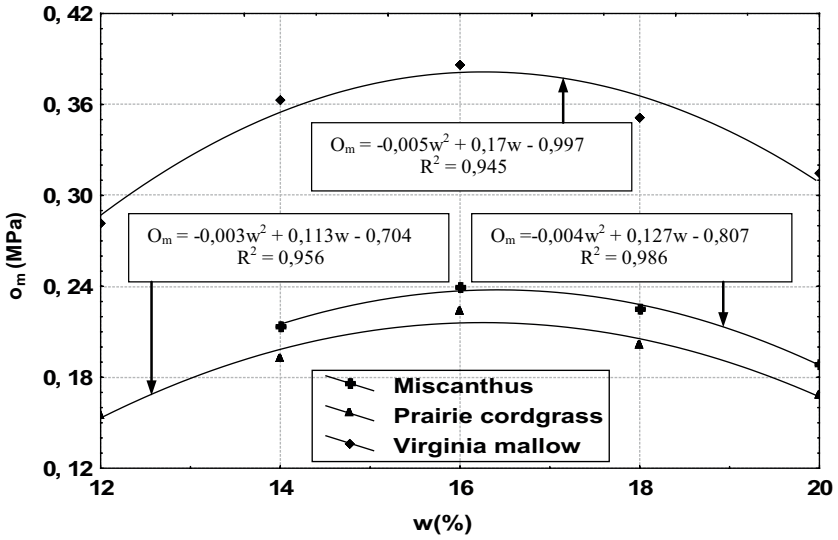

Fig. 4. Correlation between mechanical strength (O_m) and moisture content (w)

Also, in case of energy consumption, an increase in the moisture content of the loose material leads to a significant reduction in the energy expenditure required for pressing (Fig. 5).

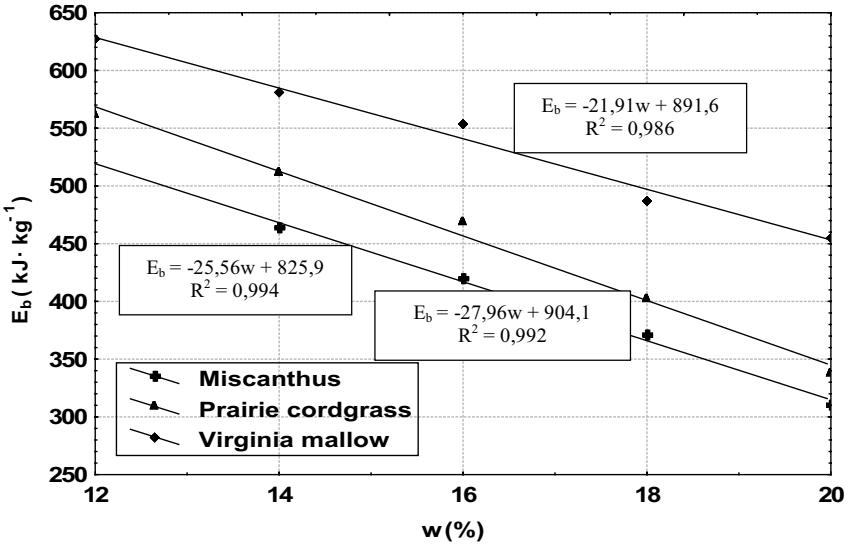

Fig. 5. Correlation between energy consumption *(E_b)* and moisture content (*w*)

The highest reduction in energy demands (40%) related to an increase in moisture content was noted for prairie cordgrass. It is also worth noting that in the case of Virginia mallow, the value of the reduction is 27%. However, it must be noted that briquettes produced with lower energy expenditure are characterized by higher moisture content, which in turn lowers their calorific value.

CONCLUSIONS

On the basis of the results of the present examination, the following conclusions can be formulated:

1. It has been found out that pressure energy consumption during pressure agglomeration is dependent both on the moisture content and the type of input material, and consequently, its physical and chemical properties.

2. The increase in moisture content of the input material in the investigated range leads to a decrease in energy required for agglomeration. The highest levels of such a reduction are seen in miscanthus and prairie cordgrass briquetting (38% and 40% respectively). In the case of Virginia mallow, the reduction is 27%.

3. The lowest energy consumption per unit needed to produce agglomerate have been noted in the case of miscanthus and are 23% lower on average than in the case of Virginia mallow briquetting.

4. It has been found that with the increase in moisture content of the input material there is an increase in mechanical durability of agglomerates. The best results in durability are obtained by Virginia mallow agglomerate.

5. A proper miscanthus briquette compacting requires the loose input material moisture content to be at the level of about 14%. In the case of prairie cordgrass and Virginia mallow, a similar quality of agglomeration is possible at lower moisture content, which was observed at 12%.

REFERENCES

Borkowska H., Styk B., 2006: Ślazowiec pensylwański (*Sida hermaphrodita* Rusby) uprawa i wykorzystanie. Wydawnictwo AR w Lublinie.

Clinton-Brown J.C., Lewandowski I., 2000: Overwintering problems of newly established *Miscanthus* plantations can be overcome by identifying genotypes with improved rhizome cold tolerance. New Phytologist, 148:287-94.

El Bassam N., 1998: Energy plant species. James and James Science Publishers, London.

Junginger M., Bolkesjø T., Bradley D., Dolzan P., Faaij A., Heinimö J., Hektor B., Leistad Ø., Ling E., Perry M., Piacente E., Rosillo-Calle F. Ryckmans Y., Schouwenberg P.P., Solberg B., Trømborg E., da Silva Walter A., de Wit M., 2008: Developments in international bioenergy trade. Biomass and Bioenergy, 32:717-729.

Kaliyan N., Morey V.R., 2009: Factors affecting strength and durability of densified biomass products. Biomass and Bioenergy, 33:337-359.

Kościk B., 2003: Rośliny energetyczne. Wydawnictwo AR w Lublinie.

Kowalczyk-Juśko A., 2007: Źródła biomasy na cele energetyczne. [in:] Bioenergetyka podkarpacka. Wydawnictwo PWSZ, Jarosław.

Kowalska A., 2010: Overview of technological methods of energy production from biomass. Teka Komisji Motoryzacji I Energetyki Rolnictwa, tom 10: 209-215.

Kulig R., Laskowski J., 2005: Wpływ zawartości tłuszczu na proces granulowania materiałów paszowych. Inżynieria Rolnicza, 7(67):59-68.

Kulig R., Laskowski J., 2006: Wpływ zawartości włókna na proces granulowania materiałów paszowych. Inżynieria Rolnicza, 5(80):365-374.

Lewandowski I., Clinton-Brown J.C., Scurlock J.M.O., Huisman W., 2000: Miscanthus: European experience with a novel energy crop. Biomass and Bioenergy, 19:209-227.

Li Y., Wu D., Zhang J., Chang L., Wu D., Fang Z., Shi Y., 2000:Measurement and statistics of single pellet mechanical strength of differently shaped catalysts. Powder Technology, 113: 176–184.

Mani S., Tabil L.G., Sokhansanj S., 2006: Effects of compressive force, particle size and moisture content on mechanical properties of biomass pellets from grasses. Biomass and Bioenergy, 30:648-654.

Niedziółka I., Szymanek M., Zuchniarz A., Zawiślak K., 2008: Characteristics of pellets produced from selected plant mixes. Teka Komisji Motoryzacji I Energetyki Rolnictwa, tom 8: 157-162.

Potter L., Bingham M.J., Baker M.G., Long S.P., 1994: The potential of two perennial C_4 grasses and a perennial C_4 sedge as lingo-cellulosic fuel crops in N.W. Europe. Crop establishment and yields in E. England. Annals of Botany, 45:111-19.

Relova I., Vignote S., León M. A., Ambrosio Y., 2009: Optimisation of the manufacturing variables of sawdust pellets from the bark of Pinus caribaea Morelet: Particle size, moisture and pressure. Biomass and Bioenergy, 33:1351-1357.

Rozporządzenie Ministra Rolnictwa i Rozwoju Wsi z dnia 14 marca 2008 r. w sprawie plonów reprezentatywnych roślin energetycznych w 2008 r.

Ruiz G., Ortiz M., Pandolfi A., 2000: Three-dimensional finite-element simulation of the dynamic Brazilian tests on concrete cylinders. Int. J. Numer. Meth. Engng., 48: 963-994.

Schenkel Y., Crehay R., Delaunois C., Schummer J., 2003: The agricultural sector and bioenergy production. Teka Komisji Motoryzacji I Energetyki Rolnictwa, tom 3: 228-235.

Spooner D.M., Cusick A.W., Hall G.E., Baskin J.M., 1985: Observations on the distribution and ecology of *Sida hermaphrodita* (L.) Rusby (*Malvaceae*). Sida, 11:215-225.

Szymanek M., Kachel-Jakubowska M., 2010: Estimation and analysis of chosen factors of the influence on quality and energy consumption at the processing of plant materials for energy purposes. Teka Komisji Motoryzacji I Energetyki Rolnictwa, tom 10: 454-463.

van Dam J., Faaij A.P.C., Lewandowski I., Fischer G., 2007: Biomass production potentials in Central and Eastern Europe under different scenarios. Biomass and Bioenergy, 31:345-366.

van Dam J., Faaij A.P.C., Lewandowski I., Van Zeebroeck B., 2009: Options of biofuel trade from Central and Eastern to Western European countries. Biomass and Bioenergy, 33:728-744.

WPŁYW WILGOTNOŚCI WYBRANYCH ROŚLIN ENERGETYCZNYCH NA PARAMETRY PROCESU BRYKIETOWANIA

Streszczenie. Przedstawiono wyniki badań przebiegu procesu aglomerowania ciśnieniowego roślin energetycznych (miskant cukrowy, spartina preriowa, ślazowiec pensylwański). Oceniono podatność badanych materiałów na proces brykietowania. Wyznaczono jednostkowe nakłady energii elektrycznej ponoszone bezpośrednio w procesie wytwarzania aglomeratów oraz określono jakość gotowego produktu. Stwierdzono, iż najniższe zapotrzebowanie energii elektrycznej występuje podczas brykietowania mączki z miskanta (średnio 412,87 $kJ \cdot kg^{-1}$), najwyższe zaś odnosi się do ślazowca i wynosi średnio 629,23 $kJ \cdot kg^{-1}$. Natomiast wytrzymałość kinetyczna aglomeratu przyjmuje najwyższą wartość w odniesieniu do brykietu otrzymanego ze ślazowca - przeciętnie 91,45%.

Słowa kluczowe: rośliny energetyczne, brykietowanie, energochłonność aglomerowania ciśnieniowego, jakość brykietów

TEKA Kom. Mot. Energ. Roln. – OL PAN, 2011, 11, 197–208

APPLICATION OF THE SELECTED TECHNIQUES OF RAPID PROTOTYPING TO THE DESIGN AND MANUFACTURE OF PROTOTYPE ELEMENTS OF MACHINES AND EQUIPMENT

Piotr Kowalski, Zbigniew Pączek, Robert Żuczek

Foundry Research Institute, 73 Zakopiańska Str., 30-418 Cracow, Poland

Summary. By using rapid prototyping techniques, prototype parts, components or finished products can be quickly manufactured. The elements of a new device can serve as an example of the practical use of this solution. The result of the studies was a short series of prototype parts. Due to the functions performed by these elements, they were made from specially selected plastics characterised by mechanical properties allowing for the initial testing of prototype. The design of parts was based on the three-dimensional computer models. Owing to the availability of the FDM Titan device, in a short time real patterns were obtained. They were used to make silicone dies which, in turn, were used for casting a short series of prototypes from plastics. The components obtained in this way were subjected to tests to check their functionality. A series of test castings was also made.

Keywords: rapid prototyping, designing of new products, metalcasting, plastics.

INTRODUCTION

In a modern market economy and competition, quick manufacture of prototypes of the highest quality becomes a must. To satisfy high requirements of customers and shorten the lead times, manufacturers are forced to use innovative methods of production, based on the computer-aided design and the latest achievements of rapid prototyping and tooling performance. For several years these issues have been the subject of research conducted by the Centre for Design and Prototyping at the Foundry Research Institute in Cracow. Until now, numerous application works for different customers have simultaneously been implemented. [7÷11]

The last decade has seen a tremendous progress in the application of computer-aided product manufacturing. The abbreviations like CAD (Computer Aided Design), CAM (Computer Aided Manufacturing), CAE (Computer Aided Engineering) are now generally known, and the opportunities offered by them are widely used by engineers in various industries [2÷6, 13].

In particular, significant progress can be seen in the rapid manufacture of new products, which is usually preceded by the need of making prototypes. This is particularly true in the automotive industry, engineering, defence, aviation and more recently in telecommunications. Metalcasting, being major supplier of components for a wide range of customers, including also the aforementioned sectors of industry, must use and uses the possibilities offered by the advanced application of CAD / CAM / CAE systems.

The most notable progress has been observed in the last few years in the field of rapid prototyping (RPS) and rapid tooling (RT). Rapid prototyping technique came into use in 1987, when the 3D Systems Company launched the first device for the manufacture of foundry patterns from liquid synthetic resin, the successive layers of which were hardened with a beam of ultraviolet laser light. In this way the technique known as stereolithography RPS was born.

Considering the benefits offered by rapid prototyping, the subsequent years witnessed its outstanding development. New techniques and stands for the manufacture of patterns were developed. Currently, rapid prototyping is seen as an obvious step in the preparation of a new product.

According to data for the year 2008 [1], the area of application of patterns/parts made by RP and RT is as follows:

- 13.7% utility models – for presentation,
- 10.0% parts of complex models,
- 15.3% visualisation (aid) in engineering studies,
- 3.4% models as a part of tooling,
- 6.5% patterns for foundry,
- 12.5% models to make prototype tools,
- 5.3% models to aid the implementation of various projects,
- 4.6% other applications.

The best-known techniques of RP and RT with their respective applications have been broadly described in information materials published by different companies offering equipment for practical implementation of these techniques, and also in numerous publications and online data. Considering the above, the presentation of these techniques has been omitted in this paper. [1,12÷22]

The general principle of RP and RT is essentially the same and consists in reproduction and successive application of very thin layers of the pattern. The shape of the formed piece is written in advance in computer memory, using a graphical editor operating in a triaxial (3D) system.

Depending on the used techniques, the pattern is usually built from liquid synthetic resin, paper, powders of different materials, wax. High precision of the manufactured patterns ensures the application of advanced optics (including laser technology) for curing the individual layers or cutting them out.

Patterns are made on specially equipped work stands, typical for a given technique. The size of the manufactured patterns is limited by the dimensions of a worktable. If larger patterns are to be made, it is sometimes possible to apply techniques which enable joining various elements reproducing parts of a workpiece. Different RP techniques have strictly determined the scope of application and precision (the accuracy of reproducing pattern shape). They differ quite obviously in the cost of the equipment and materials used.

The application of RP techniques caused revolutionary changes in the way the new production has been prepared and new equipment designed.

Currently, in the world market, a strong competition is going on within a large group of the well-known companies that offer all the available techniques of rapid prototyping, supplying the equipment, materials, maintenance and services.

The choice of an RP technique is usually determined by a number of factors, among which the following ones should be mentioned here:

- pattern dimensions,
- pattern application,
- pattern dimensional accuracy,
- pattern price.

All these factors were analysed at the Foundry Research Institute before a decision was taken about the purchase of various stands for rapid prototyping, mainly for the needs of foundry industry,

but not only. When the decision was taken to establish a Centre for Design and Prototyping at the Foundry Research Institute, the above criteria were considered, the most useful techniques of RPS were selected, and the necessary equipment was purchased.

As a result of these actions, the Centre uses the following devices and the following techniques:

- LOM
- Solidscape
- FDM
- 3Dprinting

PURPOSE AND SCOPE OF STUDY

The aim of this study was to examine the possibility of using one of the techniques of rapid prototyping (FDM - Fused Deposition Modelling) in the manufacture of parts of a prototype device. The scope of the study included design and manufacture of prototype components.

MATERIALS AND METHODS

In the studies, the FDM Titan device from Stratasys (Figure 1) was used. It enabled making patterns from plastics. The FDM Titan is a modern facility, used to create functional and visual patterns from plastics. The pattern-building process involves depositing successive layers of material fed to the worktable in semi-solid state. In this technique, the pattern material are various types of plastics, which in the form of a wire wound on a spool are supplied from trays to a head moving in the X-Y axes. In the heating elements of a thermal head unit, two nozzles are mounted: the nozzle feeding pattern material and the nozzle feeding support material. In these nozzles, the wire fed from a tray is preheated until it reaches a semi-solid state. Then the melted pattern material and support material are squeezed by nozzles onto a special base board placed on the worktable moving vertically in the Z-axis to form the first layer of a built pattern, according to horizontal cross-sections generated by an Insight programme cooperating with the FDM Titan device. With modelling of a specific layer of the item completed, the worktable is lowered by a preset thickness, and the solidified shell is acting as a support for further applied layers. The thickness of the material filament fed during pattern building depends on the nozzle type and on the type of pattern material used and can be: 0.127 mm, 0.178 mm, 0.254 mm and 0.33 mm. The worktable size is limited to 406 x 355 x 406 mm, but the built patterns have no size restrictions, since individual components of a complex structure can be combined by gluing.

Fig. 1. FDM Titan device made by Stratasys

Despite the commercial availability of many similar printers using FDM technique, the FDM Titan device is the only device in the country which enables modelling of plastics. Patterns are made from several materials like:

- ABS (acryl-nitril-butadienestyrene),
- PC (polycarbonate), PC-ISO (for medical applications),
- PPSF/PPSU (polyphenylsulphon).

The available pattern plastics can be divided into two groups, depending on the type of the used support material:

- pattern materials using broken off support (PC, PC-ISO, PPSF),
- pattern materials using support soluble in appropriate basic solutions (ABS and PC-ABS).

The proposed pattern materials are supplied in white colour, while in the case of ABS seven-colour palette is available. Additionally, it is possible to build patterns from two types of transparent materials: ABSi (three colours of transparency) and PC-ISO. As already mentioned, ABS is the material from which both colour and transparent patterns can be made, but apart from visual effects, owing to the use of soluble support, an additional advantage of this material is the ability to make complex patterns with a series of internal channels.

The second material using soluble support is the material of a trade name PC-ABS, combining the properties of ABS and PC. Patterns made from ABS and PC are characterised by relatively high strength and low shrinkage. Their basic drawback is the loss of shape at temperatures as low as 100°C.

The material offering the highest strength and temperature of plastic deformation is PPSF. At temperatures up to about 190°C, patterns made from this material do not undergo deformation, are characterised by relatively good thermal and chemical resistance, as well as environmental resistance to aggressive liquids such as unleaded petrol, engine oil, coolant and washer fluid.

Items made from these materials, apart from visual - advertising value can serve as useful parts, (otherwise called Real Parts^{TM}), as patterns for castings made in ceramic moulds by the lost foam

process or by direct moulding in traditional processes, or as master-patterns to make silicone dies for wax patterns. The ready prototype patterns can be subjected to finishing treatment by e.g. grinding or drilling; finally, to obtain the required outer surface quality, they are painted or chrome-plated.

RESULTS OF INVESTIGATIONS

Studies discussed in this article formed part of Development Project 0R00004005 executed in 2010 by the Centre for Design and Prototyping at the Foundry Research Institute in Cracow. During tests, prototype items varying in size and complexity were made. In future they will be produced by the gravity and die casting processes.

At the present stage of research, prototype castings were made by the lost wax process and vacuum casting in plaster moulds. The necessary drawing documentation of those elements was prepared in a 3D system using a SolidEdge graphical editor.

The ready drawings helped to prepare the equipment for operation and making FDM models. Prior to casting manufacture, the following technology steps were developed: filling mould cavity, casting solidification and cooling. The technology was checked using a specialised MAGMAsoft software. Below a specification of the examined items is given.

Item No. 1

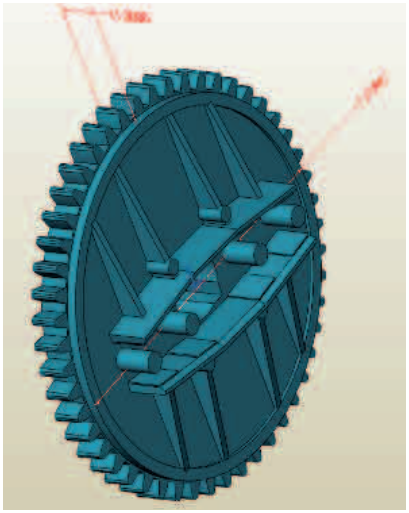

Name : Wheel
Cast material : AK7 aluminium alloy
Weight : 0,1 kg
In future this item will be made by die casting process.
The following elements were successively made: FDM model, silicone resin die and wax patterns.
Castings were made by the lost wax process.
Items were cast in ceramic molochite moulds.
Altogether 4 sets with 6 castings in each set were made.

The following checking tests were performed on castings:
– structure examinations;
– hardness measurements;
– dimensional accuracy : RPS model, die, wax pattern, casting.

Item No. 2

Name : Cross
Cast material : AK7 aluminium alloy
Weight : 0,10 kg (10 g)
In future this item will be made by die casting process.
The following elements were successively made: FDM model, silicone resin die and wax patterns.
Castings were made by the lost wax process.
Items were cast in ceramic molochite moulds.
Altogether 4 sets with 6 castings in each set were made.
The following checking tests were performed on castings:
– structure examinations;
– hardness measurements;
– dimensional accuracy : RPS model, die, wax pattern, casting.

Ceramic moulds were made on an automatic CYKLON device from MK Technology GmbH in Germany.

Photographs below present successive operations performed at this stand:
- pattern set ready for application of the first ceramic coating
- application of ceramic coating
- supporting mould with loose ceramic material
- drying of ceramic coating

Fig. 2. Pattern set ready to make a ceramic mould

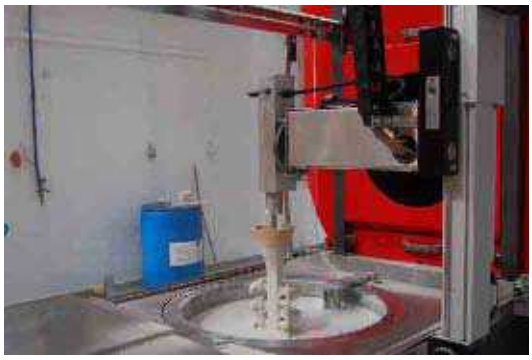

Fig. 3. Application of ceramic coating

Fig. 4. Mould supported with loose ceramic material

Fig. 5. Drying of applied ceramic coating

Item No. 3

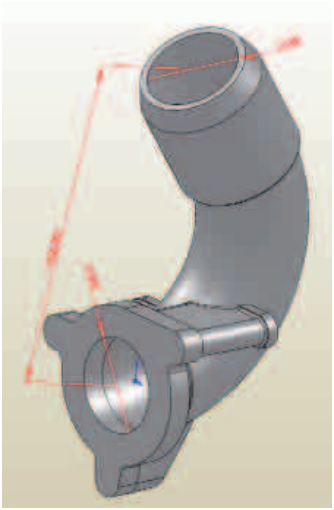

Name : Elbow
Cast material : AK7 aluminium alloy
Weight : 0,398 kg

In future this item will be made by gravity die casting process with sand core.
The following elements were successively made: FDM model, silicone resin die and wax patterns.
Castings were made by the lost wax process.
Items were cast in plaster moulds.
The following checking tests were performed on castings:
– structure examinations;
– hardness measurements;
– dimensional accuracy : RPS model, die, wax pattern, casting.

Item No. 4

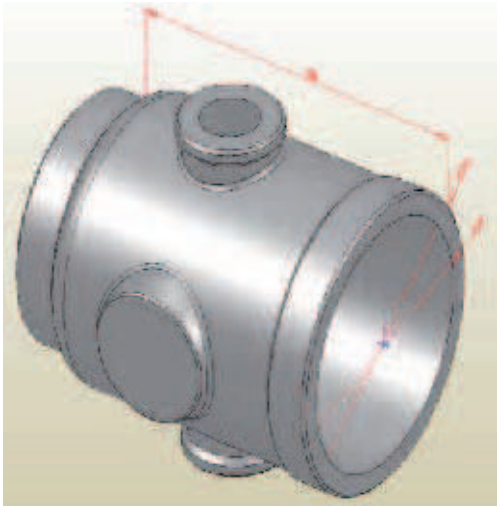

Name: Sleeve
Cast material : AK7 aluminium alloy
Weight : 0,621 kg

In future this item will be made by gravity die casting process with sand core.
The following elements were successively made: FDM model, silicone resin die and wax patterns.
Castings were made by the lost wax process.
Items were cast in plaster moulds.
The following checking tests were performed on castings:
– structure examinations;
– hardness measurements;
– dimensional accuracy : RPS model, die, wax pattern, casting.

The structure examinations and hardness measurements taken on the four prototype castings confirmed that the technical parameters corresponding to standard requirements for AK7 alloy had been obtained.

The dimensional accuracy was checked using an optical 3D scanner ATOS III. It allows for the scanning (measuring the coordinates of points) of objects with overall dimensions from several millimetres up to several metres. ATOS operating principle is that of triangulation. Two cameras observe the run of fringes in the examined item and for each camera pixel the coordinate point is calculated with high precision. The maximum number of measuring points in a single shot is 4 000 000. The time for one shot is 2 seconds. The measuring fields are 150x150 and 500x500 mm.

The use of special software enables a complete analysis of the measurement (dimensioning of the item, compatibility with CAD data, coloured map of deviations, inspection sections, etc.) Quality control is one of the areas where optical 3D scanner ATOS III is used. It enables comparing the examined object with CAD model design, or comparing two identical objects. It also enables dimensioning of arbitrary cross-sections and geometrical features. The use of automatic rotary tables enables total quality control and analysis of shrinkage,

ATOS III 3D is used in tool shops as a means for performance control, verification of processing, and tool reproduction. It also enables comparing the mould with pattern, digital recording and documentation. The 3D optical scanner using structured light emits onto the measured object a set of white light fringes characterised by a specific density of packing. The packing density of fringes enables specifying the amount of data received. With more fringes, more of data are received. These fringes are subjected to unequal distortion, and the image of the illuminated object is recorded by objective lenses mounted in the scanner head. As a result of the measurement carried out by this technique, a set of structured light fringes, lying on the surface of the object and at the time of illumination visible to both lenses, is obtained. The resulting sets of fringes are superimposed by means of reference points. So, prior to scanning, reference points are applied on patterns.

The image formed as a result of scanning is point cloud, and therefore the obtained model is subjected to polygonisation. This means that the point cloud is converted to a network of non-overlapping triangles. The created polygonal network is subjected to further processing, and the task of this processing is to remove reference points, fill surface discontinuities, and smooth them whenever possible. Thus prepared network of triangles is a model of the real object.

ATOS III programme for processing of scanned models allows reproduction of the model surface. It also allows fitting of models to each other.

The studies of dimensional accuracy made with the use of the described scanner fully confirmed the dimensional compatibility of models and castings made within the range of values expected for the ready cast elements.

CONCLUSIONS

The studies fully confirmed the applicability of FDM technique in creation of models used for the manufacture of prototype castings.

The possibility of making prototype castings using equipment available at the Centre for Design and Prototyping has been confirmed. The prototype castings can be used in verification of the design assumptions, while their lot production by selected casting technology can be undertaken as the next step.

Considering high surface quality and dimensional accuracy, models made by FDM techniques can successfully serve as prototype parts made from plastics.

REFERENCES

Development Project 0R00004005, Foundry Research Institute, Cracow 2010

WOHLERS ASSOCIATES *Wohlers Report 2009*, , Inc. Colorado, USA

OCZOŚ K.E.: *Rosnące znaczenie Rapid Manufacturing w przyrostowym kształtowaniu wyrobów*. Mechanik (2008)4, 256.

OCZOŚ K.E.: *Zastosowanie techniki Rapid Tooling do kontroli jakości wytwarzanych części samochodowych*. Mechanik (2008)12, 1022-1028.

OCZOŚ *K.E.:Rozwój kształtowania przyrostowego wyrobów*. Mechanik (2007)2,65

OCZOŚ K.E., *Rapid Prototyping - znaczenie, charakterystyka metod i możliwości*, Mechanik 1997, 70 nr 10 s.441 – 452

CHLEBUS E.: *Innowacyjne technologie Rapid Prototyping – Rapid Tooling w rozwoju produktu*. Oficyna Wydawnicza Politechniki Wrocławskiej. Wrocław 2003, s.37-42,47-57,106-140,152-158

PĄCZEK Z., KARWIŃSKI A., KROKOSZ J., PRZYBYLSKI J., PYSZ S.: *Zastosowanie technik LOM do wykonywania odlewów, możliwości, szanse, problemy*, wyd. Instytut Odlewnictwa – Kraków, Kraków, 2003

KROKOSZ J., MŁODNICKI S., GIL A., KARWIŃSKI A., PABIŚ R., ĆWIKLAK R.: *Ocena możliwości wykorzystania technik szybkiego prototypowania w odlewnictwie oraz opracowanie założeń i wykonanie serii modeli i odlewów artystycznych*, Odlewnictwo współczesne – Polska i świat 2010, nr 1, str.3-13

PYSZ S., Karwiński A., Czekaj E.: *An Analysis and Comparison of Properties of Al-Si Alloy Automotive Castings Made by Rapid Prototyping and Standard Lot Production*. TEKA Komisji Motoryzacji i Energetyki Rolnictwa – OL PAN, Tom IX, Lublin 2009, pp. 250 – 258.

Pirowski Z., Gościański M.: *Constraction and Technology of Production of Casted Shares for Rotating and Field Ploughs*. TEKA Komisji Motoryzacji i Energetyki Rolnictwa – OL PAN, Tom IX, Lublin 2009, pp. 231 – 239.

Development Project 0R00004005, Foundry Research Institute, Cracow 2010

PLICHTA J., PLICHTA S.: *Techniki komputerowe w inżynierii produkcji*. Wydawnictwo Uczelniane Politechniki Koszalińskiej, Koszalin

RUSZAJ A.: *Niekonwencjonalne metody wytwarzania elementów maszyn i narzędzi*. Wydawca IOS w Krakowie. Kraków 1999,s.288,299

BUBICZ M.: *Raport: Szybkie prototypowanie cz. I – przegląd dostępnych rozwiązań. Maszyny, materiały, zastosowania*. / Projektowanie i Konstrukcje Inżynierskie 6(09) czerwiec, 2008, p. 14 - 21.

BUBICZ M.: *Cyfrowe czy jednak fizyczne? Prototypowanie – wyzwanie XXI wieku*, Konstrukcje inżynierskie 2007, nr 1

CHOJNOWSKA L.: *Model wirtualny wsparty wydrukiem 3D*. Desing News w Mechanice i Elektronice, 2008, nr 03

PŁATEK P., Kret M.: *Techniki druku 3D – przykłady zastosowań metody FDM, warstwowego osadzania topionego materiału*. Seminarium techniki szybkiego prototypowania w cyklu życia produktu. „Mechanik" 2008, nr12.

DYBAŁA B.: *Technologie szybkiego prototypowania i wytwarzania*, W: „Raport. Rapid Prototyping & Reverse Engineering", 2010

LEWANDOWSKI J.L.: *Postęp w zakresie szybkiego prototypowania*, Przegląd Odlewnictwa 3/2001 str. 116-117

CHUA C.K., LEONG K.F., LIM C.S.: *Rapid Prototyping. Principles and Applications,* World Scientific, Singapoore 2004.

GUSTAFSON R.: *Rapid Prototyping: a tool for casting design and verification*, Mod. Casting 1999 Vol.89 nr 3 s.44-47

WUENSCHE R.: *Rapid Prototyping bei der Herstellung von Gussteilen*, Giesserei 2004 Jg.91 H.4 s.44-46

ZASTOSOWANIE WYBRANYCH TECHNIK RAPID PROTOTYPING DO WYKONYWANIA PROTOTYPOWYCH ELEMENTÓW KONSTRUKCJI MASZYN I URZADZEŃ.

Streszczenie. Dzięki zastosowaniu technik Rapid Prototyping istnieje możliwość szybkiego wytworzenia prototypowych części, podzespołów lub gotowych produktów. Przykładem zastosowania takiego rozwiązania są elementy nowego urządzenia. Efektem prowadzonych prac było uzyskanie krótkiej serii prototypowych części. Ze względu na spełniane funkcje, do wykonania ich zastało dobrane odpowiednie tworzywo sztuczne o właściwościach mechanicznych pozwalających na wstępne testowanie prototypu. Podstawą do wykonania detali były trójwymiarowe modele komputerowe. Dzięki wykorzystaniu urządzenia FDM Titan w krótkim czasie uzyskano modele rzeczywiste, następnie na ich podstawie zostały wykonane matryce silikonowe, które z kolei posłużyły do odlania krótkiej serii prototypów z tworzywa sztucznego. Tak uzyskane elementy zostały przekazane do testów w celu sprawdzenia ich funkcjonalności. Wykonano również serię odlewów z możliwością ich wykorzystania do testowania.

Słowa kluczowe: szybkie prototypowanie, projektowanie nowych wyrobów, odlewnictwo, tworzywa sztuczne.

TEKA Kom. Mot. Energ. Roln. – OL PAN, 2011, 11, 209–217

THE EFFECT OF PRELIMINARY PROCESSING ON COMPACTION PARAMETERS OF OILSEED RAPE STRAW

Ryszard Kulig, Janusz Laskowski

Department of Food Industry Machinery Operation, University of Life Sciences in Lublin

Summary. This study determines the effect of the moisture content (10% to 22%) and fractionation degree (d_{sr}=0.95 and d_{sr}=1.94 mm) of oilseed rape straw on compaction parameters under model conditions. The straw's susceptibility to compaction and the quality of the resulting briquettes were analyzed. Straw density increased with a rise in moisture content, whereas the density of the agglomerated product decreased after removal from the press die. Lower energy demand was reported during the compaction of finely ground material (average of 27.02 $J \cdot g^{-1}$) throughout the entire moisture content range. The average difference in energy demand reported at various moisture content levels reached 36%. A higher degree of straw fractionation reduced energy consumption by 14% on average.

Key words: compaction, briquetting, moisture content, degree of fractionation, oilseed rape straw.

INTRODUCTION

The achievement of stringent targets of renewable energy schemes requires the use of biofuels produced from residual crop materials. Straw shows considerable promise as crop residue biomass fuel. The straw of nearly all cereal grain species and oilseed rape can be used for energy generation. The growing demand for alternative energy sources supports productive management of oilseed rape straw which is usually chopped and incorporated into the soil through plowing.

Straw is a difficult material to handle in comparison with other energy carriers. Straw is a non-homogenous material with a lower calorific value, in particular per unit volume [3]. For this reason, straw has to be compacted into briquettes under pressure [11]. Compaction significantly reduces the cost of handling and transporting plant biomass for the needs of energy generation.

According to various research studies, the moisture content [5, 14, 15, 16, 17, 20] and fractionation degree of the processed material [1, 13] significantly affect the agglomeration of solid biofuels. Those parameters impact the compaction process [7, 9, 12, 18, 19] as well as the quality of the resulting product [2, 4, 6, 10]. Oilseed rape straw is characterized by a moisture content of 30% to 40% upon harvesting. Only wilted and dried straw can be processed, which implies that harvested straw has to be left in the field for several to more than ten days. Due to specific moisture content requirements, straw harvest dates have to be adapted to the needs of the compaction process (to eliminate additional drying or hydration of the processed material).

The objective of this study was to determine the values of parameters during the compaction of straw characterized by a different moisture content and degree of fractionation.

MATERIALS AND METHODS

The experimental materials comprised oilseed rape straw harvested in 2010. The material was ground in a H-950 hammer mill equipped with ϕ 3 and 9 mm sieves. The particle size distribution of the studied material was described to determine the average size of the produced fractions. Particle size distribution was determined in accordance with the Polish Standard PN-89/R-64798 using the SASKIA Thyr 2 laboratory screen and a set of sieves with the following mesh size: 6, 2, 2.5, 1.6, 1.0, 0.5, 0.315 and 0.1 mm. The screening time was two minutes. After screening, the produced fractions were weighed on WPE 300 scales with the precision of $\pm 10^{-2}$ g. The average size of fractionated particles (fractionation module) was calculated using the following formula:

$$d_{sr} = \frac{\sum_{i=1}^{i=n} h_i \cdot P_i}{100} \tag{1}$$

where: d_{sr}- average particle size, mm; h_i- average mesh size of two adjacent sieves, mm; P_i- fractionated residue in sieve, %; n- number of sieves.

The average size of particles fractionated in a sieve with a 4 mm mesh was 0.95 mm, and the size of material passed through a 12 mm mesh sieve was 1.94 mm.

The parameters of the straw compaction process were determined for raw material with moisture content in the range of 10% to 22% (in steps of 3% +/-0.2%). Straw was brought to the desired moisture level through hydration. The quantity of added water was determined based on the following formula:

$$M_w = M_1 \frac{W_2 - W_1}{100 - W_2} \tag{2}$$

where: M_w – weight of added water, g;
M_1 – weight of material sample, g;
W_1 – moisture content of material sample, %;
W_2 – required moisture content of material sample, %.

The samples were stored for 24 h in tight containers to evenly distribute moisture throughout the material.

The compaction process was analyzed according to the methodology proposed by Laskowski and Skonecki [8]. The mechanical properties of straw samples were observed using the Zwick Z020/TN2S tensile test machine. The samples were compacted in a pressing unit with a closed die. The compaction chamber had a diameter of 15 mm, cylinder (material) temperature was 20ºC, and piston speed was 10 mm·min^{-1}. Straw samples were compacted until the achievement of a working load equal to 20 kN. Compaction pressure was 114 MPa.

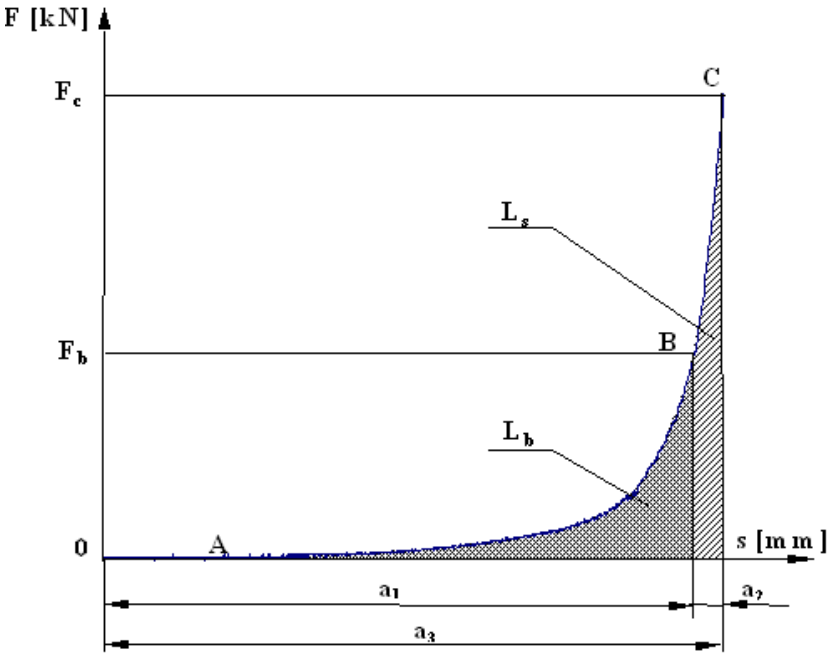

Fig. 1. Compaction characteristics: a_1–compaction, a_2-compression, a_3–pressing (Laskowski and Skonecki 2001)

The results of the analysis were used to develop a curve demonstrating the correlation between compaction force *F* and piston displacement *s*

(Fig. 1). Every compaction process was performed in three replications. The values of maximum material density in compaction chamber g_z and total compaction effort L_c were determined from the compaction curve. The above values were used to calculate the coefficient of material susceptibility to compaction k_c ($k_c = L_p \cdot (g_z - g_s)^{-1}$, where: $L_p = L_c \cdot m^{-1}$ – unitary compaction effort, m – weight of material sample, g_s – initial density of loose material. The agglomeration density of the resulting briquette was determined directly after removal from chamber g_a.

Briquette hardness was determined using the following formula:

$$T_a = \frac{F_n}{l} \tag{3}$$

where: T_a – agglomeration density, N•cm^{-1};
F_n – maximum breaking force, N;
l – briquette length, cm;

Mechanical properties were investigated using the ZWICK Z020/TN2S tensile test machine (piston speed of 10 mm·min^{-1}). The briquette was compressed transversely to the axis until breaking point, and maximum breaking force F_n was determined.

RESULTS AND DISCUSSION

The effect of moisture content on material density in the compaction chamber is illustrated in Figure 2.

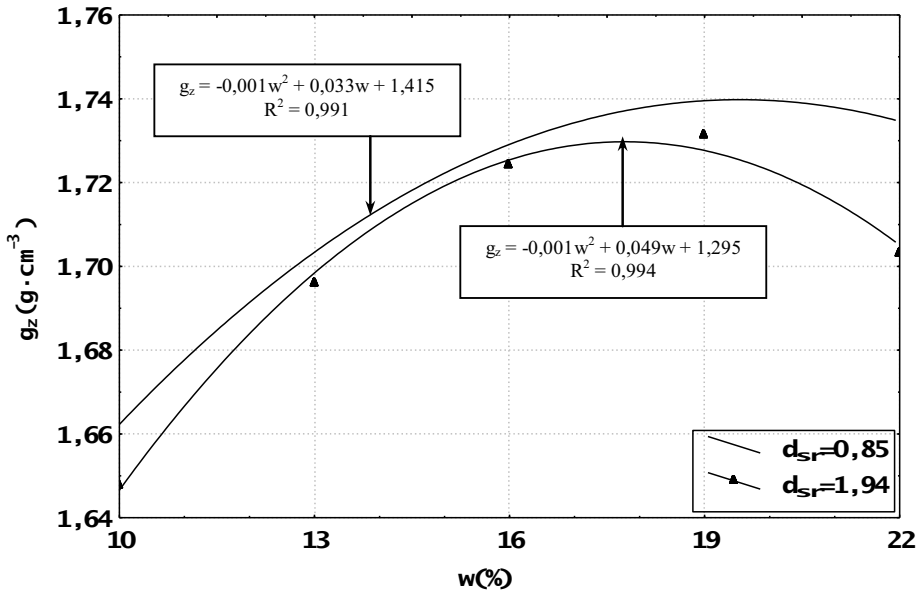

Fig. 2. Correlation between material density in the chamber (gz) and moisture content (w) at various degrees of fractionation (dsr).

The value of the studied parameter increased with a rise in the moisture content of samples characterized by a lower degree of fractionation within the entire range of tested values. Variation was determined in the range of 1.66 to 1.73 g·cm^{-3}. As regards the sample with d_{sr}=1.94 mm, the highest density (1.73 g·cm^{-3}) was noted at a moisture content of 19%. The analyzed parameter was characterized by the smallest variation (due to the effect of the degree of fractionation) at the moisture content of 13% to 19%.

The changes in agglomerate density after removal from the compaction chamber are presented in Figure 3. The highest density values were reported at 10% moisture content, and the lowest – at 22% moisture content for both the analyzed degrees of fractionation. Briquettes produced from material with d_{sr}=0.85 mm were marked by lower expansion. Product density reached 1 g•cm^{-3} at moisture content in the range of 10% to 13%. Agglomerates produced from material with d_{sr}=1.94 mm and a moisture content of 22% were characterized by the lowest density (0.71 g•cm^{-3}).

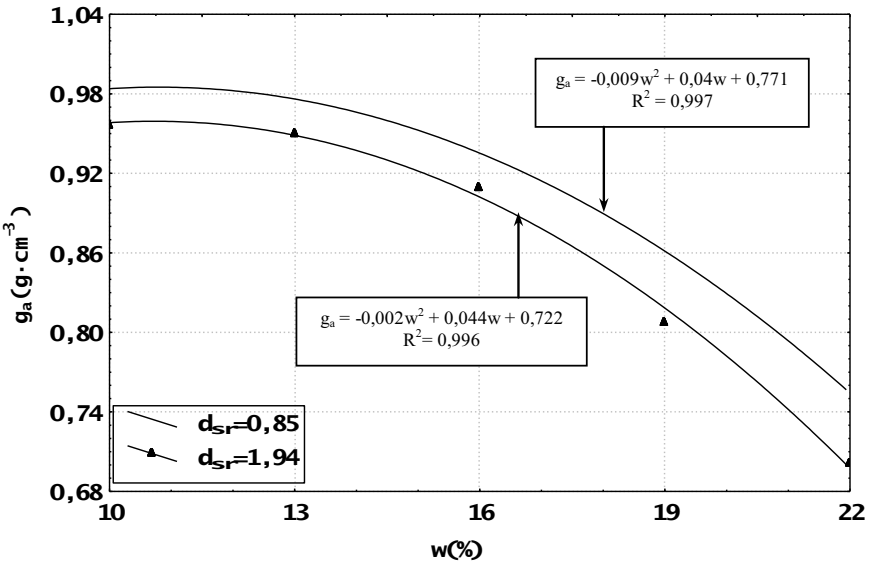

Fig. 3. Correlation between agglomerate density (g_a) and moisture content (w) at various degrees of fractionation (d_{sr})

Figures 4 and 5 demonstrate than an increase in the material's moisture content leads to higher susceptibility to compaction. It can be assumed that a higher moisture content increases the material's plasticity, thus reducing the amount of energy required for its compaction.

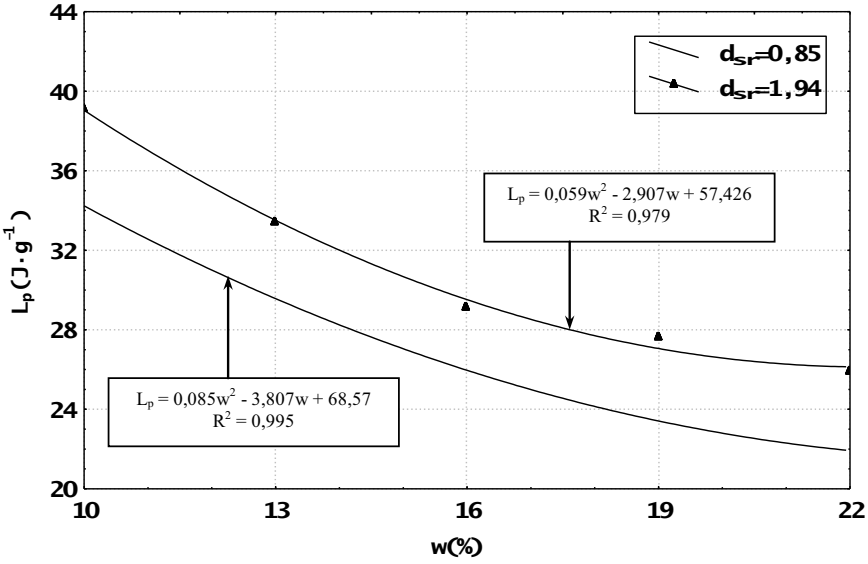

Fig. 4. Correlation between unitary compaction effort (L_p) and moisture content (w) at various degrees of fractionation (d_{sr}).

The value of the unitary compaction effort (Fig. 4) for the studied materials ranged from 21.43 to 39.15 J•g^{-1}. The highest value of parameter L_p was reported for the sample with d_{sr}=1.94 mm, agglomerated at 10% moisture content. The analyzed parameter reached the lowest value for the material with d_{sr}=0.85 mm and moisture content of 22%.

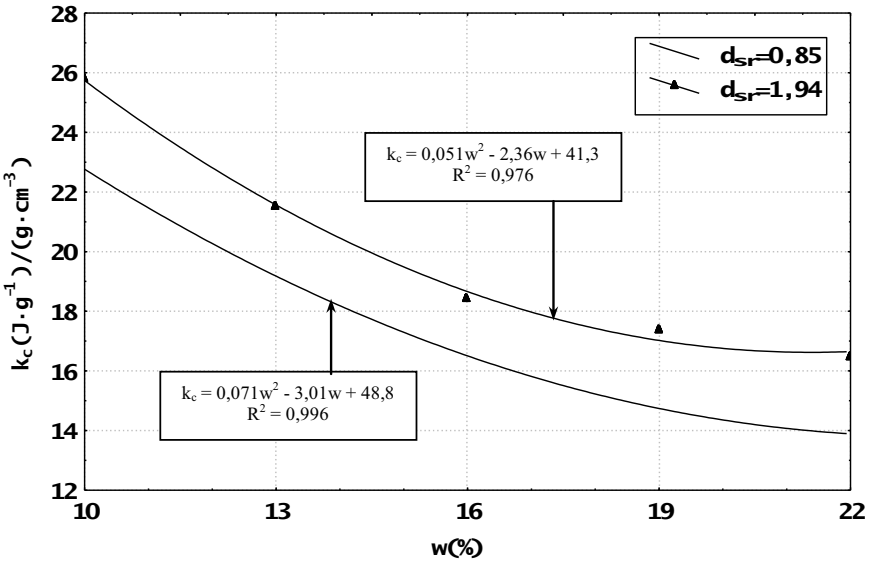

Fig. 5. Correlation between coefficient (k_c) and moisture content (w) at various degrees of fractionation (d_{sr}).

Similar correlations were observed in respect of the coefficient of susceptibility to compaction which ranged from 13.51 $(J\cdot g^{-1})\cdot((g\cdot cm^{-3}))^{-1}$ to 25.81 $(J\cdot g^{-1})\cdot((g\cdot cm^{-3}))^{-1}$ (Fig. 5).

As regards the unitary compaction effort and coefficient k_c, an increase in moisture content did not level out the differences resulting from the effect of fractionation degree. The reported differences ($p>0.05$) remained constant throughout the entire range of variation in moisture content.

The results of agglomerate hardness measurements (Fig. 6) indicate that the mechanical strength of the studied materials decreased with a rise in moisture content.

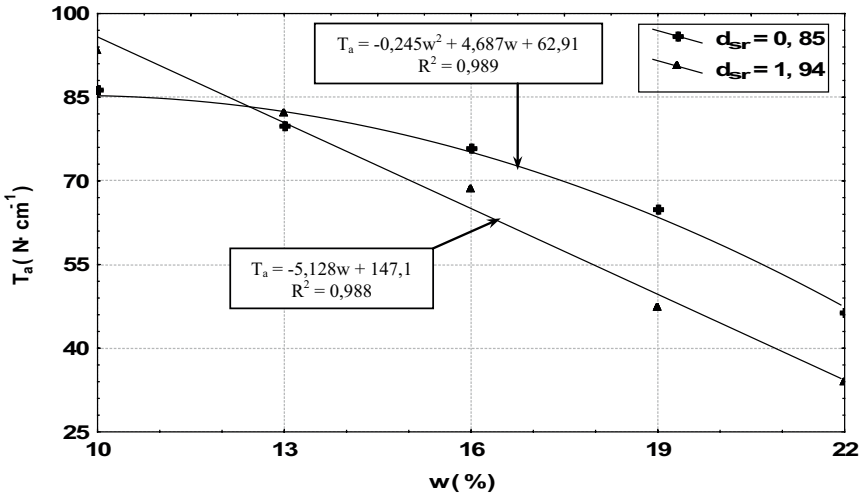

Fig. 6. Correlation between agglomerate hardness (T_a) and moisture content (w) at different degrees of fractionation (d_{sr})

Agglomerates produced from material with d_{sr}=1.94 mm were characterized by both the highest (93.32 N·cm-1) and the lowest (33.84 $N \cdot cm^{-1}$) hardness. An inversely proportional correlation was determined between moisture content and parameter T_a. In products obtained from material with d_{sr}=0.85 mm, the dynamics of decrease in hardness values increased beginning with the moisture content of 13%.

CONCLUSIONS

The following conclusions can be drawn from the results of this study:

1. The highest increase in material density in the compaction chamber was observed at the moisture content of 10% to 16%. Within the above range, the average increase in the studied parameter's value was 4.2%. A further increase in moisture content (subject to the degree of fractionation) did not result in significant changes in density (d_{sr}=0.85 mm) or led to a drop in density (d_{sr}=1.94 mm).
2. After removal from the compaction chamber, briquette density (regardless of the degree of fractionation) reached the highest values at 10% moisture content, while the lowest values were reported for the moisture content of 22%. Agglomerates produced from material with d_{sr}=0.85 mm were marked by lower expansion. The average difference resulting from the effect of fractioning degree was 3.3%.
3. An increase in the material's moisture content contributed to higher susceptibility to compaction. The average drop in the unitary demand for compaction energy (at the moisture content from 10% to 22%) was 44%, and the drop in coefficient k_c reached 44.7%.
4. An increase in the material's moisture content within the investigated range led to a decrease in agglomerate hardness. The average drop in hardness values reached 48% in materials with d_{sr}=0.85 and 79% in materials with d_{sr}=1.94 mm.

REFERENCES

Adapa P., Tabil L., Schoenau G., 2011: Grinding performance and physical properties of non-treated and steam exploded barley, canola, oat and wheat straw. Biomass and Bioenergy, Vol. 35: 549-561.

Behnke K.C., 2001: Factors influencing pellet quality. Feed Tech, 5 (4) : 19-22.

Junginger M., Bolkesjø T., Bradley D., Dolzan P., Faaij A., Heinimö J., Hektor B., Leistad Ø., Ling E., Perry M., Piacente E., Rosillo-Calle F. Ryckmans Y., Schouwenberg P.P., Solberg B., Trømborg E., da Silva Walter A., de Wit M., 2008: Developments in international bioenergy trade. Biomass and Bioenergy, vol. 32: 717-729.

Kaliyan N., Morey V.R., 2009: Factors affecting strength and durability of densified biomass products. Biomass and Bioenergy, vol. 33: 337-359.

Kulig R., Laskowski J., 2005: Wpływ procesu kondycjonowania surowców zbożowych na wybrane właściwości fizyczne granulatu. Acta Agrophysica, nr 5(2): 325-334.

Kulig R., Laskowski J., 2006: Wpływ wybranych właściwości surowców na cechy wytrzymałościowe granulatu. Inżynieria Rolnicza, nr 13(88): 251-260.

Kulig R., 2007: Effects of Conditioning Methods on Energy Consumption During Pelleting. Teka Komisji Motoryzacji I Energetyki Rolnictwa, tom 7A: 52-58.

Laskowski J., Skonecki S., 2001: Badania procesów aglomerowania surowców paszowych – aspekt metodyczny. Inżynieria Rolnicza, nr. 2(22): 187-193.

Leaver, R.H., 1988: The pelleting process. Sprout-Bauer, Muncy, PA.

Li Y., Wu D., Zhang J., Chang L., Wu D., Fang Z., Shi Y., 2000: Measurement and statistics of single pellet mechanical strength of differently shaped catalysts. Powder Technology, vol. 113: 176–184.

Mani S., Tabil L.G., Sokhansanj S., 2006: Effects of compressive force, particle size and moisture content on mechanical properties of biomass pellets from grasses. Biomass and Bioenergy, vol. 30(7): 648 - 654.

MacMahon M.J., Payne J.D., 1991: The Pelleting Handbook. Borregaard Lignotech, Sarpsborg Norway.

Relova I., Vignote S., León M. A., Ambrosio Y., 2009: Optimisation of the manufacturing variables of sawdust pellets from the bark of Pinus caribaea Morelet: Particle size, moisture and pressure. Biomass and Bioenergy; vol. 33: 1351-1357.

Skonecki S., 2010: Brykietowanie wybranej biomasy roślinnej na cele energetyczne – parametry procesu i wytrzymałość aglomeratu. Autobusy, Technika, Eksploatacja, Systemy transportowe, nr. 11: 335-345.

Skonecki S., Potręć M., 2008a: Wpływ wilgotności łusek kolb kukurydzy na parametry zagęszczania. Acta Agrophysica, 11 (3): 725-732.

Skonecki S., Potręć M., 2008b: Wpływ wilgotności słomy owsianej na podatność na zagęszczanie. Rozdział nr 9 w Monografii pod redakcją B. Dobrzańskiego, A. Rutkowskiego i R. Rybczyńskiego „Właściwości fizyczne i biochemiczne materiałów roślinnych". Wyd. Nauk. FRNA, Komitet Agrofizyki PAN, Lublin, 147-156. ISBN-13: 978-83-60489-09-3.

Skonecki S., Potręć M., 2010: Wpływ wilgotności na ciśnieniowe zagęszczanie biomasy roślinnej. Zeszyty Problemowe Postępów Nauk Rolniczych, z. 546: 341-346.

Thomas M., van Zuilichem D.J., van der Poel A.F.B., 1997: Physical quality of pelleted animal feed. 2. Contribution of processes and its conditions. Anim. Feed Sci. Tech., vol. 64: 173-192.

Thomas M., van Vliet T., van der Poel A.F.B., 1998. Physical quality of pelleted animal feed. 3. Contribution of feedstuff components. Anim. Feed Sci. Tech., vol. 70: 59-78.

Wood J.F., 1987: The functional properties of feed raw materials and their effect on the production and quality of feed pellets. Anim. Feed Sci. Tech., vol, 18: 1-17.

WPŁYW WARUNKÓW OBRÓBKI WSTĘPNEJ NA PARAMETRY PROCESU ZAGĘSZCZANIA SŁOMY RZEPAKOWEJ

Streszczenie. Przedstawiono wyniki badań nad określeniem wpływu wilgotności (od 10 do 22%) i rozdrobnienia (d_{sr}=0,95 i d_{sr}=1,94 mm) słomy rzepakowej na parametry procesu aglomerowania w warunkach modelowych. W szczególności wyznaczono podatność surowca na zagęszczanie oraz jakość uzyskiwanych aglomeratów. Stwierdzono, że wraz ze wzrostem wilgotności, rośnie gęstość materiału w komorze zagęszczania, natomiast gęstość produktu po wyjęciu z matrycy maleje. Wykazano, iż w całym zakresie wilgotności, niższe zapotrzebowanie energii występuje podczas zagęszczania materiału o wyższym stopniu rozdrobnienia (średnio 27,02 $J \cdot g^{-1}$). Przeciętna różnica w wielkości tego parametru, wynikająca z oddziaływania stopnia wilgotności wynosi 36%. Natomiast zwiększenie rozdrobnienia pozwala zredukować energochłonność procesu średnio o 14%.

Słowa kluczowe: zagęszczanie, brykietowanie, wilgotność, stopień rozdrobnienia, słoma rzepakowa.

TEKA Kom. Mot. Energ. Roln. – OL PAN, 2011, 11, 218–228

STORAGE TEMPERATURE INFLUENCE ON YOUNG MODULUS OF TOMATO SKIN

Izabela Kuna-Broniowska[1], Bożena Gładyszewska[2], Anna Ciupak[2]

[1]Department of Applied Mathematics and Informatics,
University of Life Sciences in Lublin, Akademicka 13, 20-950 Lublin, Poland
e-mail: izabela.kuna@up.lublin.pl
[2]Departments of Physics,
University of Life Sciences in Lublin, Akademicka 13, 20-950 Lublin, Poland
e-mail: bozena.gladyszewska@up.lublin.pl

Summary. Statistical analysis has been used to interpret results of studying Young modulus, critical stress vs. thickness of tomato skin of Admiro and Encore variety. The model has been based on the method of response surface regression. The possibility of prediction of Young modulus for tomato fruit stored at the temperatures 13 ºC and 21 ºC basing on changes of skin thickness and critical stress has been considered using determinant coefficient R^2 that corresponds to fitting accuracy of the model.

Key words: Young modulus, response surface, tomato fruit peel, strength of the material

INTRODUCTION

Studying mechanical properties of vegetable materials is based on the relation between the applied force and the strain caused by this action. This also allows to determine some important mechanical parameters such as Young modulus, critical strain, critical stress and Poisson ratio (Sitkei 1986).

According to the work of Voisey (1971) when calculating Young modulus one needs to assume that stress is proportional to strain and that the process is reversible. In the case of viscoelastic vegetable materials the above-mentioned conditions are rarely fulfilled. The author stresses however, that Young modulus (as experimentally determined) can be used for quantitative characterization of many vegetable products, because this parameter is independent of geometrical dimension of a sample (Dobraszczyk 1999).

Most often Young modulus is determined for small strains - occurring in compression or tension tests - as a tangent of slope angle from the stress-strain dependence in its linear region (Burgert 2006). In this way many results have been obtained for tomatoes (Matas 2004, Gladyszewska 2009), orange (Singh 2006), seed coats (Gladyszewska 2006), onions (Hole 2000), apples (Dobrzański 2003, Alamar 2008, Gladyszewska 2010). Kabas et al. (2008a) (Mohsenin 1980) studied Young modulus of tomatoes variety cherry, using Boussinesq method.

By the use of the one-axis strain method also other tomato skins have been studied and strong dependence on tomato variety has been reported (Voisey 1965, Hankinson 1979; Thompson 2001; Andrews 2002; Matas 2004; Bargel 2004; Bargel 2005; Gładyszewska 2009; Ciupak 2010a, 2010b).

MATERIALS AND METHODS

Post-harvest tomatoes were stored in a controlled environment chamber at two temperatures: 13 ºC and 21 ºC. In order to determine Young modulus in our experiments we applied the random markers method (Gładyszewska 2007) that allows to obtain results independent on sample edge deformation effects.

Each measurement was performed in 30 replications. The strips excised lengthwise from the skin of tomato fruits were measured with calipers to determine the length, width and thickness of samples before analysis. The rectangular-shaped samples had the length of 30 mm ± 0.1 mm and the width of 10 mm ± 0.1 mm. The thickness of each sample was measured under an optical microscope at 5 points in the central part of the strip on both sides. The sample was placed on a slide in the slit of a measuring table for observing its longitudinal section under an ocular microscope. Thickness was expressed as the average of 10 individual measurements with the accuracy of ± 0.05 mm.

The ends of the samples prepared directly before measurement were placed in the clamping grips of the tensile testing machine (Gładyszewska 2007). The fixed clamping grip was connected to the Megaton Electronic (AG&Co) KT-1400 tensometer with a force measurement range of 0-100 N, and the moving grip was flexibly connected to a transmission device for stretching the specimen. Using a CCD equipped with a microscope lens, the specimen was observed at 240x320 pixel resolution under 5x magnification.

The images of the stretched sample with graphite markers randomly sprayed on the sample surface and the value of the tensile force corresponding to each image were downloaded to the computer. The signal from the tensometer was transmitted to the computer with the use of an analogue-to-digital converter. The random marking method has fewer limitations and produces fewer errors than other techniques for testing the mechanical properties of biological materials. Its main advantage is that the obtained results are independent of the effects observed along the specimen's edges which are close to the clamping grips of the testing machine.

Critical stress was calculated as:

$$\sigma = \frac{F}{S} \tag{1}$$

where F [N] is a force value corresponding to the destruction of a sample, $S = a \cdot b$, *a* and *b* are thickness and width of a sample, respectively.

Knowing the strain ε_x for different stress σ one can calculate Young modulus:

$$E = \frac{\sigma}{\varepsilon_x} \tag{2}$$

where: ε_x – strain in the direction of the applied force.

The results were processed statistically using the Statistica 6 application.

RESULTS

Young's modulus is defined as a ratio of critical stress σ and strain in the direction of the applied force ε_x. Critical stress σ is a function of force value corresponding to destruction of a sample F[N] and cross-sectional area S, where = · , *a* and *b* are thickness and width of a sample, respectively. Thus, Young's modulus is a function of four variables: the force F, strain ε_x, and the thickness *a* and width *b* of the sample according to formula:

$$E = \frac{F}{a \cdot b \cdot \varepsilon_x}.$$

Determination of density function of Young's modulus requires knowledge of the distributions of other variables and does not necessarily lead to normal distribution, which is required for most statistical tests. Accordingly, there is no need to specify the density function module E, but only enough to apply the test of normality for the distribution of Young's modulus to verify the assumptions related to the method of analysis of variance. Normal distribution parameters were estimated based on a sample and hence the use of Shapiro –Wilk's test (Shapiro 1965). Type of derogation from the normal distribution of Young's module distribution was assessed by normality plots (Thode 2002).

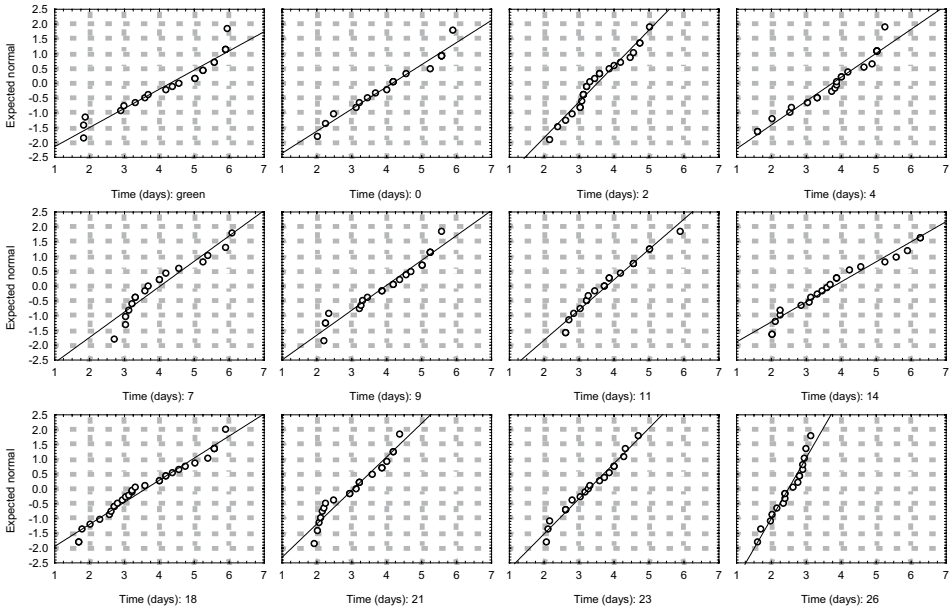

Fig. 1. Normal probability plots for Young modulus of the skin of greenhouse tomatoes cv. Admiro stored at 13°C.

Table. 1. Shapiro-Wilk test for Young's modulus

Test function	Period of storage (days)											
	green	0	2	4	7	9	11	14	18	21	23	26
Shapiro-Wilk	0.8998	0.9311	0.9488	0.9233	0.8948	0.9235	0.9429	0.9254	0.9483	0,9162	0.9581	0.9395
p- value	0.0346	0.2028	0.2557	0.0889	0.0556	0.1020	0.2715	0.0984	0.1522	0.0727	0.5350	0.2845

The results of Shapiro-Wilk test, performed at the significance level of 0.05, indicate that there are no grounds for rejecting the assumed normality of Young's modulus *E* distribution (all *p*-values are greater than 0.05) (Table 1).

Therefore, the assumption postulating a conformance between Young's modulus distribution and normal distribution seems to be fulfilled. The significance of variations in Young's modulus resulting from the studied tomato varieties, storage temperature and storage period can be examined by analysis of variance (Hinkelmann 2008). Due to space constraints, this paper presents the results of normality tests and normality plots solely for tomato fruit cv. Admiro stored at 13°C (Fig. 1).

Table 2. Univariate tests F for the Young's modulus of tomato fruit skin for two greenhouse tomato varieties

Sources of variation	SS	df	MS	F	p
Intercept	9094.21	1	9094.21	**10496.31**	0.00
Variety	155.37	1	155.37	**179.33**	0.00
Time of storage	166.99	5	33.40	**38.55**	0.00
Temperature	75.28	1	75.28	**86.88**	0.00
Variety*Time	29.99	5	6.00	**6.92**	0.00
Variety *Temperature	62.32	1	62.32	**71.92**	0.00
Temperature*Time	256.51	5	51.30	**59.21**	0.00
Variety * Temperature *Time	18.20	5	3.64	**4.20**	0.00
Error	389.89	450	0.87		

The results of the analysis of variance indicate significant differences in the mean Young modulus between varieties, temperature and storage time. Significant differences were also observed as regards interactions between the experimental factors (Table 2). Since the storage period of tomato fruits kept at various temperatures differed, further statistical analyses were carried out separately for each temperature regime. They investigated changes in Young modulus during storage and the option of modeling these changes based on stress and skin thickness values.

Table 3. Mean values of Young's modulus for tomato fruit skin cv. Encore and Admiro stored at 13 ºC and 21 ºC

Variety	Temperature	*E* Average	*E* Std. Error	*E* - 95.00%	*E* + 95.00%	N
Admiro	13 ºC	3.863	0.085	3.696	4.030	122
Admiro	21 ºC	3.791	0.086	3.621	3.960	117
Encore	13 ºC	5.743	0.086	5.574	5.912	119
Encore	21 ºC	4.213	0.087	4.042	4.384	116

The mean value of Young's modulus for tomato fruits cv. Admiro stored at the temperature of 13 ºC was 3.863 MPa, and it was a little higher in comparison with the fruit stored at 21 ºC. Tomato fruits cv. Encore were marked by higher differences in the mean values of Young's modulus which reached 5.743 MPa at 13°C and 4.213 MPa at 21°C (Table 3).

The changes in the value of Young's modulus of the skin of tomatoes cv. Admiro and Encore are shown in Fig. 2 and 3. In Admiro variety tomatoes stored at 13° C Young's modulus decreased from 4.15 MPa on harvesting day to 2.48 MPa after 26 days of storage (Fig. 2a), implying a 40% drop. As regards the fruits stored at 21°C, the values of Young's modulus decreased from 6.40 MPa on the harvesting day to 2.25 MPa after 12 days of storage (Fig. 3a).

The value of Young's modulus of the skin of tomato fruits cv. Encore stored at 13°C varied during the 28-day period of storage (Fig. 2b). In successive days of the study, the investigated parameter varied in the range of 3.73 MPa – 7.40 MPa. In the group of fruits stored at 21°C, the Young's modulus decreased from 5.79 MPa on the harvesting day to 2.98 MPa after 12 days of storage. (Fig. 3b).

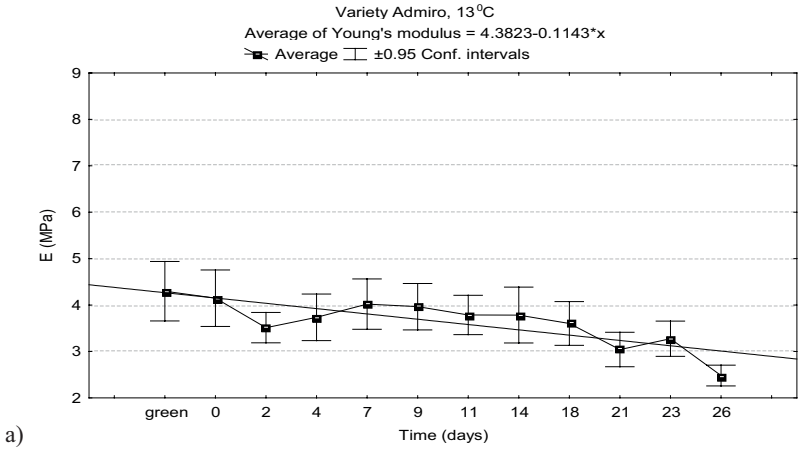

a)

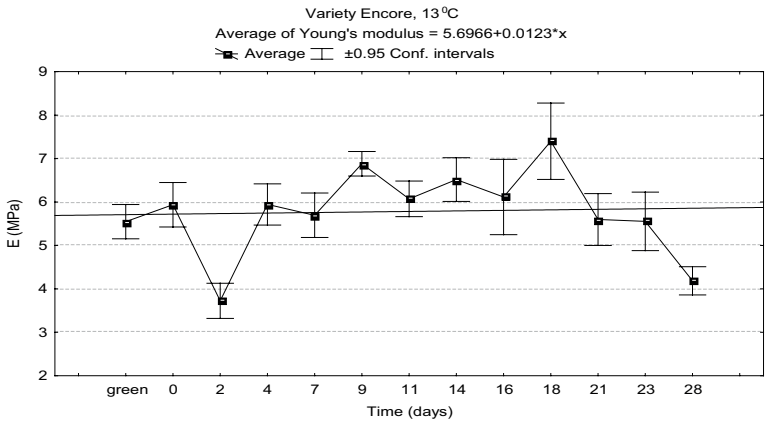

b)

Fig. 2. Mean values of Young modulus of tomato fruit skin cv. Admiro (a) and Encore (b) stored at 13°C.

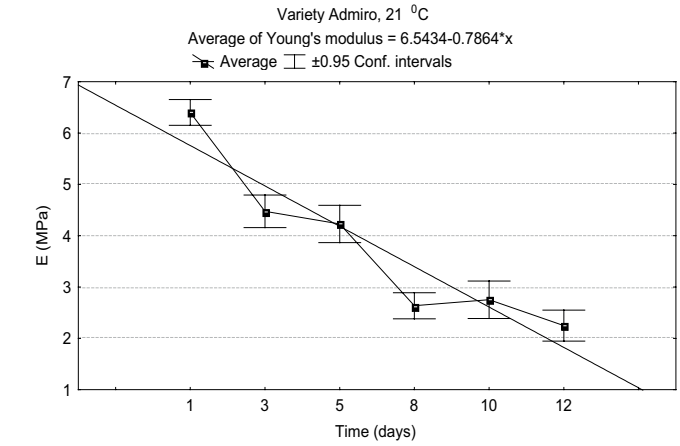

a)

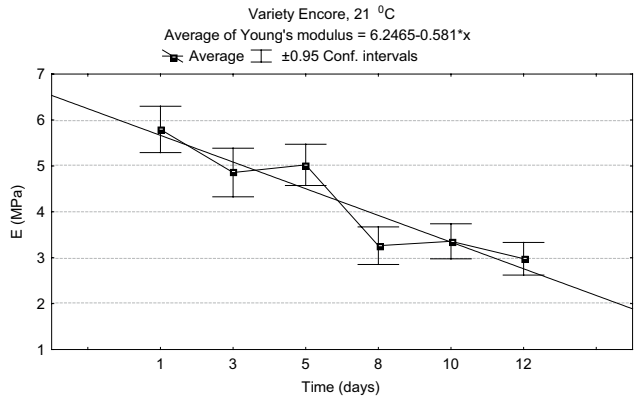

b)

Fig. 3. Mean values of Young modulus of tomato fruit skin cv. Admiro (a) and Encore (b) stored at 21°C

Table 4. Results of univariate tests of significance for a model of Young's modulus of tomato fruit skin, cv. Admiro stored at 13°C

Effect	SS	df	MS	F	p
Intercept	018	1	0.18	0.18	0.67
Time	**40.19**	**11**	**3.65**	**3.57**	**0.00**
Thickness	0.04	1	0.04	0.04	0.84
Thickness ^{2}	0.08	1	0.08	0.07	0.78
Stress	**4.73**	**1**	**4.73**	**4.63**	**0.03**
Stress ^{2}	**6.94**	**1**	**6.94**	**6.79**	**0.01**
Thickness * Stress	0.14	1	0.14	0.13	0.71
Error	241.29	236	1.02		

A curvilinear dependence was observed between Young's modulus, storage time, critical stress and skin thickness. In the fitted model (all effects method), the linear components of time and the linear and quadratic component of stress were statistically efficient (Table 4).

Thickness of skin does not significantly influence the value of Young's modulus.

Table 5. SS test results for a complete model relative to SS for the residuals, cv. Admiro stored at 13°C

	Multiple R	Multiple R^2	Adjusted R^2	SS Model	df Model	MS Model	SS Resid.
E	0.52	0.27	0.22	88.90	16	5.56	241.30

Changes in Young's modulus *E* can be predicted in 22 % (adjusted R^2) based on storage time, changes in critical stress and skin thickness. The remaining 78% of changes of this magnitude are not determined by the examined characteristics. The produced model does not fit the experimental data (Table 5) well, and it cannot be used for predicting Young's modulus.

For variety Admiro stored at 21 °C the equation describing the dependence of Young's modulus on the storage time, stress and critical thickness of the skin is an equation of the quadratic order. In the fitted model (all effects method), the linear components of time and the linear and quadratic component of stress were statistically significant (Table 6). This is the same kind of relationship as the relationship that occurs in the model for the storage temperature equal to 13 ° C (Tab. 4).

Table 6. Results of univariate tests of significance for a model of Young's modulus of tomato fruit skin, cv. Admiro stored at 21 °C

Effect	SS	Degrees of freedom	MS	F	p
Intercept	0.21	1	0.21	0.58	0.45
Time	**66.92**	**5**	**13.38**	**37.68**	**0.00**
Thickness	0.67	1	0.67	1.88	0.17
Thickness ^{2}	0.44	1	0.44	1.23	0.27
Stress	**2.95**	**1**	**2.95**	**8.30**	**0.01**
Stress ^{2}	**1.85**	**1**	**1.85**	**5.21**	**0.02**
Thickness * Stress	1.32	1	1.32	3.73	0.06
Error	37.65	106	0.35		

Tabela 7. SS test results for a complete model relative to SS for the residuals, cv. Admiro stored at 21 °C

	Multiple R	Multiple R^2	Adjusted R^2	SS Model	df Model	MS Model	SS Resid.	df Resid.	MS Resid.	F	P
E	0.93	0.87	0.86	248.97	10	24.89	37.65	106	0.35	70.1	0.00

The model obtained during the study for the peel of tomato variety Admiro, which were stored at 21 ° C fits the experimental data very well (adjusted R^2).

Changes in Young's modulus reach about 86 % due to changes of the storage time, stress and critical thickness of the skin (Table 7). In this case, a better fitting of the model was obtained than for the same variety of fruit stored at 13 ° C (Table 5).

The results of significance tests for Poisson's ratio are presented in response surface charts. This study presents a single response surface chart which is the most consistent with the best fitted model (Fig. 4).

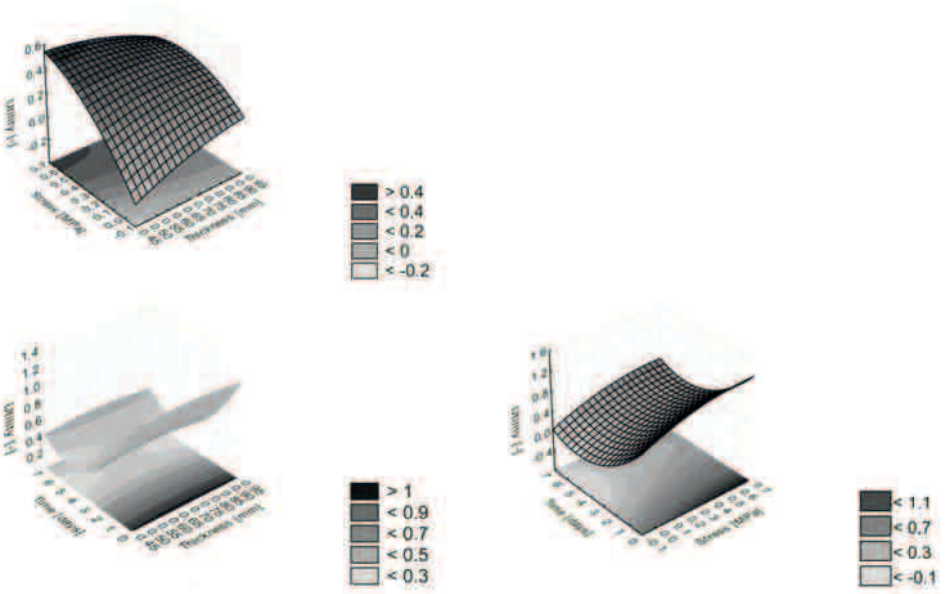

Fig. 4. Response surface - Contours for Young's modulus of tomato fruit skin, cv. Admiro stored at 21 °C

It can be assumed that the changes associated with the process of fruit ripening at room temperature, run more evenly than at 13 °C. In the summary of statistical analysis of the results obtained for the peel of tomato variety Admiro stored at two temperatures 13 °C and 21 °C it should be noted that there is need for further studies at different temperatures of storage, to determine the Young's modulus dependence on temperature conditions of storage. Changes in the value of determined parameters obtained for the skins of fruit stored at 13 °C generally proceeded without a clear trend of increase or decrease. It can not be stated unequivocally whether the reason for this is the temperature or other factors, not included in the study, which may affect the fruit firmness during storage in a climate chamber.

Table 8. Results of univariate tests of significance for a model of Young's modulus of tomato fruit skin, cv. Encore stored at 13 °C

Effect	SS	df	MS	F	p
Intercept	0.44	1	0.44	0.41	0.52
Time	**175.48**	**12**	**14.62**	**13.57**	**0.00**
Thickness	0.76	1	0.76	0.70	0.40
Thickness ^{2}	0.57	1	0.57	0.53	0.47
Stress	**7.58**	**1**	**7.58**	**7.03**	**0.01**
Stress ^{2}	**8.59**	**1**	**8.59**	**7.97**	**0.01**
Thickness * Stress	1.42	1	1.42	1.32	0.25
Error	240.34	223	1.08		

A curvilinear dependence was observed between Young's modulus, storage time, critical stress and skin thickness. This relationship can be described, due to the critical stress, as the poly-

nomial of the quadratic order. In the fitted model, the linear components of time and the linear and quadratic component of stress were statistically efficient, thickness of skin did not significantly affect the value of elastic modulus (Tab. 8).

Table 9. SS test results for a complete model relative to SS for the residuals, cv. Encore stored at 13 °C

	Multiple R	Multiple R^2	Adjusted R^2	SS Model	df Model	MS Model	SS Resid.	df Resid.	MS Resid.	F	P
E	0.70	0.49	0.45	233.57	17	13.74	240.34	223	1.08	12.75	0.00

Changes in Young's modulus *E* can be predicted in 45 % (adjusted R^2) based on storage time, changes in critical stress and skin thickness. The remaining 55 % of changes of this magnitude are not determined by the examined characteristics (Tab. 9). The produced model does not fit the experimental data (Tab. 9) well, and it cannot be used for predicting Young's modulus for tomato fruit cv. Encore stored at 13 °C.

Table 10. Results of univariate tests of significance for model of Young's modulus of tomato fruit skin, cv. Encore stored at 21 °C

Effect	SS	Degrees of freedom	MS	F	p
Intercept	0.00	1	0.00	0.00	0.97
Time	**51.24**	**5**	**10.25**	**12.77**	**0.00**
Thickness	0.36	1	0.36	0.44	0.51
Thickness ^{2}	0.44	1	0.44	0.55	0.46
Stress	0.68	1	0.68	0.85	0.36
Stress ^{2}	0.05	1	0.05	0.06	0.8
Thickness * Stress	0.28	1	0.28	0.35	0.56
Error					

In the fitted model, only the component of time was statistically efficient, the other components did not have a statistically significant impact on the change of value of Young's modulus (Table 10).

Table 11. SS test results for a complete model relative to SS for the residuals, cv. Encore stored at 21 °C

	Multiple R	Multiple R^2	Adjusted R^2	SS Model	df Model	MS Model	SS Resid.	df Resid.	MS Resid.	F	P
E	0.79	0.63	0.60	144.30	10	14.43	84.28	105	0.80	17.98	0.00

The produced model for Young's modulus *E* of cv. Admiro stored at 21 °C fits the experimental data well. Changes in Young's modulus E can be predicted in 60% (adjusted R^2) based on storage time, changes in critical stress and skin thickness (Tab. 11). The fitting of this model is much better than of the model of the same variety, stored at 13 °C (Tab. 9)

Most likely, physiological and biochemical changes occurring during fruit ripening at the higher temperatures run more clearly than in the lower temperature.

REFERENCES

Bargel H., Spatz H.-C., Speck T., Neinhuis C. 2004. Two-dimensional tension tests in plant biomechanics - sweet cherry fruit skin as a model system. *Plant Biology 6*, 432-439.

Burgert I. (2006). Exploring the micromechanical design of plant cell wall. *American Journal of Botany 93 (10)*, 1391-1401.

Chappell T. W., Hamann D. D. (1968). Poisson's ratio and Young modulus for apple flesh under compressive loading. *Transactions of the ASAE 11 (5)*, 608-610.

Ciupak A. (2010a). Wpływ warunków przechowywania owoców pomidora na mechaniczne właściwości ich skórki. Rozprawa doktorska. Uniwersytet Przyrodniczy w Lublinie.

Ciupak A., Gładyszewska B. (2010b). Właściwości mechaniczne skórki owoców pomidora w różnych temperaturach przechowywania. *Acta Agrophysica 15 (1)*, 45-54.

Dimitriadis E. K., Horkay F., Maresca J., Kachar B., Chadwick R. S. (2002). Determination of elastic moduli of thin layers of soft material using the atomic force microscope. *Biophysical Journal 82 (5)*, 2798-2810.

Dobraszczyk B. J., Vincent J. F. (1999). Measurement of mechanical properties of food materials in relation to texture: the materials approach. W Rosenthal A. J. (red.) *Food texture. Measurement and perception.* an Aspen Publication.

Dobrzański jr. B., Rybczyński R., Puchalski C. (2003). Właściwości mechaniczne skórki oraz współczynnik tarcia jabłek odmiany Gala przechowywanych w różnych temperaturach. *Acta Agrophysica 83*, 59-69.

Gładyszewska B., Stropek Z. (2010). The influence of the storage time on selected mechanical properties of apple skin. *Teka Komisji Motoryzacji i Energetyki Rolnictwa* (w druku).

Gładyszewska B., Ciupak A. (2009). Changes in the mechanical properties of the greenhouse tomato fruit skins during storage. *Technical Science 12*, 1-8.

Grotte M., Duprat F., Pietri E., Loonis D. (2002). Young's modulus, Poisson's ratio, and Lame's coefficients of Golden Dilicious apple. *International Journal of Food Properties 5 (2)*, 333-349.

Gyasi S., Fridley R. B., Chen P. (1981). Elastic and viscoelastic Poisson's ratio determination for selected citrus fruits. *Transactions of the ASAE 24 (3)*, 747-750.

Hamm E., Reis P., LeBlanc M., Roman B., Cerda E. (2008). Tearing as a test for mechanical characterization of thin adhesive films. + Suplement. *Nature Materials 7 (5)*, 386-390.

Hankinson B., Rao V. N. (1979). Histological and physical behavior of tomato skins susceptible to cracking. *Journal of the American Society for Horticultural Science 104 (5)*, 577-581.

Hinkelmann K. and Kempthorne O. 2008. Design and Analysis of Experiments. Wiley.

Hole C. C., Drew R. L., Gray D. (2000). Humidity and mechanical properties of onion skins. *Postharvest Biology and Technology 19*, 229-237.

Kabas O., Celik H. K., Ozmerzi A., Akinci I. (2008a). Drop test simulation of sample tomato with finite element method. *Journal of the Science of Food and Agriculture 88*, 1537-1541.

Matas A. J., Cobb E. D., Bartsch J. A., Paolillo jr. D. J., Niklas K. J. (2004). Biomechanics and anatomy of *Lycopersicon esculentum* fruit peels and enzyme-treated samples. *American Journal of Botany 91 (3)*, 352-360.

Mohsenin N. N. (1980). *Physical properties of plant and animal materials. I. Structure, physical characteristic and mechanical properties.* New York, London, Paris: Gordon and Breach Science Publishers.

Murase H., Merva G. E. (1977). Static elastic modulus of tomato epidermis as affected by water potential. *Transactions of the ASAE,* 594-597.

Pitts M. J., Davis D. C., Cavalieri R. P. (2008). Three-point bending: An alternative method to measure tensile priperties in fruit and vegetables. *Postharvest Biology and Technology 48*, 63-69.

Shapiro S. S., Wilk M. B. 1965. An analysis of variance test for normality (complete samples). Biometrika 52 (3-4), 591–611.

Singh K. K., Reddy B. S. (2006). Post-harvest physico-mechanical properties of orange peel and fruit. *Journal of Food Engineering 73*, 112-120.

Sitkei G. (1986). *Mechanics of Agricultural Materials.* Budapest: Akademiai Kiado.

Steffe J. F. (1996). *Rheological methods in food process engineering* . Freeman Press.

Thode H. C. 2002. Testing for normality. New York: Marcel Dekker.

Thompson D. S. (2001). Extensiometric determination of the rheological properties of the epidermis of growing tomato fruit. *Journal of Experimental Botany 52 (359)*, 1291-1301.

Voisey P. W. (1971. Modernization of texture instrumentation. *Journal of Texture Studies 2*, 129-195.

Voisey P. W., Lyall L. H. (1965). Methods of determining the strength of tomato skins in relation to fruit cracking. *Proceedings of the American Society for Horticultural Science 86*, 597-609.

ANALIZA ZMIENNOŚCI MODUŁU YOUNGA SKÓRKI OWOCÓW POMIDORA W RÓŻNYCH TEMPERATURACH PRZECHOWYWANIA

Streszczenie. Praca zawiera analizę statystyczną w celu dopasowania modelu dla modułu Younga E na podstawie naprężenia krytycznego i grubości skórki owoców pomidora odmian Admiro i Encore. Dopasowanie modelu przeprowadzono metodą regresji powierzchni odpowiedzi. Możliwość prognozowania wartości E, owoców przechowywanych w temperaturze 13 ºC i 21ºC, na podstawie zmian grubości i naprężenia krytycznego ich skórki, określono na podstawie współczynnika determinacji R^2 wyrażającego stopień dopasowania modelu.

Słowa kluczowe: moduł Younga, powierzchnia odpowiedzi, skórka owocu pomidora, naprężenia materiału

TEKA Kom. Mot. Energ. Roln. – OL PAN, 2011, 11, 229–235

THE EFFICIENCY ANALYSIS OF AN ASYNCHRONOUS GENERATOR SUPPLYING SINGLE-PHASE RECEIVER SETS IN AN AGRICULTURAL FARM

Piotr Makarski, Marek Ścibisz

Ph.D.Eng., University of Life Sciences in Lublin, Department of Technology Fundamentals

Summary. The article presents the analysis of efficiency changes of an asynchronous generator supplying single-phase receiver sets. The laboratory stand was described as well as the methodology of investigations. On the basis of the investigation results, the influence was evaluated of the generator's size and character on the efficiency of its work.

Key words: asynchronous generator, efficiency of generator

INTRODUCTION

A modern agricultural farm is usually highly mechanized. Some of the works are facilitated by machines and devices powered with electric energy. The network is the general source of electric energy due to the fact that almost the whole area of Poland is supplied with professional energy network. It has been systematically upgraded in urbanized areas and has been modernized to the present valid conditions. In rural areas the situation is less controlled.

The diffusion of energy consumers raises the individual costs of restructuring of energetic lines. The majority of these nets are guided by aerial lines. This fact has caused an increase of supply failures. The lack of possibility of bilateral lead supply, aiming at the continuous supply, results in the application of independent sources of energy.

The electric generator is the most often used spare source of electric energy. It is driven by a combustion engine. Thus, there has been observed the mechanical and then the electric processing of the burning energy. These changes have proceeded with definite efficiency together with the changes of added energy receiver sets. Therefore, the aim of the investigations was the description of energetic transformation efficiency depending on the generator's activity.

ASYNCHRONOUS GENERATOR

An asynchronous power generator consists of two basic pieces [5, 9]: stator and rotor (Fig. 1).

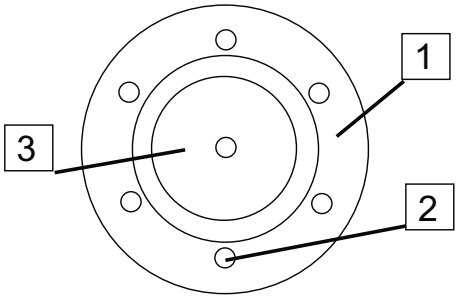

Fig. 1. The building diagram of an asynchronous machine:
1. stator, 2. stator winding, 3. rotor

Stator (1) is a motionless unit in which the winding (2) is placed. The stator winding is the source of circular whirling electromagnetic field. Rotor (3) is a movable unit placed inside the stator. From here the magnetic field influence on rotor is generated.

The magnetic field works with the speed called synchronic. It is produced due to passive energy. It is delivered to the generator from the battery of condensers.

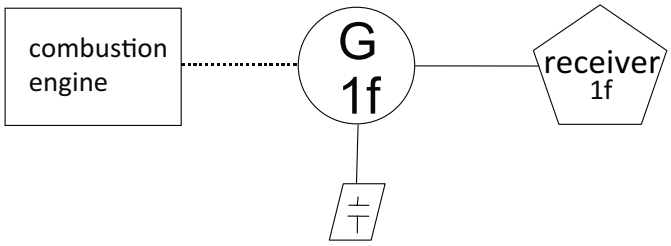

Fig. 2. The diagram of electric generator building

To be driven, the rotor needs the help of combustion engine. If the rotor of a current generator is driven with a higher speed than the synchronic speed, electric energy is generated in the winding.

LABORATORY STAND

Measurements were conducted on the laboratory stand (Fig. 3) made at the Department of Technology Fundamentals at the University of Life Sciences in Lublin. For investigations the single-phase asynchronous generator (1) was used, the type EC 2000 about the nominal power P_n = 1.7 kW, the indicative power S_n = 2 kVA, the nominal voltage U_n = 230 V and the nominal intensity of current I_n = 7.5 A.

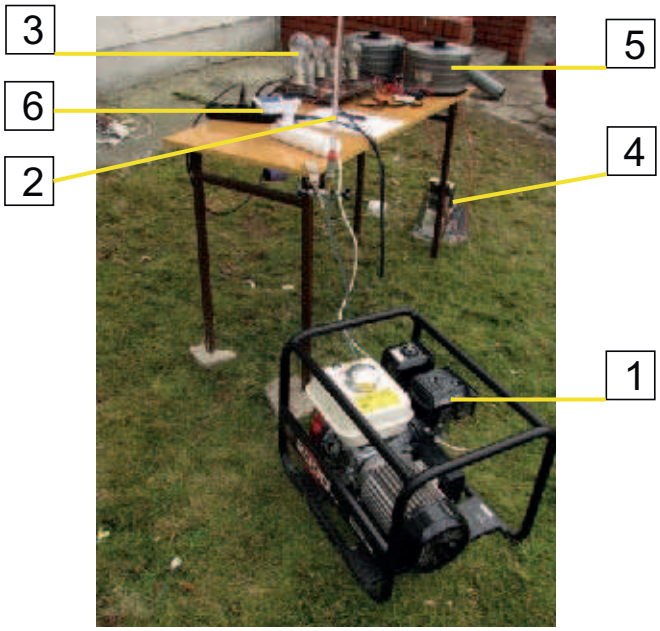

Fig.3. The laboratory stand to measure the efficiency of power generator:
1. power generator, 2. arrangement of fuel measurement, 3. the resistor duty,
4. the inductive duty, 5. autotransformers, 6. the measure of power net parameters

The fuel arrangement in the engine was modified, reinforcing the carburettor across the scaled burette (2). This allowed for the measurement of definite doses of fuel. The time of burning of the tested gob of fuel was measured using the stopper. Resistor (3) was used during the work of the generator (heating spiral casings 1000W and 1200W, bulb about power 200W, 150W, 75W and 40W) and inductive units (4) (throttles from lamps 125W and 250W). The autotransformers (5) were applied for the adjustment of the resistor and inductive work. The versatile power net measurement parameters were used for the measurement of the generator's work.(6).

METHODOLOGY

For the assessment of the efficiency of processing, the quantity of thermal energy (Q_p) received after burning the dose of fuel and the quantity of electric energy (W_p) produced in the power generator were taken into consideration. The thermal energy was evaluated on the basis of the volume (V) of the used fuel as well as the fuel's value (c_p):

$$Q_p = V * c_p, \text{ [J]}. \tag{1}$$

The quantity of electric energy W_p was marked on the basis of the measured power (P) and the time of burning (t_s) of the definite quantity of fuel (V):

$$W_p = P * t_s, \text{ [J]}. \tag{2}$$

The efficiency of processing was marked on the basis of the dependence:

$$\eta = Q_p / W_p. \tag{3}$$

The unleaded petrol Pb95 was used in the investigations. The fuel value depends both on the manufacturer and the distributor of fuel and it remains in the range of 29-38 MJ/m^3 [11, 12, 13, 14].

The fuel value was accepted as 32 MJ/m^3 [6]. It was analyzed during the burning of 5 cm^3 of the fuel.

THE RESULTS OF INVESTIGATION

In the first phase of investigations the generator was put under resistance load. The work was altered from idle state to 1.07 of the nominal power of the generator. The results of investigations are presented in Table 1.

Table 1. The investigations results of asynchronous generator put under resistance load

P, W	t_s, s	W_p, J	Q_p, J	η, -
0	27.4	0	160000	0.000
200	26.3	5267	160000	0.033
396	24.5	9681	160000	0.061
587	22.4	13129	160000	0.082
857	20.7	17718	160000	0.111
1130	18.9	21351	160000	0.133
1384	18.7	25887	160000	0.162
1709	16.0	27344	160000	0.171
1825	15.0	27441	160000	0.172

Then the resistor-inductive duty was added to the generator. It was provided with the stable value of power in the circuit circa 1000 W as well as circa 500 W and the inductive duty was altered.

The results of measurements were introduced in Tables 2 and 3.

Table 2. The investigations results of asynchronous generator for resistor - inductive duty for P≈1kW

$\cos\phi$, -	t_s, s	W_p, J	Q_p, J	η, -
0.87	20.7	21901	160000	0.137
0.90	19.9	21063	160000	0.132
1.00	18.9	19477	160000	0.122

Table 3. The investigations results of asynchronous generator for resistor - inductive duty for P≈0,5kW

$\cos\phi$, -	t_s, s	W_p, J	Q_p, J	η, -
0.50	16.0	8405	160000	0.053
0.55	18.5	9780	160000	0.061
0.65	18,9	10345	160000	0.065
0.85	20.7	11332	160000	0.071
1.00	22.4	11862	190000	0.074

THE ANALYSIS OF INVESTIGATION RESULTS

The results of the performed analysis are shown on the graphs of efficiency (η) changes due to the changes of power (P) duty or due to the changes of coefficient power ($\cos\phi$).

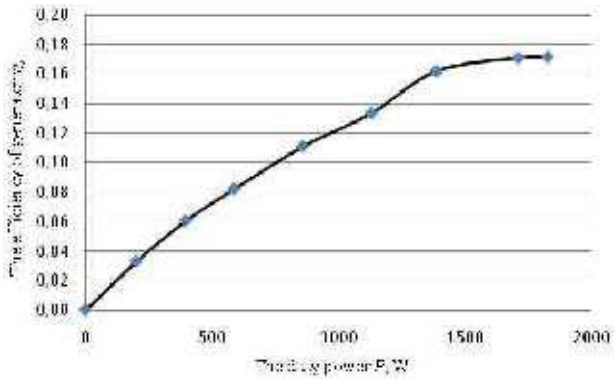

Fig. 4. Graph of efficiency changes of the generator due to the change of duty power

The growth of the generator duty causes the growth of efficiency of energy processing. The maximum efficiency 17.2 % was reached for the duty of nominal power 1.7 kW. The efficiency of energy processing (η) has grown in approximation linearly in the range of power (P) from 0 to about 1400W.

The further growth of power causes the already insignificant growth of efficiency. The change of efficiency in function of duty power for the power aggregate runs along with the efficiency of standalone electric generator in function of duty power.

For a typical generator, efficiency initially grows rapidly with duty power, however, in the wide range of duties it stays practically on the same level [2, 4]. The efficiency of the power aggregate in function of the duty moment is dominated with efficiency of combustion engine. The efficiency of combustion engine grows in function of the duty moment, initially slowly, and then after the achievement of maximum, it drops slightly [1, 7].

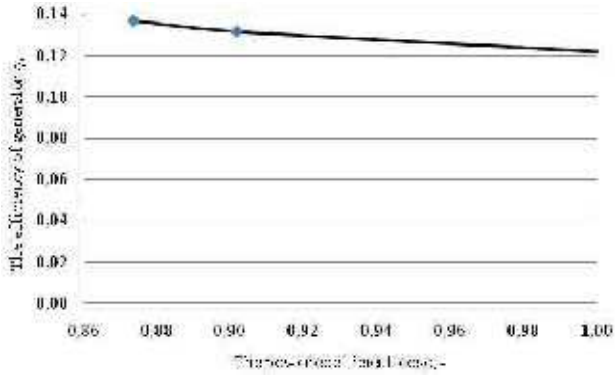

Fig. 6. The graph of efficiency changes of the generator due to change of power coefficient for duty the P ≈ 1000 W

Fig. 5 represents the change of the power efficiency of aggregate in function of power coefficient, for solid power put under load generator, even 1000W.

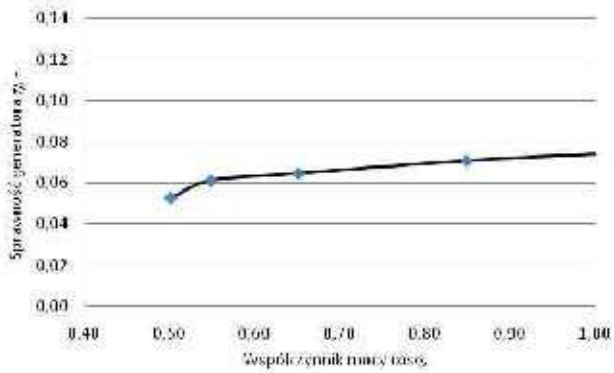

Fig. 6. The graph of efficiency changes of the generator due to change of power coefficient for duty P ≈ 500 W

The efficiency of generator grows up along with the value of power coefficient. With the growth of the *cos*ϕ from 0.5 to 1.0, the power efficiency of the aggregate grows up from 5.3 % to 7.4 %. This results in the fact, that together with the growth of power coefficient, with stable circuit power, the value of passive current diminishes, which causes the decrease of the duty losses.

CONCLUSIONS

The conducted investigations have shown that the efficiency of single-phase generator of small power is low. The maximum value reached was 17.2 %.

The most effective use of energy contained in the fuel is possible by supplying sets of resistor character. So the power generator can be used for the supplying of heat lighting or convective heating devices.

The generator efficiency is the highest by supplying duty approximate to indicative power of the generator. Therefore, from the point of view of efficiency, the power of electric aggregate needs to be correlated with the power of supplying receiver sets, so as to set the work from approximate to indicative power. However, this involves a release of pollution to the environment [3, 8, 10].

The supplying of the receiver sets with the resistor - inductive (the RL character) promotes the work efficiency of the electric generator and reduces the power coefficient. It was purposeful to use the arrangements for passive power compensation.

REFERENCES

Koniuszy A. Wskaźnik optymalizacji silników spalinowych stosowanych w rolnictwie. Silniki spalinowe, nr 1/2007 (128) PTNSS-2007-SS1-205

Koziej E., Sochoń B. 1986. Elektrotechnika i elektronika. PWN, Warszawa, ISBN 83-01-00195-X

Kwiatkowski K., Żółtowski B. 2003. Combustion engines – environmental menace. TEKA Komisji Motoryzacji i Energetyki Rolnictwa. t. III. O-PAN. Lublin.156-164

Latek W. 1987. Teoria maszyn elektrycznych WNT, Warszawa. ISBN 83-204-0887-3
Latek W. 1994. Maszyny elektryczne w pytaniach i odpowiedziach. WNT, Warszawa. ISBN 83-204-1660-4
Piekarski W., Zając G., Szyszlak J. 2006. Odnawialne źródła energii jako alternatywa paliw konwencjonalnych w pojazdach samochodowych i ciągnikach. Inżynieria Rolnicza 4
Postrzednik S., Przybyła G., Żmódka Z. 2008. Wpływ obciążenia silnika spalinowego na efektywność konwersji energii w układzie. Czasopismo techniczne M. z. 7-M. ISSN 0011-4561, ISSN 1897-6328. Wydawnictwo Politechniki Krakowskiej
Słowik T., Piekarski W., Pawlak H. 2005. Wayside relief and concentartions of selected heavy metals ions caused by motor idustry insoil. TEKA Komisji Motoryzacji i Energetyki Rolnictwa. t. V. O-PAN. Lublin. 198-204
Urbanowicz H., Nowacki Z. 1986. Napęd elektryczny w pytaniach i odpowiedziach. WNT, Warszawa. ISBN 83-204-0762-1
Wasilewski J. 2005. The influence of regulation parameters change in a fuel injection system on Nox emission levels in combustion gases of the tractor engine. TEKA Komisji Motoryzacji i Energetyki Rolnictwa. t.V. O-PAN. Lublin. 226-232
Drewno zamiast benzyny [on line]. 2011. [dostęp: 2.03.2011]. Dostępny w internecie: http://www.drewnozamiastbenzyny.pl.pl
Myszkowski S. 2010. Benzyny silnikowe [on line]. [dostęp: 3.03.2011]. Dostępny w internecie: http://www.autoexpert.pl
Nośnik energii [on line]. E-petrol. 2011. [dostęp: 2.03.2011]. Dostępny w internecie: http://www.e-petrol.pl
Właściwości fizykochemiczne [on line]. Orlen. 2011 [dostęp: 3.03.2011]. Dostępny w internecie: http://www.orlenpetrotank.pl

ANALIZA EFEKTYWNOŚCI GENERATORA ASYNCHRONICZNEGO ZASILAJĄCEGO ODBIORNIKI JEDNOFAZOWE W GOSPODARSTWIE ROLNYM

Streszczenie. W artykule przedstawiono analizę zmian sprawności generatora asynchronicznego zasilającego odbiorniki jednofazowe. Opisano stanowisko badawcze i metodykę badań. Na podstawie przeprowadzonych pomiarów dokonano oceny wpływu wielkości i charakteru obciążenia na efektywność pracy generatora.

Słowa kluczowe: generator asynchroniczny, sprawność generatora

TEKA Kom. Mot. Energ. Roln. – OL PAN, 2011, 11, 236–244

MODELLING TIRE-SOIL INTERACTION WITH THE FEM APPLICATION

Włodzimierz Malesa

Warsaw University of Technology, Faculty of Civil Engineering, Mechanics and Petrochemistry
Department of Mechanical Systems Engineering and Automation
Address: Łukasiewicza 17, 09-400 Płock, e-mail: polsw@pw.plock.pl

Summary. This article presents the application of CAD systems with the use of the finite element method (FEM) in calculations of particular parameters of the tire-soil interaction. Moreover, a distribution model of surface pressures is presented as well as calculations of stresses in the soil with the FEM application. The obtained theoretical findings resulted in a comparative analysis of the value of designated stresses with those obtained through empirical studies, carried out both in a laboratory (soil channel) and also in field conditions, conducted in the Federal Agricultural Research Center - Braunschweig (Germany).

Key words: tire-soil interaction, computer-assisted design, finite elements method, stresses in soil.

INTRODUCTION

The interaction of the drive unit with the ground is very significant not only for agrotechnological reasons, but also due to traction. Consequently, it is necessary for the drive mechanisms of machines and equipment moving on deformable ground to exert the least possible unitary pressure, and simultaneously to obtain maximum traction power in given conditions, such as pull force (P_u), or drive force (P_j). Unitary pressures occurring on the tire contact surface with the ground are directly connected with the phenomenon of their diffusion into the area on which the drive unit moves, both lengthwise and crosswise in relation to the movement direction. The range of their diffusion is a separate issue.

This study aims at applying modern methods of analysis with the application of CAD systems and FEM. This is of great importance due to economic reasons since field and laboratory research studies require incurring substantial financial costs, in view of high prices of measuring appliances and the necessity of holding a properly prepared terrain.

The influence of farming vehicles and machinery on the soil environment, through drive units, results in both the intended and side effects. The negative influence of drive units on the natural soil environment while performing activities connected with cultivating soil belong to the latter category. From this point of view, it is possible to distinguish between quantitative and qualitative deformations.

In the modern farming technology there is a tendency to increase powers of traction drive mechanisms of tractors and self-propelled farming machinery parallel to reducing the degree of soil packing (qualitative deformation). The increase in the pressure exerted on soil results in the increase in the drive force value, which directly affects the towing power value. This has caused the necessity of determining dependences describing the impact of drive mechanisms on soil. In the subject-related literature there exist numerous theoretical works and results of laboratory research concerning the issue described here.

In recent times, owing to a dynamic development of computer systems, it has been possible to apply modern numerical computer technology in order to analyze the tire-soil interaction. One of the methods applied to calculate particular parameters of the interaction between the drive mechanisms and soil is FEM (Finite Element Methods).

In this article the results of research study with the use of CAD systems have been presented, particularly the finite element method (FEM), in calculations of particular parameters of the tire-soil interaction. It was vital to verify available tools for solid modeling and FEM calculations from the perspective of their usefulness for calculating pressures in soil under particular tires while driving a farming machine.

SOLID MODELS OF DRIVE TIRES

This work presents the scope of works related to the FEM application in analyzing the propagation of stresses in the soil medium following the influence of a particular tire used for self-propelled farming machinery. Solid models of drive tires were made, including all the basic elements constituting their structure. One of the research stages was the elaboration of the model of tire-ground (soil) interaction taking into consideration the system's dynamics. Modeling the ground consisted in performing computer simulations of the tire imprint as well as in determining geometrical features of the shape left during the drive.

Then the distribution model of surface stresses was prepared, as well as calculations of stresses in the soil, with the application of the finite element method. The analysis of the obtained results in the form of chart of stresses was conducted in particular cross sections of the tire-soil geometrical model.

The theoretical findings obtained resulted in a comparative analysis of the value of designated stresses with those obtained through empirical studies, carried out both in a laboratory (soil channel) and also in field conditions, conducted in the Federal Agricultural Research Center - Braunschweig.

The tire model was made in the CAD Inventor system. Subsequent operations, such as sketching, simple and complex stretching, dragging, rounding etc. resulted in a solid which was a virtual model of the tire under examination. As the pattern for building the model, the following tire was used: Stomil 14.9-28/8PR.

THE TIRE-SOIL INTERACTION MODEL, INCLUDING THE SYSTEM DYNAMICS

The 3D tire model made in the Inventor system was used for shaping the imprint in the ground. The tire imprint was divided into a set of elementary surfaces to which forces were applied, normal and tangent components. The diagram below (Fig. 1) shows forces affecting the wheel and their distribution on the elementary surface of the imprint.

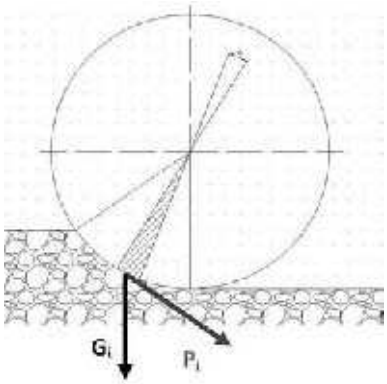

Fig. 1. Diagram of distribution of forces on a particular element of the imprint

Elementary components P_i as well as G_i were calculated according to the following dependences:

$$G_i = \frac{G}{n}$$

$$P_i = \frac{M}{nR}$$

$$P_i = \sqrt{P_{ix}^2 + P_{iy}^2}$$

$$P_{ix} = P_i \cos(i\alpha_i)$$

$$P_{iy} = P_i \sin(i\alpha_i)$$

where:

G – wheel load force,

M – moment of force imposed on the wheel,

R – tire rolling radius,

P_i – elementary force tangent to a sector of the tire contact surface with the soil occurring as a result of the moment (M) interaction

P_{ix}, P_{iy} – components of force (P_i)

α_i – elementary angle of wrap,

n – number of elementary surfaces,

i – number of an elementary surface

Figure 2 shows a fragment of the modeled imprint, formed through the tire impact on soil, which was divided into elementary surfaces. To each of these surfaces a tangent force P_i was applied, which was described by the dependence. Force (G) was distributed evenly on particular elementary surfaces of the imprint.

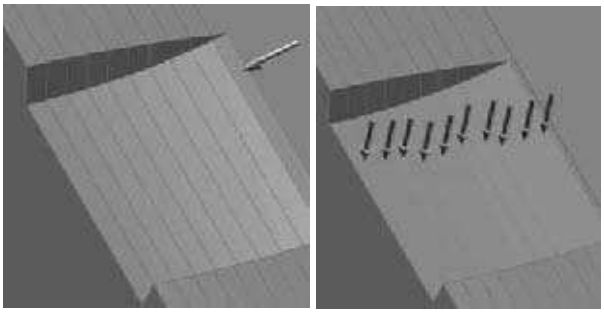

Fig. 2. Model of applying normal and tangent forces to a particular tire imprint sector

On establishing peripheral conditions, the ANSYS module of the Inventor system was used in order to determine pressures in the soil. Calculations were carried out for particular values of force (G) and moment (M).

PERFORMING CALCULATIONS OF STRESSES AND THEIR ANALYSIS WITH THE APPLICATION OF THE FINITE ELEMENT METHOD

The first case to be analyzed in the ANSYS system was the model of loading the wheel with force (G)=7kN as well as moment (M)=0 Nm, i.e. the static load test. Then, analogous calculations as in the previous case were conducted, with the difference that the moment of force (M=5000 Nm) of the tire impact on soil was taken into account. The results of the conducted calculations, as well as the trend lines determined as exponential functions (Fig. 3) show that the increase in the moment of force affecting the imprint surface causes the reduction in the value of stresses on comparable depths of the ground.

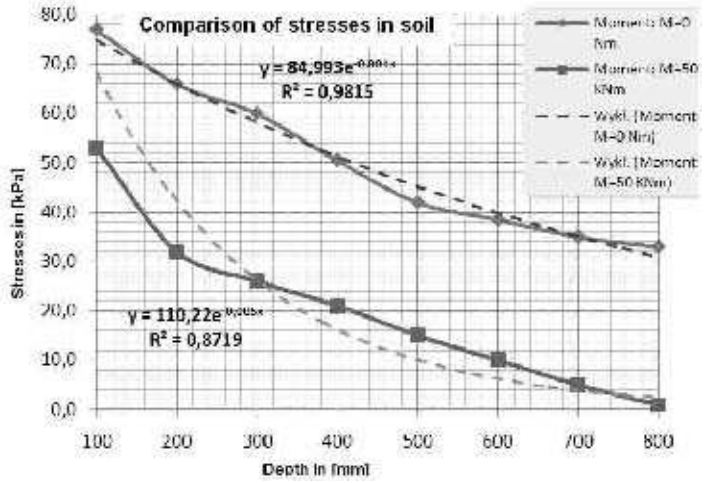

Fig. 3. Comparison of stresses in soil for the moments of 0 and 5 kNm at force G=7 kN

Then, a series of research studies were carried out for load cases analogous to the example above, with the difference that force (G) equaled 10 kN (Fig. 4).

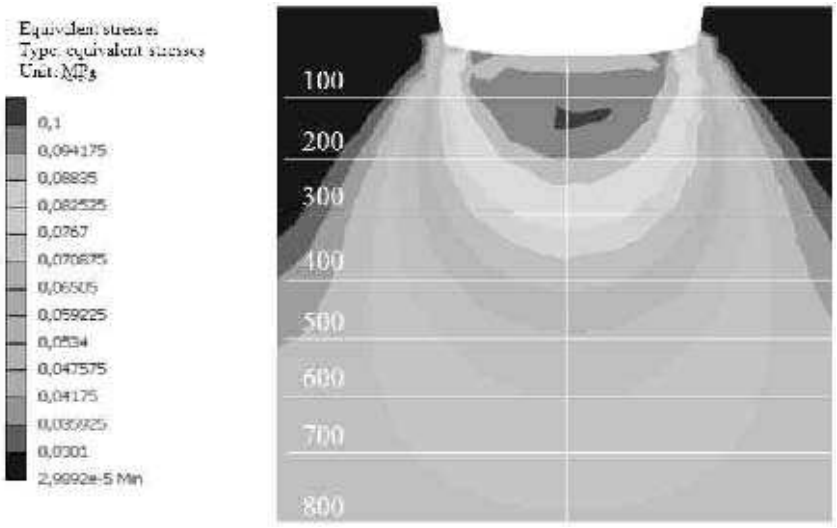

Fig. 4. Distribution of stresses in soil (M=0 Nm, G=10kN, levels in mm)

The analysis of results for the cases when (M=0 Nm, G=10kN) as well as when (M=5000Nm, G=10kN) demonstrates that also in such cases applying the moment of force results in the decrease in stresses. The difference in the value of stresses on particular ground depths approximately indicates a steady tendency, which can also be determined when observing the course of trend lines (Table 1, Fig. 5).

Table 1. Comparison of obtained results

Depth [mm]	**100**	**200**	**300**	**400**	**500**	**600**	**700**	**800**
M=0Nm, G=7kN	77.0	66.0	60.0	50.5	42.0	38.5	35.0	33.0
M=50*10^{2}Nm, G=7kN	53.0	32.0	26.0	21.0	15.0	10.0	5.0	1.0
M=0Nm, G=10kN	98.0	94.0	73.0	63.0	59.0	55.0	47.0	41.0
M=50*10^{2}Nm, G=10kN	76.0	56.0	48.0	41.0	28.0	21.0	15.0	7.0

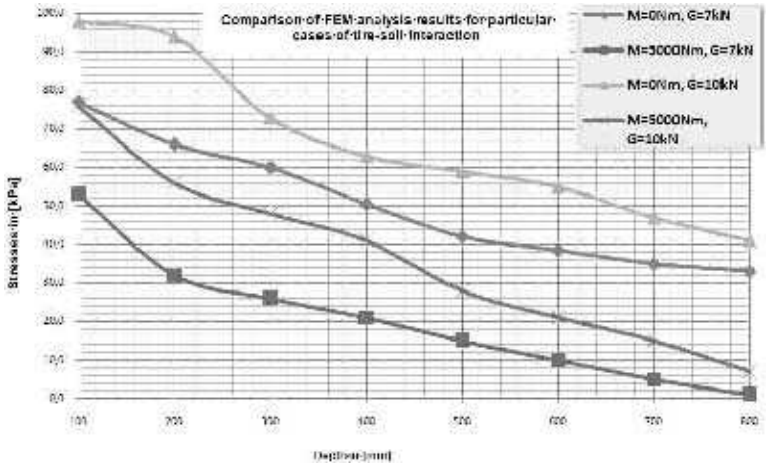

Fig. 5. Comparison of FEM analysis results for examined cases of tire-soil interaction

VERIFICATION OF CALCULATION METHODS PROPOSED THROUGH COMPARISON WITH RESULTS OBTAINED IN FIELD TESTS

The results obtained with the FEM application were compared with laboratory results carried out for the Stomil 14.9-28/8PR tire, which was modeled for the purposes of the simulation conducted with the use of the ANSYS system. The results obtained in laboratory and field tests were used for the comparative analysis.

Fig. 8. Measuring instruments in the Federal Agricultural Research Center (FAL) in Braunschweig

Source: Jakliński L.: Mechanika układu pojazd-teren w teorii i badaniach (Mechanics of vehicle-terrain systems in theory and tests) Wybrane zagadnienia (Selected issues), OWPW 2006

Laboratory and field studies were conducted in the Federal Agricultural Research Center (FAL) in Braunschweig. The sand-clay ground measuring 100m x 40m was examined. Four hydraulic pressure sensors were used for measuring pressures, buried in the soil with their measuring heads situated exactly in the center of the wheel track.

The pressures measurement results compared to the values calculated in the FEM system were presented in Table 2. The distribution of pressure values in the plane parallel to the wheel track axis at three measurement depths was presented for G=7 kN and G=10kN, at M=50Nm.

Table 2. Comparison of results obtained in laboratory tests and FEM calculations (values of stresses in [kPa])

Depth [mm]	**G=7kN**			**G=10kN**		
	P_{FEM}	**P_{meas}**	**Difference [%]**	**P_{FEM}**	**P_{meas}**	**Difference [%]**
100	77.0	85.6	10%	98.0	108.2	9%
200	66.0	59.4	11%	94.0	88.1	7%
300	60.0	44.0	36%	73.0	61.4	19%

Measurement results and those calculated with the FEM indicate significant similarity (approx. 9% error difference) for smaller ground depths. At greater depths the differences between measurements and calculations exceed even 20%, which can result from several factors:

- the geometrical model of the tire and its imprint in the ground was of insufficient accuracy,
- using approximate material properties for the ground model,
- approximate model of peripheral conditions used in FEM,
- insufficient density of the FEM grid of the calculation model (increased speed of calculations).

In order to improve the accuracy of calculations, the geometrical models of the ground and of the tire interacting with it should be better prepared in further research studies; the accuracy of the FEM model should be improved; the physical data characterizing the ground should completely correspond to the actual properties of the soil examined in laboratory conditions.

CONCLUSIONS

The results of the obtained calculations have been presented in the form of color maps, tabular comparisons and diagrams. The analysis of theoretical calculations showed a similarity of the calculated values of stresses obtained through empirical studies, carried out both in a laboratory (soil channel) and also in the field conditions, conducted in the Federal Agricultural Research Center - Braunschweig.

The application of CAD systems as well as digital simulation methods and FEM calculations in the issues under discussion gives measurable advantages, among others the ones as follow:

- a significant reduction in time needed for research and independence of the research process from weather and climatic conditions,
- relieving the research team of routine and uncreative activities - time-consuming preparation of research stands, and laborious analyses of results,
- facilitating the performance of comparative analyses of tires under examination, as well as types of ground,

- conducting reliable research studies with the application of computer systems at the stage of the tire design and drive unit, without the necessity to carry out costly and time-consuming laboratory research.

REFERENCES

Bekker M.G. Introduction to terrain-vehicle system, The University of Michigan Press, Ann Arbor 1969.

Jakliński L.: Mechanika układu pojazd-teren w teorii i badaniach (Mechanics of vehicle-terrain systems in theory and tests) Wybrane zagadnienia (Selected issues), OWPW 2006,

Jakliński L.: Modele oddziaływania koła pneumatycznego na glebę (Models of the impact of a pneumatic wheel on soil), OWPW 1999.

Jakliński L.: Monitorowanie rozkładu nacisków jednostkowych w badaniach polowych. Technika Rolnicza, Ogrodnicza, Leśna, 2004, nr 1, s.27-28

Jakliński L., Pilarczyk S.: Badanie rozkładu nacisków jednostkowych w glebie z uwzględnieniem występowania podeszwy płużnej, Journal of research and applications in agricultural engineering, Poznań 2008, vol. 53(3), str. 96.

Jakliński L., Jasiński B., Lebert M., Krzywosiński S.: Monitoring tire-soil individual stresses as contribution to soil protection, Systemy Mikroprocesorowe w Rolnictwie Międzynarodowa Konferencja – Płock 2004, s. 50-61.

Jakliński L., Pilarczyk S.: Analiza propagacji nacisków wybranych napędowych opon rolniczych, X Międzynarodowe Sympozjum Inżynierii Systemów Bioagrotechnicznych, Płock 2007, Zeszyt 6(15), s.29-33

Król K.: Metoda elementów skończonych w obliczeniach konstrukcji, Politechnika Radomska, Wydawnictwo (2006).

Kruszewski J., Gawroński W., Wittbrodt E., Najbar F., Grabowski S.: Metoda sztywnych elementów skończonych, Arkady 1975.

Kruszewski Z., Jakliński L.: Badania porównawcze opon napędowych do ciągników rolniczych 14.9-28 8PR „Stomil" i „Good Year", Sprawozdanie z pracy zleconej przez OZOS Stomil, Płock 1990.

Pytka J., Szymaniak G.: Investigations of stress state in soil under Tractor tyres, Teka Komisji Motoryzacji i Energetyki Rolnictwa IV/2004, s. 172, Wydawnictwo Oddziału PAN w Lublinie.

Rakowski G., Kacprzyk Z., Metoda elementów skończonych w mechanice konstrukcji, OWPW 2005.

Sołtyński A.: Mechanika układu pojazd-teren, Wydawnictwo Ministerstwa Obrony Narodowej, 1966.

Sommer C., Lebert M., Jakliński L., Jasiński B.: Bodenschadverdichtung Strategien und physikalischen Bodenschutz. Landtechnik no. 2, 2003.

Stasiak W.: Analiza modeli opisujących rozkład naprężeń w glebie, Journal of Research and Applications in Agricultural Engineering, Poznań, 2008, vol. 53 (2), str. 39-43.

Stasiak W., Modele propagacji nacisków w glebie generowanych przez oponę, praca doktorska, PW Płock, 2003.

Szmelter J., Dacko M., Dobrociński S., Wieczorek M.: Metoda elementów skończonych w statyce konstrukcji. Przykłady obliczeń, Arkady 1979.

Szymaniak G., Pytka J.: Effects of reduced inflation pressure and ride velocity on soil surface deformation, Teka Komisji Motoryzacji i Energetyki Rolnictwa III/2003, s. 236, Wydawnictwo Oddziału PAN w Lublinie.

Zagrajek. T., Krzesiński G., Marek P.: Metoda elementów skończonych w mechanice konstrukcji. Ćwiczenia z zastosowaniem systemu ANSYS, OWPW 2006.
Zienkiewicz O.C.: Metoda elementów skończonych, Arkady 1972.

MODELOWANIE ODDZIAŁYWANIA OPONY NA GLEBĘ Z ZASTOSOWANIEM METODY ELEMENTÓW SKOŃCZONYCH (MES)

Streszczenie. W opracowaniu przedstawiono zastosowanie systemów CAD z wykorzystaniem metody elementów skończonych (MES), w obliczeniach wybranych parametrów współpracy opony z glebą. Ponadto wykonano model rozkładu nacisków powierzchniowych oraz obliczenia naprężeń powstałych w glebie z zastosowaniem MES. W następstwie uzyskanych wyników obliczeń teoretycznych została przeprowadzona analiza porównawcza wartości wyznaczonych nacisków z uzyskanymi wynikami w trakcie badań laboratoryjnych (kanał glebowy) jak i w warunkach polowych, przeprowadzonych w Federal Reserch Centre – Braunschweig (Niemcy).

Słowa kluczowe: oddziaływanie opony na glebę, komputerowo wspomagane projektowanie, metoda elementów skończonych, propagacja naprężeń w glebie.

TEKA Kom. Mot. Energ. Roln. – OL PAN, 2011, 11, 245–251

EFFECT OF FILLERS ADDITION ON SME OF EXTRUSION-COOKING OF THERMOPLASTIC WHEAT STARCH

Thomasz Oniszczuk, Leszek Mościcki

Department of Food Process Engineering, Lublin University of Life Sciences
Doswiadczalna 44, 20-236 Lublin, Poland
E-mail: tomasz.oniszczuk @ up.lublin.pl

Summary. Results of the SME measurements during extrusion-cooking of thermoplastic wheat starch enriched with flax fibers, cellulose, and ground bark are presented in the paper. A modified single screw extrusion-cooker TS 45 with L / D = 18 and an additional cooling section of the barrel was used as the processing unit. The effect of the quantity and type of filler used in the blend containing 20% glycerol (plasticizer) and the screw speed on the efficiency of the baro-thermal process as well as energy consumption was the main target of the investigation.

Key words: thermoplastic starch, fillers, extrusion-cooking, energy consumption, SME

INTRODUCTION

The growing amount of deposited waste is a big burden to the environment. Most of plastic waste is resistant to degradation, due to polymers composition. In recent years large-scale studies have been conducted, aiming at increasing the share of starch in starch-plastic composites to the highest level, which resulted in the growth of the production of biodegradable materials used in the packaging industry[3,11].

Thermoplastic starch (TPS) based products are fully degradable and nowadays are successfully used by the rural sector in the field as well as by the food producers for food packaging [2,19]. In order to improve its physical properties and sometimes reduce the price of the finished product different fillers are added to the raw material blends in amounts from 1 to even 50%, dependently on the type of natural fibers used. The most commonly applied fibers are: flax, hemp, jute, coir, cotton, and the waste from wood industry. The important thing is, that the production of TPS-based products is possible with well known machinery and equipment used by plastic manufacturers [10,20].

In the literature many publications can be found concerning the use of starch of different origins for the production of TPS biodegradable packaging materials. Due to the importance of the problem, since 2004 large scale investigations on the processing of TPS biopolimers for packaging materials have been undertaken at the Department of Food Process Engineering, Lublin University of Life Sciences, using corn, potato and wheat starch – the most common local raw materials [1,4,12].

MATERIALS AND METHODS

The basic raw material utilized during the reported study was the wheat starch type MERIZET 200 produced by Segezha Ltd. (IR), mixed with the glycerol of 99% purity, (delivered by Odczynniki Chemiczne Lublin, PL) with the addition of the cellulose fibers vivapur type 102 (JRS GmbH, D), the flax fibers and the ground bark (both delivered by Polish rural producers).

Preparation of the mixtures

The wheat starch (16% of moisture) and other raw materials were mixed in the laboratory ribbon mixer during 20 minutes, than 6 kg samples of different composition were stored within 24 hours in the plastic bags in order to homogenize the mixtures. The share of the glycerol was 20% by weight in the mixture, the contribution of the fibers for selected blends was 0%, 10%, 20% and 30%. Immediately prior to extrusion, the prepared samples once again were mixed for 10 minutes, which guaranteed getting loose structure of the compound [8].

Extrusion

The study was performed using a modified single screw extrusion-cooker type TS 45 (ZMCh Metalchem, PL) with L / D = 18 / 1, equipped with the additional cooling section of the barrel, and a die hole diameter of 3mm. Pellets (Fig. 1) were produced using the screw speed of 60, 80 and 100 rpm. The extrusion process parameters were determined in the temperature range of 60 - 110 ° C and maintained appropriately adjusting the intensity of the flow of cooling liquid. The processing temperature was measured by thermocouples installed along the barrel; the results were recorded. The screw speed was monitored using the electronic tachometer DM-223AR Wireless [8, 16, 17, 18].

Fig. 1. TPS pellets containing 30% of the cellulose fibers and the flax fibers.

The performance testing was conducted by setting the weight of TPS pellets obtained at a given time for all the mixtures of raw materials used processed at the assumed parameters (see formula 1). The measurement was made in six repetitions for each series of tests, their average value was taken as the final result [14, 15].

$$Q = \frac{m}{t} \; [kg \cdot h^{-1}] \tag{1}$$

where: Q – the performance,
m – the mass of the extrudates obtained during the measurement [kg]

t - measurement time [h].

The Power measurement was performed using a standard wattmeter connected to the power unit of the extruder. After considering the type of the motor installed in the extruder Shraga TS - 45, appointing the load and resulting in the individual samples, the yield values obtained were converted to the specific mechanical energy index (SME), according to the formula given by Ryu [5, 6, 7, 9, 13]:

$$SME = \frac{N \cdot O \cdot P}{N_m \cdot 100 \cdot Q} \ [kWhkg^{-1}] \quad (2)$$

where: N – the screw speed [min^{-1}],
Nm - the maximum screw speed [min^{-1}],
P - power [kW],
O - motor load [%],
Q - output of the extruder [kgh^{-1}].

RESULTS

The performance of the extrusion process was directly proportional to the screw speed, the higher the turnover, the higher yield was obtained. Increasing the cellulose fiber content in the formulations influenced the decline of the process efficiency. The highest yield of 31.8 $kg \cdot h^{-1}$ was determined during the extrusion of pure TPS pellets (without the fillers addition) at the highest screw speed of 100 rpm. Other samples showed a significant impact of the screw rpm on the performance of the extrusion process, regardless of the amount of the additive.

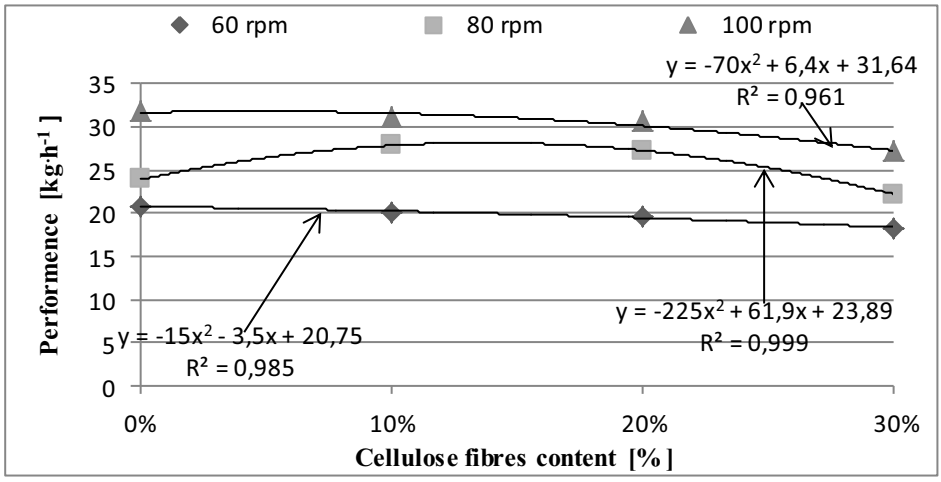

Fig. 2. Effect of cellulose fibers content and the screw speed on the efficiency of the extrusion of TPS pellets.

The lowest yield of 18.3 $kg \cdot h^{-1}$ was observed for the blend containing 30% of the cellulose fibers, processed at a 60 rpm screw speed. A similar trend was observed for the use of a filler in the

form of the flax fibers. The efficiency of the process decreased with the increasing of fiber content in the mixture. The lowest yield of 11.64 $kg \cdot h^{-1}$ was registered with the content of 30% flax fibers, processed at 100 rpm of the screw.

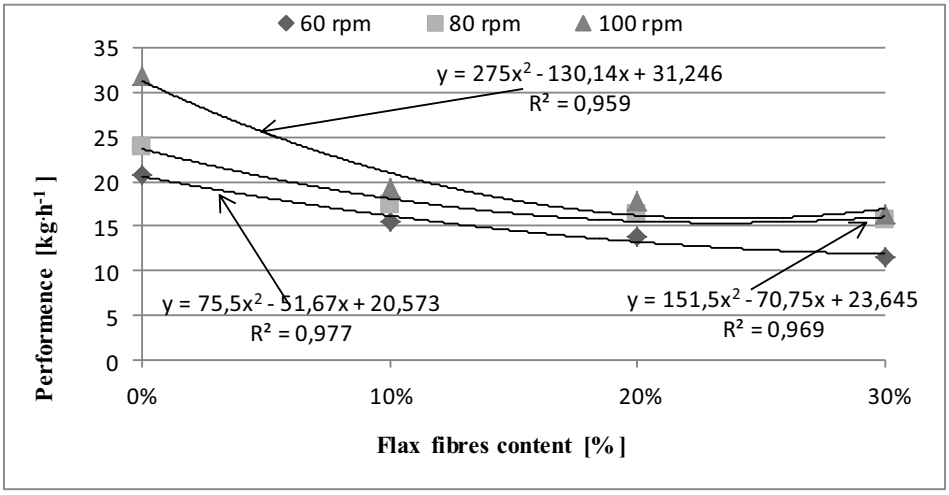

Fig. 3. Effect of flax fibers content and the screw speed on the efficiency of the extrusion of TPS pellets.

Addition of the ground bark in all kinds of mixtures resulted in a slight decrease in the efficiency of the extrusion process. Differences between the trial samples were small and amounted to little more than a 1,0 $kg \cdot h^{-1}$.

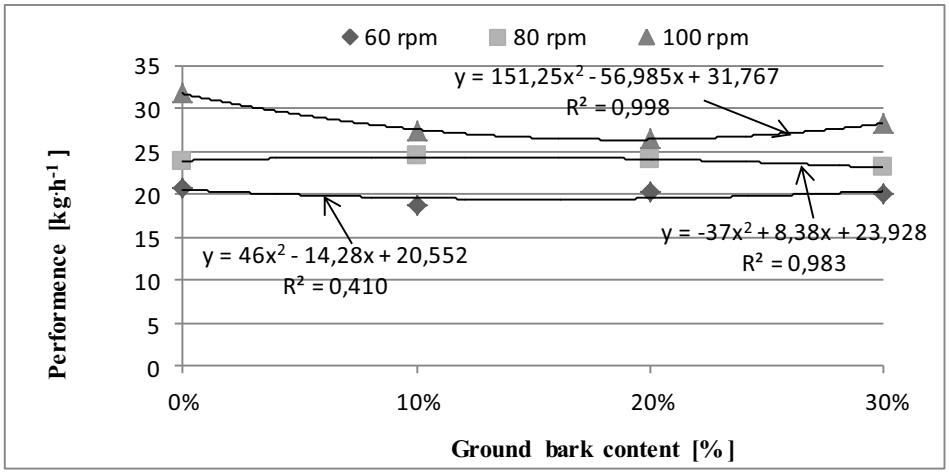

Fig. 4. Effect of ground bark content and the screw speed on the efficiency of the extrusion of TPS pellets.

The energy consumption during TPS processing depended on the screw speed used: SME value was higher with increasing of the rotation of the screw.

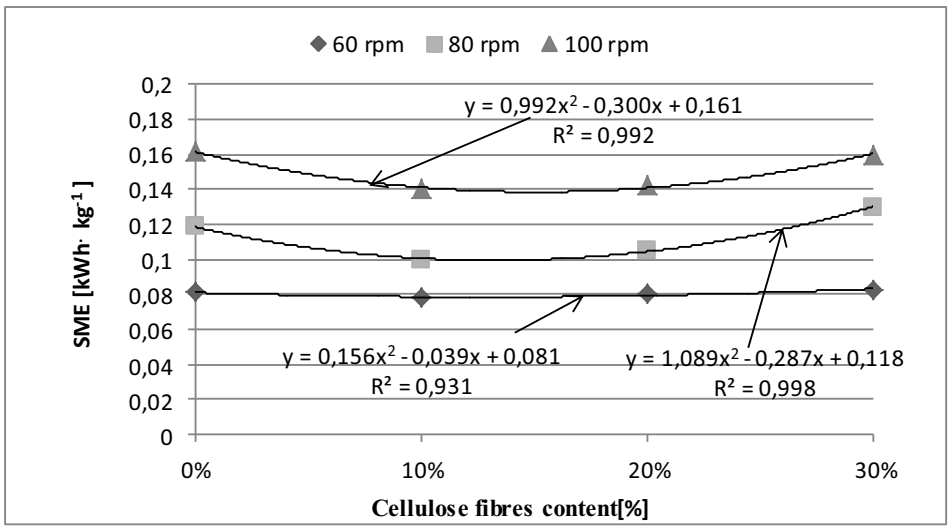

Fig. 5. Influence of cellulose fibers addition and the screw speed on SME.

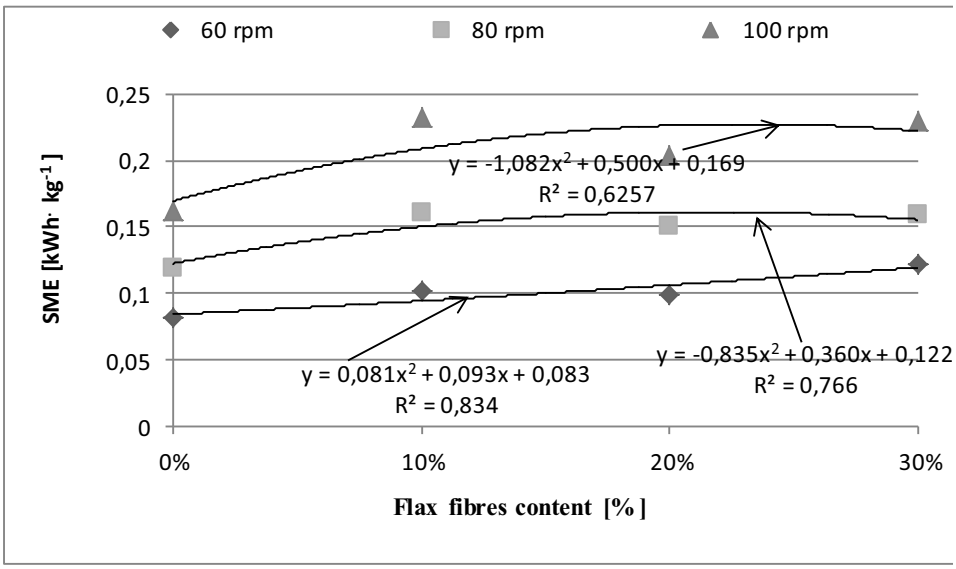

Fig. 6. Influence of flax fibers addition and the screw speed used on SME

SME was similar during the production of biopolymers containing the ground bark and the cellulose fibers. Addition of these fillers had no significant impact on the energy consumption. A bit higher value of the SME was recorded during the production of TPS pellets containing the

flax fibers. This is due to the greater length of the flax fibers and hence higher resistance during the extrusion-cooking. The highest SME value of 0.23 kWhkg^{-1} was noticed for the sample containing 30% of the flax fibers, processed at 100 rpm of the screw.

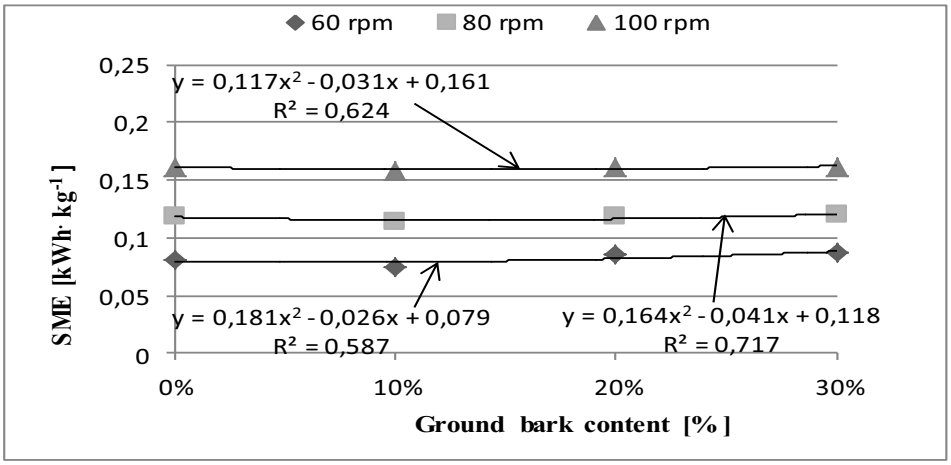

Fig. 7. Influence of ground bark addition and the screw speed on SME

CONCLUSIONS

- The performance of the extrusion-cooking of wheat thermoplastic starch was directly proportional to the screw speed applied; the higher screw rotation - the higher yield was obtained.
- Addition of the fillers affected the performance decrease and the SME increase during extrusion for all blends of raw materials used.
- The value of SME was at a similar level during extrusion of biopolymers containing cellulosic fibers and ground bark.
- The highest energy consumption of 0.23 kWh/kg was noticed in the production of the TPS pellets containing 30% of the flax fibers, processed at 100 rpm of the screw.

REFERENCES

Czerniawski B., Michniewicz J. 1998: *Opakowania Żywności.* Agro Food Technology, Czeladź.

Funke U., Bergthaller W., Lindhauer M.G. 1998: Processing and characterization of biodegradable products based on starch, *Polymer Degradation and Stability,* nr. 59, p. 293.

Janssen L.P.B.M., Mościcki L. 2006: Thermoplastic starch as packaging material, Acta Sci. Pol., Technica Agraria, 5(1).

Leszczyński W. 1999: Biodegradowalne tworzywa opakowaniowe, *Biotechnologia,* nr. 2, str. 50.

Mitrus M. 2005: Changes of specific mechanical energy during extrusion cooking of thermoplastic starch. TEKA Kom. Mot. Energ. Roln., 5, 152-157.

Mitrus M. 2006: Investigations of thermoplastic starch extrusion cooking process stability, TEKA Kom. Mot. Energ. Roln., 6A, 138-144.

Mościcki L., Mitrus M. 2001: Energochłonność procesu ekstruzji, Teka Komisji Motoryzacji i Energetyki Rolnictwa, 1, s. 186-194.
Oniszczuk T. 2006: Effect of parameters of injection moulding process on the structural properties of thermoplastic starch packaging materials, PhD Thesis, Department of Food Process Engineering, Lublin Agricultural University, Lublin.
Ryu G.H., Ng P.K.W. 2001: Effects of selected process parameters on expansion and mechanical properties of wheat flour and cornmeal extrudates, Starch, 53, 147-154.
Sikora T., Gimeza M. 2008: „Elementy towaroznawstwa", WSiP Warszawa, s. 102.
Suprakas S. R., Mosoto B. 2005: „Biodegradable polymers and their layered silicate nanocomposites: In greening the 21st century materials world", Canada Research Chair on Polymer Phisics and Nanomaterials, Chemical Engineering Department, Université Laval, Sainte-Foy, Que., Canada G1K 7P4.
Stasiek J. 2007: „Wytłaczanie Tworzyw Polimerowych, Zagadnienia wybrane", Wyd. Uczelniane Uniwersytetu Technologiczno – Przyrodniczego w Bydgoszczy, Bydgoszcz.
Wójtowicz A., Mitrus M. 2010: Effect of whole wheat flour moistening and extrusion-cooking screw speed on the SME process and expansion ratio of precooked pasta products, TEKA Kom. Mot. Energ. Roln., 10, 517-526.
Wójtowicz A. 2008: Influence of legumes addition on proceeding of extrusion-cooking process of precooked pasta, Teka Kom. Mot. Energ. Roln. – OL PAN, 8a, 209-216.
Wójtowicz A., Mościcki L. 2008: Energy consumption during extrusion-cooking of precooked pasta, Teka Kom. Mot. Energ. Roln. – OL PAN, 8, 311-318 (80:20).
Żakowska H. 1997: Materiały degradowane – alternatywa dla tradycyjnych opakowań z tworzyw sztucznych? (2). Przemysł farmaceutyczny i owocowo warzywny nr 12 str. 36-38.
Żakowska H. 2005: Recykling Odpadów Opakowaniowych wyd. Centralny Ośrodek Badawczo-Rozwojowy Opakowań, Warszawa.
Żakowska H. 2006: Światowy postęp w produkcji opakowań przydatny do kompostowania. OPAKOWANIE nr 2 str. 15-17.
Żakowska H. 2004: Ocena ekologiczna opakowań prowadzona w Cobro. Ważenie-Dozowanie-Pakowanie nr 4 str.28-30.
Żakowska H. 2003: Opakowania Biodegradowalne, wyd. COBRO Warszawa.

WPŁYW DODATKU WYPEŁNIACZY NA ENERGOCHŁONNOŚĆ EKSTRUZJI SKROBI PSZENNEJ

Streszczenie. W pracy przedstawiono rezultaty badań energochłonności procesu ekstruzji skrobi pszennej wzbogacanej dodatkami funkcjonalnymi. Określono wpływ dodatku wypełniaczy w postaci włókien lnianych, celulozowych oraz mielonej kory na wartość SME. W badaniach zastosowano zmodyfikowany ekstruder jednoślimakowy TS 45 o L/D=18 z dodatkowym chłodzeniem końcowej części cylindra urządzenia. Badano wpływ ilości oraz rodzaju stosowanego wypełniacza w mieszance zawierającej 20% gliceryny (plastyfikatora) oraz wpływ prędkości obrotowej ślimaka ekstrudera na wydajność oraz energochłonność procesu ekstruzji mieszanek skrobi termoplastycznej. Wraz ze wzrostem prędkości obrotowej ślimaka ekstrudera rosła energochłonność oraz wydajność procesu ekstruzji w przypadku wszystkich rodzajów zastosowanych mieszanek surowcowych.

Słowa kluczowe: skrobia termoplastyczna, wypełniacze, ekstruder, energochłonność

TEKA Kom. Mot. Energ. Roln. – OL PAN, 2011, 11, 252–260

PRODUCTION OF BIODEGRADABLE PACKAGING MATERIALS BY EXTRUSION-COOKING

Tomasz Oniszczuk, Leszek Moscicki

Department of Food Process Engineering, University of Life Sciences in Lublin
Doświadczalna 44, 20-236 Lublin, Poland
E-mail: tomasz.oniszczuk @ up.lublin.pl

Summary. This paper presents the results of the extrusion-cooking of the thermoplastic corn starch with fillers in the form of flax fibers, cellulose, and ground bark, using the modified single screw extrusion-cooker TS 45 (Polish design) with L / D = 18 and an additional cooling section of the barrel. The influence of the screw speed, the quantity and type of the filler used in the blends containing 20% of glycerol (plasticizer) on the performance and energy consumption of the extrusion process of thermoplastic starch (TPS) is discussed.

Key words: extrusion-cooking, biopolymers, thermoplastic starch, the extrusion-cooker.

INTRODUCTION

Along with economic development and progress of civilization throughout the world, the production of various plastics increases. Nowadays consumers are becoming increasingly sophisticated regarding the quality of products, their appearance and the quality of the packaging. Only a portion of packaging used is recycled, due to high costs and relatively low level of selective collection. The growing amount of the waste deposits is a big burden to the environment. Most of this waste is resistant to degradation, because polymers take a very long time to be decomposed in the environment [1, 4, 10, 18]. The growing awareness of eco-friendly societies and even the fashion for ecology have contributed to the development of research on the so-called biodegradable plastics. Particular attention was paid to the research group of natural materials - biopolymers produced from starch. The biopolymer is obtained after mixing the starch with a plasticizer (glycerol often), to enable the disposal of the material at a temperature lower than the decomposition temperature of starch. This form is called thermoplastic starch (TPS) [13,14,19,20], which may be complementary to alternative plastics. Unfortunately, the products made from TPS do not have wide application because of the utility of certain defects. In order to improve the physical properties of biopolymers and sometimes reduce the price of the finished product, natural fibers can be added in amount from 1 to even 50%, dependently of the fillers used in the mixture. The most commonly used fillers are: flax, hemp, jute, coir, cotton, and the waste from wood industry. The large-scale studies aiming at the increasing of the share of TPS in the production of packaging materials have been undertaken in recent years. Nowadays, a substantial growth of biodegradable materials application is noticed during the produc-

tion of various products. These products are more and more present in our houses, and manufacturers are constantly looking for newer and better technologies for their production. In addition, the fact that they can be fully degradable solves a problem for the storage of used packaging. When properly treated, they can be composted and used for agricultural or horticultural purposes. In the anaerobic process they can produce the methane gas, further used for heating or as a propellant [2,3,5,11].

MATERIALS AND METHODS

The study was performed using the single screw extrusion-cooker TS-45 (Polish design), equipped with an additional cooling system of the barrel, L / D = 18 / 1, the die of 3mm diameter, and a screw rotation 60, 80, 100 rpm (Fig. 1). Extrusion-cooking process temperature ranged from 60 till 110°C, which was determined by appropriately adjusting the intensity of the flow of cooling. The electronic tachometer DM-223AR Wireless was used to measure the screw speed; the processing temperature was measured by thermocouples installed in the barrel of the extruder, registered on the control panel.

The main component was corn starch, mixed with the glycerol (the plasticizer) and fillers in the form of: cellulose fibers, flax and ground bark, added to improve the quality of the TPS. A technical glycerol of 99% purity was added to all the prepared blends in the quantity of 20% in contrary to the fillers, which were added selectively with 0, 10, 20, and 30% content of the whole mixture weigh. The blends were mixed for 20 minutes in a laboratory ribbon blender until a homogeneous mass. After mixing, the samples were stored in sealed plastic bags for 24 hours in order to increase the penetration of the glycerol in the starch grains. Immediately prior to extrusion, the blends were again mixed for 10 minutes, which ensured obtaining a uniform and powdery mixtures fed into the extruder.

Fig. 1. Modified single screw extrusion-cooker TS-45, equipped with electric heaters and air-water cooling system of the barrel.

The performance of the extrusion-cooking was conducted by setting the weight of extrudates obtained at a given time for all the mixtures of raw materials used, processed at the assumed parameters. The performance measurement was made using an electronic timer and the WPS 210

weight in six repetitions for each series of the tests. The performance was determined by the following formula [15,16,17]:

$$Q = \frac{m}{t}\left[kg \cdot h^{-1}\right] \tag{1}$$

where:
Q - performance,
m - mass of the extrudate obtained during the measurement [kg]
t - measurement time [h].

The energy consumption measurement was performed using a standard Wattmeter connected with the power unit of the extruder. After considering the type of the Shraga motor installed in the extruder, appointing the load and resulting in the individual samples, the yield values obtained were converted to specific mechanical energy (SME), accordingly to the formula given by Ryu [6,7,8,9,12]:

$$SME = \frac{N \cdot O \cdot P}{N_m \cdot 100 \cdot Q}[kWh \bullet kg^{-1}] \tag{2}$$

where:
N – the screw speed [min^{-1}],
Nm - the maximum screw speed [min^{-1}],
P - Power [kW],
O – the motor load [%],
Q – the output of the extruder [$kg \bullet h^{-1}$].

RESULTS

During tests the significant effects of the screw speed on the efficiency of the extrusion-cooking process were observed. The performance of the extrusion process was directly proportional to the screw speed: the higher rotational speed - the higher yield was obtained. Increasing the cellulose fiber addition in the formulations influenced the decline in raw material efficiency of the extrusion process.

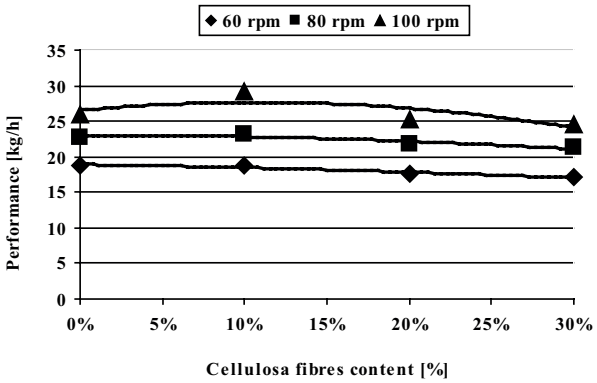

Fig. 2. The effect of the cellulose fiber's content and the screw speed on the performance of the extrusion process.

Tabl. 1. Evaluation of the results presented in Fig. 2.

Skrew rpm	Regression equations	R^2
60	$y = -4x^2 - 4,12x + 18,968$	0,81
80	$y = 75,25x^2 - 19,205x + 23,15$	0,55
100	$y = -44x^2 + 17,88x + 26,218$	0,74

The lowest yield of 17.5 $kg \cdot h^{-1}$was obtained during extrusion of the samples containing 30% of cellulose fibers, processed at the lowest screw speed (60 rpm). The increase of the screw speed resulted in a slight increase efficiency of the extrusion process, despite the growing number of cellulose fibers in the blend.

Addition of flax fibers resulted in the decline in the productivity during the extrusion process used for all blends. This was due to the greater fiber length, and the lower degree of mixing of the sample. During the processing problems appeared with the dosing of the mixture - the material blocked the inlet easily. The lowest yield of 11.28 $kg \cdot h^{-1}$was obtained during the TPS extrusion, using the additive of 30% flax fibers, processed at the lowest screw speed of 60 rpm. Increasing the fiber content in the mixture of raw flax did not have any major impact on the performance of the extrusion process. Differences between trials were minor.

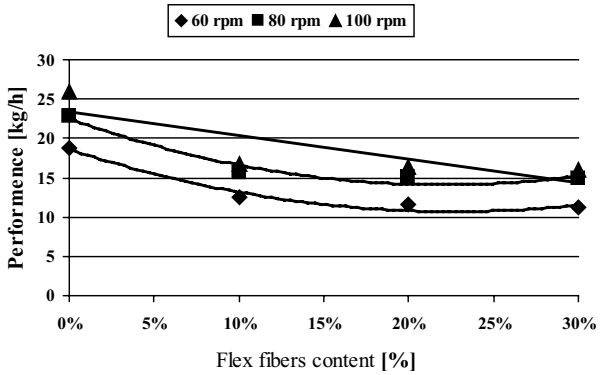

Fig. 3. The effect of the flax fiber's addition and the screw speed on the performance of the extrusion process.

Tabl. 2. Evaluation of the results presented in Fig. 3.

Skrew rpm	Regression equations	R^2
60	$y = 154x^2 - 69,8x + 18,6$	0,97
80	$y = 173x^2 - 76,22x + 22,493$	0,95
100	$y = -30,24x^2 + 23,376$	0,66

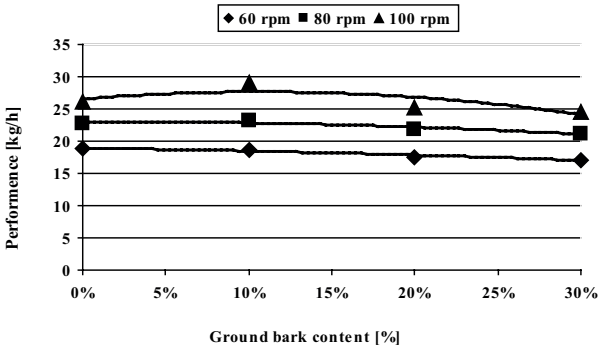

Fig. 4. The effect of the ground bark's addition and the screw speed on the performance of the extrusion process.

Tabl. 3. Evaluation of the results presented in Fig. 4.

Screw rpm	Regression equations	R^2
60	$y = -9{,}25x^2 - 3{,}535x + 18{,}922$	0,94
80	$y = -24{,}75x^2 + 1{,}115x + 22{,}962$	0,82
100	$y = -96x^2 + 20{,}64x + 26{,}544$	0,58

Similar trend was observed in the case of the blends containing 10% of the filler (ground bark and cellulose fibers). The productivity of the extrusion was bigger when fewer fillers were present. The highest yield of 29.16 $kg \cdot h^{-1}$was obtained for blends containing 10% of the ground bark at top screw speed; the lowest yield of 17.1 $kg \cdot h^{-1}$was achieved with the participation of 30% in the mixture, processed at the lowest speed of 60 rpm.

When using the extrusion-cooking technology for processing of TPS, one of the most important factor is to determine the specific mechanical energy (SME) required to obtain the unit mass of the product.

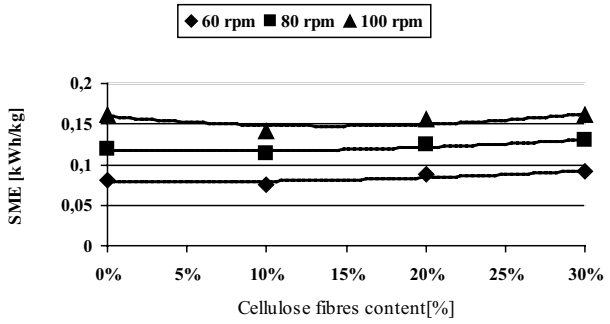

Fig. 5. Influence of the cellulose fiber's content in the mixture and the screw speed on SME

Tabl. 4. Evaluation of the results presented in Fig. 5.

Skrew rpm	Regression equations	R^2
60	$y = 0{,}221x^2 - 0{,}024x + 0{,}079$	0,73
80	$y = 0{,}248x^2 - 0{,}03x + 0{,}117$	0,82
100	$y = 0{,}598x^2 - 0{,}167x + 0{,}159$	0,57

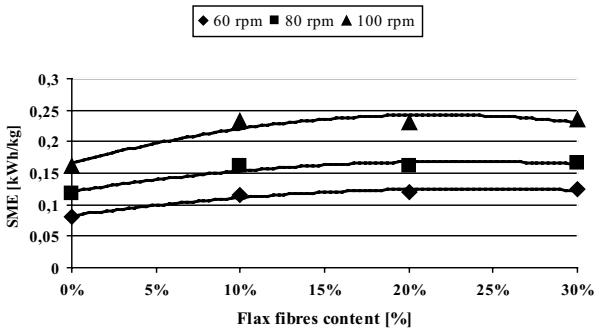

Fig. 6. Effect of the flax fiber content in the mixture and the screw speed on SME

Tabl. 5. Evaluation of the results presented in fig. 6.

Skrew rpm	Regression equations	R^2
60 obr·min^{-1}	$y = -0{,}741x^2 + 0{,}355x + 0{,}083$	0,94
80 obr·min^{-1}	$y = -0{,}899x^2 + 0{,}413x + 0{,}1211$	0,91
100 obr·min^{-1}	$y = -1{,}662x^2 + 0{,}714x + 0{,}1659$	0,90

During the extrusion process of the thermoplastic corn starch it was noticed that the energy consumption was growing with the increasing of the screw speed. The highest SME was recorded during the production of TPS pellets containing the flax fibers. This is due to greater length of the flax fibers and hence higher resistance during baro-thermal treatment, however its amount did not significantly affec the final value of the SME. The lowest value of the SME was measured during the extrusion of the samples without addition of the flax fibers (0.08 kWh•kg^{-1}), and the highest of 0.23 kWh•kg^{-1}for the sample containing 30% of the flax fibers processed at 100 rpm of the screw.

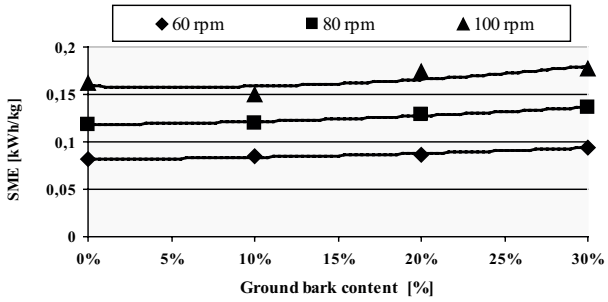

Fig. 7. Influence of the ground bark content and the screw speed on SME.

Tabl. 6. Evaluation of the results presented in Fig. 7.

Skrew rpm	Regression equations	R^2
60	$y = 0{,}094x^2 + 0{,}012x + 0{,}081$	0,98
80	$y = 0{,}148x^2 + 0{,}017x + 0{,}118$	0,98
100	$y = 0{,}362x^2 - 0{,}037x + 0{,}158$	0,62

SME measurement during the production of TPS containing cellulosic fibers and ground bark showed similar tendency. The value of SME during processing of the blends containing the ground bark was higher by 0.02 $kWh \bullet kg^{-1}$ than the blends with similar addition level of the cellulose fibers. The highest value of SME of 0.15 $kWh \bullet kg^{-1}$ was recorded during the extrusion of the samples containing cellulose fibers at 80 and 100 rpm of the screw.

CONCLUSIONS

Based on the obtained results the following conclusions can be made:

- The performance of the extrusion-cooking process was directly proportional to the screw speed; the higher rotational speed resulted in the higher capacity of the process.
- Addition of the flax fibers caused a decrease in the process efficiency for all the mixtures of raw materials used.
- 10% addition of the cellulose fiber, and the ground bark in the compound increased the efficiency of the extrusion process, while higher amount of the fillers to the level of 20 and 30% resulted in its decline.
- During the extrusion-cooking of TPS containing cellulosic fibers and ground bark the value of SME was at a similar level.
- The highest energy consumption was noticed in the production of TPS blends containing the flax fibers. That happened due to the length of the fibers and residence occurring during the processing.

REFERENCES

Czerniawski B., Michniewicz J. 1998: *Opakowania Żywności.* Agro Food Technology, Czeladź.

Fritz J., Link U., Braun R. 2001: Environmental impacts of biobased/biodegradable packaging, *Starch,* nr. 53, p. 105.

Gruin I.2003: „Materiały polimerowe", Wydawnictwo Naukowe PWN, Warszawa.

Janssen L.P.B.M., Mościcki L. 2006: Thermoplastic starch as packaging material, Acta Sci. Pol., Technica Agraria, 5(1).

Leszczyński W. 2001: Materiały opakowaniowe z polimerów biodegradowalnych, *Przemysł Spożywczy,* nr 8, str.81.

Mitrus M. 2005: Changes of specific mechanical energy during extrusion cooking of thermoplastic starch. TEKA Kom. Mot. Energ. Roln., 5, 152-157.

Mitrus M. 2006: Investigations of thermoplastic starch extrusion cooking process stability, TEKA Kom. Mot. Energ. Roln., 6A, 138-144.

Mościcki L., Mitrus M. 2001: Energochłonność procesu ekstruzji, Teka Komisji Motoryzacji i Energetyki Rolnictwa, 1, s. 186-194.

Mościcki L., Mitrus M. 2001: Przepływ energii cieplnej w ekstruderze dwuślimakowym, Teka Komisji Motoryzacji i Energetyki Rolnictwa, 1, s. 195-208.

Oniszczuk T. 2006: Effect of parameters of injection moulding process on the structural properties of thermoplastic starch packaging materials, PhD Thesis, Department of Food Process Engineering, Lublin Agricultural University, Lublin.

Oniszczuk T. 2008: „Zastosowanie Włókien Naturalnych w Produkcji Biodegradowalnych Materiałów Opakowaniowych. W: Metody fizyczne diagnostyki surowców roślinnych i produktów spożywczych. Red. B. Dobrzański jc., Wyd. Nauk. Fundacji Rozwoju Nauk Agrofizycznych, Lublin: s. 171 – 180.

Ryu G.H., Ng P.K.W. 2001: Effects of selected process parameters on expansion and mechanical properties of wheat flour and cornmeal extrudates, Starch, 53, 147-154.

Sikora T., Gimeza M. 2008: „Elementy towaroznawstwa", WSiP Warszawa, s. 102.

Suprakas S. R., Mosoto B. 2005: „Biodegradable polymers and their layered silicate nanocomposites: In greening the 21st century materials world", Canada Research Chair on Polymer Phisics and Nanomaterials, Chemical Engineering Department, Université Laval, Sainte-Foy, Que., Canada G1K 7P4.

Wójtowicz A., Mitrus M. 2010: Effect of whole wheat flour moistening and extrusion-cooking screw speed on the SME process and expansion ratio of precooked pasta products, TEKA Kom. Mot. Energ. Roln., 10, 517-526.

Wójtowicz A., 2008: Influence of legumes addition on proceeding of extrusion-cooking process of precooked pasta, Teka Kom. Mot. Energ. Roln. – OL PAN, 8a, 209-216.

Wójtowicz A., Mościcki L. 2008: Energy consumption during extrusion-cooking of precooked pasta, Teka Kom. Mot. Energ. Roln. – OL PAN, 8, 311-318 (80:20).

Żakowska H. 2005: Recykling Odpadów Opakowaniowych wyd. Centralny Ośrodek Badawczo-Rozwojowy Opakowań, Warszawa.

Żakowska H. 2004: Ocena ekologiczna opakowań prowadzona w Cobro. Ważenie-Dozowanie-Pakowanie nr. 4 str.28-30.

Żakowska H. 2003: Opakowania Biodegradowalne, wyd. COBRO Warszawa.

PRODUKCJA BIODEGRADOWLNYCH MATERIAŁÓW OPAKOWANIOWYCH METODĄ EKSTRUZJI

Streszczenie. W pracy przedstawiono rezultaty badań wpływu dodatku wypełniaczy w postaci włókien lnianych, celulozowych oraz mielonej kory na proces ekstruzji skrobi kukurydzianej. W badaniach zastosowano zmody-

fikowany ekstruder jednoślimakowy TS 45 o L/D=18 z dodatkowym chłodzeniem końcowej części cylindra urządzenia. Badano wpływ prędkości obrotowej ślimaka ekstrudera, ilości oraz rodzaju stosowanego wypełniacza w mieszance zawierającej 20% gliceryny (plastyfikatora) na wydajność oraz energochłonność procesu ekstruzji mieszanek skrobi termoplastycznej.

Słowa kluczowe: ekstruzjia, biopolimery, skrobia termoplastyczna, ekstruder.

TEKA Kom. Mot. Energ. Roln. – OL PAN, 2011, 11, 261–266

INFLUENCE OF FORCED COOLING OF THE FRICTIONAL ELEMENTS OF THE DISK BRAKE ON THE BRAKING EFFICIENCY

Yuriy I. Osenin*, Igor Sosnov*, Oksana Sergienko*, Iryna Biloborodova*

*Volodymyr Dahl East-Ukrainian National University, Lugansk, Ukraine

Summary. The article presents the results of experimental research of influence of forced liquid-air cooling of frictional elements of the disk brake on efficiency of mechanical braking. That was evaluated by the experimental estimation of the friction coefficient and integral mean temperature of interacting surfaces under different modes of operation of the cooling system and mechanical braking.

Key words: braking efficiency, cooling of the frictional contact zone, disk brake, system of liquid-air cooling.

INTRODUCTION

The operation efficiency of the frictional brake systems of the rolling stock is the main factor of safety motion, on the reliability of which a number of emergency situations on railway depends. The increase of the speed motion of the trains suggests new, stricter requirements to the operation characteristics of frictional brakes, namely, disk brakes. The main obstacle in the increase of effectiveness of the disk brake is known to be the temperature which is generated in the contact zone of the block and disk while braking [2, 6, 7]. In connection with this, forced heat energy rejection which is generated while interacting with brake elements is one of the ways of increasing effectiveness in the use of mechanical braking devices [3].

The paper presents the results of experimental research on the effectiveness of the forced heat energy system from the area of contact of frictional elements of the disk brake in the rolling stock.

EXPERIMENTAL UNIT

Experimental research of the braking process was made with the help of the laboratory stand which was worked out by the department of hoisting-and-conveying machinery of the Volodymyr Dahl East-Ukrainian National University [9]. The stand is intended for testing different designs of brake devices and checking their outlet parameters. The diagram of the experimental unit is shown in Fig. 1.

The stand gives the possibility to accumulate kinetic energy with the help of rotating disks, to fix the rotation frequency, the number of switches and the durability of the drive operation as well

as to register the following outlet parameters of the brake and the drive: the braking moment, force thrust, the time of disconnection of the brake and the drive acceleration, the time of switching and braking, the temperature of interacting surfaces, the turning angle of brake posts.

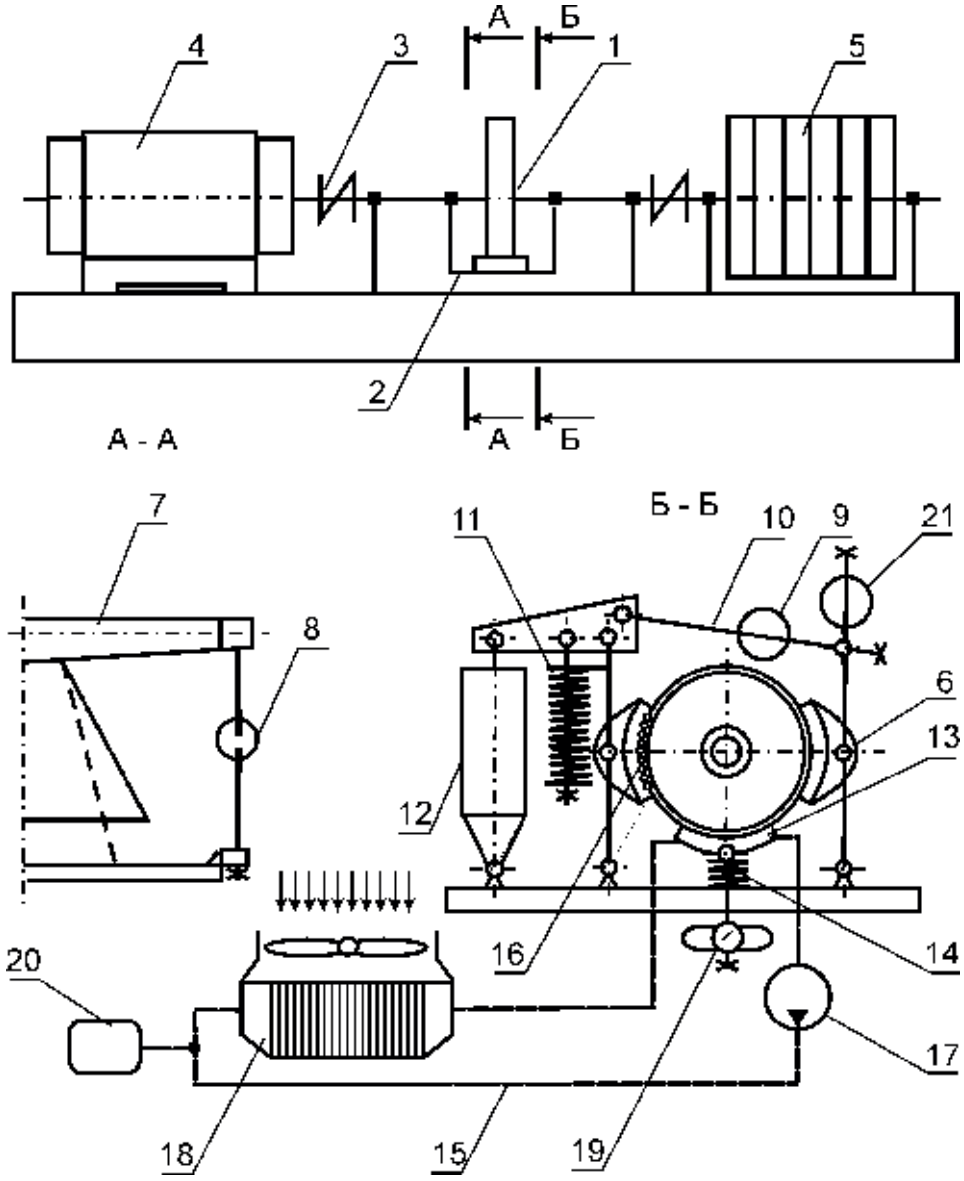

Fig. 1. Principle diagram of the experimental stand

The stand works in the following way. The brake 1 is set up on the flexible frame 2 with the help of the elastic coupling 3. The engine shaft 4 is connected with rotating mass 5 which consists

of the disks and allows for changing the moment of inertia from 8 to 60 kg·m^2 due to the attachment of the disks of flywheel mass to the shaft or disconnection from it. The frame 2 and rotating mass 5 are carried by the rolling bearings which are fastened on the posts.

A closed two-shoe brake constitutes the base of the stand ТКТГ-200. The brake locking takes place due to the forces of the compressed spring. The breaking is accomplished by an electrohydraulic pusher ТГМ-25 (corresponding positions 11 and 12 in Fig. 1).

The brake moment (the friction coefficient is defined by its value) was measured with the help of dynamometrical rings 8 (Fig. 1, А-А), which are symmetrically placed on both sides of the brake, on which the resistance strain gauges were stuck with glue. Dynamometrical rings are connected with the bed base and a rocker 7 of the flexible frame 2.

Traction force that is proportional to the pressing force of the blocks to the brake pulley was measured with the help of the transducer 9. It was made in the form of dynamometrical ring with bonded strain gauges and set up on the brake traction 10 (Fig. 1, Б-Б). Thoriation of the dynamometrical rings took place each time before the experiments and after them.

Mesh force of the frictional material of the brake blocks and brake pulley was measured by the strain gauge 21 set up on the axis of the block rotation of the brake device with self-acceleration.

The temperature of the friction surfaces was measured by seven thermocouples set up in the body of the brake block along its vertical axis.

To fulfill this task it was necessary to make the following changes in the design of the stand: a heat-remover 13 was set up, it presents the vessel whose dimensions are stipulated by the calculated quantity of heat which is to be taken from the working zone. The vessel joins the heat exchanger 18 with the help of the pipe-lines 15, the circulation of the cooling liquid was controlled by the hydraulic pump 17. A cooling locomotive section 2ТЕ116 was used as a heat-exchanger (effective area of heat-exchange makes $\approx$ 52 m^2) and it was cooled with the help of the axis fan ВОК – 4,0. The pressing of the heat-remover to the frictional disk (in this case to the brake pulley with the diameter of 200 mm) was realized by the spring 14 and checked by the dynamometer 19. A surge tank 20 was used for the compensation of the cooling liquid. A more detailed description of the cooling system and its functioning is given in the works [4, 5, 8].

The influence of the cooling system on the effectiveness of braking was evaluated by experimental determination of the friction coefficient and the temperature in the contact zone of the brake working elements under its different operation modes.

RESULTS OF EXPERIMENTAL RESEARCH

The data obtained in the process of experiments dealing with estimation of the friction coefficient between frictional surfaces of the brake block and pulley and integral mean temperature of the given surfaces are given in Fig. 2 and 3. In Fig. 2 the coefficient changes of friction-slip in the process of braking are shown (t – the time in the process of braking), Fig. 3 shows mean-volume temperatures contacting in the process of braking of frictional surfaces. Experimental values of the received quantities are marked in separate points and the theoretical values obtained in accordance with the calculation procedure are marked in full line. The procedure is worked out by the authors [5].

All the experimental values are tested with the help of Styudent criteria [1].

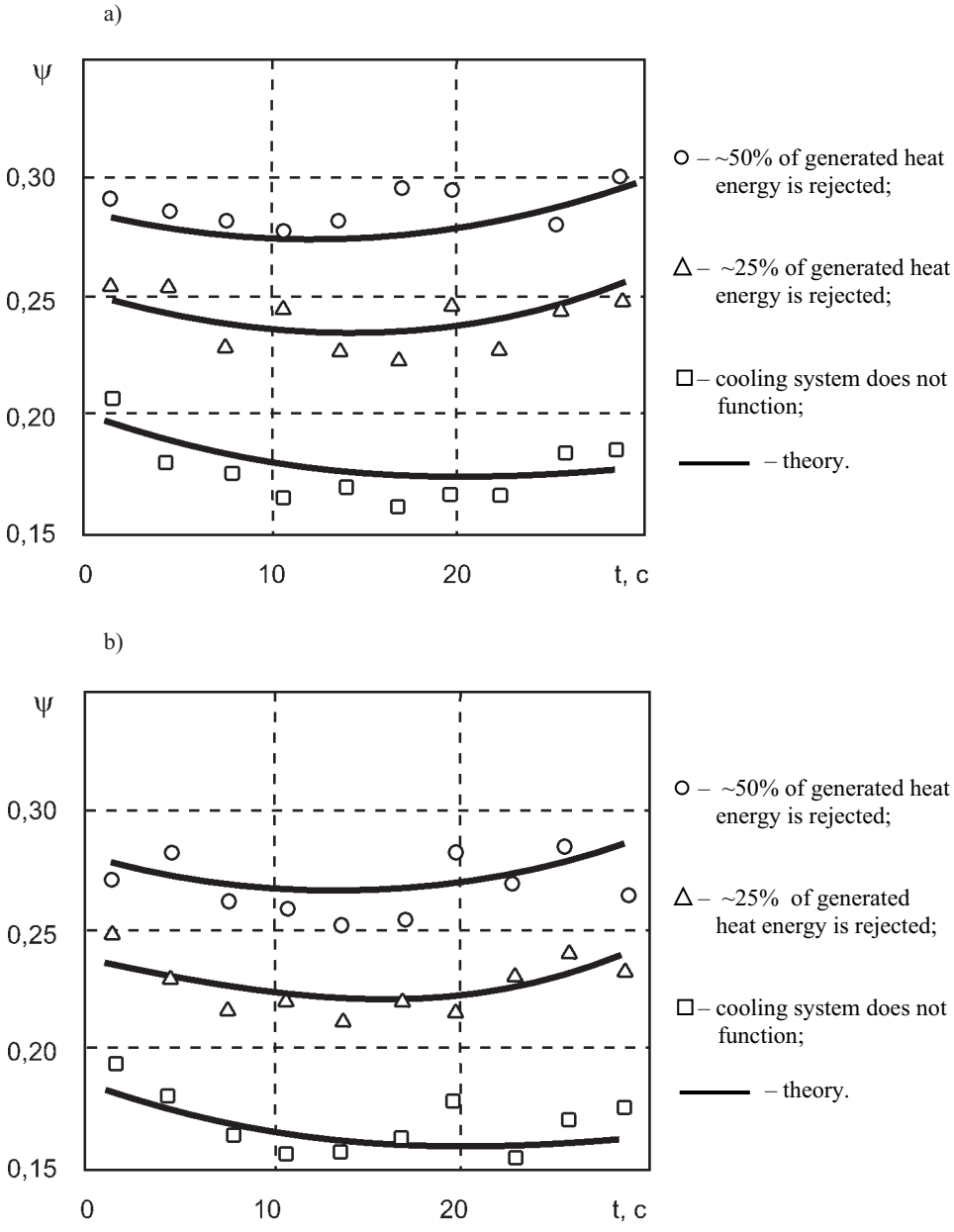

Fig. 2. Friction coefficient of frictional interacting surfaces in the process of braking; the pressing force of one brake block makes:
(a) – 1500 N; (b) – 1000 N

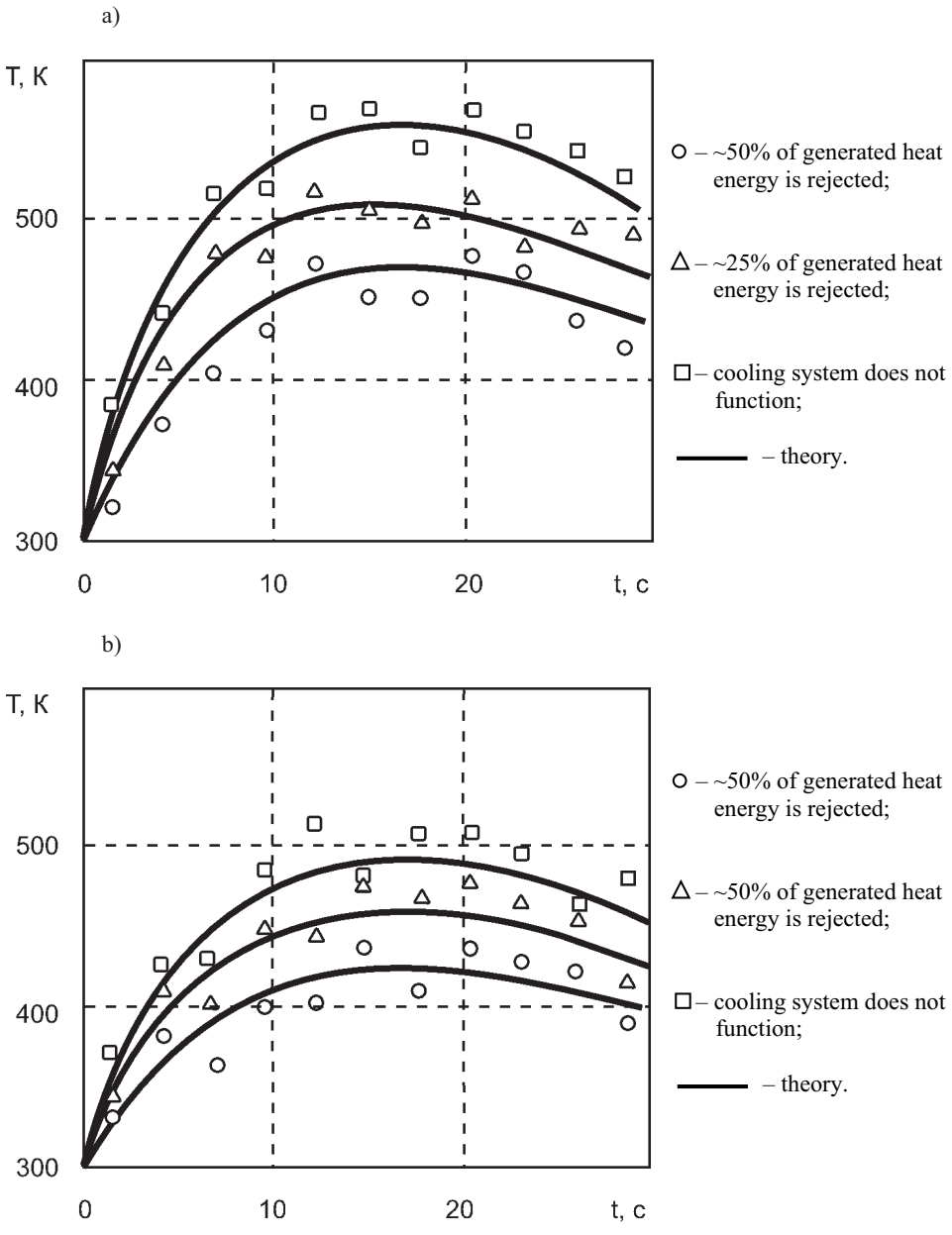

Fig. 3. Average temperature of frictional interacting surfaces in the process of braking; the pressing force of one brake block makes:
(a) – 1500 N; (b) – 1000 N

CONCLUSION

The analysis of experimental data gives the possibility to make conclusion of positive influence of the offered method of active cooling of the frictional brake on the effectiveness of braking.

The friction coefficient while using forced liquid-air cooling is about 30% higher than without its use (in the case of rejecting about 50% generated heat and pressing force of the brake block of 1500 N). Mean temperature of interacting surfaces is lower by 15% in the comparison with the case when the cooling system is absent.

REFERENCES

Adler Yu.P., Markova E.V., Granovsky Yu.V., 1976. Experiment planning in the process of optimal condition look up. M.: Science. – 255 p.

Asadchenko V.R., 2006. Automatic brakes of the rolling stock: Training appliances for higher schools of the railway transport. – M.: Route. – 392 p.

Biloborodova I.M., Osenin Yu.I., Sosnov I.I., 2009. Evaluation of main heat engineering parameters of the cooling system of the locomotive disk brake // Collection of works of the Dnepropetrovsk national university of railway transport named after V. Lazaryan, №28. – P. 7 – 12.

Biloborodova I.M., Osenin Yu.I., Sosnov I.I., 2009. Cooling system of the disk brake of transport. Patent application № 48518 dated 20.08.2009.

Biloborodova I.M., Osenin Yu.I., Sosnov I.I., 2010. Modelling of the cooling system of the locomotive disk brake. // Collection of works of the Volodymyr Dahl East-Ukrainian National University, Lugansk, №3 (145). – P.292 – 306.

Inozemtsev V.G., 1987. Brakes of the rolling stock. Questions and replies. 3-edition. – M.: Transport. – 207 p.

Parkhomov V.T., 1994. Design and brake operation. – M.: Transport. – 208 p.

Sosnov I., Sergienko O., Biloborodova I. On contact thermal resistance in the system of active effective cooling of the locomotive disk brake. // TEKA Commission of Motorization and Power Industry in Agriculture. – Liblin, Polska Akademia nauk Oddzial w Lubline, 2010. – Vol. XB. – P. 362 – 370.

Starchenko V.N., Shevchenko S.I., 2006. Measuring system for diagnostics and testing of brake devices of the transport. // Collection of works of the Volodymyr Dahl East-Ukrainian National University, Lugansk, №7 (101). – P.193 – 196.

ЭКСПЕРИМЕНТАЛЬНОЕ ИССЛЕДОВАНИЕ ВЛИЯНИЯ ПРИНУДИТЕЛЬНОГО ОХЛАЖДЕНИЯ ФРИКЦИОННЫХ ЭЛЕМЕНТОВ ДИСКОВОГО ТОРМОЗА НА ЭФФЕКТИВНОСТЬ ТОРМОЖЕНИЯ

Аннотация. В работе представлены результаты экспериментальных исследований влияния принудительного жидкостно-воздушного охлаждения фрикционных элементов дискового тормоза на эффективность механического торможения, что оценивалось путем экспериментального определения коэффициента трения и среднеинтегральной температуры взаимодействующих поверхностей при различных режимах работы системы охлаждения и механического торможения.

Ключевые слова: эффективность торможения, охлаждение зоны фрикционного контакта, дисковый тормоз, система жидкостно-воздушного охлаждения.

TEKA Kom. Mot. Energ. Roln. – OL PAN, 2011, 11, 267–273

PARAMETERS OF MODE AND CHARACTERISTICS OF THE PROCESS OF BROAD LAYERED FACING OF THE CYLINDRICAL PARTS WITH THE HELP OF SELF-PROTECTIVE DUST

A.Pakholyuk *, V.Skulskyi, I.Hordyi

Assistant Professor, Candidate of Engineering Sciences, Department of Engineering of the Lviv National Agrarian University

Summary. The aim of the given research was to establish the influence of regime parameters on the melting and facing productivity and the loss of the melted metal. It is established that sufficient uniformity of the facing metal thickness and productivity 5.8 kg/h can be obtained at the current of 400A and under condition of the electrode offset from zenith 9-11 mm. Under such conditions 12-18% of the melted metal will be flowing from the facing surface in the form of separate drops.

Key words: facing, a broad layer of the metal, shaft, dust, parameters of mode.

INTRODUCTION

The fastest-degradable parts of farm technology have a cylindrical shape and work under conditions of abrasive and other types of degradation. The area of degraded surfaces (shaft neck, surfaces for bearings etc) does not exceed 10-15% of general part area surface. Deletion of such parts involves a lot of costs invested into working metal and non-degraded surfaces are being wasted.

One of the ways of proceeding with parts resources is their renewal. The special trait of this process is that there is a need to provide the ability of renewable part to work with minimum expenses and with the minimum damage of work surfaces.

The most widely used way of renewing is facing [7, 8, 16, 18]. High properties of the metal facing can be obtained with the help of alloying [2, 12]. The effective way of introduction of alloying elements under electric bow facing is including the dusts of the alloying element into the structure of the dust wire charge or dust tape.

A wide application in farm machine building and repair industry defines the facing as the self-protective dust wire [1, 17]. It looks like an extensive tape made of light steel with the core in the form of dust mixture of alloying metals, ferro-alloys, carbides and dusts of gas and slag making substances. Such material for facing has a lot of advantages comparing with a solid wire [1, 2]. These advantages consist in an easy change of chemical structure and in the lack of protective gas or flux or mechanisms for its creation as well as in the possibility to get a great range of built up materials.

Facing a broad layered metal with a solid electrode wire of a little diameter under flux layer is obtained by transferring the electrode along cylindrical surface along the screw line or separate circular cylinders [9, 14]. To obtain a given width of the layer it is necessary to remelt metal of the previous cylinder in 50-70%, and the thermal cycle of the first and the last cylinder differ a lot [15]. So, the uniformity of chemical structure of the built-up layer and its mechanical properties appear.

The application of multi-electrode facing [3, 4] greatly complicates the process and equipment and does not guarantee the necessary quality.

Self-protective dust wire under condition of absence of additional mechanisms for flux or gas supply allows an electrode to move in an oscillating way, perpendicularly to the vector of facing speed at the width of built-up layer. This technology in comparison with the screw line facing is characterized by the high productivity of facing and uniformity of built-up metal.

The scheme of broad layered facing is shown in Fig.1. The main parameters of cylindrical parts of the facing with the cross oscillation of the electrode are: speed of the electric wire supply (V_{ws}); voltage on the bow (U_b); facing speed (V_f); average speed of the electrode oscillation (V_o); the transferring speed of the electrode end at the extreme positions (V); escape of the electrode (l_e); offset *(e)* it from zenith and radius *(R)* of electrode oscillation.

Practical application of self-protective dust wire under the facing of cylindrical parts of a little diameter is restrained by the absence of the most convenient values of these parameters.

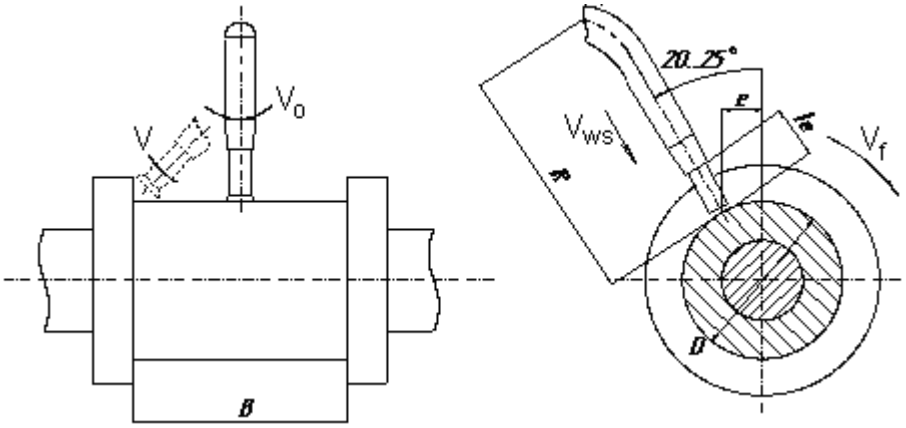

Fig. 1. The scheme of facing of cylinder surface
with the diameter *D* with the cross oscillation of electrode on the width *B*.

AIM AND METHODS

Taking into consideration the complication of the experiment along with the great quantity of crucial factors, the aim of the work was to determine the influence of the most important parameters of the regime on the productivity of the wire melting and loss of the metal. The meanings of the other parameters in the experiments were being chosen as a result of previous experiments and as a result of the constructive consideration.

The samples of the 60 mm diameter and 50 mm width made of steel St3 were faced with the self-protective dust wire ППП-Нп 30Х3Г2СМ of the 2,0 mm diameter. The wire contained 1-14%

of the dusts of gas and slag making substances. The facing was conducted with the special device, with the source of the welding current using rectifier ВДУ-506.

While conducting experiments some parameters of the regime were of permanent value: the speed of the facing – 5,5 m/h; voltage on the bow – 27 V; average speed of electrode oscillation – 213 m/h; speed of the electrode oscillation in the extreme positions – 160 m/h. Current strength was changed regulating the supply speed of the wire within a 200-400 A, escape of the electrode - 16-30 mm; offset of the electrode from zenith – 8-12 mm, oscillate radius of the electrode - 80-145 mm.

Current strength and voltage were measured with the help of ammeter and voltmeter, time of bow burning - with electric stopwatch of P-30 type up to ± 0,05 sec. Mass of the samples under investigation before and after facing was measured by weighing up to ± 1g. Mass of the built-up metal was determined as the difference of the two numbers. Special device was made to determine mass of melted wire which was adjusted on mechanism of wire supply. The device consisted of ten-toothed cam tightly joined with the mechanism of wire supply, micro-switch, enclosed in the electric circuit of impulses meter and it worked while the cam turned. One turn of the feeding roller corresponded to meter indication of 10 impulses. Mass of the wire supplied per one impulse was measured experimentally.

Coefficient of melting, facing and losses of melted metal as well as facing productivity were calculated using the following formulas:

$$\alpha_m = \frac{G_m \cdot 3600}{I_w \cdot t};\ \alpha_f = \frac{G_f \cdot 3600}{I_w \cdot t};\ \mu = \frac{G_m - G_f}{G_m} \cdot 100;\ Q_f = \frac{\alpha_f \cdot I_w}{1000}\ .$$

In the above-presented formulas:

α_m, α_f – coefficients of melting and facing, g/A h;

μ - coefficient of losses, %;

G_m – mass of melted metal, g;

G_f – mass of built-up metal, g;

I_w – power of welding current;

t – time of bow burning;

Q_f – facing productivity, kg/h.

Calculation of coefficients of melting, facing and losses of the melted metal was carried out taking into account the presence of 10-14% of dusts of gas- and slag-making components in wire.

RESULTS AND DISCUSSION

The conducted experiments and calculations have shown significant changes of the process characteristics after the change of the mentioned parameters.

At the radius of electrode oscillation of 80 mm and excepted value of other parameters, facing productivity increases while increasing strength of welding current and escape of electrode (Table 1).

A smaller influence on the productivity of facing is caused by an increase of radius of electrode oscillation (Table 2), and at the value of R=145 mm the productivity even decreases. It is obviously connected with the closing of side surface of wire on beads bulging out at the sample ends (Fig. 2) and excessive sputtering of the melted metal which is proved by the data in Table 3.

Offset of electrode from zenith considerably influences productivity of facing. Data from Table 4 have proved the increase of losses of melted metal under conditions of research by offsets of electrode from zenith by more or less than 8-9 mm. It is connected with the flow of melted metal from the welding bath in form of drops before and behind the electrode.

Table 1.Dependence of productivity of melting on the strength of welding current and escape of electrode at R = 80 mm

Current strength, A	Escape of electrode, mm	Productivity of melting, kg/h
200	16	$\frac{2,65-2,74}{2,7}$
	23	$\frac{2,88-2,93}{2,9}$
	30	$\frac{3,11-3,28}{3,2}$
300	16	$\frac{4,62-4,79}{4,7}$
	23	$\frac{5,07-5,12}{5,1}$
	30	$\frac{5,40-5,58}{5,5}$
400	16	$\frac{7,11-7,32}{7,2}$
	23	$\frac{7,85-7,96}{7,9}$
	30	$\frac{8,70-8,90}{8,8}$

Thus, estimation of correctness of choice of electrode offset from zenith can be done by evaluation of the built-up layer of metal: if thickness of layer in the middle part is smaller – offset is too large, metal flows backwards, if thickness of layer in the middle part is larger – offset is too small, metal flows forwards at certain temperatures of the heated sample.

It is worth mentioning that offset of electrode from zenith will increase after certain time of working as a result of erasing of metal opening of current-carrying terminal of nozzle. Optimal offset of electrode will happen in case when thickness of layer is the same at any point.

Dependence of productivity of facing on the strength of current and offset of electrode at excepted values of other parameters is characterized by existence of extreme value at certain values of electrode offset (Fig.3).

Table 2. Dependence of productivity of melting on the strength of welding current and radius of oscillation at escape of electrode l_e = *23 mm*

Current strength, A	Productivity of melting (kg/h) at radius of oscillation (mm)		
	80	115	145
200	$\frac{2,87-2,93}{2,9}$	$\frac{3,08-3,13}{3,1}$	$\frac{2,83-2,95}{2,9}$
300	$\frac{5,07-5,14}{5,1}$	$\frac{5,18-5,21}{5,2}$	$\frac{4,97-5,03}{5,0}$
400	$\frac{7,82-7,96}{7,9}$	$\frac{7,96-8,05}{8,0}$	$\frac{7,41-7,57}{7,5}$

Fig. 2. Appearance of built-up samples.

Table 3. The influence of strength of welding current and radius of oscillation of electrode on the losses of melted metal at escape of electrode l_e = *23 mm* and its offset from zenith *e = 8 mm*

Current strength, A	Metal losses (%) at radius of oscillation (mm)		
	80	115	145
200	$\frac{6,2-6,65}{6,4}$	$\frac{9,0-9,57}{9,3}$	$\frac{15,1-16,7}{15,8}$
300	$\frac{10,1-11,0}{10,5}$	$\frac{12,0-13,4}{12,7}$	$\frac{16,9-18,2}{17,5}$

Table 4. The influence of strength of welding current and offset of electrode from zenith on the losses of melted metal at escape of electrode l_e=*23 mm* and oscillation radius *R=80 mm*

Current strength, A	Losses of metal (%) at offset of electrode (mm)						
	0	4	8	9	10	11	12
200	13,5	8,2	6,4	8,2	10,7	13,4	16,4
300	17,1	11,8	10,5	12,1	14,9	18,1	21,2

Flow of the melted metal is the reason of such dependence. Taking into account the fact that the thickness of built-up layer should be even at the facing of thick layer of metal with cross oscillation of electrode, its offset from zenith should be chosen to obtain even thickness, allowing certain loss of melted metal at flow from welding bath back to electrode.

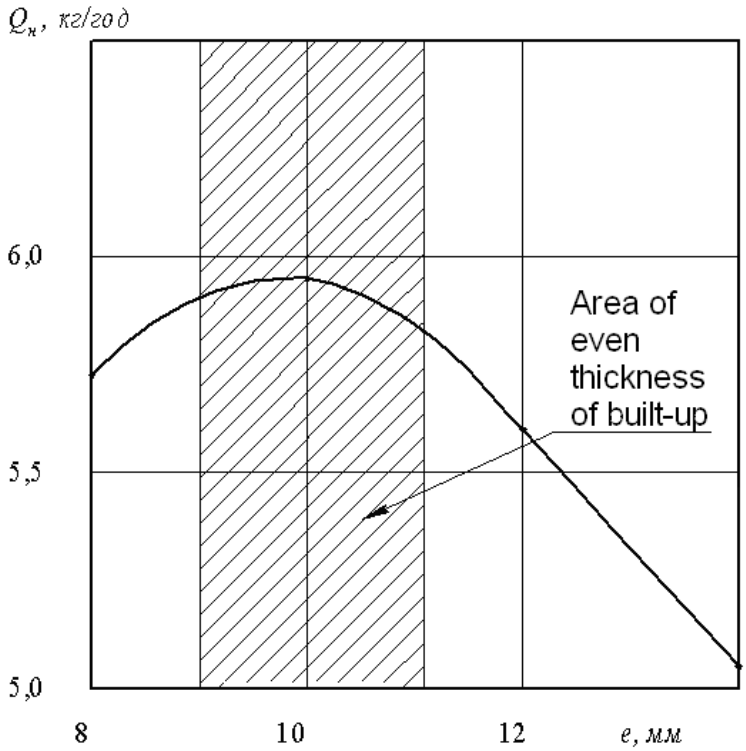

Fig. 3. The dependence of productivity of facing on the offset of electrode from zenith at strength of current 400 A, diameter sample 60 mm and layer thickness 50 mm.

SUMMARY AND CONCLUSIONS

1. Researched parameters of regime of facing of cylindrical forms with cross oscillation of self-protective dust wire considerably influence the productivity of melting and facing.
2. Maximal productivity of facing 5,8 kg/h at the speed of facing 5,5 m/h can be achieved at current 400 A and offset of electrode from zenith 9-11 mm. Increase and decrease of offset causes partial flow of metal of welding bath in form of separate drops.
3. Sufficient uniformity of thickness of built-up layer is achieved at offset of electrode from zenith 9-11 mm, when 12-18% of melted metal of welding bath will flow from built-up surface.

REFERENCES

Yuzvenko Yu.A. Dust wire for facing, - Automatic welding, 1972, page 67-71.

Technology of electric welding of metals and alloy by melting / B.E.Paton. – M.: Machine building, 1974.

Dieev V., Pichugin I. Multielectrode facing of parts of small diameter. – Machines in agriculture, 1973, №5, page 71-74.
Yudin H., Nalivkin V. Multielectrode facing of auto tractor parts. – Machines in agriculture, 1971, №1, page 63-65.
Pakholiuk A.P., Yuzvenko Yu.A., Kyrylyuk H.A., Kasatkin O.H. Optimization of the process of bow broad-layered facing of surfaces of cylinders of small diameters. – Automatic facing, 1980, №6, page 49-57.
Pakholiuk A.P., Pakholiuk O.A. Broad-layered facing of cylindrical surfaces with thin dust wire and fillets // Machine science. – 2003, № 6, page 33-35.
Bagryanskiy K.B. Electric welding and facing under ceramic gumboils. Kiev, Technique, 1976.
Khasui And., Morigaki O. Facing and metallising/ Interpret. from Japan.B.N.Popova; Edited bu B.C.Stepina, I.H Chesterkina. Moscou, Machine science, 1985.
Humeniuk I.W. Technology of the electric welding. Textbook / I.W. Humeniuk, O.W. Ivaskiv, O.W. Humeniuk. Kyiv, Deed, 2006.
Bikovskiy O.H., Pinkovskiy I.W. Reference Book of welder. Kyiv, Technique, 2002.
Prokh L. C. Reference book of welding equipment /L. C. Prokh, B.M.Shpakov, N.M.Javorskaj. Kiev, Technique, 1982.
Cheyljh A.P. Ekonomnolegirovannye metastable alloys and consolidating technologies. Mariupol, PHTU, 2009.
Kitaev A.M., Kitaev J.A. The Certificate book of welder. Moscou, Machine science, 1985.
Nikiforov H.D. Technology and equipment of welding melting / H.D Nikiforov, HW.Bobrov, W.M.Nikitin, W.W.Djchenko. Moscou, Machine science , 1978.
Machnenko W.I.,Kravcov T.H. the Thermal processes at facing of details of type of circular cylinders. Kiev, Naukova thinking, 1976.
Frumin I.I. Automatic electric bow facing. Kharkov, Metallurgizdat, 1961.
Yuzvenko Yu.A., Kyrylyuk H.A. Facing a powder-like wire. Moscou, Machine science, 1973.
Yuzvenko Yu.A., Facing. Kiev, Naukova thinking, 1976.
Common Quality Carbon Steel.Grades. DSTU 2651-94. [Actual from 1996-01-01]. Kiev, State standard of Ukraine, 1994.
Motovilin H.W. Motor-car materials: Reference book of / H.W. Motovilin, M.A. Masino, O.M. Suvorov. Moscou, Transport, 1989.

ПАРАМЕТРЫ РЕЖИМА И ХАРАКТЕРИСТИКИ ПРОЦЕССА ШИРОКОСЛОЙНОЙ НАПЛАВКИ ЦИЛИНДРИЧЕСКИХ ДЕТАЛЕЙ САМОЗАЩИТНОЙ ПОРОШКОВОЙ ПРОВОЛОКОЙ

Аннотация. Целью работы было исследование влияния параметров режима на производительности плавления и наплавки и потери расплавленного металла. Установлено, что достаточную равномерность толщины наплавленного слоя и производительность 5,8 кг/час. можно получить на токе 400 А и смещении електрода из зенита 9-11 мм При этом 12-18% расплавленного металла будет стекать из наплавляемой поверхности в виде отдельных капель.

Ключевые слова: наплавка**,** широкий слой металла, вал, порошковая проволока, параметры режима

TEKA Kom. Mot. Energ. Roln. – OL PAN, 2011, 11, 274–281

INTERNET COMPENDIUM OF SAFETY RULES FOR THE TRANSPORT OF DANGEROUS MATERIALS

Halina Pawlak, Piotr Maksym, Beata Ślaska-Grzywna*

University of Life Sciences in Lublin
Department of Technology Fundamentals,
*Department of Food Engineering and Machines

Summary. The article presents basic information about laws applicable and required for the rail transport of hazardous materials. An internet compendium of safety principles is presented and discussed, as a useful tool to apply when transporting hazardous materials, to support the acquisition, expansion and testing of knowledge in this field.

Key words: compendium, transportation, dangerous materials, safety principles

INTRODUCTION

Economic conditions force changes in the transport system. Increasingly, attention is drawn to the fast development of international transport by improving the legislative process and the organization of the transport process [1]. The changes should also include rules for the carriage of dangerous goods.

The basis of the dangerous materials transport process, inter alia, is the proper way of conduct of people who are directly involved in the implementation of the consignment of the material.

In Poland, despite the popularity of rail transport in recent years, transportation of dangerous materials by rail is about 18%, while road transport is the main method of transport of hazardous materials and involves about 81%. On the basis of reports of safety advisers, in 2007 about 100 million tons of dangerous goods were transported in Poland (on the road), and about 23 million tons (by the railway) [6].

Carriers operating rail transport of hazardous materials should pay particular attention to:

- training of persons actively engaged in the organization and the process of transporting dangerous goods;
- distribution and characteristics of hazardous materials released for transport by rail as well as their packaging and labeling;
- the operations of loading and unloading;
- shipping documentation;
- technical and operational conditions of railway vehicles, railway lines and markings;

- principles and organization of traffic at railway stations and ways of its surveillance according to the nature and extent of risks in timing and maneuvering [2, 3, 4, 12].

THE AIM AND THE RANGE OF WORK

These issues are described in the applicable legislation (laws, guidelines, station bulletins, official instructions), which contain detailed requirements for the safety of eliminating the danger to humans, environment and the proper organization of transport of hazardous materials by rail [10, 11].

Persons employed by carriers must be trained in the requirements related to such carriage and throughout the period of employment on an ongoing basis are subject to supplemental training. Changes in regulations require the conducting of periodic or ad hoc training [8, 13, 14]. For example, people involved in the filling and emptying of tanks should be trained in the requirements relating to the carriage of liquid fuels, according to the degree of their responsibilities and their duties. Training should include:

- general rules on the carriage of dangerous goods,
- specific provisions relating to their responsibilities and obligations,
- threats posed by dangerous goods, safe way of dealing with them, their protection and emergency procedures [15].

Training should be conducted prior to taking up the duties of the carriage of dangerous goods. Information on all of the trainings should be kept by the employer and employee, and verified by the new employment. Training should be supplemented periodically to reflect changes in the rules [8].

For quick access to the evolving knowledge in this area, an Internet compendium was developed on safety precautions when transporting hazardous materials.

Joomla1.5.x was used for the construction of the compendium - content management system that provides ready-made solution for building portal applications with different profiles, especially due to the availability of many additional components. As a software platform needed to run the application the following can be used: Apache, PHP scripting language and MySQL database server [7, 16].

The prepared compendium includes, among other things:

- current classification of hazardous materials, including:
  - explosives and explosive items,
  - gases,
  - inflammatory liquid materials,
  - solids, flammable, self-reactive substances and explosives, desensitized;
  - pyrophoric materials;
  - materials which, in contact with water, emit flammable gases;
  - oxidizing materials (oxidative);
  - organic peroxides;
  - toxic substances;
  - infectious materials;
  - radioactive materials;
  - corrosive materials;
  - miscellaneous dangerous substances and articles;
- safety rules;

- marking (marking principles) of rolling stock;
- example of a model sheet of hazardous chemicals;
- control questions in the form of quiz [6, 17, 18, 19, 20].

RESULTS

Examples of elements included in the compendium are presented in Figures 1, 2, 6. Additionally, Figure 5 shows a carriage for transporting hazardous materials, together with the description and the correct labeling.

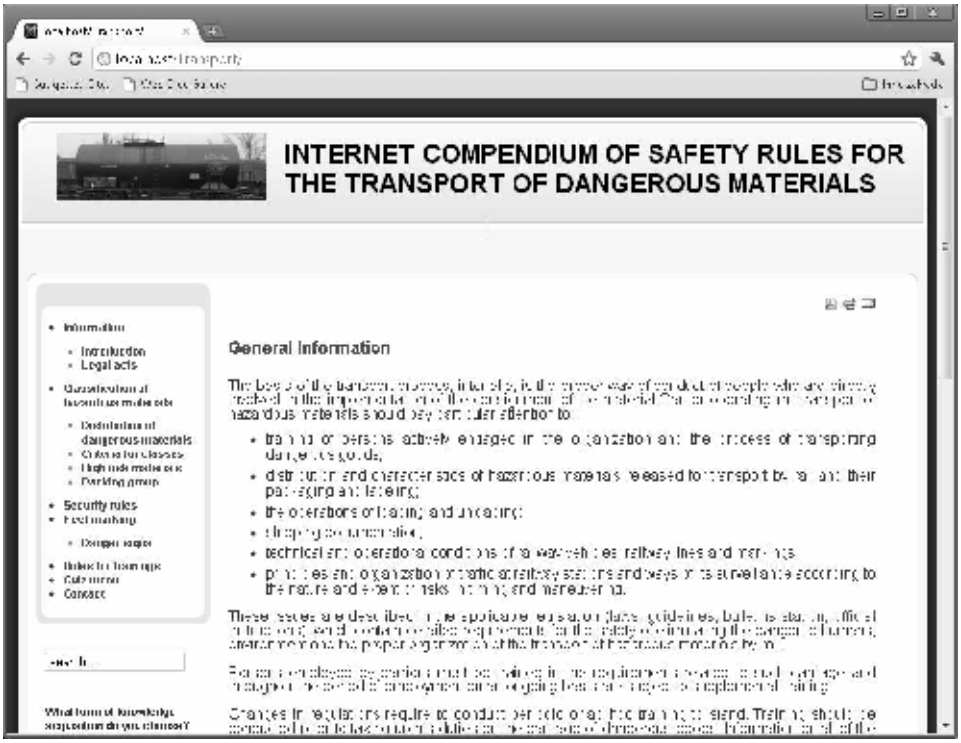

Fig. 1. Screenshot – Information

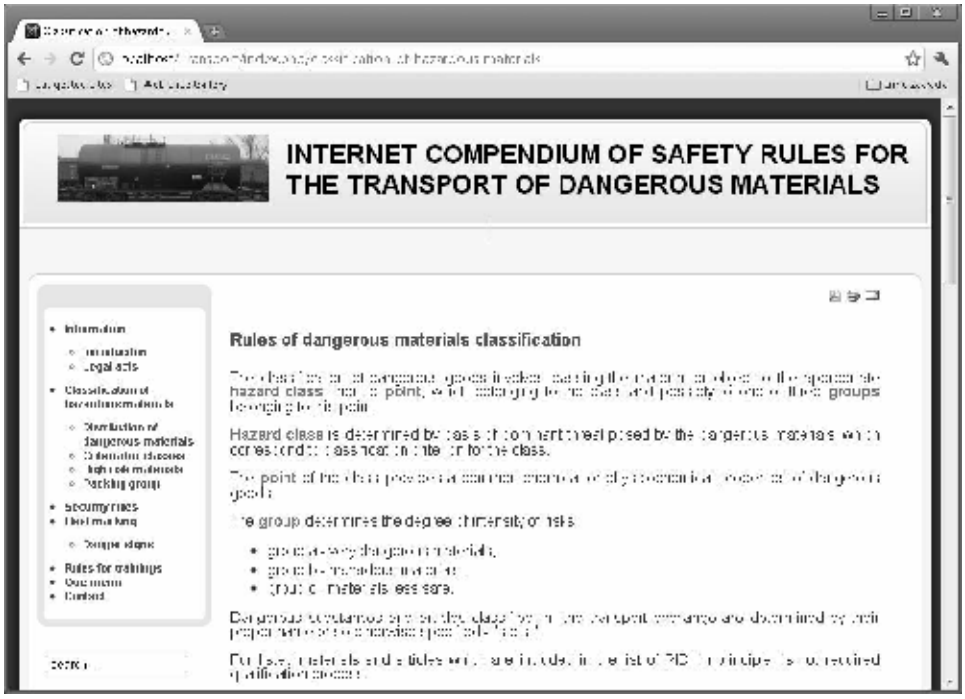

Fig. 2. Screenshot – Rules of dangerous materials classification

MARKING OF THE TRANSPORT UNIT - EXAMPLE

Proper marking of the transport unit for liquid fuel is composed of plates in orange (Fig. 3) and placards (Fig. 4). Approved method of marking is to:

- inform other participants about the existing threat,
- informing the emergency services taking action on the scene involving dangerous goods.

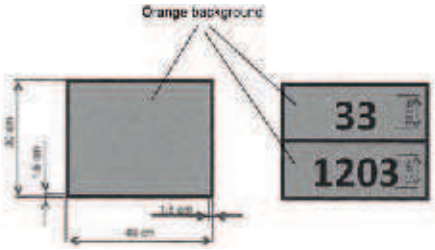

Fig. 3. Orange plates [9]

The transport unit carrying dangerous goods should be provided with two rectangular reflective plates in orange - plain or with numbers. Numbers (number) placed on the tables mean: the number in the upper part is the number of hazard identification, while the bottom - a UN number of the liquid fuel.

Fig. 4. A sample class of label 3 [9]

Transport unit carrying liquid fuel should be provided with warning stickers affixed to the carriage, with background in a contrasting color. The shape of a square rotated at an angle 45° and a side length of 25 cm. Boards and stickers should be visible, weather resistant, numbers and symbols indelible, remaining in transit in their seats and remaining legible after 15 minutes in a fire [3, 9].

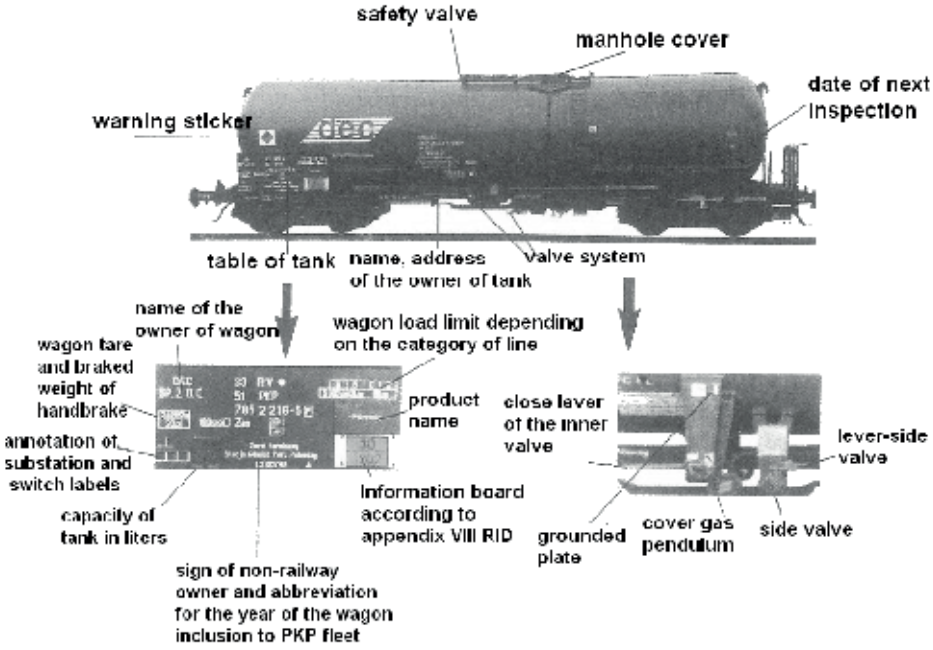

Fig. 5. Model of properly labeled carriage

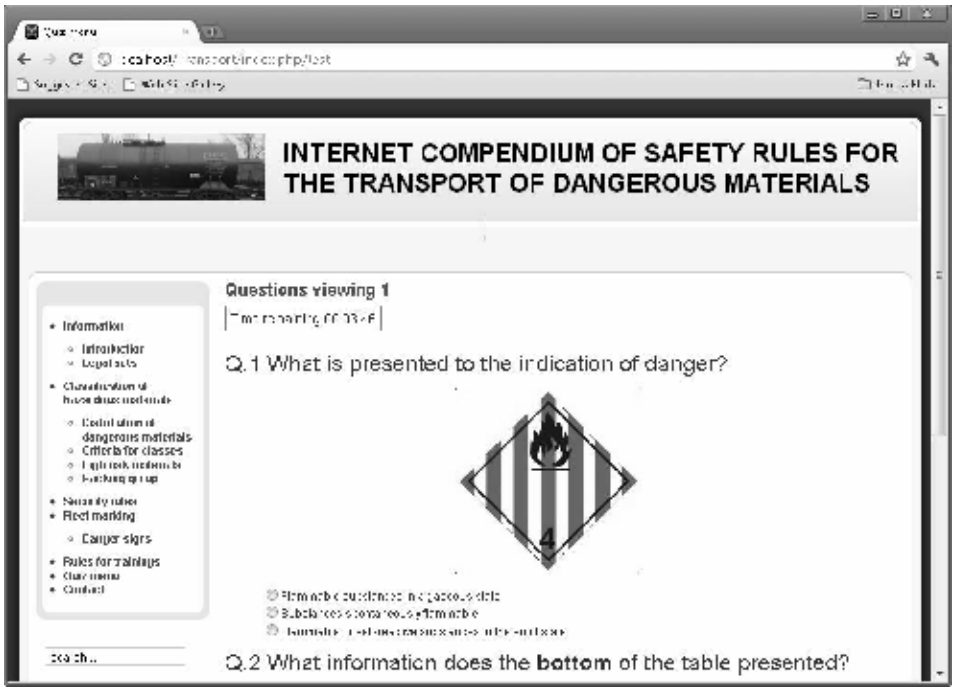

Fig. 6. Screenshot – Quiz consisting of a set of 10 diverse questions

CONCLUSIONS

The developed system is a form which complements the required training for those involved in the transportation of hazardous materials.

Building online compendium of using content management system does not require additional training on computer use, or using additional software. Access to the content is possible both via the Internet and within internal network in a company.

Ease of use of the collected information is provided by the legibility of the menu, which allows for quick access to current regulations and requirements, whether using a personal computer or mobile devices.

In addition, a simple form is provided for all users to verify their knowledge with the placed set of control questions.

Furthermore, the technology applied for the construction of the compendium allows to easily extend and customize its contents to the changing rules of carriage of hazardous materials, as well as to create a new set of control questions.

REFERENCES

Chernetskaya N., Kolodyazhnaya L.: Rational ways of development of railway transportations by international transport corridors (review). TEKA Komisji Motoryzacji i Energetyki Rolnictwa. OL PAN, 10A, 70-77

Instrukcja o technice pracy manewrowej Ir-9. http://www.plk-sa.pl/fileadmin/PDF/akty_prawne_i_przepisy/instrukcje/Ir-9.pdf

Instrukcja o postępowaniu przy przewozie koleją towarów niebezpiecznych Ir-16. http://www.plk-sa.pl/fileadmin/PDF/akty_prawne_i_przepisy/instrukcje/Ir-16.pdf

Łangowski K. 2010.: Ramy prawne bezpieczeństwa w transporcie towarów niebezpiecznych (1) – ADR. Bezpieczeństwo Pracy. Nauka i praktyka 03/2010. CIOP-PIB. Warszawa. s. 17-21

Łangowski K. 2010.: Ramy prawne bezpieczeństwa w transporcie towarów niebezpiecznych (2) – klasyfikacja. Bezpieczeństwo Pracy. Nauka i praktyka 10/2010. CIOP-PIB. Warszawa. s. 13-17

Michalik J. S., Grzegorczyk K., Gredecki S., Piękniewski M., Słomka L., Janik P., DziewulskiD., Zając S. 2009.: Zagrożenia poważnymi awariami drogowymi w transporcie drogowym niebezpiecznych chemikaliów w Polsce. Bezpieczeństwo Pracy. Nauka i praktyka 09/2009. CIOP-PIB. Warszawa. s. 6-9

Pakiet CMS Joomla. http://www.joomla.org/

Pawlak H., ŚcibiszM. 2010.: Opinion of the carriers preparation to road transportation of dangerous materials. TEKA Komisji Motoryzacji i Energetyki Rolnictwa. Vol. 10, s. 326-332

Pułkowski M., Domański W. 2010.: Bezpieczeństwo transportu drogowego paliw płynnych w cysternach – podstawowe obowiązki uczestników przewozu. Bezpieczeństwo Pracy. Nauka i praktyka 09/2010. CIOP-PIB. Warszawa. s.9-13

Przewóz towarów niebezpiecznych. http://www.utk.gov.pl/portal/pl/4/171/ Przewoz_koleja_towarow_nibezpiecznych.html

Regulamin dla międzynarodowego przewozu kolejami towarów niebezpiecznych (RID) Aneks I do Przepisów ujednoliconych o umowie międzynarodowego przewozu towarów kolejami (CIM), będący zał. C do Konwencji o międzynarodowym przewozie kolejami (COTIF)

Rozporządzenie Ministra Infrastruktury z dnia 1 maja 2004 r. w sprawie wzoru formularza rocznego sprawozdania z działalności w zakresie przewozu towarów niebezpiecznych oraz sposobu jego wypełniania (Dz. U. Nr. 118, poz. 1239)

Rozporządzenie Ministra Infrastruktury z dnia 12 lipca 2004 r. w sprawie egzaminu dla kandydatów na doradców i dla doradców do spraw bezpieczeństwa przewozu koleją towarów niebezpiecznych (Dz. U. Nr 164, poz. 1717, z późn. zm.)

Rozporządzenie Ministra Infrastruktury z dnia 21 maja 2004 r. w sprawie wzoru świadectwa do spraw bezpieczeństwa przewozu koleją towarów niebezpiecznych (Dz. U. Nr 135, poz. 1445)

Rozporządzenie Ministra Infrastruktury z dnia 21 maja 2004 r. w sprawie szczegółowych wymagań w stosunku do podmiotów prowadzących kursy początkowe i doskonalące oraz zakresu tych kursów (Dz. U. Nr 135, poz. 1446)

Środowisko pracy dla pakietu CMS Joomla. http://www.wampserver.com /en/

Umowa europejska dotycząca międzynarodowego przewozu drogowego towarów niebezpiecznych (ADR), sporządzona w Genewie 30 września 1957r. 20 marca 1975r. Dz. U. Nr 35, poz. 189

Ustawa z dnia 28 października 2002r.Przewóztowarów niebezpiecznych. Dz. U. Nr 199, poz. 1671

Ustawa z dnia 31 marca 2004 r. o przewozie koleją towarów niebezpiecznych (Dz. U. Nr 97, poz. 962, z późn. zm.)

Ustawia z dnia 28 marca 2003r. o transporcie kolejowym (Dz. U. z 2007 r. Nr 16, poz. 94)

INTERNETOWE KOMPENDIUM ZASAD BEZPIECZEŃSTWA PRACY PRZY TRANSPORCIE MATERIAŁÓW NIEBEZPIECZNYCH

Streszczenie. W artykule przedstawiono podstawowe informacje dotyczące aktów prawnych stosowanych i wymaganych przy transporcie kolejowym materiałów niebezpiecznych. Opisano i zaprezentowano internetowe kompendium z zakresu zasad bezpieczeństwa pracy przy transporcie materiałów niebezpiecznych jako narzędzie do wspomagania pozyskiwania, rozszerzania i sprawdzania wiedzy z tego zakresu.

Słowa kluczowe: kompendium, transport, materiały niebezpieczne, zasady bezpieczeństwa

TEKA Kom. Mot. Energ. Roln. – OL PAN, 2011, 11, 282–289

THE IMPACT OF INTAKE CANAL GEOMETRY ON KINEMATICS OF LOAD IN COMBUSTION CHAMBER

Piotr Piątkowski

Technical University of Koszalin, Department of Mechanical Engineering,
75-620 Koszalin, Racławicka Street 15-17, e-mail: piotr.piatkowski@tu.koszalin.pl,

Summary. The results of analysis of technical possibilities to increase engine efficiency were presented in this article. This problem was connected with kinematics properties of air inflow to the combustion chamber. The possibilities of intake airflow modulation have a positive impact on the level of engine usable parameters and emission. This issue was presented in the results of experimental research. Results of baseline research gave information about the flow resistance. On the basis of the results of experimental research the conclusions were made.

Key words: supply system, engine, combustion chamber

1. INTRODUCTION

The efficiency of engine is the highest priority during the designing of modern engines. Those questions corresponding to the decrease of fuel consumption and decrease of impact on natural environment have become extremely important. Efficiency is also important today, when intensification of transport use has had a negative impact on air clarity and economic growth and is the cause of an increase in fuel consumption.

The direction of sparkle ignition (SI) engine development was based on the development of automotive market and introduction of new technology which has given many new products. Now, the most important aims are the decrease of fuel consumption and fulfilling more and more radical norms of emission relating to toxic gases emissions as well as the keeping of high level of usable engine parameters such as torque and power.

Photochemical smoke over the city is today the „normal" effect of chemical reaction under sunrays in the big and high industrialized cities.

In most of the countries the administrative limits have been imposed on fumes emissions. The toxic gases involved are; hydrocarbons (C_nH_m), carbon monoxide (CO), nitric oxide (NO_x), molecular parts (PM) and sulfur oxide (S – mainly from the fuel pollution).

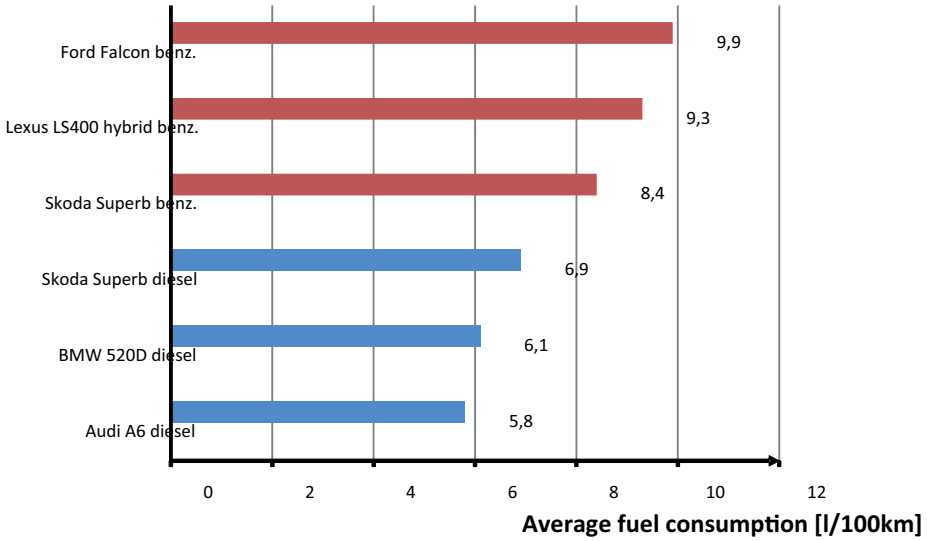

Fig. 1. Average fuel consumption by modern cars with automatic transmission[12] (test type - ADR 81)

Currently, in the phase of continuous development are systems which are able to increase energy efficiency of SI engines, as well as achieve better energy - ecological parameters. By applying a combination of a few different modern constructional systems, the considerable decrease of fuel consumption and exhaust gases emission could be achieved (Fig. 1 and 2).

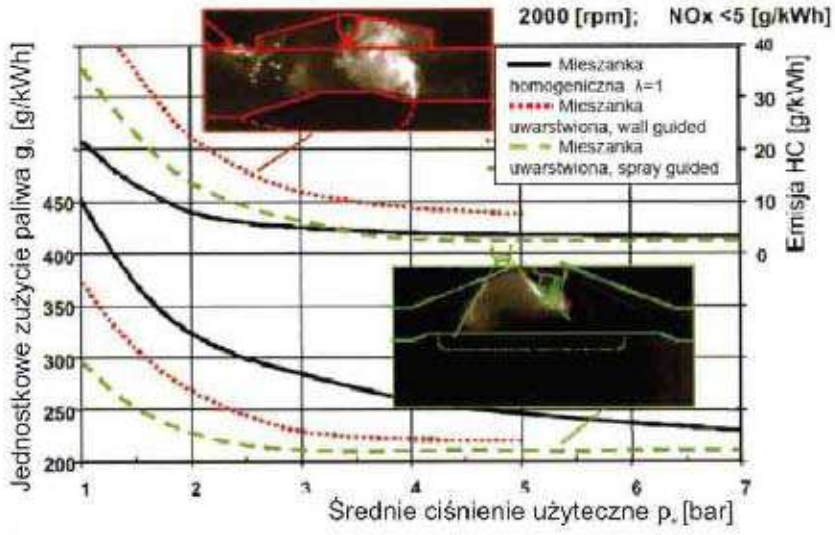

Fig. 2. Comparison of specific fuel consumption and hydrocarbons emission for GDI engine by the injection and mixture type [3]

The alternative fuels as a source of energy for the modern engine are still developed by the quality and exploitation requirements. It can be a cause of more effective use of these fuels as a renewable source of energy in the future. Apart from this, now we have many possibilities of adopting engine feeding system to specific properties of fuel [8].

These indirect measures of have helped to achieve lower levels of fuel consumption and toxic gases emissions as well as the increase (or maintaining) of engine parameters like torque and power.

Many researchers [1, 6, 7, 10] were engaged in the research on the impact of intensification of vortrex in combustion chamber on heat transfer in SI engine. Others were engaged in the research on the impact of turbulence on heat growth [2, 4, 11] and stabilization of the burning process in piston engines [5]. The results of this type of research are indicative in a different way of the impact of swirl on engine work conditions. The authors agree that the vortrex has a positive impact on air-fuel mixture formation by achievement of a more homogeneous form. This conclusion was made by the achievement of decrease of level emissions of carbon monoxides and hydrocarbons. Also, the increase of nitric oxide was achieved. However, the impact of vortrex on heat transfer was not clear. The possibilities of intensification of preliminary swirl in intake canal are seldom mentioned in research works. This intensification can be very important in cases of:

- formation of homogenous mixture,
- low RPM level,
- engines with a relatively small capacity of one cylinder
- application of alternative fuel in the engine feeding system.

2. EXPERIMENTAL STAND

The experimental stand was based on the real intake system of four strokes, four cylinders SI engine with displacement of 1598 cm. The diameter of intake canal for experimental stand was 34 mm. The cause of difference between engine and model was accessibility of tubes on the local market.

The effect of swirl was achieved by using a flexible element with the 65 mm length, width 32mm and thickness 0,4mm steel tape assembled inside the tube. The real view of this element is presented in Figure 3.

On the basis of these assumptions the airflow experimental model in the intake canal was built. The picture of experimental stand is illustrated in Figure 4.

The value of airflow resistance (Δp) was determined using the equation;

$$\Delta p = \rho \cdot g \cdot n \cdot l \text{ [Pa]}, \tag{1}$$

where;
ρ – density of liquid in manometer [g/ccm],
g – Earth acceleration [m/s^2],
n – manometer ratio,
l – number of gradations.

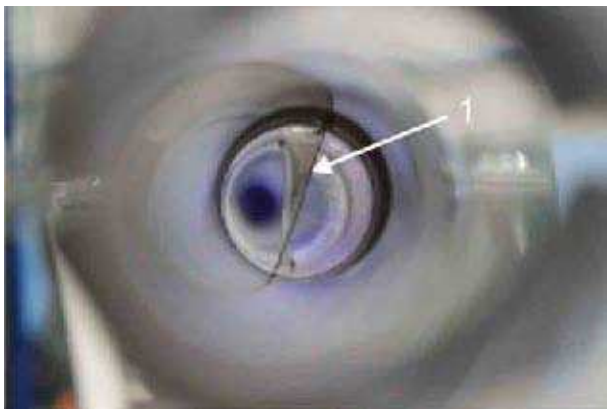

Fig. 3. The picture of canal with flexible geometry [9]; 1 – steel tape

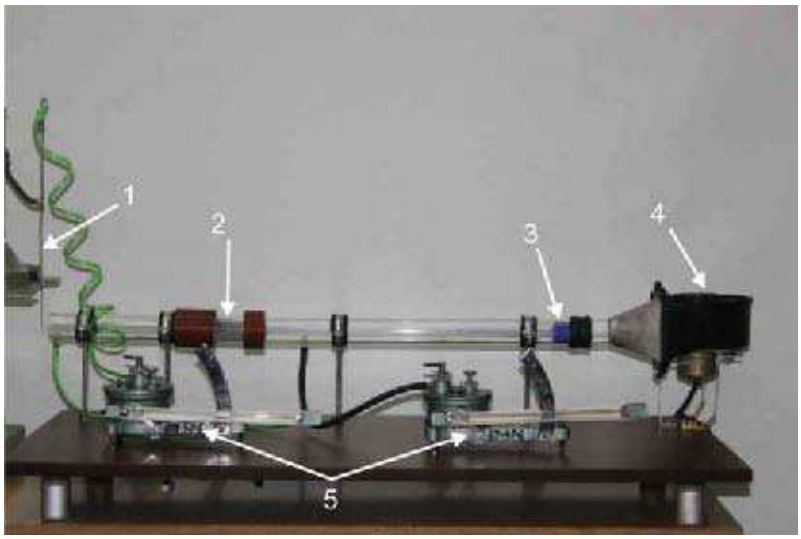

Fig. 4. The experimental stand; 1 – Prandtl's pipe, 2 – flexible tape, 3 - airflow stabilizer, 4 – ventilator, 5 – Recknagel's micro manometers

The value of velocity was achieved on the basis of dynamic pressure in two self-orthogonal planes. Measure points were based on the divided field of tube surface. The diameter of tube was divided by nine rings with 2 mm width. And so the four measure points for each ring were achieved.

The airflow velocity (v) for each measure point was calculated according to the equation;

$$v = \sqrt{\frac{2 \cdot g \cdot \rho \cdot n \cdot l}{1{,}3}} \ [\mathrm{m/s}]. \tag{2}$$

The average value of velocity for the field of tube surface was achieved from;

$$\overline{v} = \frac{1}{A} \cdot \sum_{n=1}^{9} \frac{\left(v_{n1} + v_{n2} + v_{n3} + v_{n4}\right)}{4} \cdot A_n \text{ , [m/s]}, \tag{3}$$

but;

$$A_n = \pi \cdot \frac{\left(d_{n1}{}^2 - d_{n2}{}^2\right)}{4} \text{ , [m}^2\text{]}, \tag{4}$$

where;
A – field of surface of orthogonal canal intersection [m^2],
A_n – field of surface for n –ring,
n – number of the ring,
$v_{n1\div4}$ – airflow velocity for the successive n - ring and measure point,
d_{n1} – outside diameter for n – ring,
d_{n2} – inside diameter for n – ring.

3. RESULTS OF EXPERIMENTAL RESEARCH

The research was concerned with the assessment of impact of flexible geometry canal on airflow velocity and flow resistance. Also, changing of airflow extreme of velocity positioning was important for evaluation of velocity profile. As it was mentioned, the steel tape was a flexible element of intake canal. One end of tape was fixed to the tube by the first ring, but the second end of tape could change its position by the moving of the second ring.

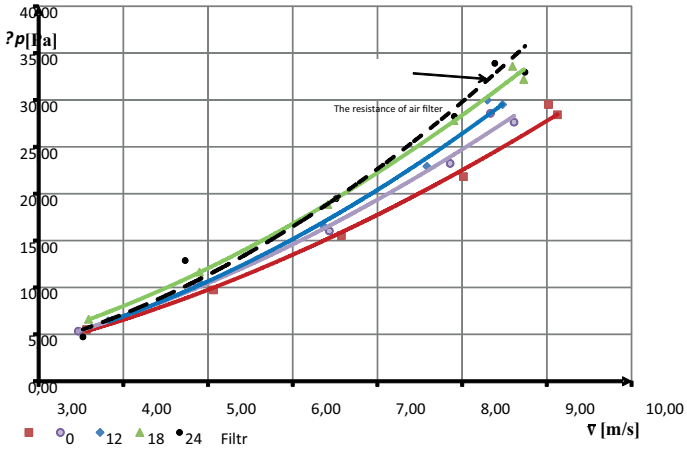

Fig. 5. The airflow resistance (Δp) by average airflow velocity ($\bar{v}$), different angle of twist tape (0, 12, 18, i 24°) and air filter flow resistance

In this way, the steel tape was twisted. The second ring was able to make the steel length's compensation. The angle of tape twist was from 0÷24°, however, the obtained average velocities were from 3,5÷9,2 m/s. The composition of experimental research results concerned the assessment of airflow resistance by average velocity and the angle of tape twist was presented in Figure 5.

A very important conclusion from the analysis of Figure 5 is that the use of flexible element of intake canal has no significant impact on airflow resistance and the airflow resistance is even lower than for the clear air filter flow. The difference between the lowest and the highest resistant value for the tape twist 24° for the achieved airflow velocity was only a bit more than 5 Pa, while the measure deviation of airflow resistance was 0,96 Pa.

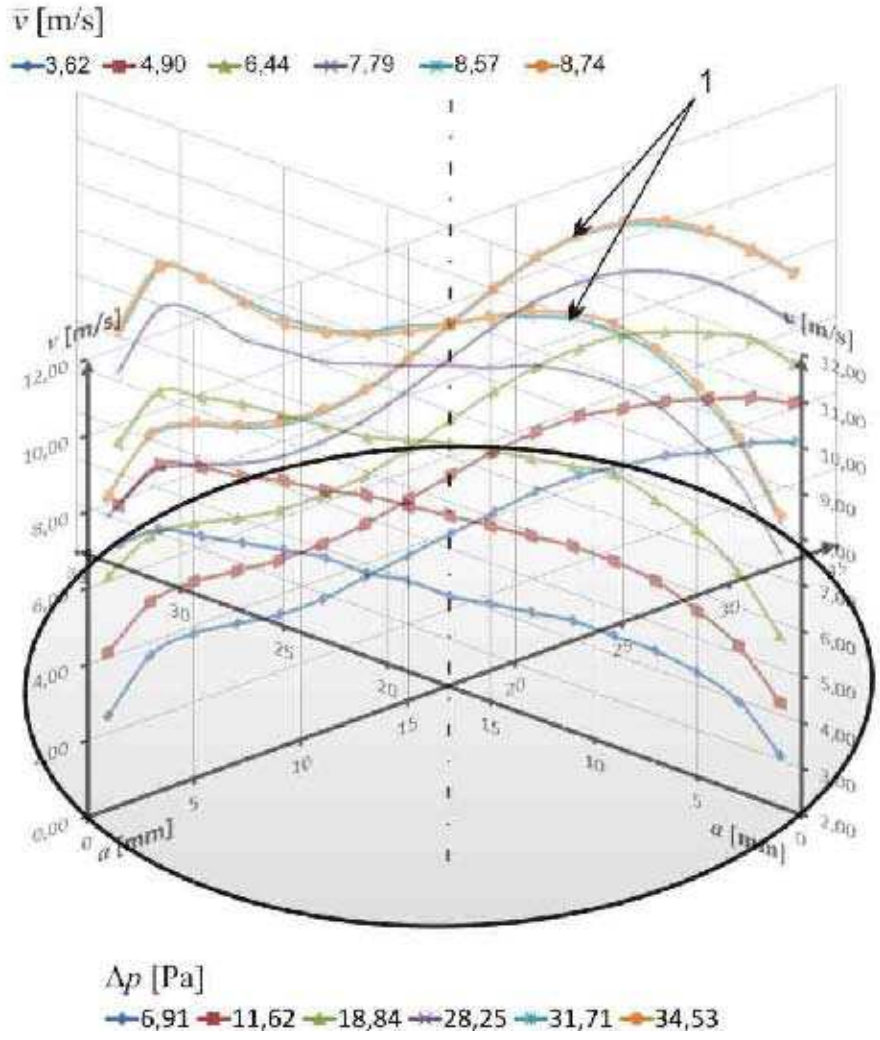

Fig. 6. The composition of velocity profiles of airflow for two mutually perpendicular planes inside the canal; 1 - the highest airflow velocity (11,2m/s)

These results are very promising for the achieved change of airflow velocity profile for the cross intersection. Suitable velocity profile can help to deliver cylinder load without the meeting with valve head and the intensity of turbulence will decrease, than it can decrease filling loses.

From the analysis of results illustrated in Figure 6 we can see that by the change of angle tape's twist, the change of airflow velocity profile was achieved. It was very effective for the angle of tape twist 24°. There the two extremes for velocity profile next to inside tube's walls appeared. This experiment can be very useful for implementation of flexible intake canal for air inflow to combustion chamber to the piston engines. In this way, we can get an insignificant increase of flow resistance (about 7%). Suitable positioning of flexible element inside intake canal for intake valves has a positive impact on the effect of load swirl penetration from intake's canal to the combustion chamber.

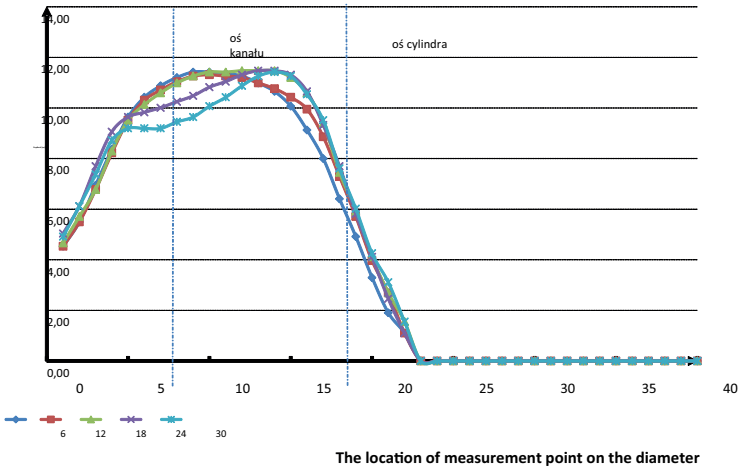

Fig. 7. The view of change of airflow velocity profile during inlet to the cylinder for parallel canal

It will be very useful for the mixture preparation. On the composition of speed profile (Fig. 6) the displacement of the minimum from the center was achieved. The cause of this was an unexpected, not axial deformation of tape during the twist – which will be dealt with during the next experimental research.

In Figure 7 the change of airflow speed profile during inlet to combustion chamber was illustrated. There we can see the positive action of swirl from intake canal, which displaced the center of intake airflow to the center of cylinder. It will be very helpful from the points of view of the mixture preparation and combustion process.

4. FINAL CONCLUSIONS

On the basis of the results of experimental research the following conclusions can be drawn:

1. Implementation of geometrically flexible element of intake canal has no significant impact on the flow resistance (even less than impact of air filter).
2. The velocity of airflow and the angle of tape twist have an impact on the kind of velocity profile change.

3. The change of airflow velocity profile can be the cause of decrease of turbulence from valve head.

4. Effect of load swirl during filling of combustion chamber has an impact on the achievement of better condition of mixture preparation (the mixture is more homogeneous)

REFERENCES

Algifri AH., Bhardwaj RK, Rao YVN.: Heat transfer in turbulent decaying swirl flow in a circular pipe. Int J Heat Mass Transfer 1988, 31(8) pp. 1563–8.

Alkidas A.C.: Combustion advancements in gasoline engines, Energy Conversion&Mana-gement, 48/2007, pp. 2751-61.

Friedl H., Kapus P.: Kierunki Rozwoju Silników ZI, Silniki Spalinowe 2/2002.

Fuerhapter A, Piock WF, Fraidl GK.: CSI – controlled auto ignition – The best solution for the fuel consumption – versus emission tradeoff? SAE Paper NO. 2003-01-0754; 2003.

Goto Y., Narusawa K.: Combustion stabilization of spark ignition natural gas engine, JSAE Review 17 (1996) pp. 251-8.

Loosley DJ.: Heat transfer from a centrally located source in a vortex flow, MSThesis, AFIT, WPAFB, 1961.

Mc Kelvey R.: Heat transfer from a heated cylinder in vortex type flow, MSThesis, AFIT, WPAFB, 1960.

Piątkowski P.: Wpływ parametrów zasilania w układach dwupaliwowych na efektywność energetyczną tłokowego silnika spalinowego, Rozprawa doktorska, Koszalin 2007.

Piątkowski P., Lewkowicz R.: Wpływ kinematyki ładunku napływającego do komory spalania na efektywność procesu spalania w silnikach tłokowych, Motrol nr 12/2010, pp. 115-121.

Yilmaz M, Comakli O, Yapici S.: Enhancement of heat transfer by turbulent decaying swirl flow. Energy Conversion Manage 1999;40:1365–76

Zhang D., Hill P.G.: Effect of swirl on combustion in a short cylindrical chamber, Combustion and Flame 106/1996, page 318-332.

http://australian-clean-energy-facts.com.

WPŁYW GEOMETRII KANAŁU DOLOTOWEGO NA KINEMATYKĘ RUCHU ŁADUNKU W PRZESTRZENI ROBOCZEJ SILNIKA TŁOKOWEGO

Streszczenie. W artykule przedstawiono wyniki badań eksperymentalnych oraz analizy literatury pod względem możliwości technicznej realizacji pracy silnika z uwagi na ograniczenie emisji spalin oraz zmniejszenie zużycia paliwa. W pracy przedstawiono zagadnienia związane z możliwością wykorzystania zjawiska zawirowania ładunku na tle uzyskiwanych wartości parametrów pracy. Zamieszczone wyniki badań eksperymentalnych przeprowadzone na stanowisku modelowym pozwoliły uzyskać odpowiedź na zagadnienia oporów przepływu oraz pozwoliły określić wnioski dotyczące technicznej możliwości implementacji do silnika badawczego.

Slowa kluczowe: system zasilania, silnik, komora spalania

TEKA Kom. Mot. Energ. Roln. – OL PAN, 2011, 11, 290–296

INCREASING THE EROSIVE WEAR RESISTANCE OF SELECTED IRON ALLOYS BY MECHANICAL STRAIN HARDENING OF STRUCTURE

Zenon Pirowski, Jerzy Olszyński, Andrzej Gwiżdż

Foundry Research Institute,
Poland, 31-418 Krakow, 73 Zakopiańska Street

Summary. The article presented here describes the initial stage of studies on the hardening potential of some selected iron alloys under the effect of internal stresses. Tests were conducted on these alloys when subjected to compressive and tensile stresses. It has been proved that tensile stresses do not cause hardening of alloy; this effect is due to the presence of compressive stresses, though their effect on the degree of work hardening may differ considerably. Investigations were also made on the erosive wear rate, regarded as a factor inducing very complex surface phenomena in castings on performance.

Keywords: iron alloys, strain hardening, wear, erosion

INTRODUCTION

Strain hardening is a phenomenon which occurs during cold plastic deformation of the processed material. It involves the continuous increase of deformation resistance. Therefore, to obtain higher deformation, the value of the deformation forces must be raised accordingly. Then the processed material undergoes hardening and decrease of its plastic properties. Many materials that are plastic by nature, under the influence of strain hardening may completely lose this property. The effect of strain hardening increases with the deformation rate. Increasing the temperature reduces the effect of strain hardening, because higher mobility of atoms facilitates “slides” and “jumps” in the atomic structure and thus reduces the possibility of the formation of dislocations. An important role in the strain hardening of materials is played by, along with dislocations, other lattice faults. Their mutual relations consist in an interaction of the stress fields. For example, the interstitial dopant atoms are attracted to the edge dislocations, and as a result of this effect the so called Cottrell atmosphere, i.e. clusters of atoms of the impurities inhibiting the movement of dislocations, is formed. Dislocations are also blocked by grain boundaries, particles of foreign phases, or other dislocations.

RESEARCH MATERIAL

As mentioned above, strain hardening is the phenomenon that occurs during cold plastic deformation of the processed material. Among the cast iron alloys, this phenomenon is mainly observed in materials with the austenitic structure. In these alloys, the strain hardening mechanism may consist, on the one hand, in blocking the movement of dislocations, especially in the presence of micro-and nanoprecipitates (e.g. nitrogen compounds) and, on the other - in initiating, under the effect of external stress, the transformation of austenite into martensite. Such alloys are, for example, cast high-manganese steels, cast chromium-nickel steels, and austempered ductile iron.

The following alloys were selected for the studies: cast Cr-Ni-Mo steel with low nitrogen content (less than 0.2%) and with high nitrogen content (about 0.4%), cast high-manganese steel and austempered ductile iron, for which a reference material was the same cast iron but without heat treatment. The chemical composition and designations of the cast alloys are compared in Table 1.

Table 1. The results of melt chemical analysis

Alloy	Chemical composition; %											
	C	Si	Mn	P	S	Cr	Ni	Mo	V	N	Mg	Cu
A	1,20	0,30	13,0	0,040	0,005	0,75	0,20		3,2	0,04		
B	0,19	0,68	5,0	0,025	0,015	24,3	5,40	3,35	1,10	0,39		
C	0,16	0,87	5,0	0,025	0,015	24,9	4,80	3,35	0,95	0,19		
D and E	3,40	2,10	0,34	0,03	0,01		1,80			0,04	0,07	1,00

MECHANICAL TESTS

Typical tensile test was performed for alloys designated with symbols A, B, C, D and E. The test was conducted on specimens pre-stressed with a force equal to 0.8 $\mathbf{F_m}$ for individual non-pre-stressed alloys.

Hardness was measured by Rockwell technique on heads of the specimens designed for mechanical tests: directly and in indentations formed by prior measurements of Brinell hardness.

Measurements were also made by Rockwell method on cross-sections of the working parts of the mechanical specimens: not subjected to external stress, and subjected to compressive stress with a force of $\mathbf{-F_m}$ value and to tensile stress with a force of $\mathbf{+F_m}$ value.

STRUCTURE EXAMINATIONS

Using a FERRIKOMP device and a magnetic technique, the content of ferromagnetic phases was measured in the specimens. The measurements were taken in the material non-pre-stressed, and then on specimens subjected to cold work with a breaking force $\mathbf{F_m}$ applied in static tensile test and with a force **F** equal to 0.8 value of the force $\mathbf{F_m}$. Tests were also carried out on specimens fractured after the preliminary application of force $\mathbf{F} = 0.8\ \mathbf{F_m}$, withdrawn after 1 minute.

Microstructure was examined under a Neophot 32 optical microscope. Colour etching technique and differential contrast were applied.

Metallographic examinations were carried out on alloys not loaded with external stress and on alloys subjected to tensile stress until specimen failure.

EROSION TESTS

Erosion tests were performed using a device of the authors' own design, which enables simultaneous testing of 27 specimens.

The erosive media successively used included water-based silica sand slurry, copper slag grit, and coal dust. Erosive wear tests were carried out each time for 40 hours (total of 120 hours). Specimens of all alloys were tested simultaneously, due to which the same experimental conditions were created and the possibility of a comparative assessment of different alloy types. As a measure of erosion resistance of various alloys, the wear rate Z/h [mg/h] was adopted, specifying the weight loss per unit time.

Tests were carried out on specimens not pre-stressed and pre-stressed with a force equal to 0.8 $\mathbf{F_m}$. The technique of pre-stressing and the magnitude of the applied stress were discussed earlier.

Summing up the results of erosive wear in three types of abrasive media, the wear rate of the specimens of the examined alloys was determined in different and changing abrasive environments.

ANALYSIS OF RESULTS

Static tensile test at room temperature, carried out on specimens not subjected to external stress and on specimens pre-stressed with a tensile force equal to 0.8 $\mathbf{F_m}$ gave no evidence in any of the investigated alloys of the visible effect of hardening.

On the other hand, the effect of hardening was observed in the examined alloys after the application of initial compressive stress due to a pressure exerted by a 10 mm dia. ball acting with a force of about 30 kN.

For the examined alloys, this effect is graphically shown in Figure 1.

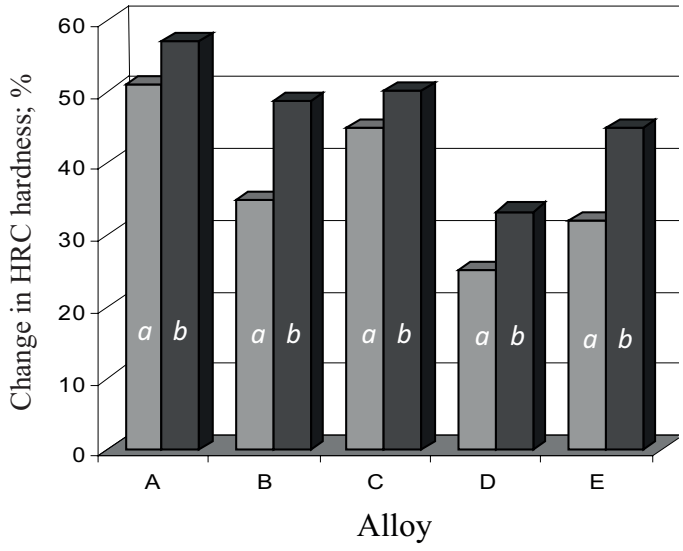

Fig. 1. Effect of compressive stress on the strain hardening of the tested alloys
a - without pre-stressing
b - in HB indentations

Rockwell hardness measurements were also used as another method for the evaluation of hardening effect in the investigated alloys. The effect of hardening was evaluated in the 8 mm dia. specimens subjected to both tensile stress acting with a force equal to + $\mathbf{F_m}$, and compressive stress acting with a force equal to **-F_m**. The results of this hardening were quantified and shown graphically in Figure 2.

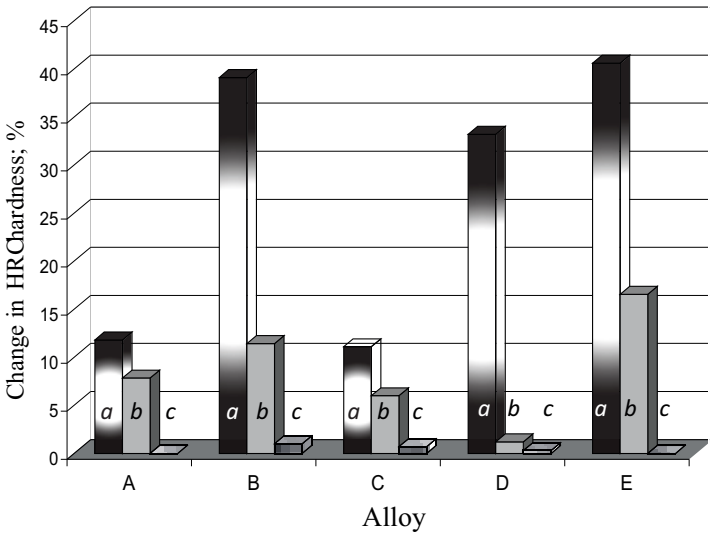

Fig. 2. Relative increase in HRC hardness in the tested alloys
a - in HB indentations
b - after application of **-Fm** compressive force
c - after application of **+Fm** tensile force

One of the hardening mechanisms can be the $\gamma \rightarrow \alpha$ transformation under the influence of external stress. Paramagnetic austenite is then transformed into ferromagnetic martensite.

In the examined alloys, the main ferromagnetic phases are ferrite, martensite, and cementite (both free and combined in pearlite). The paramagnetic phases mainly include austenite and graphite (in cast iron), occupying a small volume, especially when in the form of spheroids.

The measurements of the volume content of ferromagnetic phases showed that under the influence of external tensile stress in cast high-manganese steels and ductile iron (without austenite), the $\gamma \rightarrow \alpha$ transformation did not occur. To some extent it did occur in the cast Cr-Ni-Mo steel with high nitrogen content (0.4%) and in austempered ductile iron (ADI). This effect occurred but only under loading with a force equal to 0.8 F_m; at higher loads it occurred no longer.

A pronounced effect of $\gamma \rightarrow \alpha$ transformation under the influence of external stress was observed in cast Cr-Ni-Mo steel with low nitrogen content (0.2%). This effect, depending on the magnitude and method of application of tensile stress, caused an increase in the amount of ferromagnetic phases in this alloy from 24% to 30% or 36%, sometimes even up to 43%, i.e. by nearly 20%. This fact has been confirmed by metallographic observations.

7. CONCLUSIONS

The lack of the hardening effect observed in specimens subjected to pre-stressing with the external tensile stress acting with a force equal to **0.8 F_m** may result from the fact that the load relief for a short period of time does not lead to the aging process after cold work. This phenomenon is of a diffusive nature. To disperse Cottrell atmosphere grouped around the dislocations it is necessary to relieve the load for a period of a few months at ambient temperature or preheat the specimens to temperatures above 400°C.

The hardening effect observed with the application of compressive stress can be caused by a number of factors, including:

- a much higher deformation rate in the case of compression (up to 3 kN/s) compared with tension (0.5 kN/s) strongly favours hardening,
- specimen fracture along the grain boundaries during the tensile test releases the accumulated dislocations, resulting in relaxation of material,
- due to significant compressive stress, the intermolecular distances are reduced, which increases the cohesive forces resulting in alloy hardening.

Measurements of the amount of ferromagnetic phases in alloys before and after cold work and metallographic examinations of these alloys have shown that the $\gamma \rightarrow \alpha$ transformation occurring under the influence of external tensile stress was distinctly observed to take place only in the cast Cr-Ni-Mo steel with the addition of about 0.2% nitrogen. In other alloys (cast high-manganese steel, cast Cr-Ni-Mo steel with about 0.4% nitrogen, ADI) austenite was stable enough to practically prevent the occurrence of the transformation. In all these cases, the austenite stabilising factor was the high content of either carbon or nitrogen; in the case of ductile iron without heat treatment, austenite did not occur in the as-cast state, thus preventing the occurrence of the $\gamma \rightarrow \alpha$ transformation under these conditions (cold work at room temperature).

Comparing these results with the hardness measurements leads to a conclusion that hardening of the examined alloys under the effect of pressure did not result from the transformation of austenite into martensite, but rather generally from transformation into the α phase. The hardening was definitely stronger in a Cr-Ni-Mo steel with 0.4% nitrogen and ADI than it was in the, undergoing this transformation, cast Cr-Ni-Mo steel with 0.2% nitrogen. The reason for the observed hardening effect may therefore be the formation and concentration of dislocations at grain boundaries and on micro-and nanoparticle precipitates. The mechanism of such hardening was proposed by Orowan.

During erosive wear, the material is exposed to continuous pressure exerted by small particles of abrasive media. This pressure causes the formation of local internal stress in the examined material. In the crumple zone, cyclically variable stresses of different nature are operating. The surface microareas of the substrate are exposed to compression, stretching, bending, shear, etc. This, practically impossible to grasp, variability of stresses makes outer layers of the substrate, attacked by the particles of abrasive medium, undergo fatigue wear and tear off from the surface uncovering the successive layers.

Thus, the alloy tendency to hardening under the effect of external stress should be characteristic of its increasing resistance to erosive wear. Studies of the wear rate may, therefore, serve as a tool for validation of the results obtained by other laboratory tests.

A comparison of the erosion wear rate in corresponding specimens (prestressed with tensile stress or not) showed that pre-stressing of specimens with a force of 0.8 F_m increased in a significant way the resistance to erosive wear only in alloy B (cast Cr-Ni-Mo steel with an addition of 0, 4% nitrogen). In the case of other examined alloys, the application of this cold work did not give positive results.

The results obtained show high complexity of the hardening phenomena. The, occurring as a result of external stress, transformation of γFe into α Fe, as well as the increase in alloy hardness due to the formation of dense dislocations during cold work need not be the factors leading to an increased resistance to erosive wear. Equally important factors are: the quantitative content of different phases in the matrix (resistant austenite, non-resistant ferrite), their morphology, or the presence of possible precipitates (graphite, carbides, nitrides, intermetallic phases, etc.). These factors change the run of the process of the loss of coherence in material subjected to the effect of destructive loads.

Higher resistance to erosive wear observed in cast Cr-Ni-Mo steel with 0.4% nitrogen (35HRC) subjected to preliminary cold work, compared with the same cast steel but with a nitrogen content of about 0.2% (45 HRC), can prove that it is nitrogen that plays here the decisive role. On the one hand, nitride precipitates are formed inhibiting the dislocation movement and acting as a source of dislocation loops (Orowan mechanism), while - on the other - the presence of nitrogen as such increases the impact of Cottrell atmosphere on the movement of dislocations.

The, observed in the case of cast Cr-Ni-Mo steel with 0.2% nitrogen (alloy C), increased erosion wear rate in some abrasive media of the specimens after prestressing indicates that the $\gamma \rightarrow \alpha$ transformation occurring under the effect of pressure (the content of paramagnetic phases reduced from 76% to even 57%) need not be the transformation of austenite into martensite, as confirmed by metallographic observations.

The results of the executed studies, although marking only a preliminary step in the research, have already undergone the first practical trials. A series of the pilot castings operating as parts of agricultural machines working in soil have been produced. They successfully passed the stage of performance tests and, at present, their production is being launched in cooperation with PIMR Poznan within the framework of a Structural Project (SPO_WKP; Action 1.4.1).

REFERENCES

Masson J. M. – Fonderie – Fondeur d'Aujourd'hui, No 163, mars 1997, s. 18-42.
Pirowski Z. – Prace Instytutu Odlewnictwa, zeszyt 1-2, Kraków 1998, s. 75-87.
Czyżowicz S. - Prace IMŻ 3-4, Gliwice,1993, s. 26-38.
Malkiewicz T. – Metaloznawstwo stopów żelaza; PWN, Warszawa-Kraków, 1976, s. 299.
Schoefer E. A. – Welding Juornal; vol. 53, 1974, s. 10-12.
Pirowski Z., Tybulczuk J., Uhl W. - Acta Metallurgica Slovaca, Koszyce, 2/1999, s. 333.
Pirowski Z., Wodnicki J., Gwiżdż A. - Acta Metallurgica Slovaca, Koszyce, 2/2002, s. 381.
Przybyłowicz K. – Metaloznawstwo teoretyczne; Skrypt AGH; Kraków 1974.
P. J. Cunat: Alloying Elements in Stainless Steel and Other Chromium – Containing Alloys; Euro Inox 2004; Materiały: International Chromium Development Association; dostępne: Rue de Lisbonne F-75 008 Paris.
M. Blicharski: Inżynieria materiałowa – stal; WNT; Warszawa 2004.
S. Prowans: Metaloznawstwo; PWN; Warszawa 1988.
K. Wesołowski: Metaloznawstwo i obróbka cieplna; WNT; Warszawa 1978.
K. Przybyłowicz: Metaloznawstwo; WNT; Warszawa 2007.
Z. Pirowski: Zwiększenie odporności na zużycie erozyjne dwufazowego staliwa Cr-Ni przez dodatek azotu i innych pierwiastków międzywęzłowych; Archiwum Technologii Maszyn i Automatyzacji. Komisja Budowy Maszyn PAN Oddział w Poznaniu; vol. 26; nr 1; s. 1005-121; Poznań 2008;
Encyklopedia techniki. Metalurgia; Wydawnictwo "Śląsk"; Katowice 1978.

Pirowski Z., Olszyński J., Gościański M., Turzyński J.: Elementy maszyn rolniczych pracujących w glebie wykonane z nowoczesnych tworzyw odlewniczych; MOTROL – Motoryzacja i Energetyka Rolnictwa; Lublin 2006; t. 8, s. 169

Pirowski Z., Gościański M.: Construction and technology of production of casted shared for rotating and field ploughs: TEKA Commission of Motorization and Power Industry in Agriculture Lublin University of Technology the Volodymir Dahl East-Ukrainian National University of Ługańsk: 2009; v. IX; s. 231-239.

C. J. Smithells: Metals Reference Book; vol. 2; Butterworths, London 1967.

Stainless Steel World. Materiały internetowe: http://www.stainless-steel-world.net/pdf/11022.pdf

W. Łoskiewicz, M. Orman: Układy równowagi podwójnej stopów metali; PWN; Kraków 1955.

S. Rudnik: Metaloznawstwo; PWN; Warszawa 1978.

A. Hernas: Żarowytrzymałość stali i stopów; Wydawnictwo Politechniki Śląskiej; Gliwice 1999.

The work was partly executed under a Commissioned Research Project (PBZ-KBN-114/ T08/2004).

ZWIĘKSZENIE ODPORNOŚCI WYBRANYCH STOPÓW ŻELAZA NA ZUŻYCIE EROZYJNE POPRZEZ MECHANICZNE ODKSZTAŁCENIA STRUKTURY

Streszczenie. Artykuł opisuje początkowy etap badań na temat możliwości hartowania wybranych stopów żelaza pod wpływem naprężeń wewnętrznych. Przeprowadzono badania tych stopów w warunkach ściskania i rozciągania i udowodniono, że naprężenia rozciągające nie powodują stwardnienia stopu; na efekt ten wpływa obecność naprężeń, choć ich wpływ na stopień umocnienia może się znacznie różnić. Zbadano również tempo zużycia erozyjnego, traktowane jako czynnik indukujący bardzo złożone zjawiska powierzchniowe w powstających odlewach.

Słowa kluczowe: stopy żelaza, odkształcenia, ścieranie, erozja

TEKA Kom. Mot. Energ. Roln. – OL PAN, 2011, 11, 297–302

APPLICATION OF AN IDUCTIVE CONVERTER FOR MEASURING THE THICKNESS OF ANTI-CORROSION COATINGS IN MACHINES

Pawel Ptak[*], Tadeusz Zloto[**]

*Institute of Telecommunications and Electromagnetic Compatibility
** Institute of Machine Technology and Production Automation
Częstochowa University of Technology

Summary. The paper deals with measuring the thickness of anti-corrosion coatings. We discuss anti-corrosion treatments and various methods of testing them as well as present factors affecting measuring errors of inductive converters. Then, we describe the operation of a transformer inductive converter applied to measuring the thickness of selected anti-corrosion coatings.

Key words: inductive converters, anti-corrosion coating, measuring methods

INTRODUCTION

Corrosion is a problem affecting practically all branches of industry. Despite using more and more effective anti-corrosion treatments corrosion damages are still the most frequent causes of failure or aggravating technological parameters in many machines, devices, or constructions. Non-destructive tests of corrosion damages can contribute significantly towards assessing the technological condition of machines and construction while they are being in use. There exist a number of methods of protecting metallic elements from corrosion, including surface treatments (zinc plating, painting, bitumen coating, and others). Coatings applied for protective or decorative reasons should meet desired parameters of quality, thickness, resistance and looks. Measurements of the thickness of surface coatings are applied in automotive, electronic, metallurgical, plastic, telecommunications, aviation and food industries.

Various types of anti-corrosion treatments have to meet detailed standards concerning their properties, thickness, and testing methods. The method of applying the coating, its thickness, acceptable deviation, and measurements are determined in the technological process. Measurements can be performed by means of a number of devices and methods, which are selected depending on the specific conditions and requirements, such as access to the surface examined and properties of the substrate and coating [Beamish 2000; Biestek, Sękowski 1973; Górecka, Polański 1983; Petrilli 2001].

The measurement methods can be divided into destructive and non-destructive. Destructive methods are more universal and in many cases advantageous, whereas non-destructive methods are

recommended for measuring coating thickness when it is not possible to take a coating sample, or when destroying the coating is not advisable.

The non-destructive methods include magnetic, electromagnetic, inductive, and eddy-current testing. Most thickness gauges typically employ the eddy-current method or inductive methods. One of the most popular gauges is a transformer inductive converter used for measuring the thickness of conducting and non-conducting surface coatings on ferromagnetic substrates [Bronkiewicz, Janiczek, Ptak 2005; Bronkiewicz, Ptak 2005; Lewińska-Romicka 2001a; Lewińska-Romicka 2001b; Petrilli 2001].

APPLICATION OF THE INDUCTIVE CONVERTER FOR MESURING THE THICKNESS OF ANTI-CORROSION COATING

An inductive converter may have a single coil, in which case it is a choke converter, or two or more coils, in which case it is a transformer converter. The windings on the ferromagnetic core are elements of the choke (current transformer) with the open magnetic circuit. It is induced by alternating current of frequency from a few hundred to several thousand Hz. The magnetic circuit of the converter is closed by the coating and substrate examined, and the coating is a gap in the circuit (Fig.1). The signal coming from the inductive converter situated over the area examined depends on a number of parameters. A parameter significantly affecting the signal strength is the distance *d* from the surface tested [Janiczek 2006; Łapiński 1974; Senczyk 1994].

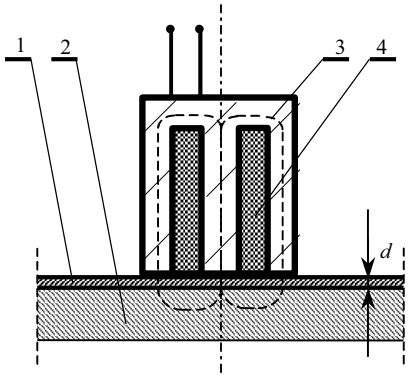

Fig. 1. Inductive converter for measuring the coating thickness; 1 - coating, 2 - substrate, 3 – magnetic flux path, 4 - windings

It can be assumed that the measuring signal corresponding to a given thickness of the coating, such as the voltage U_p for the transformer converter, depends on the quantities characterizing its construction and parameters of the element tested. The dependence can be represented as

$$U_p = f\left(d_w, d_p, \mu_w, \mu_p, \varepsilon_w, \varepsilon_p, f, I, z_1, z_2, k, A\right)$$

where
U_p - the output voltage signal of the converter,
d_w, d_p - the thickness of the coating and substrate, respectively,
μ_w, μ_p - the magnetic permeability of the coating and substrate, respectively,

ε_w, ε_p - the permittivity of the coating and substrate, respectively,
f - the frequency of the current power supply,
I - the amplitude of the power supply (current) signal,
z_1, z_2 - the number of turns in the power supply winding and in the measuring winding,
k - the construction coefficient of the converter,
A - the coefficient related to the dimensions and shape of the sample examined.

It can be therefore assumed that the voltage induced at the secondary winding depends on the coating thickness, magnetic permeability of the substrate, radius of the object curvature, the substrate thickness, area of measurement, coarseness of the surface and distance from the measuring site to the object edge. The output voltage of the inductive measuring converter depends on the coating thickness, electrical conductivity of the substrate, radius of the object curvature, thickness of the substrate, area of measurement, coarseness and distance from the measuring site from the object edge [Beamish 2000; Lewińska-Romicka 2001; Bronkiewicz, Janiczek 2004; May, Morton, Zhou, 2007; Rawa 2001].

FACTORS AFFECTING MEASURING ERRORS IN INDUCTIVE CONVERTERS

Measuring errors accompanying the use of transformer converters typically result from alternations in the feeding voltage and frequency, changes in temperature, non-linearity of characteristics, change in the impedance phase angle, accuracy of the instrument connected to the converter, insufficient sensitivity, or interference by electromagnetic fields. Changes in the feeding voltage and frequency can be usually avoided by using a good quality voltage generator, which is resistant to such kind of interference. Changes in temperature cause changes in the resistance of the windings and in order to eliminate them measuring systems are used with two inductive converters connected differentially. To ensure a sufficient sensitivity of the converter a small gap is used, which may, however, have negative consequences because when the gap is small, a change in its length affects significantly the converter sensitivity. Thus, the gap in the magnetic circuit cannot be too small if it undergoes large changes during the measurement, on the other hand, it cannot be too long to avoid large dissipation of magnetic flux [Bronkiewicz, Janiczek, Ptak 2005; Hull, John 1988; Janiczek, Ptak 2007; Miłek 2006]. The nonlinearity between an electric quantity and a nonelectric one, dependent on the changes in the gap length, can be reduced if the converter operation involves only small changes in the gap length. The magnetic circuits with the differential connection are not fully symmetrical, so errors may result from changes in the impedance phase angle. To minimize the risk of such errors, the two halves of the differential converter should be of identical construction and made of the same materials.

The measuring converter is but an element in the measuring chain so it is also essential to develop an appropriate computational algorithm which would yield the coating thickness.

The number of factors potentially increasing the uncertainty of the measurement is significant. The accuracy can be assessed by theoretical analysis and empirical testing of measuring converters [Biestek, Sękowski 1973; Łapiński 1974; Sajdera 2002; Wilson 2005].

TESTING THE INDUCTIVE TRANSFORMER CONVERTER

The tests of the measuring converter were performed on especially prepared samples with known thickness of the substrate and the coating. The substrates were ferromagnetic and the con-

verter was fed mainly by sinusoidal signals of various frequencies. Test with non-sinusoidal signals were also performed. The coatings were non-ferromagnetic conductors. The aim of the tests was to assess the usefulness and reliability of the measuring converter for measuring coating thickness without carrying out the full calibration procedure.

The tests were intended mainly to assess the performance of the converter on conductive coatings on ferromagnetic substrates. This type of measuring converter was originally designed to operate with amplitude signal, and such signals were mainly used in testing. Figs. 2 and 3 present the amplitudes of the measuring signal depending on the frequency for various thicknesses of aluminum platings and paints.

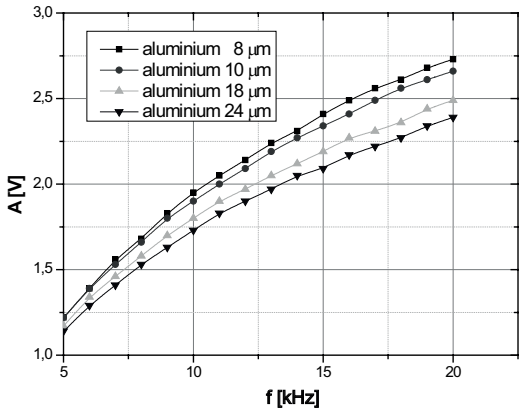

Fig. 2. Amplitudes of the measuring signal for various thicknesses of aluminum platings on 1 mm thick ferromagnetic substrate

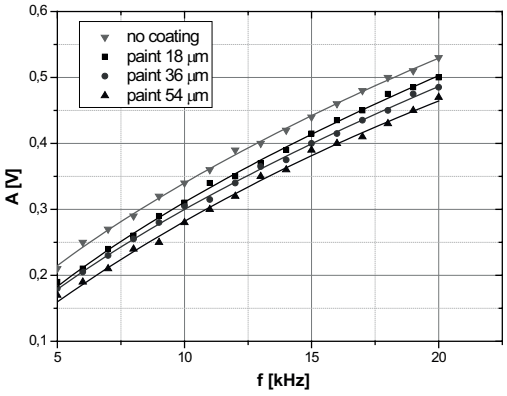

Fig. 3. Amplitudes of the measuring signal for various thicknesses of paints on 1 mm thick ferromagnetic substrate

On the basis of previous studies an instrument was designed for measuring multilayer coatings for testing and diagnostic purposes. This instrument is used for measuring the thickness of the conducting layer, e.g. zinc, together with other protective layers on power industry constructions, or on a car body in automotive industry. The total thickness of the protecting coatings can be measured

by means of the inductive method, but the thickness of the conductive layer cannot be examined in this way because it is covered by non-conductive external coatings, such as paints.

The thickness of the zinc plating under the paint layer was measured by means of the inductive transformer sensor. The tests were performed for zinc platings of 13 μm, 24 μm, 35 μm, 45 μm and 55 μm of thickness on 1mm thick ferromagnetic substrate. The thickness of the external paint was such that the total thickness of the paint and zinc plating was always 70 μm. Because of that it is known that the sensor responds only to the changes in the zinc plating thickness and not to the changes in the two-layer thickness, which is always the same. [Biestek, Sękowski 1973; Łapiński 1974; Sajdera 2002; Wilson 2005]. Fig. 4 presents the values of the voltage signal depending on the frequency for zinc coatings of various thicknesses.

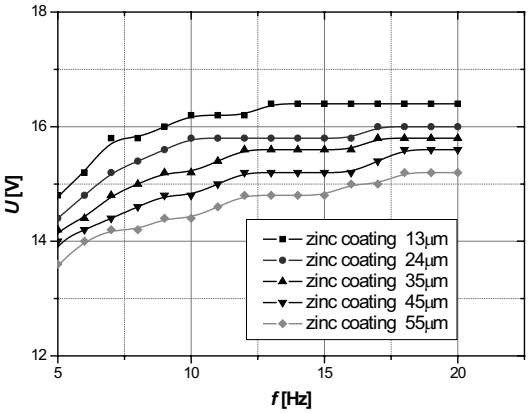

Fig. 4. Dependence of the voltage signal on the frequency for zinc coatings of various thicknesses

CONCLUSIONS

The tests performed on the inductive transformer converter lead to the following conclusions:

1. Using the inductive transformer sensor enables analysis of the zinc coating thickness. Thus, the method described can be applied for assessing corrosion in the conductive protective layer, which is not accessible for examination by means of the classical eddy-current method during exploitation. The measuring signal can be easily adjusted to the measuring probe used.
2. The inductive converter examined can be applied for measuring coatings of small thickness, as compared to the substrate thickness, with measuring signals of frequencies from 10 to 20 kHz. Since the depth of the measuring signal penetration into the coating on a ferromagnetic substrate decreases with increase in frequency, the frequency and amplitude of the signal have to be selected individually for each sample so as to maximize the measurement accuracy.

REFERENCES

Beamish D., 2000: Coating thickness measurement. Metal Finishing, Vol. 98, Issue 6.

Biestek T., Sękowski S., 1973: Metody badań powłok metalowych. Wydawnictwa Naukowo-Techniczne, Warszawa.
Borowik L., Ptak P., 2010: Diagnostyka i monitoring zabezpieczeń antykorozyjnych urządzeń elektroenergetycznych. Śląskie Wiadomości Elektryczne, nr 6, s. 52-55.
Bronkiewicz A., Janiczek R., 2004: Pomiary grubości nieferromagnetycznych warstw wierzchnich na podłożu ferromagnetycznym poprzez magnesowanie podłoża. Przegląd Elektrotechniczny, nr 2, s. 80-84.
Bronkiewicz A., Janiczek R., Ptak P., 2005: Pomiary grubości cienkich warstw. Metody i systemy komputerowe w automatyce i elektrotechnice. Wydawnictwa Politechniki Częstochowskiej, Częstochowa, s.29-32.
Bronkiewicz A., Ptak P., 2005: Wybrane aspekty metrologiczne metody pomiaru grubości warstw wierzchnich na podłożach ferromagnetycznych. Materiały V Krajowej Konferencji PES-5 Postępy w Elektrotechnice Stosowanej, Zakopane-Kościelisko, s. 283-290
Górecka R., Polański Z., 1983: Metrologia warstwy wierzchniej. WNT, Warszawa.
Hull J. B., John V. B., 1988: Non-destructive testing. Macmillan Education, London.
Janiczek R., 2006: Elektryczne miernictwo przemysłowe. Wydawnictwa Politechniki Częstochowskiej, Częstochowa.
Janiczek R., Ptak P., 2007: Przetworniki indukcyjnościowe w pomiarach grubości warstw wierzchnich. (Inductive transducers in measurements of surface layers thickness), Wiadomości Elektrotechniczne, 1 s. 86-90.
Lewińska-Romicka A., 2001a: Pomiary grubości powłok. Biuro Gamma, Warszawa.
Lewińska-Romicka A., 2001b: Badania nieniszczące. Podstawy defektoskopii. WNT, Warszawa.
Łapiński M., 1974: Pomiary elektryczne i elektroniczne wielkości nieelektrycznych. Wydawnictwa Naukowo-Techniczne, Warszawa.
May P., Morton D., Zhou E., 2007: The design of a ferrite-cored probe. Sensors and Actuators, A 136 s. 221-228.
Miłek M., 2006: Pomiary wielkości nieelektrycznych metodami elektrycznymi. Wyd. Politechniki Zielonogórskiej, Zielona Gora.
Petrilli C., 2001: The basics of coating thickness measurement. Metal Finishing, Vol 99, Issue 8, August.
Rawa H., 2001: Elektryczność i magnetyzm w technice. Wydawnictwo Naukowe PWN, Warszawa.
Sajdera N., 2002: Thickness testing. Metal Finishing, Vol 100, Supplement 1, January.
Senczyk D., 1994: Metody badania materiałów. Wyd. Politechniki Poznańskiej, Poznań.
Wilson J., 2005: Sensor Technology Handbook. Newnes, An imprint of Elsevier.

ZASTOSOWANIE PRZETWORNIKA INDUKCYJNEGO DO POMIARU GRUBOŚCI POWŁOK ANTYKOROZYJNYCH MASZYN

Streszczenie. W artykule przedstawiono zagadnienia, dotyczące pomiaru grubości powłok antykorozyjnych. Omówiono sposoby zabezpieczeń antykorozyjnych maszyn oraz metody ich badania przy zastosowaniu różnorodnych metod. Przedstawiono czynniki wpływające na błędy pomiarowe przetworników indukcyjnych. Opisano badania przetwornika indukcyjnego transformatorowego zastosowanego do pomiarów grubości wybranych warstw antykorozyjnych.

Słowa kluczowe: przetworniki indukcyjne, powłoka antykorozyjna, metodyka pomiaru

TEKA Kom. Mot. Energ. Roln. – OL PAN, 2011, 11, 303–316

THE PROBLEM OF PERFORMANCE LIFE OF STRUCTURAL ELEMENTS UNDER THE CONDITIONS OF THERMAL FATIGUE

Andrzej Pytel, Stanisław Pysz

Foundry Research Institute in Cracow, Poland

Summary. The article presents an overview of the underestimated in Poland cast iron with vermicular graphite, which can be successfully used for cast parts of machines and equipment, especially working under the conditions of thermal fatigue. Because the vermicular graphite cast iron is capable of offering much better properties than grey cast iron, it can be interchangeably used to produce various components operating in the automotive industry and as parts of agricultural machines. In addition to the literature data, comparative studies were done by the Foundry Research Institute in the scope of mechanical and thermal fatigue testing, and simulation was carried out for the cast iron with flake and vermicular graphite. Studies have been continued within the framework of the POIG.01.03.01-12-061/08-00 project. The technology being currently developed relates to high quality cast iron with spheroidal and vermicular graphite with and without the addition of alloying elements, particularly to the grade resistant to thermal fatigue. Issues discussed in this article are related with properties of the structural material which the cast iron with vermicular graphite certainly is. Examples of the application of this material should raise interest of the designers, mainly as regards possible use of this cast iron grade for different elements of agricultural machines, offering increased mechanical properties, longer life on performance, and the possibility to reduce the cast wall thickness, thereby reducing also the casting weight and production costs.

Keywords: cast iron with spheroidal graphite, cast iron with flake graphite, cast iron with vermicular graphite, castings for agriculture, computer simulation, mechanical properties, thermal fatigue

INTRODUCTION

The development of industry, particularly of the automotive and engineering applications, and a strong competition in various industrial sectors has forced engineers to develop and produce more advanced and better materials and designers to use them. Due to the use of these materials, it has become possible to increase the durability of structural elements, especially their resistance to the corrosive effects of CO, CO_2, HC, NO_x, and sulphides, which is the subject of numerous studies [1-4]. The weight and manufacturing cost reduction has also become possible, successfully combined with the improved performance qualities of the finished products. Among different alloys, the structural material which currently finds growing application in various sectors of the industry is cast iron. Its popularity has continued unchanged for many years. The development of technique faces an increasing demand for the cast iron of always higher properties. Several

varieties of cast iron have been developed, to mention as an example alloyed cast iron, malleable cast iron, ductile iron, austempered cast iron (ADI) [5-12], as well as cast iron with vermicular graphite [13-28].

In this family, the cast iron with vermicular graphite plays quite a specific role, as it has a number of undeniable advantages compared with grey and ductile irons, and its properties are somewhere between the high quality inoculated grey cast iron and ductile iron. From the historical point of view, the cast iron with vermicular or compacted graphite has been known since 1948, when it was produced for the first time [22, 23]. Because of the narrow range of stable foundry production, a large-scale use of this cast iron for complex parts such as cylinder blocks and heads was not possible until the advanced process control technologies with modern electronic measurement devices and computer systems have been developed [22]. In 2006, a new ISO 16112 standard for cast iron with vermicular graphite, using a combined nomenclature of "Cast iron with compacted (vermicular) graphite", was published. Five distinct types of this cast iron were distinguished, based on the minimum tensile strength of samples taken from the separately cast ingots. The standard distinguishes between the following grades of cast iron: ISO 16112/JV/300 (ferritic) 16112/JV/350 ISO, ISO 16112/JV/400, ISO 16112/JV/450 (pearlitic); ISO 16112/JV/500 (alloyed). This cast iron is increasingly used as a structural material for many different elements, especially in the industry making cars, tractors, agricultural machines and trains, but also in metallurgical and glass industries.

Compared with high-quality cast iron with flake graphite, the cast iron with vermicular graphite is characterised by, among others, the following beneficial features [24]:

- higher tensile strength,
- better toughness and resistance to dynamic loads,
- lower sensitivity to wall thickness (the required mechanical properties are equally well preserved in heavy castings),
- lower tendency to oxidation and swelling at high temperatures,
- better resistance to thermal fatigue.

Compared with the ferritic ductile iron, the vermicular graphite cast iron offers the following advantages:

- lower modulus of elasticity,
- lower coefficient of thermal expansion,
- higher thermal conductivity,
- higher resistance to thermal fatigue during very rapid changes in temperature cycles (heating – cooling),
- higher damping capacity,
- better machinability,
- better castability and lower tendency to the formation of shrinkage cavities,
- lower tendency of castings to deformation at high temperatures and better dimensional stability,
- lower tendency to the formation of hard spots,
- lower environmental pollution when manufactured.

GENERAL CHARACTERISTICS OF VERMICULAR GRAPHITE CAST IRON AS A STRUCTURAL MATERIAL RESISTANT TO THERMAL FATIGUE

Cast iron with vermicular graphite is mainly used for elements which should offer higher properties than the grey cast iron, alloyed grades included, can provide. Higher strength of vermicular graphite cast iron allows the casting wall thickness and hence the weight of castings to be effectively reduced. The main advantage of this material is, however, its high resistance to sudden temperature changes as well as tightness. High functional properties of this material make it applicable for elements of the machinery and equipment operating in the agricultural industry, particularly for high-temperature operation. Cast iron with vermicular graphite is one of the cast materials characterised by proper shape of the graphite precipitates. The precipitates of graphite assume the form intermediate between spheroids and flakes. The technical English literature uses the nomenclature "vermicular graphite cast iron (cast iron with worm-like graphite) or "compacted graphite cast iron"; Germans call it „Gusseisen mit Vermiculargraphit." In short, it is referred to in English literature as CGI, and in German as GGV. The cast iron designation system is included in the Polish Standard PN-EN1560: 2001, while characteristics of the graphite precipitates, the graphite shape reference samples included, are given in PN-EN ISO 945:1999 (the graphite shape reference sample type III in Fig.1 in the standard). Instructions are also available in different countries, which further define and clarify the cast iron with vermicular graphite, for example in Germany this is VDG-Merkblatt W50. In the U.S., the ASTM A842-85 specification is well-known. The basic chemical composition of the vermicular graphite cast iron is usually comprised within the following limits: C = 3,2–3,8%; Si = 2,0–3,2%; Mn = 0,1–0,7%; P up to 0,06%; S up to 0,02%. Depending on the manufacturing process, the cast iron also includes appropriate amounts of elements such as Mg, Ce, Ca, Al, Ti, Y, La. To obtain adequate performance properties, alloying elements such as Cu, Sn, Mo, V, Cr, Sn, etc. are used. The structure of metal matrix can differ, assuming the form of ferritic, ferritic-pearlitic, pearlitic, and also ausferritic (ADI with vermicular graphite.) Figures 1–3 show photographs of various structures of the cast iron with flake graphite, spheroidal graphite, and vermicular graphite (the examinations were performed under an optical microscope); Figure 2 shows a photograph of the vermicular graphite precipitates as seen under the scanning electron microscope.

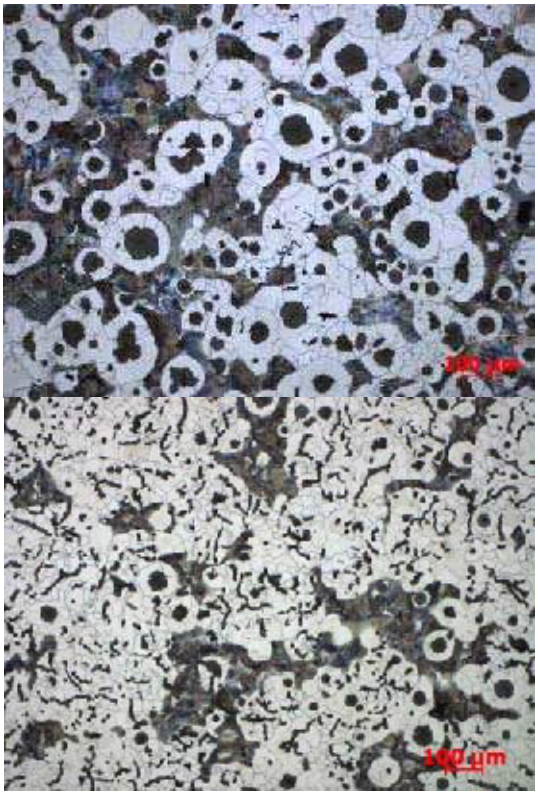

Fig. 1. Cast iron with flake graphite, spheroidal graphite and vermicular graphite

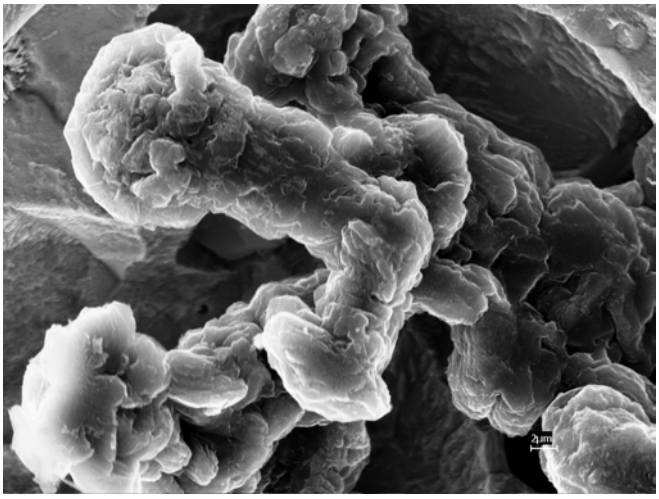

Fig. 2. Vermicular graphite (scanning photograph, 8000x)

The mechanical, physical and technological properties of vermicular graphite cast iron (when controlled by the graphite shape) are somewhere between those that characterise the cast iron with spheroidal graphite and flake graphite. Major parameters of the mechanical, physical, and casting properties of cast iron with different types of graphite and metal matrix are summarised in Table 1 [23, 24].

Table 1. Typical mechanical, physical, and casting properties of the cast iron with flake, spheroidal and vermicular graphite

Selected parameters	Unit	Grey cast iron	Ferritic vermicular graphite cast iron	Pearlitic vermicular graphite cast iron	Ductile iron
Tensile strength, R_m	MPa	100–400	min. 300	400–500	350–900
Yield strength, $R_{p0,2}$	MPa	-	min. 240	340–440	250–600
Elongation, A_5	%	max. 1,5	min. 2	1	3–30
Bending strength	MPa	300–600	600	700	800–1200
Compression strength	MPa	500–1400	min. 500	min. 600	600–1200
Hardness	HB	140–300	130–190	200–280	120–350
Impact strength (unnotched specimen)	J	6–19	max. 10	-	9–196
Impact strength (notched specimen)	J	-	max. 7	-	max. 21
Modulus of elasticity, E_0	GPa	75–155	130–160	130–170	165–185
Density	Mg/m^3	7,0–7,5	7,0	7,1	7,1–7,3
Thermal conductivity, λ (20÷200°)	W/m·K	46 - 59	38–46	34	25–38
Coefficients of linear and thermal expansion, α (20÷200°)	$K^{-1}x10^6$	11–12	11	13	11,3–13
Electrical resistance (20°C)	μΩ·m	0,5–1,0	0,7	0,8	0,5–0,7
Linear shrinkage	%	1,0–1,2	0,9–1,1	0,9–1,1	0,7–1,1
Bulk shrinkage	%	1,0–3,0	1,0–5,0	1–5	7–10

EXAMPLES OF THE APPLICATION OF CAST IRON WITH VERMICULAR GRAPHIT IN INDUSTRY INCLUDING CASTINGS FOR AGRICULTURE

The main directions in the industrial application of cast iron with vermicular graphite are as follows:

a) replacing grey cast iron and reducing casting weight through reduced cast wall cross-sections,

b) replacing alloyed grey cast iron with vermicular graphite cast iron,
c) large-lot production of different thin-walled castings characterised by properties corresponding to ductile iron of medium grade,
d) castings for operation under cyclic temperature changes, subjected to the effect of mechanical stresses.

Cast iron with vermicular graphite has found application for, among others, the following elements:

– castings for the automotive industry: heads, exhaust manifolds, brake discs, brake shoes, crankcases, connecting cables for tractors, hand brake levers [12, 13, 15, 22, 26, 27];
– castings for the shipbuilding industry: heads, covers, and cylinders for diesel engines [12, 13];
– parts of pressure fittings, such as valves, valve bodies, pipes for power hydraulics [26], and distribution systems of different weight for the high-pressure hydraulics [23];
– castings of machine parts: bearing housings, flywheels, gear housings, chain wheels [13];
– castings for the steel industry;
– castings for the automotive and agricultural industries: exhaust manifolds, brake discs, brake shoes, crankcases, connecting cables for tractors [13].

SCOPE AND PURPOSE OF RESEARCH

The aim of the studies was to demonstrate the advantages offered by the cast iron with vermicular graphite, especially as regards its mechanical properties and resistance to thermal fatigue, and possible use of this material for different structural components. The paper gives only a general outline of the research, since in the course of the executed project, an in-depth assessment of the cast materials to know their thermal fatigue behaviour and compare the properties will be possible no sooner than when the special devices for studies of this type are available. Taking the exhaust manifold casting as an example, numerical computations were made for the selected chemical composition of grey and vermicular graphite cast irons.

COMPARATIVE STUDIES OF GREY AND VERMICULAR GRAPHITE CAST IRONS

Cast iron was melted in a Radyne type medium frequency induction furnace in a crucible of 80 kg capacity (basic lining). Cast iron melts were prepared with additions of alloying elements (Mo, Cu, V, Sn, Sb), bearing in mind the fact that these elements affect the mechanical and performance properties of the cast material. Cast iron was poured into bentonite sand moulds in the form of 25 mm thick ingots. For comparative tests, ingots were cast from grey iron (melt no. 5/5882w - Tables 2 and 3) and from vermicular graphite iron (melt nos.: 031, 0.38, 6007). Both cast iron grades had a pearlitic structure.

Studies of the cast iron included:

– analysis of chemical composition,
– observations under the microscope (graphite precipitates, metal matrix structure),
– mechanical properties (R_m, A_5, HB),
– thermal fatigue behaviour,
– numerical computations of selected chemical composition of the grey and vermicular graphite cast irons used for casting of the exhaust manifold.

TESTS AND RESEARCH

The melting process was monitored and samples were taken for spectrographic studies of the chemical composition. The results of the chemical analysis are compiled in Table 2.

Table. 2. Chemical analysis compared for low-alloyed grey cast iron and cast iron after the vermicularising treatment

No.	Melt symbol	Chemical analysis of cast iron, wt.%										
		C	Si	Mn	P	S	Mg	Mo	Cu	V	Sn	**Sb**
1	5/5882w	3,7	1,70	0,23	0,025	0,020	-	0,25	0,34	0,07	0,26	0,031
2	031	3,60	2,35	0,38	0,045	0,015	0,010	0,25	0,33	0,09	0,045	0,031
3	038	3,70	2,30	0,40	0,055	0,020	0,015	0,47	-	0,27	-	0,05
4	6007	3,70	2,30	0,40	0,055	0,020	0,025	0,23	0,35	0,10	0,035	0,031

Note: melt 5/5882w – low-alloyed grey cast iron; melts: 031, 038, 6007 – vermicular graphite cast iron.

After casting of test ingots, specimens for mechanical tests were prepared. Figure 3 shows a specimen for mechanical tests.

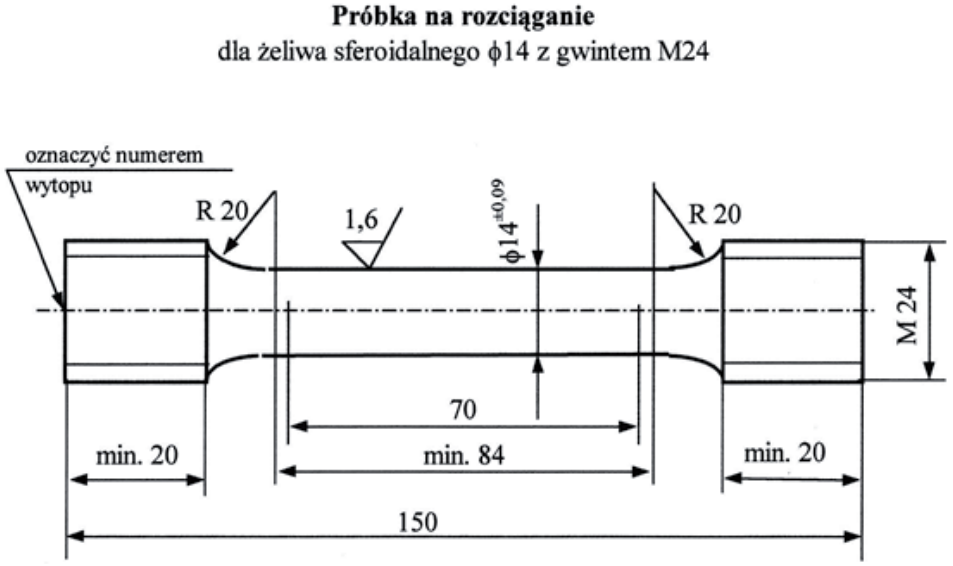

Fig. 3. Specimen for mechanical tests

After fracture of the specimens, the structural examinations of the cast material were carried out. Examples of structures obtained in low-alloyed grey cast iron and in vermicular graphite cast iron are shown in Figures 4 and 5.

Fig. 4. An example of the structure of the tested grey cast iron

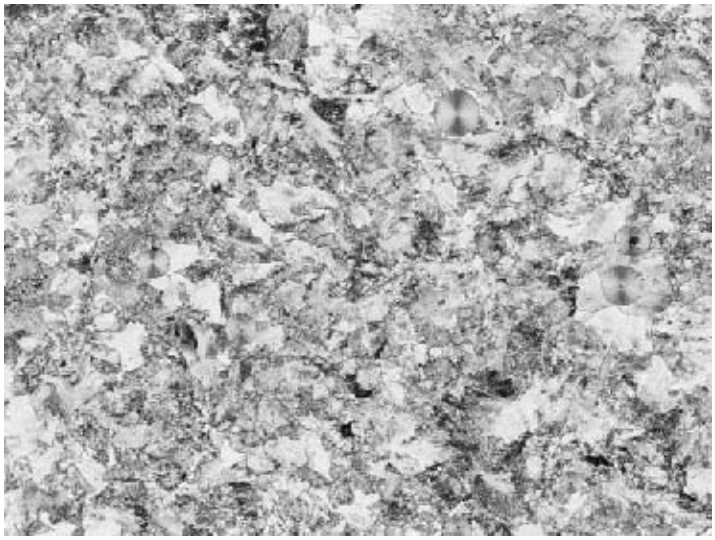

Fig. 5. An example of the structure of the tested vermicular graphite cast iron

The results of the mechanical and thermal fatigue tests of the investigated cast iron are compared in Table 3.

Table 3. The results of the mechanical and thermal fatigue tests of the investigated cast iron

No.	Symbol	Results of mechanical and thermal fatigue tests	Thermal fatigue				
		Tensile strength	Elastic limit	Yield point	Elongation	Hard-ness	Number of cycles, number of fractures
		R_m MPa	$R_{0,2}$ MPa	$R_{0,02}$ MPa	A_5 %	HB	Temperature, °C
							600
1	5/5882w	394	0	-	0	236	60(3p)
2	031	539	413	287	2,57	184	140(1p) 160(2p)
3	038	427	332	202	3,21	268	180(1p) 340(2p)
4	6007	734	522	-	8,1	285	235

Note: sample designation 5/5882 – grey cast iron

The thermal fatigue behaviour of low-alloyed grey cast iron and of the cast iron with vermicular graphite was tested on samples of own design, using a special-purpose device operating automatically in a preset cycle of heating the samples up to a temperature of 600°C and cooling in water at room temperature. The sample is shown in Figure 6, and the device for thermal fatigue testing is shown in Figure 7.

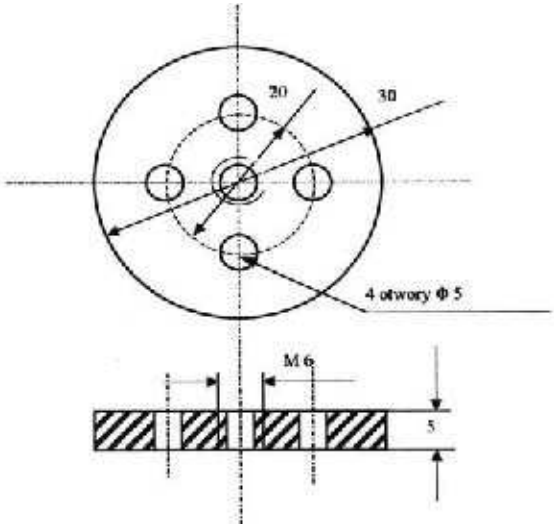

Fig. 6. Sample for thermal fatigue testing

Fig. 7. The device for thermal fatigue testing of metals

Numerical calculations were also performed for the specified chemical composition of cast iron with flake and vermicular graphite, taking as an example the casting of an exhaust manifold. All tests were conducted in accordance with current standards:

- determination of cast iron microstructure: PN-75/H-04661,
- characterisation of graphite precipitates in cast iron: PN-EN ISO 945,
- tensile testing of metallic materials: PN-EN ISO 6892-1,
- Brinell hardness test: PN-EN ISO 6506-1.

NUMERICAL CALCULATIONS PERFORMED FOR THE SPECIFED CHEMICAL COMPOSITION OF CAST IRON WITH FLAKE AND VERMICULAR GRAPHITE SHOWN ON THE EXAMPLE OF A CAST EXHAUST MANIFOLD

The numerical analysis was performed for castings made from the grey and vermicular graphite irons. The potentials offered by MAGMAIron programme were used; the programme allows predicting the final properties of castings basing on the preset boundary parameters. The MAGMAIron module uses a kinetic model of the growth and formation of microstructure, which allows taking into account the local properties of alloy, including thermo-physical changes, especially at the solidification front boundary, as a result of the segregation of elements. The following factors have also been taken into consideration: alloy composition, modification technique, phase

transformations in the solid state, the effect of silicon content on the segregation of elements, as well as the impact of major alloying elements on the solidification mode.

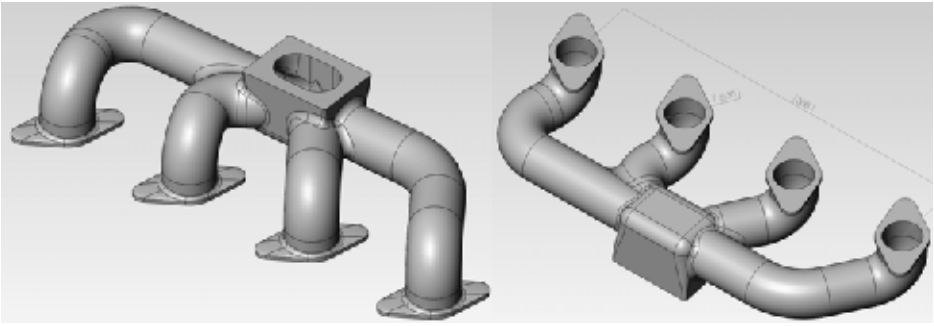

Fig. 8. Drawing of the examined exhaust manifold

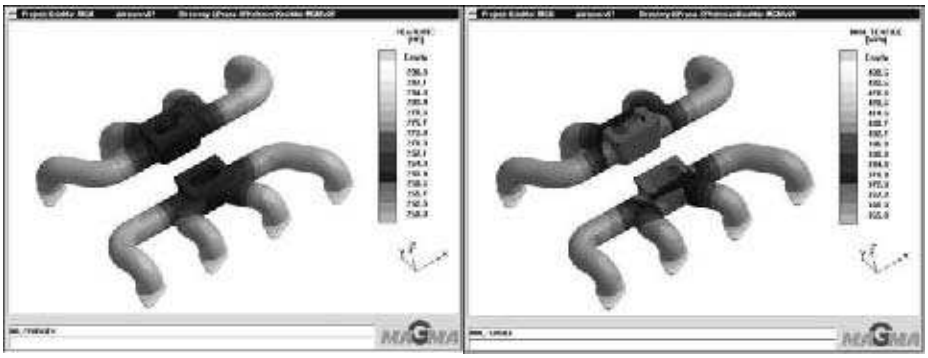

Fig. 9. The distribution of hardness and strength values in grey iron casting

Numerical calculations of the casting process of the exhaust manifold aimed at a determination of the characteristic final properties of the casting allowing for the cast material type (grey cast iron, vermicular graphite cast iron). The form and shape of graphite in the vermicular graphite cast iron determines its final properties. A ramified graphite structure free from the sharp edges increases the strength of the casting matrix. The final properties of iron castings to a large extent depend on the solidification rate. In the case of cast exhaust manifold, thin walls of 4 mm thickness prevail. This part of the grey iron casting has the final strength of about 415 MPa, while casting made of the vermicular graphite iron is capable of reaching in the same place the strength of 800 MPa. Only the area of the exhaust gas take off from the collector, which forms a hot spot, solidifies for a time much longer. Therefore, properties in this area are lower, compared to the area of thin-wall tube and the strength amounts to 370 MPa and 680 MPa for the grey and vermicular graphite cast irons, respectively.

The performed numerical analysis shows that elements operating under the demanding and periodically changing conditions, when made from the vermicular graphite cast iron can considerably prolong the time of their operation.

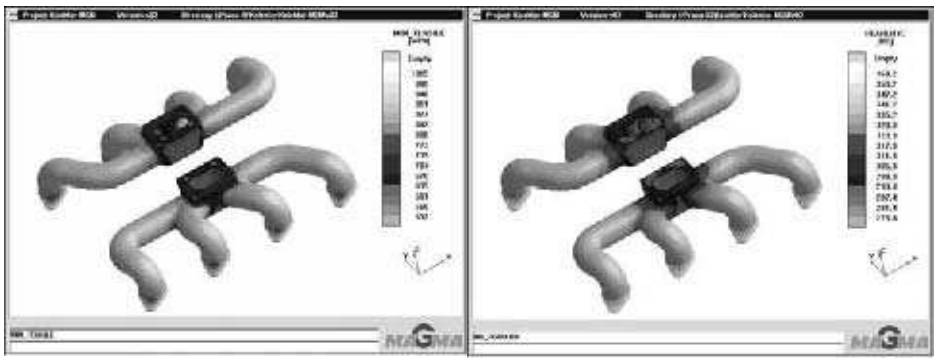

Fig. 10. The distribution of hardness and strength values in vermicular graphite iron casting

RESULTS AND DISCUSSION

Studies of the mechanical properties of low-alloy pearlitic grey cast iron and vermicular graphite cast iron showed the definitely superior properties of the vermicular graphite cast iron. Very high values of the tensile strength (539−734 MPa), elongation A_5 (2,57−8,1), and Brinell hardness (approximately 184–285 HB) were obtained in the cast iron with vermicular graphite. Higher elongation in one set of samples may be due to higher spheroidal graphite content in the structure of cast iron. Low-alloyed cast iron with pearlitic structure and lamellar graphite has the strength of about 394 MPa and a hardness of about 236 HB; the samples showed no elongation.

The microstructure of samples taken from the test ingots showed the pearlitic type cast iron (the amount of pearlite P, P98, P92) with over 70% of vermicular graphite (samples 031, 038 and 6007).

The thermal fatigue tests carried out at a temperature of 600°C confirmed longer life of samples made from the cast iron with vermicular graphite, compared to the cast iron with flake graphite (the number of heating-cooling cycles until the appearance of the first two cracks was 160 to 340 for the vermicular graphite cast iron and about 60 for the three cracks in grey cast iron.

The results provide clear evidence that, compared to grey cast iron, the vermicular graphite cast iron is a material of higher performance characteristics and as such can be successfully used for elements of machines and equipment, including items operating in the agricultural industry.

REFERENCES

Kuranc A.: A Continuous Measurement of CO, CO_2, HC and NO_x At The Work of a combustion engine fed with petrol in nstable thermal conditions, TEKA, Polish Academy of Sciences, 2005, vol. V, s. 107-115.

Kozak M., Merkisz J.: The mechanics of fuel sulphur influence on exhaust emissions from diesel engines, TEKA, Polish Academy of Sciences, 2005, vol. V, s. 96-106.

Wasilewski J.: An analysis of smoke emissions from a rape biofuel fed tractor engine, TEKA, Polish Academy of Sciences, 2006, vol. VI, s. 169-174.

Zając G.: Methyl esters of rape oil as an addition to diesel fuel, TEKA, Polish Academy of Sciences, 2009, vol. IX, s. 407-417.

Janowak J. F., Gundlach R. B.: Development of Ductile Iron for Commercial Austempering. AFS Transactions, 86 (1983), s. 377.

Kovacs B. V.: Heat Treating of Austempered Ductile Iron. AFS Transactions, 99 (1994), s.281.

Kovacs B. V.: On the Terminology and Structure of ADI, AFS Transactions, 102 (1991), s.417.

Brandenberg K. Hayrynen K. L., Keought J. R.: Austempered gears and shafs tough solutions, Applied Process Inc. Technologies Div. Livonia, Michigan, USA.

Kowalski A., Pytel A., Turzyński J.: Properties and application of new types of ausferritic cast iron. Conference Proceedings. Slovenian Fundrymen Society. Faculty of Natural Sciences and Engineering, University of Liubliana, Portoroż 12-13 September 2007.

Pirowski Z., Gościański M.: Konstrukcja i technologia wytwarzania odlewanych lemieszy do pługów obracalnych i zagonowych, MOTROL – Motoryzacja i Energetyka Rolnictwa, Lublin 2009; t. 11, s. 159-167.

Podrzucki C.: Problemy produkcji odlewów z żeliwa sferoidalnego ADI, Przegląd Odlewnictwa, 10 (1966), s. 260.

Guzik E.: Żeliwo ausferrytyczne na walce hutnicze. Konferencja Naukowo-Techniczna nt. „Kierunki rozwoju produkcji walców". Wisła-Malinka 21-23 02. 2001, s. 87.

Guzik E.: Procesy uszlachetniania żeliwa. Wybrane Zagadnienia, Archiwum Odlewnictwa, Katowice (2001) 85-89.

Podrzucki C.: Żeliwo – struktura, właściwości, zastosowanie. Tom 1 i 2, Wyd. ZG STOP, Kraków (1991).

Zych J.: Wpływ molibdenu na odporność na zmęczenie cieplne żeliwa z grafitem płatkowym, wermikularnym i sferoidalnym, XX Konferencja Wydziału Odlewnictwa AGH, Kraków (1995) 93-98.

Dawson S.: Compacted graphite iron a material solution for modern diesel engine cylinder blocks and heads. SinterCast, Sweden, China Foundry, Vol.6 no. 3, (8/2009) 241-246.

Pietrowski S.: Kompendium wiedzy o żeliwie wermikularnym, Krzepnięcie Metali i Stopów, Rocznik 2, Nr 44, PAN Katowice (2000), s. 279-292.

Pytel A., Sękowski K.: Perlitic VermicularGraphite Cast Iron, International Conference on Advances in Materials and processing Technologies, AMPT 99, Dublin, Ireland (1999), s. 1381-1388.

Pytel A.: Zmęczenie cieplne i przemiana eutektoidalna żeliwa niskostopowego z grafitem wermikularnym. Międzynarodowa Konferencja Naukowa, Żeliwo sferoidalne XXI wieku, Instytut Odlewnictwa, Kraków (2003), II/49-II56.

Sjögren T.: Influences of the graphite phase on Elastic and plastic deformation behaviour of cast irons; Department of Mechanical Engineering Component Technology – Castings School of Engineering, Jönköping University (2007).

Warrick R.J., G.G. Ellis G.G.: Development and application of enhanced compacted graphite iron for the bedplate of the new chrysler 4.7 liter v-8 engine" ; International Congress and Exposition Detroit, Michigan March 1-4, (1999).

Dawson S., Zhang F.: Compacted graphite iron - a material solution for modern diesel engine cylinder blocks and heads. Proceedings of 69th World Foundry Congress. 16-20 October 2010, Hangzhou China, s. 0359 - 0364.

Dawson S., Schroeder T.: Practical Applications for Compacted Graphite Iron AFS Transactions 2004, American Foundry Society, Des Plaines IL USA, s. 1-9.

Nechtelberger E., Puhr H. i in.: Cast Iron with Vermicular/compacted Graphite-State of the Art. Development, Production, Properties, Applications. 49kongres Odlewniczy Chicago, 1982, ref. Nr1.

Sternkopf J.: Statische und dynamische Festigkeitseigenschaften von Gusseisen mit Vermikulargraphit. Giessereitechnik, 1985, nr 9.

Nechtelberger E. i inni.: Stand und Entwicklung von Gusseisen mit Vermiculargraphit Herstellung, Eigenshaften und Anwendung. Giesserei-Praxis, 1982, nr 22.
Palmer P. V.: Future of cast metal. Foundry Trade Journal, 151 (1981), nr 3223, s. 574.
Zakharkenko E. V., Levchenko J. i in.: Otlivki iz chunguna s sharowidnym vermikularnym grafitom. Kiev. Naukowa Dumka, 1986.

This work was supported by Structural Funds operating under the Operational Programme Innovative Economy for the years 2007–2013, Measure 1.3.

ZAGADNIENIE TRWAŁOŚCI ELEMENTÓW KONSTRUKCYJNYCH PRACUJĄCYCH W WARUNKACH ZMĘCZENIA CIEPLNEGO

Streszczenie. W artykule przedstawiono ogólne dane na temat niedocenianego w kraju żeliwa z grafitem wermikularnym, które z powodzeniem nadaje się na odlewy elementów maszyn i urządzeń, szczególnie pracujących w warunkach zmęczenia cieplnego. Ponieważ żeliwo to ma lepsze właściwości od żeliwa szarego może być zamiennie wykorzystane do produkcji różnych elementów w przemyśle motoryzacyjnym i budowy maszyn dla rolnictwa. Oprócz danych literaturowych przedstawiono zarys badań porównawczych wykonanych w Instytucie Odlewnictwa w zakresie badań mechanicznych, zmęczenia cieplnego i symulacyjnych dla żeliwa z grafitem płatkowym i wermikularnym. Prace są w dalszym ciągu kontynuowane w ramach prowadzonego projektu POIG.01.03.01-12-061/08-00. Rozwijana obecnie technologia dotyczy żeliwa wysokojakościowego sferoidalnego i wermikularnego bez dodatków i z dodatkiem pierwiastków stopowych, szczególnie odpornego na zmęczenie cieplne. Przedstawione w artykule zagadnienia właściwości materiału konstrukcyjnego jakim jest żeliwo z grafitem wermikularnym i przykłady zastosowania tego tworzywa powinny wzbudzić zainteresowanie konstruktorów do wykorzystania tego tworzywa również na różne elementy maszyn rolniczych, powodując zwiększenie właściwości wytrzymałościowych odlewnych elementów, trwałości a także możliwości obniżenia grubości ścianek odlewów, a tym samym zmniejszenia ich masy i obniżenia kosztów produkcji.

Słowa kluczowe: żeliwo sferoidalne, żeliwo z grafitem płatkowym, żeliwo z grafitem wermikularnym, odlewy dla rolnictwa, symulacja komputerowa, właściwości mechaniczne, zmęczenie cieplne.

TEKA Kom. Mot. Energ. Roln. – OL PAN, 2011, 11, 317–325

MOISTURE INFLUENCE ON THE UNITARY ENERGY OF A CUTTING PROCESS OF SELECTED ENERGY PLANTS

Henryk Rode, Paweł Witkowski

Warsaw University of Technology
Faculty of Civil Engineering, Mechanics and Petrochemistry
Department of Mechanical Systems Engineering and Automation
Address: Al. Jachowicza 2/4, 09–402 Płock, Poland; e-mail: hrode@op.pl

Summary. Research results of a cutting process of selected energy plants are presented in the following case study. The study also presents the influence of a plant's moisture on the unitary energy of cutting the stems, with various diameters, of the following energy plants: Salix viminalis, Sida Hermaphrodita, Miskanthus Giganteus, Reynoutria sachalinesis and Topinambour.

Key words: cutting process, energy plants, unitary energy of cutting, moisture

INTRODUCTION

The rigorous requirements concerning environmental protection, as well as the search for ecological and cheap sources of energy cause the fact that the cultivation of energy plants is becoming more and more popular [Dreszer et al. 2003, Gradzik et al. 2003]. These plants, while being burnt, emit not much sulphur dioxide into the atmosphere and the carbon dioxide balance is almost zero because it is absorbed during the plants' growth [Grzybek 2002].The weight of the ash left after the burning process is twenty times lower. The expected and systematic increase of energy plants plantations causes the fact that the problem of the harvest and processing, which also means cutting process of the plants, is becoming quite significant. The knowledge about the influence of such factors as geometric dimensions, moisture and morphological constitution on the unitary energy of the cutting process is necessary for proper design and optimalization of this process [Frączek, Mudryk 2006, Górski 2001, Kowalski 1993, Kwaśniewski et al. 2006, Popko, Miszczuk 1989, Szymanek 2007]. It is of vital importance for the proper functioning of agricultural machines' cutting units.

THE PURPOSE OF THE RESEARCH

The cutting process of plants has been researched for many years at the Institute of Mechanical Engineering Warsaw University of Technology in Płock [Żuk 1979, Żuk 1986, Żuk, Rode 1992,]. The influence of selected parameters of the cutting unit and the plant's constitution and condition

on the quality of the cutting process and its power-consumption has mainly been concerned in the above mentioned research [Rode 2008, Rode, Szpetulski 2010].

The aim of the latest research was to determine the influence of the moisture of the selected energy plants on the power-consumption of their cutting process. The research was carried out with the usage of a laboratory station, constructed for this purpose, at the Institute of Mechanical Engineering Warsaw University of Technology in Płock. The research of the energy plants' cutting process included determining unitary energy of the cutting process of plants' stems with different diameters, without forks and with different moisture.

The notion unitary energy means the total energy needed for the realisation of the cutting process falling on the unit area of the section of the cut plant.

THE SUBJECT OF STUDY

The plants characterized by high biomass increase, high resistance to diseases and pests and with low soil requirements are cultivated for energy purposes [Baran et al. 2007, Dubas et al. 2004]. According to this, energy willow (Salix viminalis), Sida Hermaphrodita, Miskanthus Giganteus, Reynoutria sachalinesis and Topinambour were selected as representatives of such plants.

Salix viminalis is an energy willow species. It is characterized by a quick increase of timber mass (about 14 times bigger than in case of naturally grown forests) [Juliszewski et al.2006, Rudko, Stasiak 2004, Szczukowski et al.2002, Szczukowski et al.2004]. It is also characterized by very high fuel value. Its other advantages are low soil requirements, easy vegetative reproduction (shoots), resistance to frost and pests and low fertilizer and pesticides requirements (possibility of fertilization with sludge). The willow's sprouts achieve the height of even 7 metres, which is why it is the best to process them into silvers, briquettes and pellets, and then burn them in stoves. The ash weigh does not exceed 1% of the burnt weight. Moreover, it also functions as phytoremediation – soil and water natural purification of heavy metals and other chemical combinations.

Fig. 1. View of Salix viminalis' stem in a cross-section

Sida Hermaphrodita is a perennial plant with a big increase of timber mass, especially in the first year of growth. It is cultivated mainly for energy purposes, for reclamation of chemically degraded soil or in roadsides protecting other crops from transport pollution. It is also used as a raw material in pulp and paper industry. It is characterized by high resistance to soil and climate requirements. It reproduces generatively (seeds) or by vegetation (shoots) [Rutkowski 2006].

Fig. 2. View of Sida Hermaphrodita's stem in a cross-section

Miskanthus Giganteus is a grass. It has stiff blades filled with spongy core. The blades reach the height of 250 cm (great timber mass increase). It is resistant to diseases and pests. The grass does not tolerate waterlogged and marshy ground. It reproduces by vegetation (shoots) [Rutkowski 2006].

Fig. 3. View of Miskanthus Giganteus' stem in a cross-section

Reynoutria sachalinesis is a perennial plant with expansive nature. It grows to 300 cm. The empty stems look like bamboo shoots. It is characterized by great biomass increase and fuel value. Up to 580 GJ of energy can be obtained from 1 ha of crop. It accumulates heavy metals from soil. It grows in riverside bushes and flood meadows [Burnie 2005].

Fig. 4. View of Reynoutria sachalinesis' stem in a cross-section

Topinambour is a perennial plant growing to 350 cm. It is cultivated for its tubers, for alcohol and silage, and also for energy purposes. It grows on every soil and is resistant to temperature changes [Burnie 2005].

Fig. 5. View of Topinambour's stem in a cross-section

The researched plants came from the Experimental Station at the Faculty of Agriculture and Biology – University of Life Sciences in Skierniewice [Experimental Station of The Faculty of Agriculture at SGGW].

RESEARCH STATION AND THE COURSE OF RESEARCH

Research station for cutting process research is located in the laboratory at the Warsaw University of Technology in Płock [Rode, Szpetulski 2010]. It is a measuring device of pendulous type. During the cutting the plant sample is hold by the holder and is cut by a knife attached at the end of the pendulum. During the research a potential initial and final energy of the pendulum with the knife is determined. The result of a subtraction of initial and final energy determines the energy of cutting.

The plants from the plantation were selected at random. Then, they were selected according to their diameters, moisture and forks. The samples for cutting, 8 cm long, with different diameters and without forks, were prepared from the stems of energy plants. Each measurement was carried out at least 7 times [Mulas, Rumianowski 1997]. The cutting of the plant took place with the following parameters: knife velocity V = 4,7 m/s, knife edge thickness = 100 μm, type of knife edge: even with a cut from the top, knife edge angle $\alpha = 26°30'$.

RESEARCH RESULTS

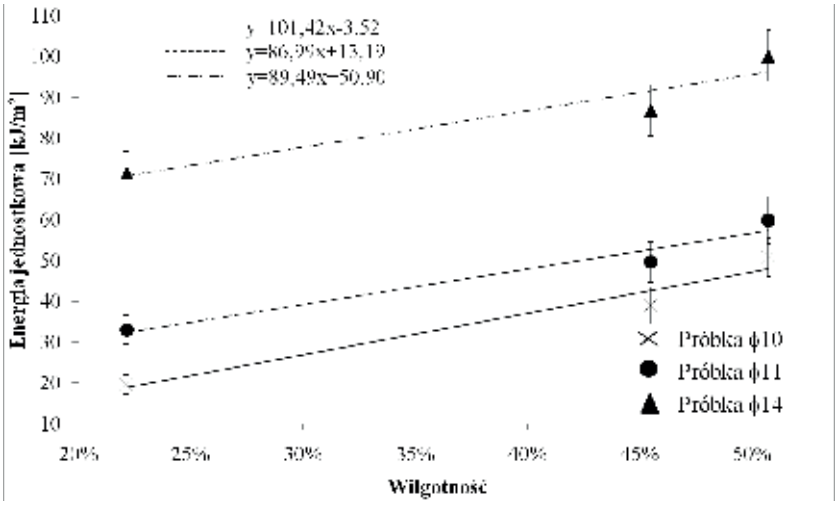

Legend: energia jednostkowa [kJ/m^2] – unitary energy, wilgotność – moisture, x- sample Ø10, ● sample Ø 11, ▲ sample Ø 14

Fig. 6. Comparison of the course of changes of unitary energy (in moisture function) of cutting the Salix viminalis's stem for 3 different diameters

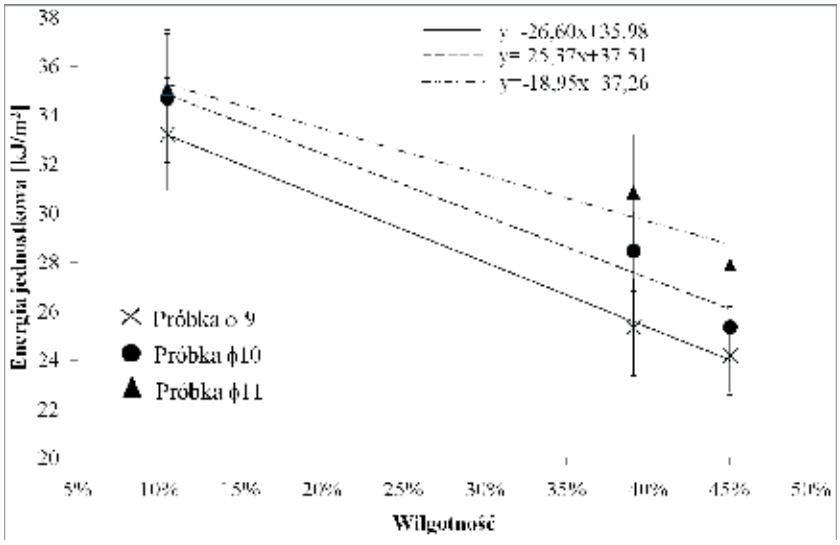

Legend: energia jednostkowa [kJ/m^2] – unitary energy, wilgotność – moisture, x- sample Ø9, ● sample Ø 10, ▲ sample Ø 11

Fig. 7. Comparison of the course of changes of unitary energy (in moisture function) of cutting the Sida Hermaphrodita's stem for 3 different diameters

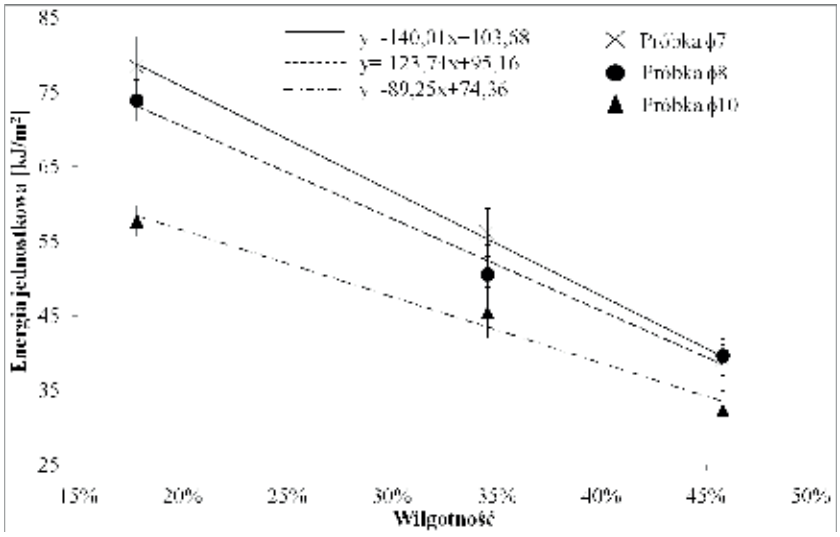

Legend: energia jednostkowa [kJ/m^2] – unitary energy, wilgotność – moisture, x- sample Ø7, ● sample Ø 8, ▲ sample Ø 10

Fig. 8. Comparison of the course of changes of unitary energy (in moisture function) of cutting the Miskanthus' stem for 3 different diameters

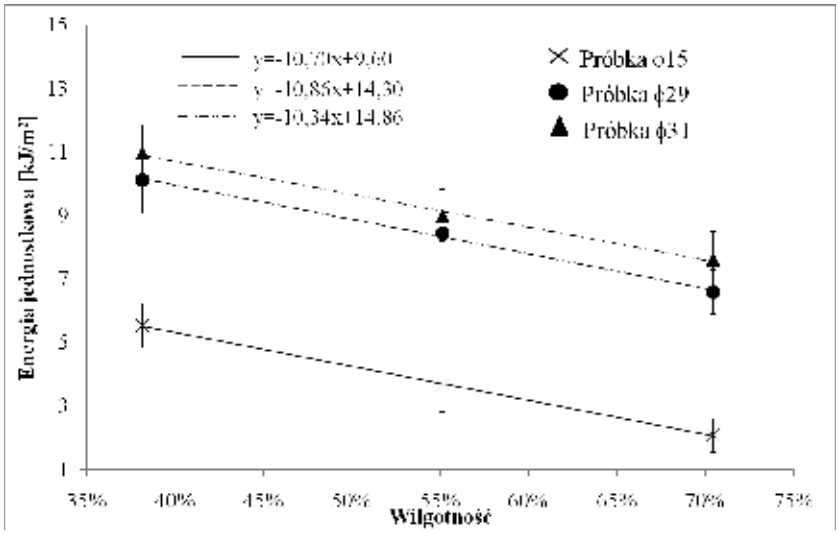

Legend: energia jednostkowa [kJ/m^2] – unitary energy, wilgotność – moisture, x- sample Ø15, ● sample Ø 29, ▲ sample Ø 31

Fig. 9. Comparison of the course of changes of unitary energy (in moisture function) of cutting the Reynoutria sachalinesis' stem for 3 different diameters

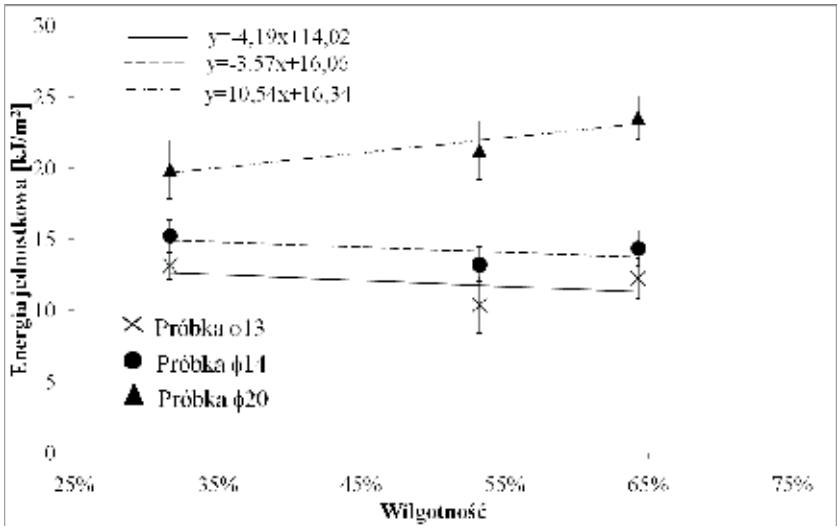

Legend: energia jednostkowa [kJ/m^2] – unitary energy, wilgotność – moisture, x- sample Ø13, ● sample Ø 14, ▲ sample Ø 20

Fig. 10. Comparison of the course of changes of unitary energy (in moisture function) of cutting the Topinambour's stem for 3 different diameters

CONCLUSIONS

1. For stems of Salix viminalis the unitary energy increases together with moisture increase. It is independent from the stems' diameter. It may be connected with the plant's constitution. In the Salix viminalis' stem's cross-section the fibrous tissue is the greatest in terms of percentage.
2. Topinamour moisture increase does not change the unitary energy of cutting process regardless of the stem's diameter. Topinambour's stem has a full cross-section.
3. The increase of moisture in the remaining plants researched has an impact on the unitary energy decrease. It may result from the fact that there is less energy needed for crushing the plants and also from the epidermis and fibrous tissues cutting resistance. Those plants' stems' cross-sections are as those of a pipe.
4. The energy of cutting of the plant decreases rapidly when the plant breaks.
5. The measurement results show, that the moisture has a significant impact on the unitary energy of cutting the plant. The less fulfilled the plant's stem is, the greater influence of moisture there is.

REFERENCES

Baran D., Kwaśniewski D., Mudryk K. 2007: Wybrane właściwości fizyczne trzyletniej wierzby energetycznej. Inżynieria Rolnicza, nr 8(96), s. 7-12.

Burnie G. i inni, 2005: Botanica. Rośliny ogrodowe. Kónemann.

Dreszer K., Michałek R., Roszkowski A. 2003: Energia odnawialna – możliwości jej pozyskiwania i wykorzystania w rolnictwie. Wydawnictwo PTIR, Kraków – Lublin –Warszawa.

Dubas J., Grzybek A., Kotowski W., Tomczyk A. 2004: Wierzba energetyczna – uprawa i technologie przetwarzania. Wyższa Szkoła Ekonomii i Administracji. Bytom.

Frączek J., Mudryk K. 2006: Metoda określenia oporów cięcia pędów wierzby energetycznej. Inżynieria Rolnicza, nr 8(83), s. 91-98.

Górski J. 2001: Proces ciecia drewna elektryczną pilarką. Rozprawy Naukowe i Monografie. Wydawnictwo SGGW, Warszawa.

Gradzik P., Grzybek A., Kowalczyk K., Kościk B. 2003: Biopaliwa. Warszawa.

Grzybek A. 2002: Biomasa jako alternatywne źródło energii. Warszawa.

Juliszewski T., Kwaśniewski D., Baran D. 2006: Wpływ wybranych czynników na przyrosty wierzby energetycznej. Inżynieria Rolnicza, nr 12(87), Kraków, s. 225-232.

Kowalski S. 1993: Badania oporów cięcia wybranych roślin. Zeszyt Prob. Post. Nauk Rol. 408, s. 297- 303.

Kwaśniewski D., Mudryk K., Wróbel M., 2006: Zbiór wierzby energetycznej z użyciem piły łańcuchowej. Inżynieria Rolnicza, nr 13(88), s. 271-276.

Mulas E., Rumianowski R. 1997: Rachunek niepewności pomiaru. WPW, Warszawa.

Popko H., Miszczuk M. 2004: Badania oporów krajania niektórych produktów spożywczych.. Zeszyt Prob. Post. Nauk Rol. 354.

Rode H. 2008: Badania procesu cięcia wybranych roślin energetycznych, Rozdział w monografii Wybrane zagadnienia mechaniki w budowie urządzeń technicznych. s. 286-297. Politechnika Warszawska, Płock.

Rode H., Szpetulski J. 2010: The study of the willow viminalis cutting process. Bioagrotechnikal Systems Engineering. vol.6(22), Płock, s. 63-75.

Rudko T., Stasiak M. 2004: Właściwości mechaniczne pędów wierzby energetycznej. III Zjazd Naukowy. Referaty i doniesienia. Dąbrowice 27-29. 09.2004.
Rutkowski L.2006:Klucz do oznaczania roślin naczyniowych Polski niżowej. Wyd. Naukowe PWN, Warszawa.
Szczukowski S., Tworkowski J., Stolarski M.J. 2004. Wierzba energetyczna. Wydawnictwo Plantpress Sp. z o.o., Kraków.
Szczukowski S., Tworkowski J., Wiwart M., Przyborowski J. 2002: Wiklina (Salix Sp.) Uprawa i możliwości wykorzystania. Wydawnictwo Uniwersytetu Warmińsko-Mazurskiego, Olsztyn.
Szymanek M. 2007: Analysis of cutting process of plant material. Teka Komisji Motoryzacji i Energetyki Rolnictwa – OL PAN, VIIA, s.107-113.
Żuk D. 1979: Określenie koniecznej prędkości elementów tnących w maszynach do ścinania źdźbeł i łodyg. Maszyny i Ciągniki Rolnicze nr 3/1979. Warszawa.
Żuk D. 1986: Proces cięcia źdźbeł zbóż. Prace Naukowe Politechniki Warszawskiej - Mechanika z. 95. Warszawa.
Żuk D., Rode H. 1992: Propozycje oceny energetycznej zespołów tnących. Prace Naukowe Politechniki Warszawskiej - Mechanika z. 152. Warszawa.

WPŁYW WILGOTNOŚCI NA ENERGIĘ JEDNOSTKOWĄ CIĘCIA WYBRANYCH ROŚLIN ENERGETYCZNYCH

Streszczenie. W pracy omówiono wyniki badań procesu cięcia wybranych roślin energetycznych. Omówiono wpływ wilgotności rośliny na energię jednostkową cięcia łodyg wierzby konopianej, ślazowca pensylwańskiego, miskantusa olbrzymiego, rdestu sachalińskiego oraz topinamburu o różnych średnicach.

Słowa kluczowe: proces cięcia, rośliny energetyczne, energia jednostkowa cięcia, wilgotnośc

TEKA Kom. Mot. Energ. Roln. – OL PAN, 2011, 11, 326–334

THE ENERGY OF A CUTTING PROCESS OF A SELECTED ENERGY PLANT

Henryk Rode

Warsaw University of Technology
Faculty of Civil Engineering, Mechanics and Petrochemistry
Department of Mechanical Systems Engineering and Automatization
Address: Al. Jachowicza 2/4, 09–402 Płock, Poland, e-mail: hrode@op.pl

Summary. Research results of a cutting process of a selected energy plant are presented in the following case study. The unitary energy of cutting stems of the multiple flowers rose with different diameters, moisture and at places on stem with and without forks was determined. The unitary energy of cutting the particular plant tissues (epidermis, fibrous, ground) was also determined.

Key words: cutting process, energy plants, unitary energy of cutting process, multiple flowers rose (Rosa multiflora)

INTRODUCTION

The correct organization of energy plant cultivation, harvest, processing and distribution requires a great knowledge not only of the plants' thermo-chemical properties but also of their mechanical properties [Frączek, Mudryk 2006]. These properties determine most of the technological processes. They have an impact on the energy consumption of the harvest and treatment processes. They also determine the construction of particular working units of agricultural machines [Kowalski 1993, Popko, Miszczuk 1989, Szot & others 1987]. The knowledge about unitary energy of cutting and the influence of determining factors such as: geometric dimensions, moisture and morphological constitution are necessary for the proper design and optimisation of any energy plant's cutting process. It is of vital importance for the proper functioning of agricultural machines' cutting units.

A laboratory station at the Institute of Mechanical Engineering - Technical University of Warsaw was built [Rode, Szpetulski 2010] in order to determine the impact of selected constructional parameters and functional cutting units used in agriculture as well as to determine the plants' properties influence on the cutting process and the quality of section. The research results will allow a better study of the energy plants cutting process and, simultaneously, will help with the optimal choice of functional and constructional parameters of functional cutting units used in agricultural machines [Szymanek 2007]. This issue is very significant at present, due to the

fact that the renewable energy received from energy plants cultivation is getting more and more important nowadays.

TESTING METHODS

The plant cutting process has been researched for many years at the Institute of Mechanical Engineering - Technical University of Warsaw in Płock [Rode 1994, Żuk 1979, Żuk 1986, Żuk 1999, Rode 1992, Żuk and Rode 1999]. The research mainly concerns the cutting unit parameters and the plants' constitution and condition impact on the cutting process and its energy consumption [Rode 2008].

The aim of the latest research was to determine the influence of the geometric dimensions and morphological constitution of selected energy plants' parameters on the energy consumption of the cutting process of these plants. The research was carried out with the usage of a laboratory station at the Institute of Mechanical Engineering - Technical University of Warsaw in Płock, which was built especially for this purpose.

The research of the energy plants' cutting process included:

- Determining unitary energy of the cutting process of plant's stems with different diameters, without forks and different moisture.
- Determining unitary energy of the cutting process of plant's stems on forks.
- Determining unitary energy of the cutting process of plant's particular tissues: epidermis, fibrous and ground.

The notion unitary energy means the total energy needed for the realisation of the cutting process falling on the unit area of the section of the cut plant.

The plants characterized by high biomass increase, high resistance to diseases and pests and with low soil requirements are cultivated for energy purposes [Baran & others 2007, Dubas & others 2004]. According to this, multiple flowers rose (Rosa multiflora) was selected as a representative of such plants.

Multiple flowers rose (Rosa multiflora) is a scrambling shrub. It is less popular and known than the energy willow [Juliszewski & others 2006, Rudko, Stasiak 2004, Szczukowski & others 2004]. Its recurved stems achieve the height of 4 – 7 meters. This species has low requirements as far as the climate and soil are concerned. Multiple flowers rose tolerates sandy soils class V and VI. It even grows on dunes. Its great advantage is its high resistance to weather, low temperatures and drought. The characteristic feature of this plant is its great annual biomass increase – up to 20t per hectare. Multiple flowers rose is commonly used for soil reclamation of soils subjected to (wind and water) erosion. The plants came from the Experimental Station at the Faculty of Agriculture and Biology – University of Life Sciences in Skierniewice [Stacja Doświadczalna Wydziału Rolnictwa SGGW].

Fig. 1. A stem of multiple flowers rose after cutting at the place without forks

Fig. 2. A stem of multiple flowers rose after cutting at the place with fork

RESEARCH STATION

Research station for the cutting process research, Fig. 3, is located in the laboratory at the Department of Mechanical Systems Engineering and Automation of the Institute of Mechanical Engineering - Technical University of Warsaw in Płock. The measuring device of pendulous type is constructed from the main plate (2) with a mast with frame (1) attached. The mast at its higher part has a pocket of shaft rotating together with the pendulum (3), to which a knife (4) is attached. A stop dog (6) serves to block the pendulum (3) in horizontal position. The main plate (2) is put on adjustable feet (7), which help with levelling the device. On the main plate, a holder of plant sample with fastening handwheel (5) is fixed. Rotary disk (8) attached to the shaft of the pendulum (3) cooperates with linear transducer, which reads the voltage value of electric signal. The transducer (9) is an electromechanical device, which changes linear motion into electric signal proportional to the shift. The linear motion is transmitted in the transducer onto a turn of a measuring drum. The signal is measured at the frequency of 400 Hz and, then, is recorded in the memory of digital recording device equipped with measurement display (10). The plant sample is hold by the holder with fastening handwheel during the cutting. The plant is cut by a knife attached at the end of the pendulum. During the research a potential initial and final energy of the pendulum with the knife is determined. The result of a subtraction of initial and final energy determines the energy of cutting.

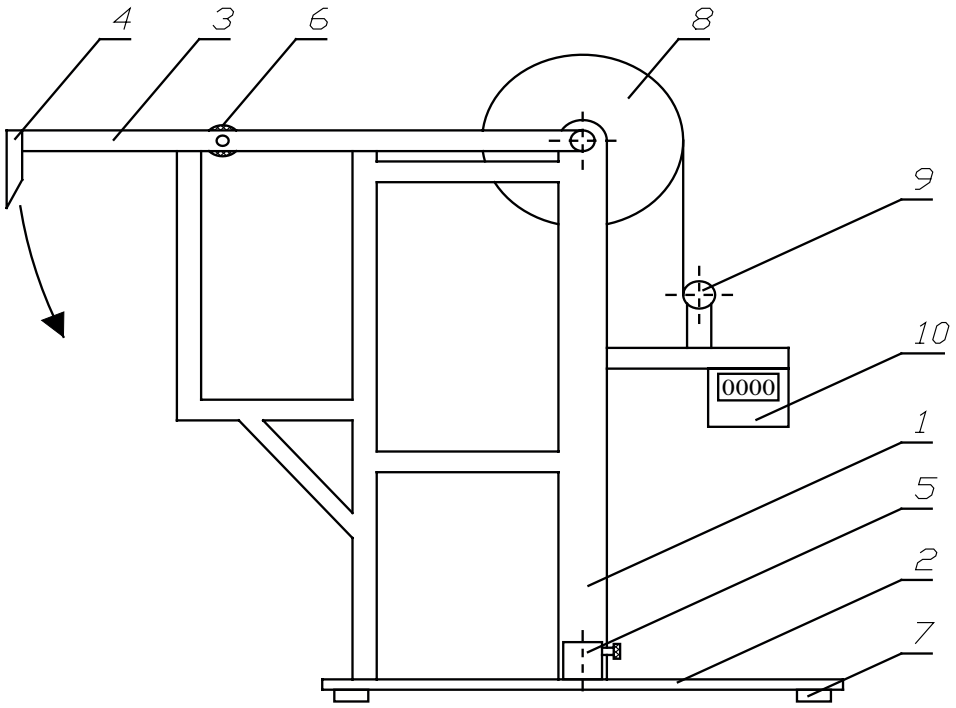

Fig. 3. Measuring device of pendulous type: 1 – mast with frame, 2 – main plate, 3 pendulum, 4 - knife, 5 – holder of plant sample with fastening handwheel, 6 – stop dog, 7 – adjustable foot, 8-rotary disk, 9 – linear transducer, 10 – digital recording device.

THE RESEARCH

The plants from the plantation were selected at random. Then, they were selected according to their diameters and forks. The samples for cutting, 8 cm long, with different diameters and with and without forks, were prepared from the stems of energy plants.

The measurement of the energy of cutting of plant samples without forks and with forks at the place of cutting were carried out, as well as the measurement of the energy of cutting particular tissues of the plant. Each measurement was carried out at least 7 times [Mulas, Rumianowski 1997]. The temperature, where the research took place, was 20^{o}C and atmospheric pressure was 1020 hPa. The plant moisture was measured by electronic moisture analyzer SARTORIUS MA 30.

The cutting of the plant took place with the following parameters: knife velocity V = 4,7 m/s, knife edge thickness = 100 μm, type of knife edge: even with a cut from the top, knife edge angle α = 26°30'.

MEASUREMENT RESULTS

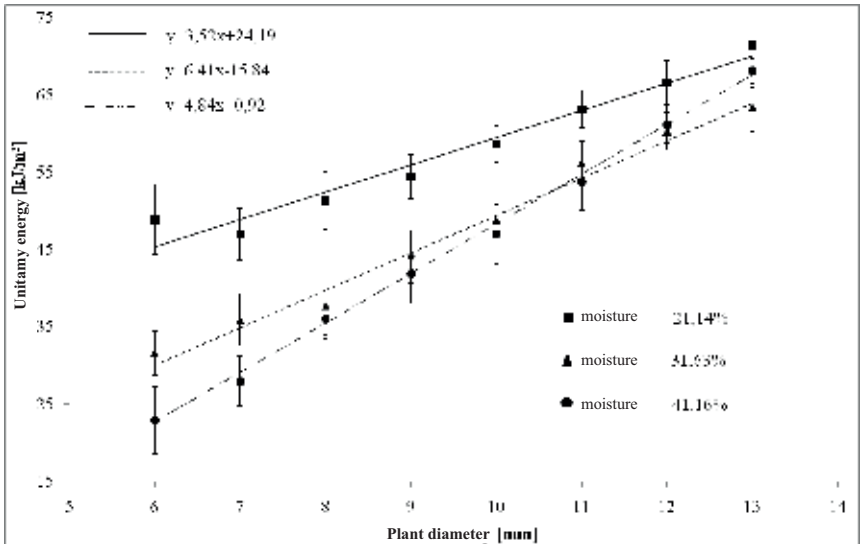

Legend: Unitary energy [kJ/m^2], ■ – moisture 21,14%, ▲ – moisture 31,63%, ● – moisture 41,16%, Stem diameter [mm]

Fig. 4. Comparison of the course of changes of unitary energy of cutting in the diameter function of the multiple flowers rose's stem without forks for 3 different moistures.

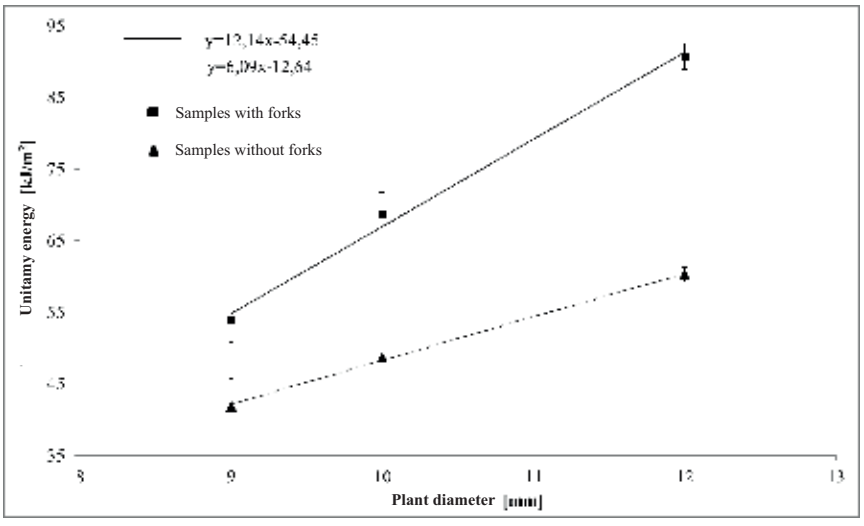

Legend: Unitary energy [kJ/m^2], ■ –stem with forks, ▲ – stem without forks, Stem diameter [mm]

Fig. 5. Comparison of the course of changes of unitary energy of cutting in the diameter function of the multiple flowers rose's stem with and without forks with moisture of 41,16%.

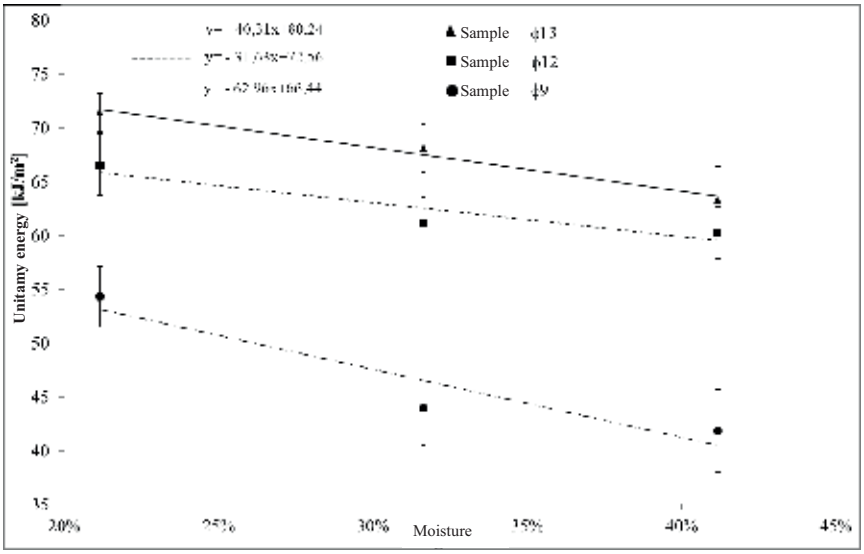

Legend: Unitary energy [kJ/m^2], ▲ – stem diameter 13 [mm], ■ – stem diameter 12 [mm], ● – stem diameter 9 [mm], Moisture [%],

Fig. 6. Comparison of the course of changes of unitary energy of cutting in the moisture function for 3 diameters of the multiple flowers rose's stem without forks

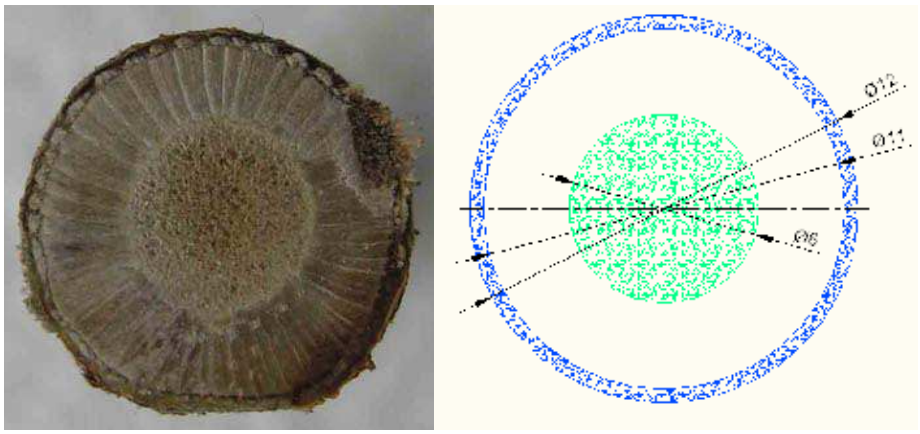

Fig. 7. Way of determining the diameters of particular tissues of the plan

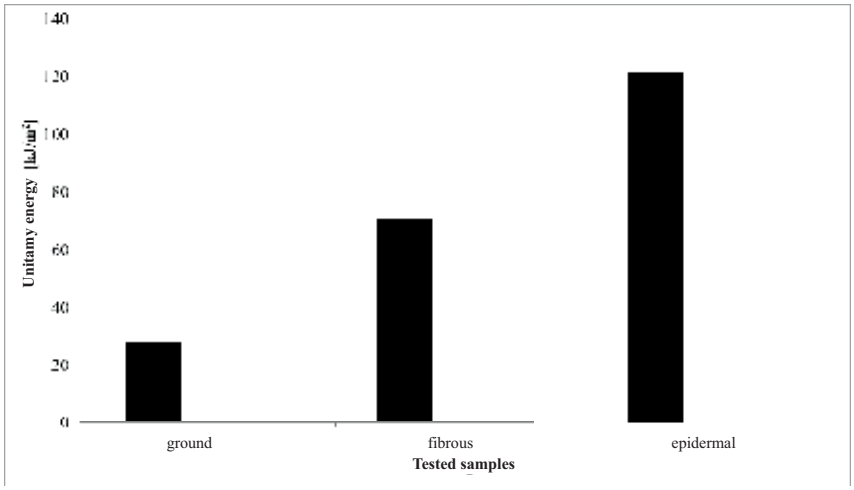

Legend: Unitary energy [kJ/m^2], left - epidermis, centre - fibrous tissue, right - ground tissue,

Fig.8. Unitary energy of cutting particular tissues of multiple flowers rose

CONCLUSIONS

1. For stems of multiple flowers rose the unitary energy increases together with the stems' diameter.
2. The unitary energy decreases together with the plants' moisture increase. This may result from the fact, that there is less energy needed for crushing the plants and the plants epidermis, fibrous and ground tissues resistance to cutting.
3. The energy of cutting of the plant decreases rapidly when the plant breaks.
4. The measurement results show the increase of unitary energy of cutting at the stem's fork. The bigger stem's diameter the bigger energy increase. In all cases the energy increased twice.
5. The greatest unitary energy is needed for epidermis cutting – twice the amount needed for the fibrous tissue cutting and several times as much as it is needed for the ground tissue cutting.

The measurement results show, that the multiple flowers rose's constitution has a significant impact on the unitary energy of cutting. Thus, upon this, it can be stated that the right choice of cutting units parameters should take the plant's morphological properties into account.

REFERENCES

Baran D., Kwaśniewski D., Mudryk K. 2007: Wybrane właściwości fizyczne trzyletniej wierzby energetycznej. Inżynieria Rolnicza, nr 8(96), s. 7-12.

Dreszer K., Michałek R., Roszkowski A. 2003: Energia odnawialna – możliwości jej pozyskiwania i wykorzystania w rolnictwie. Wydawnictwo PTIR, Kraków – Lublin –Warszawa.

Dubas J., Grzybek A., Kotowski W., Tomczyk A. 2004: Wierzba energetyczna – uprawa i technologie przetwarzania. Wyższa Szkoła Ekonomii i Administracji. Bytom.
Frączek J., Mudryk K. 2006: Metoda określenia oporów cięcia pędów wierzby energetycznej. Inżynieria Rolnicza, nr 8(83), s. 91-98.
Górski J. 2001: Proces ciecia drewna elektryczną pilarką. Rozprawy Naukowe i Monografie. Wydawnictwo SGGW, Warszawa.
Gradzik P., Grzybek A., Kowalczyk K., Kościk B. 2003: Biopaliwa. Warszawa
Juliszewski T., Kwaśniewski D., Baran D. 2006: Wpływ wybranych czynników na przyrosty wierzby energetycznej. Inżynieria Rolnicza, nr 12(87), Kraków, s. 225-232.
Kowalski S. 1993: Badania oporów cięcia wybranych roślin. Zeszyt Prob. Post. Nauk Rol. 408, s. 297- 303.
Kwaśniewski D., Mudryk K., Wróbel M., 2006: Zbiór wierzby energetycznej z użyciem piły łańcuchowej. Inżynieria Rolnicza, nr 13(88), s. 271-276.
Mulas E., Rumianowski R. 1997: Rachunek niepewności pomiaru. WPW, Warszawa.
Popko H., Miszczuk M. 2004: Badania oporów krajania niektórych produktów spożywczych.. Zeszyt Prob. Post. Nauk Rol. 354.
Rode H. 1994: Badania wpływu wybranych parametrów pracy kosiarki ze śrubowym zespołem tnącym na zużycie energii i wysokość ścierniska", VI Sympozjum im. prof. Cz. Kanafojskiego, Płock.
Rode H. 2008: Badania procesu cięcia wybranych roślin energetycznych, Rozdział w monografii Wybrane zagadnienia mechaniki w budowie urządzeń technicznych. s. 286-297. Politechnika Warszawska, Płock.
Rode H., Szpetulski J. 2010: The study of the willow viminalis cutting process. Bioagrotechnikal Systems Engineering. vol.6(22), Płock, s. 63-75.
Rudko T., Stasiak M. 2004: Właściwości mechaniczne pędów wierzby energetycznej. III Zjazd Naukowy. Referaty i doniesienia. Dąbrowice 27-29. 09.2004.
Szczukowski S., Tworkowski J., Stolarski M.J. 2004. Wierzba energetyczna. Wydawnictwo Plantpress Sp. z o.o., Kraków.
Szczukowski S., Tworkowski J., Wiwart M., Przyborowski J. 2002: Wiklina (Salix Sp.) Uprawa i możliwości wykorzystania. Wydawnictwo Uniwersytetu Warmińsko-Mazurskiego. Olsztyn.
Szymanek M. 2007: Analysis of cutting process of plant material. Teka Komisji Motoryzacji i Energetyki Rolnictwa – OL PAN, VIIA, s.107-113.
Żuk D. 1979: Określenie koniecznej prędkości elementów tnących w maszynach do ścinania źdźbeł i łodyg. Maszyny i Ciągniki Rolnicze nr 3/1979. Warszawa.
Żuk D. 1986: Proces cięcia źdźbeł zbóż. Prace Naukowe Politechniki Warszawskiej - Mechanika z. 95. Warszawa.
Żuk D., Rode H. 1992: Propozycje oceny energetycznej zespołów tnących. Prace Naukowe Politechniki Warszawskiej - Mechanika z. 152. Warszawa.
Żuk D., Rode H. 1999: Dobór parametrów śrubowego zespołu tnącego, Prace Naukowe Politechniki Warszawskiej - Mechanika z. 176. Warszaw

ENERGIA PROCESU CIĘCIA WYBRANEJ ROŚLINY ENERGETYCZNEJ

Streszczenie. W pracy omówiono wyniki badań procesu cięcia wybranej rośliny energetycznej. Wyznaczono energię jednostkową cięcia łodyg róży wielokwiatowej o różnych średnicach i różnych wilgotnościach w miej-

scach bez zgrubień i zgrubiałych (rozgałęzieniach). Wyznaczono także energię jednostkową procesu cięcia poszczególnych tkanek rośliny tj. okrywającej, włóknistej, miękiszowej.

Słowa kluczowe: proces cięcia, rośliny energetyczne, energia jednostkowa procesu cięcia, róża wielokwiatowa

TEKA Kom. Mot. Energ. Roln. – OL PAN, 2011, 11, 335–342

THE TESTING OF ENERGY EFFICIENCY OF A PROTOTYPE HYBRID SOLAR PANEL

Mariusz Sarniak

Warsaw University of Technology
Faculty of Civil Engineering, Mechanics and Petrochemistry
Department of Mechanical Systems Engineering and Automation
Address: Al. Jachowicza 2/4, 09–402 Płock, Poland
e-mail: sarniak@pw.plock.pl

Summary. The study presents results of testing of a prototype hybrid panel. The panel combines a fluid panel and photovoltaic module in one casing. The tests were performed for four positions of the hybrid panel in relation to the level and for constant southern azimuth. The tests resulted in calculation and comparison of efficiency of solar thermal and photovoltaic energy conversion for the assumed test trends.

Keywords: solar panel, photovoltaic conversion, solar thermal conversion, photovoltaic cell, photovoltaic panel.

INTRODUCTION

Numerous tests of photovoltaic modules [Pluta 2003, Smoliński 1998] proved that, in the case of use of silicon cells, the efficiency of the modules decreases, by 0.4 %, on average, for each temperature degree increment. The combination of a photovoltaic module with a fluid panel in one solar hybrid panel will improve efficiency of the photovoltaic panel as a result o decrease of its temperature and will make it possible to use the heat for heating of the agent circulating in the fluid panel. One may arrive at similar conclusions when analyzing charts presenting spectral sensitivity of photovoltaic silicon cells. It results from the charts that photovoltaic modules made of silicon cells use mainly the visible spectrum of solar radiation. In turn, solar radiation spectra with greater lengths of waves (infrared) contribute to an increase in the internal temperature of the module. Due to scarce information about the type of hybrid panels, we made an attempt to construct a prototype and perform initial tests.

THE AIM AND SCOPE OF STUDY

The aim of this study was to construct a prototype hybrid panel made of a fluid panel and photovoltaic module. Another stage of this study involved testing of energetic efficiency of photovoltaic and solar thermal energy conversion processes as well as verification of the extent, to which

the hybrid panel inclination in relation to the level affects the efficiency of both types of conversion processes. The tests were performed for four inclination angles of the panel. For each inclination, solar radiation intensity was measured.

DESCRIPTION OF THE TEST STATION

Fig. 1 presents a schematic diagram of the hybrid panel abbreviated as PV/T. The hybrid panel with the measurements of 50x100 cm includes an absorber for solar thermal conversion and four strings of 32 photovoltaic cells connected in series. The total area of photovoltaic cells equals 0.2112 m^2. The prototype structure uses monocrystalline silicon cells. The basic element of the panel used in solar thermal conversion is a copper pipe with the diameter of 6 mm and total length of 5.5 m. FS 20 polystyrene with the thickness of 30 mm was used as insulating layer for the back wall of the panel.

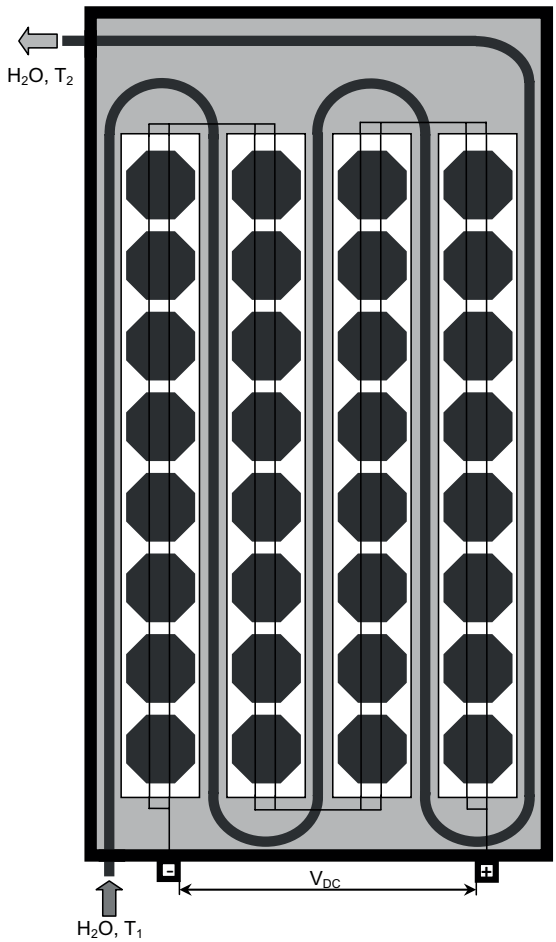

Fig. 1. The schematic diagram of PV/T hybrid panel

The flat fluid panel has a form of serpentine channels with inlet and outlet pipes extending from the enclosure. Water with stabilized temperature of T_1=296 K (23^0C) was used as an agent heated in the fluid panel. Screw terminals for direct current poles of the photovoltaic module were also extended.

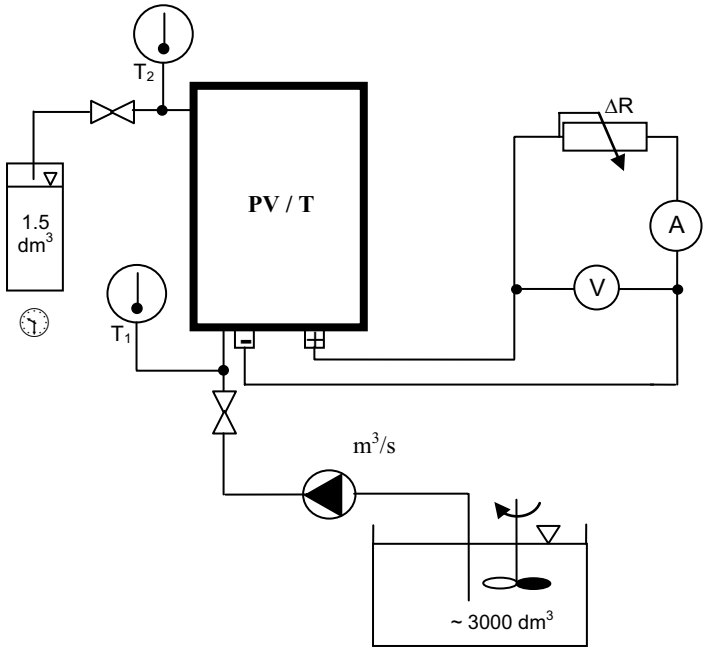

Fig. 2. A diagram of the measurement station for testing of PV/T hybrid panel

Fig. 2 presents a diagram of the measurement station for testing of the hybrid panel. The temperature of inlet and outlet water with respect to the fluid panel was determined with the use of Digital Multimeter VC 333 temperature probes with the accuracy of ±1 %. Circulation of water in the fluid panel was forced by GIRO electrical pump, model 1250.79.00. For stabilized (recurrent) flow conditions, each 1.5 dm^3 of water flowing out of the panel was measured. Measurements of the photovoltaic module (marked as PV) were made with the use of DT 9208A universal meters with the accuracy of 0.5 % for voltage range and 2 % for current intensity [Operator's manual 2006].

METHODOLOGY OF TESTS

The initial tests were performed on 9 July 2010 between $12^{00} \div 15^{00}$ in the vicinity of Płock – GPS position: 52.61 N and 19.72 E in weather conditions corresponding to complete solar operation. Upon stabilization of the flow of water through the flat fluid panel, the stream of energy obtained from the panel ($\dot{Q}_u$) was calculated as follows:

$$\dot{Q}_u = \rho_w \cdot \dot{V}_w \cdot c_w \cdot (T_2 - T_1) \quad [W], \tag{1}$$

where:
ρ_w - water density in the temperature of 298 K (25 ^{0}C) equaling to 997.04 [kg/m^3],
$\dot{V}_w$ - water volumetric flow expressed in [m^3/s],
c_w - specific heat of water for the temperature of 298 K (25^{0}C) and pressure of 1000 [hPa] equaling to 4189.9 [J/(kg×K)],
T_1 – water temperature measured on the panel inlet pipe in [K],
T_2 - water temperature measured on the panel outlet pipe in [K].

The calculations disregard irrelevant changes of water density and specific heat values depending on changes in temperature and atmospheric pressure. The measurements of efficiency of the fluid panel were performed for four angle positions with respect to the level (β): 0^0, 30^0, 60^0 and 90^0. The panel azimuth angle was placed in the southern direction. The intensity of solar radiation was measured with the use of PL-110SM solar radiation meter manufactured by Voltcraft with the measurement accuracy of ± 5 %. The meter has a CE mark [Operating instructions 2009]. During the test, humidity and temperature conditions ensuring nominal accuracy of the meter were fulfilled. The efficiency of the fluid panel (η_{kc}) was calculated as follows:

$$\eta_{kc} = \frac{\dot{Q}_u}{S_{kc} \cdot E} \cdot 100 \quad [\%], \tag{2}$$

where:
S_{kc} – active area of the fluid panel equaling to 0.5 m^2,
E – solar radiation intensity [W/m^2].

The test of the photovoltaic module involved the preparation of current and voltage characteristics for each angle position of the panel. The tests were performed with the use of methods proposed by the author of this study [Sarniak 2008]. The efficiency of the photovoltaic module (η_{PV}) was calculated as follows:

$$\eta_{PV} = \frac{I_{MPP} \cdot U_{MPP}}{S_{PV} \cdot E} \cdot 100 \quad [\%], \tag{3}$$

where:
E – as in the formula (2),
S_{PV} – active area of the photovoltaic module equaling to 0.2112 m^2
I_{MPP} – direct current intensity for maximum power point [A],
U_{MPP} – direct current voltage for maximum power point [V].

TEST RESULTS

Results of tests of the fluid panel were presented in the Table 1. The calculations were made for the fluid panel water inlet temperature of T_1=296 K (23^{0}C) as stabilized as a result of mechanical stirring and with the assumption that the active area of the panel equals to S=0.5 m^2. The measurements were repeated three times in a row and the recorded values represent arithmetic values of the measurements.

Table 1. Results of tests of the fluid panel for four angle values (β) of the hybrid panel inclination

β [^{0}]	$\dot{V}_w$ x 10^{-6} [m^3/s]	T_2-T_1 [K]	($\dot{Q}_u$) [W]	E [W/m^2]	η_{kc} [%]
0	25.42	3.1	329.24	860	19,14
30	22.73	4.0	379.77	1010	18.80
60	20.83	2.2	191.47	920	10.41
90	18.99	1.8	142.78	720	9.91

The examples of tests results for the photovoltaic module in the form of current and voltage characteristics were presented in Fig. 3. The figure shows a chart presenting I-V characteristics for the hybrid panel inclination angle of 30^0.

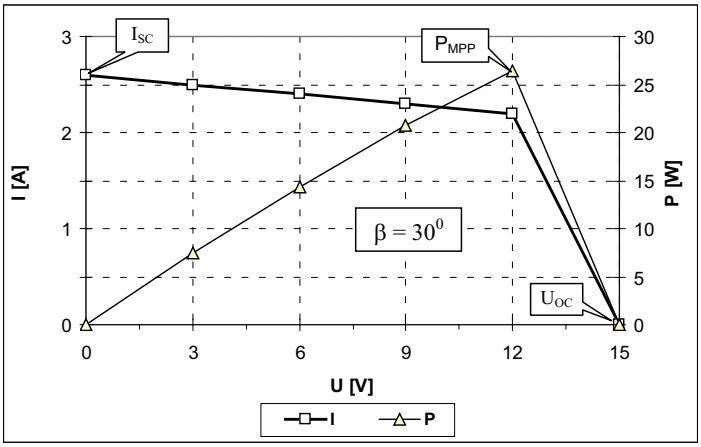

Fig. 3. The current and voltage characteristics of the photovoltaic module for the inclination angle of 30^0 in southern azimuth direction I – current, U – voltage, P – direct current power

Table 2 presents results of tests of the photovoltaic module characteristics for four values of inclination angle of the hybrid panel (β). The values were provided for characteristic points of the charts I-V: U_{OC} – open module voltage, I_{SC} – short-circuit current of the module, U_{MPP} – voltage for maximum power, I_{MPP} – current intensity for maximum power and P_{MPP} – maximum power point.

Table 2. Results of tests of basic parameters of the photovoltaic module

β [^{0}]	U_{OC} [V]	I_{SC} [A]	U_{MPP} [V]	I_{MPP} [A]	P_{MPP} [W]	E [W/m^2]	η_{PV} [%]
0	14.8	2.3	11.7	2.1	24.57	860	13.53
30	15.3	2.6	12.3	2.2	27.06	1010	12.69
60	15.1	2.4	12.1	1.9	22.99	920	11.83
90	14.6	2.2	11.1	1.7	18.87	720	12.41

In order to ensure transparency of interpretation of the results in Fig. 4, the author provided a graphic presentation of the results of tests of photovoltaic and solar thermal conversion depending on the inclination angle of the hybrid panel and solar radiation intensity. It results from the chart that the conversion process relating to the fluid panel is most affected by changes in the inclination angle and solar radiation parameters. In both cases, the greatest efficiency values are demonstrated by conversion processes for the panel inclination angles of 0 and 30 degrees.

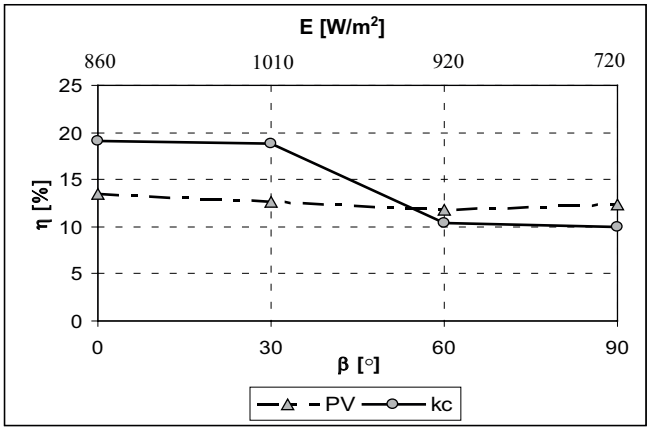

Fig. 4. Charts presenting the efficiency of photovoltaic (PV) and solar thermal (kc) conversion processes in the P/VT hybrid panel

CONCLUSIONS

1. As a result of the tests, the author states unequivocally that the combination of both photovoltaic and solar thermal conversion processes increases general efficiency of the hybrid panel, however, the efficiency will never exceed the efficiency of both the processes conducted separately.
2. A visible influence of the inclination angle changes in relation to the level of the hybrid panel upon the efficiency of the conversion processes can be observed.
3. The solar thermal conversion process conducted in the test conditions proved more sensitive to the changes of the panel inclination angle.

4. The total greatest energy stream obtained from the hybrid panel was 406.83 [W] and it reached the maximum values in both the conversion processes for the panel inclination angle of 30^0.
5. The scope of the tests should also be extended by the testing of changes of the azimuth angle in various seasons of the year and for various intensities of solar radiation.
6. The author would also recommend replacement of cells of the photovoltaic module for cells made on the basis of amorphous silicon, for which no efficiency is lost for temperature increments.

REFERENCES

Bogdanienko J. 1989: Odnawialne źródła energii. PWN, Warszawa.

Chochowski A., Czekalski D. 1999: Słoneczne instalacje grzewcze. Wydawnictwo COIB, Warszawa.

Chochowski A., Czekalski D. 2005: Pomiary pyranometryczne na stanowisku SGGW-Ursynów. Polska Energetyka Słoneczna nr 2/2005, 15-19.

Chwieduk D. 2004: Solar energy utilization. Opto-electronics Review 12 (1), 13-20.

Chwieduk D. 2006: Modelowanie i analiza pozyskiwania oraz konwersji termicznej energii promieniowania słonecznego w budynku. Instytut Podstawowych Problemów Techniki PAN, Warszawa.

Cieśliński J., Mikielewicz J. 1996: Niekonwencjonalne źródła energii. Wydawnictwo Politechniki Gdańskiej, Gdańsk.

Gronowicz J. 2008: Niekonwencjonalne źródła energii. Instytut Technologii Eksploatacji – PIB. Radom-Poznań.

Jarzębski Z. M. 1990: Energia Słoneczna, konwersja fotowoltaiczna. PWN, Warszawa.

Kaiser H. 1995: Wykorzystanie energii słonecznej. Wydawnictwo AGH, Kraków.

Klugmann E.1999: Energetyka fotowoltaiczna. PWN, Warszawa.

Klugmann E., Klugmann-Radziemska E. 1999: Alternatywne źródła energii. Energetyka fotowoltaiczna. Wydawnictwo Ekonomia i Środowisko, Białystok.

Klugmann E. Klugmann-Radziemska E. 2005: Ogniwa i moduły fotowoltaiczne oraz inne niekonwencjonalne źródła energii. Wydawnictwo Ekonomia i Środowisko, Białystok.

Lewandowski W. 2002: Proekologiczne źródła energii odnawialnej. WNT, Warszawa.

Marecki J. 1995: Podstawy przemian energetycznych. WNT, Warszawa.

Nawrocka A., Grundas S. 2010: Applications of semiconductor nanoparticles in power industry. Teka Kom. Mot. i Energ. Roln. – OL PAN, v. 10, 284–293.

Ney R. 1994: Energia odnawialna. Nauka Polska nr 1/1994.

Nowicki J. 1980: Promieniowanie słoneczne jako źródło energii. Arkady, Warszawa.

Operating instructions 2009: PL-110SM Solar Radiation Measuring Instrument, version 11/09. Voltcraft®, Lindenweg 15, D-92242 Hirschau, Germany.

Operator's manual 2006: Digital multimeter DT9208A. Zhangzhou Weihua Electronic Co., Ltd, China.

Pietruszko S. 2003: Photovoltaics in the World and in Poland. Applied Energy 74, 169-175.

Pluta Z. 2000: Podstawy teoretyczne fototermicznej konwersji energii słonecznej. Oficyna Wydawnicza Politechniki Warszawskiej, Warszawa.

Pluta Z. 2003: Słoneczne instalacje energetyczne. Oficyna Wydawnicza Politechniki Warszawskiej, Warszawa.

Sarniak M. 2006: Badanie wpływu przestrzennego ustawienia paneli fotowoltaicznych na przebiegi charakterystyk prądowo-napięciowych. Wybrane Problemy Inżynierii Mechanicznej. Instytut Inżynierii Mechanicznej w Płocku, rozdział 15 w monografii, 176-183.
Sarniak M. 2008: Podstawy fotowoltaiki. Oficyna Wydawnicza Politechniki Warszawskiej, Warszawa.
Smoliński S.1998: Fotowoltaiczne źródła energii i ich zastosowania. Wydawnictwo SGGW, Warszawa.
Tymiński J. 1997: Wykorzystanie odnawialnych źródeł energii w Polsce do 2030 roku. Aspekt energetyczny i ekologiczny. Wydawnictwo IBMER, Warszawa.
PN-EN ISO 9488: 2002: Solar energy – Vocabulary.

BADANIE EFEKTYWNOŚCI ENERGETYCZNEJ PROTOTYPOWEGO HYBRYDOWEGO KOLEKTORA SŁONECZNEGO

Streszczenie. W pracy przedstawiono wyniki badań prototypowego, hybrydowego kolektora słonecznego. Kolektor ten jest połączeniem kolektora cieczowego i modułu fotowoltaicznego w jednej obudowie. Badania przeprowadzono dla czterech położeń pochylenia kolektora hybrydowego względem poziomu i przy stałym ustawieniu azymutalnym, skierowanym w kierunku południowym. W wyniku badań obliczono i porównano sprawności procesów konwersji fototermicznej i fotowoltaicznej dla założonych warunków badań.

Słowa kluczowe: kolektor słoneczny, konwersja fotowoltaiczna, konwersja fototermiczna, ogniwo fotowoltaiczne, panel fotowoltaiczny

TEKA Kom. Mot. Energ. Roln. – OL PAN, 2011, 11, 343–353

EVALUATION OF HARVEST OF ENERGETIC BASKET WILLOW[1]

Wiktoria Sobczyk*

*University of Science and Technology AGH Cracow Poland

Summary. The aim of the investigations was the assessment of the size of harvest of five energetic basket willow clones at a plantation of the Forest Inspectorate Krzeszowice, the Forest Inspectorate Brodła branch, in the Malopolska voivodeship.

The article shows that in the years 2003, 2006 and in 2011 the highest crops of clone No. 1056 were obtained. Due to the extremely dry 2003 year the yield of this clone was evaluated as lower than in 2006. The 2011 harvest is estimated as lower than in 2006. The willow *Salix viminalis* is a plant which easily adapts to vegetation on any soil. The plant growing does not require any special cultivation treatment. By the establishment and maintenance of willow plantations it is possible to contribute to rural development, increase income and reduce unemployment in the country. Farmers are willing to undertake willow plantations if its sale at attractive prices is guaranteed.

The Polish market for biomass is formed slowly. To be able to develop fully and be profitable you need much more effort as well as technical and economic ventures.

In 2007 member countries of the European Union endorsed the "Climate package 3 x 20". By 2020 they plan 20-percent reduction in energy consumption, increase to 20% of energy produced from alternative sources and 20-percent reduction in CO_2 emissions. Europe is looking for alternatives to conventional energy sources, the combustion of which releases a greenhouse gas - carbon dioxide.

Keywords: alternative energy, energetic plants, energetic willow, clone, harvest, "Climate package 3 x 20"

INTRODUCTION

In the last twenty years Poland has undergone profound economic transformation. Energy Policy of the European Union envisages providing a reliable, affordable and environmentally friendly energy supply. Poland is adapting to these patterns and looking for new and renewable energy sources. Among the energy crops the greatest chance belongs to the energetic willow *Salix viminalis*, which can grow both on rural land and on grassland. Willow is a plant with no special cultivation needs. It can grow both in very dry, poor in nutrients areas and in very humid and fertile ones.

Cultivation of willow *Salix viminalis* contributes to the introduction of new, attractive product on the market. A 4-year old willow plantation has a 14 times higher growth, than willow growing

[1] The paper has been prepared within the AGH – University of Science and Technology – statutory research work No 11.11.100.482

at the same time in a natural forest. If crops become widespread, then in the future they will be partially completed by wood harvested from forests [8].

Willow has a growing interest among farmers and small manufacturing companies. Farmers having land of low agricultural productivity may intend to grow the willows. Growing willow on marginal land meets the expectations of growers. It does not require large inputs of labor and is characterized by low energy consumption (low demand for fertilizers and pesticides), high productivity and the ability to use standard machines.

Farmers undertake willow plantations, and specialized companies process it to biomass. Apart from energetic value willow also has great ecological advantage. It can be used to protect the environment, among others to create buffer zones along routes or for the reclamation activities in post-industrial areas [ibid.].

ENERGY SOURCES

The term 'energy source' is understood as primary energy source (not processed) of fuel, nuclear, water, Earth's interior and wind energy, solar radiation and chemical reactions. The primary source of energy for Earth is the solar radiation, with which the power of about 178 PW reaches the Earth, of which approximately 30% is reflected by the atmosphere, and more than 45% is absorbed by the land and sea. The rest is consumed in the process of photosynthesis. Throughout the ages fossil fuels have been formed: coal, peat, crude oil and natural gas.

Huge demand for energy occurred in the era of the industrial revolution. In 1980 energy consumption increased 10 times, although the number of people increased by only 2.5 times. The increase in unit consumption per capita has still been growing.

In the second half of the twentieth century coal has ceased to be a major source of energy, especially in the developed countries. For ecological reasons, it has been replaced by the petroleum and natural gas. Electricity, which played a central role in the industry and the economy, is produced mainly in thermal power plants, water, nuclear and wind [3, 7]. Thermal power plants produce over 60% of global energy. Hydroelectric plants do not pollute the environment, but require appropriate terrain and a considerable potential of water, besides they incur large costs associated with the construction of dams. Hydropower is much cheaper than thermal plants. It is also better in terms of ecology. Hydroelectric power stations provide 21% of all the electricity in the world.

Depletion of energy resources and oil crises have led the world to looking for alternative energy sources. Compared with other countries in the EU, Poland has a large technical potential of biomass and considerable resources of geothermal energy.

BIOMASS

Biomass is organic matter produced in the process of photosynthesis from solar energy, carbon dioxide and water. The origin of the biomass can be varied: field crop production, the waste found in food industry, the waste wood as well as pulp and paper mills (12, 13, 17). The production has been started of biomass for energy purposes on special plantations of fast growing trees (willow, poplar), rape, topinambur [4, 5, 19], sunflower, mallow slime, fodder beet and grass (Miscanthus giganteus) [1, 2]. A significant source of biomass is waste from animal production and waste generated in municipal (sewage sludge, household waste, waste paper) (Tab. 1).

Table 1. Characteristics of plants cultivated on energetic plantations [1]

biomethane yield (m^3/t d.m.)	production of biomethane (m^3/ha)	percentage of methane	production of biogas (m^3/ha)	cultivated plant
410	13530	85	15920	Miscanthus giganteus
410	9840	85	11580	Spartina pectinata
410	3280	85	3860	grass pasture
450	10800	83	13010	maize
410	6150	85	7240	alfalfa
840	18820	85	22140	beets (roots and leaves)
390	3120	75	4160	wheat (grain and straw)

t. d.m. - ton of dry matter

Unconventional energy sources play an important role in increasing the profitability of agriculture goods and in activation of the rural population. The particular usefulness of alternative energy sources for rural areas is due to the fact that the installations can be tailored to the needs of farmers and local communities. In the case of the wide rural areas may constitute a supplementary, economically attractive source of energy, relieving overburdened rural electricity network. The development of biofuels and biomass for heating purposes can be an incentive for the cultivation of plants for non-food purposes [9, 17].

WILLOW *SALIX VIMINALIS*

Willow *Salix viminalis* (Fig. 1) as an energy plant has raised a lot of interest, because of the high yielding. Type of *Salix* includes over 300 species that occur as trees, shrubs or dwarf shrubs. Shrub willow species are used mainly for basket-work, but fast-growing forms are assigned for energy purposes. It is possible to obtain a change in the form of certain species, depending on cultivation. Some of them (sallow) may exist in two forms simultaneously. Willows have low soil requirements, but most grow in wetlands and near watersources.

Fig. 1. Willow *Salix viminalis* [own material]

During the first period after setting up of plantations, willow *Salix viminalis* requires special care. Fast-growing weeds choke the young seedlings, even when the field in the year before planting was well prepared. Plant Protection Institute in Poznan recommends the use of herbicide, before the shoots start to grow.

Herbicide doses are dependent on the nature and development stages of weeds. These treatments can be performed during the growing season of plants after the earlier application of protectors that cover the young shoots. If chemical weed control method does not afford the desired results, it can be destroyed by mechanical means. Spacing should be expanded twice, before a strong root system of weeds is formed [14]. In the first year of growing, plants have a root system, which throughout the years develops into intense increments.

The greatest demand for minerals in the plants appears in the second year, because then there is the greatest weight gain. In subsequent years of growing the plants you do not need to apply almost any agricultural practices. Demand for fertilizers is decreasing, because they collect nutrients from the organic litter layer formed of fallen leaves [10].

The energy value of willow is comparable to pulverized coal. As we know, willow is an ecological product, so it has completely organic combustion parameters. Such characteristics make it like the fuel of the future [18].

For many years in Poland there is cultivation of willow for basket-work or honey-yielding aims, thanks to early flowering period. Crops willow *Salix viminalis* and *Salix purpurea* started about 20 years ago in order to use the energy [11]. These species are characterized by very rapid and large increase in biomass, as well as disease resistance (scab, gangrene of shoots) and harmful insects.

After the first year of growing, shoots should be cut at the height of 3 cm above the soil surface, so that they have dormant buds. If the cut bars correspond to the standards, they can be used for new plantings. In the following years harvest is made each year, whether the plants are intended for fuel pellets, the cuttings to increase the plantation or cuttings for sale. If we make a harvest every 2 or 3 years, the resulting biomass is used for heating purposes and for production of chipboard. After harvesting willow plantations should be intensively fertilized to get crops faster. Exploitation of the plantation may last up to 30 years. After the liquidation of the plantation, soil should be renovated [15, 16].

For single collection they use combine harvester or sheaf-binders. To cut willow stems on small plantations you can use special sickle (Fig. 2) or hand mower blades: exhaust or tractor.

Fig. 2. The employee of the Forest Inspectorate Brodła cuts the stems with the special sickle [own material]

PURPOSE AND METHODS

The task of the research study was to assess the economic benefits of growing willow *Salix viminalis* in Forest Inspectorate Brodła (municipality Alwernia), 30 km west of Krakow (Fig. 3). Experimental plantation was established on sandy soils.

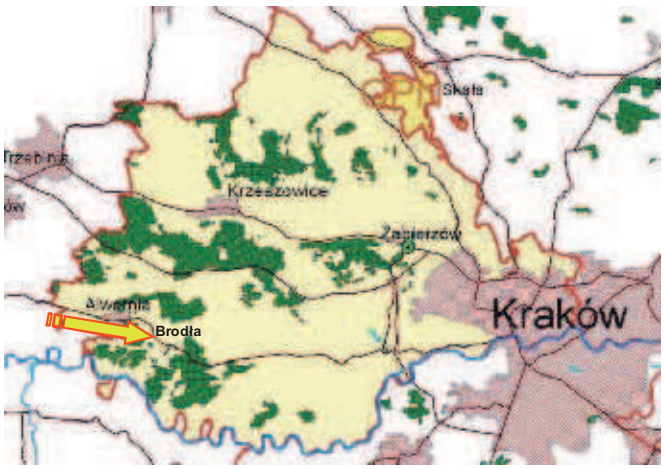

Fig.3. Location of Forest Inspectorate Brodła

Inoculated willow clones were marked by numbers: 1051, 1052, 1054, 1056, 1059, 1007, 1015 and 1033rd. In an experimental nursery (Fig. 4 and 5) planting of seedlings was carried out in six rows: at 50 cm, a length of 10 meters for each clone. Seedlings were distributed at 33 cm.

The aim of the study was the choice of clone whose yield is the largest and the most profitable. The study was realized in 2003, 2006 and in 2011. Subject to annual growth were clones with the following numbers: 1051, 1052, 1054, 1056 and 1059th.

Fig. 4. The experimental energy willow plantation in the Forest Inspectorate Brodła

Fig. 5. Author of the article near clone 1052

Both in 2003 and in 2006 a study was started from measuring the height of plants of 50 samples of each clone. The thickness of individual clones shoots was measured at the height of 100 cm plants (Tab. 2). Mean thickness of stems of each clone was calculated. The mass of individual shoots of 100 clones (t/ha) was accepted for the determination of the estimated one-year yield of individual clones (Tab. 3).

Table 2. The results of calculations of average thickness of clone shoots [own preparation]

clones	average shoot thickness [mm]
1051	6,9
1052	4,17
1054	8,6
1056	10,2
1059	9,6

Table 3. The results of the mass investigations (2003 r.)

	no. clone	member of shoots	mass [kg]
1	1051	100	14,5
2	1052	100	9,8
3	1054	100	20,5
4	1056	100	21,6
5	1059	100	16,4

In 2011 the study was limited to 15 random shoots of each clone and their height (Fig. 6) and thickness (Fig. 7 and 8). During the fieldwork it was found, that the highest shoots (average height 305 cm) belonged to clone No. 1056. This clone also had the thickest stems (Tab. 4). It can be concluded that the yield from planting clone No. 1056 will be the highest.

Fig. 6. Assessment of shoots by the author of article. The highest has a clone No. 1056

Fig. 7. Visible differences in thickness of stems of different clones; in the foreground clone No. 1056

Fig. 8. The thickest stems of clone No. 1056

Table 4. The results of investigations of the plants' height in 2011 (the empirical data)

clone no.	average height of shoots in cm	average shoot thickness (mm) at the height of 100 cm
1051	255	16
1052	267	17
1054	286	18
1056	305	22
1059	270	13
1007	not measured	not measured
1015	not measured	not measured
1033	not measured	not measured

RESULTS AND DISCUSSION

Based on the investigation [20] it was found, that in the first year of cultivation annual growth of thickness was 7 ÷ 13 mm. Measuring in 2003 showed that clone 1056 had the thickest stems (Tab. 3). One hundred shoots of clones number 1056 and number 1054 achieved the largest weight: 21,6 kg and 20,5 kg. After the weight test there were counted the shoots on the surface of 1 m^2. Since in the nursery the willow grew at the spacing of 0.5 m, the surface area of 1 m^2 included two rows. On this basis the estimated yield (in tons per 1 hectare) of individual clones in 2003 and in 2006 was calculated (Fig. 9 and 10).

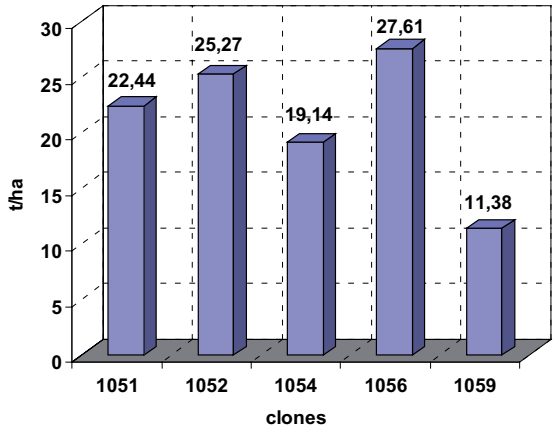

Fig. 9. Graphic interpretation of estimated yield in tons per 1 hectare of willow clones in 2003 [own preparation]

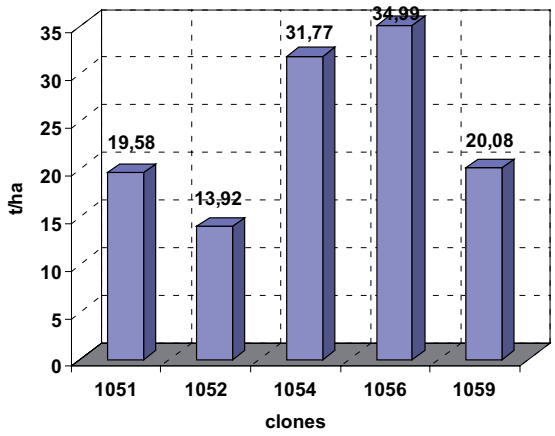

Fig. 10. Graphic interpretation of estimated yield in tons per 1 hectare of willow clones in 2006 [own preparation]

In 2011 the highest yield is expected for clones 1056 (approximately 35 tons) and 1054 (approximately 32 tons).

SUMMARY AND CONCLUSIONS

In 2003 and 2006 the highest yield was estimated for the planting of willow clone No. 1056. Therefore, to establish the potential of energy plantations you need cuttings of this clone. Willow *Salix viminalis* is a perennial which grows on almost any soil. But it has a high demand for water. The year 2003 was poor in rain, so it was estimated that the yield of willow was small: 27 t/ha [13]. However, in 2006 the estimated yield increased substantially: to 35 t/ha. Large demand of willow for water does not mean that you can overdo it. That happened in 2010, when following long rain the whole plantation was in the water for weeks. This fact may in turn cause lower yields.

A medium-sized area (0.5 ha) appropriate for the cultivation of willow *Salix viminalis* can supply each farm with fuel for all the year. A significant aspect of the rationale for setting up plantations of fast-growing willow and timber harvesting for energy purposes is the use of fallow land or land polluted by industry and thus excluded from the production of food raw materials [6]. In addition, a new product in form of chips, briquettes and pellets is introduced to the market.

In March 2007 at the summit of the European Union, the member countries endorsed the „Climate package 3 x 20". This document is a response to rising fuel prices and energy and finding alternatives to conventional energy sources, the combustion of which releases the greenhouse gas - carbon dioxide. By 2020 they assume 20-percent reduction in energy consumption and increase to 20% of energy produced from alternative sources, as well as 20-percent reduction in CO_2 emissions.

Poland has one of the largest in the EU countries potential for renewable energy resources. To be able to use it, there should be increased funding in research and technology development, and a system of funding projects should be created. This work is mainly inspired by the European Union, which for many years has supported the development of renewable energy sources.

The author would like to express sincere thanks to mgr. inż. Krzysztof Smaga [20], the employee of the Forest Inspectorate Krzeszowice, the Forest Inspectorate Brodła branch, for help in field studies, consultation and valuable suggestions.

REFERENCES

Borkowska H., Styk B., 1997: Ślazowiec pensylwański (*Sida hermaphrodita* Rusby). Uprawa i wykorzystanie. Wyd. AR, Lublin.

Borkowska H., Styk B., 2001: Ślazowiec pensylwański jako wieloletni przedplon dla niektórych gatunków roślin uprawianych na osadzie pościekowym. Materiały konferencyjne „Odpady organiczne a ochrona i produktywność agrocenozy", Lublin.

Ciechanowicz W., 2001: Bioenergia a energia jądrowa, Wyższa Szkoła Informatyki Stosowanej i Zarządzania, Warszawa.

Franków B., 2003: Uprawy energetyczne – topinambur. Materiały konferencyjne „Strategia działań na rzecz poprawy stanu środowiska naturalnego", WKTiR w Zamościu, Krasnobród.

Góral S., 1999: Słonecznik bulwiasty – topinambur. Uprawa i użytkowanie. IHAR, Radzików.

Gradziuk P., Wojtaszek Z., 2001: Alternatywne wykorzystanie gruntów rolniczych na cele niezwiązane z produkcją żywności. SGGW, Warszawa.

Hrynkiewicz A., 2002: Energia – wyzwanie XXI wieku, Wydawnictwo Uniwersytetu Jagiellońskiego, Kraków.

Jońca M., Martyn W., 2002: Uprawa wierzby i możliwości wykorzystania, Instytut Nauk Rolniczych w Zamościu, Zamość.

Kadelski L., 2005: Biopaliwa może za rok, „Motor" nr 49.

Kościk B., 2003: Rośliny energetyczne, Wydawnictwo Akademii Rolniczej, Lublin.

Kowalik P., 1995: Energetyczne wykorzystanie biomasy w Polsce - szanse i bariery, III Konferencja <Racjonalizacja użytkowania energii i środowiska>, Zakopane 1995.

Kowalska A., 2008: Overviev of technological methods of energy production from biomass. Teka Kom. Mot. Energ. Roln. - OL PAN, X, 209-215.

Kulig R., Laskowski J., 2008: Effect of conditioning parameters on pellet temperature and energy consumption in the process of plant material pressing. Teka Kom. Mot. Energ. Roln. - OL PAN, VIIIA, 105-112.

Regionalna Dyrekcja Lasów Państwowych w Krakowie, Lasy Państwowe, Nadleśnictwo Krzeszowice, Zabierzów 2003, 2011 (materiały dokumentacyjne, wywiad).

Malada A., Sobczyk W., 2005: Uprawa roślin energetycznych jako forma aktywizacji środowisk wiejskich. Zeszyty Naukowe Katedry Inżynierii Procesowej Uniwersytetu Opolskiego, zeszyt II, Opole, p. 92-98.

Małopolski Ośrodek Doradztwa Rolniczego w Krakowie, oddział w Karniowicach, materiały źródłowe, Karniowice 2009.

Niedziółka I., Szymanek M., Zuchniarz A., Zawiślak K., 2008: Characteristics of pellets produced from selected plant mixes. Teka Kom. Mot. Energ. Roln. - OL PAN, VIII, 157-163.

Szczukowski S., Tworkowski J., 1999: *Salix* – źródło odnawialnych i ekologicznych surowców. Ogólnopolski Informator Produkcji Roślin, no 9.

Szczukowski S., Tworkowski J., Stolarski M., 2004: Wierzba energetyczna, Wydawnictwo Plantpress Sp. z o.o., Wrocław.

Szeptycki A., 2001: Odnawialne źródła energii – szansa dla rolnictwa i obszarów wiejskich, w: Odnawialne źródła energii u progu XXI wieku, materiały konferencyjne, Warszawa 10–11 XII 2001.

Szurlej A., 2003: Biomasa – opłacalne i ekologiczne paliwo, „Hasło ogrodnicze", Vol. 11.

www.bni.com.pl

Wywiad środowiskowy z pracownikiem Nadleśnictwa Krzeszowice, oddział Nadleśnictwo w Brodłach, panem mgr. inż. Krzysztofem Smagą, luty 2011.

OCENA PLONOWANIA WIERZBY ENERGETYCZNEJ

Streszczenie. Celem badań była ocena wielkości plonowania pięciu klonów wierzby energetycznej z plantacji w Nadleśnictwie Brodła, woj. małopolskie. W artykule wykazano, że zarówno w latach 2003, 2006, jak i w 2011 najwyższe potencjalne plonowanie uzyska się z posadzenia klonu nr 1056. Ze względu na bardzo suchy 2003 rok plonowanie tego klonu oceniono jako niższe niż w 2006 r. W 2011 r. zakłada się słabsze zbiory niż w 2006 r. Wierzba *Salix viminalis* jest rośliną przystosowaną do wegetacji na dowolnym gruncie, a jej uprawa nie wymaga szczególnych zabiegów agrotechnicznych. Przez zakładanie i prowadzenie plantacji wierzby energetycznej można przyczynić się do rozwoju wsi, zwiększenia dochodów i zmniejszenia bezrobocia na wsi. Rolnicy będą chętnie zakładać plantacje wierzby energetycznej, jeśli będzie gwarancja sprzedaży po atrakcyjnych cenach.

Polski rynek biomasy powstaje powoli. Aby mógł się w pełni rozwinąć i być opłacalnym, potrzeba jeszcze wielu starań i przedsięwzięć technicznych i ekonomicznych.

W 2007 r. kraje członkowskie Unii Europejskiej zatwierdziły „Pakiet klimatyczny 3 x 20". Do roku 2020 zakłada się 20-procentową redukcję zużycia energii, wzrost do 20% udziału energii produkowanej ze źródeł niekonwencjonalnych oraz 20-procentową redukcję emisji CO_2. Europa poszukuje alternatywy dla konwencjonalnych nośników energii, których spalanie powoduje emisję gazu cieplarnianego – dwutlenku węgla.

Słowa kluczowe: energetyka alternatywna, rośliny energetyczne, wierzba wiciowa, klony, plonowanie, „Pakiet klimatyczny 3 x 20"

TEKA Kom. Mot. Energ. Roln. – OL PAN, 2011, 11, 354–362

THE IDENTIFICATION OF OPERATIONAL FAILURES OF THE HEATING, VENTILATION AND AIR-CONDITIONING CIRCUIT IN THE CAR BY MEANS OF THERMOVISION METHODS.

Sebastian Styła, Wiktor Pietrzyk

Department of Computer and Electrical Engineering, Lublin University of Technology,
20-618 Lublin, ul. Nadbystrzycka 38a; e-mail: s.styla@pollub.pl

Summary. The present article contains the description of proposed method for periodical inspection of the heating, ventilation and air-conditioning (HVAC) circuits by means of thermovision cameras. The methods of interpretation of the obtained results have been presented in order to carry out the diagnostics of heating circuit failures. The technical condition of the ventilation system (air supply ducts) has been evaluated without its dismantling. Furthermore, the article contains the presentation of thermovision examinations enabling the indication of the areas with the highest heat losses in an easy and fast manner for the engine as well as for the passenger cabin. This possibility is particularly important in the winter period.

Key words: thermogram, infrared measurements, heating circuit, thermovision camera, microclimate in motor vehicle.

INTRODUCTION

The comfort of travelling by cars is influenced by many factors encompassing the design solutions and the microclimate in the motor vehicle. The desirable inside temperature to be achieved will improve the travel comfort and the psycho-physical functions of both the driver and passenger will be affected positively [4, 7]. The temperature control is possible for front and rear, LH or RH seats individually, by means of modern heating and air-conditioning circuits installed in the vehicles owing to air stream stratification phenomenon. The purpose of such solution is to adapt the microclimate in the motor vehicle to the individual needs of travelling passengers.

The appropriate microclimate in a motor vehicle i.e. the temperature, its distribution and air humidity contribute among others to the following:

- pulse stabilization in travelling passengers;
- reduction of driver's reaction time;
- reduction of nervousness and hurry;
- reduction of the impact of allergic reactions thanks to the purification of supplied air (by means of anti-dust filters);

– achievement of temperature distribution optimal for the human body (warmer feet, cooler head).

The factors specified above directly contribute to the safety improvement in road traffic. Failure to meet them causes the feeling of discomfort by the driver as well as the passengers.

The optimal temperature in the passenger cabin should be included between the limits 23 – 26 °C in summer period (at outside temperature of 40 °C) and about 27 °C in winter period (at outside temperature of –20 °C) [1, 2, 7].

All inefficiencies of the heating and air-conditioning circuit, particularly in winter period can contribute to non-optimal use of thermal energy and consequently to the discontinuation of travel (e.g. as a result of panes freezing). Many years' operation of the cars leads to the electrical or mechanical failures as well as to the choking of ducts supplying the air to the vehicle interior.

THE THERMOVISION MEASUREMENTS AND THEIR ACCURACY

The quantities of additional equipment installed in motor vehicles change simultaneously with the development of the new design solutions in the cars. Their standard equipment encompasses the systems which were used a few years ago in the high class cars only. As a result of continuous technological development, the cars become more complex and problematic in case of potential repairs. Therefore, it is necessary to create new diagnostic procedures.

The thermovision examinations [13, 14, 15, 17] are used in the machines diagnostics more and more frequently. For a few years recently they have also been applied in the automotive sector, e.g. for the tyres wearing examination [10] or for qualitative evaluation of the vehicles used for food transportation [16]. The creation of fast and non-invasive methods of the technical condition evaluation for selected equipment was possible due to the relationship between the temperature conditions and the failure.

The thermovision examinations are based upon visualization of infrared radiation which is invisible for human eye and is emitted by a body with temperature higher than absolute zero. This property is defined as the emissivity factor i.e. ability of a body to hand over the energy. The emisissivity depends on the physico – chemical properties and is a unique feature of each object. The termovision camera is the device used for temperature measurement and analysis; the obtained image is called thermogram.

Owing to their advantages i.e. versatility and possibility of contactless temperature measurement, the thermovision examinations are perfectly suitable for the analysis of elements releasing certain amount of heat in course of their operation. The accuracy depends mainly on the applied method, device calibration and on the accuracy of thermovision camera. The most important are the errors associated with the applied method i.e. the following [8, 9, 11]:

– emissivity estimation errors;
– errors caused by the impact of the ambient radiation reflected by the object (e.g. solar radiation, street lighting);
– errors caused by the transmission of radiation through atmosphere;
– errors caused by the transmission of infrared radiation through the camera;
– errors caused by the impossibility of results averaging.

Owing to their values, even up to a few percent, these errors take priority in course of the termovision measurements. In course of the examinations presented in the present article, these errors have been minimized thanks to the application of an appropriate measurement procedure described in the chapter entitled "Examinations methodology".

THE HEATING, VENTILATION AND AIR-CONDITIONING (HVAC) CIRCUIT OF THE CAR

As mentioned above, the heating, ventilation and air-conditioning (HVAC) circuit performs an important role, particularly in case of unfavourable weather conditions, in the summer period (high temperature) as well as in the winter period (rain, snow, low temperature). From the functional point of view, the heating, ventilation and air-conditioning (HVAC) circuit constitutes a whole entity. The fresh air flows through the evaporator and is supplied to the interior of passenger cabin (temperature reduction) or additionally heated in the heater (temperature increase). The principle of cooperation between both the systems is illustrated in Figure 1. The "hot" or "cold" air cycle is established by means of a diaphragm which can be controlled in the mechanical mode by means of a cable or in the electrical mode by means of a mini motor.

The basic requirement to be met in the course of the designing and selection of the devices dedicated for the vehicle heating and air-conditioning is to achieve desirable temperature within assumed period of time. Owing to heat losses, the power determined for the equipment is higher than its value resulting from energy balance calculated for the specified vehicle body as well as for climatic conditions in which the car will be operated [6].

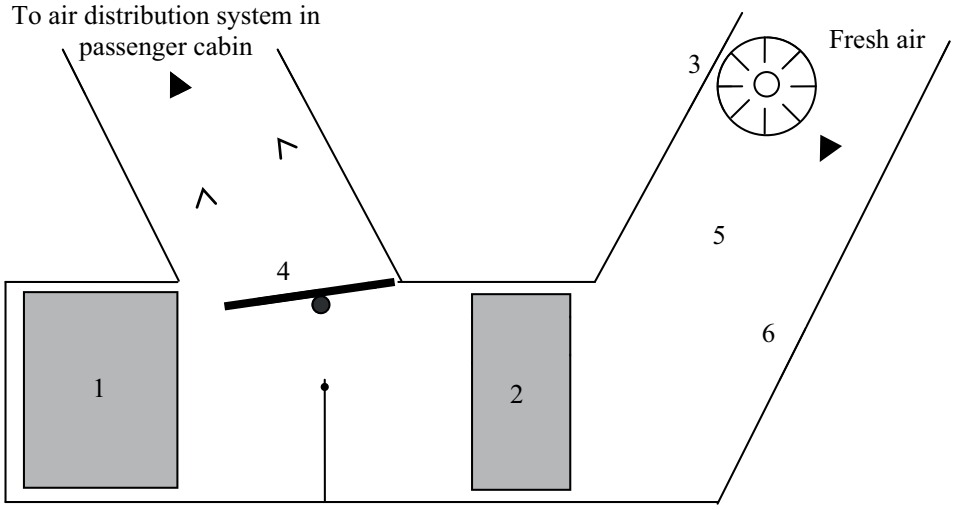

Fig. 1. The cooperation between the heating and air – conditioning system
1-heater; 2- evaporator; 3- blower; 4- hot and cold air diaphragm; 5- cold air; 6- hot air

The contemporary cars are provided with the possibility to control the temperature, humidity, air stream velocity and its stratification. The whole operation is monitored by ECC system (Electronic Climate Control) incorporating the electronic control system. The driver has the possibility to set the required operation parameters by means of the panel (Fig. 2).

Fig. 2. Control panel for the heating and air – conditioning system installed in BMW cars (1994-2001)
1- air supply to windscreen / panes; 2 - air supply to the head (driver's side); 3 - air supply to the feet (driver's side); 4 – air – conditioning automatic control (driver's side); 5 – temperature indicator (driver's side); 6 – temperature control (driver's side); 7 – air supply intensity (driver's side); 8 – defrosting function; 9 – rear pane heating; 13 – vehicle inner temperature sensor; 11 – closed loop air cycle; 12 - air – conditioning ON; 13 – temperature indicator (passenger's side); 14 – temperature control (passenger's side); 15 - – air supply intensity (passenger's side); 16 – residual heat utilization; 17 - air supply to the head (passenger's side); 18 - air supply to the feet (passenger's side); 19 – air – conditioning automatic control (passenger's side);

The basic functions of the „control panel" are: manual temperature setting by the driver and passenger separately, defrosting of the windscreen and side panes, electric defrosting of rear pane as well as closed loop cycle mode and residual heat utilization mode. In the closed loop cycle mode (pushbutton 11, Fig. 2) the diaphragm supplying fresh outside air is closed and air is circulated in the car interior in order to ensure its faster heating. The residual heat utilization mode (pushbutton 16, Fig. 2) enables the car heating after engine shutoff. The heat contained in the engine cooling medium is used for this purpose. Irrespective of differences in the construction of the heating and air – conditioning systems, the majority of their functions is identical independently on the model of the vehicle.

EXAMINATIONS METHODOLOGY

Owing to the application of an electronic system for the heating and air – conditioning circuit operation control, the diagnostics procedure is carried out by means of the diagnostic testers or by means of devices dedicated for the inspection of air – conditioning systems in the cars. The procedures and the manner of proceeding in course of repair are widely described in literature [1, 3, 5]. However, this article presents the proposal of the evaluation of the technical condition of structural elements of the vehicle which affect the maintenance of specified temperature in the car. It is impossible to detect these failures by means of a/m devices. The examinations were carried out for those parts (circuits) of vehicle which can be potentially damaged during everyday operation owing to the ageing of elements or to mechanical processes (gaskets, ventilation ducts, rear pane heating circuit etc.). This issue is particularly important in the winter period with high difference of temperatures inside and outside of vehicle. All leaks and failures can lead to the necessity of stopping the travel.

The examinations have been performed by means of ThermaCAM E45 thermovision camera manufactured by FLIR. The following criteria have been established in order to minimize the measurement inaccuracies described in the preceding chapter:

a) owing to the lack of information about the material used for the fabrication of the bodies of the cars being tested and for the fabrication of other components of the motor – car body, a black tape with known emissivity was adhesive-bonded every time onto the element being tested in order to determine the correct value of emissivity factor;

b) owing to significant impact of weather conditions on the obtained results, days selected for the examinations were characterized by the weather free of any significant meteorological changes in the course of three successive days (72 hours);
c) owing to results accuracy, the impact of atmospheric radiation and the impact of the radiation reflected from the object being tested were minimized, because the measurements were performed at night and cloudy sky, far from street lighting;
d) the measurements for semi – transparent and transparent components (car panes / windscreen) have been performed in accordance with requirements included in the literature [12] (correct value of emissivity factor and of transfer coefficient);
e) the cars under examinations were heated up to the temperature of passenger cabin i.e. about 25 °C (the difference between the inside and outside temperature was equal to about 35 °C).

It was possible to obtain objective results and to maintain the minimization of measuring error, because the criteria presented above have been met.

THE RESULTS OF EXAMINATIONS – THERMOVISION PICTURES

All damages in the scope of the heat insulation system of the car and in the scope of heating circuit, particularly in winter period, lead to non- optimal use of thermal energy. They can also cause the panes freezing and consequently the loss of visibility. The engine temperature is reduced as a result of high heat demand. Therefore, the fuel consumption is increased.

The thermograms included below represent the areas with the leaks and failures occurred as a result of everyday operation of vehicle and as a result of structural components ageing. The gaskets located between the cabin doors and the car body are the elements producing the highest heat losses (Fig. 3a). The determination of heat loss percentage is possible by means of computerized analysis of the obtained results for every location being examined (the arrows indicate the maximum heat losses in the surface under analysis - Fig. 3b).

a) b)

Fig. 3. Thermogram of the car:
a) locations of occurring heat losses;
b) Temperature values at the locations of occurring heat losses

This method is used in order to qualify an element (gasket) for potential replacement. Ar1 point (Fig. 3b) situated in the vicinity of the engine chamber represents the highest heat losses in the thermogram under analysis.

The choked ventilation ducts distributing the air in the car are frequently the reason of the heating circuit inefficiency caused by the contaminations penetrating through the cabin filter used over long period of time without replacement. Another possible reason is the physical damage of ducts occurring as a result of excessive temperature or repair works.

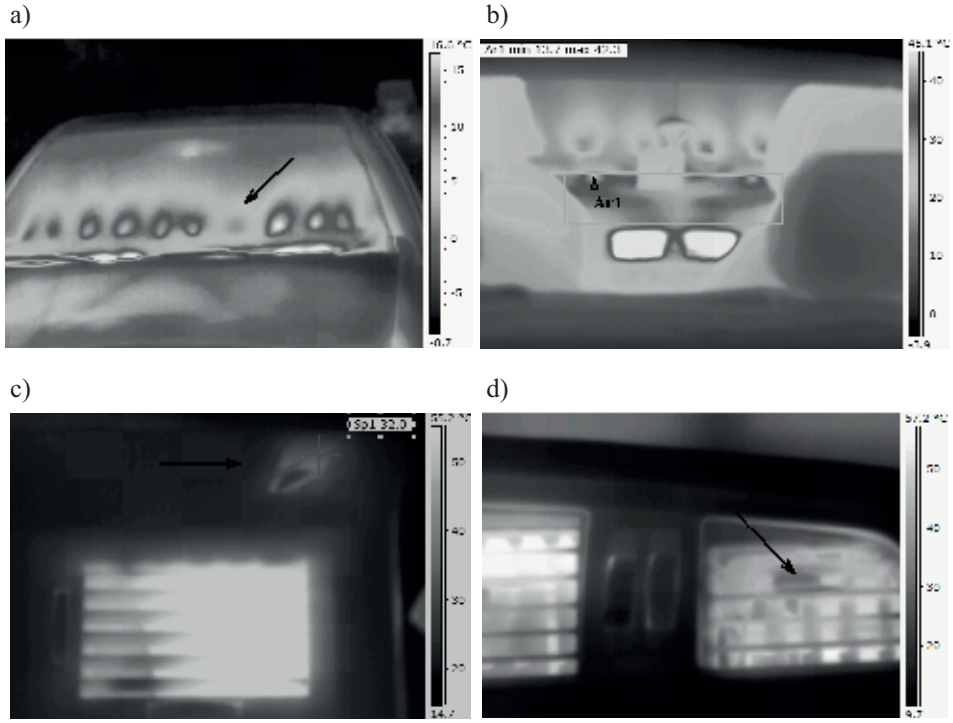

Fig. 4. Thermograms of air distribution circuit in the passenger cabin
a) windscreen; b) dashboard of the car (central panel);
c) side air grilles; d) central air grilles

The examples of the failures described above are illustrated in Figure 4:

– blocked air grille heating the windscreen causes its non-uniform defrosting (Fig. 4a) and can consequently lead to the visibility loss for the driver;
– properly heated air distribution system in the car makes it possible to perform the analysis of failures inside the ventilation ducts without dismantling e.g. dashboard (Fig. 4b). Furthermore the thermovision pictures give the opportunity to evaluate the warming – up of the dashboard i.e. a phenomenon associated with the use of proper materials and insulation elements;
– blocked side grille causes the loss of visibility in the mirrors (lack of defrosting of the windscreen areas situated in the vicinity of the mirror – Fig. 4c);
– failure (breaking) of air grille occurring in the form of non-uniform heat distribution at outlet (Fig. 4d).

The thermovision examinations make it also possible to quickly localize the physical damages causing the heat losses (Fig. 5a) and the discontinuities in the rear pane electric heating circuit of the car (Fig. 5b).

a) b)

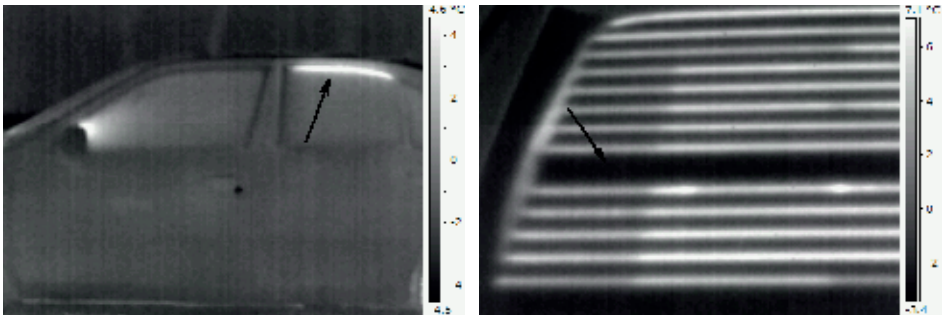

Fig. 5. Thermograms of failures
a) physical damage of the body in vicinity of rear pane,
b) discontinuity of rear pane heating path

CONCLUSIONS

1. The examinations presented in this article demonstrated that the thermovision can be used for the diagnostics of selected elements, systems or the whole circuits of motor vehicles in an easy and fast manner. The appropriate interpretation of the obtained results – thermovision pictures is the prerequisite for its application.
2. The efficient operation of the heating and air – conditioning system affects the travel comfort, reduces the driver fatigue and consequently increases the road traffic safety.
3. The method of examinations presented in this article can be applied in the summer as well as in winter period. However, the efforts should be made in order to maintain the highest possible difference between the temperature in the passenger cabin interior and outside temperature (more accurate interpretation of the results).
4. Using the thermovision cameras, it is possible to evaluate the vehicle insulation condition in a fast manner and to indicate the locations potentially endangered by failures. This method enables the detection of operational, design and technological defects of the car.
5. As a result of precise computerized analysis of the obtained results (thermograms) it is possible to classify an element or the whole system (circuit) as an inefficient component. The thermovision pictures are the diagnostic symptoms ensuring the detection of damaged location in a fast and reliable manner.
6. The thermovision examinations are an objective, non – invasive and contactless method used for the evaluation of technical condition of the heating, ventilation and air-conditioning (HVAC) circuit enabling the obtainment of diagnostic data without necessity to dismantle its individual elements.
7. The thermovision pictures can be used as database helpful in the design of new solutions, the improvement of reliability and performance of the heating, ventilation and air-conditioning circuits.

REFERENCES

Deh U.: Klimatyzacja w samochodzie, WKŁ, Warszawa, 2000.
Herner A., Diehl H. J.: Elektrotechnika i elektronika w pojazdach samochodowych, WKŁ, Warszawa, 2010.
Hinz T.: Układy klimatyzacji, Poradnik Serwisowy nr. 1/2009, Instalator Polski Sp. Z o. o., Warszawa, 2009.
Kordecka D.: Bezpieczeństwo pracy i ergonomia, CIOP, Warszawa, 1997.
Kozak P.: Klimatyzacja, Poradnik Serwisowy nr. 2/2004, Instalator Polski Sp. Z o. o., Warszawa, 2004.
Kwaśniowski S.: Ogrzewanie, wentylacja i klimatyzacja w pojazdach mechanicznych. Zasady doboru urządzeń ogrzewczych, wentylacyjnych i klimatyzacyjnych do pojazdów, Oficyna wydawnicza Politechniki Poznańskiej, Wrocław, 1995, s. 75-88.
Kwaśniowski S.: Ogrzewanie, wentylacja i klimatyzacja w pojazdach mechanicznych. Wymagania w zakresie mikroklimatu we wnętrzach pojazdów oraz kabin maszyn roboczych, Oficyna wydawnicza Politechniki Poznańskiej, Wrocław, 1995, s. 7-19.
Madura H.: Pomiary termowizyjne w praktyce, PAK, Warszawa, 2004.
Maldaque X.: Nondestructive evaluation of materials by infrared thermography, Springer-Verlag, London, 1993.
Minkina W.: Pomiary termowizyjne – przyrządy i metody, Wydawnictwo Politechniki Częstochowskiej, Częstochowa, 2004.
Minkina W. A., Rutkowski P., Wild W. A.: Podstawy pomiarów termowizyjnych. Część II – Współczesne rozwiązania systemów termowizyjnych, błędy metody, PAK 1/2000, Warszawa, 2000, s. 11-14.
Minkina W. A.: Podstawy pomiarów termowizyjnych. Część IV – Pomiar temperatury ciał półprzezroczystych i poprzez te ciała, PAK 1/2000, Warszawa, 2000, s. 5-8.
Orzechowski T.: Technika pomiarów termowizyjnych w diagnostyce maszyn, PAK 4/2002, Warszawa, 2002, s. 18-20.
Polczyk S., Różański L.: Thermographic Diagnosis Station of Machines. 7th International DAAAM Symposium, Wienna, 1996, s. 351-352.
Poloszyk S., Różański L.: Termowizyjna diagnostyka maszyn technologicznych, PAK 1/2000, Warszawa, 2000, s. 15-18.
Rohatka T., Bińczak K.: Termowizja w identyfikacji eksploatacyjnych uszkodzeń układów termoizolacyjnych do transportu żywności, Motrol'2009, Lublin, 2009, s. 170-175.
Więcek B., Lis M., Zwolenik S., Danych R., Wajman T.: Zastosowanie termowizji w badaniach nieniszczących i w mikroelektronice, PAK 11/2002, Warszawa, 2002, s. 8-12.
PN-E-01005:1990 „Technika świetlna – terminologia".
ASTM E1213 - 97(2009) Standard Test Method for Minimum Resolvable Temperature Difference for Thermal Imaging Systems.
ASTM E1311 - 89(2010) Standard Test Method for Minimum Detectable Temperature Difference for Thermal Imaging Systems.
http://www.flir.com
http://www.landinst.com
http://www.infratec.de

IDENTYFIKACJA USZKODZEŃ EKSPLOATACYJNYCH OBWODU OGRZEWANIA, WENTYLACJI I KLIMATYZACJI SAMOCHODU Z WYKORZYSTANIEM TERMOWIZJI

Streszczenie. W niniejszym artykule zaproponowano metodę okresowej kontroli obwodów ogrzewania, wentylacji i klimatyzacji z zastosowaniem kamer termowizyjnych. Przedstawiono sposoby interpretacji otrzymanych wyników w celu zdiagnozowania uszkodzeń obwodu ogrzewania. Dokonano oceny stanu technicznego instalacji wentylacyjnej (kanałów doprowadzających powietrze) bez jej demontażu. W artykule przedstawiono ponadto badania termowizyjne, które pozwalają w szybki i łatwy sposób wskazać miejsca występowania największych strat ciepła zarówno silnika, jak i kabiny pasażerskiej, co jest szczególnie ważne w okresie zimowym.

Słowa kluczowe: termogram, pomiary w podczerwieni, obwód ogrzewania, kamera termowizyjna, mikroklimat w pojeździe

TEKA Kom. Mot. Energ. Roln. – OL PAN, 2011, 11, 363–372

THE PROBLEMS IN FIBRE OPTIC COMMUNICATION IN THE COMMUNICATION SYSTEMS OF VEHICLES

Sumorek Andrzej, Buczaj Marcin

Ph.D. Eng., Department of Computer and Electrical Engineering,
Lublin University of Technology, Poland

Summary. The diversification of technical solutions occurred as a result of almost thirty years of evolution of the communication systems between the mechatronic systems in motor vehicles. The vehicles are equipped with the conventional cable connections between the switches and actuators as well as with advanced data exchange networks. These networks show more and more similarities to computer networks. They are the new solutions; even their classification has been created a few years ago (class D). Therefore the personnel engaged in the scope of functional programming and vehicles servicing encounter the problems associated with networks operation. The purpose of the article is to present the principles of functioning of the basic networks with the medium in the form of an optical fibre. Particular emphasis has been placed on the detection of failures consisting in the damage of communication node and optical fibre.

Key words: Media Oriented Systems Transport, Domestic Digital Bus.

INTRODUCTION

The systematics associated with networks classification presented in the year 1994 contained 3 types of networks. Such systematics was also presented in 2007 in literature in 2007 [12]. This approach has been established as a result of the standardization introduced by SAE J1850 [5, 10]. Three classes of communication systems have been specified in SAE J1850. The applications group associated with bus throughput is used as the criterion of subdivision. The increase of the vehicles users' requirements enforced the increase of the networks throughput and the launching of two new additional classes of networks indicated as C+ and D or Infotainment [7]. The summary of essential parameters for individual classes is presented in Table 1 [2, 19].

The networks and communication busses with lower throughput are built on the basis of standard copper conductors. Their topology can be diversified. There are simple systems in the form of linear bus as well as the systems in star configuration. The ring topology is rarely applied. The combination consisting of point-to-point connections, linear buses and star buses is more popular than ring topology. The optical fibre performs the role of medium in the networks with higher throughput. Its use is almost obligatory in D class (MOST, D2B buses) or optional in C+ class (FlexRay, Byteflight buses). The introduction of fibre optic communication into the vehicles networks and the introduction of fibre optic solutions into the telecommunication was based upon the same factors.

The possibility to achieve high throughput of data exchange (> 1 Gb/s) is the principal factor justifying the introduction of fibre optic solutions. The price of the vehicle subassemblies would be significantly increased in case of such throughput level achieved in traditional vehicles communication networks operating in difficult working conditions (wide range of temperature and humidity changes, vibration). The transmission security is automatically improved as a result of fibre optic technology. On the one hand an optical fibre is resistant to electromagnetic interference and on the other hand it does not generate any interference potentially affecting the operation of other devices. The achievement of similar throughputs of fibre optic and "copper" buses is possible at smaller diameters of the wires. The diameters of fibre optic cables, smaller than the diameters of copper cables result in reduced weight of vehicle and, consequently in reduced fuel consumption in course of the vehicle operation. Unfortunately, there are some additional problems introduced by the fibre optic connections of high-speed communication buses; said problems are described in further parts of this article.

Table 1. The classification of bus communication systems [2, 19]

Diagnostic	
Typical application	Testers, analysers
Throughput	< 10 Kb/s
Example of bus (network)	ISO 9141 K-Line
Class A	
Typical application	Electronic elements included in the motor vehicle body, connections of circuits and actuators
Throughput	< 25 Kb/s
Example of bus (network)	LIN, SAE J1587
Class B	
Typical application	Electronic systems included in the motor vehicle body, connections of controllers in the systems of additional equipment of motor vehicle
Throughput	25÷125 Kb/s
Example of bus (network)	CAN low-speed
Class C	
Typical application	Power transmission system and running gear; connections of controllers in the power transmission and chassis system, real time systems
Throughput	125Kb/s÷1 Mb/s
Example of bus (network)	CAN high-speed
Class C+	
Typical application	Real time systems; power transmission and safety system; „X-by-wire" control
Throughput	1÷10 Mb/s
Example of bus (network)	FlexRay, Byteflight
Class D / Infotainment	
Typical application	Multimedia, connections of controllers in telematics systems
Throughput	>10 Mb/s
Example of bus (network)	MOST, D2B

COMMUNICATION USING „MOST" BUS

The connections in ring topology prevail in multimedia networks. Such topology is also applied in Domestic Digital Bus (D2B) and in Media Oriented Systems Transport (MOST) buses. Domestic Digital Bus has been created in 1992 and was promoted by the group of companies i.e. Matsushita, Philips and Optical Chip Consortium [8]. At the moment this bus is not developed. This solution was applied at the turn of the 20th and the 21st century in the vehicles: Mercedes S class and Jaguar X-type. MOST bus is the successor of Domestic Digital Bus (D2B). The works associated with this bus have been commenced in the year 1998 by the following companies: Audi, BMW, Daimler -Chrysler, Becker Automotive and Oasis Silicon [2, 4, 20, 21]. The problems encountered by the designers and users of D2B bus at that time are the problems associated with MOST bus at the moment. MOST Cooperation Association informs that MOST bus has been used by 16 manufacturers of motor vehicles in more than 90 models in the year 2010 [13]. The fibre optic cable is the basic communication medium of MOST bus ensuring required throughput of this bus. It is possible to integrate 64 multimedia slaves in ring topology (Fig. 1) [4, 21]. The possible slaves are: control panel, radio and TV tuners, CD and DVD players; amplifiers systems; navigation system, phones, telephone assistance systems (e.g. Tele-Aid, Automatic Collision Notification, Stolen Vehicle Recovery), voice control systems, game consoles, displays for the passenger on the front and rear seat.

The role of the master node is performed by one of elements of the ring. The task of the master consists in the events management on the bus (timing master function) i.e. in generation of communication frames [6, 21]. The frames are handed over by other nodes (slaves) in unchanged form or in a form supplemented with individual data. The communication is possible with the speed of 25 or 50 Mb/s in accordance with specification [21]. The members of the MOST consortium assure that it is possible to changeover to third generation of bus in a smooth manner and to ensure the communication speed of 150 Mb/s [13, 16]. Another function of the ring management consists in the addressing of bus slaves and is assigned to „network master" node. Four groups of addresses (logical, physical, group and broadcast addresses) determined by the addresses master are used in further communication between the nodes. The third management function consists in the informing, reservation and release of resources required for synchronous communication. This function is called „connection master". The configuration with all three managing functions performed by single physical device is possible in practice; most often in the form of the vehicle console control module [2].

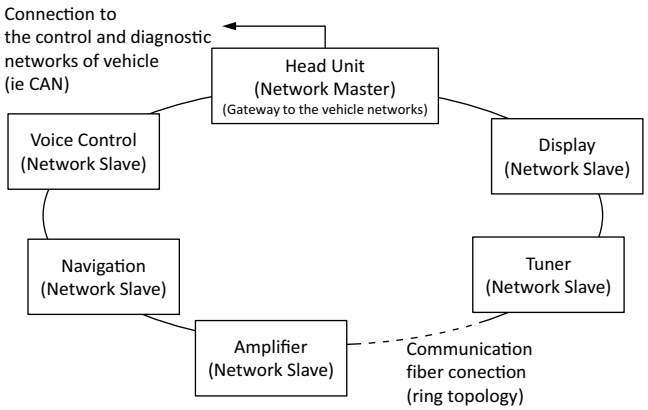

Fig. 1. Typical topology of MOST bus [2, 6, 20, 21]

After startup of the bus devices, the addressing of slaves is performed by „network master". The next step consists in the reservation of synchronous channels by the slaves requiring synchronous communication (audio and video data) as considered by the „connection master" in its table. Since then „timing master" is responsible for the distribution of communication frames (Fig. 2).

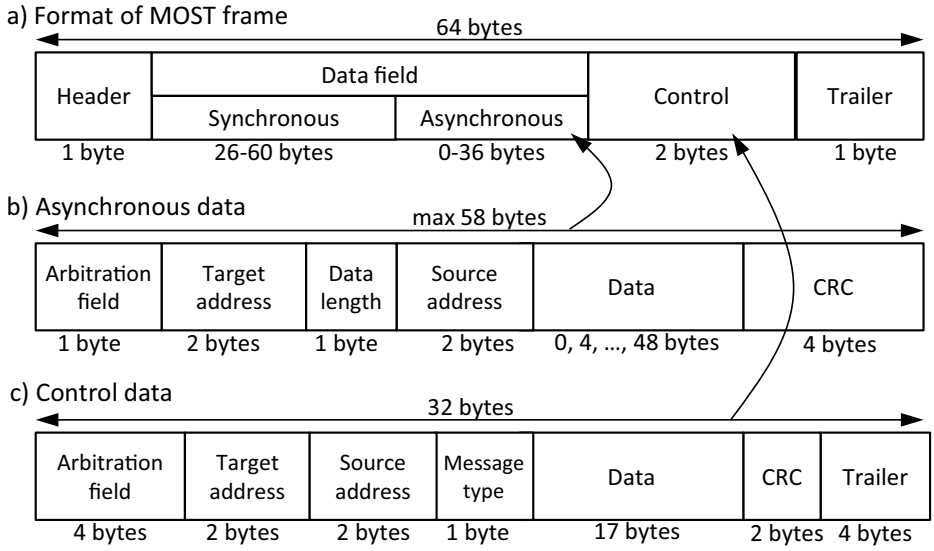

Fig. 2. Data format [4, 20, 18, 21]

The communication unit of MOST bus is defined as the block consisting of 16 frames (Fig. 2a). The following data are transferred in the framework of a single frame:

- synchronous data – audio and video data being transferred in reserved channels of the frame data field (Fig. 2a). The size of the synchronous data field is configured in the frame header and has the impact on the size of asynchronous field;
- asynchronous data – packages of non-multimedia data i.e. the information about the compositions being played; GPS data, computer network packages. They are packaged in the frames in accordance with structure illustrated in Fig. 2b and transferred in an asynchronous data field. The asynchronous packages are subdivided into smaller parts and transferred in several frames. In case of attempted access to the bus by several devices simultaneously, the arbitration is performed by means of initial fields of package. The package with the highest priority is directed to the frame which is practically associated with the lowest binary number in the arbitration field;
- control data – data required for network functioning control and for the devices functions control. Their required arbitration and subdivision are similar to those required for asynchronous data (Fig. 2c).

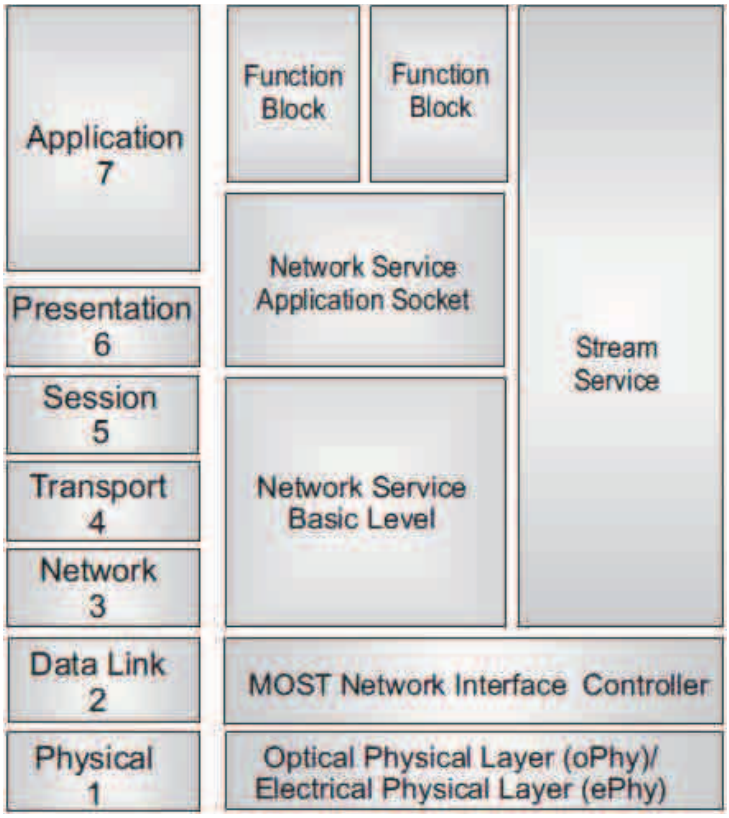

Fig. 3. MOST layers in the ISO-OSI model [4]

One of the features inherited by MOST bus from D2B bus consists in the method of its description, manner of the bus specification preparation. One layer or only a few of selected layers of protocol are often defined for CAN or LIN buses [1, 9, 15, 14]. In case of MOST bus, the specification encompasses the elements from the lowest physical layer up to the commands from application layer (Fig. 3). It is possible to support the complex devices originating from various manufacturers thanks to precise description of the addressing, services, functions and commands (Function Blocks).

BUS FAILURES AND METHODS OF THEIR DETECTION

As a result of the use of fibre optic cables in MOST bus and thanks to the protections applied in the protocol frames (Fig. 2), the average rate of errors for MOST bus is equal to 10^{-10} [21]. In case of secure CAN protocol, the average rate of errors is equal to 10^{-11} in case of situations with superimposing artificial errors resulting in the reduction of undetected rate of errors of 10^{-7} [21, 17].

There are 3 principal reasons of potentially occurring problems in the bus functioning:

– incorrect bus functioning as a result of incorrect software (incompatible version of the slave software, erroneous function call);

– corruptions or lack of communication resulting from the failure of master or slave node of the bus (power supply voltage out of permissible range; physical damage of the node;
– corruptions or lack of communication resulting from the failures of fibre optic cables.

The first one of three specified groups of errors can be extremely difficult to detect in case of rarely occurring errors without significant importance. Lack of repeatability of the problems and their incidental occurrence prevents their elimination by means of simple methods applied in workshop practice. In case of persistently occurring error, the errors can be detected by means of the network traffic recorder. For example the Data Logger manufactured by Telemotive AG – model „the blue PiraT 150M6-C2LE" can be used for the recording and further analysis of the traffic on MOST bus. The Data Logger is provided with an interface enabling the connection of tester to optical network MOST150 and the recording of control messages, bus status information, bus data packages. The additional interfaces are provided to enable the recording of the activity of other devices in the vehicle, because the recorder is provided with 4 inputs of CAN protocol, 2 inputs for LIN protocol, 4 serial interfaces and four Ethernet ports.

The second one of three specified groups of errors results from the partial or total failure of one of nodes. In case of damaged „time master" or „network master" any correct startup of the network and its functioning is impossible. In case of additionally failed gateway to diagnostic network, any network diagnostics is completely impossible. In such case the replacement of the node performing the role of "master" and the replacement of gateway is the only possible solution. In other cases it is necessary to detect the slave nodes deforming or locking the optical signal. In this case the procedure is similar to that applied in case of the elimination of fibre optic cables failures .

The third group of errors results from the failures of fibre optic cables. Their result consists in the reduction of luminous flux or its decay. The failures consist in:

– broken conductor or conductor plug;
– excessive bending angle of fibre optic conductor;
– scratching or cracks on the fibre optic cable sheath;
– contamination of contact surfaces in the connector.

Fig. 4. Typical failures of fibre optic cables: bending, damage of sheath, damage of fibre [11]

The sole efficient method preventing the operation interruptions of the fibre optic bus built in ring topology consists in the application of nodes with many transmitters and receivers supporting several rings simultaneously or in an additional cable connection between the nodes (Fig. 5) [3, 21].

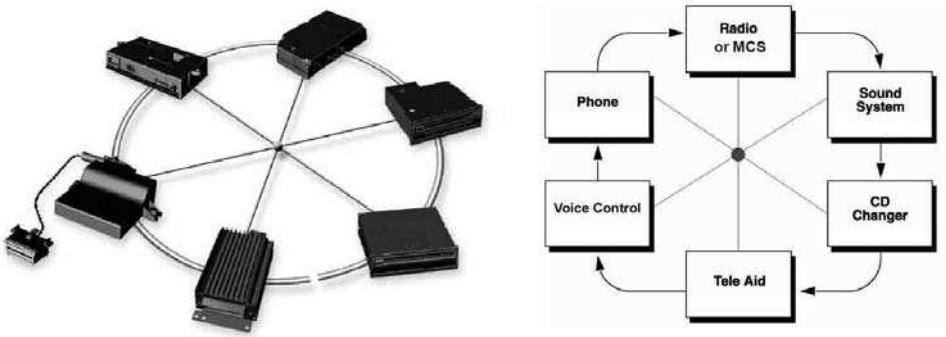

Fig. 5. Optical ring bus aided by means of copper star configuration. MOST bus in AUDI car (on the left) [4]. D2B bus in Mercedes car (on the right) [11]

There are two methods of use of an additional cable connection. The first method consists in the use of cable connection for the application of an independent diagnostic protocol (e.g. CAN). This protocol makes it possible to perform the complete diagnostics of the nodes irrespective of optical protocol. Another method originates from D2B bus and is based upon the information supplied from master node and concerning the configuration (sequence) of devices in the ring. In this method, after decoupling of optical bus, a diagnostic wake-up signal is sent by the master node and the slave nodes respond in the form of electric signals in the sequence conforming with the order of the devices occurring in the list. The lack of an "electric" response of the node indicates its failure (Fig. 6).

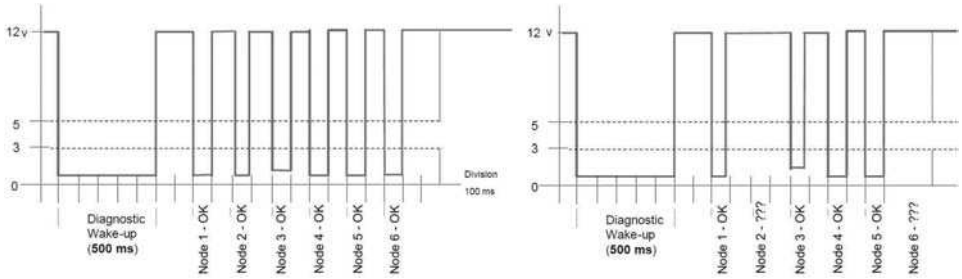

Fig. 6. Response to diagnostic wake – up in D2B bus. Efficient nodes (on the left), the second and sixth nodes failed (on the right) [11]

The evaluation of the fibre optic connections status is impossible by means of the method consisting in the use of an additional electric connection for diagnostic purposes. The partial and complete failures of the fibre optic ring can lead to the ring de-synchronization, problems with the execution of "ring lock" operation and unsuccessful network startup, lack of communication resulting from the fibre optic conductor discontinuity. The evaluation of the network node, fibre optic cable failure is possible by means of one or two fibre optic testers (Fig. 7).

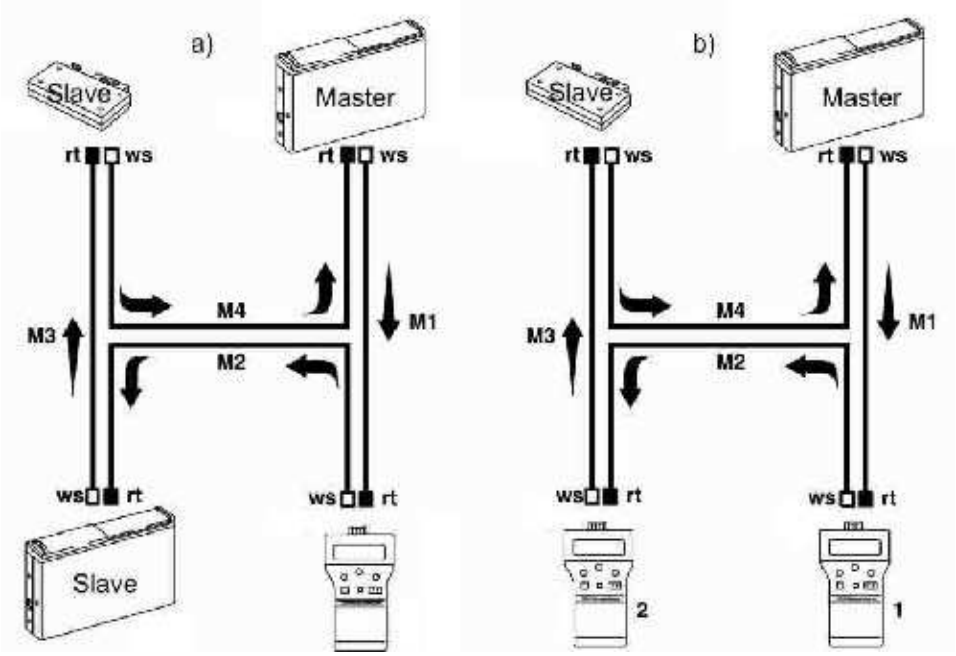

Fig. 7. Testing of bus elements of by dedicated testers [11]

The evaluation of the node failure by means of the fibre optic tester consists in the replacement of "suspected" node by tester. An optical signal is transmitted by the tester operating in "by-pass" mode. If the remaining network components are able to support each other after such replacement, the eliminated element is inefficient.

The use of two testers is required for the evaluation of fibre optic cable. One of them performs the function of a standard source of luminous flux and another is used as the illumination meter. Therefore it is possible to determine if the signal level is optimal for specified type of connection or if the replacement of the fibre optic conductor is required.

CONCLUSIONS

The summary of problems presented above and accompanying to the optical networks functioning in vehicles is based upon Media Oriented Systems Transport and Domestic Digital Bus. The both buses are operated in ring topology. The fibre optic communication makes it possible to achieve higher transmission rates as well as to reduce the impact of electromagnetic interference and its emission. The following operation problems occur in case of application of a fibre optic bus in the vehicle:

1. It is important to maintain the value of the fibre optic cable arc under its limit value which is approximately equal to 25 mm. The luminous flux is reduced and bus operation becomes problematic if this limit value is exceeded.
2. A special device for the terminals connection is required in case of the fibre optic cable failure. Therefore a good practice consists in the replacement of the failed fibre optic cable.

3. In contrast to the typical linear or star cable buses, the knowledge of the route of fibre optic cables forming the ring is necessary in order to localize the failure.
4. In order to localize the failures of the optical ring bus in an easy manner, it is necessary to support this bus by means of an additional communication ring or by means of a standard cable connection in star topology and to plan an emergency procedure.
5. Low-skilled service personnel will be practically unable to eliminate the failure which is not displayed as a legible result obtained from an automatic auto-detection procedure.

REFERENCES

Bosch R. GmbH, 1991: CAN Specification. Version 2.0, Stuttgart.

Bosch R. GmbH, 2008: Sieci wymiany danych w pojazdach samochodowych, Warszawa, Wydawnictwa Komunikacji i Łączności.

Fechner B., 2010: Timing master faults. Elektronik automotive, 3/2010, p. 29-31.

Grzemba A., 2008: MOST - The Automotive Multimedia Network, Frazis Verlag GmbH.

International Organization for Standardization, 1994: ISO 11519-3 Road Vehicles – Low Speed Serial Data Communication – Part 3: Vehicle Area Network (VAN).

Kaparuk J., 2010: Pokładowe systemy diagnostyczne OBD i EOBD oraz sieci transmisji danych. Wybrane zagadnienia. Cz. 1, Poradnik serwisowy, 4/2010, Warszawa, Wydawnictwo Instalator Polski.

Leen G., Hefferman D., 2000: Talking to the car. The Engineneer, http://www. theengineer.co.uk/news/talking-to-the-car/285325.article, 5 October 2000.

Leen G., Heffernan D., 2002, Expanding Automotive Electronic Systems. Computer, vol 35.

LIN Consortium, 2006: LIN Specification Package Revision 2.1, http://www.lin-subbus.org/index.php?pid=7&lang=en&sid=40196e2bfe83bdc51aa65e0d4f79ef26.

Lupini C.A., 2010: In-Vehicle Networking Technology for 2010 and Beyond, SAE International, USA.

Mercedes Benz, 2004: Domestic Digital Bus (D2B). Technical training materials - 416 HO D2B (CooksonI), Mercedes-Benz USA.

Merkisz J., Mazurek S., 2007: Pokładowe systemy diagnostyczne pojazdów samochodowych, Warszawa, Wydawnictwa Komunikacji i Łączności.

MOST Cooperation, 2010: Annual Achievement Report 2010. http://www.mostcooperation. com/publications/brochures_newsletters/latest/index.html?do180739=download.

Sumorek A., 2010: Safe Communications Among Vehicle Sub-assemblies on the Basis of the Embedded Functions of CAN Protocol, Teka Komisji Motoryzacji i Energetyki Rolnictwa, vol. X, s. 432-439.

Sumorek A., Buczaj M., 2010: Przyszłość magistrali Local Interconnect Network, Motrol - Motoryzacja i Energetyka Rolnictwa, tom 12, s. 145-157.

Thiel C., 2010: From Germany into the whole wide world. Elektronik automotive, 3/2010, p. 6-7.

Tran E., Koopman P. (advisor), 1999: Multi-Bit Error Vulnerabilities in the Controller Area Network Protocol. Carnegie Mellon University. Pittsburgh.

Widerski T., 2005: Samochodowe sieci informatyczne. Poradnik serwisowy, 5/2005, Warszawa, Wydawnictwo Instalator Polski.

Widerski T., Kędzierski J., 2004: Samochodowe sieci informatyczne (CAN), Auto Moto Serwis, 4/2004, Warszawa, Wydawnictwo Instalator Polski, s. 38-42.

Widerski T., Kędzierski J., 2004: Samochodowe sieci informatyczne (MOST), Auto Moto Serwis, 6/2004, Warszawa, Wydawnictwo Instalator Polski, s. 35-37.

Zimmermann W., Schmidgall R., 2008: Magistrale danych w pojazdach. Protokoły i standardy, Warszawa, Wydawnictwa Komunikacji i Łączności.

PROBLEMY KOMUNIKACJI ŚWIATŁOWODOWEJ W SYSTEMACH KOMUNIKACYJNYCH POJAZDÓW

Streszczenie. Efektem prawie trzydziestu lat ewolucji systemów komunikacji pomiędzy układami mechatronicznym pojazdów jest zróżnicowanie rozwiązań technicznych. W pojazdach można spotkać zarówno tradycyjne połączenia kablowe pomiędzy przełącznikami i elementami wykonawczymi jak i zaawansowane sieci wymiany danych. Sieci te wykazują coraz więcej podobieństw do sieci komputerowych. Są to rozwiązania nowe, które jeszcze kilka lat temu nie miały nawet swojej klasyfikacji (klasa D). W związku z tym, osoby zajmujące się programowaniem funkcjonowania i serwisem pojazdów napotykają problemy przy pracy z sieciami. W artykule przestawiono zasady funkcjonowania podstawowych sieci z medium w postaci włókna światłowodowego. Nacisk został położony na mechanizm wykrywania uszkodzeń polegających na uszkodzeniu węzła komunikacyjnego oraz włókna światłowodowego.

Słowa kluczowe: Media Oriented Systems Transport, Domestic Digital Bus.

TEKA Kom. Mot. Energ. Roln. – OL PAN, 2011, 11, 373–385

FLY ASH IN AGRICULTURE - MODERN APPLICATIONS OF COAL COMBUSTION BY-PRODUCTS

Dominika Katarzyna Szponder[*], Kazimierz Trybalski[*]

[*]Department of Environmental Engineering and Mineral Processing,
Faculty of Mining and Geoengineering, AGH University of Science and Technology,
Al. Mickiewicza 30, 30-059 Krakow, Poland.

Summary. Although alternative energy sources are gaining increasing importance, fossil fuels, especially coal, play a significant role in the global energy production. Unfortunately, coal combustion generates a large amount of Coal Combustion Products (CCPs), including fly ash. Fly ash has substantial negative effect on environment, while its properties could make it a desired secondary raw material in many industry branches. Due to the large amount of fly ash produced in recent years, the researchers have been searching for new, unconventional methods of FA utilization.

Fly ash can be used in agriculture, because it has special physical and chemical properties. FA has a unique structure and contains almost all the nutrients necessary for proper plants growth and development. First of all, fly ash is used as a mineral fertilizer which improves the physical, chemical and biological properties of soils. It can also be applied as an agent, which increases plant growth and amount of the obtained yields. In addition, fly ash is used to reduce the amount of heavy metals accumulated in plants and to limit the spread of diseases.

Although fly ash application in agriculture has many benefits, there are some disadvantages connected with this application (for example heavy metals and radionuclides contamination of soils and surface waters, soil salinity). In addition, there is also risk associated with lack of information on the long-term effects of fly ash application on soil quality and environment. Therefore, it is necessary to continue research on this topic to clarify the effects of the fly ash addition to the soil on agricultural production and the environment.

In this publication the authors determined the usefulness of FA and the limits of its use in agriculture. They also presented the modern applications of CCPs in agriculture, as well as evaluated the benefits and risks associated with this type of FA application.

Key words: fly ash, coal combustion products, agriculture, soil quality, fertilization, soil contamination.

INTRODUCTION

Although alternative energy sources are gaining increasing importance, fossil fuels, especially coal, play a significant role in the global energy production. Around $3.5 \cdot 10^9$ Mg of coal is mined in the world annually, which accounts for almost 38% of the world's electricity source [Ram and Masto 2010]. In Poland, the production of electricity and heat is also based on the thermal processing of bituminous coal and lignite in power plants.

Unfortunately, coal combustion generates a large amount of wastes in the form of Coal Combustion Products (CCPs). This group of wastes includes fly ash, slag, ash-slag mixture, microspheres, bottom ash from fluidized bed, gypsum and other wastes from flue gases desulfurization. Among them, fly ash (FA) deserves special attention because it has a substantial negative effect on the environment, while its properties could make it a desired secondary raw material in many industry branches [Szponder and Trybalski 2009b].

FA is a mineral residue from coal combustion. It leaves the boiler with the flue gases and then is captured by dust collectors (mainly electro-filters). It was estimated that $5.5 \cdot 10^8$ Mg of FA is produced each year in the world (most of all in China, USA and India) [Ram and Masto 2010], while in Poland approximately $4.2 \cdot 10^6$ Mg was generated in 2009. FA shows a wide variation in their physical, chemical and mineralogical properties which depend on the nature of fuel (bituminous coal, lignite, biomass, etc.), conditions of combustion, type of emission control devices, storage and handling methods. Specific physical, chemical and mineralogical properties and massive formation of FA allows for its wide use as raw material in many industry areas. In the same time, disposal and storage of FA is associated with high costs and a considerable burden for the environment. Traditionally, most of this secondary raw material is used in building industry, ceramics, road construction or mining. In recent years new, unconventional methods of FA utilization were found in the chemical industry, environmental engineering or agriculture [Pandey and Singh 2010, Szponder and Trybalski 2009a].

In this publication the authors determined the usefulness of FA and the limits for its use in agriculture. They also presented some modern applications of CCPs in agriculture, as well as evaluated the benefits and risks associated with this type of FA application.

PROPERTIES OF FLY ASH

Fly ash is inorganic residue from coal combustion in power boilers. FA has a high morphological, phase and chemical composition diversity depending on the use of different methods of combustion (conventional and fluidized bed boilers), the composition of fuels (bituminous coal, lignite, biomass), a high dispersion of minerals in fuels and the dynamics of thermal processes. There are three basic groups of FA – silicate fly ash (sFA), aluminium fly ash (aFA) and calcium fly ash (cFA) [Szponder and Trybalski 2009b]. The most important properties of fly ash are presented in Table 1 [Sobik-Szołtysek and Janecka 2006].

Table 1. Selected properties of fly ashes [Sobik-Szołtysek and Janecka 2006].

Designation	Unit	Fly Ash		
		Silicate	Aluminium	Calcium
Specific density	[kg/m^3]	2500 – 4500	2000 – 4000	2000 – 4000
Specific surface by Blaine	[cm^2·cm^{-3}]	2250 – 2450	2250 – 2450	2250 – 2450
Permeability	[m/s]	10^{-10} – 10^{-7}	> 10-7	10^{-11} – 10^{-8}
SiO_2	[% by weight]	38 – 58	40 – 50	25 – 56
$A1_20_3$	[% by weight]	15 – 31	30 – 35	5 – 18
Fe_2O_3	[% by weight]	4.5 – 15	5 – 12	4.5 – 8
CaO	[% by weight]	1.7 – 10	2 – 4	12 – 41
MgO	[% by weight]	0.2 – 5	1 – 3	0.8 – 7
Na_2O	[% by weight]	0.3 – 1.5	0.5 – 1.5	0.1 – 1.5
K_2O	[% by weight]	0.3 – 3.7	1.5 – 3	0.25 – 3

SO_3	[% by weight]	0.2 – 2	0.4 – 1	3.1 – 10
Cr	[ppm]	90 – 240	80 – 110	100 – 110
Cd	[ppm]	0.2 – 0.7	0.8	< 2
Cu	[ppm]	80 – 190	55 – 75	40 – 100
Ni	[ppm]	30 – 200	–	–
Pb	[ppm]	20 – 380	50 – 80	25 – 45
Zn	[ppm]	30 – 1100	110 – 140	90 – 220
Roasting loss	[% by weight]	2 – 10	0.5 – 2	0.5 – 2

Physical Properties

Generally, fly ash is light gray to black in colour (depending on the amount of unburned carbon and organic matter residue). Some time it can be light brown to dark brown in colour (mostly from brown coal and biomass combustion). FA consists of fine, glassy particles, which range in particle size from 0.01 to 100 μm. Their composition is dominated by spherical grains (mineral or amorphous), either solid (pirospheres), hallow (cenospheres) or filled with smaller amorphous particles (plerospheres). These grains appear individually, or in the form of aggregates. In addition, there is a large group of irregular, highly porous, rounded or sharp-edged grains in FA (carbon residue and soot). FA has low bulk density, high surface area and light texture [Ahmaruzzaman 2010].

Chemical Properties

The major chemical components of FA include oxides of silicon, aluminium, iron and calcium (95 - 99%). In addition, FA contains secondary components in the form of oxides of Ti, P, Mg, S, Na and K (0.5 - 3.5%) and unburned carbon (roasting loss). This waste also contains trace elements like Mn, B, Ba, Cu, Sr, Ni, Cr, Zn, Cd, Co, Mo, V, Se, Pb, As, etc. (0.1 - 0.3%) and radioactive elements like ^{40}K, ^{226}Ra i ^{232}Th. The pH of FA is usually in the range from 4.5 to 12.0, depending on the sulfur content in coal and on combustion and desulphurization technology. Wastes in which the ratio of Ca to S is lower than 2.5 are acidic in nature, and those with a ratio higher than 2.5 are alkaline [Szponder and Trybalski 2009a, Pandey and Singh 2010, Feng i in. 2006].

Mineralogical Properties

In its mineralogical structure, FA contains primarily amorphous substances in the form of silicon-aluminium glass (80%). It contains also a few crystalline phases such as gypsum ($CaSO_4 \cdot 2H_2O$), mullite ($3Al_2O_3 \cdot 2SiO_2$), quartz (SiO_2), magnetite (Fe_3O_4), anhydrite ($CaSO_4$), ettringete ($3CaO \cdot Al_2O_3 \cdot 3CaSO_4 3 \cdot 32H_2O$), opaline SiO_2, hematite (Fe_2O_3), lime (CaO), chlorite, feldspar, and spinel ($FeAl_2O_4$) [Ahmaruzzaman 2010, Szponder and Trybalski 2009a].

Fly Ash Properties Significant for Application in Agriculture

Because of its favorable physical and chemical properties fly ash has been used in agriculture and forestry for more than thirty years. The specific and bulk density, particle size, porosity, water holding capacity, surface area and chemical composition are the most important physicochemical

properties of FA allowing for utilization in agriculture. FA contains most of the necessary plant nutrients (except of nitrogen and organic carbon, which are oxidized in the combustion process). This deficiency is compensated by high concentrations of phosphorus, which by reaction with aluminum, iron and calcium contained in the alkaline FA, can be easily absorbed by plants. Significant amount of macro- and micronutrients in FA utilized in agriculture improves soil fertility, which encourages the crops growth. Moreover, FA with large amounts of amorphous aluminosilicate glassy spheres is great addition to the clay soil, and considerably improves its properties. At the same time, calcium-rich alkaline FA is very useful for neutralizing acidic soils. Because of these and other physical and chemical properties of FA, its application in agriculture improves soil fertility [Pandey and Singh 2010, Singh et al. 2010].

Despite these favorable characteristic, environmental concern has been raised as to the potential risk FA may pose to plants and consumers. These disadvantages are connected mainly with heavy metals presence in FA. Those metals can be accumulated in crops and may be poisonous to final consumers. Furthermore, traces of radionuclides contained in this waste present a risk to crops [Singh et al. 2010].

APPLICATIONS OF FLY ASH IN AGRICULTURE

In agriculture, fly ash can be utilized in many different ways. First of all, it is used as a mineral fertilizer which improves the physical, chemical and biological properties of soils. Also, it can be applied as an agent which increases plant growth and the amount of obtained yields. In addition, FA is used to reduce the amount of heavy metals accumulated in plants and to limit the spread of diseases.

Soil Quality Improvement

The influence of fly ash application on physical, chemical and biological properties of soil and its quality has been carefully examined [Ram and Masto 2010, Singh et al. 2010, Pandey and Singh 2010, Ferreira et al. 2003, Ciećko et al. 2009, Właśniewski 2009, Fulekar 1993, Gracia i in. 1995, Phung et al. 1979, Lai et al. 1999, Menon et al. 1993, Kalra et al. 1997, Vincini et al. 1994].

FA addition to soil significantly alters its structure. Because FA particles are small and have specific shapes (e.g., hollow spheres), it causes the formation of pores and voids in the soil structure. The changes in soil structure are related to such changes in its physical properties as bulk density, porosity, hydraulic conductivity, water holding capacity and aeration. These properties have a direct impact on the nutrients availability in the soil, its biological activity, and plant germination and growth. Another property of FA, which improves soil quality, is the presence of pozzolanic minerals such as Ca and Si in FA. This property affects the soil bulk density, porosity and its ability to retain water [Ram and Masto 2010]. For example, research [Fulekar 1993] showed that the addition of a large dose of FA (600 $t{\cdot}h^{-1}$) to acid clay soil, causes a significant improvement in soil texture and its physical and chemical properties. An the same time, the addition of a large amount of FA (200 - 400 $t.h^{-1}$) to sandy-clay soil results in a significant improvement of its bulk density, acidity, gas permeability and water holding capacity [Gracia et al. 1995].

The addition of FA to soil has a significant effect on its chemical properties. Fly ash, especially alkaline FA, contains large amounts of Ca and is used to reduce soil acidity. If FA contains significant amounts of silicate minerals such as mullite, it forms silicic acid, which neutralizes hydrogen ions in the soil. Adequate pH in soil has a significant effect on the chemical components bioavailability, and thus directly and indirectly affects plant growth [Ram and Masto 2010]. Fly

ash successfully replaces limestone and dolomite in soil pH regulation. For example, some studies [Phung et al. 1979] showed that the addition of 1 kg of alkaline FA has the same effect on soil pH and calcium bioavailability as the addition of about 0.2 kg of pure $CaCO_3$.

Fly ash also provides minerals which are essential for soil, such as P, K, B, Ca, Mg, Mn, Zn, carbonates, bicarbonates and sulfates. Micro and macro elements delivered to soil in the FA have a positive effect on plant growth and upgrade its agronomic properties [Ram and Masto 2010]. For example, Lai et al. [Lai et al. 1999] found out that the concentrations of Mg, B, K and P increased in the soil which contained about 5 - 10% of FA. Also, Menon et al. [Menon et al. 1993] noted that in the crops growing on the medium containing FA, the concentration of biogenic elements, such as K, Ca, Mg, S, Zn and B, is higher than in the traditionally grown plants.

An effect of FA on the soil's biological and biochemical properties has not been thoroughly studied. There is no information on the biological processes and the impact of too low or too high FA concentration on the soil's biological properties. Although FA does not directly affect the biological activity of the soil, it changes soil texture what may lead to intensification of biological processes in soil [Ram and Masto 2010]. For example, some studies [Kalra et al. 1997] showed that 5% concentration of FA in soil increased microbial activity, while addition of larger amounts of FA inhibited biological processes. However, research conducted by Vincini et al. [Vincini et al. 1994] showed that concentration of FA in soil higher than 10% still enhanced microbial activity in soil. The impact of FA on microbial activity is inconclusive. It is generally accepted that small amounts of FA have little effect on microbial activity and larger FA concentration in soil inhibits microorganisms.

Plant Growth and Yield Increase

The application of fly ash for soil fertilization is associated with plant growth and yield increase. FA contains almost all minerals necessary in the metabolic processes of plants. The influence of FA application on plant growth and production yield rate has been studied by many researchers [Ajaz and Tiyagi 2003, Khan and Khan 1996, Singh and Agrawal 2010, Singh et al. 2010, Iyer and Scott 2001]. In most cases, the addition of FA to soil increases plant growth as well as the minerals and nutrients uptake.

For example, Khan and Khan [Khan and Khan 1996] conducted a study on the impact of FA on tomatoes growth. They were trying to determine the most suitable dose of FA in the soil. In the experiment they used the following doses of FA: 0, 10, 20, 30, 40, 50, 60, 70, 80, 90 and 100%. The research showed that in the soil which contained from 20 to 80% of FA, the growth of shoots and roots increased by 40 - 90%. In the sample which contained 100% of FA, plant growth increased by app. 5%. The most optimal soil contained 50 - 60% of FA.

In their studies Ajaz and Tiyagi [Ajaz and Tiyagi 2003] determined the effect of different concentrations of FA (0, 10, 25, 50, 75, 90 and 100%) on cucumbers growth and quality parameters (length, fresh and dry weights, leaf area). Parameters improvement took place when the soil contained 10 - 50% of FA. The fresh weight of cucumber increased maximally by 115% at the soil mixture which contained ¼ of FA and ¾ of soil. The production of cucumber decreased at the concentration of FA in the soil above 50%.

Other researchers [Singh and Agrawal 2010] examined the effects of different concentrations of FA addition to soil on the growth of three cultivars of mung bean. The use of fly ash had a positive influence on the mung bean growth and the crops productivity. 10% concentration of FA in the soil turned out to be the best for cultivars M. Jyoti and M. Janpriya (40.6 and 33.9% growth increase), while 5% concentration was the most beneficial for cultivar M. Jagriti (29.5% growth increase). The

researchers concluded that the differences in the effects of FA application on the growth of mung bean may indicate a genetic base for variability.

As it was demonstrated in the examples, the addition of FA to soil has various effects on plant growth and yields. These parameters depend both on the amount of added FA and on plant characteristics.

Stabilization of Soil Contaminated with Heavy Metals

Lately, increased attention has been paid to the possibility of stabilization (chemical immobilization) of soil contaminated with heavy metals by applying fly ash. Stabilization minimizes the mobility of heavy metals, so these contaminations are not transported into deeper soil layers and into groundwater any longer. In addition, after immobilization of phytotoxic trace elements it will be possible to restore fertility to highly contaminated soils [Singh et al. 2010, Pandey and Singh 2010, Ayala et al. 1998].

Research [Ciccu et al. 2001, Ciccu et al. 2003] showed that fly ash addition to soil bounces metals and reduces their transport susceptibility, as well as helps to restore the natural soil properties. Stabilization of metals is based on such phenomena as adsorption, complexation and (co) precipitation. It was found out that for the immobilization of heavy metals alkaline FA (high sorption capacity) and zeolites synthesized from FA could be used.

Kumpiene et al. [Kumpiene et al. 2007] investigated the use of a mixture of fly ash and peat as an additive to soils contaminated with heavy metals. They found that mobility and bioavailability of metals such as Cu and Pb in soil is significantly reduced by using this agent.

Other researchers [Cornell and Schwertmann 2003] proved that the iron oxides contained in the fly ash can absorb significant quantities of metals from soil. In this case, high soil pH is required, because the amount of contamination adsorbed by iron oxide decreases with decreasing pH.

Fly ash is an effective, inexpensive and environmentally friendly additive for stabilization of soils contaminated with heavy metals.

Agricultural Diseases Control

Fly ash can be successfully used in agricultural diseases control. Several studies were carried out in this field [Pandey et al. 2009, Narayanasamy and Gnanakumar 1989, Narayanasamy and Gnanakumar 2005, Sankari and Narayanasamy 2007, Eswaran and Manivannan 2007, Mendki et al. 2001]. These studies show that FA can be used as a potential insecticide in agricultural areas. FA could be also used as an active carrier in certain insecticide formulations like dust, wettable powder and granules [Pandey et al. 2009].

In their studies, Narayanasamy and Gnanakumar [Narayanasamy and Gnanakumar 1989, Narayanasamy and Gnanakumar 2005, Sankari and Narayanasamy 2007] confirmed the insecticidal properties of FA (especially FA from lignite) against pests such as Epilachna, Spodoptera, Lepidoptera and Coleoptera. They developed the FA application in pests control in rice, vegetables (eggplant, okra, tomato, cauliflower, bitter gourd, etc.), and stored grain. They also determined the bio-efficiency of FA-based pesticides. The most effective against insects were pesticides, which contained FA and turmeric or neem seed kernel.

Eswaran and Manivannan [Eswaran and Manivannan 2007] studied the effect of fly ash from lignite on viral disease of papaya leaves. They applied a treatment which included various concentrations of FA administered at different days after planting. It turned out that the most effective was

double application of around 2 kg of FA from lignite on the plant 90 and 120 days after planting. This treatment significantly reduced the amount of the virus and the disease spreading. The authors concluded that the use of FA from lignite has significantly improved plant resistance mechanism and increased the fruit production.

The study [Mendki et al. 2001] shows that fly ash can be used as a safe insecticide in the pulses storage. The addition of 1 kg of FA at 5000 kg of seeds protects them against pests (especially Callosobruchus chinensis) for 16-18 months.

These and other scientific researches confirm that fly ash can effectively control various pests infesting plants, especially vegetables, both in laboratory and field conditions.

Forestry

Fly ash can also be used in forestry. Primarily it can be used to change the acidic pH of forest run, especially in the forest which grows on soil with small amount of nutrients (e.g. sandy soils). Usually in this type of forest tree species such as P. deltoids, D. sissoo, Eucalyptus sp, Melia Azadirachta, Casuarina cunninghamiana miq., etc. are present. In his research, Riekerk [Riekerk 1984] proved that the addition of fly ash to poorly drained sandy soil can increase the pH of the run from 4.7 to 6.0 and can double the growth rate of pine trees.

FA can be used to increase biomass production. Soils with minerals and nutrients deficiency are fertilized by FA additives. FA may be applied as a filler for soils in forest nurseries [Pandey i in. 2009].

Additionally, certain species of trees can be planted on reclaimed FA landfills. During land reclamation, many species like D. sissoo, Albizia Lebbeke, Eucalyptus hybrid, Acacia and Tamarindus are planted on soils, which contain large amounts of FA. This brings mutual benefits. On one hand, the land contaminated with FA is restored. On the other hand, very fast-growing tree species, planted on landfills, provide large amounts of biomass, which can be used in industry, and bring economic benefits [Pandey et al. 2009].

Floriculture

It is advisable to use fly ash in floriculture and ornamental plant production. FA contains all nutrients which are necessary for proper plant growth. However, it also contains heavy metals which are toxic for living organisms. As ornamental plants are not consumed by humans and animals, they can be fertilized by FA, even if they contain heavy metals [Pandey et al. 2009].

FA can also be used for ornamental plants and storage of their cuttings, for pot cultivation, and especially for hydroponics cultivation. This type of cultivation traditionally uses sphagnum peat, pine bark, coir dust, perlite and vermiculite, which are generally acidic (pH app. 4.0) and contain limited amounts of minerals. Therefore, liming materials (dolomite, calcitic limestone, etc) are used to adjust the pH. Additionally, the shortage of minerals and nutrients is supplemented by the addition of artificial fertilizers. Since alkaline FA is widely available, it can be used to replace liming materials, previously used in the cultivation of ornamental plants. This innovative solution brings mutual benefits, because firstly it significantly reduces the cost of ornamental plants and flowers cultivation, and secondly it is a great method for ecologically and economically justified FA utilization [Pandey et al. 2009].

RISKS CONNECTED WITH FLY ASH APPLICATION IN AGRICULTURE

Although fly ash application in agriculture has many advantages, there is a risk associated with it. The primary disadvantage of this utilization is the possibility of contamination of soils and surface waters with heavy metals and radionuclides, and change in soil salinity. In addition, there is also a risk associated with lack of information about the long-term effects of fly ash application on soil quality and environment.

Heavy Metals Contamination

The main concern of fly ash application in agriculture is the presence of heavy metals in FA. This waste contains many potentially toxic elements such as As, Cu, Zn, Cd, Pb, Co, Mo, Mn, Hg, Ni, Cr, Se, B, etc. [Pandey and Singh 2010]. The risk of pollution depends on the mobility of these elements. These heavy metals can be leached from soils, which contain particularly large amounts of FA, and can lead to pollution of land, groundwater, rivers and lakes. Many studies [Ram and Masto 2010, Singh et al. 2010, Pandey and Singh 2010, Ferreira et al. 2003] show that 5 to 30% of heavy metals present in FA are leachable. The most leachable elements are Cd, Cu and Pb. In addition, improperly conducted agricultural practices may affect the leaching of toxic elements from soils fortified with fly ash.

Unfortunately, there are still not many researches on the effects of FA on biological properties of soil. However, it is known that at higher concentrations of FA in soil, heavy metals may become more active and prevent microbial activity in the soil [Ram and Masto 2010]

For example, studies conducted in England [Tolle et al. 1983] indicate that some elements in high concentration are toxic to plants and animals. They point out that in plants grown in soils fertilized with FA, concentrations of elements such as B, Mo, As and Se were above the level considered toxic to animals and humans.

Pollution with Radioactive Isotopes

Fly ash also contains certain amounts of radioactive elements such as ^{238}U, ^{232}Th, ^{40}K, ^{226}Ra, ^{210}Pb, ^{228}Ra, ^{222}Ru i ^{220}Ru (radionuclides of uranium and thorium series). During the combustion process radioactive isotopes accumulate in the FA. Therefore, FA contains slightly elevated concentrations of these elements compare to the surrounding rocks and soils [Pandey and Singh 2010].

Studies conducted by Goyal et al. [Goyal et al. 2002] proved that in soil containing up to 24% FA, the activity levels of gamma emitting radionuclides such as ^{40}K, ^{226}Ra i ^{228}Ac, remained in permissible limits, despite local differences in the level of radiation. Also, ground water was not contaminated with radionuclides. However, due to the high harmfulness of these pollutants on living organisms, FA should be used in agriculture with caution.

Soil Salinity

The application of fly ash (especially unweathered FA) as additive to soil can cause an increase of its salt content. Also, the salinity in the surrounding water reservoirs and ground water will increase. Salinity increases because of high concentration of totally dissolved solids, total

hardness, cations and anions in FA leachates (mainly Ca^{2+}, Na^{+}, F^{-}, Cl^{-}, SO_4^{2+}, OH^{-} and $CO_3^{2+)}$ [Ram and Masto 2010].

The salinity increase can induce salt stress in plants. Different plant species respond in different way to salinity increase in soil. Plants can be classified, accordingly, as tolerant, moderately tolerant or moderately sensitive. The soluble ions can harm plants by direct toxic effects and also through significant changes in osmotic potential. For example, an elevated level of Na^{+} reduces soil permeability, hydraulic conductivity, and infiltration by changing the soil structure. It also leads to erosion water logging, and surface runoff. High levels of inorganic and organic colloids can be released, which might transport contaminants such as pesticides, heavy metals and radionuclides [Sumner et al. 1998]. Therefore, crop productivity is decreasing with increasing salinity for most plants [Ferreira et al. 2003].

Although salinity and associated toxicity is a major limitation in the FA application in agriculture, the processes of FA weathering lead to significant reduction in a soluble salts concentration. Studies conducted by [Haynes 2009] showed that in FA after 3 years of weathering, the salt concentration dropped rapidly. In weathered FA the soluble salts concentration is no longer a limitation in its application in agriculture.

Long Term Effect of Fly Ash Application on Soil

Despite progress in the research, still little is known about the long-term effects of fly ash on soil. A universal method for the determination the leaching of toxic elements from fly ash is still missing, and most studies on this subject are based on industrial FA landfills rather than FA agricultural applications.

The similar situation applies to research connected with transport of soluble salts, heavy metals, radionuclides and other pollutants in soil fertilized with FA. As a result of interaction between FA and soil, pollutants behavior in FA – soil mixture, can vary considerably from their behavior in the pure FA.

Also, the processes of weathering of FA can have unpredictable effects on soil quality in the long term. These processes may lead to: changes in pH of the soil, decreases in Al and Si solubility through precipitation of non-crystalline aluminosilicates or clays with a low Al / Si molar ratio (storage of heavy metals), and production of secondary minerals (hydrated calcium silicate, hydrated calcium aluminosilicate, ettringite) in soil. As a result the porosity of the soil is reduced and its biological functions are disturbed [Ram and Masto 2010].

CONCLUSIONS

Fly ash is a valuable secondary raw material, which is widely used in industry. A lot of research, including the one mentioned in this article, has indicated that FA can also be successfully used in agriculture.

FA can be used in agriculture, because it has unique physical and chemical properties. FA has a unique structure and contains almost all the nutrients necessary for proper plants growth and development. The application of FA in agriculture improves soil texture, reduces soil bulk density, improves water holding capacity, optimizes pH value, increases buffering capacity, increases soil aeration, percolation and water retention in the area of plant growth, reduces crush formation, provides macronutrients such as K , P, Ca, etc., provides micronutrients such as Fe, Zn, Cu, Mo, B, etc., reduces consumption of other additives (lime, fertilizers), reduces the mobility and availability

of heavy metals and has insecticidal properties as well [Pandey and Singh 2010]. It improves soil quality and increases yields. The amount and method of FA introduction into soil depends on its type, the type of crops, the prevailing climatic conditions, as well as the properties of FA.

Although FA utilization in agriculture has many advantages, there is a risk associated with its biological use. The main risk factor is that FA contains toxic elements (heavy metals, radioactive isotopes) and large amounts of dissolved salts. These substances can be leached from FA. Leaching can cause soil and water salinity, unfavorable changes in soil pH, increase of heavy metals mobility and availability and their accumulation in plants [Singh et al. 2010]. Therefore, caution must be taken with fly ash application in agriculture.

It is also important to continue and extend research concerning the effect of FA application in agriculture on crops and environment. Firstly, research should be carried out on the long-term impact of FA on soil properties, microbial activity and diversity as well as crops quality. Furthermore, the fate of toxic compounds contained in FA (including heavy metals and radionuclides) should be carefully investigated, both in the laboratory and field. Also, potential contaminants leaching from soil enriched with fly ash and their impact on the surrounding environment should be continuously monitored.

Acknowledgements

This work was financed from the 2010 – 2013 budget for scence research as a research project.

REFERENCES

Ahmaruzzaman M., 2010: A review on the utilization of fly ash. Progress in Energy and Combustion Science 36, 327 – 363.

Ajaz S., Tiyagi S., 2003: Effect of different concentrations of fly-ash on the growth of cucumber plant, Cucumis sativus. Archives of Agronomy and Soil Science 49, 457 – 461.

Ayala J., Blanco F., Garcia P., Rodriguez P., Sancho J., 1998: Austrian fly ash as a heavy metals removal material. Fuel 77 (11), 1147 – 1154.

Ciccu R., Ghiani M., Peretti R., Serci A., Zucca A., 2001: Heavy metal immobilization using fly ash in soils contaminated by mine activity. www.flyash.info/2001/mining1/06perett.pdf.

Ciccu R., Ghiani M., Serci A., Fadda S., Peretti R., Zucca A., 2003: Heavy metal immobilization in the mining-contaminated soils using various industrial wastes. Minerals Engineering 16, 187 – 192.

Ciećko Z., Żołnowski A. C., Kulmaczewska J., Chełstowski A., 2009: Effect of successive doses of drainage from coal ash to soil acidity (Wpływ następczy melioracyjnych dawek popiołów z węgla kamiennego na kwasowość gleby). Zeszyty problemowe postępów nauk rolniczych 535, 73 – 83.

Cornell R. M., Schwertmann U., 2003: The Iron Oxides: Structure, Properties, Reactions, Occurrences and Uses. Second ed. Wiley-VCH, Weinheim.

Eswaran A., Manivannan K., 2007: Effect of foliar application of lignite fly ash on the management of papaya leaf curl disease. Acta Horticulturae (ISHS) 740, 271– 275.

Feng Y. J. , Li F., Wang X. L., Liu X. M., Zhang L. N., 2006: Principal Chemical Properties of Artificial Soil Composed of Fly Ash and Furfural Residue. Pedosphere 16(5), 668-672.

Ferreira C., Ribeiro A., Ottosen L., 2003: Possible applications for municipal solid waste fly ash. Journal of Hazardous Materials B96, 201 – 216.

Fulekar M. H., 1993: The pH effects on leachability of fly-ash heavy metals: laboratory experiment. Indian Journal of Environmental Protection 13, 185 – 192.

Goyal D., Kaur K., Garg R., Vijayan V., Nanda S. K., Nioding A., Khanna S., Ramamurthy V., 2002: Industrial fly ash as a soil amendment agent for raising forestry plantations. In: Taylor P. R. (Ed.), 2002. EPD Congress and Fundamental of Advanced Materials for Energy Conversion, TMS Publication, Warrendale, PA, 251 – 260.

Gracia G., Zabaleta I., Canibano J. G., Gyeyo M. A., 1995: Use of coal ash/mine waste in agriculture; their properties fromagriculture point of view. Coal Abstracts 95, 32 – 46.

Haynes R. J., 2009: Reclamation and revegetation of fly ash disposal sites -challenges and research needs. Journal of Environmental Management 90, 43 – 53.

Iyer R.S., Scott J.A., 2001: Power station fly ash — a review of value-added utilization outside of the construction industry. Resources, Conservation and Recycling 31, 217 – 228.

Kalra N., Joshi H. C., Chaudhary A., Chaudhary R., Sharma S. K., 1997: Impact of fly ash incorporation in soil on germination of crops. Bioresource Technology 61, 39 – 41.

Khan M. R., Khan M. W., 1996: The effect of fly-ash on plant growth and yield of tomato. Environmental Pollution 92, 105 – 111

Kumpiene J., Lagerkvist A., Maurice C., 2007: Stabilization of Pb and Cu contaminated soil using coal fly ash and peat. Environmental Pollution 145, 365 – 373.

Lai K. M., Ye D. Y., Wong J. W. C., 1999: Enzyme activities in sandy soil amended with sewage sludge and coal fly ash. Water, Air, & Soil Pollution 113, 261 – 272.

Mendki P. S., Maheshwari V. L., Kothari R. M., 2001: Fly-ash as a post-harvest preservative for five commonly utilized pulses. Crop Protection 20, 241 – 245.

Menon M. P., Sajwan K. S., Ghuman G. S., James J., Chandra K., 1993: Fly ash-amended compost as a manure for agricultural crops. Journal of Environmental Science and Health, Part A: Environmental Science and Engineering 28, 2167 – 2182.

Narayanasamy P., 2005: Prospect of use of fly-ash as a dust insecticide and a carrier in pesticide formulation. In: Proceedings of the National Seminar Cum Business Meet on Use of Fly-ash in Agriculture. FAUP, TIFAC, DST, New Delhi, 50 – 57.

Narayanasamy P., Gnanakumar D., 1989: A. Lignite fly-ash: a nonpolluting substance for tackling pest problems. In: Devaraj KV (ed), 1989: Progress in pollution research. University of Agricultural Sciences, Bangalore, 201 – 206.

Pandey V. C., Abhilash P.C., Singh N., 2009: The Indian perspective of utilizing fly ash in phytoremediation, phytomanagement and biomass production. Journal of Environmental Management 90, 2943 – 2958.

Pandey V. C., Singh N., 2010: Impact of fly ash incorporation in soil systems. Agriculture, Ecosystems and Environment 136, 16 – 27.

Phung H. T., Lam H. V., Page A. L., Lund L. J., 1979: The practice of leaching boron and soluble salts from fly ash-amended soils. Water, Air, & Soil Pollution 12, 247 – 254.

Ram L. C., Masto R. E., 2010: An appraisal of the potential use of fly ash for reclaiming coal mine spoil. Journal of Environmental Management 91, 603 – 617.

Riekerk H., 1984: Coal-ash effects on fuel-wood production and runoff water quality. Southern Journal of Applied Forestry 8, 99 – 102.

Sankari S. A., Narayanasamy P., 2007: Bio-efficacy of fly-ash based herbal pesticides against pests of rice and vegetables. Current Science 92, 811 – 816

Singh A., Agrawal S. B., 2010: Response of mung bean cultivars to fly ash: Growth and yield. Ecotoxicology and Environmental Safety 73/ 8, 1950 – 1958.

Singh R. P., A.K. Gupta, Ibrahim M. H., Mittal A. K., 2010: Coal fly ash utilization in agriculture: its potential benefits and risks. Review Environmental Science Biotechnology 9, 345 – 358.

Sobik-Szołtysek J., Janecka B., 2006: Analysis of the possibilities of unconventional fly ash utilization (Analiza możliwości zagospodarowania popiołów lotnych metodami niekonwencjonalnymi). Ochrona Powietrza i Problemy Odpadów 40 (6), 184 – 193.

Sumner M. E., Miller W. P., Kookana R. S., Hazelton P., 1998: Sodicity, dispersion, and environmental quality, Sodic Soils: Distribution, Properties, Management and Environmental Consequences. In: Sumner M.E., Naidu R. (Eds.), 1998. Oxford University Press, New York, 149 – 172.

Szponder D. K., Trybalski K., 2009a: Identification of the fly ash properties by using different methods and equipments (Określanie właściwości popiołów lotnych przy użyciu różnych metod i urządzeń badawczych). Górnictwo i Geoinżynieria, 33/4, 287 – 298.

Szponder D. K., Trybalski K., 2009b: Influence of fly ash structure, phase and diversification of chemical composition on their utilization process. 13th Conference on Environment and mineral processing: 4.–6. 6. 2009, Ostrava, Czech Republic, Part I, VSB – Technical University of Ostrava, Faculty of Mining and Geology, Institut of Environmental Engineering; Ostrava, 121 – 127.

Tolle D. A., Arthur M. F., Van Voris P., 1983: Microcosm/field comparison of trace element uptake in crops grown in fly ash amended soil. Science of the Total Environment 31, 243 – 263.

Vincini M., Carini F., Silva S., 1994: Use of alkaline fly ash as an amendment for swine manure. Bioresource Technology 49, 213 – 222.

Właśniewski S., 2009: Effect of fertilization with fly ash from coal on selected chemical properties of sandy soil and yield of Atos (Wpływ nawożenia popiołem lotnym z węgla kamiennego na wybrane właściwości chemiczne gleby piaszczystej i plonowanie owsa). Ochrona Środowiska i Zasobów Naturalnych 41, 479 – 488.

POPIOŁY LOTNE A ROLNICTWO – NOWOCZESNE ZASTOSOWANIA UBOCZNYCH PRODUKTÓW SPALANIA

Streszczenie. Pomimo ciągle rosnącego znaczenia alternatywnych źródeł energii, paliwa kopalne, w tym przede wszystkim węgiel kamienny i brunatny, odgrywają znaczącą rolę w globalnej gospodarce energetycznej. Niestety w procesach przetwarzania węgli na energię powstają uboczne produkty spalania, w tym popioły lotne. Odpady te w znaczący sposób oddziaływają negatywnie na środowisko naturalne, ale jednocześnie posiadają specyficzne właściwości umożliwiające ich wykorzystanie w przemyśle. Ze względu na bardzo duże ilość powstających popiołów lotnych, w ostatnich latach poszukuje się nowych, niekonwencjonalnych zastosowań dla tych odpadów.

Ponieważ popioły lotne posiadają unikalną strukturę, a także zawierają w swoim składzie prawie wszystkie składniki odżywcze niezbędne dla prawidłowego wzrostu i rozwoju roślin, zwrócono uwagę na możliwość ich utylizacji w rolnictwie. Przede wszystkim stosuje się je jako substytut nawozu mineralnego do poprawy właściwości fizycznych, chemicznych i biologicznych gleb. Jednakże odpady te są również wykorzystywane jako środek zwiększający wzrost roślin i ilość otrzymywanych plonów. Ponadto, za pomocą popiołów lotnych zmniejsza się ilość metali ciężkich akumulowanych w roślinach czy też kontroluje rozprzestrzenianie chorób. Jednakże, ze stosowaniem popiołów lotnych w rolnictwie związane są pewne zagrożenia (m. in. skażenie gleb i wód powierzchniowych metalami ciężkimi i izotopami promieniotwórczymi, zasolenie gleb). Ponadto istnieje ryzyko związane z brakiem informacji na temat wpływu długotrwałego stosowania popiołów lotnych na jakość gleb i środowiska. W związku z tym celowe wydaje się podjęcie badań zmierzających do dokładnego określenia wpływu dodatku popiołów lotnych do gleb na produkcje rolniczą i środowisko naturalne.

W tej publikacji, autorzy podjęli się próby określenia właściwości popiołów lotnych umożliwiających i ograniczających wykorzystanie popiołów lotnych w rolnictwie. Przedstawili także nowoczesne zastosowania tych ubocznych produktów spalania w rolnictwie, a także ocenili korzyści i zagrożenia płynące z tego typu utylizacji.

Słowa kluczowe: popiół lotny, uboczne produkty spalania, rolnictwo, jakość gleb, nawożenie, zanieczyszczenie gleb.

TEKA Kom. Mot. Energ. Roln. – OL PAN, 2011, 11, 386–396

SIMPLIFIED CALCULATION OF COMBUSTION PROGRESS IN THE IC ENGINE

Stanisław Szwaja

Institute of Internal Combustion Engines and Control Engineering,
Czestochowa University of Technology, Armii Krajowej 21, 42-201 Częstochowa,
e-mail: szwaja@imc.pcz.czest.pl

Summary. A simplified method for MFB (Mass Fraction Burnt) determination on the basis of Energy Conservation Law has been presented in the paper. At first, cumulative heat as a function of the crank angle is computed as result of solving the mentioned law. Next, the cumulative heat after normalizing can be treated as the MFB function. Additionally, computation of the specific heat c_p/c_v ratio has also been conducted and the obtained results lead to the conclusion that accuracy in determining the c_p/c_v does not significantly influence the shape of the normalized MFB profile. Following the presented computational method, combustion phases 0-10%MFB and 10-90%MFB are also charged with a marginal error.

Keywords: combustion engine, heat release rate, MFB

INTRODUCTION

Results from several works [1,2,3,4,5] concerning modeling 3-D combustion process in the internal combustion (IC) reciprocating engine with the aid of sophisticated methods including CFD technique lead to the conclusion that a simplified analysis based on empirical data from this combustion process can be sufficient for scientific purposes. However, there are also problems with this analysis particularly touching measurement methods for the TDC (Top Dead Centre) determination and in-cylinder pressure signal processing [6,7,8,9,10]. The simplified method for determining combustion progress in the IC engine is based on the Energy Conservation Law. Thus, the heat released during fuel combustion in the internal combustion engine can be described with the following equation on the basis of this principle:

$$\delta Q_{ch} = dU_s + \delta Q_{ht} + dW + \sum h_i dm_i \tag{1}$$

where:
δQ_{ch} – heat released from combustion,
dU_s – internal energy of the fluid filling the engine cylinder,
δQ_{ht} - heat transferred to the engine walls,
$dW = pdV$ - work done by the fluid to the environment,

$\sum h_i dm_i$ - crevices losses in energy.

The internal energy increment considered as total differential from a product of mass m and the specific heat c_v and temperature T of the working fluid can be expressed by the equation:

$$dU_s = d(mc_v dT) = mc_v dT + mTdc_v + c_v Tdm = mc_v dT + c_v Tdm \tag{2}$$

Assuming that the c_v is constant and there is no mass transfer out of the closed cylinder space $dm_i = 0$, dU_s can be determined as follows:

$$dU_s = mc_v dT \tag{3}$$

Hence, after rearranging the equation (1), its form is obtained for the net heat released δQ_{net}, which is not influenced by heat losses δQ_{ht} to cylinder walls.

$$\delta Q_{net} = \delta Q_{ch} - \delta Q_{ht} = dU_s + d \tag{4}$$

Next, taking the differential form of the equation of state as follows

$$Vdp + pdV = mRdT \tag{5}$$

then, rearranging it to the form

$$mc_v dT = \frac{c_v}{R}(Vdp + pdV) \tag{6}$$

then, substituting it to the equation (3) and then to the equation (4) we finally obtain the equation (7)

$$\delta Q_{net} = \left(\frac{c_v}{R}\right) Vdp + \left(\frac{c_v}{R} + 1\right) pdV \tag{7}$$

Considering the relations (8), (9) and (10) between the universal gas constant R and both the specific heats c_p and c_v at constant pressure and constant volume, respectively,

$$R = c_p - c_v \ (8), \ \gamma = \frac{c_p}{c_v} \ (9), \ \frac{c_v}{R} = \frac{1}{\gamma - 1} \tag{10}$$

the final equation for the net heat δQ_{net} over the crank angle increment $d\theta$ can be derived as follows:

$$\frac{dQ_{net}}{d\theta} \cong \left(\frac{1}{\gamma - 1}\right) p\frac{dV}{d\theta} + \left(\frac{\gamma}{\gamma - 1}\right) V\frac{dp}{d\theta} \tag{11}$$

where:

γ – ratio of the specific heats (c_p/c_v) at constant pressure and constant volume, respectively,

p – in-cylinder combustion pressure,

V – in-cylinder volume,

θ – crank angle (CA) deg,

Q_{net} – net heat released during combustion.

The equation (11) is applied for heat release rate (HRR) determination in the IC engine [5,11,12,13,14].

In accordance with this equation, combustion progress can be expressed by the cumulative heat Q_{net}, which can be determined through integrating it over the θ.

If someone assumes that the Lower Heating Value (LHV) of the fuel does not change at elevated pressure and temperature, then the heat released from combustion process can be expressed as a product of the fuel *LHV* and the fuel mass burnt $M_F(\theta)$. Thus, progress in combustion can be quantitatively described by the normalized function as the MFB (Mass of fuel Fraction Burnt) defined as follows:

$$\mathrm{MFB}(\theta) = \frac{\mathrm{M_F}(\theta)}{\mathrm{M_T}} = \frac{\mathrm{Q_{net}}(\theta)}{\mathrm{Q_{net}}} \tag{12}$$

where:

M_F – mass of the fuel burnt since start of combustion up to the current crank angle θ,

M_T – total mass of the fuel burnt in the single combustion event.

Although the MFB function is often used in the engine combustion analysis, difficulties as pointed in [15,16,17,18,19] might be encountered for anyone who wants to compute progress in combustion in the internal combustion (IC) engine on the basis of this equation (11). As far as both the $p(\theta)$ and $V(\theta)$ are known values, then the solution of the equation can be easily obtained. The problem appears in case when accurate determination of the γ (c_p/c_v) ratio is required. There are several methods for calculating the γ. In general, these methods are based on empirical results. Gatowski et al. [20] proposed the γ can be determined as follows:

$$\gamma = 1.38 - 0.08 \cdot \frac{(\mathrm{T} - 300)}{1000} \tag{13}$$

where:

T - temperature of the in-cylinder working fluid in K.

There are slightly different formulas for the γ determination in the [21] and [22].

$$\gamma = 1.338 - 6 \cdot 10^{-5}\mathrm{T} + 10^{-8}\mathrm{T}^2 \tag{14}$$

$$\gamma = 1.38 - \mathrm{k_1 e}^{\left(\frac{\mathrm{k_2}}{\mathrm{T}}\right)} \tag{15}$$

where: k_1 and k_2 are constants from the range (0.2 - 900).

As anyone can notice, these equations are also functions of temperature.

Furthermore, the γ can be determined directly, following its definition on the basis of separate calculation of the c_p and c_v. In this case both the c_p and c_v can be determined from e.g. the NASA polynomials. During combustion, relation between burnt and unburnt air-fuel mixture varies, that contributes to change in the γ. Thus, the γ is changing from the γ_u to the γ_b which stand for the unburnt and burnt mixture, respectively. To compute the final γ for the total burnt and unburnt compounds of the fluid filling the engine cylinder, the mass-based ratio between burnt and unburnt content have to be provided. As the combustion progress requires γ value for its computation, thus both combustion progress represented by the released heat and the γ can be determined from an iteration process. As mentioned, the total γ of burnt and unburnt species can be determined on the basis of their mass fractions. Therefore, the MFB profile for the combustion progress is required. The most well-known function for MFB calculation is the empirical formula developed by Rassweiler and Withrow [23]. It is presented in the equation (16).

$$\mathrm{MFB}_{\theta} = \frac{\sum_{\theta} \Delta p_{\theta}}{\sum \Delta p_{\mathrm{begin-end}}} \tag{16}$$

where:
θ – crank angle,
Δp_{θ} – corrected pressure rise with respect to combustion,
begin – end – location of begin and end of combustion.

However, the difficulty has to be faced with the proper determination of the end of combustion, which is necessary for the MFB computation. Brunt et al. [24] assumed that the end of combustion is located at the maximum of $pV^{1.15}$.

RESULTS AND DISCUSSION

The main aim of the paper is to show that the combustion progress in the IC engine can be expressed by the normalized cumulative net heat represented by the MFB function. In that case no one takes care about determining the γ with relatively high accuracy. Unlike the MFB, which is considered as pure empirical formula, the cumulative net heat is obtained through applying Energy Conservation Law for that purpose. Although normalized net heat cannot be managed as the MFB profile due to neglecting heat transfer to walls and the crevice effect, it can be applied as well as the empirical MFB formulas for the MFB determination. Furthermore, such approach is justified with respect to theory.

For example, combustion of hydrogen at stoichiometric ratio with exhaust gas recirculation (EGR) of 20% (by mass) was taken into analysis. The combustion pressure was acquired from the IC spark ignited CFR engine (displacement = 611cm^3) working at compression ratio (CR) of 10 with spark timing (ST) of 6 deg before TDC at rotational speed of 900rpm. In Figure 1 the in-cylinder combustion pressure vs crank angle is plotted. As seen, there are pressure fluctuations on the combustion pressure as a result of hydrogen combustion instabilities.

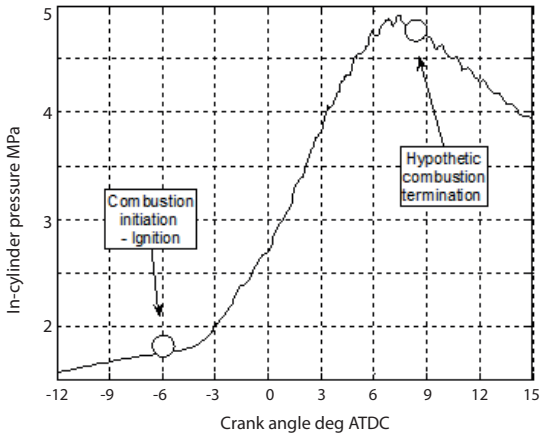

Fig. 1. In-cylinder combustion pressure history of hydrogen combustion at stoichiometric ratio with 20%EGR in the CFR engine with compression ratio of 10 and spark timing of 6 deg before TDC

As far as combustion progress is going on the chemical composition of the gases filling the combustion chamber is also varying from air and fuel (hydrogen and EGR gases) at the start of combustion to exhaust gases when combustion is completed. Hence, the $\gamma = c_p/c_v$ ratio is also changing with the in-cylinder gas chemical composition change, as it is plotted in Figure 2.

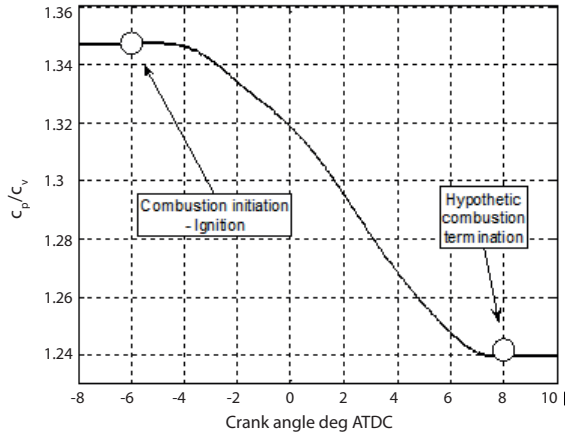

Fig. 2. Estimated γ (cp/cv) of the in-cylinder gases during combustion of H2+air+20%EGR in the CFR engine (CR = 10, ST = -6 deg ATDC) vs crank angle

To show the impact of the γ on the heat release calculation and further, on the MFB function, four cases of various γ were taken for the analysis. They are shown in the table 1.

Table 1: Four cases of the γ taken for MFB calculation

No.	$\gamma = c_p/c_v$	@ temperature	Air-fuel mixture composition
1	1.396 (constant)	25°C (NTP)	Hydrogen+air_{stoic}+20%EGR
2	1.347 (constant)	900K (temperature at the ignition)	Hydrogen+air_{stoic}+20%EGR
3	Varied from 1.34 to 1.24	Varied from 900K to 2500K	Hydrogen+air_{stoic}+20%EGR
4	$\gamma = n$, Constant, assumed as polytrophic index n of compression	Uknown	Hydrogen+air_{stoic}+20%EGR

In the case 4 the γ is assumed to be the polytrophic index n of the compression process in the piston engine following the equation (17).

$$\gamma = \frac{\log \frac{p_0}{p_i}}{\log \frac{v_i}{v_0}} \tag{17}$$

where:

p_0, v_0 - pressure and volume at spark timing, respectively,

p_i, v_i - pressure and volume at point i located before the spark timing with p_0, v_0,
i - 1, 2, 3 - index of the point i with p_i, v_i taken for γ computation (Fig. 3).

As shown in Figure 3 the compression process in the *log p – log v* coordinating system is represented by almost the straight line. As the in-cylinder pressure increases with the in-cylinder volume decrease, the average temperature of the in-cylinder gases also increases, which causes higher heat transfer rate to the engine cooling system, therefore the instantaneous polytrophic index n decreases with compression process approaching the ignition point expressed by the p_0, v_0 coordinates. Thus, someone can assume that the polytrophic index n can be similar to the γ when it is calculated at the end of the compression stroke eg. assuming the data for p_0, v_0, and p_1, v_1.

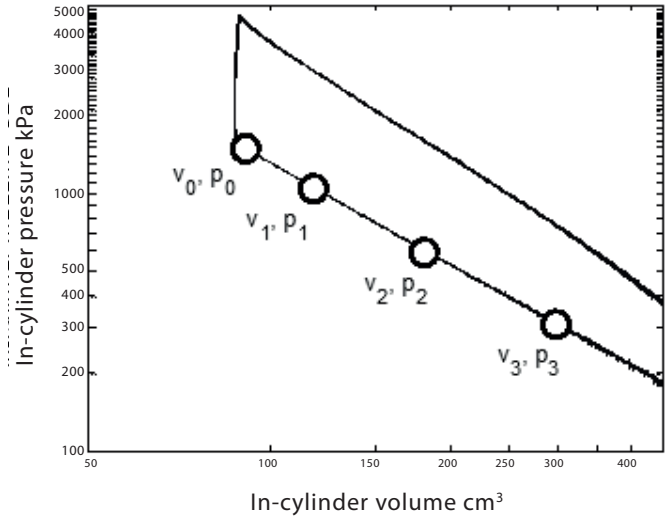

Fig. 3. p-v diagram in log scale with points marked for polytrophic index computation

Following the equation (11), the heat release rate (HRR) was calculated using the real combustion pressure. Due to differentiating the $dp/d\theta$ expression, undesired influence of pressure fluctuations on the heat release appeared. To avoid this shortcoming, low-pass filtering the combustion pressure with the cut-off frequency of 3.5 kHz was applied. Then, the pressure fluctuations were eliminated from the combustion pressure trace. As a result, the computed HRR curve was smooth, as presented in Figure 4a, in which the HRR vs crank angle computed with 3 different γ (c_p/c_v) values is presented. As expected, higher γ results in lower HRR. Another feature can also be observed Figure 4a . It was found that all the three curves were similar in shape to each other, even though they were computed with different γ's. Furthermore, cumulative net heat profiles for these γ ratios (Figure 4b) also look similar to each other. The noticeable difference is in the maximum HRR and maximum cumulative heat, which is justified if anyone assumes that coefficients $\gamma/(\gamma+1)$ and $1/(\gamma+1)$ (Eq.11) can vary with γ change.

a)

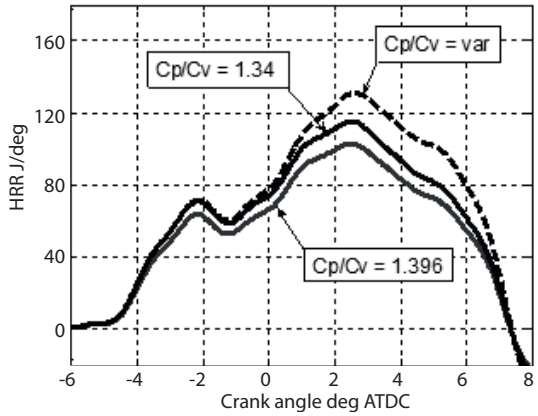

b)

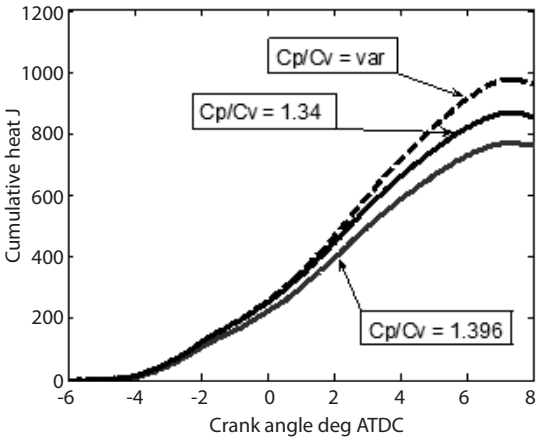

Fig. 4. HRR vs crank angle (a), cumulative net heat vs crank angle (b)

The difference in the cumulative heat between these curves presented in Figure 4b can be reduced if they are recalculated to normalized interval from 0 to 1, as shown in Figure 5a. Figure 5b depicts zoom onto 0.5 of the MFB. In the percentage scale this value corresponds to 50%MFB. There are limits in the MFB profile, which are particularly important in the analysis of the combustion process. They divide the combustion process into combustion phases as follows:

– 0-0.1MFB (0-10%MFB) – first combustion (or pre-combustion) phase,
– 0.1-0.9MFB (10-90%MFB) – main combustion phase – it is treated as combustion duration when expressed in CA deg.

0.5MFB (50%MFB) is treated as the centre of combustion. In its crankshaft location half of the fuel amount has been burnt.

The curve calculated for the γ varying with combustion progress (Table 1, case No.3) was considered as the most accurate to the real heat release, so it was taken as the reference trace to the others. As seen, the largest difference occurs for location of 0.5MFB (50%MFB) and it equals approximately to 0.16 CA deg. As far as the 0.1MFB and 0.9MFB are concerned, they are shifted to the same direction and the offset is almost the same. Thus, the combustion duration as measured from 0.1 to 0.9MFB might be charged with insignificant error when compared to the real 0.1-0.9MFB combustion phase.

a)

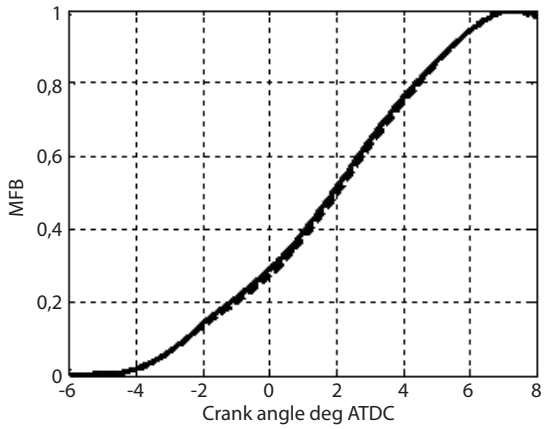

b)

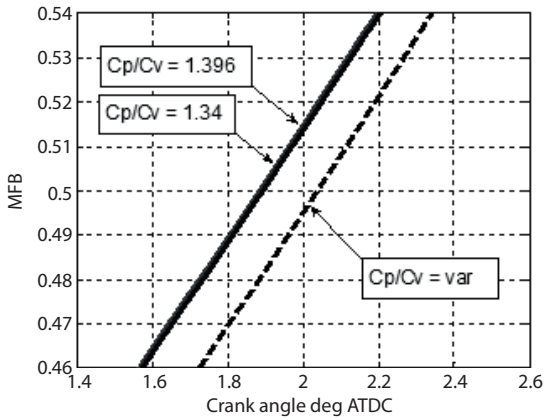

Fig. 5. MFB profile (a), zoom to 0.5MFB (b)

As mentioned, there are several difficulties in calculating the γ (c_p/c_v ratio), so, the polytrophic index n of the compression stroke can be applied instead of the specific ratio γ as recommended by Tunestal [25]. As determined, the polytrophic index $n = 1.34$ of the combustion pressure trace

data taken at the end of the compression stroke does not vary remarkably when compared with the $\gamma = 1.347$ for the combustible mixture. Satisfactorily good compatibility between γ and n in this case comes from low heat transfer between walls and the in-cylinder fluid at the end phase of the compression stroke.

CONCLUSIONS

Progress in combustion determined as the normalized cumulative net heat on the basis of the Energy Conservation Law can be considered as good as the other methods for heat release rate (HRR) and MFB analysis in the IC engine. It provides several advantages such as satisfactory accuracy and simplified calculation, in which $\gamma = c_p/c_v$ ratio can be calculated as the compression polytrophic index directly determined from the compression pressure trace. Such assumption does not charge the final results with significant errors. Additionally, normalized net heat can be considered as substitution for the MFB, which usually is empirically determined. This approach for combustion progress analysis was successfully applied for combustion knock in the hydrogen fuelled IC engine [26].

REFERENCES

Tutak W., Jamrozik A.: Modelling of the thermal cycle of gas engine using AVL FIRE Software, COMBUSTION ENGINES/Silniki Spalinowe, No. 2/2010 (141), pp. 105-113, 2010.

Tutak W.: Thermal Cycle of Engine Modeling with Initial Swirl Process Into Consideration, COMBUSTION ENGINES/SILNIKI SPALINOWE, 1/2008 (132), pp. 56-61, 2008.

Kociszewski A.: Numerical analysis of spark plugs number influence on selected parameters of combustion in piston engine, COMBUSTION ENGINES, 1, (132), pp. 50-55, 2008.

Kociszewski A.: Three-dimensional modelling and experiment on combustion in multipoint spark ignition engine, MEMSTECH'2009, 22-24 MEMSTECH 2009, V-th International Conference Perspective Technologies and Methods in Mems Design, 22 - 24 April 2009, Polyana-Svalyava (Zakarpattya), UKRAINE, pp. 20-23, 2009.

Kociszewski A.: Numerical modelling of combustion in SI engine fuelled with methane, COMBUSTION ENGINES, 4/2009 (139), pp. 45-54, 2009.

Jamrozik A., Kociszewski A., Tutak W.: Dokładność pomiarów indykowania silnika spalinowego, Czasopismo Pomiary Automatyka Kontrola PAK 2009 nr 12, pp. 1030-1036, 2009.

Jamrozik A., Kociszewski A., Tutak W.: Błędy indykowania silnika ZI z dwustopniowym systemem spalania, Journal of KONES Powertrain and Transport, Vol. 16, No. 4, pp. 179-193, European Science Society of Powertrain and Transport Publication, Warsaw 2009.

Tutak W.: Interpretacja wyników pomiaru prędkości przepływu ładunku w komorze spalania tłokowego silnika spalinowego, Pomiary Automatyka Kontrola, Vol.54, nr 2, pp. 67-70, 2008.

Gruca M.: Cyfrowy system do analizy wykresu indykatorowego w czasie rzeczywistym, Zeszyty naukowe Politechniki Częstochowskiej nr 162, MECHANIKA z. 26, pp. 276-286, 2006.

Gruca M.: Zastosowanie światłowodowego czujnika do dynamicznego wyznaczanie GMP tłoka, Fragment w monografii: Silniki gazowe; wybrane zagadnienia. Wyd. Politechniki Częstochowskiej, pp.256-267, 2010.

Jamrozik A.: Modelling of two-stage combustion process in SI engine with prechamber, MEMSTECH 2009, V-th International Conference PERSPECTIVE TECHNOLOGIES AND METHODS IN MEMS DESIGN, Lviv-Polyana, pp. 13-16, UKRAINE 22 - 24 April 2009.

Jamrozik A., Tutak W.: Modelling of combustion process in the gas test engine, Proceedings of the VI-th International Conference MEMSTECH 2010 PERSPECTIVE TECHNOLOGIES AND METHODS IN MEMS DESIGN, pp. 14-17, Lviv – Polyana 2010.

Tutak W., Jamrozik A.: Numerical analysis of some parameters of gas engine, Teka Commission of Motorization and Power Industry in Agriculture, Volume X, pp. 491-502, Polish Academy of Science Branch in Lublin, Lublin 2010.

Cooney C.P., Yeliana, Worm J.J., Naber J.D.: Combustion Characterization in an Internal Combustion Engine with Ethanol−Gasoline Blended Fuels Varying Compression Ratios and Ignition Timing, Energy Fuels, 23 (5), pp. 2319–2324, 2009.

Bitar E.Y., Oppenheim A.K., Schock H.J.: Model for control of combustion in a piston engine, SAE paper 2006-01-0401, 2006.

Zhu G., Daniels C.F., Winkelman J.: ‚MBT timing detection and its closed-loop control using in-cylinder pressure signal, SAE paper 2003-01-3266, 2003.

M Mittal, G Zhu, H Schock: Fast mass-fraction-burned calculation using the net pressure method for real-time applications, Proceedings of the Institution of Mechanical Engineers, Part D: Journal of Automobile Engineering, 223, 3, pp. 389-394, 2009.

K Kar K., Stone R., Raine R., Thorwarth H.: Analysis of combustion in a small homogeneous charge compression assisted ignition engine, DOI: 10.1243/146808705X60834, Int. J. Engine Res. Vol. 7, pp. 237-253, IMechE 2006.

Jankowski A., Czerwiński J.: Memorandum of prof. A.K.Oppeheim and example of application of the Oppeheim correlation (OPC) for the heat losses during the combustion in IC engine, Journal of Kones Powertrain and Transport, Vol. 17, No.2, pp.181-194, 2010.

Gatowski J.A., Balles E.N., Chun K.M., Nelson F.E., Ekchian J.A., Heywood F.B.: A heat release analysis of engine pressure data, SAE Paper No: 841359, 1984.

Brunt M.F.J., Rai H., Emtage A.L. The calculation of heat release energy from engine cylinder pressure data, SAE Paper No: 981052, 1998.

Egnell R.: Combustion diagnostics by means of multizone heat release analysis and NO calculation, SAE Paper No: 981424, 1998.

Rassweiler G.M., Withrow L.: Motion pictures of engine flames correlated with pressure cards, SAE Paper No: 380139, 1938.

Brunt M.F.J., Emtage A.L.: Evaluation of burn rate routines and analysis errors, SAE Paper No: 970037, 1997.

Tunestal P.: Self-tuning gross heat release computation for internal combustion engines, Control Engineering Practise, 17, pp. 518-524, 2009.

Szwaja S, Jamrozik A.: Analysis of Combustion Knock in the SI Engine, COMBUSTION ENGINES/Silniki Spalinowe, Mixture Formation Ignition Combustion, Nr 2009-SC2, pp. 128 -135, June 2009

UPROSZCZONA METODA OBLICZANIA POSTĘPU SPALANIA W SILNIKU O SPALANIU WEWNĘTRZNYM

Streszczenie. W artykule przedstawiono uproszczoną metodę obliczania MFB (części spalonej masy) w oparciu o zasadę zachowania energii. Początkowo, ciepło skumulowane w funkcji kąta obrotu wału korbowego jest obliczane w wyniku rozwiązania powyższej zasady. Dalej, skumulowane ciepło po normalizacji może być traktowane jako funkcja MFB. Ponadto, wyliczono też stosunek ciepła właściwego c_p/c_v , a uzyskane wyniki prowadzą do wniosku, że dokładność w określaniu c_p/c_v nie wpływa znacząco na kształt znormalizowanego

profilu MFB. Ponadto, przy zastosowaniu przedstawionej metody obliczeniowej, fazy spalania 0-10% MFB i 10-90% MFB są obciążone marginalnym błędem.

Słowa kluczowe: silnik spalinowy, szybkość uwalniania ciepła, MFB (część spalona masy)

TEKA Kom. Mot. Energ. Roln. – OL PAN, 2011, 11, 397–406

NUMERICAL ANALYSIS OF THE IMPACT OF EGR ON THE KNOCK LIMIT IN SI TEST ENGINE

Wojciech Tutak

Institute of Internal Combustion Engines and Control Engineering
Czestochowa University of Technology, Tel.: 34 3250555,
Armii Krajowej Av. 21, 42-201 Czestochowa
Email: tutak@imc.pcz.czest.pl,

Summary. The paper presents results of modelling of the thermal cycle of the SI test engine using AVL FIRE software. Results are presented of impact of exhaust gas recirculation on the knock limit, thermal efficiency and mean indicated pressure of the test engine. Modelling was done for the test engine powered by gasoline. This engine runs at a constant speed. The engine is designed for lean mixtures combustion. The paper presents results of optimizing ignition advance angle of the engine with EGR with the detection of knock process. The knock process was modelled with the use of AnB model.

Key words: internal combustion engine, thermal cycle, modelling, combustion, knock, exhaust gas recirculation

INTRODUCTION

Engines are designed to maximize power and economy while minimizing exhaust emissions. In some engines, a fraction of the engine exhaust gases is recycled to the intake to dilute fresh mixture for control of NOx emission [6]. In order to reduce the in-cylinder temperature, a charge dilution must be done. One of the effective methods used to dilute the fresh charge is to recycle some part of the exhaust gases back into the cylinder. This method is called exhaust gas recirculation (EGR). Using EGR will lead to a decrease in the in-cylinder temperature and a decrease in knocking tendency. This method makes possible to improve advance timing to achieve higher thermal efficiency compared to engines operating on mixtures without fraction of recycled exhaust gas. In addition, EGR will reduce the in-cylinder NO_x production [11]. Shizuo and all [13] investigeted the effects of EGR on direct injection gasoline engine. They confirmed that an appropriate volume of EGR improves fuel economy and HC emission. This phenomenon is presumably due to the intake temperature increase by EGR, which improved the flame propagation in the relatively lean area of the air-fuel mixture, which is not uniformly distributed. Excessive EGR induces deterioration of fuel economy and HC emission prior to occurrence of misfire. The limit to the volume of EGR is presumably due to the worsened flame propagation associated with reduced oxygen concentration, not to the worsening ignition performance [13]. Amr and Saiful [11] have investigated a supercharged natural gas SI engine with exhaust gas recirculation. They havev confirmed that the

increase of the percentage of EGR dilution in the inlet mixture decreases the oxygen concentration, and consequently, it decreases the combustion rate significantly. For instance, the increase of EGR dilution from 0% to 10% at atmospheric inlet conditions increased the total combustion duration from about 74 deg to 95 deg. The maximum tolerable EGR dilution limit increased from about 10% to 12%. The use of cooled EGR with a dilution rate ranged from 20% to 30% depending on engine speed suppressed engine knocking and allowed using high inlet pressure condition at relatively high compression ratio values. Cooled EGR has the potential of reducing the maximum burned gas temperature and consequently NO emission in high compression ratio conditions [11]. The improvement in fuel consumption with increasing EGR is due to three factors: firstly, reduced pumping work; secondly, heat loss to the cylinder walls; and thirdly, a reduction in the degree of dissociation in the gases burned at high temperature [14]. Li and all [15] presented the experimental study results carried out on an electronically controlled fuel injection „stoichiometric gasoline engine" by using cold EGR and increasing compression ratio to improve fuel economy and reduce emissions. They stated that stoichiometric mixture is not an economical mixture for gasoline engines and its use may lead to poor fuel economy and, consequently, an increase in CO_2 emission. It is an important topic to improve the fuel economy of gasoline engines and make them operate at stoichiometric air–fuel ratio without deteriorating emissions from the engines [15]. An investigation was carried out to improve both fuel economy and emissions on gasoline engine at stoichiometric ratio by using cold EGR to suppress the knocking and increasing in compression ratio of the engine [15]. In addition, they stated that when the compression ratio was increased from 8 to 11.8 and EGR ratio as well as air swirl ratio of the engine were optimized, the fuel economy was improved by 5.3% and the NOx and (NOx + HC) emission was decreased by 54.8% [15].

Knock is an abnormal combustion process occurring in SI engines. It is characterized by the occurrence of pressure oscillations. This phenomenon can destroy piston, exhaust valves or rings. Due to this disadvantageous effect it is important to avoid knock phenomenon but on the other hand, due to efficiency reasons, it is desirable to work as close to knock combustion as possible. The most accepted theory that explains engine knock is the auto-ignition theory [6]. The auto-ignition theory states that when the fuel–air mixture in the end gas region ahead of the flame front is compressed to sufficiently high pressure and temperature, the fuel oxidation process can occur in parts or in the entire end gas region. This releases the chemical energy in the end gas region at extremely high rates resulting in high local pressures. The non-uniform pressure distribution inside the combustion chamber causes pressure waves or shock waves to propagate across the chamber causing noise which is known as knock [6].

DESCRIPTION OF THE ECFM COMBUSTION MODEL

Turbulent combustion process is based on the conservation equations of chemical reaction flows. A variety of combustion models is available and successful calculations have been conducted. The CFM (Coherent Flame Model) has been successfully used for modelling the process of combustion in spark ignition engines. The ECFM-3Z (Extended Coherent Flame Model 3-Zones) model belongs to a group of advanced models of the combustion process in a compression ignition engine. For several years it has been successfully used, constantly modified and improved by many researchers [19]. Together with turbulence process sub-models (e.g. the k-zeta-f), exhaust gas component formation, knock combustion and other sub-models, they constitute a useful tool for modelling and analysis of the thermal cycle of the compression ignition internal combustion engine.

Modelling of combustion process was carried out using an advanced model of combustion. ECFM (Extended Coherent Flame Model) model was used based on the phenomenon of turbulent

mixing zone of air, fuel and exhaust. The ECFM has been developed in order to describe combustion in spark ignition engines. This model allows the modelling of the combustion process of air-fuel mixtures with EGR effect and NO formation. The model relies on description of unburned and burnt zones of the gas. A turbulent premixed combustion zones are characterised by chemical time scale, integral length scale and turbulence intensity. In reciprocating internal combustion engines the chemical time scales are much smaller in comparison to the turbulent scales. The concept of combustion model is based on a laminar flamelet idea, whose velocity and thickness are mean values, integrated along the flame front. The thickness of the flame front layer depends on the pressure, the temperature and content of unburned fuel in the fresh zone. In addition, it is assumed that reaction takes place within relatively thin layers that separate the fresh unburned gas from the fully burnt gas. This model uses a 2-step chemistry mechanism for the fuel conversion [1]:

$$C_nH_mO_k + \left(n + \frac{m}{4} - \frac{k}{2}\right)O_2 \rightarrow nCO_2 + \frac{m}{2}H_20 \Rightarrow C_7H_{13} + \left(7 + \frac{13}{4}\right)O_2 \rightarrow 7CO_2 + \frac{13}{2}H_20 \quad (1)$$

$$C_nH_mO_k + \left(\frac{n}{2} - \frac{k}{2}\right)O_2 \rightarrow nCO + \frac{m}{2}H_2 \Rightarrow C_7H_{13} + \left(\frac{7}{2}\right)O_2 \rightarrow 7CO + \frac{13}{2}H_2 \quad (2)$$

where: n, m, k – number of the atoms of carbon, hydrogen and oxygen in the fuel, respectively. Hydrocarbon C_7H_{13} was taken as a fuel.

The reaction (2) of formation of CO and H_2 is taken into account for stoichiometric and fuel-rich mixtures, while for lean mixtures this reaction is omitted. The unburned gas phase consists of 5 main unburned species: fuel, O_2, N, CO_2 and H_2O. At the burnt gas phase it is assumed that no fuel remains. The burnt gas is composed of 11 species, such as O, O_2, N, N_2, H, H_2, CO, CO_2, H_2O, OH and NO.

To model the formation of the nitrogen oxides Zeldovich extended mechanism was used. To detect the knock process, which may occur in the modeled engine, the knock model AnB was used. The model is based on the knowledge of the auto-ignition delay. This knock model is based on two equations. It was especially constructed for the extended coherent combustion flame model. The first equation determines the fuel consumption y_{fu} during auto-ignition process and the second equation defines the ignition delay θ [1].

$$\frac{\partial y_{fu}}{\partial t} = y_{fu}c_1 e^{-\frac{T_a}{T_{gb}}}, \quad (3)$$

where: c_1 – constant, T_a – the activation temperature, T_{gb} – the local temperature of the burnt gas.

The second equation defines the ignition delay θ:

$$\theta = A\left(\frac{RON}{100}\right)^{c_2} p^n e^{\frac{B}{T_{fr}}}, \quad (4)$$

where: *RON* – fuel octane number, limited up to 140, used in the ignition delay expression, c_2 – constant, p – pressure in bar, T_{fr} – the local temperature of the fresh gas in K, n - pressure exponent in the ignition delay expression, A - pre-exponential factor in the ignition delay expression due to auto-ignition (Arrhenius approach) and B - activation temperature in the ignition delay expression.

MODELLING RESULTS

Modelling of the thermal cycle of the test spark ignition engine in the AVL FIRE program was carried out. The object of investigation was a spark ignition S320ER internal combustion engine fed with gasoline. The engine was operated at a constant speed of 1000 rpm. The work investigates the influence of EGR on engine operating parameters, on NO content in the exhaust gases and reduces engine knocking phenomena. The study was conducted for the excess air ratio equal to 1.2. The choice of this point of operation was dictated by the fact that in these conditions, the engine was working properly, the knock phenomenon occurred at the larger angles of ignition advance.

The percentage of exhaust gases recycled back to the engine intake (%EGR) was calculated as a percentage of the total inlet mass flow rate as follows:

$$\%\mathrm{EGR} = \frac{\dot{m}_{\mathrm{EGR}}}{\dot{m}_{\mathrm{a}} + \dot{m}_{\mathrm{f}} + \dot{m}_{\mathrm{EGR}}}, \tag{5}$$

where: $\dot{m}_{EGR}$ is mass rate of EGR, $\dot{m}_a$ is mass rate of air, $\dot{m}_f$ is mass rate of fuel, respectively in kg/s.

One of the parameters determining the performance of the combustion process in the engine is the indicated work.

$$p_i = \frac{\sum_{180}^{540} \frac{p_n + p_{n+1}}{2}(V_{n+1} - V_n)}{V_s} \tag{6}$$

where p_n, p_{n+1} are instantaneous values of the pressure in the cylinder [MPa], V_n, V_{n+1} are instantaneous values of the cylinder volume [m^3], V_s is displacement volume [m^3].

The average value of the indicated efficiency, expressed in % is equal to:

$$\eta_i = \frac{p_i V_s}{Q} 100\%, \tag{7}$$

where Q is total heat supplied to the engine [MJ].

The heat supplied to the engine cylinder:

$$Q = \frac{V \rho W}{0.5 n t}, \tag{8}$$

where V is volume of gasoline delivered to the engine cylinder [m^3], ρ is density of gasoline [kg/m^3], W is calorific value of gasoline [MJ/kg], n is speed engine [rpm], t is time consumption of gasoline delivered to the engine cylinder [min].

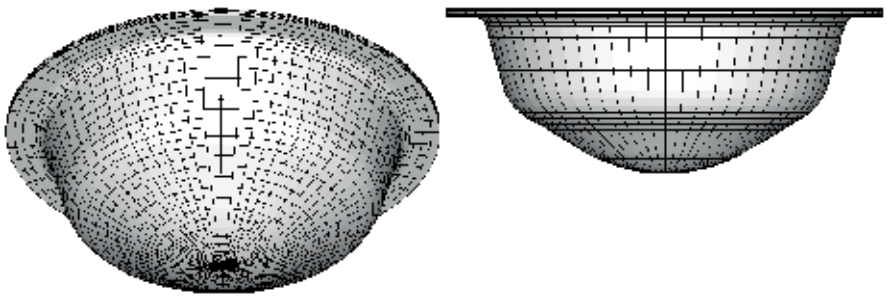

Fig. 1. The computational mesh for combustion chamber

Table 1. Modelling parameters

Engine rotational speed	-	1000 rpm
Cylinder bore	-	120 mm
Stroke	-	160 mm
Connecting-rod length	-	275 mm
Squish	-	2 mm
Initial pressure for 180 deg before TDC	-	0.9 MPa
Initial temperature for 180 deg before TDC	-	310 K
Lambda	-	1.2
EGR	-	0-12.5%
Fuel	-	C_7H_{13}
FIRE sub-models		
Turbulence model	-	k-zeta-f
Combustion model	-	Coherent Flame Model ECFM
NO formation model	-	Extended Zeldowich Model
Knock model	-	AnB

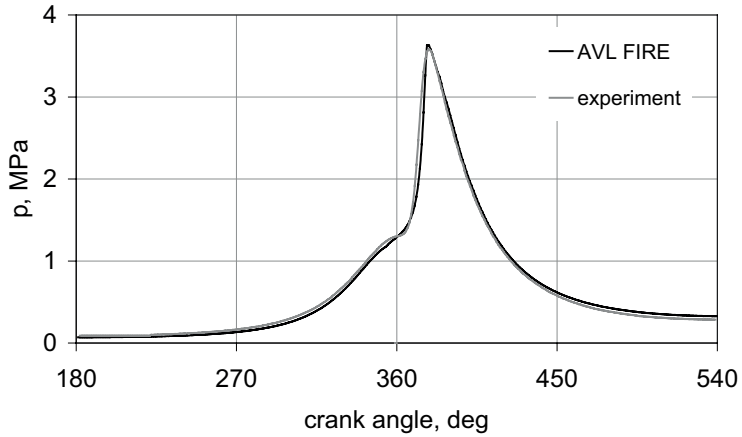

Fig. 2. Courses of pressure obtained by indicting of real test engine and by modeling using FIRE software

Computations were conducted for the angle range from -180 deg CA before TDC (top dead center) to 180 deg CA (crank angle) after TDC. The mesh of the modelled combustion chamber (Fig. 1) of the S320ER test engine consisted of nearly 30000 computation cells. Two-layered wall boundary layer was considered. Model tests were carried out in FIRE software. In the first stage of model calibration was made by comparing the changes of pressure courses from the real test engine with the course obtained by the FIRE software modeling. Result of calibration of the model is presented in Fig. 2. The variation of combustion pressures is shown, obtained as a result of indicating the real test engine and modelling with AVL FIRE software, respectively, for the same initial conditions and settings and spark advance timing. Designated engine efficiency is the gross efficiency, the modelling does not include charge exchange loop.

Fig. 3 presents the results of engine thermal cycle optimization in terms of advance angle, for the conditions without EGR.

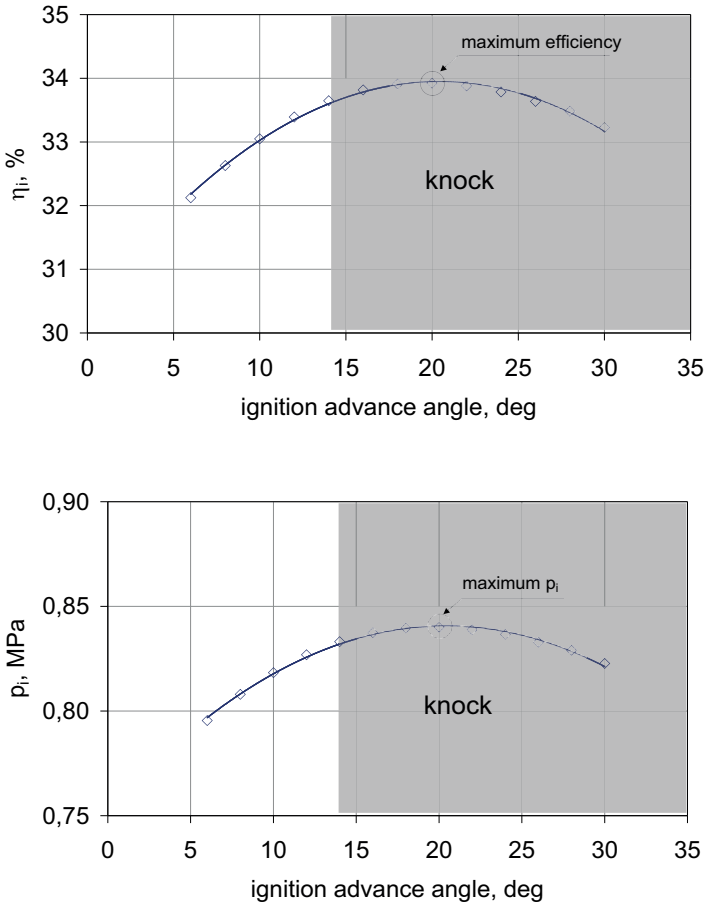

Fig. 3. Indicated thermal efficiency and mean indicated pressure of modelled test engine with marked knock area, without EGR

The gray area indicates the conditions for the occurrence of knock in the test engine. Maximum efficiency possible to obtain, without the danger of knock, was 33.7% and mean indicated pressure is 0.83 MPa. The test engine, thus, can operate with a maximum angle of ignition advance equal to 14 deg before TDC. Further enhancing of the value of the angle of ignition advance causes knock, which can contribute to engine damage.

Fig. 4 shows a comparison of the indicated thermal efficiency curves obtained for a different EGR ratio and for a fixed angle of ignition advance, equal to 10 deg before TDC, ignition timing for maximum efficiency and conditions limited by knock onset. It turned out that for the modelled test engine, the curve that determines knock limit is quite close to the curve that determines the maximum engine efficiency.

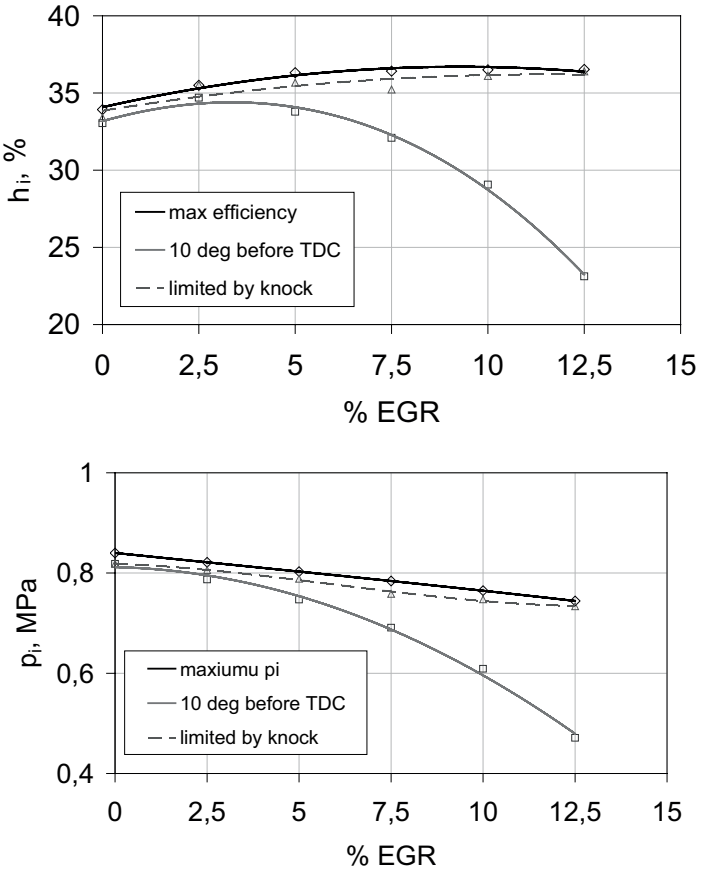

Fig. 4. Indicated thermal efficiency and mean indicated pressure

The test engine, of course, cannot work under conditions where there is danger of knock phenomena occurrence. For maximum EGR ratio, equal to 12%, an increase of indicated thermal efficiency was observed from 23% do 36.4%. This was due to change in the angle of ignition advance. For maximum efficiency, at 12.5% EGR, the ignition advance should be changed to 60 deg before TDC. Unfortunately, this resulted in the occurrence of knock phenomenon. The maximum ignition timing for these conditions could be below 50 deg before TDC. Optimizing the ignition angle has also a positive effect on the value of the mean indicated pressure. For the constant ignition angle equal to 10 deg and 12.5% EGR ratio, the value of the mean indicated pressure was 0.47 MPa and for the optimized ignition angle equal to 50 deg, TDC reached 0.74 MPa.

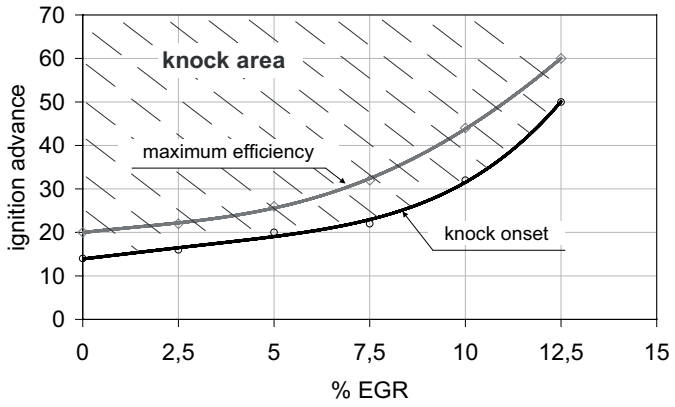

Fig. 5. Curves of spark ignition advance for the maximum value of thermal indicated efficiency and limited by knock phenomenon onset

Fig. 5 shows the area of knock combustion of the test engine. The impact is illustrated of ignition advance angle and EGR ratio on the test engine performance. The curve called „knock onset" refers to the critical angle of ignition at which knock in the combustion process of the test engine begins. The second curve defines the ignition angles for which the maximum efficiency could be achieved but because of the danger of knock phenomenon it cannot be achieved.

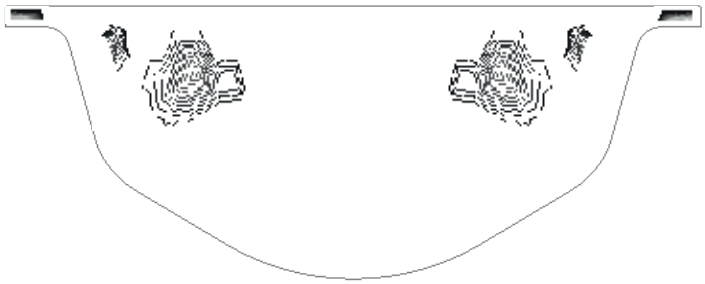

Fig. 7. Places of knock onset in the combustion chamber of the test engine $\lambda = 1.2$ for and ignition advance 20 deg before TDC

Fig. 7 shows the areas for the formation of a knocking in the modeled combustion chamber for ignition advance angle of 20 deg after TDC. These areas are located near the surface of the piston squeezing surface.

CONCLUSIONS

A small exhaust gas ratio in a fresh load causes an increase in engine thermal efficiency. For the modelled test engine 2.5% EGR ratio caused an increase in the efficiency of about 1.7%. Increasing share of EGR in the fresh charge decreased value of mean indicated pressure. Limit value of EGR ratio for the modelled engine was 12.5%. With greater participation of EGR ratio combustion process slowed down too much and thus operation of engine was no longer effective.

Changing the timing advance caused a considerable improvement in engine operating parameters. Limit values were determined by the occurrence of knock process. Exhaust gas recirculation not only has a positive effect on the reduction of NO in exhaust gases, but also reduces the possibility of knock onset. Engine equipped with exhaust gas recirculation system should be able to change the ignition angle, depending on the ratio of the exhaust gases recirculation.

REFERENCES

AVL FIRE, VERSION 2009ICE *Physics & Chemistry. Combustion, Emission, Spray, Wallfilm*. Users Guide, 2009.

Baumgarten C.: *Mixture Formation in Internal Combustion Engines*. Springer-Verlag Berlin Heidelberg 2006.

Colin O., Benkenida A.: *The 3-Zones Extended Coherent Flame Model (ECFM3Z) for Computing Premixed/Diffusion Combustion*. Oil & Gas Science and Technology 2004.

Gunabalan A., Tamilporai P., Ramaprabhu R., *Effects of injection timing and EGR on DI diesel engine performance and emission – using CFD*, Journal of Applied Sciences 10 (22), p. 2823-2830, 2010.

Hélie1 J., Trouvé A.: *A modified coherent flame model to describe turbulent flame propagation in mixtures with variable composition*. Proceedings of the Combustion Institute, Volume 28, Issue 1, 2000, Pages 193-201. Revue de l'Institut Français du Pétrole.

Heywood J. B.: *Internal combustion engine fundamentals*. McGraw-Hill, 1988.

Rychter T., Teodorczyk A.: *Modelowanie matematyczne roboczego cyklu silnika tłokowego.* PWN, Warsaw 1990.

Szwaja S, Jamrozik A.: *Analysis of Combustion Knock in the SI Engine*. SILNIKI SPALINOWE/ Combustion Engines, Mixture Formation Ignition & Combustion, Nr 2009-SC2, June 2009.

Warnatz J, Maas U., Diable R. W.: *Combustion. Physical and Chemical Fundamentals, Modeling and Simulation, Experiments, Pollutant Formation*. Springer, 2006.

Tatschl R., Priesching P., Ruetz J.: *Recent Advances in DI-Diesel Combustion Modeling in AVL FIRE – A Validation Study*. International Multidimensional Engine Modeling User's Group Meeting at the SAE Congress April 15, 2007 Detroit, MI.

Amr I., Saiful B.: *Optimization of a natural gas SI engine employing EGR strategy using a two-zone combustion model*. Fuel 87 (2008) 1824–1834.

Erjiang H., Zuohua H., Bing L., Jianjun Z., Xiaolei G.: *Experimental study on combustion characteristics of a spark-ignition engine fueled with natural gas–hydrogen blends combining with EGR*. International Journal of Hydrogen Energy, 34 (2009, 1035-1044).

Shizuo S., Daisaku S., Takanori U., Hiroyuki S.: *Effects of EGR on direct injection gasoline engine*. JSAE Review 19 (1998) 223-228.

Abd-Alla G.H.: *Using exhaust gas recirculation in internal combustion engines: a review*. Energy-Conversion and Management 43 (2002) 1027–1042.

Li W., Wang Y., Zhou L., Su L.: *Study on improvement of fuel economy and reduction in emissions for stoichiometric gasoline engines*. Applied Thermal Engineering 27 (2007) 2919–2923.

Tutak W., Jamrozik A., Kociszewski A., Sosnowski M., *Numerical analysis of initial swirl profile influence on modelled piston engine work cycle parameters*. SILNIKI SPALINOWE/ Combustion Engines, Mixture Formation Ignition & Combustion, 2007-SC2, s. 401-407, rys. 11, poz. bibl. 8, 2007.

Jamrozik J. Tutak W.: *Numerical analysis of some parameters of gas engine*. Motorol 2010. TEKA Kom.Mot.Energ.Roln. - OL PAN Vol.10, s.491-502, 2010.

Cupiał K., Sosnowski M, Jamrozik A, Kociszewski A., Tutak W.: *Flame Kernel Formation Around a Spark Plug of SI Engine Using KIVA-3V with Standard and Newly Developed Ignition Model*. Silniki Spalinowe R.46 nr SC2, s.203-206.

Nande, A., Szwaja, S. and Naber, J.: *Impact of EGR on Combustion Processes in a Hydrogen Fuelled SI Engine*. SAE Technical Paper, 2008, doi:10.4271/2008-01-1039.

Kociszewski A.: *Three-Dimensional Modelling and Experiment on Combustion in Multipoint Spark Ignition Engine.* Proceedings of the 5th International Conference MEMSTECH'2009. Perspective Technologies and Methods in Mems Design. Lviv - Polyana, Ukraine. s.20-23, 2009.

Jamrozik A., Tutak W.: *Modelling of combustion process in the gas test engine*. Perspective Technologies and Methods in Mems Design, MEMSTECH, Lviv - Polyana, Ukraine. s. 14-17, 2010

Tutak W., Jamrozik A., Kociszewski A., Sosnowski M.: *The influence of initial swirlprofile on modelled piston engine work cycle parameters*, XIV Ukrainian-PolishConference on "CAD in Machinery Design. Implementation and Educational Problems." CADMD`2006, Polyana, Ukraine, 22-23 May 2006, s. 118-121, rys. 10, tab. 1, poz. bibl. 7

Jamrozik A., Tutak W., Kociszewski A., Sosnowski M.: *Numerical Analysis of Influence of Prechamber Geometry in IC Engine with Two-Stage Combustion System on Engine Work Cycle Parameters*, Journal of KONES Powertrain and Transport, Vol 13, No 2, s. 133-142, rys. 14, tab. 2, poz. bibl. 9, European Science Society of Powertrain and Transport Publication, Warsaw 2006.

Kociszewski A., Jamrozik A., Tutak W., Sosnowski M.: *Computational Analysis and Experimental Research into Lean Mixture Combustion in Multi-Spark Plug SI Engine*, Journal of KONES Powertrain and Transport, Vol 13, No 3, s. 123-130, rys. 13, poz. bibl. 8, European Science Society of Powertrain and Transport Publication, Warsaw 2006.

NUMERYCZNA ANALIZA WPŁYWU EGR NA GRANICĘ SPALANIA STUKOWEGO W BADAWCZYM SILNIKU SPALINOWYM

Streszczenie. W pracy przedstawiono wyniki modelowania obiegu cieplnego tłokowego silnika spalinowego z wykorzystaniem programu FIRE. Modelowano obieg silnika o zapłonie iskrowym z procesem recyrkulacji spalin. Analizowano wpływ udziału EGR na zmniejszenie toksyczności spalin oraz na ograniczenie obszaru pracy silnika, w którym występuje spalanie stukowe. Okazało się, że dzięki optymalizacji obiegu silnika z EGR pod względem kąta wyprzedzenia zapłonu, w badanym silniku, osiągnięto takie wartości kąta zapłonu, dla którego nie występuje jeszcze spalanie stukowe a jednocześnie osiąga się parametry zbliżone do optymalnych.

Słowa kluczowe: silnik spalinowy, obieg cieplny, badanie, spalanie stukowe, recyrkulacja spalin

TEKA Kom. Mot. Energ. Roln. – OL PAN, 2011, 11, 407–414

NUMERICAL ANALYSIS OF SOME PARAMETERS OF SI INTERNAL COMBUSTION ENGINE WITH EXHAUST GAS RECIRCULATION

Wojciech Tutak

Institute of Internal Combustion Engines and Control Engineering
Czestochowa University of Technology, Tel.: 34 3250555, Armii Krajowej 21, 42-201 Czestochowa
Email: tutak@imc.pcz.czest.pl,

Summary. The paper presents results of modelling of the thermal cycle of SI test engine using AVL FIRE software. The results are presented of the influence of exhaust gas recirculation on some engine parameters e.g. indicated thermal efficiency and mean indicated pressure. The knock phenomenon was taken into account. The engine parameters were limited by knock combustion process. It turned out that several percent of exhaust gases turned back into the cylinder which is beneficial not only for NO concentration but also has a favorable impact on knock combustion limit.

Key words: internal combustion engine, combustion, knock, exhaust gas recirculation

INTRODUCTION

Contemporary engines are designed to minimize exhaust emissions while maximizing power and economy. One of possible methods of doing this is exhaust gas recirculation. A fraction of the engine exhaust gases is recycled to the intake to dilute fresh mixture for control of NO_x emission [6]. This method is called exhaust gas recirculation, in short EGR. The recycled gases reduce the in-cylinder temperature and cause a decrease in knocking tendency.

Amr and Saiful[1] experimentally investigated the use of the stoichiometric air–fuel mixture with exhaust gas recirculation technique in a spark-ignition natural gas engine. Engine performance and NO emissions were studied for both atmospheric and supercharged inlet conditions. It was found that the use of EGR has a significant effect on NO emissions. NO emissions decreased by about 50% when EGR dilution increased from zero with an inlet pressure of 101 kPa to close to the misfire limit with an inlet pressure of 113 kPa. In addition, the use of EGR effectively suppressed abnormal combustion which occurred at higher inlet pressure. The use of higher inlet pressure in the presence of EGR improved engine performance significantly. NO emissions decreased by about 12% when 5% of EGR dilution was employed with an inlet pressure of 113 kPa compared to using undiluted stoichiometric inlet mixture with an inlet pressure of 101 kPa [1]. In recent years an increase is observed in the petroleum price. It has led to more interest in alternative fuels like DME. Wang and Zhou [2] confirmed that the properties of DME provide a potential for a large EGR ratio

in an engine. Their experimental results indicate that NO_x emission can be reduced by about 40% at a large EGR share without visible smoke and deterioration in thermal efficiency of DME engine. However, CO emission increases with the rise of EGR share. A commercial oxidation catalytic converter was used to investigate its influence on CO emission. Additionally, they prove that DME vehicle engine can meet stricter emission regulations with an EGR integrated system and oxidation catalytic after treatment [2]. Bin Huang and co-workers [3] have investigated the cycle-by-cycle variations in a spark ignition engine fueled with natural gas–hydrogen blends combined with exhaust gas recirculation. The effects of EGR ratio and hydrogen fraction on an engine's cycle-by-cycle variations were analyzed. The results showed that the cylinder peak pressure, the maximum rate of pressure rise and the indicated mean effective pressure decrease and the cycle-by-cycle variations increase with the increase of EGR ratio. A slight influence of EGR ratio on indicated mean effective pressure was observed at low EGR ratios while large influence of EGR ratio on indicated mean effective pressure was demonstrated at high EGR ratios [3]. Pradeepa and Sharma have taken into account the renewable fuel JBD suitable for diesel engines [4]. Diesel engines running on JBD were found to emit higher nitrogen oxides, NO_x. Hot EGR, a low cost technique of exhaust gas recirculation, was effectively used in that work to overcome this environmental penalty. Practical problems faced while using a cooled EGR system were avoided with hot EGR. Results indicated higher nitric oxide emissions when a single cylinder diesel engine was fuelled with JBD, without EGR. NO emissions were reduced when the engine was operated under hot EGR levels of 5–25%. However, EGR level was optimized as 15% based on adequate reduction in NO emissions, minimum possible smoke, CO, HC emissions and reasonable brake thermal efficiency. Smoke emissions of JBD in the higher load region were lower than diesel, irrespective of the EGR levels. However, smoke emission was higher in the lower load region. CO and HC emissions were found to be lower for JBD irrespective of EGR levels. Combustion parameters were found to be comparable for both fuels [4]. Erjiang and coworkers [5] have conducted an experimental investigation on the influence of different hydrogen fractions and EGR rates on the performance and emissions of a spark-ignition engine. The results showed that massive EGR introduction decreases the engine power output. However, hydrogen addition can increase the power output at large EGR operation. Effective thermal efficiency showed an increasing trend at small EGR rate and a decreasing trend with further increase of EGR rate [5]. For a specified hydrogen fraction, NO_x concentration was decreased with the increase of EGR rate and this effectiveness becomes more obvious at high hydrogen fraction. HC emission was increased with the increase of EGR rate and it decreased with the increase of hydrogen fraction. CO and CO_2 emissions showed little variations with EGR rate, but they decreased with the increase of hydrogen fraction. The study showed that natural gas–hydrogen blend combining with EGR can result in high-efficiency and low-emission spark-ignition engine [5]. Shizuo and all [7] investigeted an effect of EGR on direct injection gasoline engine. They confirmed that an appropriate volume of EGR improves fuel economy and HC emission. This phenomenon is presumably due to the intake temperature increase by EGR, which improves the flame propagation in the relatively lean area of the air-fuel mixture, which is not uniformly distributed [7]. Abd-Alla in his work presented a summary of the possibility of using exhaust gas recirculation in a spark ignition engine. He confirmed that in spark ignition engines, substantial reductions in NO concentrations are achieved with 10–25% EGR. However, EGR also reduces the combustion rate, which makes stable combustion more difficult to achieve. At constant burn duration and brake mean affective pressure, the brake specific fuel consumption decreases with increasing EGR [8].

MODELLING RESULTS

Modelling of the thermal cycle of the test spark ignition engine in the AVL FIRE program was carried out. The object of investigation was a spark ignition S320ER internal combustion engine fed with gasoline. The engine was operated at a constant speed of 1000 rpm. Exhaust gas recirculation was taken into account. An influence was analyzed of EGR on engine operating parameters, NO concentration in the exhaust gases and reduction of engine knocking phenomena. The paper presents the thermal cycle parameters for the conditions of constant ignition advance and the optimized angles.

The percentage of exhaust gases recycled back to the engine intake (%EGR) was calculated as a percentage of the total inlet mass flow rate. Geometric mesh of combustion chamber of modeled test engine is presented in the paper "Numerical analysis of the impact of EGR on the knock limit in SI test engine". The verification results and modelling parameters are also presented in the above-mentioned paper. Figure 1 shows changes in the indicated thermal efficiency and mean indicated pressure for the modeled engine depending on the EGR ratio. It turned out that small exhaust gas content in a fresh load causes an increase in engine efficiency. For modeled engine 2.5% EGR ratio caused an increase in the efficiency. The maximum obtained efficiency was 34.7%. Of course, with increasing participation of EGR in the fresh charge the value of mean indicated pressure decreased. With the increasing EGR there was a higher than 2.5% decline in engine efficiency.

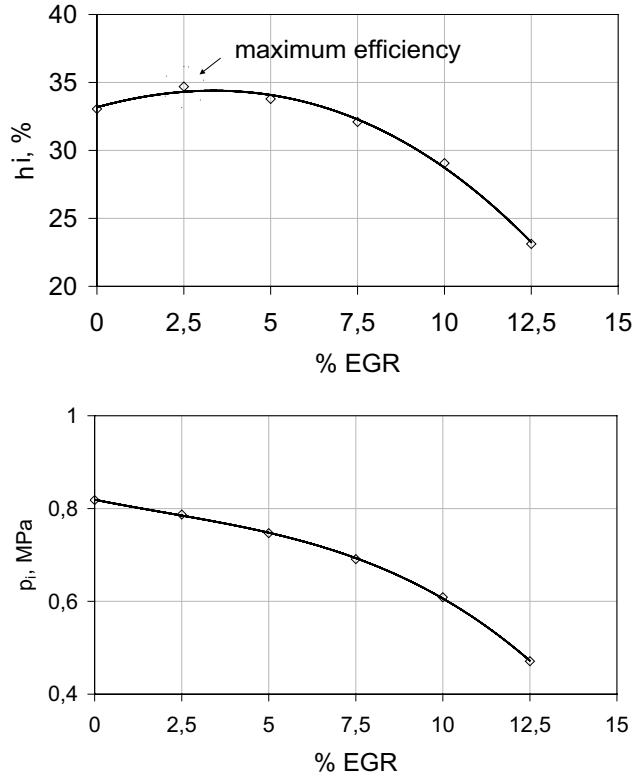

Fig. 1. Courses of indicated thermal efficiency and mean indicated pressure for constant spark advance timing equal to 10 deg before TDC

Figure 2 shows the value of mean indicated pressure for a fixed advance angle and the optimized conditions. It turns out that it is appropriate to increase the advance angle for increased participation of recycled gases in the fresh charge. For 12.5% increase of EGR the ignition advance angle allowed for an increase of mean indicated pressure by over 35 % from 0.47 MPa to 0.74 MPa

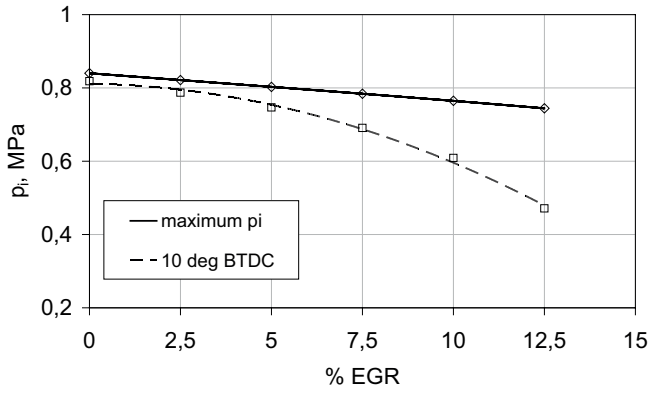

Fig. 2. Mean indicated pressure for constant ignition angle 10 deg before TDC and for optimized conditions at different shares of EGR, λ=1.2

Engine running without EGR reached the indicated efficiency equal to 33%. For 12.5% EGR ratio the indicated thermal efficiency dropped to 23%. Results were obtained for the test engine running with a constant angle of ignition advance.

The solid line in Fig. 3 represents the maximum pressure obtained for the conditions in which there was no knock combustion.

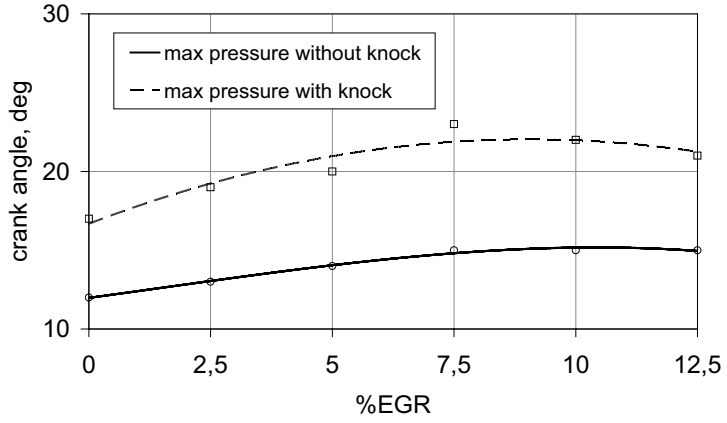

Fig. 3. The angle of the maximum combustion pressure for the conditions with and without knocking for different EGR shares

The dashed line represents the hypothetical value of the maximum pressure obtainable in the research engine, the limitation is the occurrence knock process.

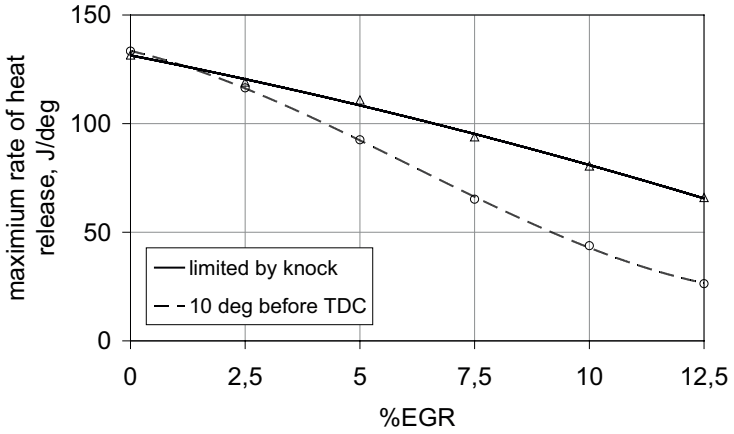

Fig. 4. Maximum rate of heat release for condition limited by knock onset and for constant ignition advance equal to 10 deg before TDC

Fig. 4 shows the dependence of rate of heat release to the conditions of constant advance angle and the optimized conditions. From Fig. 3 it can be concluded that the maximum heat release rate decreases with the increase of percentage EGR share. The increase of EGR dilution in the mixture decreases the in-cylinder oxygen concentration and, consequently, it reduces the heat release rate.

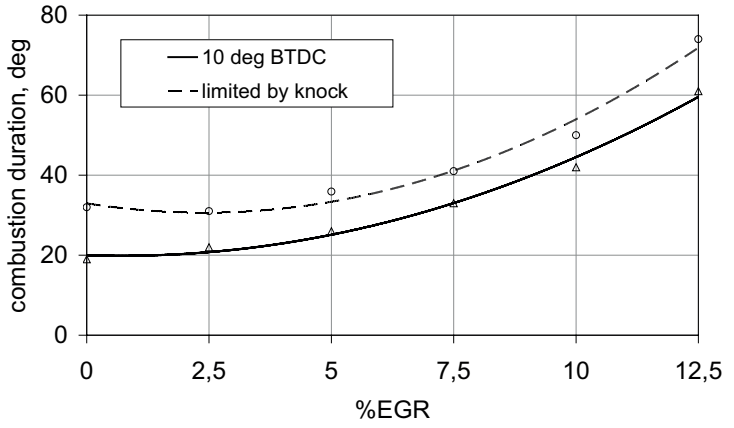

Fig. 5. Effect of EGR on the combustion duration angle for conditions: ignition advance equal to 10 degrees before TDC and the conditions for optimum ignition angle restricted by knock combustion onset

The combustion duration was calculated as the crank angle interval from the spark ignition to the end of combustion where the heat release reaches its maximum [1]. The increase of EGR share decreases the oxygen concentration which slowed down the combustion rate and increased combustion duration.

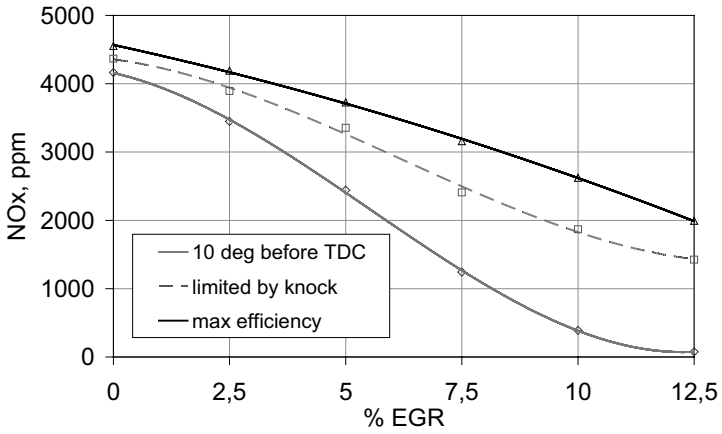

Fig. 6. Curves of NOx concentration depending on EGR percentage share

Figure 6 shows the impact of EGR ratio on NO content in the exhaust gases. With the increase in the share of exhaust gases in a fresh load it causes an decrease of NO in the exhaust gases. For the test engine NO concentration in the exhaust gas can be reduced by using 12.5% of EGR and the ignition angle about 50 deg before TDC. Under these conditions the drop of NO concentration from 4450 ppm to 1460 ppm can be achieved.

Due to the concentration of NO in the exhaust gas it is preferable not to make changes in the value of ignition angle, but it involves a significant deterioration in the thermodynamic parameters of engine cycle. For optimal conditions, without knock combustion, 12.5% of EGR reduced NO in the exhaust by more than 65%.

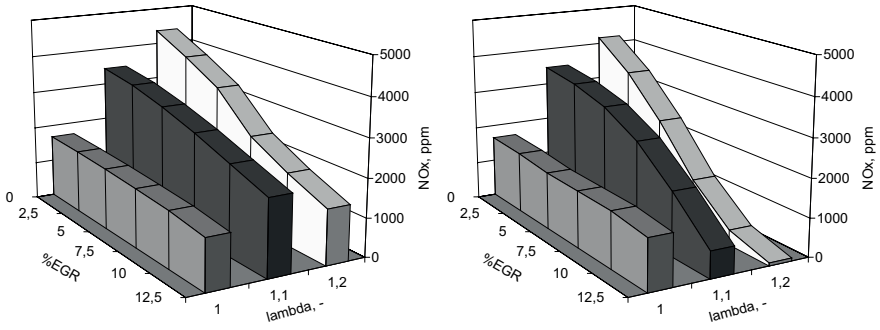

Fig. 7. NO concentration: a) in optimized conditions (max p_i and η_i),
b) constant ignition angle equal to 10 deg BTDC

Fig. 7 shows the NO concentration in the exhaust gases for different coefficients of excess air. Without optimizing the thermal cycle engine by changing the angle of advance a significant reduction of nitrogen oxides was achieved using EGR. On the other hand, a decrease followed of thermodynamic parameters of the engine cycle (Fig. 7b). Optimizing the thermal cycle of an engine with EGR in conditions of angle advance caused a smaller reduction of NO in the exhaust. How-

ever, it had a beneficial effect on the engine performance. This is the most evident for the excess air ratio equal to 1.2.

CONCLUSION

The paper presents the problem of optimizing the thermal cycle of a piston engine with exhaust gas recirculation. Achieving maximum thermodynamic parameters of the test engine cycle is limited by the occurrence of knock phenomenon. Maximum mean indicated pressure equal to 0.83 MPa was obtained for the test engine, without EGR. In the case of 12.5% EGR the maximum value of p_i reached a value 0.74MPa with more than 60% decrease in NO content. Exhaust gas recirculation is beneficial not only in reducing the toxicity of exhaust gases but also by effectively shifting the formation of the knock limit.

REFERENCES

Amr I., Saiful B.: *An experimental investigation on the use of EGR in a supercharged natural gas SI engine*. Fuel, Vol. 89, Issue 7, July 2010, Pages 1721-1730.

Wang Y., Zhou L.: *Experimental study on exhaust emissions from a multi-cylinder DME engine operating with EGR and oxidation catalyst*. Applied Thermal Engineering, Vol. 28, Issue 13, September 2008, Pages 1589-1595.

Bin H., Erjiang H., Zuohua H., Jianjun Z., Bing L., Deming J.: *Cycle-by-cycle variations in a spark ignition engine fueled with natural gas–hydrogen blends combined with EGR* . International Journal of Hydrogen Energy, 2009

Pradeepa V., Sharma R.P.: *Use of HOT EGR for NOx control in a compression ignition engine fuelled with bio-diesel from Jatropha oil*. Renewable Energy, Vol. 32, Issue 7, June 2007, Pages 1136-1154.

Erjiang H., Zuohua H., Bing L., Jianjun Z., Xiaolei G. Bin H.: *Experimental investigation on performance and emissions of a spark-ignition engine fuelled with natural gas–hydrogen blends combined with EGR*. International Journal of Hydrogen Energy, Vol. 34, Issue 1, January 2009, Pages 528-539.

Heywood J. B.: *Internal combustion engine fundamentals*. McGraw-Hill, 1988.

Shizuo S., Daisaku S., Takanori U., Hiroyuki S.: *Effects of EGR on direct injection gasoline engine*. JSAE Review 19 (1998) 223-228.

Abd-Alla G.H.: *Using exhaust gas recirculation in internal combustion engines: a review*. Energy Conversion and Management 43 (2002) 1027–1042.

AVL FIRE, VERSION 2009ICE *Physics & Chemistry. Combustion, Emission, Spray, Wallfilm*. Users Guide, 2009.

Szwaja S, Jamrozik A.: *Analysis of Combustion Knock in the SI Engine*. SILNIKI SPALINOWE/ Combustion Engines, Mixture Formation Ignition & Combustion, Nr 2009-SC2, June 2009.

AVL FIRE, VERSION 2009ICE *Physics & Chemistry. Combustion, Emission, Spray, Wallfilm*. Users Guide, 2009.

Tatschl R., Priesching P., Ruetz J.: *Recent Advances in DI-Diesel Combustion Modeling in AVL FIRE – A Validation Study*. International Multidimensional Engine Modeling User's Group Meeting at the SAE Congress April 15, 2007 Detroit, MI.

Jamrozik A., Tutak W.: *Modelling of combustion process in the gas test engine*. Perspective Technologies and Methods in Mems Design, MEMSTECH, Lviv - Polyana, Ukraine. s. 14-17, 2010.

Jamrozik J. Tutak W.: *Numerical analysis of some parameters of gas engine*. Motrol 2010

Tutak W. Jamrozik A.: *Modeling of thermal cycle of gas engine using AVL FIRE software.* Silniki Spalinowe 2010

Jamrozik A., Tutak W., Kociszewski A., Sosnowski M.,: *Numerical Analysis of Influence of Pre-chamber Geometry in IC Engine with Two Stage Combustion System on Engine Work Cycle Parameters*, Journal of KONES Powertrain and Transport, Vol 13, No 2, s. 133-142, rys. 14, tab. 2, poz. bibl. 9, European Science Society of Powertrain and Transport Publication, Warsaw 2006.

Tutak W., Jamrozik A., Kociszewski A., Sosnowski M.: *The influence of initial swirlprofile on modelled piston engine work cycle parameters*, XIV Ukrainian-PolishConference on "CAD in Machinery Design. Implementation and Educational Problems." CADMD`2006, Polyana, Ukraine, 22-23 May 2006, s. 118-121, rys. 10, tab. 1, poz. bibl. 7.

Kociszewski A., Jamrozik A., Tutak W., Sosnowski M.: *Computational Analysis and Experimental Research into Lean Mixture Combustion in Multi-Spark Plug SI Engine*, Journal of KONES Powertrain and Transport, Vol 13, No 3, s. 123-130, rys. 13, poz. bibl. 8, European Science Society of Powertrain and Transport Publication, Warsaw 2006.

ANALIZA NUMERYCZNA WYBRANYCH PARAMETRÓW PRACY SILNIKA ZI Z RECYRKULACJĄ SPALIN

W pracy przedstawiono wyniki modelowania obiegu cieplnego tłokowego silnika spalinowego o zapłonie iskrowym z uwzględnieniem recyrkulcaji spalin. Modelowanie przeprowadzono z wykorzystaniem propgramu FIRE. Analizowano wpływ EGR na tokyczność spalin z uwzględnieniem granicy spalania stukowego. Określono wpływ recyrkulacji spalin na długość procesu spalania.

TEKA Kom. Mot. Energ. Roln. – OL PAN, 2011, 11, 415–421

THE INVESTIGATIONS OF THE INFLUENCE OF FUEL CONSUMPTION ON THE CHANGES OF SELECTED PARAMETERS OF THE LUBRICANT IN DIESEL ENGINES

Piotr Wanke

Warsaw University of Technology
Faculty of Civil Engineering, Mechanics and Petrochemistry
Department of Mechanical Systems Engineering and Automation
Address: Jachowicza 2/4, 09 – 402 Płock, Poland
e-mail: pwanke@pw.plock.pl

Summary. The paper presents the results of comparative investigations of changes in dynamic viscosity and dielectric constant of the lubricant in diesel engines fueled with Ekodiesel Plus 50B and Ekoterm Plus under real operating conditions.

Keywords: diesel fuels, engine lubricants, dynamic viscosity, dielectric constant.

INTRODUCTION

The real operating conditions of kinematic pairs in diesel engines (CI) depend on a variety of factors. The possibilities of occurrence of excess loads, high air dustiness, unprofessional and irregular maintenance, failure to use fuels to applicable standards (use of cheaper replacements) and fuels recommended by the manufacturers can result in unpredictable changes in the lubricant properties in the oil ducts. The design requirements, technologies of manufacturing of materials and parts in the kinematic pairs as well as mutual tribological relations during operation – much dependent on the quality of the applied lubricants and fuels – determine the course of the abrasive loss process in the said kinematic pairs of diesel engines and self-propelled machinery [Wanke, Koniuszy 2009, Wanke 2010]. The most difficult to define are the changes in the lubricating conditions in the slide areas of critical pairs related to a continuous deterioration of the rheological and qualitative parameters of the engine lubricants, resulting from the dissolution and dissipation of pollutants as well as fuel leaks through the piston rings [Szczerek, Wiśniewski 2000]. That is why in day-to-day operation the changes in the properties of the engine lubricant should be monitored between the scheduled maintenance inspections. The intervals recommended by the manufacturers due to various operating conditions are not always necessary to apply. Through a realization of periodic diagnostics of selected lubricant parameters for given operating conditions we can determine new

oil change criteria, which is economically justifiable – particularly in professional applications. For central lubrication systems an appropriate selection of engine lubricant (particularly its properties and parameters) for the actual operating conditions can have a decisive influence on the optimization of the durability potential of the whole power train [Wajand J. A., Wajand J. T. 2000, Jakóbiec 2001 a, b, Olszewski i in. 2004, Bocheński 2005].

One of the more important issues in recent years in the field of durability optimization and reliability maximization in diesel engines in operation – discussed by authors of many publications – has been the use of fuels compliant with the manufacturer specifications and applicable standards [Mucha 2000, Oleksiak 2001 a, b, Baczewski K., Kałdoński T. 2004, PN-EN 590:2006]. In older generation of engines – engines of a lower fuel system sensitivity to the quality of fuel – very often different replacement fuels were used of unpredictable impact on the changes of the quality of the engine lubricant, thus on the durability and reliability of the engine [Kowalski 2006].

In relation to the presented conditions the authors, in the comparative tests, have undertaken to explain whether the amount of used fuel influences the rheological properties of the diesel engine lubricant (farm tractors) under real operating conditions. The authors particularly attempted to explain whether the observed changes of the selected engine lubricant properties can lead to a modification of the recommended service interval plan and, in extreme cases, whether they can lead to pathology in the wear of the critical friction pairs particularly those operating under slide friction.

The here presented results are a second part of the earlier publication of the author [Wanke 2010] and were collected simultaneously in the same field experiment under real operating conditions of the tractors.

RESEARCH METHODOLOGY

In the operational comparative investigations the authors tested two Ursus 1614 farm tractors manufactured in the years 1992÷1993 fitted with the Z 8602.1 engines after a rebuild performed in the beginning of 2006 before the start of the agricultural season. The tests were carried out in the agricultural season 2008 from 3 March to 6 December. The initial mileage of the first tractor marked A (fueled with Ekodiesel Plus 50B – diesel oil) equaled to 689,4 motor hours (mth) and the second marked B (fueled with Ekoterm Plus – heating oil) 703,6 motor hours counting from the engine rebuild. Directly prior to the initiation of the tests the engines were filled with the oil of the same grade SAE 15W/40, API CG-4, ACEA 96 E2/B2/A2 [Podniało 2002] and a diagnostics was performed according to the manual. Based on the obtained results of the inspection the engines were deemed parametrically acceptable – technically operative [URSUS 1614 Wheeled Farm Tractors 1992].

The monitored tractors belonged to one owner and were operated in the same farm simultaneously on the same fields at the same time adequately to their tractive effort for works related to soil cultivation, fertilization and crops transportation. Based on the performed diagnostics and analysis of the conditions it was assumed that both tractors were in a similar initial state and operated under similar operating conditions, which makes the test results comparable.

The oil samples for the comparative tests were taken according to a preset procedure – the same for each of the operated tractors. The first sample – the base sample was taken from the packaging when the oil was delivered to the workshop. The second one was taken directly upon finishing of the first day of operation. Then, the oil sample was taken regularly approximately every 1000 dm^3 of used fuel until the oil change. Each of the samples was marked. The oil samples were taken through the dipstick slot with the use of a syringe and a hose of the capacity of $50 \cdot 10^{-6}$ m^3, accuracy $\pm 5 \cdot 10^{-7}$ m^3, directly upon the finishing of the tractor operation. Immediately after the tak-

ing of the sample the syringe and the hose were thoroughly cleaned in a thinner and dried. The oil attrition was topped up. In the period of the experiment the amount of consumed fuel was recorded from the indications of the flow meters with the accuracy of $\pm 10^{-3}$ m^3.

For each of the taken samples the dynamic viscosity and the dielectric constant were measured three times in a steady temperature of T = 293 K and then the average values and standard deviations were calculated. For the marking of the viscosity a digital rotational viscosity meter was used – Brookfield DV-II+ with an ultra thermostatic chamber controlled by a PC computer with Rheocalc 32 installed. The measurement was carried out according to the [PN-EN ISO 3104:2004] standard and the recommendations of the manufacturers of the viscosity meter with the accuracy $\pm 10^{-2}$ mPa·s [Brookfield DV-II+ User Manual 2008]. For the determining of the changes in the quality of the oil a Lubrisensor device was used that, thanks to the absolute changes in the value of the dielectric constant (accuracy $\pm 10^{-1}$), enables detection of 3 groups of operational pollutants of the engine oil (group I – oxides and sediments, dirt, products of fuel combustion, acids; group II – water, coolant, metal parts; group III – fuel). The dielectric constant grows or lowers proportionally to the changes in the concentration of the pollutants present in the oil. The direction of the sway of the indicator towards „+" or „–" and the value of the indication determined the group of the pollutants and their amount. The evaluation of the condition of the tested oil consisted in calibrating of the device against a reference sample (fresh oil) and measuring of the changes of the dielectric constant for the tested samples taken from the engine [Lubrisensor User Manual 2000, Olszewski 2001]. The obtained results of the comparative tests were then correlatively and regressively analyzed on the significance level of $\alpha = 0.05$.

DISCUSSION OF THE TEST RESULTS

Based on the statistical analysis of the results a significant impact (significance level of α = 0,05) was observed of the amount and quality of the used fuel on the changes of the rheological and quality parameters of the engine lubricant of the grade SAE 15W/40 API CG-4. A very strong positive (directly proportional dependence of the dielectric constant – Fig. 2) and negative correlation (indirectly proportional dependence of the dynamic viscosity – Fig. 1) has been observed as a function of the amount of the used fuel and the multiple correlation – type R(z/xy) (Fig. 3). The comparison of the coefficients of the directions of the regression lines indicates that the unit drop of the dynamic viscosity of the lubricant – grade SAE 15W/40 API CG-4 in the engine fueled with diesel oil (Fig. 1, straight line) is approximately 10% lower than in a comparable engine fueled with heating oil (Fig. 1, dotted line). In the case of the relative changes in the dielectric constant it has been observed that the unit increment of the analyzed parameter is approximately 33% higher than in the case of engine B fueled with heating oil (Fig. 2, dotted line).

During the comparative operational measurements of the changes in the quality of the engine oils with the use of Lubrisensor in the case of all samples taken directly from the oil sump in the tested range of operation only the pollutants from group I have been observed. The pollutants from groups II and III (water, coolant, metal particles and fuel) were not detected by the device. This could confirm the earlier formulated assumption (at the beginning of the comparative investigations) that the engines were fully operational parametrically upon inspection as per the recommendation of the manufacturer. An important effect of the performed tests is the increment of the dielectric constant – clearly seen in figures 2 and 3 (as compared with the reference oil) only in the first oil samples

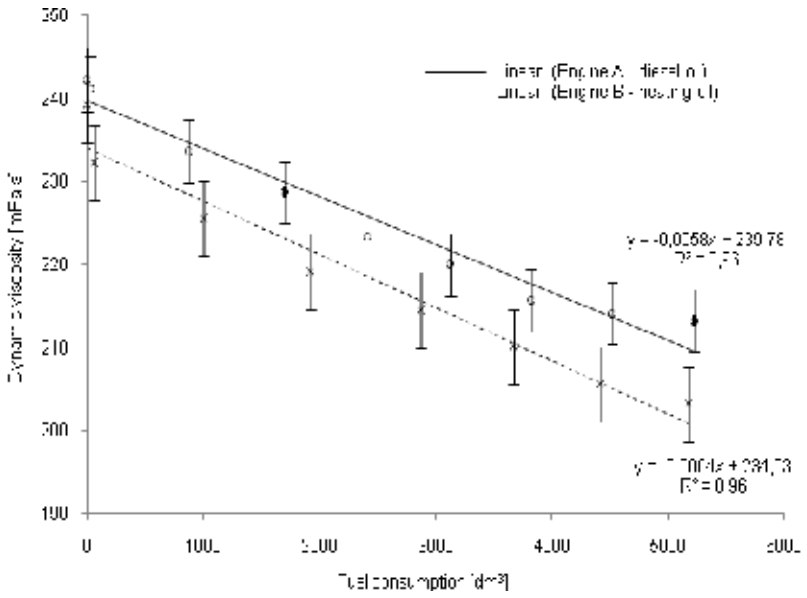

Fig. 1. The comparison of the regression lines of the changes in the dynamic viscosity of the engine oil – grade SAE 15W/40 API CG-4 as a function of fuel consumption (constant measurement temperature T = 293 K)

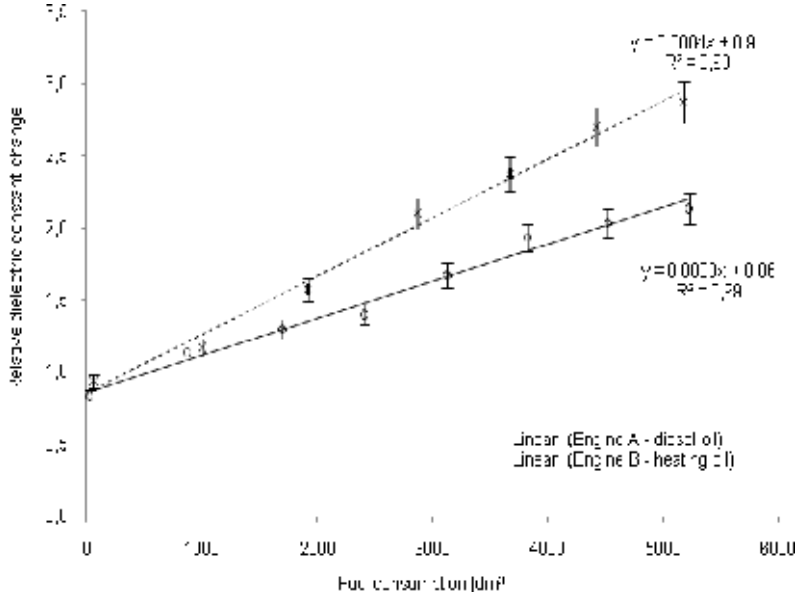

Fig. 2. The comparison of the regression lines of the relative changes of the dielectric constant of the engine oil – grade SAE 15W/40 API CG-4 as a function of fuel consumption (constant measurement temperature T = 293 K)

taken from the engines upon consuming of 29 dm^3 (tractor A) and 60 dm^3 (tractor B) of fuel respectively at a simultaneous drop in the dynamic viscosity of up to 17% when fueled with Ekoterm Plus (fig. 3). Such a significant change after only one day of operation may indicate an excess amount of pollutants (carbon sediments, tar) inside the engine and oil ducts and may necessitate engine flushing at the nearest oil change.

The results shown in Fig. 1, 2 and 3 of periodic monitoring of the changes of the selected rheological and qualitative properties of the engine oil - grade SAE 15W/40 API CG-4 as a function of fuel consumption realized under real operating conditions of the farm tractors constituted a basis for the extension of the oil change interval recommended by the manufacturer (recommended 200 mth of operation) [URSUS 1614 Wheeled Farm Tractors 1992]. Throughout the whole agricultural season (field works and transport) at the fuel consumption of 5226 dm^3 – for engine A fueled with Ekodiesel Plus 50B – and 5180 dm^3 for engine B fueled with Ekoterm Plus the excess of the admissible changes of the dynamic viscosity and the dielectric constant was not observed against fresh oil despite the extension of the oil change interval by approximately 80% and 60% respectively [Wanke 2010].

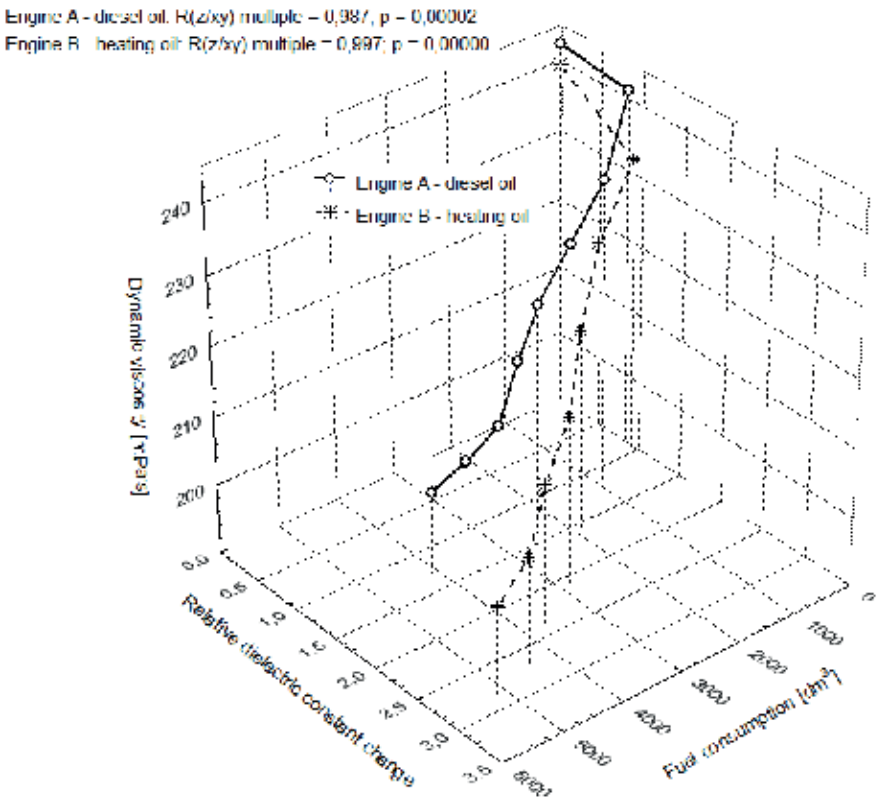

Fig. 3. The graph of the spread of the values with the lines of the dynamic viscosity changes and the dielectric constant of the engine oil – grade SAE 15W/40 API CG-4 as a function of fuel consumption (multiple correlation indicators included of constant temperature of T = 293 K)

Based on the discussed nature of the changes of the dynamic viscosity and the dielectric constant of the engine oil – grade SAE 15W/40 API CG-4 as a function of quantity (also depending on the quality) of the used fuel a supposition was formulated of a possibility of a significant extension of the oil change intervals for the Z 8602.1 engines until the boundary values are reached as defined in the change ±25% (dynamic viscosity) [Bocheński 2005] and 3.5÷4.0 (dielectric constant) [Sobańska-Górska, Zajkowski 1995].

CONCLUSIONS

1. The Z 8602.1 engine fueling with Ekoterm Plus accelerates the unit growth of the dielectric constant by approximately 33% and results in an approximately 10% faster drop in the dynamic viscosity of the engine oil – grade SAE 15W/40 API CG-4 as a function of the amount of consumed fuel as compared to the fueling with Ekodiesel Plus 50B. This indicates a significant acceleration of the engine oil parameters deterioration that may lead to the deterioration of the lubricating conditions and an accelerated wear of the friction pairs through the reduction of anti wear oil properties used in the friction surfaces of the kinematic pairs in the engine.
2. Unit changes in the values of the dynamic viscosity and the dielectric constant in the compared samples of the engine oil are very strongly correlated (on the significance level of $\alpha = 0.05$) with the amount and quality of the consumed fuel.
3. Periodic monitoring of the engine oil conditions in the Z 8602.1 engines – in operational conditions – allows for an extension of the oil change interval depending on the local operating conditions measured by the amount of fuel used during an operation.

REFERENCES

Baczewski K., Kałdoński T. 2004: Paliwa do silników o zapłonie samoczynnym. WKŁ, Warszawa.
Bocheński C. 2005: Paliwa i oleje smarujące w rolnictwie. Wydawnictwo SGGW, Warszawa.
Instrukcja obsługi. Lepkościomierz cyfrowy Brookfield DV–II+, 2008.
Instrukcja obsługi. Lubrisensor, 2000.
Instrukcja obsługi. Kołowe ciągniki rolnicze URSUS 912, 914, 1012, 1014, 1222, 1224, 1614. Wydawnictwo ZSL, Warszawa 1992.
Jakóbiec J. 2001 a: Zmiany właściwości użytkowych olejów silnikowych w warunkach eksploatacji (cz. 1). Paliwa Oleje i Smary w Eksploatacji, nr 83, 25–28.
Jakóbiec J. 2001 b: Zmiany właściwości użytkowych olejów silnikowych w warunkach eksploatacji (cz. 2). Paliwa Oleje i Smary w Eksploatacji, nr 84, 30–32.
Kiernicki Z. 2010: Some properties of the diesel fuelled with the fuel from plastic waste. Teka Kom. Mot. i Energ. Roln. – OL PAN, v. 10, 153–162.
Kowalski K. 2006: Użytkowanie pojazdów wojskowych w warunkach niedoboru paliw bazowych. Eksploatacja i Niezawodność, nr 4, 16–21
Mucha J. 2000: Jakość oleju napędowego a eksploatacja silnika. Paliwa Oleje i Smary w Eksploatacji, nr 79, 36–38
Oleksiak S. 2001 a: Ocena smarności olejów napędowych (cz. 1). Paliwa Oleje i Smary w Eksploatacji, nr 88, 36–38
Oleksiak S. 2001 b: Ocena smarności olejów napędowych (cz. 2). Paliwa Oleje i Smary w Eksploatacji, nr 89, 35–38

Olszewski W. 2001: Możliwość oceny stanu jakości oleju silnikowego podczas eksploatacji za pomocą pomiaru własności dielektrycznych. Journal of Kones. Combustion Engines, nr 3–4, 95–101.

Olszewski W., Maciąg A., Janik R. 2004: Ocena wpływu czasu eksploatacji na właściwości użytkowe olejów silnikowych. Problemy Eksploatacji nr 1, Instytut Technologii Eksploatacji, Radom.

Podniało A. 2002: Nowe specyfikacje olejów silnikowych. Paliwa, Oleje i Smary w Eksploatacji, nr 100, 38 – 40

Sobańska-Górska K., Zajkowski R. 1995: Eksploatacyjna weryfikacja przydatności przyrządu Lubrisensor do szybkiego określania optymalnego czasu pracy oleju silnikowego. Instytut Transportu Samochodowego, Warszawa.

Szczerek M., Wiśniewski M. 2000: Trybologia i trybotechnika. Wydawnictwo Instytutu Technologii Eksploatacji, Radom.

Wajand J.A., Wajand J.T. 2000: Tłokowe silniki spalinowe średnio- i szybkoobrotowe. WNT, Warszawa.

Wanke P., Koniuszy A. 2009: An analysis of wear of slide pairs lubricated by class CC 30 lubricants mixed with diesel fuels. Teka Kom. Mot. i Energ. Roln. – OL PAN, v. 9, 370–376

Wanke P. 2010: A study on fuel quality impact on the changes of selected lubricant parameters in self-ignition engines. Teka Kom. Mot. i Energ. Roln. – OL PAN, v. 10, 2010, 503–508

PN-EN ISO 3104:2004: Przetwory naftowe. Ciecze przezroczyste i nieprzezroczyste. Oznaczanie lepkości kinematycznej i obliczanie lepkości dynamicznej.

PN-EN 590:2006: Paliwa do pojazdów samochodowych. Oleje napędowe. Wymagania i metody badań.

BADANIA WPŁYWU ZUŻYCIA PALIWA NA ZMIANY WYBRANYCH PARAMETRÓW OLEJU SMARNEGO W SILNIKACH Z ZAPŁONEM SAMOCZYNNYM

Streszczenie. W pracy omówiono wyniki badań porównawczych zmian lepkości dynamicznej i stałej dielektrycznej oleju smarnego w funkcji zużycia paliwa, w silnikach z zapłonem samoczynnym, zasilanych paliwem Ekodiesel Plus 50B i Ekoterm Plus w rzeczywistych warunkach eksploatacji.

Słowa kluczowe: paliwa do silników z zapłonem samoczynnym, oleje silnikowe, lepkość dynamiczna, stała dielektryczna

TEKA Kom. Mot. Energ. Roln. – OL PAN, 2011, 11, 422–429

THE ASSESSMENT OF THE QUALITY OF SPRAY NOZZLES BASED ON THE SPRAY GEOMETRY

Cezary Wiśniewski

Warsaw University of Technology
Faculty of Civil Engineering, Mechanics and Petrochemistry
Department of Mechanical Systems Engineering and Automation
Address: Jachowicza 2/4, 09–402 Płock, Poland, e-mail: wis@pw.plock.pl

Summary. The transverse spray uniformity is very often used to assess spray quality. The value of the spray uniformity index (the coefficient of variation) is estimated on the basis of laboratory tests, carried out on the grooved table. The functional parameters of nozzles have direct influence on the value of this index. The differences between the actual and the nominal values of the parameters might have a significant influence on the quality of the spray during field works.

This study presents an analysis of the results of tests on the quality of flat fan nozzles used for fields spraying. The quality was evaluated on the basis of a statistical analysis of functional parameters characterizing the geometry of the spray stream. The obtained results allowed drawing conclusions and making comments on the influence of the spray nozzle quality on the spray process. The conclusions and remarks might be useful for the nozzle manufacturers.

Keywords: workmanship quality, nozzle, functional parameter, spray, quality evaluation

1. INTRODUCTION

Field crop spraying is one of the most frequently used agricultural and technical procedures particularly during vegetation of plants. Pesticides are poisons and can cause many dangers not only for the sprayer operator but also for outsiders and for other life forms in the environment [19]. Therefore, the use of minimal pesticide inputs and only when they are necessary is essential. The tests conducted in Poland and abroad are aimed at the minimization of the use of chemical preparations to the extent ensuring high quality and effectiveness of the procedure. The analyses of research work [4, 8, 19] showed that a lot of factors connected with the structure of sprayers, their functions and use, properties of the working liquid, atmospheric conditions and agricultural and technical conditions affect the quality and effectiveness of the procedure.

The spraying quality is evaluated on the basis of a non-uniform transverse distribution of the spray (the coefficient of variation), the values of which are calculated with the use of results of measurements performed on a grooved table (patternator). The spray uniformity index value is directly influenced by volumes and distribution of the liquid in grooves of the table depending on

functional parameters of nozzles, including, the intensity of outflow of the technological liquid and the values of angles characterizing geometry of the spray stream. The relevance of the parameters is confirmed by the fact that for example the nominal values of the spray stream angle and liquid outflow rate are provided in nozzle type designations and spray nozzle selection instructions. The issue of evaluation of workmanship quality of the flat fan nozzles was tackled in several studies [21-24]. However, in order to supplement and update the evaluation, it is necessary to perform an analysis of quality, again considering the spray angle and the stream asymmetry angle in relation to the spray nozzle symmetry axis perpendicular to the sprayed area.

Due to the influence of special causes (assignable causes) and natural variability (chance causes of variation) of each production process [12], it is practically impossible to obtain spray nozzles with nominal value of the spray stream angle and ideal angle symmetry for the entire population. However, neither manufacturer information relating to spray nozzles used in agriculture nor any Polish standards provide admissible ranges of variability of the parameters, which do not affect the spray quality. Few manufacturers of industrial spray nozzles guarantee that the stream angle will not be changed by more than ±5° [5]. The tests [9] showed that the spray stream angle value, which is smaller than the nominal value, may lead to formation of liquid droplets greater than the assumed ones and, at the same time, worse coverage of plants with pesticides. Besides, as the computer simulations showed, a small asymmetry of the spray angle may (in some configurations of distribution of the spray nozzles on the spray boom) lead to a great value of the coefficient of variation for the boom [16].

2. LABORATORY TESTS

The laboratory tests were performed in the year 2003, on new, serial production flat fan nozzles used in spraying because of their great usability [1, 20]. For the selected type of spray nozzles and the liquid operating pressure of 0.3 MPa, the nominal values of the functional parameters are shown in Table 1.

Table 1. The nominal values of the functional parameters

Functional parameter	Nominal value
liquid outflow rate	$Q_{nom} = 2 \times 10^{-5}\ m^3\ s^{-1}$
spray stream angle	$\alpha_{nom} = 110°$
asymmetry angle (the angle between the stream symmetry axis and the nozzle symmetry axis)	$\beta_{nom} = 0°$

The tests were performed in accordance with recommendations presented in the standards [6, 7] and methodology of tests of tractor pressure sprayers [25]. The tests covered 300 flat fan nozzles mounted one by one on the spraying boom placed at the height of 0.5 m above the measuring table (patternator). The measurements were repeated three times in a row for each of the nozzles and for the same testing conditions. The tests involved measurements of intensity of the liquid outflow and video recording of the spray stream emitted by each of the nozzles. The detailed description of the test stand, the testing method and the preparation of the test data are presented in the studies [2, 3, 11].

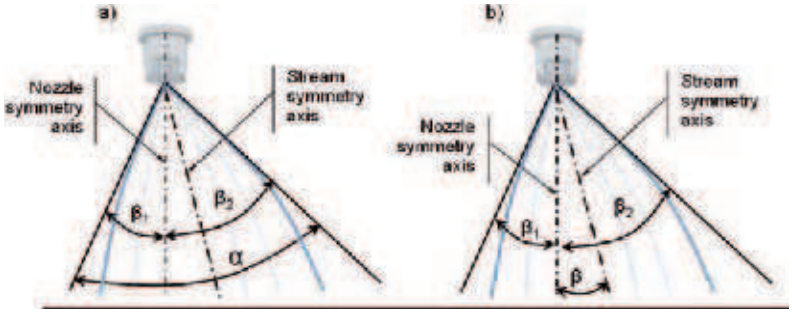

Fig. 1. Illustration of the method of angle determination in the spray stream: a) α - the liquid spray angle, where: $\alpha=\beta_1+\beta_2$, b) β - asymmetry angle, where: $\beta=0.5|\beta_2-\beta_1|$, β_1,β_2 – angles of the left and right parts of the spray stream in relation to the nozzle symmetry axis perpendicular to the sprayed surface [22]

The values of α and β angles characterizing the geometry of the spray stream (Fig. 1) were determined with the use of computer processing and statistical analysis of the recorded video images of the spray streams. The value of α angle was determined between the slant heights of the elliptical cone in the upper part of the stream before bending of the slant heights in the bottom part (Fig. 1a). This method of determination of liquid spray angle in the flat fan nozzle is commonly used by manufacturers and research centers [1]. The value of β angle has been calculated using the absolute value of the difference between β_1 and β_2 angles (Fig. 1b).

3. THE ANALYSIS OF TEST RESULTS

The data of the liquid spray angle and spray stream symmetry angle were subject to computer processing and statistical analysis. The analysis was aimed at the obtainment of assessment of the statistics describing trial empirical data and assessment of the compliance of the empirical data with the nominal values provided by manufacturers of nozzles. As a result of 300 trial evaluations of average spray angles and asymmetry, the basic statistical location and differentiation measures were determined (Table 2).

Table 2. The values of statistical location and differentiation measures of the empirical distribution for the liquid spray angle α and asymmetry angle β for flat fan nozzles [22]

Measure	Value	Measure	Value		
	Angle α	Angle β		Angle α	Angle β
Average	103.5°	0.96°	Maximum	107.5°	2.75°
Median	103.7°	0.84°	Minimum	97.1°	0.1°
Mode	104.3°	0.6°	Range	10.4°	2.65°
Variance	3.598	0.283	Lower quartile	102.15°	0.55°
Standard deviation	1.897°	0.535°	Upper quartile	104.95°	1.30°
Standard error	0.110°	0.031°	Coefficient of variation	1.83%	55.88%

When analyzing the results (Table 2) in terms of statistical location measures (e.g. average, median, mode, quartiles), it should be stated that:

- The average spray angle of the liquid emitted by the nozzle was 103.5º and was lower from the nominal value provided by the manufacturer (110º). The average symmetry angle value ($\beta_{śr}$=0.96º) also indicated that an average nozzle was characterized by asymmetry of the spray stream.
- Assuming that the tested nozzles represent a random collection of all nozzles of the type, the obtained average values should be interpreted with errors of 0.110º for angle α and 0.031º for angle β respectively.
- Half of the nozzles tested was characterized by liquid spray angles exceeding 103.7º and asymmetry angles exceeding 0.84° (median values).
- The dominant angle (mode value) in the spray nozzle test was α angle with the value of 104.3° and β angle with the value of 0.6°.
- Most typical nozzles used in the test were such nozzles, for which liquid spray angle values fell within the range of 102.15° and 104.95° (between the lower and upper quartile of α angle) and such nozzles, for which asymmetry angles fell within the range of 0.55° and 1,3° (between the lower and upper quartile of β angle).

When analyzing the calculated values (Table 2) of empirical characteristics of distribution (e.g. standard deviation, coefficient of variation), it may be stated that:

- The average differentiation (standard deviation) of the liquid spray angle was 1.897°, which, as expressed relatively (coefficient of variation), corresponds to approx. 1.83% of the arithmetic average. Such a low value of the variability coefficient proves a considerable homogeneity of nozzles in terms of deviation of the angle values from the average value.
- The average differentiation (standard deviation) of the asymmetry angle was 0.535°, which, as expressed relatively (coefficient of variation), corresponds to approx. 55.88% of the arithmetic average. Such a high value results from a considerable standard deviation (0.535°), which, in relation to the average value (0.96°) proves a considerable differentiation of the nozzles in terms of deviation of the angle values from the average value.

The above-mentioned observations are illustrated in a graphic presentation of the distribution series composed of the analyzed data (Fig. 2 and 3).

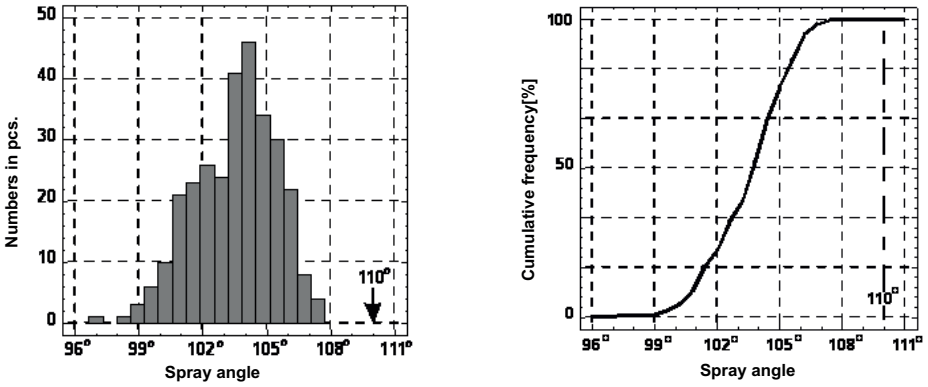

Fig. 2. A histogram of numbers and a cumulative frequency curve for the testing of data of the liquid spray angle (α) with indicated level of the nominal value 110° [22]

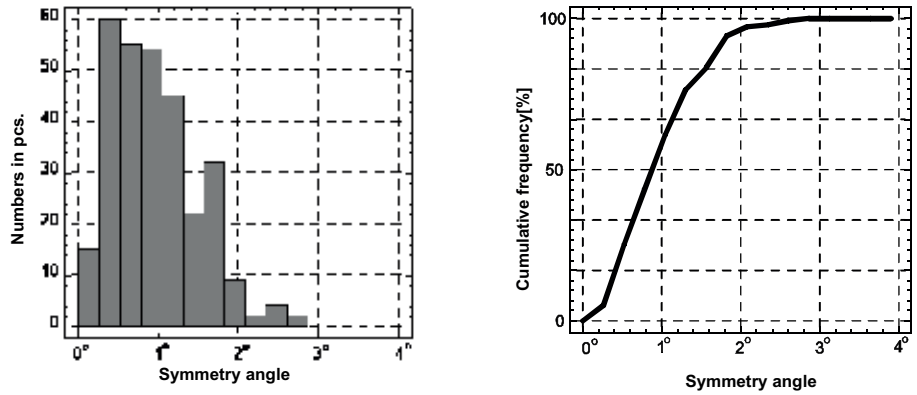

Fig. 3. A histogram of numbers and a cumulative frequency curve for the esting of data of the liquid stream asymmetry angle (β)

By treating the tested sample of nozzles as representative for the entire population of nozzles of the type and taking into account large numbers of the sample (300 elements), it may be assumed that the tested nozzles are characterized by the liquid spray angle value lower than that indicated by the manufacturer. This assumption is justified because 100% of the nozzles tested were characterized by liquid spray angle values lower than the nominal value of 110°.

The difference observed between the average value of the sample ($\beta_{śr}$=0.96°) and the assumed nominal value of the liquid stream asymmetry angle (β_{nom} = 0°) does not require any verification in terms of statistical relevance due to the fact that 100% of the values in the large samples composed of 300 elements were greater than 0°.

4. CONCLUSIONS

The conducted analysis aimed at the evaluation of the workmanship of new serial production flat fan nozzles. The obtained results and conclusions can be useful for the nozzle manufacturers and to formulating standards and quality requirements.

By adopting a definition of the quality quoted in the standard [17] as "degree, to which a set of inherent characteristics (...) fulfils requirements (...)", it may be stated that the considered functional parameters constitute the characteristics (inherent characteristics) of nozzles affecting correct spraying procedures (in accordance with the equipment specified in the standards, for example). An inadequate quality level of nozzles may result in a failure to fulfill the user's expectations related to the effectiveness and costs of the procedure or may cause negative impact on the natural environment.

The statistical test performed on a large randomly collected sample of flat fan nozzles enabled an evaluation of the statistical values characterizing the population of nozzles in terms of some functional parameters. In characterizing the population of nozzles, attention should be paid to the following main conclusions:

- Average values of α and β angles differ considerably (in terms of statistics) from the values indicated by the manufacturer. The difference shows that the production process of nozzles was out of control and that the influence of assignable causes resulted in the movement of the process mean (desirable nominal value) to the undesirable value.
- The nozzles were characterized by a high homogeneity in terms of deviation of angle α from the average value (1.83%) and showed great differentiation for angle β (55.9%). The great value of the coefficient of variation for angle β shows that the production process was unstable and the dispersion of the angle β values in the population of nozzles was considerable.
- Due to the confirmed deviation of the values of α and β angles from the nominal values, it would be purposeful for manufacturers to indicate admissible values of the deviations in order to provide unambiguous evaluation of the quality of nozzles and eliminate nozzles that do not comply with the manufacturer specifications.

The above-mentioned comments enable an evaluation quality of flat fan nozzles, although the evaluation is not unambiguous and it depends on an adopted criterion. The unambiguity of the evaluation results particularly from the absence of available data relating to tolerance ranges for α and β angles that could guarantee good quality of spraying. As regards the tolerance ranges for the angles, one may consider Shewhart's criteria [18], however, the adoption of this approach would require a verification in the form of additional laboratory tests and simulation analyses.

From the practical point of view, the quality of the evaluated spraying was based on a non-uniform transverse distribution of the spray as determined for the spraying boom, and depended, to a great extent, on the order in which nozzles are mounted in the boom – a fact to which the study [16] referred. This results from non-uniform "overlapping" of asymmetrical cones of the spray streams across the width of the spraying boom. Additionally, in the case of the liquid spray angle, a considerable difference between the actual value and the nominal value of the angle may lead to formation of droplets even greater than the assumed ones and, at the same time decrease of the degree of coverage of crops with a pesticide. Besides, the value of the angle, which is lower than the nominal value of the angle, will lead to a decrease of the transverse range of the spray streams for the spraying boom located at the height recommended by the manufacturer in the manual.

Considering the above-mentioned comments, it may be stated that taking into account the statistical analysis of the liquid spray angle values and stream asymmetry only as well as conclusions resulting from the analysis, the quality of workmanship of the nozzles (compliance with the nominal

values) may be evaluated unequivocally as unsatisfactory. However, there is still an open issue of evaluation of the influence of low quality workmanship of nozzles on the quality of spraying, which may be determined upon testing of the relation between the indicator of the spraying quality and variability of functional parameters of the nozzles mounted in the spraying boom.

Future trend in the studies should involve such tests that would allow detecting the causes of deviation of the functional parameter values of nozzles from the nominal values. The causes may result from inappropriate quality of production or inappropriate structure of the nozzles causing high sensitivity of functional parameters to insignificant random changes in the workmanship quality. The tests may consider an analysis of the internal structure of a nozzle, including the influence of accuracy of the surfaces inside the nozzle chambers and channels or shaping of the chambers and channels for the purposes of variability of the functional parameters.

REFERENCES

An Engineer's Guide to Spray Technology Bulletin. No. 498 2000 [on line]: Last updated: 2000-06-30. [Accessed: 2006-04-10]. Available at: http://service.spray.com/web/register/ view_lit.asp?code=B498.

Dwiliński L., Michalak G., Pietrzyk J. 1999: Automatyzacja pomiarów nierównomierności oprysku na stole wielorowkowym. VI Międzynarodowe Sympozjum nt.: Ekologiczne aspekty mechanizacji nawożenia, ochrony roślin, uprawy gleby i zbioru roślin uprawnych, IBMER, Warszawa, 147-152.

Dwiliński L., Michalak G., Pietrzyk J. 2001: Opracowanie metodyki badań rozpylaczy płaskostrumieniowych z wykorzystaniem zautomatyzowanego stanowiska laboratoryjnego. Sprawozdanie z pracy badawczej nr 503G/7703/2311/001, PW WBMiP, Płock.

Gajtkowski A. 1978: Wskaźniki określające jakość rozpylenia cieczy w opryskiwaczach polowych. Maszyny i Ciągniki Rolnicze, nr 7-8, 25-27.

H.IKEUCHI&Co.,Ltd. 2011: Accuracy Guarantee on Spray jets. In: www.kirinoikeuchi.co.jp Technical Information [on line]. [Accessed: 2011-02-14; 18:00]. Available at: http://www.kirinoikeuchi.co.jp/eng/technical_information/accuracy_guarantee_on_spray_nozzles.html.

ISO 5682-1:1996 Equipment for crop protection - Spraying equipment - Part 1: Test methods for spray jet nozzles.

ISO 5682-2:1997 Equipment for crop protection - Spraying equipment - Part 2: Test methods for hydraulic spray jets.

Kamiński E. 1987: Postęp techniczny w ochronie roślin. Mechanizacja Rolnictwa, nr 9, 18-20.

Matthews G.A. 2004: How was the pesticide applied? Crop Protection, nr 23, 651-653.

Michalak G. 2003: Wpływ parametrów funkcjonalnych rozpylaczy na jakość oprysku. rozprawa doktorska, Politechnika Warszawska WBMiP, Płock.

Michalak G. 2006: Metodyka badań parametrów funkcjonalnych rozpylaczy. Wybrane Problemy Inżynierii Mechanicznej, Politechnika Warszawska, Instytut Inżynierii Mechanicznej, Płock, 133-139.

Montgomery D.C. 2005: Introduction to Statistical Quality Control, John Wiley and Sons, New York.

Nozzle product guide 2009 [on line]: Last updated: 2009-08-26. [Accessed: 2011-02-14]. Available at: http://www.hardi-international.com/en/SalesInfo/~/media/PDF/INT/Nozzles/ nozzle_catalogue_GB.ashx.

Ozkan H. E., Reichard D. L., Ackerman K. D. 1992: Effect of orifice wear on spray patterns from fan nozzles. Trans. ASAE, Vol. 35, nr 4, 1091-1096.

Philips I. C., Miller P. C. H. 1999: Field and wind tunnel measurements of the airborne spray volume downwind at single flat–fan nozzles. Journal of Agricultural Engineering Research, Vol. 72, nr 2, 161-170.

Pietrzyk J. 2006: Ocena wpływu parametrów rozpylaczy na jakość oprysku metodą komputerowej symulacji. Wybrane Problemy Inżynierii Mechanicznej, Politechnika Warszawska, Instytut Inżynierii Mechanicznej, Płock, 94-103.

PN-EN ISO 9000:2006. Systemy zarządzania jakością. Podstawy i terminologia.

PN-ISO 8258+AC1:1996. Karty kontrolne Shewharta.

Sawa J. 2009: Risk assessment of the performance of plant protection. Teka Komisji Motoryzacji i Energetyki Rolnictwa – OL PAN, v. 9, 277–284.

Szulc T. 1996: Badania nad doborem końcówek rozpylających opryskiwaczy polowych i wpływ ich zużycia na jakość oprysku. PIMR Poznań, Pr. PIMR: Vol. 41, nr 4, 61-66.

Wiśniewski C. 2003: Ocena jakości wykonania rozpylaczy płaskostrumieniowych na podstawie wybranego parametru funkcjonalnego. Przegląd Techniki Rolniczej i Leśnej, nr 8/2003, 10-12, 19.

Wiśniewski C. 2006: Ocena jakości wykonania rozpylaczy płaskostrumieniowych na podstawie badania ich parametrów funkcjonalnych. Wybrane Problemy Inżynierii Mechanicznej, Politechnika Warszawska, Instytut Inżynierii Mechanicznej, Płock, 120-130.

Wiśniewski C. 2008: Ocena jakości wykonania rozpylaczy płaskostrumieniowych. Wybrane Zagadnienia Mechaniki w Budowie Urządzeń Technicznych, Politechnika Warszawska, Instytut Inżynierii Mechanicznej, Płock, 319-330.

Wiśniewski C. 2010: Ocena jakości wykonania rozpylaczy na podstawie parametrów funkcjonalnych. Problemy Eksploatacji, nr 2/2010 (77), 49-56.

Zasiewski P. 1993: Metodyka badań ciągnikowych opryskiwaczy ciśnieniowych. IBMER, Warszawa.

OCENA JAKOŚCI ROZPYLACZY NA PODSTAWIE BADANIA GEOMETRII STRUGI OPRYSKU

Streszczenie. Jakość oprysku bardzo często oceniana jest na podstawie jego poprzecznej równomierności. Wartość wskaźnika nierównomierności oprysku (współczynnika zmienności) szacowana jest metodą badań przeprowadzanych w warunkach laboratoryjnych na stole rowkowym. Na wartość tego wskaźnika bezpośredni wpływ mają wartości parametrów funkcjonalne badanych rozpylaczy. Różnice pomiędzy wartościami rzeczywistymi i nominalnymi tych parametrów mogą w istotny sposób wpływać na jakość oprysku podczas prac polowych.

W pracy przedstawiono ocenę wyników badań jakości wykonania rozpylaczy płaskostrumieniowych, stosowanych w opryskiwaczach polowych. Oceny dokonano na podstawie analizy statystycznej wartości parametrów funkcjonalnych charakteryzujących geometrię strugi oprysku. Na podstawie uzyskanych wyników sformułowano wnioski dotyczące jakości wykonania rozpylaczy oraz uwagi związane z wpływem tej jakości na jakość oprysku. Wnioski i uwagi mogą być przydatne dla producentów rozpylaczy rolniczych.

Słowa kluczowe: jakość wykonania, rozpylacz, parametr funkcjonalny, oprysk, ocena jakości

TEKA Kom. Mot. Energ. Roln. – OL PAN, 2011, 11, 430–440

INFLUENCE OF EXTRUSION-COOKING PROCESS PARAMETERS ON SELECTED MECHANICAL PROPERTIES OF PRECOOKED MAIZE PASTA PRODUCTS

Agnieszka Wójtowicz

Department of Food Process Engineering, Faculty of Production Engineering,
University of Life Sciences, Doświadczalna 44, 20-280 Lublin, agnieszka.wojtowicz@up.lublin.pl

Summary. The paper presents the results of measurements of selected mechanical properties of precooked pasta made from maize flour using variable parameters of extrusion-cooking process. The different level of water addition to maize flour was used due to the moisture content from 30 to 34%. Processing of maize pasta products was performed at the temperature ranged 80-100°C on single-screw modified extrusion-cooker TS-45 with L/D = 18:1 using a differentiated screw speed: 60, 80, 100 and 120 rpm. Depending on the screw speed and the dough moisture content selected tensile properties and extension characteristics of hydrated products by elongation tests of precooked maize pasta products were determined. A higher screw speed and moisture content lowered load at tensile strength and increased extension at break during elongation tests. Similar tendencies were observed for tensile strain at break and tensile strain at tensile strength. Precooked maize pasta due to its acceptable texture and tensile properties may be an attractive product for consumers on a gluten-free diet.

Key words: extrusion-cooking, maize pasta, gluten-free pasta, extension, tensile

INTRODUCTION

In recent years, the world is constantly increasing the production of pasta products from raw materials other than flour and semolina flour such as rice, corn, barley, oats, fortified compound additives (Jurga, 2002). In the production of traditional pasta, the high level of addition of these raw materials to semolina or wheat flour results in deteriorating of gluten structure and decreases the physical properties of pasta products. It may occur that the reduction of the strength and plasticity of wet forms of pasta during pressing will industrially increase their stickiness and dry matter loss during cooking. Therefore, in conventional, industrially manufactured pasta, an acceptable addition of high-starchy raw materials to wheat flour or semolina pasta or noodles should not be higher than 10%. Application of extrusion-cooking to pasta processing give the possibilities to use many different raw materials, also gluten-free, for precooked or instant pasta (Huber 1998, Li Vasanthan 2003, Wang 1999, Wójtowicz 2008, 2010, Wójtowicz Mitrus 2010, Wójtowicz Mościcki 2009)

Preparation of gluten-free pasta is a challenging task for the food technologist, because of the lack of gluten which is formed when wheat is used as the starting material (Bryant et al., 2001). Gluten is the main contributor to dough development during mixing and extrusion, and thus prevents disaggregation of pasta during cooking in boiling water. It has been suggested that the lack of gluten can be overcome by blending pre-gelatinized starch or corn flour before adding water, or by gelatinizing some of the starch during mixing or extruding. Extrusion is a suitable process for producing snack foods for consumers with celiac disease, as starch is the main component providing the desirable expanded structure in the final product (Camire 1990, Ding 2005, Wójtowicz 2011). In the formulation of gluten-free pasta, it has been suggested that the production process should be altered, for example by pre-gelatinizing the gluten-free starch during mixing or extruding to denature the protein and protect the starch from rupturing during cooking (Charutigon 2008, Chillo 2007, Gallager 2008 Lai 2001).

The only effective way for treating celiac disease is a strict adherence to a gluten-free diet, the patients are not allowed to eat any bread, cereal or other food made with wheat, rye, barley, triticale and oat flour or ingredients, or by-products made from those grains, processed foods that contain wheat and gluten-derivatives as thickeners and fillers, for example hot dogs, salad dressings, canned soups/dried soup mixes, processed cheese, cream sauces, and medications that use gluten as pill or tablet binders (Niewinski 2008). Gluten removal results in major problems for processing and many gluten-free products available on the market are of low quality, exhibiting poor mouthfeel and flavor. This presents a major challenge to the cereal technologist to search for alternatives to gluten in the manufacture of gluten-free food products (Gallager 2004, Yoenyongbuddhagal, S., Noomhorm, A. 2002).

For the evaluation of mechanical properties of food products many tests may be performed according to instrumental measurements (Raina 2005, Ross 2006). There are several methods which have been used to measure the rheological properties of dough in extension: simple uniaxial extension, where dough is stretched in one direction; and biaxial extension, where the dough is stretched in two opposing directions. One of the oldest and most widely used test methods to measure material properties is the uniaxial tensile test. A strip of material is clamped at both ends and pulled apart at a fixed rate in a suitable testing machine, and the force measured at the same time as the displacement of the object. The force is generally plotted against the displacement (extension) to give a force–extension curve (Dobraszczyk 2003).

Mechanical and dynamic-mechanical properties of cereal-based products have been investigated by several research groups. Moreover, some model has been developed to study the relations between cooked pasta and mechanical properties. It is known that the evolution of mechanical parameters is related to the hydration process during cooking and overcooking as well as starch gelatinization. In particular, the mechanical behavior is described through the changes occurring in the elastic modulus and the tensile strength. (Cafieri et al. 2010). Elongation at break is the recorded strain at the moment of rupture of the sample and is expressed as the elongation percentage with respect to the original length. (Chillo 2009)

The aim of this work was an evaluation of processing parameters influence on selected mechanical properties of gluten-free maize precooked pasta.

MATERIALS AND METHODS

Maize flour was used in the tests (protein - 5.13%, fat - 1.4%, ash - 0.45%, fiber - 2.0%). The raw material was moistened by proper water addition and mixed for a final dough moisture content 30, 32 and 34%. After mixing and resting compounds were processed using the modified

single screw TS-45 extrusion-cooker (Metalchem, Gliwice, Poland) with screw length to diameter ratio L/D=18:1, compression ratio - 3:1, equipped with additional glycol cooling section just before the die, at the temperature ranged from 80 to 105°C. Pasta products were shaped for threads with application of a forming die with 12 holes 0.8 mm in diameter. Gluten-free pasta products were processed at different screw speed at the level of 60, 80, 100 and 120 rpm. After a while, the drying samples were stored in plastic bags before testing.

Pasta elongation was tested with Tensile Kiefer Dough and Gluten Extensibility Rig equipment of Instron 5564 apparatus with head 50N (Stable Micro Systems Ltd., UK). Tests were performed in Food and Bioprocess Engineering Group, Wageningen University (the Netherlands). Tension test speed 3.3 $mm \cdot s^{-1}$ was set. Single pasta tread after 5 minutes of hot water hydration was placed on the testing table and held under plastic cover during the test. During the tensile tests load at break, extension at break, tensile stress at break, tensile strain at break, tensile stress at tensile strength, and true stress at tensile strength were evaluated using computer program. Values on curves are means of five replications.

The results were analyzed using the statistical software Statistica 6.0, examining the relationships between the moisture content of raw materials and screw rpm to all the tested processing parameters. Analysis of variance was conducted at the confidence level of 95% (p=0.05), significance of differences was assessed by Duncan's range test.

RESULTS

The results of measurements of strength characteristics of gluten-free pasta processed at varied screw speed and different moisture content of maize flour dough (30-34%) showed dependency on both the moisture content of raw materials and screw rotations applied during the extrusion. It was observed that increasing the moisture content of maize flour causes a significant increase in the value of extension at break, elongation at break, and to reduce stress during stretching. In this case, little effect was used during extrusion screw rotation of maize precooked pasta on rheological properties determined in tensile tests. Correlation coefficients for these dependencies are shown in Table 1.

Table 1. Correlation coefficients of rheological parameters of maize pasta, depending on the moisture content ranged 30-34% of raw materials and the screw speed of 60-120 rpm.

Parameter	Tensile strain at break [$mm \cdot mm^{-1}$]	Tensile stress at break [MPa]	Extension at break [mm]	Load at tensile strength [N]	Tensile strain at tensile strength [$mm \cdot mm^{-1}$]	Tensile stress at tensile strength [MPa]	True stress at tensile strain [kPa]
Moisture content [%]	0,554	-0,173	0,534	-0,475	0,418	-0,605	0,253
Screw speed [rpm]	0,284	0,362	0,173	-0,309	0,217	-0,243	-0,182

The values of tensile strain at break increased with increasing screw speed applied during extrusion-cooking of maize pasta. Similarly, the increased initial moisture content of maize flour

resulted in the increase of the value of this parameter. Relationships between processing parameters and tensile strain at break of maize precooked pasta are shown in Fig. 1.

Load at tensile strength measured with the use of the Kiefer Dough and Gluten Extensibility Rig showed the lowest value of the load during extension for gluten-free pasta processed using high-moisture dough and high screw rotational speed. However, low screw speed and the highest moisture applied during the extrusion-cooking of maize pasta resulted in the highest value of load at tensile strength. A similar range of results was obtained for maize pasta extruded at the highest speed and lowest initial moisture content of maize flour. The results of measurements of load at tensile strength are summarized in Fig. 2.

Carini et al. 2009 tested extruded and laminated pasta products. Force at rupture (maximum force (N) required to shear the sample) in the range from 10 till 14 N were obtained for extruded and laminated fresh pasta and extensibility (deformation at breakage (mm)) in the range from 9 ot 11 mm were obtained. The extruded pasta was characterized by higher extensibility and force at rupture. They also tested an influence of mixing system on mechanical properties of pasta. Different mixers affecting the physicochemical properties were observed more markedly in the extruded than in laminated products. Fresh extruded pasta was less extensible and harder than the laminated one (carini 2010)

Li and others (2008) tested mechanical properties of wheat protein dough and they assumed that extensibility at rupture decreased when the glutenin, insoluble glutenin, soluble glutenin, and glutenin macropolymer were added, and decreased systematically with increasing levels of these fractions. However, extensibility at rupture increased when the monomeric protein, albumin-globulin, and gliadin were added, and increased systematically with increasing levels of these fractions.

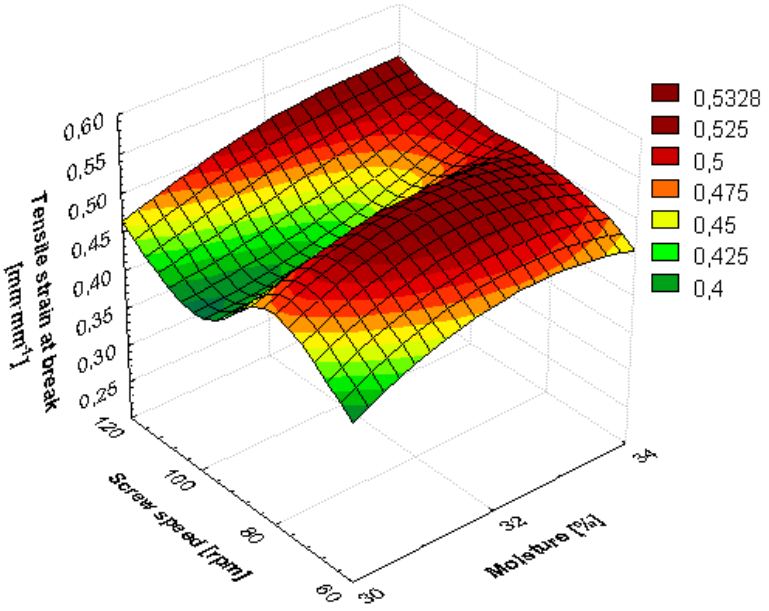

Figure 1. Tensile strain at break during elongation test of precooked maize pasta processed at different screw speed and initial moisture content.

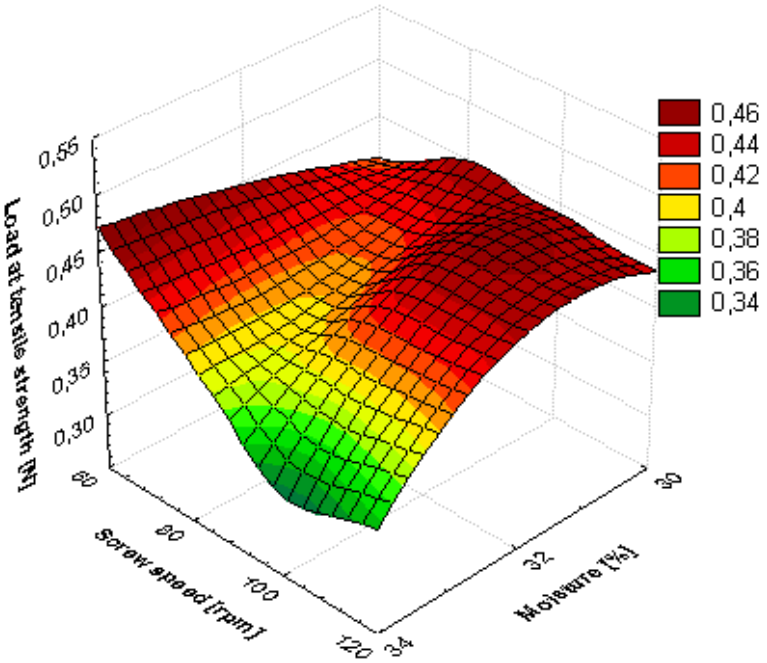

Figure 2. Load at tensile strength of precooked maize pasta processed at different screw speed and initial moisture content during elongation test.

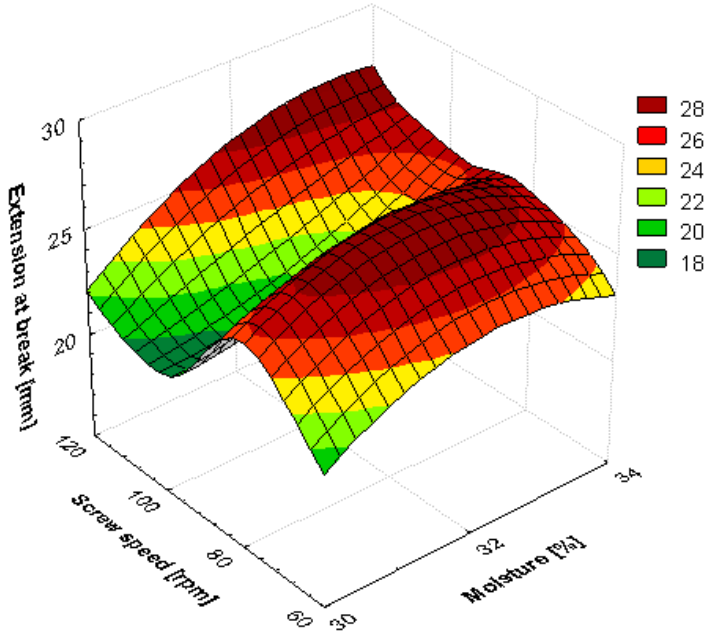

Figure 3. Extension at break during elongation test of precooked maize pasta processed at different screw speed and initial moisture content.

The values of extension at break indicate a diverse flexibility of maize pasta during the tensile test. Extension at break was dependent on the screw speed used during the extrusion-cooking, the higher the extrusion screw speed used for pasta processing, the greater extension until rupture (Fig. 3). The smallest differences between the measurements were determined for examining of extruded maize pasta with initial moisture content of 30%, the higher the moisture content of maize flour was set, the greater differences in flexibility – products prepared with the highest screw speed used during extrusion at the highest moisture content of raw materials showed the highest values of extension, which suggested that they were the most flexible.

During the test, the true stress at tensile strain indicated the effects of extrusion screw speed and moisture content of raw materials on the value of true stress of maize pasta - stress underwent reduction using the low speed screw extrusion at low initial moisture content of raw materials and at the highest screw speed and high moisture content of maize flour (Fig. 4). The most stable results, about 1300 kPa, in assessing of this parameter, were obtained for extruded precooked maize pasta processed with the initial moisture content of 32% - in this case there was no significant effect of screw speed on true stress at tensile strain values.

Figure 5 presents the results of tensile stress at tensile strength evaluated for maize pasta extruded at different extrusion screw speeds and moisture content of raw materials. It was found that for this parameter the lowest tensile stress values were obtained for maize pasta processed at the highest speed screw and high-moisture maize flour - 34%. Other measurements showed no significant difference, tensile stress at tensile strength ranged from 0.53 to 0.58 MPa. This shows a similar resistance to the stretching of maize precooked pasta.

Zardetto and others (2009) tested extruded and sheeted pasta and they observed the extruded pasta samples were tougher than the sheet-rolled pasta. Cooking the pasta resulted in less toughness and more hardness, and a significant increase in the extensibility of both samples.

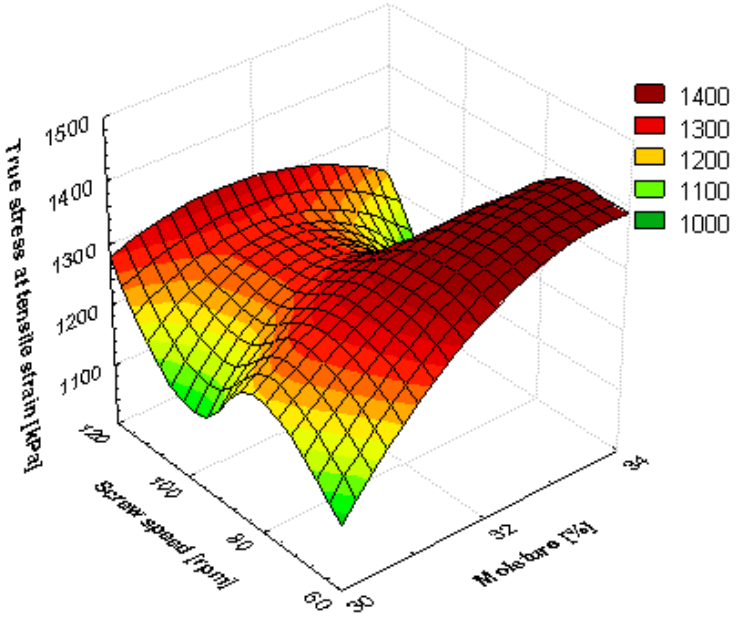

Figure 4. True stress at tensile strain during elongation test of precooked maize pasta processed at different screw speed and initial moisture content.

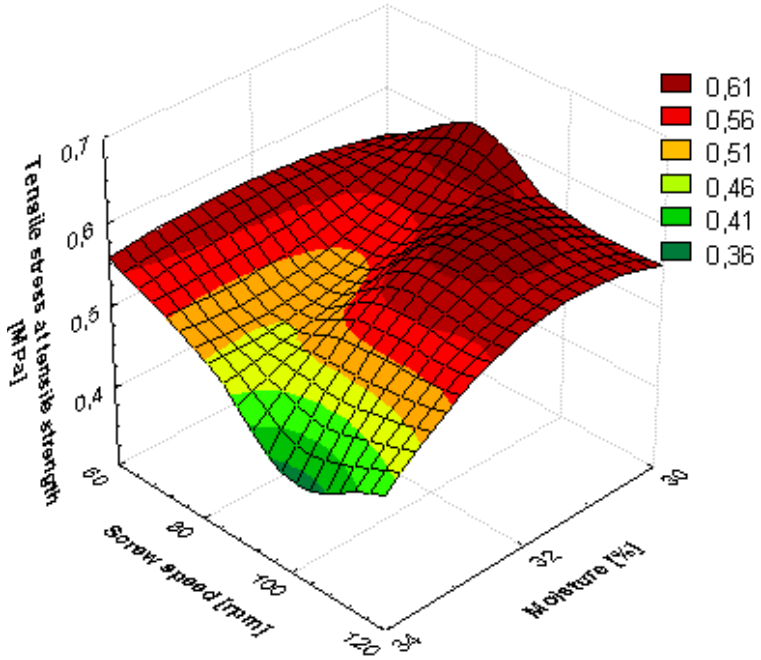

Figure 5. Tensile stress at tensile strength of precooked maize pasta processed at different screw speed and initial moisture content during elongation test.

Values of tensile stress at break, evaluated in a tensile test varied depending on the screw speed during extrusion-cooking of maize pasta and the initial moisture content of flour. Tensile stress at break was about 6-fold higher than the tensile stress at tensile strength, the results obtained in the study of this parameter ranged from 2.1 to 3.2 MPa. This demonstrates the high resistance of extruded maize pasta at break. The measurement results are presented in graphical form in Figure 6. Low resistance to breaking pasta products were only recorded for products processed at the lowest screw speed during extrusion-cooking. The most resistant to rupture were gluten-free maize pasta produced using 100 and 120 rpm with the initial moisture content of flour 30-32%. Low values of tensile stress at break were observed for pasta with low tensile strain at tensile strength during extension tests.

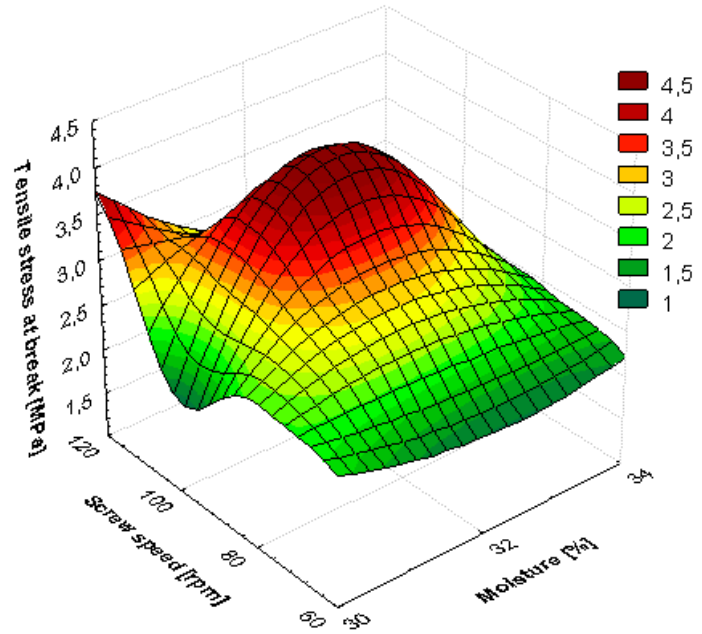

Figure 6. Tensile stress at break of precooked maize pasta processed at different screw speed and initial moisture content during elongation test.

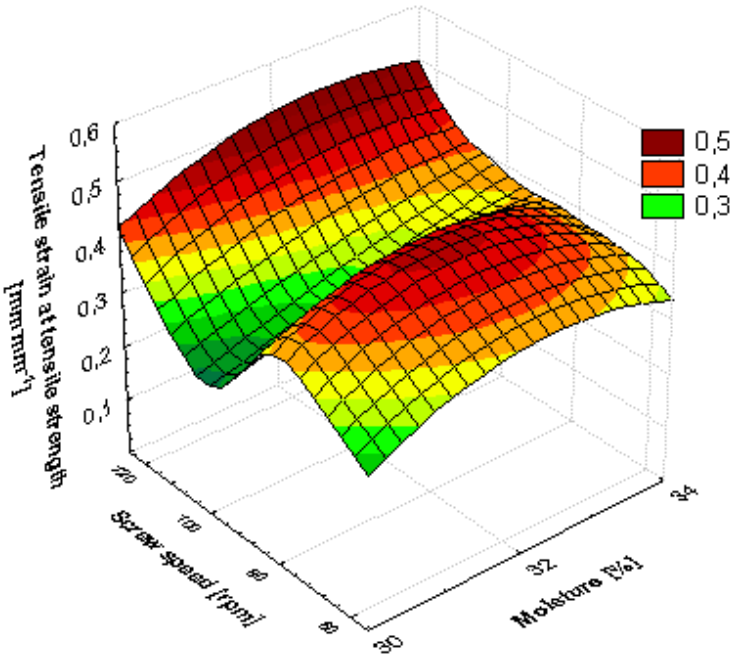

Figure 7. Tensile strain at tensile strength of precooked maize pasta processed at different screw speed and initial moisture content during elongation test.

The values of tensile strain at tensile strength of maize gluten-free pasta are illustrated in Fig. 7. Within the results of this parameter significant differences depending on the moisture content of raw materials and the screw speed during the extrusion-cooking of maize pasta were observed. Smallest deformation was observed for pasta processed at the lowest moisture content of maize flour, independently on the screw rotation, which may prove too low moisturizing of raw materials to obtain stable structure of pasta under tension and these pasta products underwent rupture very easy. Increasing humidity of raw materials to 32% resulted in the occurrence of larger tensile strain depending on the extrusion speed - the higher screw speed used during the extrusion-cooking, the higher values of tensile strain at tensile strength were obtained. The most significant differences were observed during testing pasta processed with initial moisture of maize flour 34%, in these products an influence of screw speed on tensile stress at tensile strength was very important.

CONCLUSIONS

The mechanical properties of precooked maize pasta processed by extrusion-cooking using modified single screw extruder TS-45 varied, according to the processing conditions: resistance for elongation and tensile of pasta increased with increasing screw speed during processing. It was observed that increasing the moisture content of maize flour causes a significant increase in the value of extension at break and tensile strain at break, and reduction of tensile stress at tensile strength and tensile stress at break. In this case, little effect of varied screw rotations was noted on the mechanical properties of maize precooked pasta determined in tensile tests. Precooked maize pasta, due to its acceptable texture and tensile properties, may be an attractive product for producers and consumers on a gluten-free diet.

Acknowledgements

This scientific work was supported by Polish Ministry of Science and Higher Education founds on science in the years 2008-2010 as a research project N N312 162334.

REFERENCES

Bryant, R.J., Kadan, R.S., Champagne, T.E., Vinyard, B.T., Boykin, D., 2001. Functional and digestive characteristics of extruded rice flour. Cereal Chemistry 78, 131–137.

Camire, M., Camire, A., Krumhar, K., 1990. Chemical and nutritional changes in foods during extrusion. Food Science and Nutrition, 29(1), 35-57.

Carini E., Vittadini E., Curti E., Antoniazzi F., Viazzani P.: Effect of different mixers on physico-chemical properties and water status of extruded and laminated fresh pasta, Food Chemistry 122 (2010) 462–469

Carini E., Vittadini E., Curti E., Antoniazzi F.: Effects of different shaping modes on physico-chemical properties and water status of fresh pasta, Journal of Food Engineering 93 (2009) 400–406

Charutigon C., Jitpupakdree J., Namsree P., Rungsardthong V., 2008. Effects of processing conditions and the use of modified starch and monoglyceride on some properties of extruded rice vermicelli. LWT - Food Science and Technology, 41,4, 642–651.

Chillo S., Iannetti M., Civica V. , Suriano N., Mastromatteo M., Del Nobile M.A.: A study of the relationship between the mechanical properties and the sensorial optimal cooking time of spaghetti, Journal of Food Engineering 94 (2009) 222–226

Chillo, S., Laverse, J., Falcone, P.M., Del Nobile, M.A., 2007. Effect of carboxymethylcellulose and pregelatinized corn starch on the quality of amaranthus spaghetti. Journal of Food Engineering, 83, 492–500.

Ding Q.B., Ainsworth P., Tucker G., Marson H., 2005. The effect of extrusion conditions on the physicochemical properties and sensory characteristics of rice-based expanded snacks. Journal of Food Engineering, 66, 283–289.

Dobraszczyk B.J., Morgenstern M.P.: Rheology and the breadmaking process, Journal of Cereal Science 242 38 (2003) 229–245

Gallagher E. Formulation and nutritional aspects of gluten-free cereal products and infant foods in: Gluten-Free Cereal Products and Beverages (eds. Arendt E., Dal Ballo F.) , Academic Press, Elsevier Inc., 2008, 321-341 ISBN: 978-0-12-373739-7

Gallagher E., Gormley T.R.. Arendt E.K.: Recent advances in the formulation of gluten-free cereal-based products, Trends in Food Science & Technology 15 (2004) 143–152

Huber G.R., 1998. Extrusion cooking applications for precooked pasta production, North Dakota, USA.

Lai Hsi-Mei, 2001. Effects of rice properties and emulsifiers on the quality of rice pasta. Journal of the Science of Food and Agriculture, 82, 203-216.

Li J.H., Vasanthan T., 2003. Hypochlorite oxidation of field pea starch and its suitability

Li Y., Zhu R., Tian J.: Influence of wheat protein contents and fractions on dough rheological properties as determined by using a reconstitution method, Agricultural Sciences in China, 2008, 7(4): 395-404

Mościcki L., Mitrus M., Wójtowicz A., 2007. Technika ekstruzji w przemyśle rolno-spożywczym, PWRiL, Warszawa.

Niewinski M., 2008. Advances in celiac disease and gluten-free diet. Journal of the American Dietetic Association108, 4, 661-672.

Raina C. S., Sukhcharn Singh, Bawa A. S. Saxena D. C., 2005. Effect of vital gluten and gum arabic on the textural properties of pasta made from pre-gelatinised broken rice flour, Food Science and Technology International, 11, 433-442.

Ross A., 2006. Instrumental measurement of physical properties of cooked Asian wheat flour noodles. Cereal Chemistry, 83(1), 42–51.

Wang N., Bhirud P., Sosulski F., Tyler R., 1999. Pasta – like product from pea flour by twin – screw extrusion. Journal of Food Science, 4, 671-678.

Wójtowicz A. 2010 Błyskawiczne makarony bezglutenowe – charakterystyka cech użytkowych i tekstury, w: Wpływ procesów technologicznych na właściwości materiałów i surowców roślinnych, red. Witrowa-Rajchert D., Lenart A., Rybczyński R., Wydawnictwo Naukowe FRNA, Komitet Agrofizyki PAN, Lublin, 2010, 117-134, ISBN 978-83-60489-17-8.

Wójtowicz A., 2007. Effect of monoglyceride and lecithin on cooking quality of precooked pasta. Polish Journal of Food and Nutrition Sciences, 57, 3A, 157-162.

Wójtowicz A.: 2011. Precooked pasta in: Extrusion-Cooking Techniques. Applications, Theory and Sustainability (eds. Moscicki L), Wiley-VCH, Weinheim, Germany, ISBN 978-3-527-32888-8

Wójtowicz, A. 2008. Influence of legumes addition on proceeding of extrusion-cooking process of precooked pasta. TEKA Commision of Motorization and Power Industry in Agriculture, 8a, 209-216

Wójtowicz, A., Mitrus, M. 2010. Effect of whole wheat flour moistening and extrusion-cooking screw speed on the SME process and expansion ratio of precooked pasta products, TEKA Commision of Motorization and Power Industry in Agriculture, 2010, 10, 517-526

Wójtowicz, A., Mościcki, L. (2009). Influence of extrusion-cooking parameters on some quality aspects of precooked pasta-like products, Journal of Food Science, 74(5), E226-233.

Yoenyongbuddhagal, S., Noomhorm, A. 2002. Effect of raw material preparation on rice vermicelli quality, Starch/Starke, 54, 534–539.

Zardetto S., Dalla Rosa M.: Effect of extrusion process on properties of cooked, fresh egg pasta, Journal of Food Engineering, 92, 1, 2009, 70-77

WPŁYW PARAMETRÓW PROCESU EKSTRUZJI NA WYBRANE WŁAŚCIWOŚCI MECHANICZNE PODGOTOWANYCH MAKARONÓW KUKURYDZIANYCH

Streszczenie. W artykule przedstawiono wyniki pomiarów wybranych właściwości mechanicznych makaronów błyskawicznych z mąki kukurydzianej przy zmiennych parametrach procesu ekstruzji. Zastosowano zróżnicowany dowilżania mąki kukurydzianej do zawartości wilgoci od 30 do 34%. Ekstruzję produktów makaronowych z kukurydzy przeprowadzano w temperaturze 80-100 ° C, na ekstruderze jednoślimakowym TS-45 z L / D = 18:1, przy użyciu zróżnicowanych prędkość ślimaka: 60, 80, 100 i 120 obr. / min. W zależności od szybkości ślimaka i wilgotności ciasta ustalono wybrane właściwości wytrzymałościowe i właściwości rozciągania uwodnionych produktów makaronowych z kukurydzy. Wyższa prędkość ślimaka i wilgotność obniża wytrzymałość na obciążenia i zwiększa ilość przerwań podczas badań rozciągania. Podobne tendencje zaobserwowano dla napięcia przy obciążaniu i wydłużaniu. Wstępnie gotowany makaron z maki kukurydzianej, ze względu na właściwą strukturę i elastyczność, może być atrakcyjnym produktem dla konsumentów na diecie bezglutenowej.

Słowa kluczowe: ekstruzja, makaron kukurydziany, makaron bezglutenowy, wydłużanie, rozciąganie

TEKA Kom. Mot. Energ. Roln. – OL PAN, 2011, 11, 441–449

INFLUENCE OF EXTRUSION-COOKING PROCESS PARAMETERS ON SELECTED PHYSICAL AND TEXTURAL PROPERTIES OF PRECOOKED MAIZE PASTA PRODUCTS

Agnieszka Wójtowicz

Department of Food Process Engineering, Faculty of Production Engineering,
University of Life Sciences, Doświadczalna 44, 20-280 Lublin, agnieszka.wojtowicz@up.lublin.pl

Summary. The paper presents the results of measurements of selected physical and mechanical properties of precooked pasta made from maize flour using variable parameters of extrusion-cooking process. The different level of water addition to maize flour was used due to the moisture content from 30 to 34%. Processing of maize pasta products was performed at the temperature ranged 80-100°C on single-screw modified extrusion-cooker TS-45 with L/D = 18:1 using a differentiated screw speed: 60, 80, 100 and 120 rpm. Depending on the screw speed and the dough moisture content selected physical, textural and tensile properties of precooked maize pasta products were determined, like the expansion ratio, hardness of dry pasta, firmness and extension characteristics of hydrated products due to elongation tests. The expansion ratio of pasta increased with increased rpm applied during processing, the use of higher moisture content of raw materials affect the limiting expansion ratio of maize precooked pasta products. SME values ranged from 0.17 to 0.34 $kWh \cdot kg^{-1}$ and were strongly dependent the screw speed rotations during the extrusion-cooking of pasta. Hardness and firmness of maize precooked pasta products increased with the increase of the screw speed. Precooked maize pasta may be a valuable product for the nutrition as gluten-free carbohydrates source, because of its texture and convenience, especially for the consumers with celiac disease diet.

Key words: extrusion-cooking, maize pasta, gluten-free pasta, expansion ratio, SME, texture

INTRODUCTION

Extrusion technique can be used to produce precooked or instant pasta and noodles which require any cooking and only hydration in hot water for several minutes. Modern systems of thermoregulation can produce a desired level of starch gelatinization, while screw variable speed and the proper geometry of plasticizing zone is able to formation a stable products' structure in contact with water and after preparation for consumption. According to extrusion-cooking process conditions, preservation and packaging of pasta are significantly simplified, the drying time is reduced, which reduces production costs. Equally important advantage is the ease of production, since the process does not require highly efficient dryers, or gelatinization by steam spraying or bath cooking [10, 20, 27]. Modifying of the process parameters allows formation the quality characteristics of extruded products, and the greatest influence on these characteristics of the finished products are the raw materials used, their moisture content and extrusion-cooking parameters, i.e. screw speed, temperature and pressure.

Extruded precooked gluten-free pasta can be a perfect complement to offer products for people on gluten-free diet without using any additional functional substances, and the convenience of the products allows the easy preparation for consumption by hydration in hot water without cooking. Extrusion causes complete or partial destruction of crystalline structure of starch due to gelatinization process as well as protein denaturation and the formation of complexes between starch and fats, and proteins and fats [1, 3, 7]. Thermal and mechanical interaction occurring during extrusion-cooking causing these changes can be used to produce a wide range of products based on starch, such as snacks, modified starches, breakfast cereals, instant porridge for children and dietetic food products [9, 14, 15].

Corn (maize) or rice products play an important role in the nutrition of people with gluten intolerance (celiac disease), which cannot consume products made from commonly used materials based on wheat, rich in gluten [6, 16]. Maize or rice pasta, traditionally made with the dough additional processing (steaming or frying) characterized glassy cross-section, firm consistency after cooking, limited cooking losses and colour characteristic for the raw material used. Sometimes, from technological reasons, some additives are used, like methylcellulose or diglycerides or other emulsifiers for proper pasta structure formation without presence of gluten [21]. However, availability of gluten-free pasta products on Polish market is limited. Specific physicochemical properties of raw materials of corn and rice, such as high starch content, no gluten, hypoallergenic and delicate flavor make them very desirable in the production of extrudates and a new generation of products and convenience foods intended for specific audiences [2].

Due to instant characteristics of precooked gluten-free pasta, its preparation for consumption is very easy by hot water hydration without cooking. For high starch gelatinization, which results in the stabile shape and soft texture of final products, pasta dough should be processed at temperature of 90-95°C to achieve proper starch gelatinization level and shape-keeping properties, than has to be quickly cooled down to prevent products' expansion. The extrusion-cooking treatment because of complex thermal and mechanical treatment, gives the gluten-free pasta specific characteristics of precooked products, which may be classified as convenient foods [12].

The aim of this work was an evaluation of processing parameters influence on selected physical and textural properties of gluten-free maize precooked pasta.

MATERIALS AND METHODS

As the raw material maize flour was used (protein - 5.13%, fat - 1.4%, ash - 0.45%, fiber - 2.0%). Raw material was moistened by proper water addition and mixed for final dough moisture content 30, 32 and 34%. After mixing and resting compounds were processed using the modified single screw TS-45 extrusion-cooker (ZMCh Metalchem, Poland) with screw length to diameter ratio L/D=18:1, compression ratio - 3:1, equipped with additional glycol cooling section just before the die, at the temperature ranged from 80 to 105°C. Pasta products were shaped for threads with application a forming die with 12 opens 0.8 mm in diameter. Gluten-free pasta products were processed at different screw speed at the level of 60, 80, 100 and 120 rpm. After short drying samples were stored in plastic bags before testing.

Based on the data collected during multiple trials the energy requirement of extrusion-cooking process was evaluated at different screw speed and with different initial moisture content of raw material. Power consumption was measured using standard register connected to extruder's motor during processing of each recipe at different screw speed used. After the consideration of motor load and process output ($kg \cdot h^{-1}$), the SME (specific mechanical energy) values ($kWh \cdot kg^{-1}$) were calculated on the base of method described by Wójtowicz [22, 25].

The expansion ratio index of precooked maize pasta was designated as the ratio of the diameter of the pasta thread to a diameter of forming die opens (0.8 mm) [25, 26]. Measurements of pasta diameter were performed with a caliper with digital display with an accuracy of 0.01 mm. The measurements were made in 15 replications, as final result the average of the measurements was taken into account.

Universal testing machine Zwick BDO-FB0.5TH (Zwick GmbH & Co., Germany) was used for texture evaluation. For hardness of dry products the Warner-Bratzler steel blade with 3 mm thick and 60 mm long, double-face truncated at an angle 45° was used. Hardness of dry pasta processed under different screw rpm was measured as breaking force (N) for single pasta during breaking test as mean of 10 replications. Hardness was evaluated as maximum force at break [8]. Texture of hydrated products after 5 minutes of hot water hydration for firmness evaluation was measured as maximum force (N) during test in five-blade Kramer cell, where 100g of hydrated pasta was placed and double compression test was performed with a head speed 100 mm·min^{-1}. *TestXpert*® 10.11 program was used for curves analysis, depend on moisture of raw materials and processing screw speed [28].

Results were analyzed using the statistical software Statistica 6.0, examining the relationships between the moisture content of raw materials and screw rpm to all tested parameters. Analysis of variance was conducted at a confidence level of 95% (p=0.05), significance of differences was assessed by Duncan's range test.

RESULTS

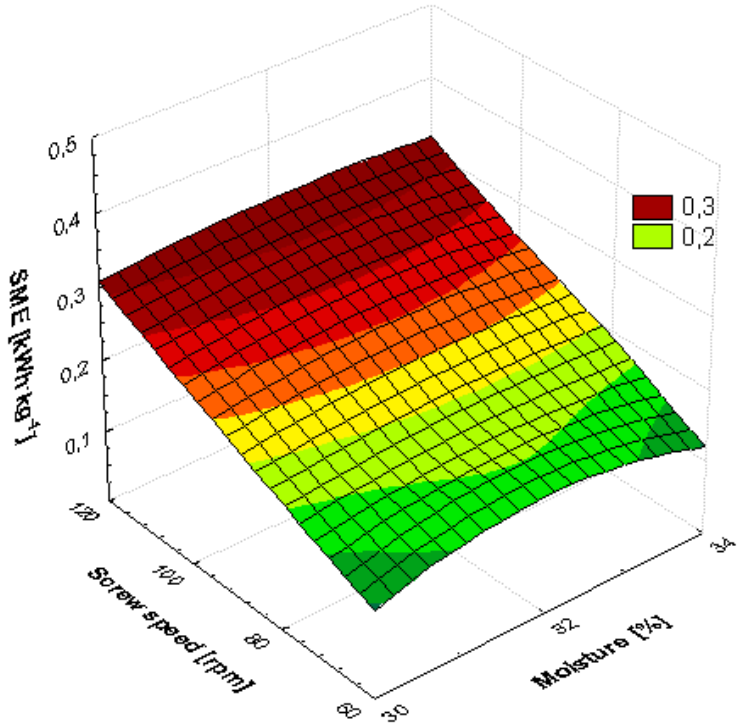

Figure 1. Specific mechanical energy registered for precooked maize pasta processed at different screw speed and initial moisture content of raw materials.

All the results were analyzed in three dimension arrangement and correlation coefficients were set both for influence of moisture content of the dough and screw speed used during the extrusion-cooking. SME values, designated as the specific mechanical energy during extrusion of maize precooked pasta ranged from 0.17 to 0.34 $kWh \cdot kg^{-1}$ and depended mainly on the screw speed used during processing (Fig. 1). The higher screw speed was used, the higher the SME were determined for maize pasta. There were no significant effects of the moisture content on SME values of maize precooked pasta.

Hot water hydration time for ready-to-eat properties of maize precooked pasta varied from 4 to 6 minutes and any traditional cooking was needed. Low expansion of precooked products is preferable because of its short preparation time. The expansion ratio results of maize precooked pasta products not exceed 1.8 (Fig. 2). This parameter evaluated for maize precooked pasta processed at varied screw speed and raw materials moisture content was dependent on both of these process conditions. The higher extrusion-cooking screw speed was applied, the higher expansion ratio was observed with a high correlation coefficient (r=0.8). The lowest expansion was noted for maize pasta processed at 30 and 34% of dough moisture content and lowest screw speed. Increasing of dough moisture content processed at higher screw speed lowered products' expansion. Higher screw speed applied during the extrusion-cooking increased pasta expansion and therefore longer the time of hot water hydration was observed.

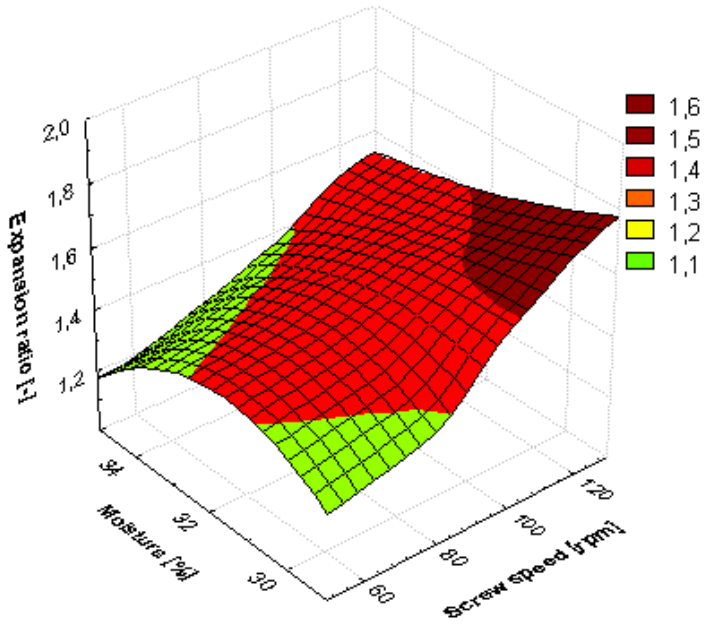

Figure 2. The expansion ratio of precooked maize pasta processed at different screw speed and initial moisture content of raw materials.

Textural features of both dry pasta and cooked or hydrated products are very often seen as quality indicators. Instrumental methods for evaluation of hardness, firmness, cohesiveness, adhesiveness and stickiness of pasta products primarily utilize cutting and compression tests using universal testing machines [4, 5, 11, 17, 18, 30]. For measuring the hardness of pasta and noodles

cutting test may be used by setting the maximum forces required to destroy the samples [13, 23, 29], and to measure the characteristics of the cooked products' texture it can be used Kramer cell, which make it possible to identify a series of measurements in the double compression tests wide range of textural characteristics, depending on the software used for analysis and interpretation of measurement results [24].

Hardness of instant dry pasta made from maize flour is shown in Figure 3. Hardness of dry gluten-free pasta was strongly affected by extrusion screw speed applied (r=0.87); it was the most important factor responsible for higher hardness of pasta products. At 100 and 120 rpm and low moisture level hardness was the highest. Hardness of dry pasta lowered with increased water addition and lower screw speed applied. The moisture content of the dough was less important factor according to maize pasta hardness (Figure 3).

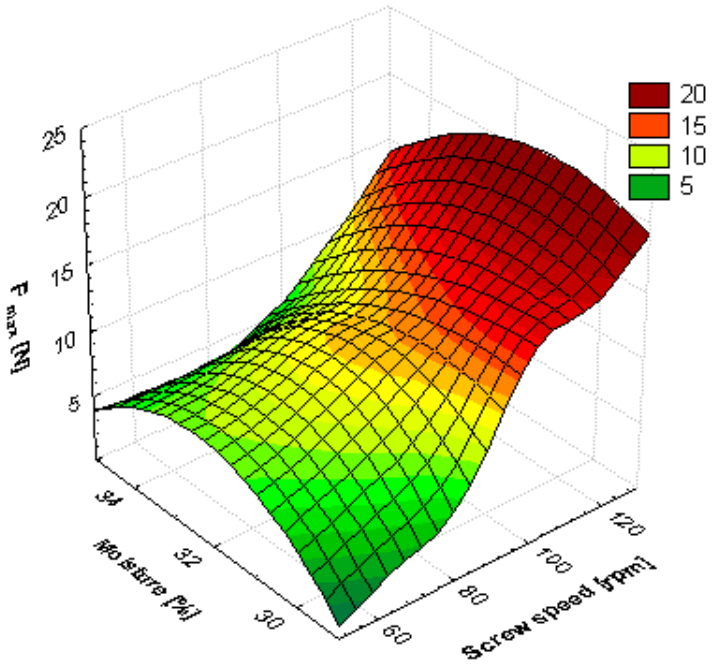

Figure 3. Hardness of precooked maize pasta processed at different screw speed and initial moisture content.

The texture of pasta prepared for consumption by a few minutes or longer cooking or by hot water hydration allows the assessment of the characteristics of flexibility, elasticity and stickiness of pasta and noodles [17, 19]. The use of five-blade Kramer cell gives the possibility for a series of measurements in the compression-shearing tests and determination of a wide range of textural characteristics, depending on the software used for analysis and interpretation of measurement results [28]. Figure 4 shows an example texture measurement profile during evaluation the texture of maize precooked pasta upon hydration.

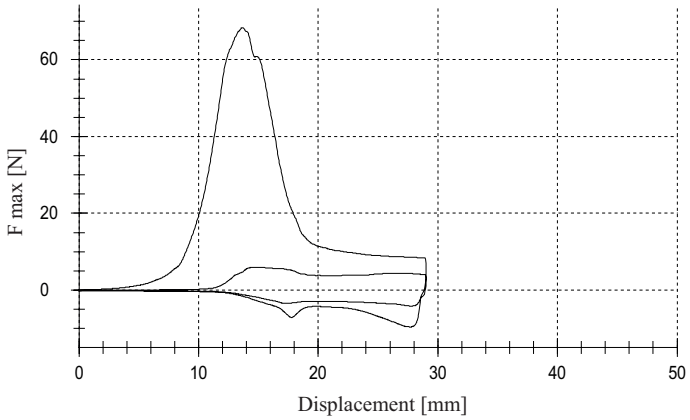

Figure 4. Sample of texture measurement of maize precooked pasta after 5 minutes of hot water hydration (30% of moisture content, screw speed 80 rpm).

Firmness evaluated in the double compression test showed significant effect of extrusion-cooking screw speed on the gluten-free pasta firmness (r=0.78). Increasing the moisture content of raw material caused a slight decrease of firmness of pasta corn after hydration when screw speed not exceed 100 rpm (r =- 0.36). At highest rpm an influence of moisture content of raw materials was important with correlation coefficient r=-0.6. Firmest consistency was observed for maize pasta processed at 120 rpm and 30% of dough moisture (Fig. 5). The higher screw speed was used during extrusion-cooking, the firmer the products were obtained.

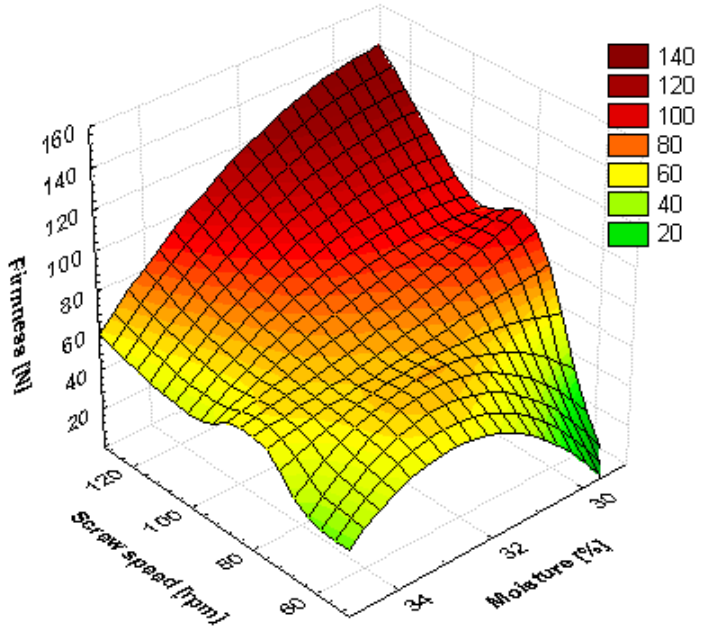

Figure 5. Firmness of precooked maize pasta processed at different screw speed and initial moisture content.

CONCLUSIONS

A study of the influence of processing parameters like screw speed and dough moisture content during the extrusion-cooking of precooked maize pasta allowed to establish the relationships between process parameters and product characteristics. The use of the proper moisture content of raw materials and processing intensity for maize precooked pasta using modified single screw extruder TS-45 influenced the low expansion ratio which decreased as the moisture content of the material increased. The SME requirements increased with increasing of extrusion screw speed, which increased the expansion of pasta products. Precooked maize pasta products were ready for consumption after 4-6 minutes hydration in hot water. After hydration gluten-free precooked pasta showed stabile consistency, low stickiness and acceptable firmness. Precooked gluten-free maize pasta may be valuable for the nutrition, because of its texture and convenience as carbohydrates source, especially for the consumers with celiac disease diet.

Acknowledgements

This scientific work was supported by Polish Ministry of Science and Higher Education founds on science in the years 2008-2010 as a research project N N312 162334.

REFERENCES

Abecassis J., Abbou R., Chaurand M., Morel M. H., Vernoux P., 1994: Influence of extrusion conditions on extrusion speed, temperature and pressure in the extruder and on pasta quality. Cereal Chemistry 71, 3, 247 – 253.

Bryant R.J., Kadan R.S., Champagne T.E., Vinyard B.T., Boykin D. 2001: Functional and digestive characteristics of extruded rice flour. Cereal Chemistry 78, 131–137.

Camire, M., Camire, A., Krumhar, K., 1990: Chemical and nutritional changes in foods during extrusion. Food Science and Nutrition, 29(1), 35-57.

Charutigon C., Jitpupakdree J., Namsree P., Rungsardthong V. 2008: Effects of processing conditions and the use of modified starch and monoglyceride on some properties of extruded rice vermicelli. LWT - Food Science and Technology, 41,4, 642–651.

Chillo S., Laverse J., Falcone P.M., Del Nobile M.A., 2007: Effect of carboxymethylcellulose and pregelatinized corn starch on the quality of amaranthus spaghetti. Journal of Food Engineering, 83, 492–500.

Counts D.R., Sierpina V.S., 2006: Celiac Disease/Gluten Intolerance. EXPLORE, 2, 1, 43-45

Ding Q.B., Ainsworth P., Tucker G., Marson H., 2005: The effect of extrusion conditions on the physicochemical properties and sensory characteristics of rice-based expanded snacks. Journal of Food Engineering, 66, 283–289.

Guinea G.V., Rojo F.J., Elices M., 2004: Brittle failure of dry spaghetti. Engineering Failure Analysis, 11, 705–714.

Hagenimana A., Ding X., Fang T., 2006: Evaluation of rice flour modified by extrusion cooking. Journal of Cereal Science, 43, 38–46.

Huber G.R., 1998: Extrusion cooking applications for precooked pasta production, North Dakota, USA.

Lai Hsi-Mei, 2001: Effects of rice properties and emulsifiers on the quality of rice pasta. Journal of the Science of Food and Agriculture, 82, 203-216.

Li J.H., Vasanthan T., 2003: Hypochlorite oxidation of field pea starch and its suitability for noodle making using an extrusion cooker. Food Research International, 36, 381–386.

Martinez C., Ribotta P., León A., Añón C., 2007: Physical, sensory and chemical evaluation of cooked spaghetti. Journal of Texture Studies, 38, 666–683.

Mercier C., Linko P, Harper J.M., 1998: Extrusion Cooking, AACC, Minnesota, USA.

Mościcki L., Mitrus M., Wójtowicz A., 2007: Technika ekstruzji w przemyśle rolno-spożywczym, PWRiL, Warszawa.

Niewinski M., 2008: Advances in celiac disease and gluten-free diet. Journal of the American Dietetic Association108, 4, 661-672.

Raina C. S., Sukhcharn Singh, Bawa A. S. Saxena D. C., 2005: Effect of vital gluten and gum arabic on the textural properties of pasta made from pre-gelatinised broken rice flour. Food Science and Technology International, 11, 433-442.

Ross A., 2006: Instrumental measurement of physical properties of cooked Asian wheat flour noodles. Cereal Chemistry, 83(1), 42–51.

Sozer N., Dalgıc A.C., Kaya A., 2007: Thermal, textural and cooking properties of spaghetti enriched with resistant starch. Journal of Food Engineering, 81, 476–484.

Wang N., Bhirud P., Sosulski F., Tyler R., 1999: Pasta – like product from pea flour by twin – screw extrusion. Journal of Food Science, 4, 671-678.

Wójtowicz A., 2007: Effect of monoglyceride and lecithin on cooking quality of precooked pasta. Polish Journal of Food and Nutrition Sciences, 57, 3A, 157-162.

Wójtowicz A., 2008: Influence of legumes addition on proceeding of extrusion-cooking process of precooked pasta. TEKA Commision of Motorization and Power Industry in Agriculture, 8a, 209-216

Wójtowicz A., 2010: Błyskawiczne makarony bezglutenowe – charakterystyka cech użytkowych i tekstury, w: Wpływ procesów technologicznych na właściwości materiałów i surowców roślinnych, red. Witrowa-Rajchert D., Lenart A., Rybczyński R., Wydawnictwo Naukowe FRNA, Komitet Agrofizyki PAN, Lublin, 2010, 117-134, ISBN 978-83-60489-17-8.

Wójtowicz A., 2011: Precooked pasta. in: Extrusion-Cooking Techniques. Applications, Theory and Sustainability (eds. Moscicki L), Wiley-VCH, Weinheim, Germany, 2011, 99-117, ISBN 978-3-527-32888-8.

Wójtowicz A., Mitrus M., 2010: Effect of whole wheat flour moistening and extrusion-cooking screw speed on the SME process and expansion ratio of precooked pasta products. TEKA Commision of Motorization and Power Industry in Agriculture, 2010, 10, 517-526

Wójtowicz A., Mościcki L., 2008: Energy consumption during extrusion-cooking of precooked pasta. TEKA Commision of Motorization and Power Industry in Agriculture, 8, 311-318.

Wójtowicz A., Mościcki L., 2009: Influence of extrusion-cooking parameters on some quality aspects of precooked pasta-like products. Journal of Food Science, 74(5), E226-233.

Wójtowicz A., Mościcki L., 2010: Evaluation of selected quality characteristics and texture of gluten-free precooked pasta. Proceedings of 5th International Congress Flour-Bread'09, Osijek, Croatia, 126-134.

Yalla S., Manthey F., 2006: Effect of semolina and absorption level on extrusion of spaghetti containing non-traditional ingredients. Journal of the Science of Food and Agriculture, 86, 841–848.

Yoenyongbuddhagal S., Noomhorm A. 2002: Effect of raw material preparation on rice vermicelli quality, Starch/Starke, 54, 534–539.

WPŁYW PARAMETRÓW PROCESU EKSTRUZJI NA WYBRANE CECHY FIZYCZNE I TEKSTURĘ PODGOTOWANYCH MAKARONÓW KUKURYDZIANYCH

Streszczenie. W artykule przedstawiono wyniki pomiarów wybranych właściwości fizycznych i tekstury kukurydzianych makaronów błyskawicznych ekstrudowanych przy zmiennych parametrach procesu. Zastosowano zróżnicowany poziom dowilżenia mąki kukurydzianej do wilgotności od 30 do 34%. Ekstruzję podgotowanych makaronów kukurydzianych przeprowadzono w temperaturze 80-100°C z zastosowaniem zmodyfikowanego ekstrudera jednoślimakowego TS-45 z L / D = 18:1 przy użyciu zróżnicowanych prędkość ślimaka: 60, 80, 100 i 120 obr·min^{-1}. W zależności od obrotów ślimaka i wilgotności ciasta przeprowadzono ocenę wybranych właściwości fizycznych, tekstury i cech wytrzymałościowych podgotowanych makaronów kukurydzianych, m.in. zapotrzebowanie SME, wskaźnik ekspandowania promieniowego, twardość makaronów suchych i jędrność uwodnionych produktów bezglutenowych. Wskaźnik ekspandowania makaronu wzrastał w miarę zwiększania prędkości ślimaka stosowanych podczas ekstruzji, zastosowanie wyższych wilgotności surowców wpłynęło na ograniczenie ekspandowania podgotowane makaronów kukurydzianych. Wartości SME wahały się od 0,17 do 0,34 kWh·kg^{-1} i były głównie uzależnione od obrotów ślimaka podczas ekstruzji makaronu. Twardość oraz jędrność podgotowanych makaronów kukurydzianych zwiększały się wraz ze wzrostem zastosowanej prędkości obrotowej ślimaka. Podgotowany makaron kukurydziany może być cennym żywieniowo produktem jako bezglutenowe źródło węglowodanów, ze względu na jego teksturę i wygodę przygotowania, zwłaszcza dla konsumentów chorych na celiakię wymagających diety bezglutenowej.

Słowa kluczowe: ekstruzja, makaron kukurydziany, makaron bezglutenowy, ekspandowanie, SME, tekstura

TEKA Kom. Mot. Energ. Roln. – OL PAN, 2011, 11, 450–456

ESTIMATION OF BIODIESEL FUEL ON THE BASIS OF RAPE OIL AND ISOPROPYL ALCOHOL

Victor Zaharchuk, Valentyna Tkachuk, Oleg Zaharchuk

Lutsk National Technical University, Lutsk, Ukraine

Summary. The article is devoted to the analysis of operating properties of biodiesel fuels, in particular thermal energy indexes on the basis of which a conclusion is made about the prospects and advantages of application of biodiesel fuel on the basis of rape oil and isopropyl alcohol.

Key words: biodiesel fuel, diesel engine, toxicity, isopropyl esters, rape oil.

INTRODUCTION

Presently in our state there is a large park of the wheeled transport vehicles and agricultural vehicles with diesels which work on the diesel fuel (DF) of mineral oil origin. However, from facts of numerous sources, supplies of mineral oil accessible on our market can be sufficient only to the year 2015, therefore the cost of diesel fuel will be constantly growing. In such situation the use of alternative fuels becomes economically justified. In addition, the automobile industry is one of the greatest polluters of the environment. Application of alternative fuels will allow for a significant decrease of the harmful fumes emission from diesels and improvement of the ecological situation in cities and rural settlements. Application of alternative fuels which are made from renewable sources will allow for the promotion of Ukraine's independence from the imported energy resources.

One of the basic ways of solving the complicated situation is adaptation of diesels for work on alternative fuels. Such fuels are: compressed natural gas, dimethyl esters (DME) and biofuel, in particular methyl esters of rape oil (MERO). Natural gas is approximately two times cheaper than diesel fuel. However, for making a diesel work on natural gas its substantial re-equipment is required into a gas diesel or into a gas engine with spark lighting. Thus a gas diesel works on the mixture of natural gas and diesel fuel, for it has a considerably more difficult system of feeding compared to the diesel. As to gas engines with spark lighting, their researches are not yet completed.

This publication aims at a determination and analysis of effective calculation indexes of a diesel working on different biofuels.

MATERIALS AND RESEARCH

Recently, a wider application has been found by alternative biofuels on the basis of vegetable oils. Biodiesel fuel, i.e. methyl and ethyl esters of vegetable oils, whose most widespread form is rape oil, belongs to such fuels. Research on fuels made from vegetable oils is conducted by the well-known motor-building firms of the USA, Great Britain, Germany, Sweden, Japan. Presently, more than 6,5 million t biofuel is made in Europe. Work is conducted concerning the application of esters of vegetable oils as diesel fuel on territories of the former USSR. There should be mentioned: MVTU named after Bauman, MSAU named after Goryachkina, Klaipeda University, National University of Bioresources and Environmental Management of Ukraine, KHPI and others.

Application of biodiesel fuel requires no changes in the construction of engine. Tests showed the increase of expenditure of biodiesel fuel to 10%, which can be explained by the lower combustion temperature. At the same time the emission of fumes with harmful compounds is diminished [1].

A traditional biodiesel fuel is made with the use of methyl alcohol which is highly toxic and dangerous for the health of people. Its possible concentration in the air around the working area reaches 5 mgs/m, whereas for ethanol it reaches 1000 mgs/m. It is a substantial negative factor from the standpoint of ecological safety at the production of biofuel (especially in the conditions of agricultural production) and its use, in fact through the effects of destruction a selection from the biofuel of methyl alcohol is possible, especially at deviation from normal work of the fuel system of engine. Also, the lack of methyl ether is that it is an aggressive enough matter in relation to precise materials of engine parts (metals, rubber). Therefore, at its application replacement of fuel tanks, fuel hoses and gaskets is required, with the ones made from material approved by MERO, and also more frequent replacement of motor oil.

A biodiesel fuel can also be made with the use of ethyl spirit (EERO). But such a fuel has a fairly high cost due to the high cost of ethyl spirit. In addition, the reaction of esterification with an ethyl spirit is considerably slower.

RESULTS OF RESEARCH

In the Lutsk National Technical University a new biodiesel fuel is created with the use of isopropyl alcohol instead of methyl. This type of alcohol has insignificant toxicity and aggressiveness. The fuel is obtained by the reaction of pre-esterification of rape oil with an isopropyl alcohol in presence an alkaline catalyst. Optimum correlation of components of new biofuel is certain according to a mathematical design. The search of optimum parameters was carried out, utilizing a three-factor experiment. As a parameter of optimization the temperature of freezing (t_{freez}) of biofuel is chosen (Fig 1).

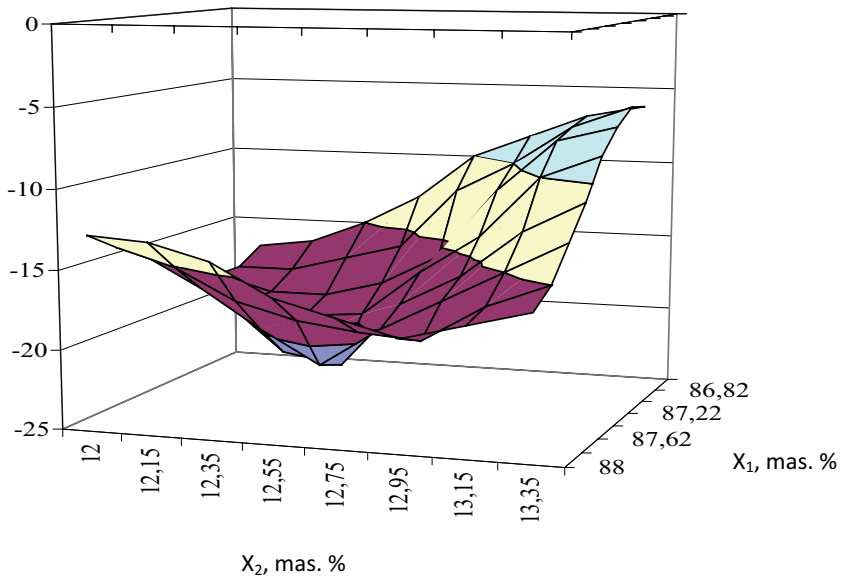

Fig. 1. Dependence of the biofuel freezing temperature on the maintenance of rape oil (X_1) and isopropyl alcohol (X_2)

Elementary composition (content of carbon C, hydrogen H and oxygen O) of isopropyl ester of rape oil (IERO) was certain in accordance with maintenance of acids in rape oil [2]: ester of erucic acid - 50,0 %, by an oleic- 29,0 %, linoleic - 15 %, other esters of other acids. The experimental values of operating properties of biodiesel fuels were compared to the requirements of DSTU, as diesel fuel «L» is easily soiled (Table 1).

Table 1. Comparative description of indexes of operating properties of diesel and biodiesel fuels

№	Name of index	Method of tests	Norm of DSTU 3868-99	Diesel fuel	Biodiesel fuel	
					MERO	IERO
1.	Cetane number	DSTU 3868-99	not below 45	47	48	49
2.	Density, g/sm^3 at 15°C	DSTU 3900-99	no more than 0,860	0,84	0,88	0,88
3.	Kinematic viscosity at 40°C, sSt	DSTU 33-00	3,0-6,0 at 20 C	5,4	5,6	16,1
4.	Acidity, mg KOH on 100 sm^3	GOST 5985-79	no more than 5,0	2,7	-	-
5.	Temperature of freezing, °C	GOST 20287-91	no more than -10	-14	-12	-22

The new fuel has the best consumer characteristics, in particular, lower temperature of freezing. It obtained the toxicological and sanitary passport, its technical properties were developed and

ratified. In the private enterprise «Limeks Invest» the industrial endorsement of the production of the offered biofuel is carried out. In the near future the stand tests of diesel will be conducted on such fuel.

For comparison and estimation of effective indexes of diesel D-240 during its work on oil diesel fuel and biodiesel fuels in the conditions of identical middle effective pressure, the computer calculation of its work cycle was executed for the nominal mode. The initial data for calculation are presented in Table 2, and results of calculation in Table 3.

It is obvious from the calculations that the less carbon in the molecules of biodiesel fuels the lower the combustion temperature. For the obtainment of identical effective power of diesel during its work on oil diesel fuel and biodiesel fuels a specific effective expense of fuel will be large in the case of the use of biofuels. In addition to some worsening of indexes of diesel during work on biodiesel fuels their large viscidity is a negative factor, compared to an oil fuel. Investigation revealed its worst atomization by sprayers. Therefore some researchers recommend using biodiesel fuel in mixtures with diesel fuel (30% biodiesel and 70% DF).

Table 2. Results of calculation of effective indexes of diesel during its work on different fuels

№	Index	Fuel			
		DF	MERO	EERO	IERO
1	Elementary composition, %: C H O	 87 12,6 0,4	 77,5 12,0 10,5	 77,54 12,04 10,42	 76,28 13,16 10,05
2	In theory necessary amount of air for combustion of 1 kg of fuel, kg	14,45	12,70	12,73	12,98
3	Lower temperature of combustion, MJ/kg	42,44	37,50	37,56	38,33
4	Coefficient of surplus of air	1,5	1,5	1,5	1,5
5	Middle effective pressure, MPa	0,694	0,698	0,698	0,699
6	Effective coefficient	0,350	0,350	0,350	0,350
7	Specific effective expense of fuel, g/kW*h	242,63	274,54	274,06	268,05
8	Effective power, kW	60,43	60,76	60,76	60,88

But among biodiesel fuels IERO has the highest combustion temperature and the least expense of fuel, which advantageously distinguishes it from MERO and EERO. The presence of oxygen in the molecules of biodiesel fuels allows for the intensification of the process of combustion. Other effective indexes of engine on condition of increase of specific effective expense of fuel are identical.

Viscosity of IERO is higher compared with the proper value of normative requirements, which can hamper the passing of fuel through filters, deteriorate the working of fuel sprayers and worsen mixing. It can be considered as the lack of IERO. Therefore, at low temperatures it is expedient to utilize such fuel in mixtures with an oil diesel fuel. On the other hand, higher viscosity of fuel will provide good greasing of the diesel fuel apparatus parts. The solidification temperature of IERO is 2 times lower than in MERO. In fact it enables to use such fuel in a winter period at the temperature reaching -22˚C, while the standard is to - 12˚. Acidity in IERO is absent so that it is not a corrosive agent. Ash content in IERO stays within the limits of norm which points out to low content of mineral ash in this fuel.

Biodiesel fuel, and above all IERO, is safer from the viewpoint of ecology. As experiments showed, biodiesel leak in water does not affect living organisms. In addition, it is fully biodegradable –it is decomposed in soil or in water by microorganisms within 28 days. The conducted toxi-

cological and hygienic researches of IERO allowed to draw the conclusion that this fuel belonged on average to the 4th class of danger (the lowest class).

The stand tests of diesel of D-240 were conducted during its work on IERO and oil DF, the loading descriptions of which were obtained as a result (Fig. 2). It is evident from the test results that the power Ne of diesel during work on these fuels is practically identical. In the case of work of diesel on IERO the increase of specific expense of fuel remains within the range of 4…6 % as a result of lower combustion temperature and increase of nitrogen oxides concentration NOx in exhaust gases through higher content of oxygen in a biopropellant. The rejection of sizes of other compared indexes (for example exhaust smoking of D of exhaust gases) is within the limits of possible accuracy of their measurement.

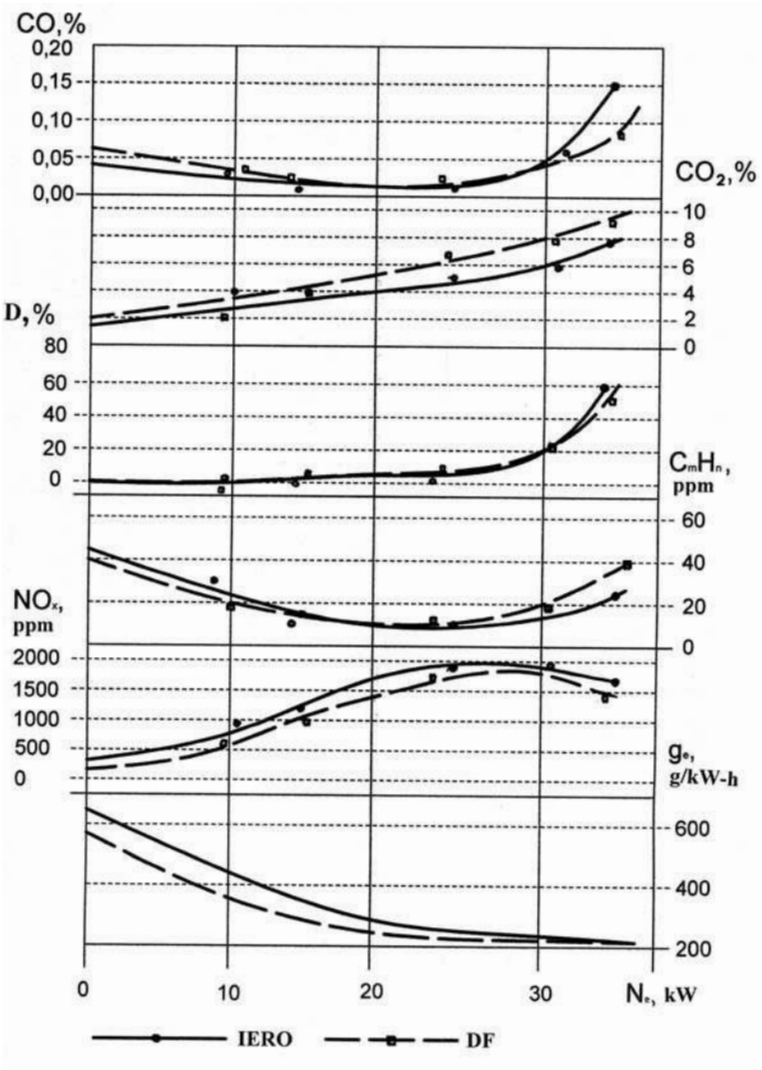

Fig. 2. Loading characteristics of diesel D-240 (n = 1500 rpm)

Biodiesel fuel practically does not contain sulphur, which is why an engine working on this fuel has a zero level of SO2 emissions, and this advantageously distinguishes it from the diesel in which the emissions of sulphur oxides cause substantial environmental damage. It is especially topical for our state, because in the diesel fuels produced in our petroleum refinery factories the sulphur contents significantly exceed the admissible norms. An important advantage of engines working on biodiesel fuel are low emissions of dioxide carbon which is instrumental in the formation of the greenhouse effect on the Earth. It is explained by the fact that there is less carbon in biodiesel fuel than in oil fuels.

CONCLUSIONS

The analysis of operating properties of biodiesel fuels shows that the new biodiesel fuel has a lower temperature of freezing than methyl ester of rape oil and is characterized by toxicity and aggressiveness comparable to ethyl esters of rape oil, but is considerably cheaper. The results of the experimental findings confirm that the new environmentally clean biofuel has improved consumer characteristics and is suitable for production and use in transport.

REFERENCES

Adamenko O., Visochanskiy V., Letko V., Mikhayliv M., 2001: Alternative fuels and other untraditional energy sources. Ivano-Francovsk, 432 p. (in Ukrainian).

Tkachuk V., 2007: Biopropellant as perspective energy saving resource//The Scientific news of Institute of management and economy the «Galichina academy». Special issue of materials IV international scientific and technical conference the rence "Ecological and economic problems of European Region of Carpathians «EEPKE 2007». Ivano-Francovsk, p. 32-37. (in Ukrainian).

Maslo V., 2005: Ways of development of production of biodiesel in Ukraine//Announcer of agrarian science. № 10, p. 78-80. (in Ukrainian).

Markov V., Gayvoronskiy A., Devyanin S., Ponomarev E., 2006: Rape oil as alternative fuel for a diesel//Motor industry. - № 2, 8.

Marchenko A., Prokhorenko A., Osetrov A., 2004: A comparative estimation of efficiency of application of vegetable fuels is in the diesel engine of origin//Combustion engines. Khar'kov: NTU «KHPI»- № 3, p. 46-51. (in Ukrainian).

Marchenko A., Minak A., Slabun I., 2003: Results of researches of working process and toxicity of diesel working on the fuels of plant origin// Combustion engines. Khar'kov: NTU «KHPI». № 2, p. 33-40. (in Ukrainian).

Marchenko A., Strokov A., Minak A., 2002: Toxicity of working gases of diesel at the use of fuels of phytogenic// Combustion engines. Khar'kov: NTU «KHPI»- № 1, p. 22-25. (in Ukrainian).

Mel'nichuk M., 2009: Technical problems biodiesel production in Ukraine//Announcer of national university of Life and Environmental Sciences of Ukraine. Prod. p. 141-154.

Zabarniy G., 2006: Thermodynamics efficiency and resources of liquid biopropellant in Ukraine: Monograph/ Zabarniy G., Kudrya S., Kondratyuk G. K. 226 p..

Cossack V., 2007: Determination of content of methyl esters of fatty acids in a diesel fuel by the methods of chromatography-spectroscopy/ IV a scientific and technical conference is «Advancement in oil and gas and to petrochemical industry». Lvov. p. 137-138. (in Ukrainian).

Letko V., 2000: Application of alternative fuels in combustion engines / M.: MADI. 311 p.

Tyutyunnikov B., Bukhshtab Z., 1992: Chemistry of fats. M. 448 p.
Biodiesel Zieht Stark An // of Produktion., 2002. - № 13. S. 4.
Tkachuk V., 2007: Improvement of physical and chemical indexes of biofuels due to the use of frapeseed oil izopropilesteriv/Collection of theses of lectures V scientific and technical conference «Advancement in oil and gas and to petrochemical industry» (on September, 11-14 in 2007). Lvov. p. 220-222.
Chulkov P., 1998: Motor fuels: resources, quality, substitutes. M. 416 p.
Terent'ev G., 1989: Motor of fuel from alternative sources of raw materials. M. 271 p.
Zakharchuk V., 2007: Bases of theory, construction and calculation of motor-car engines. Lutsk: LDTU. 216 p.
Devyanin S., Markov V., Semenov V., 2007: Vegetable oils and fuels on their basis for diesel engines. Kharkiv, 452 (in Ukrainian).
Fizer L., Fizer M., 1966: Organic chemistry. Moscow, 782 p. (in Russian).
Zakharchuk V., 2010: Application of alternative fuels in diesel engines. Kiev. №2, p. 26-28 (in Ukrainian).

OCENA WŁAŚCIWOŚCI EKSPLOATACYJNYCH PALIWA OLEJU NAPĘDOWEGO BIO NA PODSTAWIE OLEJU RZEPAKOWEGO I ALKOHOLU IZOPROPYLOWEGO

Streszczenie. Artykuł dotyczy analizy właściwości eksploatacyjnych paliwa napędowego bio, szczególnie temperatury tężenia, na podstawie której omówiono perspektywy i zalety alkoholu izopropylowego z oleju rzepakowego.

Słowa kluczowe: olej napędowy bio, diesel, toksyczność, alkohol izopropylowy, olej rzepakowy.

TEKA Kom. Mot. Energ. Roln. – OL PAN, 2011, 11, 457–466

THE PROPOSED METHODOLOGY FOR ANALYSIS OF ECOLOGICAL PROBLEMS CONCERNING THE TECHNICAL INFRASTRUCTURE OF MOTOR TRANSPORT

Edyta Zielińska, Kazimierz Lejda*

* Rzeszów University of Technology, the Faculty of Mechanical Engineering and Aeronautics

Summary. The most crucial threats found in facilities of the technical infrastructure of motor transport have been presented in the article. There are also issues concerning modelling an ecological strategy using a taxonomic method for the technical infrastructure as well as applied methods and techniques selected depending on particular problems and chosen objectives. The article describes criteria and basic assumptions of the taxonomic method as well as its application to assess ecological issues.

Keywords: technical infrastructure of motor transport, ecological problems, taxonomic method

INTRODUCTION

Nowadays motor transport plays a very important role in shaping the world's economy. It gives an easy access to modern products and technologies on all continents, thus improving effectiveness of each country's functioning [11]. However, the share of the individual regions of the world in the international trade traffic and the industrial cooperation is dependent on the technical condition of basic elements of motor transport, i.e. transport means and their infrastructure.

To keep transport means in a suitable technical condition, an adequate technical infrastructure of motor transport is required, equipped with specialty tools and diagnostic devices. The service and repair operations performed for internal combustion transport means in the technical infrastructure affect the proper operation of vehicles, but also generate pollution, which has a negative effect on the natural environment [3,14].

The ecological aspect of the subject matter is really crucial; sadly, the analysis of the actual status confirms that these issues are paid little attention to in technical infrastructures of motor transport. The problem related to the protection of environment is located at the bottom of the priority list for technical infrastructures. The economic effect from selling services, supported by expenditures on the marketing sphere and focused on maximisation of profits is still of the dominant significance [17]. The situation in the technical infrastructure can only be improved by appropriate normalisations and legal regulations, which are in force in the EU and which Poland will have to conform to as well.

ECOLOGICAL THREATS CONCERNING THE TECHNICAL INFRASTRUCTURE OF MOTOR TRANSPORT

The dynamic development of motor transport has had an adverse influence on the natural environment in recent years, because it has contributed to deterioration of conditions for living, working and relaxing as well as to the generation of important ecological problems of global range, i.e. acid rains, pollution of water and global warming [1,4]. The influence of motor transport on the environment may have a socio-economical character connected with the economic growth of individual regions, as well as a physical one, connected with multiple serious threats. The most important dangers are [20]:

- air pollution with toxic components of exhaust fumes,
- atmosphere pollution with used tyres and road surface products as well as dusts emerging from utilization of clutch and brake linings,
- a toxic influence of engine fuels during transport, distribution, storage and operation in motor vehicles,
- pollution of soil and water with washing and maintenance agents for a car body,
- a danger of leakages of fuels, oils and operating fluids,
- a noise and a road surface vibration danger caused by movement of vehicles,
- pollution of the natural environment caused by the recycling of retired vehicles and frequent replacing of spare parts (gaskets, filter cartridges etc.)

The pollutants from exhaust fumes of motor vehicles are the greatest burden for the atmosphere, due to the effect of combustion of various kinds of fuels containing many toxic compounds [15]. Pollutants generated in technical infrastructures of motor transport, which are the key elements in the system for proper operation of vehicles, also have a negative influence on the natural environment. The wide range of services of the technical infrastructure which cause pollution are warranty, periodic and according to a client's requirements inspections, comprehensive or selective diagnostics of functional blocks, periodic technical inspections, routine or accident repairs, sale or rent of vehicles as well as possible collecting of retired vehicles for recycling [5,6,10].

A technical infrastructure of motor transport functioning within a network structure of a given automotive consortium or a trade and service organisation is characterized by an established specificity imposed by the administration of these companies, resulting from the accepted concept for management. However, all these companies share similar ecological problems. The most crucial ecological threats concerning the technical infrastructure of motor transport are as follows [19]:

- air pollution with exhaust fumes in places for servicing or repairing vehicles (operating engines),
- noise emission in aforementioned places (operating engines),
- management and possible recycling of operating fluids (motor oil, gear oils, brake and power steering oils, brake fluid, cooling fluids, AC fluids etc.),
- management of used and replaced units, subsets and elements (steel elements, non-iron metals, polymers, rubber elements etc.) during inspections or repairs,
- protection of the environment against harmful influence of disposal sites for used vehicles designated for recycling.

The issue of environment protection, as one of basic factors for development of motor transport, goes unnoticed by an individual user or owner of a vehicle. The primary values for an individual owner of a motor vehicle resulting from marketing research, have been specified in Fig.1

Protection of the environment against the effects of development of motor transport gains a priority only in the social context, which includes the following actions [7,12]:

- protecting the environment against the effects of production and operation of vehicles, as well as the influence of the technical infrastructure of motor transport,
- reducing material and energy consumption as well as costs of production and operation of vehicles,
- increasing reliability and durability of vehicles,
- reducing material, energy and recycling costs of retired vehicles.

The influence of the aforementioned factors on the state of environment is not always directly visible. Their mutual relations are very complex, and environment is affected by many subjects, directly or indirectly, independently or dependently on each other. Durability and reliability of motor vehicles have a clear influence on the environment as well, because these qualities, among other things, cause reduction in the quantity of waste products from operation of vehicles. The material and energy consumption of production and operation processes also have a measurable influence on the environment, as well as the way of management of retired vehicles. The influence of costs of these processes on the environment is the least visible, however, it is to be remembered that pro-ecological actions are very expensive and the balance of finances is subjected to the same economic regulations in every social structure.

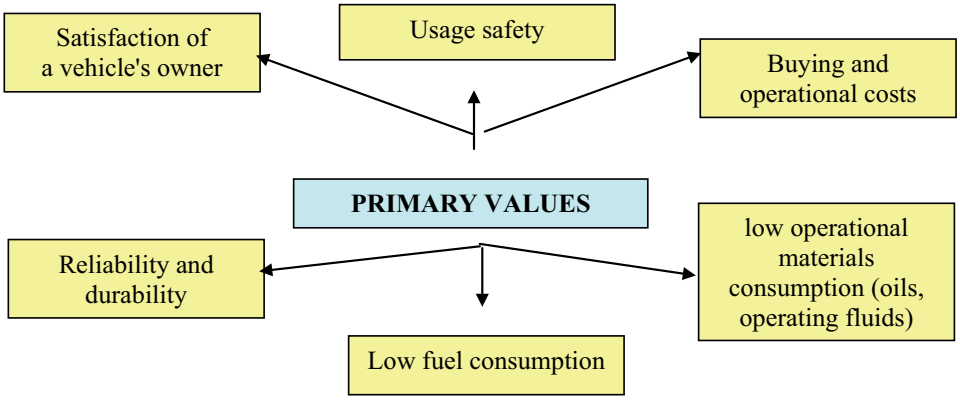

Fig. 1. Primary values for an owner of a motor vehicle

MODELLING LOGISTIC PROCESSES IN THE TECHNICAL INFRASTRUCTURE OF MOTOR TRANSPORT

Planning and controlling a logistic process in the technical infrastructure of motor transport requires a proper construction of its model. It should enable coordination between organisational units of every activity, tracking the process realisation time, the analysis of costs, the assessment of involvement and responsibility of individual units, relations between them, material goods movement, information flow, payments etc.

Different methods and techniques can be used to model logistic processes in the technical infrastructure of motor transport, chosen depending on particular problems and objectives. A model based on a taxonomic method can be employed to realize the established goals connected with the issue of the environment protection [2,8]. The choice of this method is appropriate mainly because the parameters which appear in the descriptions of technological issues and are expressed in different measurement units can be normalized receiving dimensionless values. The taxonomic method

enables the dendritic arrangement, which mirrors the location of a given technology better within a multidimensional space of parameters, so it is more transparent than optimisation methods. Generally, the taxonomic method is employed in natural science to good effect. In technical applications, projects which grasp comprehensively the issues of using taxonomic methods appear very rarely [9]. Using this method to develop a logistic system with an ecological aspect in mind, establishes a new quality for technical applications.

Methodology and the range of studies

To assess pro-ecological actions in progress in the technical infrastructure of motor transport, 15 companies have been chosen including car showrooms, fuel and repair stations, specialist car garages, depots, municipal and intercity transport, transport and spedition companies etc. The acquisition of the information regarding the selected parameters of a pro-ecological assessment (Table 1) has run into serious difficulties in some companies, due to the lack of properly kept documentation, treatment of waste as a total without selection with regard to the type, competence of employees responsible for this issue etc. Repeatedly, the information has been acquired from the additional analyses of statistical data relative to the quantity of performed inspections, repairs and other services within specified time [16].

Table 1. The parameters for a pro-ecological assessment of the technical infrastructure of motor transport selected for analysis

No.	PARAMETER SYMBOL	PARAMETER TYPE	MEASUREMENT UNIT
1	P1	Emission of volatile components from exhaust fumes (CO, HC, NO_x) to atmosphere	[kg/year]
2	P2	Emission of carbon dioxide ($CO_{2)}$ to atmosphere	[kg/year]
3	P3	Used tyres and rubber elements waste	[kg/year]
4	P4	Select plastics waste	[kg/year]
5	P5	Select non-iron metals waste	[kg/year]
6	P6	Iron metals waste	[kg/year]
7	P7	Select glass and ceramics waste	[kg/year]
8	P8	Select lubricant waste (motor and gear oils)	[dm^3/year]
9	P9	Other select operating fluids (cooling, brake, wiper and AC fluids)	[dm^3/year]
10	P10	Asbestos brake and clutch linings	[kg/year]
11	P11	Lead and NiCad batteries	[kg/year]
12	P12	Paint and lacquer waste removed during lacquering	[kg/year]
13	P13	Total quantity of material waste	[kg/year]
14	P14	Overall “quality” of generated waste	[0-1]*

15	P15	Emission of noise to surroundings (on average)	[dB]
16	P16	Level of pro-ecological investments per year	[thousands/PLN]
17	P17	Employment at jobs connected with ecological activities	[quantity of people]
18	P18	Level of employees' training in an ecological aspect	[0-1]**
19	P19	Implementation of management logistics system in an ecological aspect	[0-1]***
20	P20	Monitoring system and procedures for studies on threats to environment	[0-1]****
21	P21	Energy demand with reference to pro-ecological works (on average)	[kWh/month]

*0 - lowest, 1- highest; ** 0 - lowest, 1 - highest; *** 0 - lack of system, 1 - system implemented; **** 0 – lack of system, 1 - existing system

In the chronological order, the study methodology has included the following scope of tasks [18]:

- establishing and acquiring the cooperation of transport companies,
- analysing the kinds of services taking into consideration pro-ecological aspects in selected companies,
- selecting parameters for a pro-ecological assessment, which are possible to analyse and common for the studied companies,
- gathering data for established parameters for a pro-ecological assessment from every company,
- performing calculations using the taxonomic method,
- preparing a dendrite presenting the smallest differences between individual parameters for all studied companies,
- analysis of the study results.

The calculations have been performed using the taxonomic method for 15 companies (technologies), characterized by 21 parameters selected for analysis, using the following procedure*:

- determination of values of individual parameters for each technology according to the accepted measurement units (acc. table 1),
- addition of 4 exemplary technologies bearing WP2, WP13, WP14, WP21 (Table 2) signatures,
- design of the total dendrite for all 15 pro-ecological technologies, illustrating the accepted study procedure.

Multiple consultations with technical supervision and directly with the employees engaged in specific work types in the selected companies allowed to gain the most reliable and adequate values for individual parameters for each of the 15 technologies. The most essential parameters, because of a pro-ecological assessment of the technical infrastructure of motor transport, have been assigned exemplary technologies, choosing WP2 (emission of carbon dioxide to atmosphere), WP13 (total quantity of material waste), WP14 (overall "quality" of waste) and WP21 (the amount of energy demand).

* applicable to this article

THE STUDY RESULTS

Using the taxonomic method to assess pro-ecological problems in the technical infrastructure of motor transport allows for the description of a large amount of parameters in order to perform their proper analysis and correct reasoning [13]. While drawing conclusions from the performed analysis for the dendritic arrangement, the basic role is played by the sequence of connected points and the values of average differences between these points. Proximity and grouping of the particular technologies indicate the similarity among the examined parameters. In the final effect, the calculation results using the taxonomic method have enabled the construction of a dendrite, presenting distances within the space of the examined parameters (Fig. 2).

The constructed total dendrite for the differentiation of the technology for all the 15 selected companies enables to draw the following conclusions:

- with reference to CO_2, in the group of low emissions, the No. 6 technology has the lowest value, which under the project assumptions concerning the building of the technical infrastructure means that the other companies should aim at obtaining the values similar to the WP2 exemplary technology, or implement the existing and proved technology in the company, encoded under No. 6.
- among the companies of the lowest values of the sum of waste, the most advantageously located is the No. 4 technology, because it appears a short taxonomic distance away from the WP13 exemplary technology,
- the least harmful influence of waste on the natural environment is indicated by the company encoded as No. 2, which is located a short taxonomic distance away from the WP14 exemplary technology within the taxonomic space,
- from among the surveyed companies, the No. 8 technology shows the lowest energy consumption, which means that it is the least energy-intensive and appears very close to the WP21 exemplary technology within the taxonomic space.

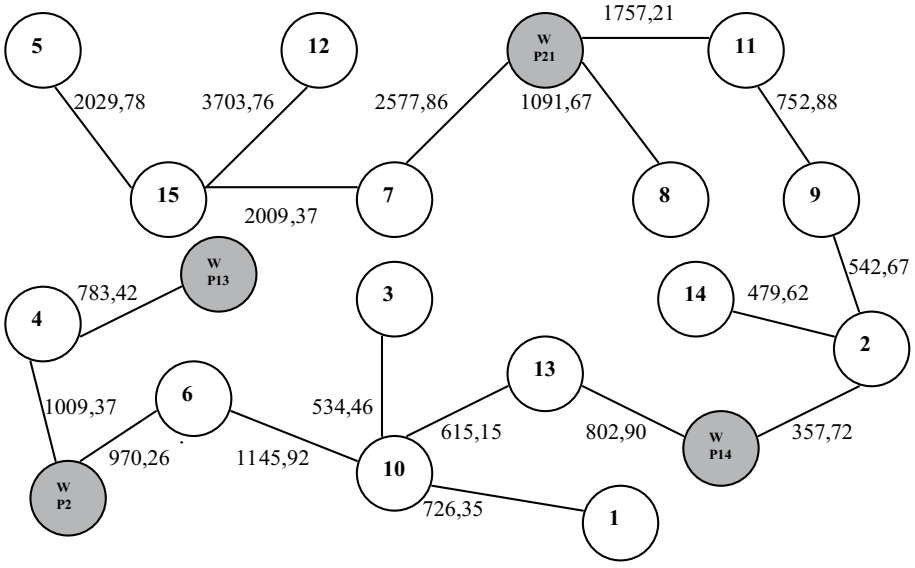

Fig. 2. The total dendrite for the differentiation of the technology for all of the 15 surveyed companies

Table 2. The total list of parameters for all of the surveyed companies

P / T	P1	P2	P3	P4	P5	P6	P7	P8	P9	P10	P11	P12	P13	P14	P15	P16	P17	P18	P19	P20	P21
min																					
max																					
min lub max		896,29											#######	0,87							250,00
60 % min		537,78											#######	0,52							150,00
1	131	929	10 809	1 016	2 119	26 696	1 720	3 867	3 976	3 667	4 032	615	58 518	0,35	60	41	4	0,20	0,95	0,67	800
2	90	1 328	7 279	1 209	1 787	31 339	1 666	6 996	3 755	4 614	4 134	594	63 372	0,72	78	66	4	0,85	1,00	0,79	900
3	71	1 679	6 637	1 098	2 982	29 997	1 406	4 693	4 306	1 666	2 399	662	55 846	0,27	68	36	5	0,49	0,66	0,95	950
4	46	1 000	5 233	402	698	17 245	856	2 816	1 630	1 992	914	197	31 982	0,26	110	76	2	0,98	0,17	0,13	600
5	136	2 647	9 533	1 807	2 866	78 595	2 504	5 587	5 362	4 115	2 527	619	113 516	0,13	120	85	6	0,26	0,71	0,73	975
6	52	1 221	7 489	970	2 651	19 658	1 559	6 716	3 660	3 265	1 987	332	48 288	0,49	79	79	3	0,28	0,69	0,50	740
7	248	3 017	13 336	2 814	3 378	58 771	2 771	9 248	3 157	6 978	5 200	771	106 424	0,31	69	92	7	0,27	0,89	0,11	250
8	142	1 921	8 261	1 916	2 930	41 464	2 571	12 316	4 747	4 142	6 111	504	84 961	0,87	50	75	5	0,97	0,60	0,18	1000
9	70	1 395	5 656	1 240	2 050	33 823	952	8 341	1 952	4 104	3 388	777	62 282	0,59	62	36	4	0,45	0,76	0,92	430
10	70	896	6 263	529	1 290	28 544	790	6 044	4 063	3 032	4 325	543	55 423	0,70	122	78	4	0,75	0,96	0,54	740
11	114	1 093	4 300	1 275	1 212	39 882	1 040	6 772	3 299	2 928	2 051	472	63 230	0,18	54	66	3	0,63	0,56	0,94	800
12	250	4 329	21 099	2 751	6 179	88 923	2 693	15 982	8 884	8 079	5 384	1 354	161 326	0,19	58	58	9	0,30	0,78	0,49	940

13	126	2 247	4 764	1 407	2 430	27 656	1 420	8 677	4 122	3 389	2 596	552	57 013	0,64	89	70	4	0,36	0,23	0,80	800
14	73	1 444	8 766	849	1 770	30 114	1 836	6 207	6 054	5 242	3 749	922	65 510	0,25	48	37	6	0,60	0,60	0,78	850
15	145	2 309	18 288	1 605	3 124	70 040	3 124	8 838	4 403	7 838	6 102	1 532	124 893	0,13	116	92	9	0,95	0,83	0,60	900
WP2	**53**	**672**	**4 697**	**397**	**967**	**21 408**	**592**	**4 533**	**3 047**	**2 274**	**3 244**	**407**	**41 568**	**1**	**92**	**59**	**3**	**1**	**1**	**1**	**555**
WP13	**34**	**750**	**3 925**	**301**	**524**	**12 933**	**642**	**2 112**	**1 222**	**1 494**	**686**	**148**	**23 987**	**1**	**82**	**57**	**2**	**1**	**1**	**1**	**450**
WP14	**106**	**1 441**	**6 196**	**1 437**	**2 197**	**31 098**	**1 928**	**9 237**	**3 560**	**3 106**	**4 583**	**378**	**63 721**	**1**	**37**	**56**	**4**	**1**	**1**	**1**	**750**
WP21	**186**	**2 262**	**10 002**	**2 111**	**2 534**	**44 078**	**2 078**	**6 936**	**2 368**	**5 233**	**3 900**	**578**	**79 818**	**1**	**52**	**69**	**6**	**1**	**1**	**1**	**187,5**

P – parameters, T – technology

CONCLUSIONS

Currently, the most pressing problem is the protection of the natural environment against the effects of the dynamic development of motor transport, the functioning of which causes many serious threats. Technical infrastructures of motor transport have a large share in the degradation of the environment, due to diagnostic inspections, routine and periodic maintenance, repairs and other kinds of services concerning vehicles which are performed there (e.g. car washes, paint shops etc.).

To assess these extremely important ecological issues, the taxonomic method can be used, which enables the dendritic arrangement mirroring the location of the examined factors within a multidimensional space of parameters [13,16]. The realisation of the subject matter presented in this article makes it possible to formulate the following conclusions of a general character:

- arranging pro-ecological technologies in the technical infrastructure of motor transport, using the taxonomic method is an effective way to find the point determined by the defined criteria within the space of the selected parameters,
- verification of the results for a differentiation of pro-ecological technologies with the dendritic arrangement method is possible with the help of the diagonal matrix of Czekanowski [17],
- the dendritic arrangement using the taxonomic method and the matrix one using the Czekanowski's method give concurrent results with reference to pro-ecological technologies in the technical infrastructure of motor transport [17].

As opposed to all kinds of optimization methods, which in reality only allow for a linear arrangement of the examined ecological problems, taxonomy enables the dendritic arrangement, which mirrors the location of the examined factors better within a multidimensional space of parameters.

REFERENCES

Born S., Sonzogni W.: Integrated environmental management: strengthening the conceptualization. Environmental Management, Nº19 (2)/1998.

Borys T.: Zastosowanie metod taksonomicznych. Wyd. Akademii Ekonomicznej, Seria „TAKSONOMIA", Zeszyt 1, Wrocław 1994.

Chaciński J., Jędrzejewski Z.: Zaplecze techniczne transportu samochodowego. Wyd. Komunikacji i Łączności, Warszawa 1982.

Chłopek Z., Danilczyk W., Gutowski J., Kruczyński S.: Ocena transportu drogowego w zakresie energochłonności i zanieczyszczenia środowiska – propozycje kierunkowe rozwoju. Materiały II Konferencji nt. „Racjonalizacja użytkowania energii i środowiska", Szczyrk 1994.

Lejda K.: Selected problems in car recycling. Polish Academy of Sciences – Brench in Lublin, TEKA, Vol. IV, Lublin 2003.

Lejda K.: Problemy recyklingu ogumienia pojazdów. Mat. IV Międzynarodowej Konf. Naukowej nt. „Problemy recyklingu", Rogów 2005.

Lejda K.: Recykling motoryzacyjny w wybranych krajach Unii Europejskiej. Mat. XVII Międzynarodowej Konf. Naukowej SAKON'06 nt. „Metody obliczeniowe i badawcze w rozwoju pojazdów samochodowych i maszyn roboczych samojezdnych. Zarządzanie i marketing w motoryzacji", Rzeszów-Przecław 2006.

Matusek M., Bartnicki M.: Metoda porównań międzyzakładowych z wykorzystaniem metod taksonomicznych. Zeszyty Nauk. PŚl, Nr 1597, Gliwice 2003.

Młodak A.: Analiza taksonomiczna w statystyce regionalnej. Wyd. DIFIN, Warszawa 2006.

Oprzędkiewicz J., Stolarski B.: Technologia i systemy recyklingu samochodów. Wyd. PWN, Warszawa 2003.
Rydzkowski W., Wojewódzka-Król K.: Transport. Wyd. Naukowe PWN, Warszawa 2009.
Stefanowicz T.: Wstęp do ekologii i podstaw ochrony środowiska. Wyd. Politechniki Poznańskiej, Poznań 1996.
Stolarski B.: Metody taksonomiczne w technologii samochodów. Wyd. Politechniki Krakowskiej, Kraków 1990.
Uzdowski M., Abramek K., Garczyński K.: Eksploatacja techniczna i naprawa. Wyd. Komunikacji i Łączności, Warszawa 2003.
Wojciechowska A., Wojciechowski T.: Motoryzacyjne zanieczyszczenie środowiska. Zeszyty Naukowe Politechniki Łódzkiej, Bielsko-Biała 1990.
Zielińska E.: Możliwość wykorzystania metody taksonomicznej do opracowania modelu zarządzania ekologicznego w zapleczu technicznych środków transportu. Materiały Międzynarodowej Konferencji Naukowej SAKON'06 nt. „Metody obliczeniowe i badawcze w rozwoju pojazdów samochodowych i maszyn roboczych samojezdnych; Zarządzanie i marketing w motoryzacji", Rzeszów-Przecław 2006r.
Zielińska E.: Logistyka zaplecza technicznych środków transportu samochodowego w aspekcie problemów ekologicznych. Rozprawa doktorska, Uniwersytet Przyrodniczy w Lublinie, Lublin 2008.
Zielińska E., Lejda K.: Wykorzystanie metody taksonomicznej do oceny problemów ekologicznych w zapleczu technicznym transportu. Czasopismo Logistyka Nº 1/2009 - wersja elektroniczna – CD.
Zielińska E., Lejda K.: Analiza i modelowanie procesów logistycznych w zapleczu technicznym transportu samochodowego w aspekcie problemów ekologicznych. Oficyna Wydawnicza Politechniki Rzeszowskiej, (s. 219), Rzeszów 2010.
Zielińska E., Lejda K.: Ecological problems of transport vehicle. Polish Academy of Sciences – Branch in Lublin, TEKA, Vol. X, Lublin 2010.

PROPONOWANA METODYKA ANALIZY PROBLEMÓW EKOLOGICZNYCH W ZAPLECZU TECHNICZNYM TRANSPORTU SAMOCHODOWEGO

Streszczenie. W artykule przedstawione zostały najistotniejsze zagrożenia występujące w obiektach zaplecza technicznego transportu samochodowego. Zaprezentowane zostały zagadnienia dotyczące modelowania metodą taksonomiczną strategii ekologicznej w zapleczu technicznym oraz stosowane metody i techniki dobierane w zależności od konkretnych problemów oraz wybranych celów. Wymieniono kryteria i podstawowe założenia metody taksonomicznej oraz jej aplikację do oceny zagadnień ekologicznych.

Słowa kluczowe: zaplecze techniczne transportu samochodowego, problemy ekologiczne, metoda taksonomiczna

TEKA Kom. Mot. Energ. Roln. – OL PAN, 2011, 11, 467–474

LOAD OF THE HYDROSTATIC SLIPPER IN AXIAL PISTON PUMPS

Tadeusz Zloto, Konrad Kowalski

Institute of Machine Technology and Production Automation
Częstochowa University of Technology

Summary. The paper presents an analysis of the load of hydrostatic slippers in axial piston machines and describes the load of the basic mating surfaces. The hydrostatic load and relief of the slipper was studied with reference to the fundamental mathematical relationships. The results of simulation calculations of the slipper's twisting moment during its operation depending on the angular velocity, working pressure of the slipper's mass, and the coefficient of friction occurring between the swash plate in the pressure zone of the pump were obtained in the MathCad software. Their graphic representations are also shown.

Key words: piston pump, hydrostatic slipper, twisting moment.

INTRODUCTION

The reliability and durability of volumetric hydraulic piston machines crucially hinges on the condition of hydrostatic supports. Under the normal operating conditions the hydrostatic slipper should 'float', i.e. the fluid friction conditions should occur in the gap between the slipper and the swash plate, which takes over the load. The hydrostatic slipper in axial piston machines is of relatively small size and transfers large loads in demanding conditions. The swash plate is inclined at a certain angle with respect to the piston axis. The fact that the piston load is located off the axis, the presence of friction and inertia load can turn the slipper over.

No satisfactory mathematical model of the whole process of designing hydrostatic slippers has been developed so far. Manufacturers of hydraulic pumps must therefore rely on laborious experimental studies, assuming some kind of a trade-off between losses resulting from leakages and the slipper's wear-out [Brzuchowski, Kertynska and Kraszewski 1974, Osiecki L. 1998, Renius 1973]. The increasing demand for new types of pumps and for improving their performance necessitates developing universal and reliable constructions of high efficiency.

SLIPPER'S LOAD IN AN AXIAL PISTON PUMP

Fig**.** 1 presents the load of an axial piston pump. The force F_p coming from the pressure in the cylinder block acts upon the front surface of the piston. The dynamic force F_a acts upon the

piston system of the mass m_c (of the piston and slipper). The force F_a depends on the linear acceleration and mass of the piston system. The friction force F_T acts against the reciprocating movement of the piston, the directions of the two are opposite.

The normal force of the piston acts upon the slipper. The magnitude of the force is:

$$F_N = \frac{0.25\pi \cdot d^2 \cdot p_1 + F_T + F_{spr} + m_c \omega^2 r_p \operatorname{tg}\alpha \cos\varphi}{\cos\alpha} \tag{1}$$

where:

p_1 – the pressure in the cylinder block,
F_{spr} – the force of the spring pressing the slipper,
F_T – the friction force between the piston and the cylinder,
m_c – the mass of the piston system,
r_p – the radius of cylinder distribution in the cylinder block,
α – the swash plate inclination angle,
φ – the current angle of the cylinder block rotation .

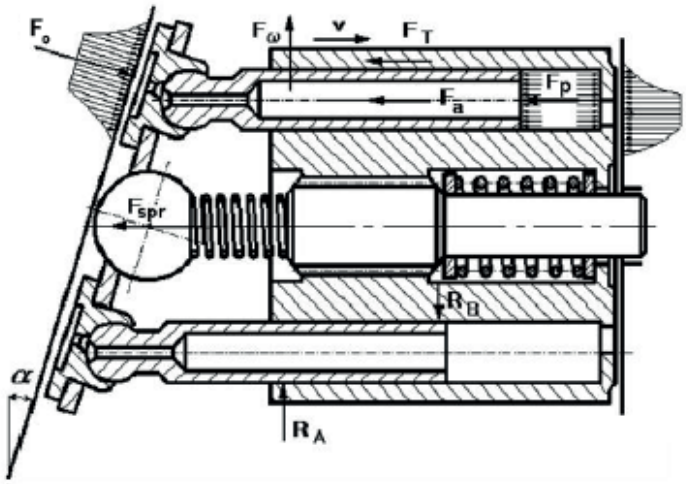

Fig. 1. Load of an axial piston pump

When a specific model (continuous or discrete) of the piston load and the friction coefficient μ_t are assumed, it is possible to find the reactive forces (Fig. 1) and friction occurring between the piston and the cylinder in accordance with [Kogl 1995, Oiecki A. 1998, Stryczek 1995]:

$$F_T = \mu_T \left(R_A + R_B \right) \tag{2}$$

HYDROSTATIC RELIEF OF THE SLIPPER

The slipper performs the task of transferring all the axial forces acting upon the piston system, and it is desirable to minimize energy losses and wear-out, and to maximize reliability within the full range of the pump operating parameters [Balas 1976, Osiecki A. and Osiecki L. 1998, Osiecki,

Niegoda 1976]. The slipper surface can have various shapes [Jerszow 1974, Jerszow B., Hiljuta and Jerszow Sz. 1993]. Regardless of the shape, there should be a central neck connecting the slipper with the piston pressure chamber.

In every typical slipper (Fig.2) an internal and external radius can be distinguished. The geometrical parameters of the slipper should be selected in such a way that the load carrying force resulting from the hydrostatic pressure field takes over 90 – 95 % of the normal load and the hydrodynamic force takes over the other 5 –10 % of the load [Baszta 1971]. In the derivation of the formula for the pressure change on the slipper sealing surface it is assumed that the mating surfaces are smooth, the flow is laminar and isothermal. The pressure change in a typical slipper is:

$$p = p_o \frac{\ln \frac{r_2}{r}}{\ln \frac{r_2}{r_1}} \tag{3}$$

where:

p, p_o - the pressures along the slipper radius and in the slipper chamber, respectively,
r_2, r, r_1 - the external, current, and internal radius of the slipper, respectively.

The repulsive force of a typical hydrostatic slipper is [Szydelski, Olechowicz 1986]:

$$F_o = p_o \frac{\pi}{2} \cdot \frac{r_2^2 - r_1^2}{\ln \frac{r_2}{r_1}} \tag{4}$$

The slipper construction affects power losses. The total power loss consists of the power lost due to leakage and friction loss. The crucial parameter is the gap height h_s (Fig. 2). With the increase in h_s the mechanical losses decrease, the volumetric losses, however, dramatically increase. Mechanical losses can be reduced by reducing the surfaces surrounding the gap. Slippers with additional bearing surfaces also contribute to minimizing mechanical losses by enabling significant hydrodynamic effects on a flat surface [Baszta, Zajczienko 1969, Lachner 1974].

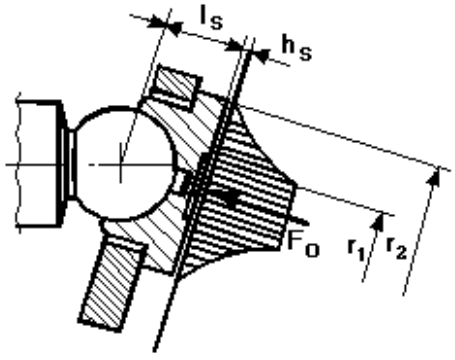

Fig. 2. Hydrostatic relief of the slipper

It is more difficult to design an axial piston pump of variable yield, in which it is necessary to transfer variable loads, resulting from the changes in the inclination angle α of the swash plate.

RESULTS OF THE SIMULATIONS OF THE SLIPPER LOAD

The twisting moment of the slipper was calculated for the pump of the typical dimensions and rated parameters as of those produced in Poland (p_{nom} = 32 MPa, Q = 45 l/min, n_{nom} = 1500 rotations/min). In the calculation model of the twisting moment, friction occurring between the slipper and the swash plate and centrifugal inertia force of the slipper were taken into consideration. The friction was obtained as a product of the force pressing the slipper towards the swash plate (obtained, in turn, as the difference of the normal force coming from the piston and the slipper hydrostatic relief) and the friction coefficient μ_s. The value of the friction coefficient was established empirically as μ_s = 0,003 [Niegoda 1977]. It was assumed that the pressure drop between the cylinder and the slipper operating chamber was 10 % (Cp = 0.9) [Ivantysyn J. and Ivantysynova M. 2001].

The value of friction was obtained as:

$$F_{TS} = \mu_S \left[\frac{0.25\pi d^2 p_1 + F_T + F_{spr} + m_c \omega^2 r_p tg\alpha \cos\varphi}{\cos\alpha} - C_p \frac{\pi p_1}{2} \left(\frac{r_2^2 - r_1^2}{\ln \frac{r_2}{r_1}} \right) \right. \tag{5}$$

and the value of the centrifugal inertia force of the slipper as:

$$F_{\omega s} = m_s \left(\frac{\omega \cos\alpha}{\cos^2\varphi + \cos^2\alpha \cdot \sin^2\varphi} \right)^2 \cdot r_p \sqrt{1 + tg^2\alpha \cos^2\varphi} \tag{6}$$

The resultant force acting upon the slipper was obtained as a geometrical sum of the projections of the component forces in the set of coordinates *xy*:

$$F_W = \sqrt{F_{WX}^2 + F_{WY}^2} \tag{7}$$

After substituting and bringing the inertia force onto the plane on which the slipper and the swash plate mate:

$$F_W = \sqrt{\left(-F_{TS} \cos\varphi + F_{\omega s} \cdot \frac{l_s}{l_{sc}} \sin\varphi \right)^2 + \left(F_{TS} \sin\varphi + F_{\omega s} \cdot \frac{l_s}{l_{sc}} \cos\varphi \right)^2} \tag{8}$$

where:

l_s – the distance between the coupling centre and the mating surface,

l_{sc} – the distance between the gravity centre and the mating surface.

The slipper's twisting moment is:

$$M_S = l_s \left| \begin{array}{l} \left\{ -\mu_s \left[\dfrac{0.25\pi d^2 p_1 + F_T + m_c \omega^2 r_p tg\alpha \cos\varphi}{\cos\alpha} - C_p \dfrac{\pi p_1}{2} \left(\dfrac{r_2^2 - r_1^2}{\ln \dfrac{r_2}{r_1}} \right) \right] \cos\varphi + \right. \\ \left. + m_s \left(\dfrac{\omega \cos\alpha}{\cos^2\varphi + \cos^2\alpha \cdot \sin^2\varphi} \right)^2 r_p \sqrt{tg^2\alpha \cdot \cos^2\varphi + 1} \dfrac{l_{sc}}{l_s} \sin\varphi \right\} + \\ + \left\{ \mu_s \left[\dfrac{0.25\pi d^2 p_1 + F_T + m_c \omega^2 r_p tg\alpha \cos\varphi}{\cos\alpha} - C_p \dfrac{\pi p_1}{2} \left(\dfrac{r_2 - r_1}{\ln \dfrac{r_2}{r_1}} \right) \right] \sin\varphi + \right. \\ \left. + m_s \left(\dfrac{\omega \cos\alpha}{\cos^2\varphi + \cos^2\alpha \cdot \sin^2\varphi} \right)^2 r_p \sqrt{tg^2\alpha \cdot \cos^2\varphi + 1} \dfrac{l_{sc}}{l_s} \cos\varphi \right\} \end{array} \right| \tag{9}$$

In Eq. (9) the variable friction F_T being a function of the cylinder block rotation angle and occurring between the piston and the cylinder was calculated on the basis of a newly developed simulation model, which will be discussed in detail in subsequent publications.

Fig. 3 presents the dependence of the slipper twisting moment on the angular velocity of the cylinder block for the pressure zone.

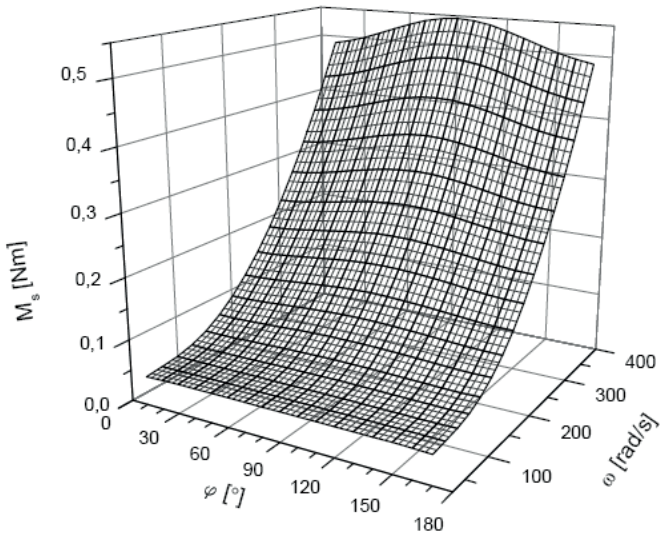

Fig. 3. Twisting moment of the slipper as a function of the angular velocity of the cylinder block for the pressure zone

As can seen in Fig. 3, the influence of the angular velocity ω on the slipper twisting moment M_s is significant. Fig. 4 shows that the impact of the pressure on the twisting moment of the slipper is insignificant.

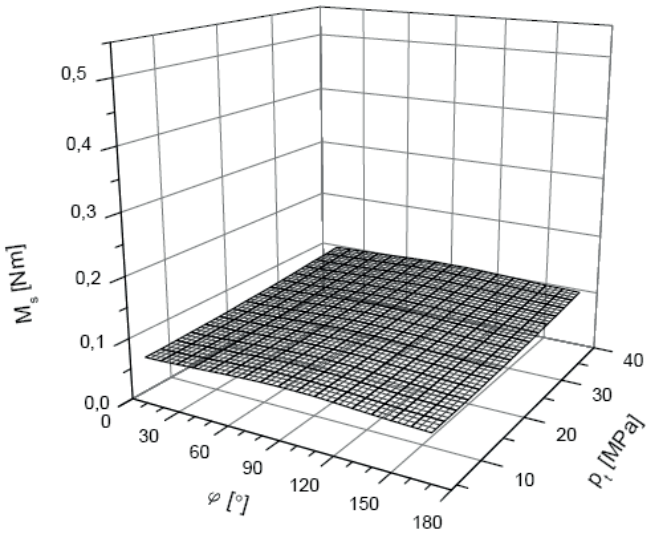

Fig. 4. Values of the slipper twisting moment depending on the pressure in the pressure zone

Fig. 5 shows values of the twisting moment depending on the slipper mass. For pressures zone, changes in the slipper mass affect the value of the twisting moment significantly.

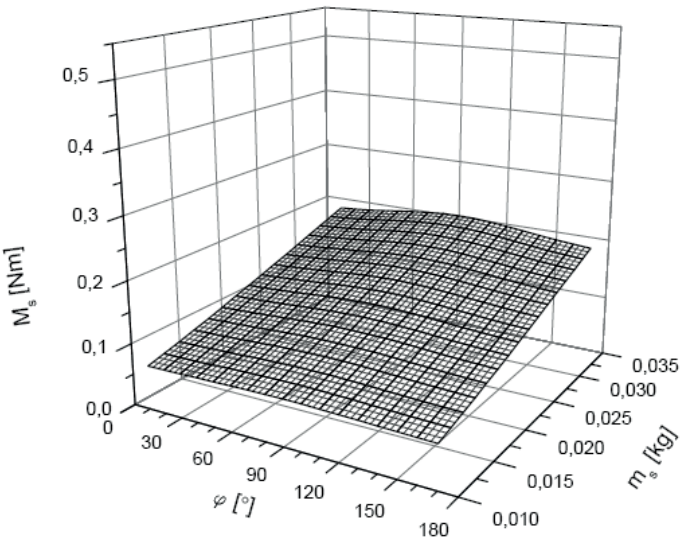

Fig. 5. Values of the twisting moment depending on the slipper mass for the pressure zone

In Fig. 6 the values of the slipper twisting moment are presented as a function of the friction coefficient for friction occurring between the slipper and the swash plate.

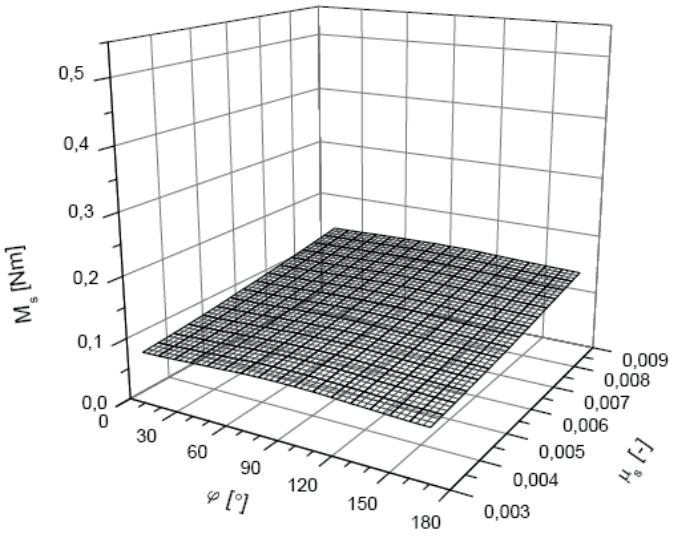

Fig. 6. Values of the slipper twisting moment depending on the friction coefficient for friction occurring between the slipper and the swash plate in the pressure zone

It can be observed that the friction coefficient affects the twisting moment significantly. The other construction parameters, such as the piston system mass, the spring pressing force, or exploitation parameters, such as the swash plate inclination angle, or friction between the piston and cylinder only slightly affect the value of the twisting moment.

CONCLUSIONS

The following conclusions can be formulated on the basis of the study:

- the decisive factor affecting the value of the twisting moment is the angular velocity of the cylinder block,
- the calculation model employed in the study is adequate for determining the influence of the basic construction and exploitation parameters of the pump on the slipper twisting moment,
- the accuracy of the twisting moment value obtained in the calculations crucially depends on friction occurring between the slipper and the swash plate. The relevant friction coefficient can be obtained only empirically.

REFERENCES

Balas W.,1976: Łożyska hydrostatyczne w osiowych pompach tłokowych. Przegląd Mechaniczny, nr 11.

Baszta T. M., 1971: Maszinostroitielnaja gidrawlika. Maszinostrojenie, Moskwa.
Baszta T.M., Zajczienko I. Z. 1969: Objemnyje gidrawliczieskije priwody. Maszinostrojenie, Moskwa.
Brzuchowski E., Kertyńska H., Kraszewski D., 1974: Wyniki badań modelowych oraz analiza wpływu tarcia na stan obciążenia elementów łożysk hydrostatycznych. Przegląd Mechaniczny, nr 21.
Ivantysyn J., Ivantysynova M., 2001: Hydrostatic Pumps and Motors. Akadmia Books International, New Delhi.
Jerszow B. I., 1974: Otżymajuszczaja siła w torcowom zazorie niekotorych gidrawliczieskich ustrojstw. Wiestnik Maszinostrojenia, nr 5.
Jerszow B. I., Hiljuta I. M. Jerszow Sz. B.,1993: Ispytanie podpiatnikow aksjalnych maszyn. Wiestnik Maszinostrojenia, nr 1.
Kogl Ch., 1995: Versterbale hydrostatische Verdrangereinheiten im Drehzahl – und Drehmomentregelkreis am Netz mit angepaβtem Versorgungsdruck. Dissertation RWTH, Aachen.
Lachner H., 1974: Hydrostatische Lagerungen in Axialkolbenmasinen. Oldhydraulik und Pneumatik, nr 8.
Niegoda J., 1977: Badanie możliwości zastosowania tłoków z bezprzegubowym
podparciem hydrostatycznym w pompach i silnikach wielotłoczkowych osiowych. Rozprawa doktorska, Politechnika Gdańska.
Osiecki A., 1998: Hydrostatyczny napęd maszyn. WNT, Warszawa.
Osiecki A., Osiecki L., 1998: Prace rozwojowe nad nową konstrukcją pomp wielotłoczkowych osiowych. Przegląd Mechaniczny, nr 4.
Osiecki L., 1998: Badanie zjawisk zachodzących w zespole tłoczek – stopka hydrostatyczna – dławik śrubowy maszyny wielotłoczkowej osiowej. Rozprawa doktorska, Politechnika Poznańska.
Osiecki A., Niegoda J.,1976: Tarcie w węźle tłoka maszyn wielotłoczkowych osiowych. Przegląd Mechaniczny nr 6.
Renius K.T., 1973: Experymentelle Untersuchungen an Gleitschuhen von Axialkolbenmaschinen. Olhydraulik und Pneumatik, 17 nr3.
Stryczek S., 1995: Napęd hydrostatyczny. WNT, Warszawa.
Szydelski Z., Olechowicz J., 1986: Elementy napędu i sterowania hydraulicznego i pneumatycznego. Warszawa.

OBCIĄŻENIE STOPEK HYDROSTATYCZNYCH MASZYN WIELOTŁOCZKOWYCH OSIOWYCH

Streszczenie. W opracowaniu przedstawiono analizę obciążenia stopek hydrostatycznych występujących w maszynach wielotłoczkowych osiowych. Przykładowo opisano obciążenie podstawowych par kinematycznych pompy wielotłoczkowej osiowej. Przeanalizowano obciążenie jak i odciążenie hydrostatyczne stopki ze wskazaniem użycia podstawowych zależności matematycznych. Wyeksponowano graficznie rezultaty obliczeń symulacyjnych w programie MathCad momentu skręcającego stopkę podczas jej pracy w zależności od prędkości kątowej, ciśnienia roboczego masy stopki i współczynnika tarcia występującego pomiędzy stopką a tarczą pochylną w przedziale strefy tłocznej.

Słowa kluczowe: pompa tłoczkowa, stopka hydrostatyczna, moment skręcający.

SPIS TREŚCI